Electromagnetic Wave Propagation in Turbulence

Evaluation and Application of Mellin Transforms

SECOND EDITION

Richard J. Sasiela

SPIE
PRESS
Bellingham, Washington USA

Library of Congress Cataloging-in-Publication Data

Sasiela, Richard J., 1940-2007
Electromagnetic wave propagation in turbulence : evaluation and application of Mellin transforms / Richard J. Sasiela. -- 2nd ed.
p. cm.
Includes index.
ISBN 978-0-8194-6728-7
1. Electromagnetic waves--Transmission. 2. Atmospheric turbulence. 3. Mellin transform. 4. Numerical calculations. I. Title.

QC665.T7S27 2007
539.2--dc22

2007004557

Published by

SPIE—The International Society for Optical Engineering
P.O. Box 10
Bellingham, Washington 98227-0010 USA
Phone: 360.676.3290
Fax: 360.647.1445
Email: spie@spie.org
www.spie.org

Printed in the United States of America.

Cover photo: provided with permission of Lincoln Laboratory, Massachusetts Institute of Technology

To my wife Joan whose love and support has meant so much

Contents

Preface to the first edition

This book is directed at two audiences: those interested in problems of electromagnetic wave propagation in turbulence and those interested in evaluating integrals. For the first group, the text provides a systematic way to obtain analytic answers to problems in which the scintillation is small and there are no nonlinear effects due to high optical powers. For those interested in evaluating integrals, the integration method is explained in separate chapters. In the chapters containing examples of wave propagation in turbulence, the problem is quickly reduced to one of evaluating an integral, and can be viewed as examples of the integration technique.

To address these two audiences, this book develops a systematic way of expressing solutions to problems of electromagnetic wave propagation in turbulence in integral form. It also develops Mellin transform techniques that are used to evaluate these integrals. This technique has three major advantages over others: 1) it is applicable to a wide range of problems; 2) the application of the technique is straightforward; and 3) the answers are expressed in analytic form. Mellin transform and hypergeometric functions have been a scientific backwater and are used regularly by only a few people. That is a shame for several reasons. Mellin transforms allow a deeper understanding of infinite series. Knowing the Mellin transform of a function is tantamount to knowing its infinite series. Mellin transform techniques, which require an understanding of hypergeometric functions, enable one to deepen his or her understanding of elementary and transcendental functions. In addition to this pedantic usefulness, it is a natural way to solve several types of problems that have wide applicability. For instance, Mellin transforms permit one to perform integrations that are very difficult to perform by other means. They enable one to solve boundary value problems in spherical and cylindrical coordinates with the same ease that Fourier transform techniques afford in solving differential equations with constant coefficients. The self-similar characteristic of Mellin transforms leads to applications in image, radar and acoustic processing, and chaos and fractal theory.

The major part of this book develops and applies a method for evaluating integrals analytically and expressing the result either as infinite series or as a sum of generalized hypergeometric functions. At first look, the method to evaluate integrals is formidable, and the final results look very complicated. It has been suggested that results from a numerical integration can be obtained more quickly. One has to overcome these prejudices. It is true that the formalism is difficult to learn because it uses mathematical techniques that are generally unfamiliar to most scientists, but that was not a valid excuse for not learning other difficult techniques, which are part of a standard scientific education. If

the formalism produces results that are useful, one should be willing to overcome the initial difficulty.

This technique has indeed proved to be very useful! The expressions for the power series, although lengthy to write down, are easily and quickly evaluated using the recursion relation for gamma functions. Recently several computer algebra programs have acquired the ability to evaluate generalized hypergeometric functions, to which the power series are equivalent. In this context the results are no more difficult to evaluate and plot for specific cases than results expressed in terms of more familiar functions such as sinusoids and exponentials. The analytic form of the answer uncovers the natural parameters of a problem and gives one insight into how important a parameter is — an insight that is difficult to develop with numerical techniques. Integrands that contain the difference of two almost equal quantities, a condition that leads to difficulties in numerical integration, are handled in the complex plane by simply deforming an integration path past a pole. Because the technique is algorithmically based, one can develop a computer algebra program that automatically evaluates these integrals, in which case the user would not need to learn the details of the technique to get an analytic answer and to generate curves for specific ranges of parameter values. The development of such a program is being investigated. Just as scientific calculators made tables of trigonometric functions and logarithms obsolete, such a computer program would do the same to most material in integral tables. It would also allow one to evaluate many integrals that are not in the integral tables.

This technique was originally developed to evaluate integrals one encounters when solving problems of electromagnetic wave propagation in turbulence. The technique enables one to solve problems in terms of integrals that are generated with filter functions that multiply the turbulence spectrum. Problems that take days to solve when one starts from first principles can often be solved in less than an hour with appropriate filter functions and Mellin transform techniques.

The techniques given in this book were developed over several years in the high-energy beam-control and propagation group at MIT Lincoln Laboratory. I would like to thank MIT Lincoln Laboratory for providing the opportunity to work on challenging problems for which this technique was developed, for the freedom to pursue research in this area, and for the chance to interact with people interested in helping to develop this technique. This work was sponsored by the Strategic Defense Initiative through the Department of the Air Force under Contract No. F19628-90-C-0002.

I chose to solve many of the problems to illustrate the method developed in this book. I did not do a comprehensive literature search to see if these problems were previously solved. I apologize if I have left out relevant references.

Several people provided ideas that enabled me to develop the technique. Lee Bradley first suggested the possible usefulness of Mellin transform techniques and the existence of the Marichev text. He also suggested the use of Gegenbauer polynomials in addressing the anisoplanatism problem. The technique of eval-

uating integrals in several complex planes was developed in collaboration with John Shelton.

Many people had a hand in suggesting what material to include, and how it should be organized. I would like to especially thank Jonathan Shonfeld for carefully reading the first draft and suggesting many organizational changes. I have had many suggestions from Robert Kramer, Hernan Praddaude, Ronald Parenti, and Charles Primmerman. Fred Knight was very helpful in converting the text into LaTeX. Jim Eggert was particularly helpful since he was willing to read the text during several stages of the evolution of this book and made many useful suggestions. The series editor Professor Hermann Haus and the Springer-Verlag editor Helmut Lotsch made helpful suggestions on how the material should be presented. I want to thank Bill Breen, Ed Sullivan, Dave Tuells, Kevin Walsh, and their staff for producing the figures, converting them into Postscript, and printing the final copy. Sue Richardson and Katharine Krozel provided useful editorial help.

A book like this that contains so much new material and has so many complicated equations is very difficult to make error free. I would appreciate hearing any comments you have on the material or errors you have found in the text. My E-mail address is Sasiela@ll.mit.edu.

Writing a book takes a tremendous investment in time and energy that is no longer available for home life. I thank my wife Joan for being so understanding during this period.

October, 1993 Richard Sasiela
Lexington, Massachusetts

Comments about the second edition:

The first edition was published by Springer-Verlag. This edition corrects typographical errors in that edition. The treatment of tilt of uncollimated beams was incorrect in Sections 4.5, and 4.6 because a γ that should have multiplied the diameter was missing. It was pointed out by Jan Herrmann that it was necessary to use the local tilt in these sections.

As pointed out by Byron Zollars, there were some internal inconsistencies with 2π factors in the development of the general formula for variance due to turbulence. This affected some intermediate formulas in Chapters 2 and 3.

Since the propagation of focused beams has become more important, this case has been treated more carefully and extensively.

The derivation of the basic equations for variance and the removal of Zernike terms is developed more carefully.

Many problems can be solved by using the filter functions for variance. For more complicated problems one needs to start with the filter functions for phase or log-amplitude and develop the variance filter functions from these. Several examples on how to do this are illustrated.

Computer algebra programs have become more powerful and many of the integrals can now be solved with these programs. Solving these problems by hand is time consuming and error prone. Having these programs to do this part of the analysis is very helpful.

Typically, one is interested in the Strehl ratio. Analytic solutions are obtained for the variances. The approximations for the Strehl ratio using the phase variance do not give accurate results for many cases of interest. The use of filter functions in the structure function is elaborated in this edition. The problem of finding the Strehl ratio when the structure function is a function of aperture position is addressed. Examples of solving for the Strehl ratio numerically are given.

Chapter 6 of the original book discussed other uses for Mellin transforms. This chapter was not needed for the development of the subsequent chapters. Since I have nothing new to add on this subject, the chapter was eliminated because of the additional topics that were addressed.

I want to thank Ronald Parenti who I have worked with on turbulence problems for over 30 years. Our recent collaboration with Professors Larry Andrews and Ronald Philips has been very productive.

Recent computer code results indicate that the calculation of the scintillation for finite beams based on Rytov theory is in error. The beam wave theory predicts a dip in the scintillation index for Fresnel number around unity. Code results predict a smaller dip. Apparently, the perturbation theory that starts with a diffraction-limited beam on axis is incorrect. In the region of error the tilt can be comparable to the beam diameter. In addition, the focus term caused by turbulence causes a change in beam size, which violates the diffraction-limited assumption. Various authors have corrected the Rytov scintillation by separately including the effects of jitter and beam spreading.

I want to thank Seth Trotz for solving the many problems encountered in converting this document into LaTeX 2_ε. Also, I want to thank Eric P. Magee and his students for pointing out errors in the draft copy of this edition.

Beth Huetter of SPIE helped to correct errors and produce a uniform format.

This work was sponsored by the Department of the Air Force under Air Force Contract FA8721-05-C-0002. Opinions, interpretations, conclusions, and recommendations are those of the author and are not necessarily endorsed by the United States Government.

February, 2007 Richard Sasiela
Lexington, Massachusetts

Glossary

$(a)_k$	Pochhammer symbol
$A(\boldsymbol{\kappa}, z)$	Amplitude of second wave
$B_\phi(d)$	Phase correlation function
c	normalized wavenumber, speed of light
C_n^2	Turbulence strength
$C_p^\lambda(x)$	Gegenbauer polynomial
D	Aperture diameter
D_i	Inner diameter of annulus
D_s	Diameter of a finite source
$\mathcal{D}(\mathbf{d}, \boldsymbol{\rho})$	Structure function of total turbulence
D_c	Characteristic source diameter for scintillation averaging
$\mathcal{D}_v(\mathbf{r})$	Structure function of velocity
$\mathcal{D}_n(\mathbf{r})$	Structure function of atmospheric density
$\mathcal{D}_\phi(\mathbf{d}, \boldsymbol{\rho})$	Structure function of phase
$\mathcal{D}_\chi(\mathbf{d}, \boldsymbol{\rho})$	Structure function of log-amplitude
$E_n(\boldsymbol{\kappa}, z)$	Normalized axial correlation function of turbulence
$f(\kappa)$	Normalized turbulence spectrum
$F(\Omega_1, \ldots, \Omega_k)$	$(n_1!)^{\Omega_1} \cdots (n_k!)^{\Omega_k}$
$F(\gamma\boldsymbol{\kappa})$	Aperture filter function
F_N	Fresnel number
${}_pF_q[(a);(b);z]$	Generalized hypergeometric function
$g(k)$	Hill Spectra
$g(\boldsymbol{\rho})$	Aperture weighting function
$G(\gamma\boldsymbol{\kappa})$	Complex aperture filter function
$G_{p,q}^{m,n}\left[z \middle\vert \begin{matrix} a_1, \ldots, a_p \\ b_1, \ldots, b_q \end{matrix}\right]$	Meijer's G-function
H	End altitude of propagation path
$H_{p,q}^{m,n}\left[z \middle\vert \begin{matrix} (a_1, \alpha_1), \ldots, (a_p, \alpha_p) \\ (b_1, \beta_1), \ldots, (b_q, \beta_q) \end{matrix}\right]$	Fox's H-function
$J_\nu(x)$	Bessel function
$\mathbf{k}$	Three-dimensional propagation vector $(\boldsymbol{\kappa}, k_z)$

k_0	$2\pi/\lambda$, wavenumber
k_z	Propagation vector along propagation direction
$K(\alpha)$	Modulation transfer function of a circular aperture
$K_\nu(x)$	Modified Bessel function of the third kind
L	End point of propagation path
L_i	Inner scale with definition $L_i = 2\pi/\kappa_i$
L_{in}	Inner scale with definition $L_{in} = 5.92/\kappa_i$
L_o	Outer scale
$n(\mathbf{r})$	Variation of air density with position
$P(\gamma, \kappa, z)$	Diffraction parameter
r_o	Coherence diameter of a plane wave
r_{os}	Coherence diameter of a spherical wave
R_o	Radius of curvature of beam wave at the source
$s,\ s_n,\ t$	Complex variables
$S(p_1, \ldots, p_k)$	$\sum_{n_1=p_1}^{\infty} \cdots \sum_{n_k=p_k}^{\infty} \frac{(-1)^{n_1+\cdots+n_k}}{n_1! \cdots n_k!}$
$S_\phi(\omega)$	Power spectral density of phase
$S_\chi(\omega)$	Power spectral density of log-amplitude
SR	Strehl ratio
t	Time or second complex variable
$\mathbf{u}_z$	Unit vector in propagation direction
$U(x)$	Heaviside unit step function
v_n	n^{th} velocity moment of turbulence
v_g	Wind ground speed
$v(h)$	Wind speed as a function of height
W_o	$1/e^2$ radius of beam wave
$Z(m, n)$	Zernike polynomial
$\alpha(h)$	Normalized atmospheric density versus altitude
γ	Propagation parameter
$\Gamma[x]$	Gamma function
$\delta(x - a)$	Dirac delta function
Δn_0	Difference of refractive index between two colors
θ_o	Isoplanatic angle
θ_χ	Characteristic source angle for scintillation reduction
θ_s	Angle subtended by a finite source
κ	Transverse wavenumber
κ_i	Wavenumber of inner scale
κ_o	Wavenumber of outer scale

λ	Wavelength
μ_m	m^{th} turbulence moment
μ_m^+	m^{th} upper turbulence moment
μ_m^-	m^{th} lower turbulence moment
$\nu(\boldsymbol{\kappa}, z)$	Fourier transform of refractive index variations
$\boldsymbol{\rho}$	Two-dimensional transverse spatial vector
τ	Time delay between measurement and correction
$\varphi(\boldsymbol{\rho}, z)$	Phase variation due to turbulence
$\varphi R(\boldsymbol{\rho}, z)$	Phase related quantity
$\Phi_1(\boldsymbol{\rho}, z)$	Total variation of the turbulence fluctuations
ψ	Psi or digamma function
$\chi(\boldsymbol{\rho}, z)$	Log amplitude due to turbulence
$\chi R(\boldsymbol{\rho}, z)$	Log-amplitude related quantity
ω	Radian frequency of turbulence variation
$\zeta(s)$	Riemann zeta function

Chapter 1

Introduction

Solving problems of wave propagation in turbulence is a field that occupies the services of a small group of researchers. The methods used in this community and the results obtained are not generally known by researchers in other communities. The main reason is that the field is considered difficult, and if there is not an obvious need to investigate the effects of turbulence, they are neglected. The difficulty arises from the need to solve stochastic differential equations. Advances made by Tatarski and Rytov reduce problems to multiple integrals. These integrals are often difficult to evaluate since fractional exponents of functions appear in integrands. The final step in most cases is to evaluate these integrals numerically and to present the results as parametric curves. Many cases are run to develop some insight into how a quantity of interest varies with parameters. Becoming an expert in this field requires a great deal of time to become familiar with these graphical results so that one has some insight into various effects.

As pointed out above, there is a formalism for reducing a problem to quadratures. This process is lengthy, and there are several ways of doing it. Different workers use different methods to get at the same result. This makes it difficult for the novice to understand the literature and to realize that there is some underlying order. This discourages a person with only a casual interest from developing a facility in this field. It was to make the solution of these problems more algorithmic that the methods expounded in this book were developed.

In this book I use the Rytov approximation to reduce a very general problem to a triple integral. I develop techniques that allow one to evaluate these integrals analytically.

The integrals that one encounters contain products of functions of which one or more is a Bessel function. Workers in the field look for these integrals in integral tables, and if unsuccessful, resort to numerical analysis. Even numerically, some of these integrals are difficult to evaluate. The integrand is often either the product of a function that goes to infinity multiplied by one that goes to zero at one of the integration limits, or the difference of two functions that each lead to a divergent integral. Great care must be exercised in evaluating these integrals.

The techniques developed in this book provide a recipe for obtaining analytical solutions. There is a saying, "You don't get something for nothing." Indeed, there is a price to be paid for being able to solve these problems more easily: The

method uses mathematical techniques that are not generally taught to physicists and engineers, and one has to be willing to learn these techniques. One has to become familiar with Mellin transforms, gamma functions, generalized hypergeometric functions, asymptotic techniques, and pole-residue integration in one or more complex planes. Once these techniques are mastered, one can quickly solve complicated problems of wave propagation in turbulence. In addition, learning these techniques has some important ancillary benefits that are also discussed in this book. The techniques can be applied to most integrals in tables. In addition, one can easily evaluate integrals that are not in the tables. Since complicated integrals appear in many fields, the technique has wide applicability. Also Mellin transform techniques can be applied to solve differential and integral equations and have found many other applications as well.

An objection voiced against this method is that expressing an integral in terms of generalized hypergeometric functions is not very useful. The argument against the use of these functions is rapidly fading with the increasing accessibility of personal computers. These functions can be evaluated easily with recursion relations; in addition, they have become even easier to use since the introduction of computer algebra programs on personal computers that manipulate these functions just as easily as trigonometric functions. It is easy to evaluate expressions in which these functions appear, and there is no reason to eschew them any more than Bessel functions.

1.1 Book Plan

In this book I systematize the solution of many practical problems in wave propagation through turbulence. In Sec. 2 of this chapter the Mellin transform and the Mellin convolution integrals are introduced. A short table of Mellin transforms that are used to solve propagation problems in turbulence is also given.

In Chap. 2 the Rytov approximation for wave propagation is introduced as is the concept of the turbulent spatial spectrum. I describe a fairly general problem of wave propagation in turbulence that is solved with the Rytov approximation. This problem involves the difference between the log-intensity or phase of two waves that can be propagating in different directions or be displaced from each other and have different focal distances. I show that solutions to problems of this kind can be reduced to triple integrals; one integral along the propagation direction and two along the spatial transform wavenumbers of the wave. Most problems encountered in practice are special cases of this general problem.

For the Rytov approximation to be valid, the log-amplitude variance σ_χ^2 must be less than approximately 0.35. Above that value the scintillation is referred to as saturated, and it does not increase much with increasing propagation distances. The formulas using the Rytov approximation incorrectly result in scintillation values that continue to grow without bound. Even when the Rytov derived formulas give a log-amplitude variance result above the saturated value,

the values obtained for the phase variance are generally valid, and the methods given in this book give correct answers.

For some problems, such as those that rely on the amplitude returns for tracking or in which one must determine the bit-error rate in an optical communications system, one needs the probability distribution function of the amplitude. For aperture diameters small compared to the coherence diameter, the main effect is amplitude fluctuations in the receive aperture since phase fluctuations are small. In this case it is found that the log-amplitude fluctuations are Gaussian and thus the intensity has a log-normal distribution that is specified by the single parameter of the scintillation index. For very large diameters the amplitude is the sum of a large number of terms that have a random phase. This leads to a negative exponential distribution of the intensity.

In the intermediate range of diameter the situation is more complicated. The tilt of the beam can produce displacements that are comparable or larger than the beam diameter. The scintillation and the intensity distribution function depend on the degree of tracking. The distribution function is characterized by several parameters. It has not been derived analytically and is typically specified by fits to data generated by computer simulations. This has led to semi-heuristic formulas for these parameters that are given in *Parenti et al.* (2006).

In addition, the first-order Rytov solution cannot be used in the saturated region. For these problems, one approach is to use a wave-optics code in which the wave is propagated forward in a computer simulation. Another approach is to use amplitude statistics that have been obtained experimentally or by computer simulations. *Nakagami* (1960) found that the amplitude distribution is gamma-gamma. The scintillation in the saturated region is surprisingly dependent on the outer scale size and is strongly affected by the inner scale size. The use of a semi-heuristic approach to determining this distribution is given in *Andrews* (2001) and *Tyson* (2002).

The second order statistics that are examined in this book are sufficient for finding the variances and power spectral densities of quantities of interest. One needs to find the fourth-order moments to determine the distribution functions. Methods of doing that and analyzing saturated scintillation are not discussed in this book.

Variations in the amplitude for coherent illumination are produced not only by scintillation, but also from speckle. This coherent interference effect can be important. It has been treated elsewhere and is not considered in this book.

In the unsaturated region, the expression for the variance of the phase or log-amplitude of a wave propagating from $z = 0$ to $z = L$ is of the form

$$\sigma^2 = 0.2073\, k_0^2 \int_0^L dz\, C_n^2(z) \int d\boldsymbol{\kappa}\, f(\kappa)\, g\left(\boldsymbol{\kappa}, z\right), \tag{1.1}$$

where $k_0 = 2\pi/\lambda$ with λ the propagation wavelength, $C_n^2(z)$ is the turbulence strength, $f(\kappa)$ is the normalized turbulence spectrum in transverse spatial trans-

form space, and $g(\boldsymbol{\kappa}, z)$ is a filter function that depends on the particular problem. The κ integration is over the entire two-dimensional space.

Different problems simply necessitate the use of different filter functions. There is the simple interpretation that for a particular problem the original turbulence spectrum is filtered. One must then integrate over the residual spectrum and along the path to find the variance.

By making a change of the spatial spectrum variables in these integrals to two new variables, one of which is frequency, one can find the power spectral density for the particular problem.

There are characteristic categories of problems. The characteristic filter functions are derived in Chap. 3. For example, the filter functions for Zernike modes, such as piston and tilt on filled and annular apertures, are derived. I show that relative displacement of two waves (anisoplanatism) can be represented as a filter function. Filter functions corresponding to a finite size source or a finite size receiver are also derived. The difference between the phase of a focused and a collimated wave affects the performance of many interesting systems, and filter functions for this problem are also evaluated.

Many applications discussed in this book are for adaptive-optics systems. An adaptive-optics system tries to correct for the effects of turbulence in an object's image or in the projection of a laser beam, and its effect on the turbulence also can be represented by filter functions. A generic system is shown in Fig. 1.1.

As I have said, this formalism reduces problems to a triple integral. The evaluation of the double integral in wavenumber space is discussed in detail in this book and the method presented has applications in many fields. The evaluation of the one remaining integral over the propagation path can be done analytically for some turbulence distribution models and is performed numerically for others. There are no numerical difficulties with this last integral.

The evaluation of these integrals is considered in Chap. 4 for the simplest problems in which the solution is obtained by table lookup of Mellin transforms. These integrals are of the form

$$\int_0^\infty dx\, h(x)\, x^a, \tag{1.2}$$

where $h(x)$ is typically a trigonometric or Bessel function or the square of one, or it is an algebraic function. In general the integral can be performed analytically when the function is any Meijer G-function. These integrals lead to important results for the effect of turbulence on wave propagation; for example, tilt jitter or other Zernike modes, residual phase variance due to a finite-bandwidth adaptive-optics system, and scintillation.

In order to solve more difficult problems, integrals whose integrand contains the product of two functions must be evaluated. These integrals contain one free parameter and are evaluated by using the Mellin convolution theorem to convert the integral in real space into one in the complex plane. These integrals are of the form

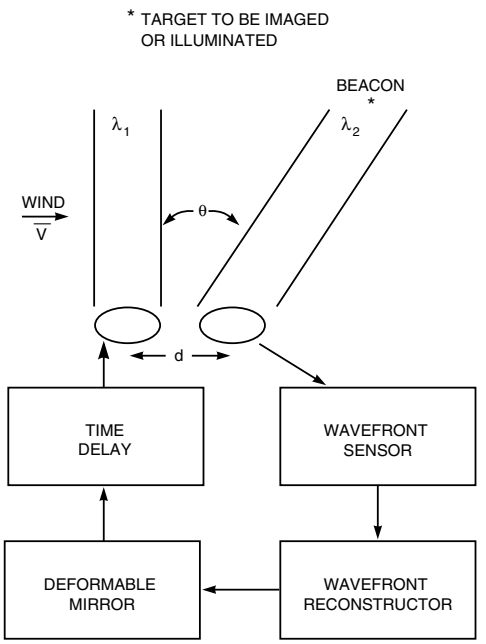

Figure 1.1. An adaptive-optics system. A beacon sends a beam through the atmosphere, and the turbulence impresses a phase aberration on it. This phase front is sampled by a wavefront sensor, which typically responds to local wavefront tilts in sections of the aperture referred to as subapertures. Phase is reconstructed from tilts in a wavefront reconstructor, and its conjugate is impressed on a deformable mirror. This mirror is in the path of the imaging or beam projection system, with the net result that turbulence phase aberrations are corrected.

$$\int_0^\infty dx\, h(x)\, g\,(x/y)\, x^a, \tag{1.3}$$

where y is the free parameter, and the functions are of the same type as in (1.2).

The method for evaluating this integral, which uses pole-residue integration, is developed in Chap. 5 for a positive-real parameter. The case of non-positive and complex parameters is developed in Chap. 9. Asymptotic solutions are developed. Some programs such as Mathematica from Wolfram Research, Inc. evaluate these integrals. The asymptotic results are not provided, and there may be difficulty evaluating some of the functions for large values of the parameter; these values are often required for the z integration. The evaluation of these integrals analytically is time consuming and error prone. When Mathematica can be used it is a a great aid, which enables solutions and power series representations to be found quickly.

In Chap. 6 I address a host of important problems in wave propagation through turbulence in which the integral is of the form in (1.3). The follow-

ing results are obtained: It is shown that the finite outer scale of turbulence can have a significant effect on tilt jitter. The effect of inner scale is shown to limit the maximum tilt that can be measured on a small aperture. It is also shown that the inner-scale size can significantly reduce the scintillation. Tilt on an annulus is considered, and it is shown that tilt jitter does not change much from that of a filled aperture until the central obscuration becomes very large. The scintillation measured from a finite size source or by a finite size receiver is shown to be considerably reduced from that of a point source or point receiver. Expressions for characteristic sizes of the source or receiver that significantly reduce scintillation are developed. The power spectral density of turbulence caused by wind transport or receiver motion is calculated. I calculate how scintillation is affected by an adaptive-optics system. The correlation function of focus is evaluated. The residual phase is calculated when one corrects the turbulence on a collimated beam by using a focused source as a reference. The general solution for Zernike anisoplanatism is given. The residual piston and tilt for distributed and offset sources are calculated.

In addition to calculating wave variances, one can use these techniques to find the Strehl ratio as discussed in Chap. 7. Analytical expressions for the Strehl ratio cannot be calculated for every case of interest. For that reason, an approximation is derived for the Strehl ratio with anisoplanatism that is much better than the Maréchal approximation. This formula is applied to anisoplanatism caused by parallel displacement, angular displacement, time displacement, chromatic displacement, and the combination of several such effects. Beam shapes for these cases are calculated in Chap. 11.

For many problems the various approximations for the Strehl ratio are not valid. In addition, when tilt is removed the structure function is a function of position, and the simpler formula to calculate the Strehl ratio is not applicable. These problems must be solved by numerical techniques. Examples of doing that are given in Sec. 7.5.

Propagation of a Gaussian wave results in integrals that have complex or negative parameters. The theory to evaluate these integrals is developed in Chap. 8 and applied in Chap. 9 to the scintillation of a Gaussian beam.

For more complicated problems there can be two or more parameters in the integral. These integrals are of the form

$$\int_0^\infty dx\, h(x)\, g_1\left(x/y_1\right) \ldots g_N\left(x/y_N\right) x^a, \tag{1.4}$$

where the functions h and g are of the same type as in (1.3). These integrals can be converted into integrals in several complex planes with the Mellin convolution theorem. Pole-residue techniques apply to this class of problems. There are complications in trying to decide which poles in the multidimensional space one should include when evaluating residues. A procedure is given in Chap. 10 that makes the process straightforward. I also develop a technique to evaluate both the series and steepest-descent contributions to an asymptotic solution.

For these more complicated problems, the series solutions sometimes do not converge for all parameter ranges. The source of this difficulty is illustrated in Chap. 10 by an integral whose integrand is a product of exponentials. A series of examples is then considered in Chap. 11. Several sample integrals in two or more complex planes are evaluated, and the results are shown to agree with integral tables. I then turn to four problems in wave propagation through turbulence that cover all parameter regions: Tilt anisoplanatism with outer scale is evaluated, and the effect of outer scale is shown to be not as large as its effect on pure tilt. The method of solution shows clearly where this difference arises. Tilt with both inner and outer scale present is calculated. The solution is shown to agree with earlier work when either effect is eliminated. Next, the low-frequency regime of the tilt power spectrum is shown to be the most greatly affected by outer scale. Finally, the phase structure and correlation functions with non-zero inner and outer scales are calculated.

In Chap. 12 I consider the beam shape for several problems. Appendix A gives the Mellin transforms for familiar functions that were not encountered in turbulence problems. Some commonly used functions are expressed as generalized hypergeometric functions in Appendix B.

1.2 Introduction to Mellin Transforms

In this section I introduce the Mellin transform, and discuss a few of its properties. The Mellin transform $H(s)$ of the function $h(x)$ is defined as

$$h(x) \rightarrow H(s) \equiv \mathcal{M}\left[h\left(x\right)\right] \equiv \int_0^\infty \frac{dx}{x} h(x)\, x^s. \tag{1.5}$$

The inverse transform is

$$h(x) = \frac{1}{2\pi i} \int_C ds H(s)\, x^{-s}. \tag{1.6}$$

The integration path is a straight line extending from $\eta - i\infty$ to $\eta + i\infty$ and crossing the real axis at a value of s for which the integral in (1.5) converges. The allowed values of η typically lie in a finite range and are specified in the Mellin transform tables. The Mellin transform tables may be augmented with the following three properties that are derivable from the Mellin transform definition:

$$h(a\, x) \rightarrow a^{-s} H(s), \quad a > 0, \tag{1.7}$$

$$x^b h(x) \rightarrow H(s+b), \text{ and} \tag{1.8}$$

$$h\left(x^p\right) \rightarrow H(s/p)/\left|p\right|, \quad p \neq 0. \tag{1.9}$$

For the general case one finds

$$x^b h\left(ax^p\right) \rightarrow \frac{1}{|p|\, a^{(s+b)/p}} H[(s+b)/p], \quad p \neq 0.$$

These relations are repeatedly used throughout the book to extend Mellin transforms from the tables to new functions. For instance, the Mellin transform of a Gaussian function is found from that of the exponential given in eq. 1.47 by the use of eq. 1.9 with $p = 2$ to obtain

$$\mathcal{M}\left[\exp\left(-x^2\right)\right] = 0.5\,\Gamma[s/2],$$

and eq. 1.7 with $a = 1/b$ to obtain

$$\mathcal{M}\left\{\exp\left[-\left(x/b\right)^2\right]\right\} = 0.5\, b^s \Gamma[s/2]. \tag{1.10}$$

The Mellin transform is the Laplace transform in the logarithm of the variable x. This is why the Mellin transform is sometimes referred to as the *log-polar transform*. The transform of an object that is scaled in size by a factor b is related to the unscaled transform by

$$H(s) = \int_0^\infty \frac{dx}{x} h(bx)\, x^s = b^{-s} \int_0^\infty \frac{dy}{y}\, h(y)\, y^s. \tag{1.11}$$

This scaling factor has magnitude unity if s is confined to the imaginary axis. This is analogous to the way a time shift results in the multiplication of a Fourier transform by a complex scaling factor. This scaling property makes Mellin transforms convenient for the analysis of chaos and of acoustical, radar, and visual signals.

Gamma functions appear repeatedly in this work, and I highlight a few of their properties. The gamma function is defined as

$$\Gamma\left[s\right] = \int_0^\infty dx\, \exp(-x)\, x^{s-1} = \sum_{n=0}^{\infty} \frac{(-1)^n}{n!} \frac{1}{s+n} + \int_1^\infty dx\, \exp(-x)\, x^{s-1}. \tag{1.12}$$

The argument s can be complex. The last integral is entire and the only singularities of the gamma function are simple poles at the negative integers $-n$ with residue $(-1)^n/n!$. The reciprocal of the gamma function can be shown to be an entire function; therefore, the only singularities of the ratio of gamma functions come from the numerator. *This property is central to allowing one to easily evaluate integrals in the complex plane whose integrand is the ratio of gamma functions.*

As one recalls from the Cauchy residue theorem in complex variable theory, the value of an integral in the complex plane that contains only simple poles within the closed integration region is equal to $2\pi i$ times the sum of the residues at the enclosed poles. If $f(z)$ does not have any singularities, then

$$\oint dz\, \frac{f(z)}{z - z_0} = 2\pi i f(z_0), \tag{1.13}$$

when the integration path, which encircles the pole in a clockwise fashion, encloses the pole at $z = z_0$. The value of the integral is equal to zero when the pole is not enclosed in the integration path.

Plots of the gamma function and its reciprocal are shown in Fig. 1.2. The

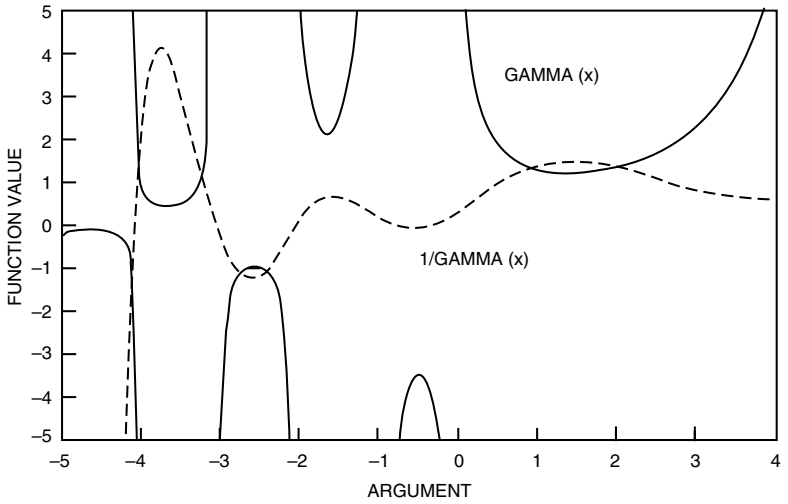

Figure 1.2. Gamma function and its reciprocal versus its argument.

recursion relation for gamma functions is

$$\Gamma[a+1] = a\Gamma[a]. \tag{1.14}$$

With the relation $\Gamma[1] = 1$, for integer a this gives $\Gamma[a+1] = a!$. With this relation the gamma function at noninteger values can be evaluated on some hand calculators.

If the argument of s in all the gamma functions is unity, then the integral can be expressed as a sum of generalized hypergeometric functions. This form is desirable because these functions can be plotted by standard computer programs. To change a gamma function argument with an integer multiplier to a gamma function with a unity factor, one uses the Gauss-Legendre multiplication formula

$$\Gamma\,[my] = m^{my-1/2}(2\pi)^{(1-m)/2} \prod_{k=0}^{m-1} \Gamma\,[y + k/m]. \tag{1.15}$$

The particular case of $m = 2$ is

$$\Gamma\,[2\,y] = 2^{2y-1}\Gamma\,[y]\,\Gamma\,[y + 1/2]\,/\sqrt{\pi}. \tag{1.16}$$

To convert an argument with negative s to one with positive s, one uses the duplication formula

$$\Gamma\,[1-s]\;\Gamma\,[s] = \pi/\sin(\pi\,s). \tag{1.17}$$

For $s > 1$, the gamma function can be approximated by Stirling's formula

$$\Gamma[s] \sim \sqrt{2\pi}\, s^{s-1/2} \exp(-s) \left[1 + 1/(12\, s) + 1/(288\, s^2) + \cdots\right], \quad |\arg\{s\}| < \pi. \tag{1.18}$$

Table 1.1 is a list of Mellin transforms that are used to evaluate integrals encountered in wave propagation through turbulence. Additional Mellin transforms are given in Appendix A. These are only a small fraction of the 1200 transforms available in closed form. The notation of *Marichev* (1983) and *Slater* (1966) for the ratio of gamma functions used throughout the book is

$$\Gamma\left[\begin{matrix}\alpha_1, \ldots, \alpha_m \\ \beta_1, \ldots, \beta_n\end{matrix}\right] \equiv \frac{\Gamma[\alpha_1]\ \Gamma[\alpha_2] \ldots \Gamma[\alpha_m]}{\Gamma[\beta_1]\ \Gamma[\beta_2] \ldots \Gamma[\beta_n]}. \tag{1.19}$$

A new notation is introduced in eq. 1.50 in the Mellin transform table: An asterisk after a term in the gamma function signifies that the integration path passes between the first and second poles of that gamma function. The notation $\left(*^N\right)$ indicates that the integration path passes between the N^{th} and $N + 1^{st}$ poles of the gamma function. No asterisk indicates that all poles are on one side of the integration path.

The table contains the Mellin transform of the Heaviside unit step function, defined by

$$\begin{aligned} U(x) &= 1 \ \text{ for } x > 0, \text{ and} \\ U(x) &= 0 \ \text{ for } x \le 0. \end{aligned} \tag{1.20}$$

This function can be used to convert integrals with finite limits into ones with infinite limits that can be evaluated with the techniques developed in this book.

Mellin transforms are used in three ways to solve turbulence problems:

1. To evaluate integrals by table lookup.
2. To find a series representation for a function.
3. To evaluate complicated integrals.

The first application of Mellin transforms is simple yet important. Some integrals are easy to evaluate directly from the Mellin transforms. For instance, from eq. 1.48 one finds that

$$\int_0^\infty dx\, x^a \sin(x) = 2^a \sqrt{\pi}\, \Gamma\left[\begin{matrix} a/2 + 1 \\ 1/2 - a/2 \end{matrix}\right], \qquad \text{Re}\{a\} < 0. \tag{1.21}$$

This technique is used to evaluate all the integrals in Chap. 4.

For some problems, i.e. those concerning anisoplanatic effects, one has to obtain the Mellin transform of the difference between a function and the first term of its power series. It is easy to show such a Mellin transform is that of the original function, except the integration path has moved over one pole. This is the analytic continuation of the integral. To illustrate, consider the transforms given in eq. 1.51 and eq. 1.57

$$\mathcal{M}\left[J_0(x)-1\right]=\lim_{\varepsilon\to 0}\left\{2^{s-1}\Gamma\left[\begin{matrix}s/2\\-s/2+1\end{matrix}\right]-\frac{1}{s+\varepsilon}+\frac{1}{s-\varepsilon}\right\},\quad 0<\mathrm{Re}\left\{s\right\}<\varepsilon.$$

The integration path and pole location are shown in Fig. 1.3.

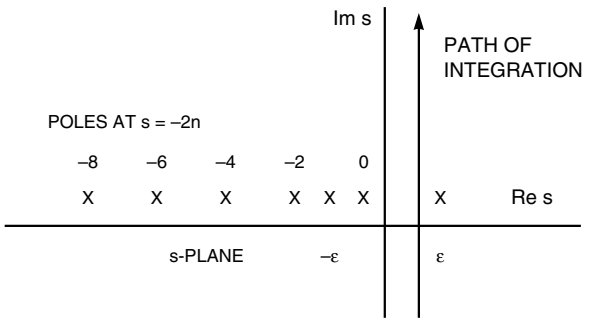

Figure 1.3. Pole locations and integration path for the Bessel function integration. For clarity, pole locations are displaced from the real axis in this and subsequent figures.

The poles continue periodically as $\mathrm{Re}\left\{s\right\}$ goes to minus infinity. For clarity in this figure and all subsequent ones the pole locations are slightly displaced from their true positions on the real axis.

In the limit, the poles at $s=0$ and $s=-\varepsilon$ additively cancel. The net result is that the integration path can now cross the real axis anywhere between the poles at $s=0$ and at $s=-2$ without changing the value of the integral. Therefore, the Mellin transform is equal to

$$\mathcal{M}\left[J_0(x)-1\right]=2^{s-1}\Gamma\left[\begin{matrix}s/2*\\-s/2+1\end{matrix}\right],\qquad -2<\mathrm{Re}\left\{s\right\}<0. \tag{1.22}$$

In this case with the asterisk notation, the strip in complex space in which the transform is valid is completely defined, and the explicit statement of the restrictions on $\mathrm{Re}\left\{s\right\}$ is redundant. This expression can be viewed as the analytic continuation of the integral of the Bessel function.

It is obvious how to extend this result to that in which the first m terms of the power series are subtracted from the function. In that case, the integration path moves past m poles of the original function, and this is indicated by $(*)^m$.

As a more difficult example, consider the integral of a power of the radial coordinate times a function that is related to the optical transfer function for a circular aperture obtained by *Fried* (1967). This integral occurs in the evaluation of many turbulence problems, and by using the unit step function one can put it in the form of a Mellin transform as

$$I(q) = \int_0^1 d\alpha\, \alpha^{q+1} K(\alpha)$$
$$= \int_0^\infty d\alpha\, \alpha^{q+1} \frac{16}{\pi} \left[\arccos(\alpha)\, U(1-\alpha) - \alpha \left(1-\alpha^2\right)^{1/2} U(1-\alpha) \right].$$

The Mellin transform for the first function is found from eq. 1.58 if one replaces s by $q+2$. This changes the condition for convergence to $\mathrm{Re}\{q\} > -2$. The Mellin transform of the second integral is found from eq. 1.55 if one replaces s by $q+3$ and also uses eq. 1.9. The condition for convergence of this term is $\mathrm{Re}\{q\} > -3$. For convergence of the entire integral, the more restrictive condition on the first function applies. Since $\Gamma[1/2] = \sqrt{\pi}$, the integral is equal to

$$I(q) = \frac{4}{\sqrt{\pi}} \left\{ \Gamma \left[\begin{matrix} q/2+\frac{3}{2},\, -q/2-1 \\ q/2+2,\, -q/2 \end{matrix} \right] - \Gamma \left[\begin{matrix} q/2+\frac{3}{2} \\ q/2+3 \end{matrix} \right] \right\}, \qquad \mathrm{Re}\{q\} > -2.$$

Using the gamma function recursion relation given in eq. 1.14, one obtains

$$I(q) = \frac{8}{\sqrt{\pi}} \frac{1}{q+2} \Gamma \left[\begin{matrix} q/2+\frac{3}{2} \\ q/2+3 \end{matrix} \right], \qquad \mathrm{Re}\{q\} > -2. \tag{1.23}$$

The second application of Mellin transforms is to find an infinite series for a function from its inverse Mellin transform. Consider the exponential function, whose Mellin transform is given by eq. 1.47 as the gamma function. In Chap. 5 it is shown that the integration path for the inverse transform of the exponential function can be closed in the left-half plane without changing the value of the integral. Residues at the poles at $s = -n$ for $n = 0, 1, 2, \ldots$ contribute to the integral to obtain

$$\exp(-x) = \frac{1}{2\pi i} \int_C ds\, \Gamma[s]\, x^{-s} = \sum_{n=0}^{\infty} \frac{(-1)^n}{n!} x^n. \tag{1.24}$$

This is the standard power series for the exponential function.

As a second more difficult example of obtaining a power series, consider $K_\nu(x)$, which is the modified Bessel function of the third kind with imaginary argument that is sometimes referred to as a Macdonald function. When ν is not an integer, the poles are simple, and the integration path can be closed in the left-half plane where there are two sets of poles at $s = -\nu - 2n$ and $s = \nu - 2n$ for $n = 0, 1, 2, \ldots$. The residues at these poles give

$$K_\nu(x) = \frac{1}{4}\frac{1}{2\pi i}\int_C ds\,\Gamma[s/2+\nu/2,\ s/2-\nu/2]\,(x/2)^{-s}$$
$$= \frac{1}{2}\sum_{n=0}^{\infty}\frac{(-1)^n}{n!}\left\{\left(\frac{x}{2}\right)^{2n+\nu}\Gamma[-n-\nu]+\left(\frac{x}{2}\right)^{2n-\nu}\Gamma[-n+\nu]\right\}$$
$$= \frac{1}{2}\left\{\frac{z^{1/2}\Gamma[-\frac{1}{3}]}{3^{1/3}}\,{}_0F_1\left[\frac{4}{3},\frac{z^3}{9}\right]+\frac{3^{1/3}\Gamma[\frac{1}{3}]}{z^{1/2}}\,{}_0F_1\left[\frac{2}{3},\frac{z^3}{9}\right]\right\}. \tag{1.25}$$

This result is used in Chap. 2. The Mellin transform of $K_\nu(x)$ has double poles when ν is an integer. The residues at these poles can be calculated with the technique presented in Sec. 5.3 to give

$$K_\nu(x) = \frac{1}{4}\frac{1}{2\pi i}\int_C ds\,\Gamma[s/2+\nu/2,\ s/2-\nu/2]\,(x/2)^{-s}$$
$$= \sum_{n=0}^{\infty}\frac{(-1)^{\nu+1}}{n!\,(n+\nu)!}\left(\frac{x}{2}\right)^{2n+\nu}[\ln(x/2)-\psi(n+1)/2-\psi(\nu+n+1)/2]$$
$$+\frac{1}{2}\sum_{n=0}^{\nu-1}\frac{(-1)^n}{n!}\left(\frac{x}{2}\right)^{2n-\nu}\Gamma[-n+\nu], \tag{1.26}$$

where $\psi(x)$ is the logarithmic derivative of the gamma function.

The third and most important application of Mellin transforms in this book is the evaluation of more complicated integrals via the Mellin convolution theorem. Consider the Mellin transform of

$$h(x) = \int_0^\infty \frac{dy}{y}\,h_0(y)h_1(x/y). \tag{1.27}$$

Use the Mellin transform definition, and interchange the integration order to obtain

$$\mathcal{M}[h(x)] = \int_0^\infty \frac{dy}{y}\,h_0(y)\int_0^\infty \frac{dx}{x}\,h_1(x/y)\,x^s.$$

Letting $w = x/y$, one obtains

$$\mathcal{M}[h(x)] = \int_0^\infty \frac{dy}{y}\,h_0(y)\,y^s\int_0^\infty \frac{dw}{w}\,h_1(w)\,w^s = H_0(s)\,H_1(s).$$

Note that in eq. 1.27 the integration variable in the second function appears in the denominator. Thus for a typical problem in which the function has the variable in the numerator, in the Mellin transform table value of the second function one needs to make the substitution $s \to -s$ by using eq. 1.9 with $p = -1$.

Therefore, the value of the original integral obtained from the inverse Mellin transform relation is

$$h(x) = \frac{1}{2\pi i} \int_C ds\, H_0(s)\, H_1(s)\, x^{-s}. \tag{1.28}$$

The Mellin convolution theorem can be applied if the Mellin transform of each function in the integrand exists. Actually, the theorem applies even if this condition is not true for one function if the second function decays fast enough. This is discussed in Chap. 9.

The convolution theorem can be generalized to integrals that contain the product of $N+1$ functions with N parameters. Consider such an integral

$$h(x_1, x_2, \ldots, x_N) = \int_0^\infty \frac{dy}{y}\, h_0(y) h_1(x_1/y) \cdots h_N(x_N/y)\,. \tag{1.29}$$

Take the Mellin transform in each of the N parameters, and interchange the integration order to obtain

$$\begin{aligned}&\mathcal{M}\left[h(x_1, x_2, \ldots, x_N)\right]\\ &= \int_0^\infty \frac{dy}{y}\, h_0(y) \int_0^\infty \frac{dx_1}{x_1}\, h_1(x_1/y)\; x_1^{s_1} \ldots \int_0^\infty \frac{dx_N}{x_N}\, h_N(x_N/y)\; x_N^{s_N}.\end{aligned}$$

Make the substitutions $w_1 = x_1/y, \ldots, w_N = x_N/y$ to obtain

$$\begin{aligned}&\mathcal{M}\left[h(x_1, x_2, \ldots, x_N)\right] \equiv H(s_1, s_2, \ldots, s_N)\\ &= \int_0^\infty \frac{dy}{y}\, h_0(y)\, y^{s_1+s_2+\cdots+s_N} \int_0^\infty \frac{dw_1}{w_1}\, h_1(w_1)\; w_1^{s_1} \ldots \int_0^\infty \frac{dw_N}{w_N}\, h_N(w_N)\; w_N^{s_N}.\end{aligned}$$

This last expression is equivalent to

$$H(s_1, s_2, \ldots, s_N) = H_0(s_1 + s_2 + \cdots + s_N)\, H_1(s_1) \cdots H_N(s_N)\,. \tag{1.30}$$

The value of the original integral is equal to the inverse Mellin transform in the N complex variables given by

$$h(x_1, \ldots, x_N) = \frac{1}{(2\pi i)^N} \int_{C_1} \ldots \int_{C_N} ds_1 \ldots ds_N\, H(s_1, \ldots, s_N)\; x_1^{-s_1} \ldots x_N^{-s_N}. \tag{1.31}$$

Methods of evaluating this integral are considered in Chap. 11.

A considerable part of this book is devoted to obtaining convergent and asymptotic series for the integrals in eq. 1.28 and eq. 1.31 and applying these techniques to a host of problems in Chaps. 6, 7, 8, 10, 12, and 13.

1.3 Higher Transcendental Functions

Many answers to problems considered in this book are expressed as sums of generalized hypergeometric functions. Some are expressed as a Meijer G function and as a Fox H-function. The answers are abstracted from infinite sums; rules to convert these sums into generalized hypergeometric functions are given here. The definition of the generalized hypergeometric function is

$$ {}_pF_q\left[(a);(b);z\right] \equiv {}_pF_q\left[\begin{array}{c}(a);z\\(b)\end{array}\right] \equiv \sum_{k=0}^{\infty} \frac{(a_1)_k\,(a_2)_k \ldots (a_p)_k}{(b_1)_k\,(b_2)_k \ldots (b_q)_k} \frac{z^k}{k!}, \tag{1.32} $$

where $(a) = a_1, a_2, \ldots, a_p$, $(b) = b_1, b_2, \ldots, b_q$, and the Pochhammer symbol is defined as

$$ (a)_k = \frac{\Gamma[a+k]}{\Gamma[a]},\ (a)_0 = 1. \tag{1.33} $$

This generalized hypergeometric function is equal to unity when $z = 0$. For $p = q+1$, this series always converges if $|\,z\,| < 1$, and it also converges for $z = 1$ if $\mathrm{Re}\left\{\sum_{i=1}^{p} a_i - \sum_{i=1}^{q} b_i\right\} < 0$. If $p < q+1$, it converges for all z. If $p > q+1$, it does not converge, yet it is useful as an asymptotic series.

The generalized hypergeometric function is a generalization of the Gauss hypergeometric function ${}_2F_1\left[\alpha,\beta;\gamma;z\right]$, which is defined as

$$ {}_2F_1\left[\alpha,\beta;\gamma;\ z\right] \equiv F\left[\alpha,\beta;\gamma;z\right] \equiv \sum_{k=0}^{\infty} \frac{(\alpha)_k\,(\beta)_k}{(\gamma)_k} \frac{z^k}{k!}. \tag{1.34} $$

Specific convergence criteria on the unit circle can be given for this function:

1. If $0 < \mathrm{Re}\left\{\alpha+\beta-\gamma\right\} < 1$, the series converges on the unit circle except at $z = 1$.
2. If $\mathrm{Re}\left\{\alpha+\beta-\gamma\right\} < 0$, the series converges absolutely for $z \le 1$.
3. If $\mathrm{Re}\left\{\alpha+\beta-\gamma\right\} \ge 1$, the series diverges on the entire unit circle.

Most functions encountered in physics are special cases of Gauss's hypergeometric function. Examples are given in Table 1.2. Additional functions that are represented as hypergeometric functions are given in Appendix B.

For most functions we deal with such as sines, cosines, exponentials, Bessel functions, etc., there is one power series that applies for any value of the function's argument. For many of the solutions of turbulence problems $p = q+1$, and there is a different power series expansion for small and large values of the argument.

The underlying function may be continuous and have continuous derivatives at the point that the power series representation must be switched. The function $1/(1+x)$ is an example of such a function.

$$\frac{1}{1+x} = \sum_{k=0}^{\infty}(-x)^k = \sum_{k=0}^{\infty}\frac{\Gamma[k+1]}{k!}(-x)^k = \sum_{k=0}^{\infty}\frac{(1)_k}{k!}(-x)^k = {}_1F_0[1,-x], \quad x<1$$
$$= \frac{1}{x}\sum_{k=0}^{\infty}(-x)^{-k} = \frac{1}{x}\sum_{k=0}^{\infty}\frac{(1)_k}{k!}(-x)^{-k} = \frac{1}{x}{}_1F_0[1,-1/x], \quad x>1. \tag{1.35}$$

The function $1/(1+x)$ does not do anything unusual at $x=1$; however, a different series is needed for values less than 1 and for values greater than 1. The complication arises because there is a pole at $x=-1$, which results in the function in the complex plane having a branch cut starting at $z=-1$ and going to infinity.

In performing an integration by using Mellin transforms, one can develop formulas that are valid for $z<1$ and for $z>1$. As an alternative, one can convert Gauss's hypergeometric function that is valid for $z<1$ to one valid for $z>1$ by using the transformation formula

$${}_2F_1\left[\alpha,\beta;\gamma;\ z\right] = \frac{\Gamma[\gamma]\Gamma[\beta-\alpha]}{\Gamma[\beta]\Gamma[\gamma-\alpha]}(-1)^{\alpha}z^{-\alpha}{}_2F_1\left[\alpha,\alpha+1-\gamma;\alpha+1-\beta;\ 1/z\right]$$
$$+\frac{\Gamma[\gamma]\Gamma[\alpha-\beta]}{\Gamma[\alpha]\Gamma[\gamma-\beta]}(-1)^{\beta}z^{-\beta}{}_2F_1\left[\beta,\beta+1-\gamma;\beta+1-\alpha;\ 1/z\right]. \tag{1.36}$$

The generalized hypergeometric function can be evaluated with a recursion relation. The function is expressed as

$${}_pF_q\left[(a);(b);z\right] = \sum_{k=0}^{\infty}c_k,$$

with

$$c_0 = 1, \text{ and } c_{k+1} = \frac{(a_1+k)\cdots(a_p+k)}{(b_1+k)\cdots(b_q+k)}\frac{z}{(k+1)}\,c_k. \tag{1.37}$$

The generalized hypergeometric function can be expressed as a Mellin-Barnes integral in the form

$${}_pF_q\left[(a);(b);z\right]$$
$$= \Gamma\begin{bmatrix}b_1,b_2,\ldots,b_q\\a_1,a_2,\ldots,a_p\end{bmatrix}\frac{1}{2\pi i}\int_{\eta-i\infty}^{\eta+i\infty}ds\,(-z)^s\,\Gamma\begin{bmatrix}a_1+s,\ldots,a_p+s,\ -s\\b_1+s,\ldots,b_q+s\end{bmatrix}, \tag{1.38}$$

where the integration path lies to the left of the poles of $\Gamma[-s]$ and to the right of all poles of the remaining numerator gamma functions. *From this relation, it is evident that the Mellin transform of any function that can be represented as a generalized hypergeometric function is expressible as a ratio of gamma functions.*

The Mellin transform of the generalized hypergeometric function is equal to

$$\begin{aligned}&\mathcal{M}\left\{{}_pF_q\left[(a);(b);z\right]\right\}\\&=(-1)^s\Gamma\left[\begin{matrix}b_1,b_2,\ldots,b_q\\a_1,a_2,\ldots,a_p\end{matrix}\right]\Gamma\left[\begin{matrix}a_1-s,\ldots,a_p-s,\ s\\b_1-s,\ldots,b_q-s\end{matrix}\right].\end{aligned}$$

A further generalization of the generalized hypergeometric function is the Fox H-function defined as

$$\begin{aligned}&H_{p,q}^{m,n}\left[z\left|\begin{matrix}(a_1,\alpha_1),\ldots,(a_p,\alpha_p)\\(b_1,\beta_1),\ldots,(b_q,\beta_q)\end{matrix}\right.\right]\\&=\frac{1}{2\pi i}\int\limits_C ds\,z^s\frac{\prod\limits_{i=1}^{n}\Gamma\left[1-a_i+\alpha_i s\right]\prod\limits_{j=1}^{m}\Gamma\left[b_j-\beta_j s\right]}{\prod\limits_{k=m+1}^{q}\Gamma\left[1-b_k+\beta_k s\right]\prod\limits_{r=n+1}^{p}\Gamma\left[a_r-\alpha_r s\right]},\end{aligned}\tag{1.39}$$

where all the poles of an individual gamma function are on one side of the integration path. If the coefficients of s are rational, the solution can be expressed as a Meijer G-function defined as

$$G_{p,q}^{m,n}\left[z\left|\begin{matrix}a_1,\ldots,a_p\\b_1,\ldots,b_q\end{matrix}\right.\right]=\frac{1}{2\pi i}\int\limits_C ds\,z^s\frac{\prod\limits_{i=1}^{n}\Gamma\left[1-a_i+s\right]\prod\limits_{j=1}^{m}\Gamma\left[b_j-s\right]}{\prod\limits_{k=m+1}^{q}\Gamma\left[1-b_k+s\right]\prod\limits_{r=n+1}^{p}\Gamma\left[a_r-s\right]},\tag{1.40}$$

where all poles of an individual gamma function are again on one side of the integration path.

The computer programs Maple and Mathematica can deal with generalized Hypergeometric functions and Meijer's G-functions. Therefore, once the results are expressed in terms of these functions, they can be further manipulated and plotted for specific cases.

These programs can find the value of the integrals that lead to these functions. When there is one solution that applies to all parameter ranges, $p\neq q+1$, there are often numerical difficulties in evaluating the function for large values of the argument. In this case, an asymptotic solution is required. These computer programs do not find the asymptotic solution, and they must be found using methods such as those described in this book. They also do not find solutions when there are more than one parameter.

For some problems the answer is expressed as a generalized hypergeometric function minus unity. This can be expressed simply as a different generalized hypergeometric function. Consider

$${}_pF_q\left[(a);(b);z\right]-1=\sum_{k=1}^{\infty}\frac{(a_1)_k\,(a_2)_k\ldots(a_p)_k}{(b_1)_k\,(b_2)_k\ldots(b_q)_k}\frac{z^k}{k!}.\tag{1.41}$$

Let $k\rightarrow k+1$ and note that from the definitions

$$(a)_{k+1}=\frac{\Gamma\left[a+1+k\right]}{\Gamma\left[a\right]}=(a+1)_k\,\frac{\Gamma\left[a+1\right]}{\Gamma\left[a\right]}=a\,(a+1)_k\,,\quad\text{and}$$

$$(k+1)! = k!\,\frac{(2)_k}{(1)_k}.$$

Therefore,

$${}_pF_q\left[(a);(b);z\right] - 1 = z\,\frac{\prod_{n=1}^{p} a_n}{\prod_{n=1}^{q} b_n}\,{}_{p+1}F_{q+1}\left[(a+1),1;(b+1),2;z\right]. \tag{1.42}$$

This relation is used in Chaps. 6 and 7.

The result of evaluating the Mellin convolution integral with pole-residue integration for problems in propagation through turbulence is generally one or more summations that contains ratios of gamma functions. As an example, consider a typical summation

$$\sum_{n=0}^{\infty} \frac{(-1)^n}{n!}\,\Gamma\left[\begin{matrix} n+w,\ -n+r \\ n+h,\ n+p \end{matrix}\right] P^{2n}. \tag{1.43}$$

This infinite series can be converted into a generalized hypergeometric function by using the function definition, and the duplication formula for gamma functions given in eq. 1.17. I will express such a summation as $K\ {}_pF_q\left[(a)\,;(b)\,;z\right]$. The rules for obtaining this representation are:

1. The coefficient K is equal to the value of the $n = 0$ term. In this case

$$K = \Gamma\left[\begin{matrix} w,\ r \\ h,\ p \end{matrix}\right]. \tag{1.44}$$

2. The arguments in the gamma function for which the sign of the index n is positive, i.e., $n+w,\ n+h$, and $n+p$, lend their n-independent constants to arguments of the hypergeometric function. Those in the numerator appear before the first semicolon (they are the a_i terms), and those in the denominator appear after it (those are the b_j terms).
3. The arguments in the gamma function for which the sign of the summation index n is negative lend minus their n-independent constants, plus one, to arguments of the hypergeometric function. (The argument of this type in the example is $-n+r$. The argument to insert in the hypergeometric series is $-r+1$.) If the argument was in the numerator, it appears after the first semicolon. Those in the denominator appear before the first semicolon.
4. The magnitude of the parameter z is the quantity in the summation raised to the index power n. (In eq. 1.43 the parameter is P^2.) The sign of the parameter is positive if the number of gamma function arguments with negative n is odd. It is negative if the number is even. The sign is positive in the example since there is one argument with negative index.
5. The subscripts before and after the function symbol are referred to as the order of the generalized hypergeometric function. The quantity before the F symbol is the number of terms before the first semicolon. The quantity after the F symbol is the number of terms between the first and second semicolons.

Using these rules the summation in eq. 1.43 is equal to

$$\sum_{n=0}^{\infty} \frac{(-1)^n}{n!} \Gamma \left[\begin{matrix} n+w, & -n+r \\ n+h, & n+p \end{matrix} \right] P^{2n} = \Gamma \left[\begin{matrix} w, & r \\ h, & p \end{matrix} \right] {}_1F_3 \left[w; -r+1, h, p; P^2 \right]. \tag{1.45}$$

The third volume of the three-volume reference work by *Prudnikov, Brychkov*, and *Marichev* (1990) contains an extensive list of equivalences between generalized hypergeometric functions and more familiar functions.

Table 1.1. Mellin Transforms that are useful for turbulence problems.

$$h(x) \to \mathcal{M}\left[h(x)\right] \equiv H(s) = \int_0^\infty \frac{dx}{x}\, h(x)\, x^s \tag{1.46}$$

$$\exp(-x) \to \Gamma\left[s\right], \quad \mathrm{Re}\left\{s\right\} > 0 \tag{1.47}$$

$$\sin(x) \to 2^{s-1}\sqrt{\pi}\,\Gamma\left[\begin{matrix}1/2+s/2\\ 1-s/2\end{matrix}\right], \qquad |\,\mathrm{Re}\left\{s\right\}\,| < 1 \tag{1.48}$$

$$\cos(x) \qquad \to 2^{s-1}\sqrt{\pi}\,\Gamma\left[\begin{matrix}s/2\\ 1/2-s/2\end{matrix}\right], \qquad 0 < \mathrm{Re}\left\{s\right\}\, < 1 \tag{1.49}$$

$$\sin^2\left(x^2\right) \quad \to -\frac{\sqrt{\pi}}{8}\,\Gamma\left[\begin{matrix}s/4*\\ 1/2-s/4\end{matrix}\right], \qquad -4 < \mathrm{Re}\left\{s\right\} < 0 \tag{1.50}$$

$$J_\nu(x) \quad \to 2^{s-1}\Gamma\left[\begin{matrix}s/2+\nu/2\\ \nu/2+1-s/2\end{matrix}\right], \qquad -\mathrm{Re}\left\{\nu\right\} < \mathrm{Re}\left\{s\right\} < 3/2 \tag{1.51}$$

$$J_\nu^2(x) \quad \to \frac{1}{2\sqrt{\pi}}\,\Gamma\left[\begin{matrix}s/2+\nu,\, 1/2-s/2\\ \nu+1-s/2,\, 1-s/2\end{matrix}\right], \quad -2\mathrm{Re}\left\{\nu\right\} < \mathrm{Re}\left\{s\right\} < 1 \tag{1.52}$$

$$J_\nu(x)\, J_{\nu+1}(x) \to \frac{1}{2\sqrt{\pi}}\,\Gamma\left[\begin{matrix}s/2+\nu+1/2,\, 1-s/2\\ \nu+3/2-s/2,\, 3/2-s/2\end{matrix}\right], \qquad -1-2\mathrm{Re}\left\{\nu\right\} < \mathrm{Re}\left\{s\right\} < 2 \tag{1.53}$$

$$(1+x)^{-p} \quad \to \frac{\Gamma[s,\, p-s]}{\Gamma[p]}, \qquad 0 < \mathrm{Re}\left\{s\right\} < \mathrm{Re}\left\{p\right\} \tag{1.54}$$

$$(1-x)^{a-1}U(1-x) \quad \rightarrow \Gamma[a]\,\Gamma\left[\begin{matrix} s \\ s+a \end{matrix}\right], \quad \mathrm{Re}\{a\} > 0,\ \mathrm{Re}\{s\} > 0 \tag{1.55}$$

$$(x-1)^{a-1}\,U(x-1) \rightarrow \Gamma[a]\Gamma\left[\begin{matrix} 1-a-s \\ 1-s \end{matrix}\right],$$
$$\mathrm{Re}\{a\} > 0,\ \mathrm{Re}\{a+s\} < 1 \tag{1.56}$$

$$1 \quad \rightarrow \lim_{\varepsilon\to 0}\left(\frac{1}{s+\varepsilon} - \frac{1}{s-\varepsilon}\right), \qquad -\varepsilon < \mathrm{Re}\{s\} < \varepsilon \tag{1.57}$$

$$\arccos(x)\,U(1-x) \rightarrow -\frac{\sqrt{\pi}}{4}\,\Gamma\left[\begin{matrix} s/2+1/2,\ -s/2 \\ s/2+1,\ 1-s/2 \end{matrix}\right], \qquad \mathrm{Re}\{s\} > 0 \tag{1.58}$$

$$U(1-x) \quad \rightarrow \Gamma\left[\begin{matrix} s \\ s+1 \end{matrix}\right], \qquad \mathrm{Re}\{s\} > 0 \tag{1.59}$$

$$U(x-1) \quad \rightarrow \Gamma\left[\begin{matrix} -s \\ 1-s \end{matrix}\right], \qquad \mathrm{Re}\{s\} < 0 \tag{1.60}$$

$$K_\nu(x) \quad \rightarrow 2^{s-2}\,\Gamma\left[s/2+\nu/2,\ s/2-\nu/2\right], \quad \mathrm{Re}\{s\} > |\mathrm{Re}\{\nu\}| \tag{1.61}$$

$$J_\mu(x)\,J_\lambda(x) \rightarrow \frac{1}{2\sqrt{\pi}}\,\Gamma\left[\begin{matrix} s/2+\frac{\mu+\lambda}{2},\ \frac{1}{2}-s/2,\ 1-s/2 \\ 1-s/2+\frac{\mu+\lambda}{2},\ 1-s/2+\frac{\mu-\lambda}{2},\ 1-s/2+\frac{\lambda-\mu}{2} \end{matrix}\right],$$
$$-\mathrm{Re}\,\{\mu+\lambda\} < \mathrm{Re}\{s\} < 1 \tag{1.62}$$

$$\delta(x-a) \quad \rightarrow a^{s-1} \tag{1.63}$$

$$K\,(x) \rightarrow \qquad \frac{8}{\sqrt{\pi}}\frac{1}{s}\Gamma\left[\begin{matrix} s/2+\frac{1}{2} \\ s/2+2 \end{matrix}\right], \qquad \mathrm{Re}\{s\} > 0 \tag{1.64}$$

$U\,(x)$ is the Heaviside unit step function; $K_\nu\,(x)$ is the Bessel function of third kind; $\delta\,(x)$ is the Dirac delta function; and $K(x)$, defined in eq. 1.23, is a constant times the optical transfer function on a circular aperture. An asterisk next to a gamma function entry indicates that the integration path passes between the first and second poles of that gamma function.

Table 1.2. Examples of the Gauss hypergeometric function.

$$\ln(1+z) = z\,{}_2F_1[1,1;2;-z]\,, \quad |z|<1 \tag{1.65}$$

$$\left(1+\sqrt{1-z}\right)^{1-2a} = 2^{1-2a}\,{}_2F_1[a,a-1/2;2a;z]\,, \quad |z|<1 \tag{1.66}$$

$$(1-z)^{-a} = {}_1F_0[a;z]\,, \quad |z|<1 \tag{1.67}$$

$$\exp(z) = {}_0F_0[z] \tag{1.68}$$

$$\sin(z) = z\,{}_0F_1\left[\tfrac{3}{2};-z^2/4\right] \tag{1.69}$$

$$\cos(z) = {}_0F_1\left[\tfrac{1}{2};-z^2/4\right] \tag{1.70}$$

$$\arcsin(z) = z\,{}_2F_1\left[1/2,1/2;3/2;z^2\right] \tag{1.71}$$

$$\arctan(z) = z\,{}_2F_1\left[1/2,1;3/2;-z^2\right] \tag{1.72}$$

$$\cos(v\arcsin z) = {}_2F_1\left[v/2,-v/2;1/2;z^2\right] \tag{1.73}$$

$$\sinh(z) = z\,{}_0F_1\left[\tfrac{3}{2};z^2/4\right] \tag{1.74}$$

$$\cosh(z) = {}_0F_1\left[\tfrac{1}{2};z^2/4\right] \tag{1.75}$$

$$J_\nu(z) = \left(\frac{z}{2}\right)^\nu \frac{1}{\Gamma[\nu+1]}\,{}_0F_1\left[\nu+1;-z^2/4\right] \tag{1.76}$$

REFERENCES

1. Andrews, L. C., Philips, R. L., Hopen, C. Y, *Laser Beam Scintillation with Applications*, SPIE Press, Bellingham, Wash., (2001).
2. Fried, D. L., "Optical Heterodyne Detection of an Atmospherically Distorted Signal Wave Front", Proc. IEEE, **55**, (1967) pp. 57–67.
3. Marichev, O. I., *Integral Transforms of Higher Transcendental Functions*, Ellis Horwood Limited, Chichester, England, (1983).
4. Nakagami, M., "The m distribution – a general formula of intensity distribution of rapid fading", *Statistical Methods in Radio Wave propagation*, W. C. Hoffman, ed., Pergamon, New York, (1960), pp. 3–36.
5. Prudnikov, A. P., Brychkov, Y. A., Marichev, O. I., *Integrals and Series*, Gordon and Breach Science Publishers, New York, (1990).
6. Slater, L. J., *Generalized hypergeometric functions*, Cambridge University Press, London-New York, (1966).
7. Tyson, R. K., "Bit-error rate for free-space adaptive optics laser communications", *J. Opt. Soc. Am. A*, **19**, (2002) pp. 753–758.
8. Parenti, R. R., Sasiela, R, J,. Andrews, L. C., Philips, R. L., "Modeling the PDF for Irradiance of an uplink beam in the presence of beam wander",*Atmospheric Propagation III*, Proc. of SPIE, Vol. 6215, (2006), 621508.

Chapter 2

Basic Equations for Wave Propagation in Turbulence

Turbulence has a large effect on electromagnetic wave propagation that can be described by stochastic differential equations. In this chapter these equations are solved with the Rytov approximation, and the main result is given in eq. 2.110, which is the starting point for all turbulence problems considered in this book. This equation is used to find phase and log-amplitude variances. These expressions are modified to obtain expressions for the power spectral density, given in eq. 2.134, beam profile given in eq. 2.161, and Strehl ratio, which is the ratio of on-axis intensity to that of a diffraction-limited wave, in eq. 2.163.

Turbulence effects arise from atmospheric refractive index variations that cause both large and small scale variations of electromagnetic-wave propagation. There are both a steady decrease of air density with altitude that causes refraction of the waves and local inhomogeneities that have a more complicated effect. The steady part of the refractive index variation $n(\mathbf{r})$ can be estimated from

$$n(\mathbf{r}) - 1 = 77.6 \times 10^{-6} \left(1 + 7.52 \times 10^{-3}/\lambda^2\right) P(\mathbf{r})/T(\mathbf{r}), \qquad (2.1)$$

where λ is the propagation wavelength in μm, P is pressure in millibars, T is temperature in degrees Kelvin, and $\mathbf{r}$ is three-dimensional spatial position. At sea level $n(\mathbf{r}) - 1$ is approximately equal to 3×10^{-4}.

In addition to this steady density variation, there are stochastic changes. Stochastic temperature variations in the air are the source of quivering images that we sometimes see. Since the atmosphere has constant pressure locally, these temperature variations cause density variations that in turn lead to refractive index variations, causing the bending and scattering of light rays. Most often these temperature variations are generated by a temperature differential between the earth and the adjoining atmosphere. In daytime, the earth is hotter than the air; this causes air closer to the ground to be hotter than that above. This negative temperature gradient bends light rays that are parallel to the earth upwards and, if strong enough, results in inverted images of the sky. This *mirage* is a common occurrence in deserts or along heated asphalt on sunny days. Stronger temperature gradients can result in the appearance of additional images.

During nighttime, temperature gradients can be positive, resulting in downward bending of light rays enabling one to see objects below the horizon and

elevating images of objects that are on the horizon. (This phenomenon is called *looming*.)

The effects of turbulence are very significant at optical frequencies since the changes in refractive index cause path changes on the order of a micrometer. At radar frequencies one can usually neglect the effect of turbulence; however, there can be situations in which it is important. At low elevation angles the effect of turbulence is more pronounced; however, even this larger effect is not significant at centimeter wavelengths. However, moisture in the air and clouds and rain showers can have significant variations in refractive index that can produce measurable effects such as signal fading and angular jitter. The theory presented here can be used in this case once a spatial spectrum of these disturbances is developed.

2.1 Turbulence Spectra

Mirages and looming are due to large scale temperature gradients that can persist for some time. Much more commonly, temperature inversions lead to smaller scale effects that fluctuate more rapidly. For typical sizes of turbulence blobs (turbules), the Reynolds number is much greater than 1, and laminar air flow is unstable, which results in the breakup of stratified air layers into smaller blobs. Often on a hot day one can see the swirling of heated air as eddies cascade down in size. This process produces smaller and smaller eddy sizes until dissipation effects become important at a scale called the inner scale, at which point rotational energy is rapidly dissipated and flow becomes laminar. This causes a rapid decrease in spectral energy at small scales.

Different methods must be used to analyze the effects on wave propagation of large- and small-scale atmospheric temperature variations. A gradual decrease in air density with height and the dispersive characteristics of air can separate white light into spectra so that starlight at low elevation angles sometimes appears to have distinct colors. (This dispersive effect also causes the green part of the sun's spectrum to set after the red part, producing the "green flash".) These density variations last for extended periods of time, and their effect on wave propagation can be analyzed with ray optics in which density along the propagation path can be assumed to remain constant with time.

Mirages are caused by variations in air density close to the earth. Air in this region has some turbulence characteristics that cause variations in the mirage shapes; however, major features of mirages can also be determined with ray-optics propagation in a deterministic atmosphere.

Small scale fluctuations also affect wave propagation in the atmosphere and produce detectable effects. With the unaided eye, one can see scintillations in starlight as well as in street lights at some distance. Turbulence has a profound effect on the ability of astronomers to separate images of two objects that are close together. In a vacuum, resolving power of a mirror increases linearly with diameter. In the atmosphere, resolution increases until a certain diameter and

then remains almost the same with increasing diameter. Thus we are led to the important concept of atmospheric coherence diameter. At sea level this diameter is about 2–15 cm at visible wavelengths. At higher elevations, at certain sites, this diameter can be tens of centimeters and is the main reason that large astronomical telescopes are located on mountain tops. Making telescope diameters larger than the coherence diameter increases the amount of light collected but hardly increases resolution for objects whose recording takes more than a fraction of a second. For smaller times images are speckled, and they contain information up to the diffraction limit of the full diameter. In some circumstances, by using elaborate processing of short term images, it is possible to resolve objects that are separated by the telescope's vacuum resolution (*Goodman* 1985).

Turbulence effects are stochastic in nature, and to characterize them in detail, one must solve the wave equation with a stochastic refractive index. This is treated in this book.

I now turn to the standard phenomenology of atmospheric turbulence. Eddy distributions at the largest sizes, where energy enters the cascade process, is highly dependent on local topography and absorption characteristics of the earth's surface, and on distribution of winds and temperature aloft. Once eddies are formed and break up into smaller eddies, the eddy size distribution follows universal laws. *Kolmogorov* (1941) and *Obukhov* (1941) were first to derive the distribution law for the relative amount of turbulence at various scale sizes in the region that is referred to as the inertial subrange. This range encompasses scale sizes from, typically, 1 millimeter to 10 meters. One can obtain this law from dimensional analysis.

Turbulence theory makes heavy use of the mean square value of the difference of a quantity at two points, i.e., the structure function. For the turbulent air speed v this is defined to be

$$\mathcal{D}_v(\mathbf{r}) = \left\langle [v(\mathbf{a}) - v(\mathbf{a}+\mathbf{r})]^2 \right\rangle, \tag{2.2}$$

where angle brackets indicate an ensemble average.

Evolution of turbulence can be analyzed with the Navier-Stokes hydrodynamic differential equations. In the inertial subrange, where dissipation is not important, Kolmogorov and Obukhov made the key assumption that the structure function of air speed is isotropic and a function solely of separation $\mathbf{r}$ and rate of energy deposition per unit mass ε, i.e.,

$$\mathcal{D}_v(\mathbf{r}) = \mathcal{D}_v(r) = f(r, \varepsilon). \tag{2.3}$$

The units of ε are $m^2/\sec^3$, and by Buckingham's Pi theorem *Langhaar* (1980) the only form the solution can assume is the combination of ε and r that have units of velocity squared. Therefore, the isotropic structure function must be

$$\mathcal{D}_v(r) = e^2(\varepsilon r)^{2/3}, \qquad r \gg L_{in}, \tag{2.4}$$

where e^2 is a constant, and L_{in} is the "inner scale." This is the "two-thirds power law".

For very small separations the Reynolds number is small and friction dominates, causing rotational velocity to be dissipated, thus resulting in laminar flow. For laminar flow, the average velocity can be expanded into a Taylor series about any point. The constant terms cancel, and because velocity is assumed to be isotropic, the linear terms also cancel; therefore, the leading term is

$$\mathcal{D}_v(r) = b^2 r^2, \qquad r \ll L_i. \tag{2.5}$$

Close to the ground the turbulence may not have evolved to isotropic Kolmogorov turbulence. In that case the following analysis would not apply.

In the region of greatest interest, the inertial subrange, the two-thirds power law contains all information on turbulence of practical importance. Even though this relation is simple, it is not easy to exploit for several reasons. First, it is not straightforward to incorporate this relation into Maxwell's equations. The Rytov approximation given below overcomes this difficulty.

Second, the steps necessary to obtain quantities of interest such as second moments or Strehl ratios are lengthy and not intuitive. I show in the next section that many specific problems are special cases of a general problem that is set up and reduced to integrals, thereby making this step straightforward.

Third, many integrals that typically arise diverge because this form of the structure function is unphysical both at small and large turbulence scales. The structure function is modified below to overcome these difficulties.

Fourth and last, these integrals are difficult to evaluate analytically, and numerical methods are often used. This reduces one's physical insight into the behavior of the solution as a function of the size of the parameters. Modifications of the structure function to remove infinities results in integrals that are even more difficult to evaluate. Mellin transform techniques that are developed in this book allow one to analytically evaluate these integrals, thus enabling one to see how solutions depend on parameters.

To solve stochastic propagation problems it is convenient to analyze problems in Fourier space. For example, the expression for the phase and log-amplitude variance in Sec. 2.3 requires the correlation function of the transverse Fourier transform of density fluctuations. Now derive statistics of density fluctuations in Fourier space. In position space the structure function of density is given by

$$\mathcal{D}_n(\mathbf{r}) = \left\langle [n(\mathbf{a}) - n(\mathbf{a}+\mathbf{r})]^2 \right\rangle. \tag{2.6}$$

It can be shown that with the concept of conservative passive additives *Tatarski* (1971) that this structure function has the same variation with distance as the structure function for velocity, and is expressed as

$$\mathcal{D}_n(r) = C_n^2 r^{2/3}, \qquad r \gg L_i, \text{ and} \tag{2.7}$$

$$\mathcal{D}_n(r) = C_n^2 \frac{b^2}{e^2} r^2, \qquad r \ll L_i, \tag{2.8}$$

where C_n^2 measures turbulence strength.

A relation between the turbulence spatial spectrum and the structure function of density is found below. First, I develop some general Fourier relations in spherical coordinates. The spatial spectrum of a quantity is found from the 3-dimensional Fourier transform

$$\Psi(\mathbf{k}) = \frac{1}{(2\pi)^3} \iiint d\mathbf{r}\, \cos(\mathbf{k}\cdot\mathbf{r})\, \psi(\mathbf{r}), \tag{2.9}$$

where integration is over all space, and $\mathbf{k}$ is the total propagation vector, which consists of a two-dimensional transverse component $\boldsymbol{\kappa}$ and a component, k_z, along the propagation vector. Thus,

$$\mathbf{k} = \boldsymbol{\kappa} + \mathbf{u}_z\, k_z, \tag{2.10}$$

where $\mathbf{u}_z$ is a unit vector in the axial direction. The three-dimensional spatial vector is also expressed as a transverse component $\boldsymbol{\rho}$ and an axial component z as

$$\mathbf{r} = \boldsymbol{\rho} + \mathbf{u}_z\, z. \tag{2.11}$$

The exponential $\exp(i\mathbf{k}\cdot\mathbf{r})$ is replaced by $\cos(\mathbf{k}\cdot\mathbf{r})$ in eq. 2.9 because $\Psi(\mathbf{k})$ is an even function of $\mathbf{k}$.

The inverse Fourier relation is

$$\psi(\mathbf{r}) = \iiint d\mathbf{k}\, \cos(\mathbf{k}\cdot\mathbf{r})\, \Psi(\mathbf{k}). \tag{2.12}$$

If this function is assumed to be isotropic, then this relation can be reduced to a simpler form. The integral can be expressed in spherical coordinates as

$$\Psi(k) = \frac{1}{(2\pi)^3} \int_0^{\pi}\int_0^{2\pi}\int_0^{\infty} r^2 \sin(\theta)\, dr\, d\theta\, d\phi\, \cos(\mathbf{k}\cdot\mathbf{r})\, \psi(r).$$

The $\mathbf{k}$ vector is considered to be along the z-axis; therefore, $\mathbf{k}\cdot\mathbf{r} = kr\cos(\theta)$, as is shown in Fig. 2.1.

Using the relation

$$\frac{d}{d\theta}\sin[kr\cos(\theta)] = -\cos[kr\cos(\theta)]\; kr\sin(\theta),$$

one can perform the two angle integrations to give

$$\Psi(k) = \frac{1}{2\pi^2 k} \int_0^{\infty} r\, dr\, \sin(kr)\, \psi(r). \tag{2.13}$$

Similarly, the angle integrations can be performed in the inverse transform to give

$$\psi(r) = \frac{4\pi}{r} \int_0^{\infty} k\, dk\, \sin(kr)\, \Psi(k). \tag{2.14}$$

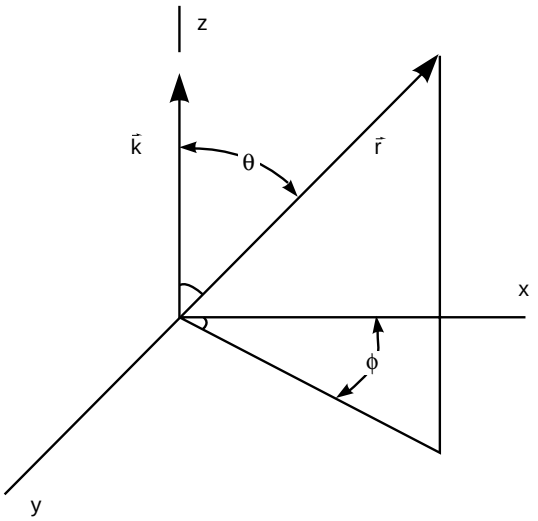

Figure 2.1. Spherical coordinate system.

Obtain a relation between the structure function and the density distribution $n_1(\mathbf{r})$, by setting $\psi(\mathbf{r})$ to the density correlation function

$$\psi(\mathbf{r}) = \langle n_1(\mathbf{a})\, n_1(\mathbf{a}+\mathbf{r})\rangle\,. \tag{2.15}$$

It has been assumed that the structure function is only a function of the separation. In general $\mathcal{D}_n(\mathbf{r})$ is also a function of $\mathbf{a}$. For a stochastic process with stationary increments (that is one in which the difference in values of the process at two positions is stationary) the dependence on $\mathbf{a}$ is through a slowly varying multiplicative factor. As long as the scale length of this variation is much longer than the correlation distance of turbulence, the error in this derivation is small.

Since a displacement in real space corresponds to a phase shift in Fourier space, one can express the density structure function as

$$\mathcal{D}_n(\mathbf{r}) = \iiint d\mathbf{k}\,|1-\exp(i\mathbf{k}\cdot\mathbf{r})|^2\Psi(\mathbf{k}) = 2\iiint d\mathbf{k}\,[1-\cos(\mathbf{k}\cdot\mathbf{r})]\,\Psi(\mathbf{k})\,. \tag{2.16}$$

Assuming isotropic turbulence, one can express this as

$$\mathcal{D}_n(r) = 8\pi\int_0^\infty k^2\,dk\,\left[1-\frac{\sin(kr)}{kr}\right]\Psi(k)\,. \tag{2.17}$$

To obtain the inverse Fourier relation, note that

$$\frac{\partial}{\partial r}r^2\frac{\partial\mathcal{D}_n(r)}{\partial r} = 8\pi r\int_0^\infty dk\,k^3\,\sin(kr)\,\Psi(k)\,.$$

The inverse sine transform gives the desired relation between the turbulence spectrum and structure function as

$$\Psi(k) = \frac{1}{(2\pi k)^2} \int_0^\infty dr \, \frac{\sin(kr)}{kr} \frac{\partial}{\partial r} r^2 \frac{\partial \mathcal{D}_n(r)}{\partial r}. \tag{2.18}$$

If the structure function with two-thirds power law given in eq. 2.7 is inserted into this integral and evaluated with eq. 1.21, then one obtains the three-dimensional Kolmogorov turbulence spectrum

$$\Psi(k) = \frac{5\,\Gamma[5/6]}{2^{4/3}\,\pi^{3/2}\,9\,\Gamma[2/3]} C_n^2\, k^{-11/3} = 0.0330054\, C_n^2\, k^{-11/3}. \tag{2.19}$$

As discussed above, the derivation is strictly valid only if C_n^2 does not depend on position. Later I will relax this restriction by allowing C_n^2 to vary slowly along the propagation path.

There are no convergence difficulties when one performs calculations with the structure function and its spatial spectrum; however, it will be seen that the phase variance of a propagating wave turns out to be infinite. The infinity comes at very small spatial wavenumbers. In a physical situation, phases and intensities are uncorrelated at large separations; therefore, the structure function must approach a constant at large separations. There are many ways of achieving this, and a convenient one is to write the turbulence spectrum as

$$\Psi(k) = 0.033\, C_n^2 \left(k^2 + \kappa_o^2\right)^{-11/6}, \tag{2.20}$$

where

$$\kappa_o = 2\pi / L_o. \tag{2.21}$$

L_o is the outer-scale size. (Some authors, e.g., *Fante* (1975), omit the 2π.) This spectrum with outer scale included is called the von Kármán spectrum. If the outer scale is allowed to grow without bound the spectrum reduces to eq. 2.19).

The structure function is found by inserting this spectrum into eq. 2.17. To evaluate the integral, the integrand is broken into two parts. The first part is evaluated with the Mellin transform in eq. 1.54 and the relation in eq. 1.9 to give

$$I_1 = 0.264\,\pi\, C_n^2\, \kappa_o^{-11/3} \int_0^\infty \frac{dk}{k}\, k^3 \left[\left(\frac{k}{\kappa_o}\right)^2 + 1\right]^{-11/6} = 1.0468\, C_n^2\, \kappa_o^{-2/3}.$$

The second integral is evaluated with the Mellin convolution theorem given in eq. 1.28 and the Mellin transforms given in eq. 1.48 and eq. 1.54 as

$$I_2 = -0.264\,\pi\, C_n^2\, \kappa_o^{-11/3} \int_0^\infty \frac{dk}{k}\, k^2 \sin(kr) \left[\left(\frac{k}{\kappa_o}\right)^2 + 1\right]^{-11/6}$$

$$= -0.264\,\pi\, C_n^2\, \kappa_o^{-11/3} \frac{\sqrt{\pi}}{r^2\,\Gamma[11/6]} \frac{1}{2\pi i} \int_C ds \left(\frac{\kappa_o r}{2}\right)^{-s} \Gamma\left[s/2 + \tfrac{3}{2}, s/2 + \tfrac{11}{6}\right].$$

Make the replacement $s \to s - 10/3$ and recognize the integral as the inverse Mellin transform of $K_{1/3}(\kappa_o r)$ given in eq. 1.61, where $K_{1/3}(x)$ is the modified Bessel function of the third kind with imaginary argument. The structure function of density is

$$\mathcal{D}_n(r) = C_n^2 r^{2/3} \left\{ (\kappa_o r)^{-2/3} \left[1.0468 - 0.62029 (\kappa_o r)^{1/3} K_{1/3}(\kappa_o r) \right] \right\}. \quad (2.22)$$

The effect of outer scale is contained in the term in braces that multiplies the structure function with infinite outer scale. This factor is plotted in Fig. 2.2. The structure function has been reduced by 5% when the separation is 1/25 of the outer scale.

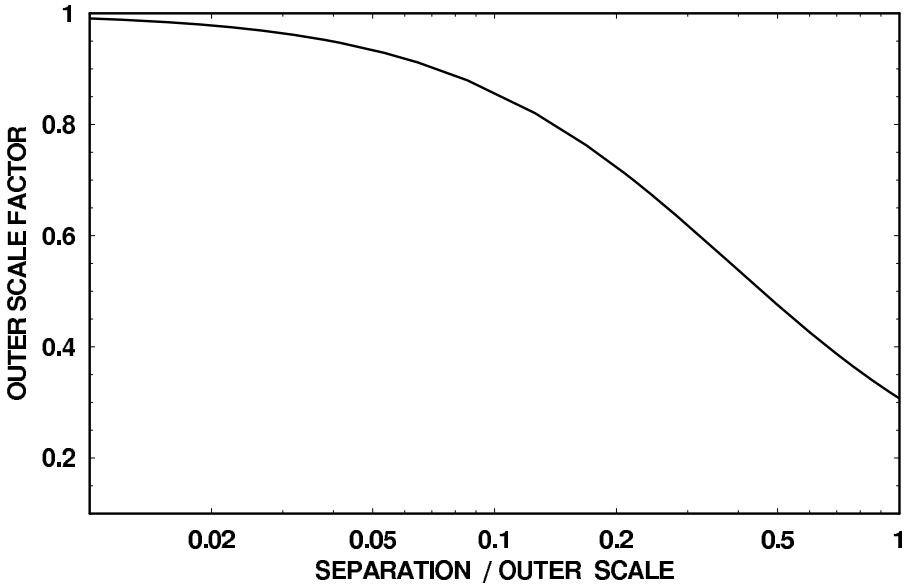

Figure 2.2. Effect of outer scale on the structure function versus the ratio of separation to outer scale.

This form of the structure function reduces to the two-thirds power law given in eq. 2.7 for small separations. This is shown with the small argument approximation of the power series given in eq. 1.25. The first two terms of the expansion are

$$K_{1/3}(x) \approx \frac{x^{-1/3}}{2^{2/3}} \Gamma\left[\tfrac{1}{3}\right] + \frac{x^{1/3}}{2^{4/3}} \Gamma\left[-\tfrac{1}{3}\right], \qquad x \ll 1.$$

The value of $\Gamma[1/3]$ is 2.6789, and the value of $\Gamma[-1/3]$ is -4.0624. With these values one obtains eq. 2.7.

For very large separations the modified Bessel function is vanishingly small, and the structure function reduces to the constant

$$\mathcal{D}_n(r) = 1.0468\, \kappa_o^{-2/3} C_n^2, \qquad \kappa_o r \gg 1. \quad (2.23)$$

The shape of the spectral region of the von Kármán spectrum in which outer scale has a significant effect has no universal theoretical justification. Measurements made over a wheat field by *Kamai* et al. (1972) support this spectral form. *Greenwood* and *Tarazano* (1974) made some measurements of turbulence spectra in areas not as topographically smooth, and their data more closely supports a model in which the turbulence spectrum is

$$\Psi(k) = 0.033\, C_n^2 \left(k^2 + k\kappa_o\right)^{-11/6}. \tag{2.24}$$

A spectrum that has been used recently because it results in more tractable integrals and has similar properties to the von Kármán spectrum is

$$\Psi(k) = 0.033\, k^{-11/3} C_n^2 \left\{1 - \exp\left[-\left(k/2\kappa_o\right)^2\right]\right\}. \tag{2.25}$$

In this book the von Kármán spectrum is used except when tilt with outer scale is found for both the von Kármán and Greenwood spectra. Qualitative behavior is the same in the two cases.

There are also difficulties at large wavenumbers. From the hydrodynamic equations it can be shown that the above spectra require infinite energy dissipation due to the rapid increase in dissipation with decreasing scale size. Physically, below a certain scale size dissipative effects force the velocity to be laminar. This leads to a rapid decrease in the spectrum with decreasing scale size. Several ad hoc models are used for the spectrum in this inner scale region; the Gaussian form used in this book for some problems is referred to as the Tatarski spectrum.

A spectrum with both inner scale and von Kármán outer scale — the modified von Kármán spectrum — is

$$\Psi(k) = 0.033\, C_n^2 \left(k^2 + \kappa_o^2\right)^{-11/6} \exp\left(-k^2/\kappa_i^2\right), \tag{2.26}$$

where

$$\kappa_i = 2\pi/L_i = 5.91/L_{in}. \tag{2.27}$$

L_{in} is the commonly used inner scale. I occasionally use L_i to simplify equations. The two are related by $L_{in} = 0.94\, L_i$. The spectrum is shown in Fig. 2.3.

Greenwood and *Tarazano* (1974) and *Gurvich* et al. (1974) noted that the turbulence does not decay as rapidly as that predicted by the Kolmogorov spectrum in the region just before it starts its rapid decay due to inner scale effects. *Hill* (1978) did a hydrodynamic analysis to derive a spectrum in the region where inner scale is significant, and found a slight peak before an exponential decay. *Frehlich* (1992) has modeled the spectrum as

$$\Psi(k) = 0.033\, C_n^2 \left(k^2 + \kappa_o^2\right)^{-11/6} g\,(k), \tag{2.28}$$

where a 4-term approximation for $g\,(k)$ is

$$g\,(k) = \exp\left(-\delta\, |k|\, L_{in}\right) \sum_{n=0}^{4} a_n \left(|k|\, L_{in}\right)^n. \tag{2.29}$$

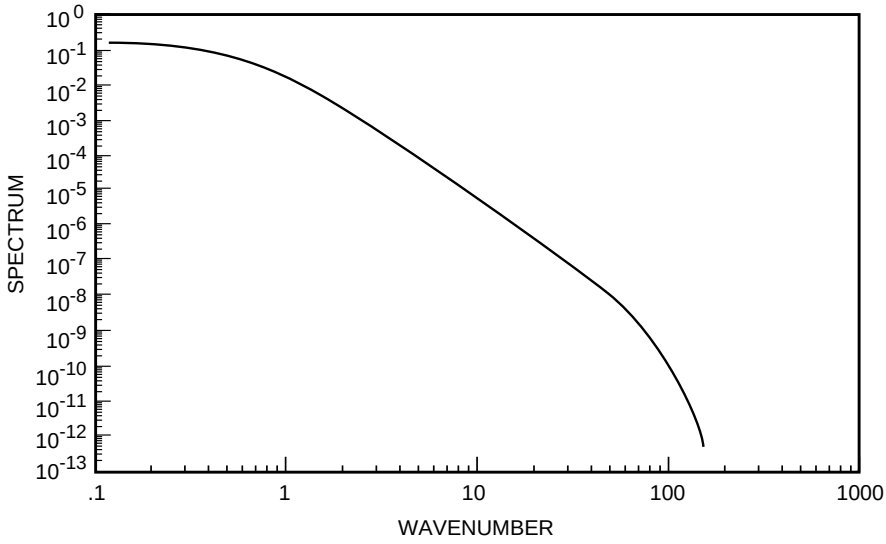

Figure 2.3. Von Kármán spectrum with inner and outer scale present normalized by $0.033\, C_n^2$. The value of κ_i is equal to $2\pi/0.1$, and the value of κ_o is equal to $2\pi/10$. The presence of the outer scale causes the spectrum to approach a constant at low wavenumbers. The inner scale causes the spectrum to decay faster than Kolmogorov turbulence at high wavenumbers. The spectrum has an $-11/3$ power law behavior in the inertial subrange at intermediate wavenumbers.

The constants are given by $\delta = 1.1090$, $a_0 = 1$, $a_1 = 0.70937$, $a_2 = 2.8235$, $a_3 = -0.28086$, and $a_4 = -0.08277$. This function is plotted versus the Tatarski function $\exp\left[-(kL_{in}/5.92)^2\right]$ in Fig. 2.4.

The spectrum given in eq. 2.26 is used in this book for tilt calculations because it is not physically unreasonable and is mathematically convenient. The spectrum given in eq. 2.28 can produce a significantly different scintillation at short ranges than the modified von Kármán spectrum, and it should be used in those calculations. The difference between the scintillation with these two spectra is considered in Sec. 7.9.

If the Tatarski spectrum is inserted into the integral for the structure function in eq. 2.17, then the expression can be evaluated with the Taylor series of the sinusoid and a term by term integration. Because each series term produces an integral that is absolutely convergent, this method is valid. For very small separations the first term of the expansion gives the most significant contribution as $1-\sin(kr)/kr \approx (kr)^2/6,$ for $r \ll L_i$. This is the only factor in the integrand on the separation; therefore, for very small separations the structure function has the required quadratic dependence on separation as given in eq. 2.5. The exponential decay is not unique in this regard; any function with rapid decay produces the correct form of structure function for small separations.

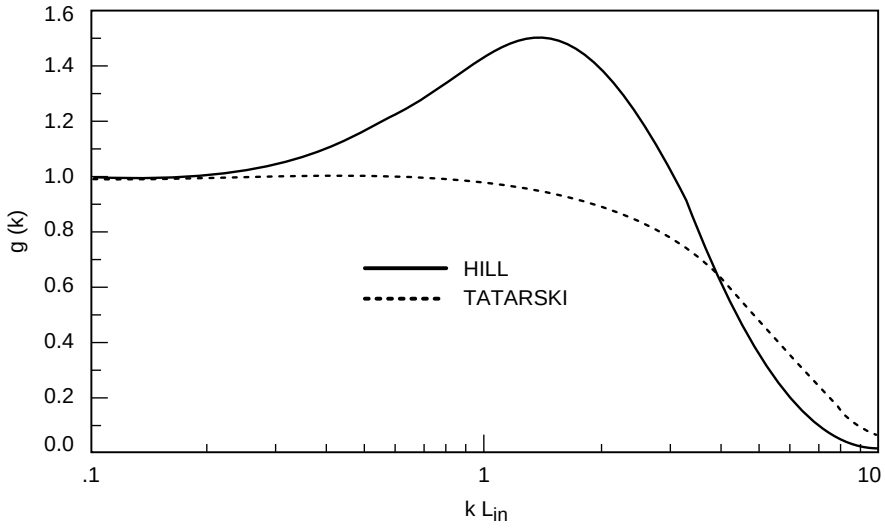

Figure 2.4. Factor that multiplies the Kolmogorov turbulence spectrum in the Tatarski and Hill models of inner scale.

In the analysis performed in this book the two-dimensional Fourier transform is used heavily. It is convenient to use the space coordinate for the direction of wave propagation and to use the Fourier transform of the transverse coordinates. The relationship between the three- and two-dimensional spectra is found by taking the Fourier transform in the propagation coordinate space, and by using the evenness of the spectrum to obtain

$$\Psi(k) = \frac{C_n^2(z)}{2\pi} \int_0^\infty dz' \, E_n(\boldsymbol{\kappa}, z') \cos(k_z z') \,, \tag{2.30}$$

where $E_n(\boldsymbol{\kappa}, z')$ is the Fourier transform in the transverse coordinates of the normalized fluctuations of the covariance of the refractive index. *Notice that the turbulence strength is now allowed to vary along the propagation path.* The inverse Fourier relation obtained with the use of eq. 2.15 is

$$C_n^2(z) \, E(\boldsymbol{\kappa}, z) = \frac{1}{(2\pi)^2} \int d\boldsymbol{\rho}'' \exp(-i\boldsymbol{\kappa} \cdot \boldsymbol{\rho}'') \, \langle n_1(0,0) \, n_1(\boldsymbol{\rho}'', z) \rangle \,. \tag{2.31}$$

A normalized turbulence spectrum $\tilde{f}(\kappa, k_z)$ is defined by

$$\Psi(k) \equiv 0.033 \, C_n^2(z) \, \tilde{f}(\kappa, k_z). \tag{2.32}$$

The two-dimensional spectrum is found by setting $k_z = 0$ to obtain

$$\Psi\left(k\right)|_{k_z=0} \equiv 0.033\, C_n^2\left(z\right) f(\kappa) = \frac{C_n^2\left(z\right)}{2\pi} \int\limits_0^\infty dz'\, E_n\left(\boldsymbol{\kappa}, z'\right). \tag{2.33}$$

The normalized spectrum $f(\kappa)$ is used in the book. For the modified von Kármán spectrum it is

$$f(\kappa) = \left(\kappa^2 + \kappa_o^2\right)^{-11/6} \exp\left(-\kappa^2/\kappa_i^2\right). \tag{2.34}$$

When inner and outer scale are negligible the spectrum is

$$f(\kappa) = \kappa^{-11/3}. \tag{2.35}$$

While $E_n\left(\boldsymbol{\kappa}, z\right)$ is never explicitly needed in this book, it is assumed that it decays rapidly with z. Therefore, it is instructive to derive it for the modified von Kármán spectrum to see its spatial variation.[1]

In Sec. 2.3 the correlation function of the transverse Fourier transform of refractive index fluctuations $d\nu\left(\boldsymbol{\kappa}, z\right)$ is required. This is evaluated with the results given above. The Fourier-Stieltjes relation between the refractive index and its transform is given by

$$n_1(\boldsymbol{\rho}, z) = \int d\nu\left(\boldsymbol{\kappa}, z\right) \exp\left(i\boldsymbol{\kappa}\cdot\boldsymbol{\rho}\right). \tag{2.39}$$

The inverse transform is

$$d\nu\left(\boldsymbol{\kappa}, z\right) = \frac{d\boldsymbol{\kappa}}{\left(2\pi\right)^2} \int d\boldsymbol{\rho}\, n_1(\boldsymbol{\rho}, z) \exp\left(-i\boldsymbol{\kappa}\cdot\boldsymbol{\rho}\right).$$

The correlation function of the transverse Fourier transform of refractive index fluctuations is

[1] $E_n\left(\boldsymbol{\kappa}, z\right)$ can be found from eq. 2.30 by multiplying both sides of the equation by $\cos\left(k_z z\right)$ and integrating over k_z from 0 to infinity. The k_z integration yields a delta function $\delta(z - z')$, which enables the z integration to be performed with the result

$$E_n\left(\boldsymbol{\kappa}, z'\right) = 0.2073 \int\limits_0^\infty dk_z\, \left(\kappa^2 + \kappa_0^2 + k_z^2\right)^{-11/6} \cos\left(k_z z'\right) \exp\left(-\kappa^2/\kappa_i^2\right). \tag{2.36}$$

For zero inner scale, this integral can be evaluated to obtain

$$E_n\left(\boldsymbol{\kappa}, z\right) = \frac{0.2073\sqrt{\pi}\, K_{\frac{4}{3}}\left(\sqrt{\kappa^2 + \kappa_0^2}\, z\right)}{2^{\frac{4}{3}}\, \left(\kappa^2 + \kappa_0^2\right)^3\, z^{\frac{7}{3}}\, \Gamma\left(\frac{11}{6}\right)}. \tag{2.37}$$

For large arguments of the modified Bessel function, one can use its asymptotic value, $K_\nu(x) \sim \sqrt{\pi/2x}\exp(-x)$, to obtain

$$E_n\left(\boldsymbol{\kappa}, z\right) \sim \frac{0.2073\pi\, \exp\left(-\sqrt{\kappa^2 + \kappa_0^2}\, z\right)}{2^{\frac{11}{6}}\, \left(\kappa^2 + \kappa_0^2\right)^{13/2}\, z^{\frac{17}{6}}\, \Gamma\left(\frac{11}{6}\right)}. \tag{2.38}$$

Therefore, $E_n\left(\boldsymbol{\kappa}, z\right)$ has exponential decay for large values of z, and its value is reduced significantly in a distance of a turbulence wavelength.

$$\langle d\nu\left(\boldsymbol{\kappa}, z'\right)\, d\nu^{*}\left(\boldsymbol{\kappa}', z''\right)\rangle$$
$$= \frac{d\boldsymbol{\kappa}\, d\boldsymbol{\kappa}'}{(2\pi)^4}\int d\boldsymbol{\rho}\int d\boldsymbol{\rho}' \exp\left[-i\left(\boldsymbol{\kappa}\cdot\boldsymbol{\rho}-\boldsymbol{\kappa}'\cdot\boldsymbol{\rho}'\right)\right]\,\langle n_1\left(\boldsymbol{\rho}, z'\right) n_1\left(\boldsymbol{\rho}', z''\right)\rangle\,.$$

Make the change in variables $\boldsymbol{\rho}-\boldsymbol{\rho}'=\boldsymbol{\rho}''$ and $\boldsymbol{\rho}'=\boldsymbol{\rho}'$ to give

$$\langle d\nu\left(\boldsymbol{\kappa}, z'\right)\, d\nu^{*}\left(\boldsymbol{\kappa}', z''\right)\rangle$$
$$= \frac{d\boldsymbol{\kappa}\, d\boldsymbol{\kappa}'}{(2\pi)^4}\int d\boldsymbol{\rho}''\int d\boldsymbol{\rho}' \exp\{-i\left[\boldsymbol{\kappa}\cdot\boldsymbol{\rho}''-\left(\boldsymbol{\kappa}-\boldsymbol{\kappa}'\right)\cdot\boldsymbol{\rho}'\right]\}\,\langle n_1(\boldsymbol{\rho}'+\boldsymbol{\rho}'', z')\, n_1(\boldsymbol{\rho}', z'')\rangle\,. \tag{2.40}$$

Assume the correlation function is a function of the coordinate difference times a slowly varying function of position along the propagation path as

$$\langle n_1(\boldsymbol{\rho}'+\boldsymbol{\rho}'', z')\, n_1\left(\boldsymbol{\rho}', z''\right)\rangle = C_n^2\left[\left(z'+z''\right)/2\right]\langle n_n\left(0,0\right) n_n\left(\boldsymbol{\rho}'', z'-z''\right)\rangle\,,$$

where $n_n\left(\boldsymbol{\rho}, z\right)$ is a normalized density fluctuation and $C_n^2(z)$ is the turbulence strength. Insert this relation into eq. 2.40. The integration over $\boldsymbol{\rho}'$ gives $(2\pi)^2\,\delta\left(\boldsymbol{\kappa}-\boldsymbol{\kappa}'\right)$. Use the relation in eq. 2.31 to find the expected value as

$$\langle d\nu\left(\boldsymbol{\kappa}, z'\right)\, d\nu^{*}\left(\boldsymbol{\kappa}', z''\right)\rangle$$
$$= E_n\left(\boldsymbol{\kappa}, |z'-z''|\right) C_n^2\left[\left(z'+z''\right)/2\right]\,\delta\left(\boldsymbol{\kappa}-\boldsymbol{\kappa}'\right) d\boldsymbol{\kappa}\, d\boldsymbol{\kappa}'. \tag{2.41}$$

This relation is used to find the expected value of second moments.

2.2 Rytov Approximation

Determining the turbulence effect on wave propagation requires one to solve Maxwell's equations with a refractive index that is stochastic. This cannot be done exactly. An approach that uses geometric optics was first introduced by *Chernov* (1960) to solve this problem. It was soon realized that this approximation requires $L < L_i^2/\lambda$ where L is the propagation distance and λ is the propagation wavelength. This has a very limited range of applicability. It was Rytov who proposed an approximation that included diffraction effects; this resulted in a wider range of validity. This approximation could be used to obtain second moments of quantities. *Tatarski* in two seminal books (1961, 1971) codified this method and obtained solutions to a large variety of problems. His results agreed well with experiments.

Since Tatarski's books were written, many problems have been solved as interest in wave propagation in turbulence expanded because of new technologies and areas of application. These areas include sending information on optical beams close to the ground, remote sensing of the atmosphere on earth and planets, correcting atmospheric distortion to allow better resolution in optical images, and sending laser beams efficiently through the atmosphere. The last

two applications require correction of atmospheric distortion by adaptive-optics systems. To correct distortion one must measure phase along a path that is close in angle to the actual path along which the laser beam propagates. How small this angle must be to obtain a good correction leads to the important concept of the isoplanatic angle. In this book anisoplanatism refers to any effect that causes a difference in the propagation paths of two waves.

When propagating laser beams parallel to the ground, one found that scintillation increased with increasing turbulence as the Rytov theory predicted until a certain level was reached, at which point the measured scintillation saturated. To solve problems in the saturation region a more complicated propagation theory was developed that allowed multiple scattering of the wave as discussed by *Strohbehn* (1978). Fortunately, even when the scintillation is saturated, Rytov theory typically gives the correct answer for phase disturbances, thus allowing one to treat many problems of practical interest. Intensity fluctuations in the saturation region are not considered in this book.

As the power in the laser beam increases, the air column along the propagation path heats up from energy absorption by the air. The lateral wind or beam slewing moves this heated air out of the beam in a time referred to as the wind clearing time. The resulting nonuniform temperature distribution across the beam diameter can be shown to be equivalent to a negative lens that causes the beam to expand. This "thermal blooming" is predicted by the nonlinear wave equation and has been extensively studied. Computer simulations are typically used to model the nonlinear interaction. Instabilities can set in when the laser power is high. The theory of this instability is described by *Schonfeld* (1992), and laboratory confirmation of the instability is described by *Johnson* and *Primmerman* (1989). Thermal blooming is not considered in this book. Additional information on saturated turbulence and thermal blooming is in *Strohbehn* (1978).

The average results obtained here are long-term averages. In the short term, the second moments can vary, an effect referred to as intermittency. Its effect on wave propagation is discussed in *Tatarski* and *Zavorotnyi* (1985).

To solve for effects of turbulence in the low-power regime, one starts with Maxwell's equations

$$\nabla \times \boldsymbol{\mathcal{E}}(\mathbf{r},t) = -\frac{\partial \boldsymbol{\mathcal{B}}(\mathbf{r},t)}{\partial t}, \tag{2.42}$$

$$\nabla \cdot \boldsymbol{\mathcal{E}}(\mathbf{r},t) = q(\mathbf{r},t)/\varepsilon(\mathbf{r},t), \tag{2.43}$$

$$\nabla \times \boldsymbol{\mathcal{B}}(\mathbf{r},t) = \mu_o \boldsymbol{\mathcal{J}}(\mathbf{r},t) + \mu_o \varepsilon(\mathbf{r},t) \frac{\partial \boldsymbol{\mathcal{E}}(\mathbf{r},t)}{\partial t}, \quad \text{and} \tag{2.44}$$

$$\nabla \cdot \boldsymbol{\mathcal{B}}(\mathbf{r},t) = 0, \tag{2.45}$$

where $\boldsymbol{\mathcal{E}}(\mathbf{r},t)$ is the electric field, $\boldsymbol{\mathcal{B}}(\mathbf{r},t)$ is the magnetic field, $\varepsilon(\mathbf{r},t)$ is the permittivity, μ_o is the magnetic permeability, $\boldsymbol{\mathcal{J}}(\mathbf{r},t)$ is the current density, and $q(\mathbf{r},t)$ is the charge density. Assume there is a time-harmonic variation of the fields

$$\boldsymbol{\mathcal{E}}(\mathbf{r},t) = \exp(-i\omega t)\, \mathbf{E}(\mathbf{r}). \tag{2.46}$$

$\mathbf{E}(\mathbf{r})$ can also vary with time but the time scale of variation is much longer than the harmonic variation. The air density affects the refractive index as

$$\varepsilon(\mathbf{r}) = \varepsilon_0 n^2(\mathbf{r}), \tag{2.47}$$

where the refractive index $n(\mathbf{r})$ for air is given in eq. 2.1. The wave equation describing the electric field derived from the above relations is

$$\nabla^2\mathbf{E}(\mathbf{r}) + k_0^2 n^2(\mathbf{r})\,\mathbf{E}(\mathbf{r}) - 2i\frac{k_0}{c}\frac{\partial\left[n^2(\mathbf{r})\ \mathbf{E}(\mathbf{r})\right]}{\partial t} + 2\nabla\{\mathbf{E}(\mathbf{r})\cdot\nabla\ln\left[n(\mathbf{r})\right]\} = 0,$$

where the free space wavenumber is given by $k_0 = \omega/c = 2\pi/\lambda$, and c is the speed of light in vacuum. The nonsinusoidal variation of the field with time is suppressed. If the rate of change of $\mathbf{E}(\mathbf{r})$ with time is much less than the sinusoidal variation $\exp(-i\omega t)$, then the third term is negligible compared to the first two. For optical and radar frequencies this condition is satisfied. In addition, if the propagation wavelength λ is much less than the inner scale, then the last term that produces coupling between the different polarization components of the electric field can be neglected. For visible wavelengths, typical inner-scale sizes of a millimeter satisfy this condition, in which case one obtains a scalar equation for each of the electric field components separately. The equation for one component is

$$\nabla^2 u(\mathbf{r}) + k_0^2 n^2(\mathbf{r})\ u(\mathbf{r}) = 0. \tag{2.48}$$

In the Rytov method the solution is expressed as

$$u(\mathbf{r}) = \exp\left[\Phi(\mathbf{r})\right]. \tag{2.49}$$

This leads to the nonlinear Riccati equation

$$\nabla^2\Phi(\mathbf{r}) + \left[\nabla\Phi(\mathbf{r})\right]^2 = -k_0^2 n^2(\mathbf{r}). \tag{2.50}$$

If it is assumed that the magnitude of the air-density inhomogeneity is small, the refractive index is

$$n(\mathbf{r}) = 1 + \delta n_1(\mathbf{r}), \tag{2.51}$$

where $\delta n_1(\mathbf{r}) \ll 1$, and δ was inserted into the expression to show smallness. This Riccati equation can be solved by a perturbation method in which it is assumed that the solution can be written as a power series in δ,

$$\Phi(\mathbf{r},\delta) = \Phi_0(\mathbf{r}) + \delta\,\Phi_1(\mathbf{r}) + \delta^2\,\Phi_2(\mathbf{r}) + \cdots. \tag{2.52}$$

This expansion is the basis of the Rytov approximation. If instead, the field $u(\mathbf{r})$ were expanded into a series, then that would be the Born approximation. The Rytov approximation leads to the log-amplitude having Gaussian statistics while the Born approximation leads to Rician statistics. The Rytov approximation agrees better with experimental results and is the reason it is used.

By inserting this into eq. 2.50 and by separating the equations based on the power of δ, one obtains a system of equations that has been explored by *Schmeltzer* (1967).

$$\nabla^2 \Phi_0 (\mathbf{r}) + \nabla \Phi_0 (\mathbf{r}) \cdot \nabla \Phi_0 (\mathbf{r}) = -k_0^2, \tag{2.53}$$

$$\nabla^2 \Phi_1 (\mathbf{r}) + 2 \nabla \Phi_0 (\mathbf{r}) \cdot \nabla \Phi_1 (\mathbf{r}) = -2 k_0^2 n_1 (\mathbf{r}), \tag{2.54}$$

$$\nabla^2 \Phi_2 (\mathbf{r}) + 2 \nabla \Phi_0 (\mathbf{r}) \cdot \nabla \Phi_2 (\mathbf{r}) = -k_0^2 n_1^2 (\mathbf{r}) - \nabla \Phi_1 (\mathbf{r}) \cdot \nabla \Phi_1 (\mathbf{r}), \text{ and} \tag{2.55}$$

$$\nabla^2 \Phi_m (\mathbf{r}) + 2 \nabla \Phi_0 (\mathbf{r}) \cdot \nabla \Phi_m (\mathbf{r}) = - \sum_{p=1}^{m-1} \nabla \Phi_p (\mathbf{r}) \cdot \nabla \Phi_{m-p} (\mathbf{r}). \tag{2.56}$$

For these equations to be valid one requires

$$|\nabla \Phi_{n+1} (\mathbf{r})| \ll |\nabla \Phi_n (\mathbf{r})|. \tag{2.57}$$

This condition gives this method the alternate name of "the method of smooth perturbations." I retain only the first two terms. Express the lowest-order term in the form

$$u_0(\mathbf{r}) = \exp [\Phi_0 (\mathbf{r})]. \tag{2.58}$$

Eq. 2.53 is equivalent to one for a wave undisturbed by turbulence,

$$\nabla^2 u_0(\mathbf{r}) + k_0^2 u_0(\mathbf{r}) = 0. \tag{2.59}$$

If I set

$$\Phi_1(\mathbf{r}) = W_1 (\mathbf{r}) / u_0(\mathbf{r}) = W_1 (\mathbf{r}) \exp(-\Phi_0), \tag{2.60}$$

the solution to second order is

$$u_1 (\mathbf{r}) = u_0 (\mathbf{r}) \exp [\Phi_1(\mathbf{r})]. \tag{2.61}$$

To obtain $\Phi_1(\mathbf{r})$ one must determine $W_1 (\mathbf{r})$. Substituting the second part of eq. 2.60 into eq. 2.54 and using eq. 2.53 to simplify the expression gives

$$\nabla^2 W_1 (\mathbf{r}) + k_0^2 W_1 (\mathbf{r}) = -2 k_0^2 n_1(\mathbf{r}) u_0 (\mathbf{r}). \tag{2.62}$$

The solution to this linear differential equation with constant coefficients is obtained with the Green's function for free space propagation as

$$\Phi_1(\mathbf{r}) = \frac{2 k_0^2}{u_0 (\mathbf{r})} \int dV' u_0 (\mathbf{r}') n_1(\mathbf{r}') G (|\mathbf{r} - \mathbf{r}'|), \tag{2.63}$$

where the integration is over the source volume denoted by primed coordinates.

The Green's function in spherical coordinates is

$$G (|\mathbf{r} - \mathbf{r}'|) = \frac{1}{4\pi |\mathbf{r} - \mathbf{r}'|} \exp (i k_0 |\mathbf{r} - \mathbf{r}'|). \tag{2.64}$$

The perturbed field is

$$\Phi_1(\mathbf{r}) = \frac{k_0^2}{2\pi u_0(\mathbf{r})} \int dV' \, u_0(\mathbf{r}') \, n_1(\mathbf{r}') \, \frac{\exp(ik_0 |\mathbf{r} - \mathbf{r}'|)}{|\mathbf{r} - \mathbf{r}'|}. \tag{2.65}$$

The requirement that the second term of the expansion must be much greater than the sum of the remaining terms leads to the requirement that

$$k_0^{7/6} \int_0^L dz \, C_n^2(z) \, z^{5/6} < 1. \tag{2.66}$$

As shown in Sec. 4.7 this is the same as requiring log-amplitude fluctuations to be small. It has generally been found that the Rytov approximation gives a good approximation to the log-amplitude variance σ_χ^2 in the regime

$$\sigma_\chi^2 < 0.35. \tag{2.67}$$

At full saturation the maximum value of σ_χ^2 is 0.6. Even though the Rytov value for log-amplitude is not valid when this inequality is not satisfied, the solution for the phase *for collimated beams* has been shown to be valid.

2.3 Phase and Log-Amplitude Variances

In this section I will develop general relations for phase and log-amplitude variances that are used throughout the book to solve turbulence problems. To cover the cases of collimated and spherical waves, variances of the log-amplitude and phase are derived for a Gaussian wave with the approach of *Ishimaru* (1969). Once these quantities are found in the general case, the remainder of the derivation will be performed for infinite waves to reduce the complexity of the analysis and to obtain formulas specific for the infinite wave case, which is typically of most interest. The general case is considered in Chap. 10. The free-space propagation of the lowest-order Gaussian mode has been considered in many places, and the appropriate expression for the field of a wave propagating in the z direction whose focus is at $z = 0$ is

$$u_0(\boldsymbol{\rho}, z) = \frac{A}{1 + i\alpha z} \exp\left[ik_0 z - \frac{k_0 \alpha \rho^2}{2(1 + i\alpha z)}\right], \tag{2.68}$$

where $\mathbf{r} = \boldsymbol{\rho} + \mathbf{u}_z z$, and

$$\alpha = \alpha_r + i\,\alpha_i = \lambda/\pi w_o^2 + i/R_o. \tag{2.69}$$

The parameter R_o is the radius of beam curvature at the source. It is equal to infinity for a collimated beam. At a radius equal to w_o at the source, the intensity has dropped to $1/e^2$ of its value on axis. If the wave were propagating from a focus at $z = L$ to $z = 0$, then one can obtain the expression for the field by substituting $L - z$ for z in the above expression.

The above Gaussian mode is the lowest mode of an infinite set. The general form of a mode in cartesian coordinates is given in *Milonni* (1988) as

$$\begin{aligned}\mathcal{E}_{mn}(x,y,z) &= \frac{Aw_0}{w(z)} H_m\left(\sqrt{2}\frac{x}{w(z)}\right) H_n\left(\sqrt{2}\frac{y}{w(z)}\right) \\ &\quad \times \exp\left\{i\left[kz-(m+n+1)\tan^{-1}(z/z_0)\right]\right\} \\ &\quad \times \exp[ik(x^2+y^2)/2R(z)]\exp[-(x^2+y^2)/w^2(z)], \end{aligned} \tag{2.70}$$

where $H_m\left(\sqrt{2}x/w(z)\right)$ are Hermite polynomials and $w(z) = |1 + i\alpha z|$.

If one had a top-hat distribution (uniform distribution within a given diameter), then to find the field in space one would have to expand the distribution into the appropriate Gaussian modes and consider the propagation of each mode. The higher-order modes will diffract away sooner, so that at very large distances the only mode that is important is the fundamental mode. No higher order modes are addressed in this book.

I use the paraxial assumption: which for the source located at $z = 0$ and the observation point located at $z = L$, the term in the exponential of the Green's function is expanded to obtain

$$\frac{\exp(ik_0\,|\mathbf{r}-\mathbf{r}'|)}{|\mathbf{r}-\mathbf{r}'|} \approx \frac{1}{(L-z')}\exp\left\{ik_0(L-z')\left[1+\frac{|\boldsymbol{\rho}-\boldsymbol{\rho}'\,|^2}{2\,(L-z')^2}-\frac{|\boldsymbol{\rho}-\boldsymbol{\rho}'|^4}{8\,(L-z')^4}\right]\right\}. \tag{2.71}$$

If the source were located at $z = L$ and the observation point were located at $z = 0$, then one can obtain the expression for the field by substituting $L - z$ for z in the above expression.

If one assumes that the distance to the source is much larger than the transverse coordinate, which requires $|\boldsymbol{\rho}-\boldsymbol{\rho}'|^4 \ll (L-z')^3\lambda$, then the last term in braces can be neglected. This approximation can also be used to find an additional restriction on the applicability of the turbulence solution. The smallest turbulence sizes are the order of the inner scale; therefore, the maximum scattering angle is λ/L_i, and the maximum deviation of the beam from boresight is $\lambda\,L/L_i$. Therefore, the paraxial assumption gives the requirement that $L \ll L_i^4/\lambda^3$. For inner scale sizes of a millimeter or more, the range over which the assumption is valid is very large, and the condition is satisfied for most problems.

After substituting eq. 2.71 and eq. 2.68 into eq. 2.65, and performing some algebraic manipulation, one finds that the turbulence-induced disturbance is

$$\Phi_1(\boldsymbol{\rho}, L) = \int_0^L dz' \int d\boldsymbol{\rho}'\, h\,(\boldsymbol{\rho}' - \gamma\,\boldsymbol{\rho}, L, z')\; n_1\,(\boldsymbol{\rho}', z')\,, \text{ where} \tag{2.72}$$

$$h\,(\boldsymbol{\rho}' - \gamma\,\boldsymbol{\rho}, L, z') = \frac{k_0^2}{2\pi}\frac{\exp\left\{ik_0\left[(\boldsymbol{\rho}'-\gamma\,\boldsymbol{\rho})^2/2\gamma\,(L-z')\right]\right\}}{\gamma\,(L-z')}, \text{ and} \tag{2.73}$$

$$\gamma = \frac{1 + i\alpha\, z'}{1 + i\alpha\, L}. \tag{2.74}$$

Note that $\gamma = 1$ at $z = L$. For other values of z for infinite waves the value of γ can be less than or greater than unity depending on whether the beam is smaller or larger than the beam at $z = L$.

It will be shown that the value of γ using the above definition can be negative for some choices of R_0. Just as for propagation in free space where one needs to choose the correct sign of $(k^2)^{1/2} = \pm k$, one needs to choose the sign of γ so that the wave moves in the correct direction. In these problems one does not encounter the complication of having the wave and group velocities being in opposite directions. We have chosen the signs so that $\exp(ikz)$ represents a wave traveling in the positive z direction and $\exp(-ikz)$ represents a wave traveling in the negative z direction. With the use of γ we will see that the equivalent expression is $\exp(i\gamma\kappa\rho)$. Just as we can choose either the plus or the minus sign of k, one has the same situation with γ. To keep the wave direction consistent, one needs to choose the root of γ^2 whose real part is positive. Therefore, when the Fresnel number is infinite and the value of γ calculated using eq. 2.77 is real and negative, then one should change its sign to be positive, which is why the absolute value sign is applied to the real part in the following equation.

Using eq. 2.74 the real and imaginary parts of γ can be expressed as

$$\begin{aligned} \gamma_r &= \left| \frac{1 - \alpha_i(L + z) + |\alpha|^2 z\, L}{1 + |\alpha|^2 L^2 - 2\alpha_i\, L} \right| \\ &= \left| \frac{F_N(1 - z/R_0)(1 - L/R_0) + F_N^{-1}\, z/L}{F_N(1 - L/R_0)^2 + F_N^{-1}} \right|, \quad \text{and} \end{aligned} \tag{2.75}$$

$$\gamma_i = -\frac{\alpha_r(L - z)}{(1 - \alpha_i L)^2 + (\alpha_r\, L)^2} = -\frac{1 - z/L}{F_N(1 - L/R_0)^2 + F_N^{-1}}. \tag{2.76}$$

Note that the imaginary part of γ goes to zero for both large (infinite plane wave) and small (point source) Fresnel numbers. The Fresnel number, $F_N = \mathrm{Re}\,(1/\alpha L) = \pi W_o^2/\lambda L$, is equal to infinity for plane waves and zero for point sources.

Therefore, for propagation from $z = 0$ to $z = L$ the value of γ is equal to unity for infinite plane waves ($W_o \to \infty, \alpha = 0$), and equal to z/L for spherical waves ($W_o \to 0, \alpha = \infty$) (corresponding to a point source at $z = 0$). In these cases the imaginary part of γ is zero.

If the source were located at $z = L$ and the wave propagated towards $z = 0$, one obtains the appropriate relations by using the substitution $z' \to (L - z')$ in the above equations, to obtain

$$\gamma = \frac{1 + i\alpha\,(L - z')}{1 + i\alpha\, L}. \tag{2.77}$$

Note that $\gamma = 1$ at $z' = 0$.

The value of propagation parameter γ is equal to unity for plane waves, and equal to $(L - z)/L$ for spherical waves (corresponding to a point source at $z = L$).

One can easily show that when the imaginary part is non-zero, then its value is negative for both propagation directions.

When the wave is being focused and we need to change the sign of the real part of γ, then in this case we need to make the sign of the imaginary part of γ negative. This results in the intensity increasing in the direction of propagation as it should for a focused beam.

To find variances, the method of spectral expansion is used, in which quantities are expressed as Fourier-Stieltjes integrals of the transverse coordinates. Refractive-index fluctuations are represented in eq. 2.39 as

$$n_1(\boldsymbol{\rho}, z) = \int d\nu(\boldsymbol{\kappa}, z) \exp(i\boldsymbol{\kappa} \cdot \boldsymbol{\rho}), \tag{2.78}$$

where the integral is over the two-dimensional transverse wavenumber space. The requirement that the refractive index is real leads to

$$d\nu(\boldsymbol{\kappa}, z) = d\nu^*(-\boldsymbol{\kappa}, z). \tag{2.79}$$

If eq. 2.78 is substituted into the expression for turbulence-induced fluctuations given in eq. 2.72, and the substitution $\boldsymbol{\rho}' - \gamma\,\boldsymbol{\rho} \rightarrow -\boldsymbol{\rho}'$ is made, one obtains

$$\begin{aligned} \Phi_1(\boldsymbol{\rho}, L) &= \int_0^L dz' \int d\nu(\boldsymbol{\kappa}, z') \int d\boldsymbol{\rho}'\, h(\boldsymbol{\rho}' - \gamma\,\boldsymbol{\rho}, L, z') \exp(i\boldsymbol{\kappa} \cdot \boldsymbol{\rho}') \\ &= \int_0^L dz' \int d\nu(\boldsymbol{\kappa}, z')\, H(\boldsymbol{\kappa}, L, z') \exp(i\gamma\,\boldsymbol{\kappa} \cdot \boldsymbol{\rho}), \end{aligned} \tag{2.80}$$

where $H(\boldsymbol{\kappa}, L, z)$ is the Fourier transform of $h(\boldsymbol{\rho}, L, z)$, and with the use of eq. 2.73 it is given by

$$H(\boldsymbol{\kappa}, L, z) = \int d\boldsymbol{\rho}'\, h(\boldsymbol{\rho}', L, z) \exp(-i\boldsymbol{\kappa} \cdot \boldsymbol{\rho}') = i k_0 \exp[-i P(\gamma, \kappa, z)]. \tag{2.81}$$

The evaluation in eq. 2.81 relied on the Fourier transform relation

$$\int_{-\infty}^{+\infty} dx\, \exp\left(iax^2 + ibx\right) = \sqrt{-\frac{\pi}{ia}} \exp\left(-ib^2/4a\right). \tag{2.82}$$

The integral was written as the product of two integrals in the x and y directions, and the Fourier transform relation was applied to each integral.

For a wave infinite in extent that propagates from $z = 0$ to $z = L$, the diffraction parameter is equal to

$$P(\gamma, \kappa, z) = \frac{\gamma \kappa^2 (L - z)}{2\, k_0}. \tag{2.83}$$

One sees that a contribution from $z = 0$, which is furthest from the observation point at $z = L$ has a greater diffraction contribution than points closer to the observation point as expected.

For propagation from $z = L$ to $z = 0$

$$P(\gamma, \kappa, z) = \frac{\gamma \kappa^2 z}{2\, k_0}. \tag{2.84}$$

These are three cases to be considered. Let the diameter of the aperture at $z = 0$ be D_1 and that at $z = L$ be D_2. The first case is a converging beam from $z = 0$ to $z = L$ for which $D_1 > D_2$. The second case is a diverging beam from $z = 0$ to $z = L$ for which $D_1 < D_2$. The last case is a converging beam that goes to a focus between $z = 0$ and $z = L$.

For the first case using similar triangles one finds that the focal distance is

$$R_0 = -\frac{LD_1}{D_2 - D_1}, \text{ and} \tag{2.85}$$

$$\gamma = \frac{D_1 + (D_2 - D_1)\, z/L}{D_2}. \tag{2.86}$$

For the second case using similar triangles one finds that

$$R_0 = \frac{LD_1}{D_1 - D_2}, \text{ and} \tag{2.87}$$

$$\gamma = \frac{D_1 - (D_1 - D_2)\, z/L}{D_2}. \tag{2.88}$$

For the last case

$$\alpha = i/R_0, \text{ and} \tag{2.89}$$

$$\gamma = |R_0 - z|/(R_0 - L),\ R_0 < L. \tag{2.90}$$

As R_0 approaches L the beam becomes smaller and diffraction effects must be considered, that is, the imaginary part of γ becomes important when the difference between L and R_0 is less than $4W_0^2/L$.

The values of γ and $P(\gamma, \kappa, z)$ for the various propagation conditions for the infinite wave case are summarized in Table 2.1. For small Fresnel numbers the solutions approach the point source case; for large values they approach the infinite plane-wave case.

For instance, for very large Fresnel numbers and the wave focused $1/N^{th}$ of the distance from $z = 0$ to $z = L$, the curvature is $R_0 = L/N$, and

$$\gamma = \left| \frac{(1 - Nz/L)}{(1 - N)} \right|,\ N > 1. \tag{2.91}$$

The value of γ is equal to $|1/(1 - N)|$ at $z = 0$. The fact that the absolute value of γ is less than unity close to the source affects the value of the scintillation.

One needs to be careful when calculating the scintillation at the focus. *Ishimaru* (1978) p. 383 pointed out that Rytov theory at the focus is only valid for scintillation values that are lower than those for a collimated beam. This occurs because the phase disturbances on the wave affect the size of the focused spot.

Table 2.1. Propagation Functions for the General Case and for Plane and Spherical Waves.
For intermediate values of the Fresnel number γ is complex and beam wave analysis must be used. One needs to choose the root of γ^2 whose real part is positive.

Propagation Direction	Wave Type	γ	Diffraction Parameter $P(\gamma, \kappa, z)$
$0 \to L$	General Case	$(1 + i\alpha z)/(1 + i\alpha L)$	$\gamma\kappa^2(L - z)/2k_o$
$0 \to L$	Plane wave	1	$\kappa^2(L - z)/2k_o$
$0 \to L$	Spherical Focus at R_0	$\lvert R_0 - z\rvert/\lvert R_0 - L\rvert,\ R_0 \neq L$	$\kappa^2\lvert R_0 - z\rvert(L - z)/2k_o\lvert R_0 - L\rvert$
$L \to 0$	General Case	$[1 + i\alpha(L - z)]/(1 + i\alpha L)$	$\gamma\kappa^2 z/2k_o$
$L \to 0$	Plane wave	1	$\kappa^2 z/2k_o$
$L \to 0$	Spherical Focus at $L - R_0$	$\lvert L - R_0 - z\rvert/\lvert L - R_0\rvert$	$\kappa^2 z\lvert L - R_0 - z\rvert/2k_o\lvert L - R_0\rvert$

Away from the focus one does not encounter these difficulties. The condition he gives is

$$0.762\, C_n^2\, k_0^2\, L\, W_0^{5/3} \ll 1. \tag{2.92}$$

In this formulation using γ, as pointed out by Ishimaru, the effective wavenumber is $\gamma\kappa$ rather than κ as can readily be seen in the last part of eq. 2.80. In general, the effective wavenumber is complex. In comparing results obtained with this method to others that do not use this approach, one must make the substitution of κ for $\gamma\kappa$ in this solution to get the same form.

Notice that $H(\boldsymbol{\kappa}, L, z)$ is an even function of kappa. Also, the real part of the exponent on the far right in eq. 2.81 is not greater than zero for long ranges, which causes the integrand in eq. 2.80 to go to zero at infinity for any angular orientation even though $\exp(i\gamma\,\boldsymbol{\kappa}\cdot\boldsymbol{\rho})$ diverges for some angles.

Log-amplitude $\chi(\boldsymbol{\rho}, z)$ and phase $\varphi(\boldsymbol{\rho}, z)$ fluctuations are real quantities defined by the relation

$$\Phi_1(\boldsymbol{\rho}, z) \equiv \chi(\boldsymbol{\rho}, z) + i\phi(\boldsymbol{\rho}, z). \tag{2.93}$$

Therefore,

$$\chi(\boldsymbol{\rho}, z) = \frac{1}{2}\left[\Phi_1(\boldsymbol{\rho}, z) + \Phi_1^*(\boldsymbol{\rho}, z)\right], \text{ and} \tag{2.94}$$

$$\phi(\boldsymbol{\rho}, z) = \frac{1}{2i}\left[\Phi_1(\boldsymbol{\rho}, z) - \Phi_1^*(\boldsymbol{\rho}, z)\right]. \tag{2.95}$$

Now specialize to the point source and the infinite beam case for which γ is real; this leads to simpler expressions. Derivations for complex waves, given in Chap. 10, differ at this point because γ is complex. By substituting eq. 2.80 into eq. 2.94 and eq. 2.95 and by using the evenness with respect to kappa, one finds

$$\chi(\boldsymbol{\rho}, L) = k_0 \int_0^L dz' \int d\nu(\boldsymbol{\kappa}, z') \sin\left[P(\gamma, \kappa, z')\right] \exp(i\gamma\,\boldsymbol{\kappa}\cdot\boldsymbol{\rho}), \text{ and} \tag{2.96}$$

$$\phi(\boldsymbol{\rho}, L) = k_0 \int_0^L dz' \int d\nu(\boldsymbol{\kappa}, z') \cos[P(\gamma, \kappa, z')] \exp(i\gamma \boldsymbol{\kappa} \cdot \boldsymbol{\rho}). \tag{2.97}$$

For the phase difference between two waves one has

$$\phi(\boldsymbol{\rho}, L) = k_0 \int_0^L dz' \int d\nu(\boldsymbol{\kappa}, z') \times \{\cos[P(\gamma_1, \kappa, z')] \exp(i\gamma_1 \boldsymbol{\kappa} \cdot \boldsymbol{\rho}) - \cos[P(\gamma_2, \kappa, z')] \exp(i\gamma_2 \boldsymbol{\kappa} \cdot \boldsymbol{\rho})\}. \tag{2.98}$$

The last three expressions apply to a single point in space. To generalize this, there are three types of problems that are of interest. The first is the one considered above, in which case the above equation applies.

The second type of problem requires one to solve for the amplitude of a particular mode. In that case, the phase on an aperture is multiplied by the mode weighting function, $g(\boldsymbol{\rho})$, and then the resulting phase is integrated over the aperture.

Define a weighting function $G(\gamma\boldsymbol{\kappa})$ that is a constant factor times the Fourier transform of $g(\boldsymbol{\rho})$

$$G(\gamma\boldsymbol{\kappa}) = \int d\boldsymbol{\rho}\, g(\boldsymbol{\rho}) \exp(i\gamma\boldsymbol{\kappa} \cdot \boldsymbol{\rho}), \tag{2.99}$$

where the integration is performed over the aperture for a receiver or over all space for a Gaussian wave.

The phase in this case is

$$\phi R(\boldsymbol{\rho}, L) = k_0 \int_0^L dz' \int d\nu(\boldsymbol{\kappa}, z') \cos[P(\gamma, \kappa, z')] G(\gamma\boldsymbol{\kappa}). \tag{2.100}$$

The expression no longer depends on $\boldsymbol{\rho}$; however, the same notation is retained for the convenience of enabling the same expression to be used for the three cases. To obtain the radial dependence of this mode, the phase expression must be multiplied by $g(\boldsymbol{\rho})$ to obtain

$$\phi R(\boldsymbol{\rho}, L) = k_0 \int_0^L dz' \int d\nu(\boldsymbol{\kappa}, z') \cos[P(\gamma, \kappa, z')] G(\gamma\boldsymbol{\kappa}) g(\boldsymbol{\rho}). \tag{2.101}$$

The three cases can be written as

$$\phi R(\boldsymbol{\rho}, L) = k_0 \int_0^L dz' \int d\nu(\boldsymbol{\kappa}, z') \cos[P(\gamma, \kappa, z')] \hat{G}(\gamma\boldsymbol{\kappa}), \tag{2.102}$$

where the value of the filter function is:

Case 1 $\hat{G}(\gamma\boldsymbol{\kappa}) = \exp(i\gamma\boldsymbol{\kappa} \cdot \boldsymbol{\rho})$—Phase at a point

Case 2 $\hat{G}(\gamma\boldsymbol{\kappa}) = G(\gamma\boldsymbol{\kappa})$—Mode amplitude on an aperture

Case 3 $\hat{G}(\gamma\boldsymbol{\kappa}) = G(\gamma\boldsymbol{\kappa}) g(\boldsymbol{\rho})$—Radial dependence of a mode on an aperture

In the next chapter filter functions are found for various types of problems in which a single transverse filter function in the receiver plane is present. If one has the product of several filter functions in real space that each depend on the radial coordinate in the receiver plane, then care must be exercised in some cases. The presence of anisoplanatism that depends only on z in the presence of another filter function is not such a case, since anisoplanatism introduces a multiplication by a phase-shift term in $\boldsymbol{\kappa}$ space and does not introduce a radial function other than in the exponent. Even if an aperture average of the anisoplanatism is needed, that is not considered a second filter function in the following discussion since all the displacements are phase shifts in the integral in eq. 2.99, which is the Fourier transform of the phase multiplied by a filter function. A finite size source, which introduces a filter function in the transmitter plane also can be considered as an independent filter function.

A problem requiring two filter functions would be to determine the slope of the amplitude on an aperture that has an apodization function. In this case, the two filter functions are the one for tilt and the one for the apodization function. A discussion of how to derive a composite filter function for the product of filter functions is considered in the footnote.

No problems requiring the product of filter functions are addressed in this book. We consider problems in which the only non-anisoplanatic filter function is that of a Zernike mode. The complex problems addressed in this book owe their complexity due to anisoplanatic effects and the addition of inner and outer scale. [2]

Another situation that can arise occurs when the anisoplanatic offset is a function of the receive aperture position. In that case, for an offset $a\boldsymbol{\rho}$, eq. 2.99 gives

$$\int d\boldsymbol{\rho}\; g(\boldsymbol{\rho}) \exp(i\gamma\boldsymbol{\kappa}\cdot\boldsymbol{\rho}) \exp(i\gamma\boldsymbol{\kappa}\cdot a\boldsymbol{\rho}) = G(\gamma(1+a)\boldsymbol{\kappa}). \tag{2.104}$$

The phase- and log-amplitude related quantities resulting from applying the filter function are

$$\begin{bmatrix} \phi R(\boldsymbol{\rho}, L) \\ \chi R(\boldsymbol{\rho}, L) \end{bmatrix} = k_0 \int_0^L dz' \int d\nu\,(\boldsymbol{\kappa}, z')\, \hat{G}\,(\gamma\,\boldsymbol{\kappa}) \begin{bmatrix} \cos\left[P\,(\gamma, \kappa, z')\right] \\ \sin\left[P\,(\gamma, \kappa, z')\right] \end{bmatrix}. \tag{2.105}$$

I shall only give the derivation of the variance of a phase-related quantity explicitly. Since the only difference between the phase- and log-amplitude related

[2] If there are two transverse filters, $g_1(\boldsymbol{\rho})$ and $g_2(\boldsymbol{\rho})$, that are multiplied in real space, then the convolution theorem can be used to find the filter function in κ space. If $G_1(\boldsymbol{\kappa})$ and $G_2(\boldsymbol{\kappa})$ are the Fourier transforms of the individual filter functions, then the composite filter function is

$$G(\boldsymbol{\kappa}) = \int d\boldsymbol{\kappa}_1\; G_1(\boldsymbol{\kappa}_1 - \boldsymbol{\kappa}) G_2(\boldsymbol{\kappa}_1). \tag{2.103}$$

It is obvious how to generalize this result to obtain the filter function for the product of any number of filter functions as

$$G(\boldsymbol{\kappa}) = \int \ldots \int d\boldsymbol{\kappa}_1 \ldots d\boldsymbol{\kappa}_{N-1}\; G_1(\boldsymbol{\kappa}_1 - \boldsymbol{\kappa}) G_2(\boldsymbol{\kappa}_2 - \boldsymbol{\kappa}_1) \ldots G_{N-1}(\boldsymbol{\kappa}_{N-1} - \boldsymbol{\kappa}_{N-2}) G_N(\boldsymbol{\kappa}_{N-1}).$$

expressions is in the trigonometric factor, the expression for the log-amplitude variance will be written at the end by inspection.

Up to now only a single wave has been considered. Generalize this to the case of finding the difference between the phase of two waves that can have different values of γ. The analysis of two beams applies, for example, to adaptive-optics systems. This will allow one to consider the difference between displaced waves, counterpropagating waves, and also the difference between spherical and plane waves. Let the second wave be multiplied by a quantity $A(\boldsymbol{\kappa}, z)$ that can be a function of the axial coordinate and transverse wavenumber. If this multiplier is zero, one is back to the single wave case, and if it is an exponential with imaginary exponent linear in separation distance, this corresponds, by definition, to anisoplanatism. The two-wave case can also express the output of a measurement system being applied to an outgoing beam. Finally, let the aperture weighting factor be different for each wave. A typical geometry for this situation is shown in Fig. 2.5. The result for the three cases is

$$\phi R(\boldsymbol{\rho}, L) = k_0 \int_0^L dz' \int d\nu\,(\boldsymbol{\kappa}, z') \times \left\{ \hat{G}_1\,(\gamma_1 \boldsymbol{\kappa}) \cos\left[P_1\,(\gamma_1, \kappa, z')\right] - A\,(\boldsymbol{\kappa}, z')\,\hat{G}_2\,(\gamma_2 \boldsymbol{\kappa}) \cos\left[P_2\,(\gamma_2, \kappa, z')\right] \right\}. \quad (2.106)$$

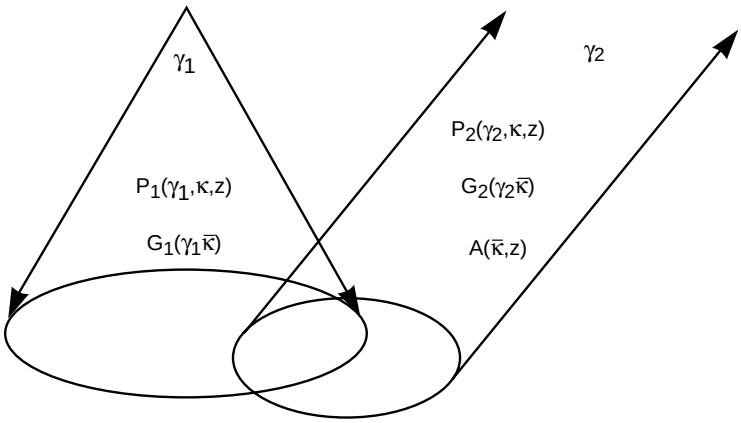

Figure 2.5. Geometry of focused and collimated beams of different diameters propagating in different directions with a separation that depends on the axial coordinate.

The second moment of $\phi R(\boldsymbol{\rho}, L)$ is found by multiplying the phase or log-amplitude by its complex conjugate and calculating the expected value. The only stochastic quantity on the right is the refractive index; therefore, the second moment of the phase-related quantity is

$$\sigma_{\phi R}^2 = \langle \phi R(L)\, \phi R^*(L) \rangle = k_0^2 \int_0^L dz' \int_0^L dz'' \iint \langle d\nu\,(\boldsymbol{\kappa}, z')\; d\nu^*\,(\boldsymbol{\kappa}\,', z'') \rangle$$
$$\times \left\{ \hat{G}_1\,(\gamma_1 \boldsymbol{\kappa})\, \cos\,[P_1\,(\gamma_1, \kappa, z')] - A\,(\boldsymbol{\kappa}, z')\, \hat{G}_2\,(\gamma_2 \boldsymbol{\kappa}) \cos\,[P_2\,(\gamma_2, \kappa, z')] \right\}$$
$$\times \left\{ \hat{G}_1^*\,(\gamma_1 \boldsymbol{\kappa}') \cos\,[P_1^*\,(\gamma_1, \kappa', z'')] - A^*\,(\boldsymbol{\kappa}', z'')\, \hat{G}_2^*\,(\gamma_2 \boldsymbol{\kappa}\,') \cos\,[P_2^*\,(\gamma_2, \kappa', z'')] \right\}. \tag{2.107}$$

The ensemble average can be simplified with the relation given in eq. 2.41 as

$$\langle d\nu\,(\boldsymbol{\kappa}, z')\; d\nu^*\,(\boldsymbol{\kappa}', z'') \rangle = E_n\,(\boldsymbol{\kappa}\,, |z' - z''|)\; C_n^2\,[(z' + z'')\,/2]\; \delta\,(\boldsymbol{\kappa} - \boldsymbol{\kappa}')\; d\boldsymbol{\kappa}\, d\boldsymbol{\kappa}', \tag{2.108}$$

where $C_n^2(z)$ is a normalizing function that is proportional to the strength of turbulence, and $E_n\,(\boldsymbol{\kappa}, |z' - z''|)$ is the two-dimensional spectra of the covariance of the density fluctuations.

The presence of the delta function in eq. 2.108 allows the integration over one transverse spectral coordinate to be performed directly. To eliminate an axial integral, change the axial coordinates into sum and difference coordinates as $z_- = z' - z''$, and $z = (z' + z'')\,/2$. This changes the integration region from that of Fig. 2.6a to the diamond shaped region of Fig. 2.6b. Perform the integration over $\boldsymbol{\kappa}'$ in eq. 2.107 to give

$$\sigma_{\phi R}^2 = k_0^2 \int\int_{Diamond} dz_-\, dz\, C_n^2(z) \int d\boldsymbol{\kappa}\, E_n\,(\boldsymbol{\kappa}, |z_-|)$$
$$\times \left[\hat{G}_1\,(\gamma_1 \boldsymbol{\kappa}) \cos\,(1, 1, +) - A\left(\boldsymbol{\kappa}, z + \frac{z_-}{2}\right) \hat{G}_2\,(\gamma_2 \boldsymbol{\kappa}) \cos\,(2, 2, +) \right]$$
$$\times \left[\hat{G}_1^*\,(\gamma_1 \boldsymbol{\kappa}) \cos\,(1, 1, -) - A^*\left(\boldsymbol{\kappa}, z - \frac{z_-}{2}\right) \hat{G}_2^*\,(\gamma_2 \boldsymbol{\kappa}) \cos\,(2, 2, -) \right], \tag{2.109}$$

where the first argument of the cosine indicates the subscript of P, the second argument the subscript of γ, and the sign refers to the sign of $z_-/2$ in $\cos\,[P_a\,(\gamma_b, \kappa, z \pm z_-/2)]$. *Tatarski* (1971) discusses in detail how to eliminate

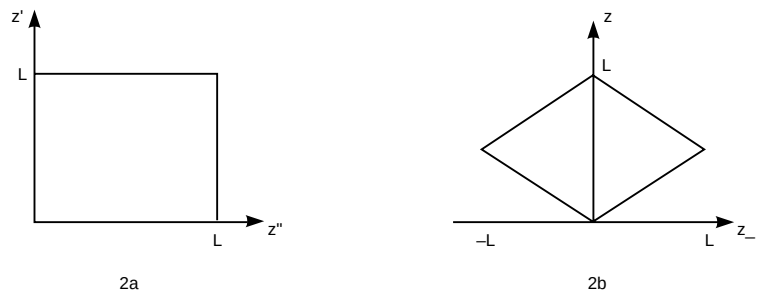

Figure 2.6. The regions of integration: (2a) original, and (2b) transformed.

one axial integration for the single wave case. His arguments extend to the two

wave case. The integration over z_- is similar to that given in eq. 2.31 except for two apparent differences; the integration in eq. 2.33 extends to infinity, while the integration above has finite limits, and there are other functions in the integrand that depend on z_-. These differences can be circumvented. The correlation function of real turbulence only has significant values over a range of tens of meters, a distance that is typically very small compared to the entire integration path.

Tatarski (1971) shows that as long as the inner scale is much larger than the wavelength, then the variation of the trigonometric term with z_- is not significant. To eliminate the dependence on z_- in the other integrand terms, one can expand the functions in Taylor series about the point where the difference coordinate is zero. The relative magnitude of the first two terms of a Taylor series is on the order of z_-/S, where S is the distance over which the function being expanded significantly changes its magnitude. For the functions in the integrand, the distance S is either the length of the propagation path or the Fresnel distance. As long as this distance is much larger than the correlation length, the first order term of the expansion is small compared to the zeroth order term. With that approximation, which is good for most practical problems, one can neglect the difference coordinate when it is added or subtracted from the sum coordinate. This assumption makes the correlation function the only one that depends on z_-. I have checked this assumption for several problems, and the error is typically on the order of one part in a million. For any specific problem one should determine if the above assumptions are violated.

The difficulty with the finite integration limits are now resolved with standard arguments: Since the correlation function is even in z_-, the integral is twice the value obtained with only the right-hand side of the diamond. The only part of the diamond-shaped area that contributes significantly to the integral is a thin strip close to the vertical axis, since the correlation function falls off very rapidly with distance along the horizontal axis. Previously in this chapter, it was shown that for the von Kármán spectrum that $E_n(\boldsymbol{\kappa}, z)$ decays significantly in a distance of a wavelength of the turbulence. For typical outer scale values, the largest correlation is 100 meters or less. Therefore, the diamond-shaped area can be extended horizontally to infinity without significantly affecting the value of the integral. This allows the limit of the z_- integration to be changed to infinity, and the integral can be evaluated with eq. 2.33.

The same derivation can be performed for log-amplitude related quantities. The result is

$$\begin{aligned}
&\begin{bmatrix} \sigma^2_{\phi R} \\ \sigma^2_{\chi R} \end{bmatrix} = 0.2073\, k_0^2 \int_0^L dz\, C_n^2(z) \int d\boldsymbol{\kappa}\, f(\kappa) \\
&\times \left\{ \hat{G}_1(\gamma_1 \boldsymbol{\kappa}) \begin{bmatrix} \cos(1,1) \\ \sin(1,1) \end{bmatrix} - A(\boldsymbol{\kappa}, z)\, \hat{G}_2(\gamma_2 \boldsymbol{\kappa}) \begin{bmatrix} \cos(2,2) \\ \sin(2,2) \end{bmatrix} \right\} \\
&\times \left\{ \hat{G}_1^*(\gamma_1 \boldsymbol{\kappa}) \begin{bmatrix} \cos(1,1) \\ \sin(1,1) \end{bmatrix} - A^*(\boldsymbol{\kappa}, z)\, \hat{G}_2^*(\gamma_2 \boldsymbol{\kappa}) \begin{bmatrix} \cos(2,2) \\ \sin(2,2) \end{bmatrix} \right\}, \quad (2.110)
\end{aligned}$$

where the first argument of the cosine (sine) indicates the subscript of P and the second argument the subscript of γ in $\cos\left[P_a\left(\gamma_b,\kappa,z\right)\right]$ $\left(\sin\left[P_a\left(\gamma_b,\kappa,z\right)\right]\right)$ and $0.2073 = 2\pi\, 0.033$. *The last expression is the central relation of this chapter.*

Notice that γ appears both in the filter function and the sine and cosine terms. In the next chapter it will be shown that in filter functions γ is usually associated with the aperture diameter D in the form γD. For the filter function one can usually include the effect of focused beams with the alternative approach of using the actual beam diameter along the propagation path in the filter function and not including γ. However, one must remember if that approach is used, then one also needs to consider how changing γ affects the trigonometric terms.

This expression is the starting point for solving many turbulence problems. One can consider the variance of the difference of either the phase or log-amplitude of two waves, each of which can be propagating up or down, have different diameters, be displaced from each other with a displacement that changes along the propagation direction, have different amplitudes, and have different values of γ.

The entire quantity multiplying the turbulence spectrum can be looked upon as a filter function of that spectrum. This concept is central to the formulation of solutions to different problems. If one is correcting turbulence, then the filter function must have a magnitude of less than unity for the correction to be effective. Sometimes there are regions of κ where this is not true. In those regions it is best to suppress the correction, if possible.

Note that often one is interested in calculating phase-related quantities in which the turbulence effects are all in the very near field, for which case, one can set the cosine terms equal to unity, thereby simplifying the evaluation of the integral. For large apertures this approximation is generally valid.

The phase and log-amplitude distributions are Gaussian in the region where the Rytov approximation is valid. The distribution of the amplitude is, therefore, log-normal. Since the intensity is the square of the amplitude, the variance of the logarithm of intensity is four times that of log amplitude, χ

$$\sigma^2_{\ln\, I} = 4\sigma^2_\chi. \tag{2.111}$$

Specific cases of the general formula for variances given above that are of interest in different problems are found by setting various terms equal to zero. These specific formulas are given in eq. 2.112–eq. 2.124. For instance, if there is only one beam, then the weighting function $A\left(\boldsymbol{\kappa},z\right)$ is zero, and the general formula reduces to

$$\begin{bmatrix}\sigma^2_{\phi R}\\ \sigma^2_{\chi R}\end{bmatrix} = 0.2073\, k_0^2 \int_0^L dz\, C_n^2(z) \int d\boldsymbol{\kappa}\, f(\kappa) \begin{bmatrix}\cos^2\left[P\left(\gamma,\kappa,z\right)\right]\\ \sin^2\left[P\left(\gamma,\kappa,z\right)\right]\end{bmatrix} \hat{F}\left(\gamma\boldsymbol{\kappa}\right), \tag{2.112}$$

where

$$\hat{F}\left(\gamma\boldsymbol{\kappa}\right) = \hat{G}\left(\gamma\boldsymbol{\kappa}\right)\, \hat{G}^*\left(\gamma\boldsymbol{\kappa}\right). \tag{2.113}$$

Let us look at this for the three cases. For Case 1 $\hat{F}\left(\boldsymbol{\kappa}\right) = 1$. For Case 2 $\hat{F}\left(\boldsymbol{\kappa}\right) = \hat{G}\left(\gamma\boldsymbol{\kappa}\right)\hat{G}^*\left(\gamma\boldsymbol{\kappa}\right)$. For Case 3 $\hat{F}\left(\boldsymbol{\kappa}\right) = \hat{G}\left(\gamma\boldsymbol{\kappa}\right)\hat{G}^*\left(\gamma\boldsymbol{\kappa}\right) g^2(\boldsymbol{\rho})$.

For Case 3 the variance varies over the aperture. The aperture-averaged variance is $\int d\boldsymbol{\rho}\ \hat{F}(\boldsymbol{\kappa}) = \hat{G}(\gamma\boldsymbol{\kappa})\,\hat{G}^*(\gamma\boldsymbol{\kappa}) \int d\boldsymbol{\rho}\ g^2(\boldsymbol{\rho}) = \hat{G}(\gamma\boldsymbol{\kappa})\,\hat{G}^*(\gamma\boldsymbol{\kappa})$, which is the same expression as Case 2.

The expression above for a specific problem looks different than the equivalent expression obtained when the problem is solved by other methods: however, the expressions are equivalent. One can obtain the other form by making the substitution $\gamma\kappa \rightarrow \kappa$. So, for instance, performing that substitution in the last equation, one obtains

$$\begin{bmatrix} \sigma^2_{\phi R} \\ \sigma^2_{\chi R} \end{bmatrix} = 0.2073\, k_0^2 \int_0^L dz\, C_n^2(z) \gamma^{5/3} \times \int d\boldsymbol{\kappa}\ \left[f(\kappa/\gamma)/\gamma^{11/3} \right] \begin{bmatrix} \cos^2\left[P(\gamma, \kappa/\gamma, z)\right] \\ \sin^2\left[P(\gamma, \kappa/\gamma, z)\right] \end{bmatrix} \hat{F}(\boldsymbol{\kappa}). \quad (2.114)$$

Expressions for various specific cases are now given. If there are two beams with weighting on the phase or log-amplitude differing by a real multiplier, i.e., $A(\boldsymbol{\kappa}, z)$ is real, and whose values of γ are equal, then

$$\begin{bmatrix} \sigma^2_{\phi R} \\ \sigma^2_{\chi R} \end{bmatrix} = 0.2073\, k_0^2 \int_0^L dz\, C_n^2(z) \int d\boldsymbol{\kappa}\, f(\kappa) \times \begin{bmatrix} \left\{\cos\left[P_1(\gamma, \kappa, z)\right] - A(\boldsymbol{\kappa}, z) \cos\left[P_2(\gamma, \kappa, z)\right]\right\}^2 \\ \left\{\sin\left[P_1(\gamma, \kappa, z)\right] - A(\boldsymbol{\kappa}, z) \sin\left[P_2(\gamma, \kappa, z)\right]\right\}^2 \end{bmatrix} \hat{F}(\gamma\boldsymbol{\kappa}). \quad (2.115)$$

If there are two beams whose centers coincide along the path with equal beam weighting, whose values of γ are equal, but where different aperture modes are wanted, then

$$\begin{bmatrix} \sigma^2_{\phi R} \\ \sigma^2_{\chi R} \end{bmatrix} = 0.2073\, k_0^2 \int_0^L dz\, C_n^2(z) \int d\boldsymbol{\kappa}\ f(\kappa) \times \begin{bmatrix} \cos^2\left[P(\gamma, \kappa, z)\right] \\ \sin^2\left[P(\gamma, \kappa, z)\right] \end{bmatrix} \left| \hat{G}_1(\gamma\boldsymbol{\kappa}) - \hat{G}_2(\gamma\boldsymbol{\kappa}) \right|^2. \quad (2.116)$$

If there are two beams whose centers coincide along the path with equal weighting of phase and log-amplitude, whose values of γ differ, but where different aperture modes are wanted *and diffraction can be neglected,* then

$$\sigma^2_{\phi R} = 0.2073\, k_0^2 \int_0^L dz\, C_n^2(z) \int d\boldsymbol{\kappa}\, f(\kappa) \left| \hat{G}_1(\gamma_1\boldsymbol{\kappa}) - \hat{G}_2(\gamma_2\boldsymbol{\kappa}) \right|^2. \quad (2.117)$$

This is an important case. When the tilt difference between two waves is required, one can use the tilt filter function given in the next chapter to obtain

$$\sigma^2_{\phi R} = 0.2073\, k_0^2 \int_0^L dz\, C_n^2(z) \int d\boldsymbol{\kappa}\, f(\kappa) \left| \frac{4J_2(\gamma_1\kappa D/2)}{\gamma_1\kappa D/2} - \frac{4J_2(\gamma_2\kappa D/2)}{\gamma_2\kappa D/2} \right|^2. \quad (2.118)$$

When the phase difference between two waves is wanted, eq. 2.117 reduces to

$$\sigma_{\phi R}^2 = 0.2073\, k_0^2 \int_0^L dz\, C_n^2(z) \int d\boldsymbol{\kappa}\, f(\kappa) \left|\exp\left(i\gamma_1\, \boldsymbol{\kappa}\cdot\boldsymbol{\rho}\right) - \exp\left(i\gamma_2\, \boldsymbol{\kappa}\cdot\boldsymbol{\rho}\right)\right|^2 . \tag{2.119}$$

Two situations of this case are considered in the next chapter. In one, a wave that emanates from a focus at L is received and a collimated beam is transmitted. In the second, a beam emanating from a focus at L is received and a beam focused at the same place is transmitted. The situation is elaborated by considering an offset of the beams and a finite size source. For a finite source, the phase from each point in the source must be integrated to obtain the full contribution.

For the case of one beam being collimated for which $\gamma = 1$ and the second being focused at L for which $\gamma = 1 - z/L$, the above equation reduces to

$$\sigma_{\phi R}^2 = 0.4146\, k_0^2 \int_0^L dz\, C_n^2(z) \int d\boldsymbol{\kappa}\, f(\kappa) \left[1 - \cos(\boldsymbol{\kappa}\cdot\boldsymbol{\rho} z/L)\right] . \tag{2.120}$$

Note that the variance varies over the receive aperture through the cosine term. The variance is zero in the center of the aperture. Because of this aperture dependence, the standard assumption of the variance being independent of aperture position in the calculation of the Strehl ratio is not valid. The general consequences of this issue are addressed in Sec. 2.5. For this case it will be found that the structure function is independent of position.

The phase variance can be integrated over the receive aperture of diameter D to obtain the aperture-averaged filter function given in eq. 3.64, which is the limit of allowing the source size and offset to go to zero.

$$F\left(\boldsymbol{\kappa}\right) = 2\left[1 - 2\,\frac{J_1\left(\kappa D z/2L\right)}{\kappa D z/2L}\right] . \tag{2.121}$$

Consider the difference between two beams of equal amplitude that are displaced from each other. A displacement in real space $\mathbf{d}$, which can be a function of z, is equivalent to a phase shift in transform space; therefore

$$A\left(\boldsymbol{\kappa}, z\right) = \exp\left(i\,\boldsymbol{\kappa}\cdot\mathbf{d}\right) , \tag{2.122}$$

where $\mathbf{d}$ is the distance between the beam centers of the two waves, which can be a function of z. The anisoplanatic filter function $A\left(\boldsymbol{\kappa}, z\right)$ is the same for collimated and focused beams with the same displacement of beam centers.

If there are two beams displaced from each other by a distance $\mathbf{d}$ that have the same propagation constant, and of which the same aperture-averaged mode is wanted, one obtains

$$\begin{bmatrix} \sigma^2_{\phi R} \\ \sigma^2_{\chi R} \\ \sigma^2_R \end{bmatrix} = \begin{bmatrix} \mathcal{D}_\phi(\mathbf{d}) \\ \mathcal{D}_\chi(\mathbf{d}) \\ \mathcal{D}(\mathbf{d}) \end{bmatrix} = 0.2073\, k_0^2 \int_0^L dz\, C_n^2(z) \int d\boldsymbol{\kappa}\, f(\kappa) \times \begin{bmatrix} \cos^2[P(\gamma,\kappa,z)] \\ \sin^2[P(\gamma,\kappa,z)] \\ 1 \end{bmatrix} F(\gamma\boldsymbol{\kappa})\; 2[1-\cos(\boldsymbol{\kappa}\cdot\mathbf{d})], \tag{2.123}$$

where σ_R^2 is the sum of the phase and log-amplitude variances, and $\mathcal{D}_\phi(\mathbf{d})$, $\mathcal{D}_\chi(\mathbf{d})$, and $\mathcal{D}(\mathbf{d})$ are the structure functions for phase, log-amplitude, and their sum, respectively.

The same approach used to find anisoplanatic effects can be used to find the covariance functions for phase and log-amplitude related quantities as

$$\begin{aligned} &\begin{bmatrix} B_{\phi R}(\mathbf{d}) \\ B_{\chi R}(\mathbf{d}) \end{bmatrix} = \left\langle \begin{matrix} \phi R(\boldsymbol{\rho}+\mathbf{d})\;\; \phi R(\boldsymbol{\rho}) \\ \chi R(\boldsymbol{\rho}+\mathbf{d})\;\; \chi R(\boldsymbol{\rho}) \end{matrix} \right\rangle = 0.2073\, k_0^2 \int_0^L dz\, C_n^2(z) \int d\boldsymbol{\kappa}\, f(\kappa) \\ &\times [G_1(\gamma_1\boldsymbol{\kappa})\;\alpha - A(\boldsymbol{\kappa},z)\; G_2(\gamma_2\boldsymbol{\kappa})\;\beta] \\ &\times [G_1^*(\gamma_1\boldsymbol{\kappa})\,\alpha - A^*(\boldsymbol{\kappa},z)\; G_2^*(\gamma_2\boldsymbol{\kappa})\,\beta]\cos(\boldsymbol{\kappa}\cdot\mathbf{d}), \end{aligned} \tag{2.124}$$

where

$$\alpha = \begin{bmatrix} \cos[P_1(\gamma_1,\kappa,z)] \\ \sin[P_1(\gamma_1,\kappa,z)] \end{bmatrix}, \text{and}\;\; \beta = \begin{bmatrix} \cos[P_2(\gamma_2,\kappa,z)] \\ \sin[P_2(\gamma_2,\kappa,z)] \end{bmatrix}. \tag{2.125}$$

In a similar fashion, the equivalent of eq. 2.110—eq. 2.123 can be found for the correlation function.

The same method of analysis as used above can be applied to find the aperture-averaged second moment of the product of phase and log-amplitude related quantities. For a single wave the relation is

$$\sigma^2_{\phi\chi R} = 0.1037\, k_0^2 \int_0^L dz\, C_n^2(z) \int d\boldsymbol{\kappa}\, f(\kappa)\, \sin[2\,P(\gamma,\kappa,z)]\, F(\gamma\boldsymbol{\kappa}). \tag{2.126}$$

With a unity filter function this can be evaluated to give

$$\sigma^2_{\phi\chi} = 2.10\, k_0^{7/6} \int_0^L dz\, C_n^2(z)\, (\gamma z)^{5/6}. \tag{2.127}$$

In Chap. 4 the scintillation variance is found to be

$$\sigma^2_{\chi} = 0.5631\, k_0^{7/6} \int_0^L dz\, C_n^2(z)\, (\gamma z)^{5/6}. \tag{2.128}$$

The value of the cross variance between amplitude and phase is 3.73 times the variance of amplitude. For some problems it is stated that the cross correlation

term is negligible compared to the sum of the phase and amplitude variances. That normally is true. For zero outer scale size, the phase variance is infinite because there is infinite energy in the long wavelength turbulence. If a finite outer scale is inserted, then the phase variance is finite. For reasonable values of outer scale, the phase variance is still considerably larger than the cross variance.

2.4 Power Spectral Density

Deleterious effects of turbulence (such as beam jitter) are ameliorated by designing suitable beam-control systems. For example, in order to design a tracking system with a certain level of performance requires one to know the frequency spectrum of jitter. Taylor's frozen-turbulence assumption is used in such calculations. It assumes that atmospheric-turbulence disturbances do not change in typical time scales of interest, but are transported frozen across the aperture by wind or telescope slewing. With this assumption, one can transform the spatial-spectrum variables given in eq. 2.110 into temporal-frequency variables ω and c. In particular, let

$$\omega = \boldsymbol{\kappa} \cdot \mathbf{v}(z). \tag{2.129}$$

Set up the local coordinate system so that the wind velocity across the propagation path, whose magnitude is given by $v(z)$, is in the x direction so that $\omega = \kappa_x v(z)$. Therefore,

$$d\kappa_x = \frac{d\omega}{v(z)}. \tag{2.130}$$

Make the additional change of variables

$$c^2 = \frac{\kappa_y^2 v^2(z)}{\omega^2} + 1, \tag{2.131}$$

from which follows

$$\kappa = \frac{\omega c}{v(z)}, \quad \text{and} \quad d\kappa_y = \frac{\omega}{v(z)} \frac{c\,dc}{\sqrt{c^2 - 1}}. \tag{2.132}$$

The last change of variables was selected to produce a unity Jacobian and an integrand for which a Mellin transform exists. Express the relation for variance given in eq. 2.110 as functions of these two new variables ω and c. Interchange the order of integration so that the omega integration is performed last, and express the integrals over omega and c, whose limits go from $-\infty$ to $+\infty$, as each double the value of an integral from 0 to $+\infty$. After these steps, the general formula for variance can be expressed as an integral over ω. Power spectral density $S(\omega)$ is related to variance σ^2 as

$$\begin{bmatrix} \sigma_{\phi R}^2 \\ \sigma_{\chi R}^2 \end{bmatrix} = \frac{1}{\pi} \int_0^\infty d\omega \begin{bmatrix} S_\phi(\omega) \\ S_\chi(\omega) \end{bmatrix}. \tag{2.133}$$

As an example, consider the power spectral density for a single wave that is given in eq. 2.112 for a wave propagating from $z = 0$ to $z = L$. If the filter function depends on the magnitude of κ and filtering $F_f(\omega)$ due to a servo system is also included, then the residual power spectral density is

$$\begin{bmatrix} S_\phi(\omega) \\ S_\chi(\omega) \end{bmatrix} = 2.606\, k_0^2\, \omega\, F_f(\omega) \int_0^L dz\, \frac{C_n^2(z)}{v^2(z)} \int_0^\infty dc\, \frac{c\, U(c-1)}{\sqrt{c^2-1}}$$
$$\times f\left[\frac{\omega\, c}{v\,(z)}\right] \begin{bmatrix} \cos^2\left[\gamma\omega^2 c^2 (L-z)/2v^2(z)\, k_0\right] \\ \sin^2\left[\gamma\omega^2 c^2 (L-z)/2v^2(z)\, k_0\right] \end{bmatrix} F\left[\frac{\gamma\,\omega\, c}{v\,(z)}\right]. \qquad (2.134)$$

The servo filter function $F_f(\omega)$ is the modulus squared of the frequency filter function of a servo system

$$F_f(\omega) = G_f(\omega) G_f^*(\omega). \qquad (2.135)$$

For instance, in a tracking system $F_f(\omega)$ is found from the frequency response of the tracking-mirror servo system. The Heaviside step function is defined in eq. 1.20. The c integration is easily evaluated with Mellin transform techniques for common problems. Examples are considered in Secs. 4.8, 7.7, and 12.6.

Just as an offset in the spatial domain of $\mathbf{d}$ is represented by a filter function $\exp\left[i\boldsymbol{\kappa}\cdot\mathbf{d}\right]$, a time delay t_d has a filter function $\exp[i\omega t_d]$. The filter function for the coherent addition of two signals each with half the power of one signal is $(1+\cos[wt_d])/2$.

More complicated problems can be analyzed. For instance, consider the situation in Fig. 2.7. The signal tilt is tracked using a receive aperture of diameter D_r with a servo response $G_f(\omega)$. The tilt is applied to an aperture of diameter D_t offset by a distance $\mathbf{d}$ and angle $\boldsymbol{\theta}$. The frequency content and phase variance of the difference of the two tilts is found by using the filter function for tilt given in eq. 3.22 and the filter function for anisoplanatism to give

$$\sigma^2 = 849 \int_0^\infty \frac{d\omega}{\omega} \int_0^L dz\, C_n^2(z) \int_0^\infty \frac{dc}{c} \frac{U(c-1)}{\sqrt{c^2-1}} f\left[\frac{\omega\, c}{v\,(z)}\right] \left| G_f(\omega) \frac{J_2\left(\frac{\omega c D_r}{2v(z)}\right)}{D_r^2} \right.$$
$$\left. - \frac{J_2\left(\frac{\omega c D_t}{2v(z)}\right)}{D_t^2} \exp\left[\frac{i\omega}{v(z)}\left(\theta_x z + d_x + (\theta_y z + d_y)\sqrt{c^2-1}\right)\right] \right|^2 \cos^2\left[\frac{\omega^2 c^2 (L-z)}{2v^2(z) k_0}\right]. \qquad (2.136)$$

2.5 Beam Shape and Strehl Ratio

Second moments are sufficient for many problems. For others the analysis must be carried further. In this section, expressions for beam shape and Strehl ratio

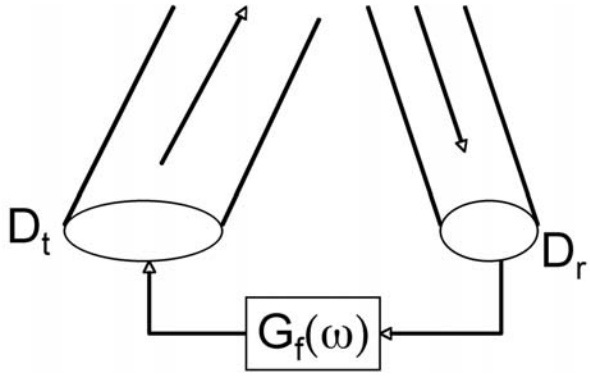

Figure 2.7. Illustration of a system that is tracking an object with a servo system and applies that tilt to a displaced aperture of a different diameter.

are found in terms of phase and amplitude structure functions for an unobscured circular aperture with a uniform and a Gaussian amplitude distribution.

The extended Huygens-Fresnel approximation to beam propagation described by *Fante* (1985) that applies to collimated beams is used; it results in the following formula for a component of electric field at a distance z from a source

$$E(\boldsymbol{\rho}) = \frac{1}{i\lambda z}\int d\boldsymbol{\rho}' E(\boldsymbol{\rho}') \exp\left[\frac{i\pi}{\lambda z}(\boldsymbol{\rho}-\boldsymbol{\rho}')^2 + \chi(\boldsymbol{\rho},\boldsymbol{\rho}',z) + i\phi(\boldsymbol{\rho},\boldsymbol{\rho}',z)\right], \tag{2.137}$$

where the dependence of both the log-amplitude $\chi(\boldsymbol{\rho},\boldsymbol{\rho}',z)$ and phase fluctuations $\phi(\boldsymbol{\rho},\boldsymbol{\rho}',z)$ on the source plane at $\boldsymbol{\rho}'$ and measurement plane at $\boldsymbol{\rho}$ (see Fig. 3.1) are explicitly shown. The axial dependence of electric field is not explicitly shown. Intensity is found by multiplying the field by its complex conjugate.

In the paraxial approximation that applies to waves that are confined to a small distance about the propagation direction—a condition that holds for laser-beam propagation—second-order terms in $\boldsymbol{\rho}'$ are negligible.

The intensity is given by

$$E(\boldsymbol{\rho})E^*(\boldsymbol{\rho}) = \frac{E^2}{(\lambda z)^2}\int d\boldsymbol{\rho}'' \int d\boldsymbol{\rho}' E(\boldsymbol{\rho}'')\, E(\boldsymbol{\rho}') \exp\left\{\frac{i2\pi}{\lambda z}[\boldsymbol{\rho}\cdot(\boldsymbol{\rho}''-\boldsymbol{\rho}')] + \delta\right\},$$

where $\delta = \chi(\boldsymbol{\rho},\boldsymbol{\rho}'',z) + \chi(\boldsymbol{\rho},\boldsymbol{\rho}',z) + i[\phi(\boldsymbol{\rho},\boldsymbol{\rho}'',z) - \phi(\boldsymbol{\rho},\boldsymbol{\rho}',z)]$.

I am interested in the ensemble average of this intensity. Assume that the phase and log-amplitude fluctuations are Gaussian in character. This is not true for the log-amplitude except for low turbulence levels; however, since the phase variance dominates the structure function it is a good approximation. I use a general result for Gaussian statistics where A and B are independent Gaussian variables

$$\begin{aligned}&\langle \exp(\alpha A + \beta B)\rangle \\ &= \exp\left[\frac{\alpha^2}{2}\left\langle (A-\langle A\rangle)^2\right\rangle + \alpha\langle A\rangle + \frac{\beta^2}{2}\left\langle (B-\langle B\rangle)^2\right\rangle + \beta\langle B\rangle\right],\end{aligned} \tag{2.138}$$

where angle brackets denote ensemble average.

Let

$$\boldsymbol{\alpha} = (\boldsymbol{\rho}'' - \boldsymbol{\rho}')/D, \tag{2.139}$$

and

$$\boldsymbol{\alpha}' = (\boldsymbol{\rho}'' + \boldsymbol{\rho}')/2D. \tag{2.140}$$

Introduce the covariance of the log-amplitude as

$$C_\chi(\boldsymbol{\alpha}D, \boldsymbol{\rho}') = \langle [\chi(\boldsymbol{\rho}'') - \langle\chi(\boldsymbol{\rho}'')\rangle]\,[\chi(\boldsymbol{\rho}') - \langle\chi(\boldsymbol{\rho}')\rangle]\rangle. \tag{2.141}$$

The structure function of log amplitude can be expressed as

$$\mathcal{D}_\chi(\boldsymbol{\alpha}D, \boldsymbol{\rho}') = \langle [\chi(\boldsymbol{\alpha}D + \boldsymbol{\rho}') - \chi(\boldsymbol{\rho}')]^2\rangle = 2[C_\chi(0, \boldsymbol{\rho}') - C_\chi(\boldsymbol{\alpha}D, \boldsymbol{\rho}')]. \tag{2.142}$$

Turbulence does not change the average energy in the beam; it just redistributes it. To obtain an important result, choose $\alpha = 0$, $\beta = 2$ and $B = \chi$ in eq. 2.138. Then, the left hand side, which is the average normalized energy, is equal to unity, and the expression in the exponential on the right must equal zero. This leads to the requirement that the average log-amplitude is equal to the log-amplitude correlation

$$\langle\chi(\boldsymbol{\rho}')\rangle = -\langle [\chi(\boldsymbol{\rho}') - \langle\chi(\boldsymbol{\rho}')\rangle]^2\rangle = -C_\chi(0, \boldsymbol{\rho}'). \tag{2.143}$$

If one starts with the basic equations for log-amplitude, this is a result that requires second-order Rytov theory to derive. In first-order Rytov theory the average value of $\chi(\boldsymbol{\rho})$ in eq. 2.96 is zero.

Two other results that will be needed are

$$\begin{aligned}
&\langle [\chi(\boldsymbol{\rho}') + \chi(\boldsymbol{\rho}'')]\,[\phi(\boldsymbol{\rho}') - \phi(\boldsymbol{\rho}'')]\rangle \\
&= \cdots \mathrm{Re}\,[\exp(i\boldsymbol{\kappa}\cdot\boldsymbol{\rho}') + \exp(i\boldsymbol{\kappa}\cdot\boldsymbol{\rho}'')]\,[\exp(i\boldsymbol{\kappa}\cdot\boldsymbol{\rho}') - \exp(i\boldsymbol{\kappa}\cdot\boldsymbol{\rho}'')]^* \\
&= \mathrm{Re}\,\{1 - 1 - \exp[i\boldsymbol{\kappa}\cdot(\boldsymbol{\rho}' - \boldsymbol{\rho}'')] + \exp[i\boldsymbol{\kappa}\cdot(\boldsymbol{\rho}'' - \boldsymbol{\rho}')]\} \\
&= 0,
\end{aligned} \tag{2.144}$$

$$\begin{aligned}
&\langle [\chi(\boldsymbol{\rho}'') - \langle\chi(\boldsymbol{\rho}'')\rangle + \chi(\boldsymbol{\rho}') - \langle\chi(\boldsymbol{\rho}')\rangle]^2\rangle + 2\langle\chi(\boldsymbol{\rho}')\rangle \\
&= \langle [\chi(\boldsymbol{\rho}'') - \langle\chi(\boldsymbol{\rho}'')][(\chi(\boldsymbol{\rho}') - \langle\chi(\boldsymbol{\rho}')\rangle]\rangle + \langle [\chi(\boldsymbol{\rho}') - \langle\chi(\boldsymbol{\rho}')\rangle]^2\rangle - 2C_\chi(0, \boldsymbol{\rho}') \\
&= C_\chi(\boldsymbol{\alpha}D, \boldsymbol{\rho}') + C_\chi(0, \boldsymbol{\rho}') - 2C_\chi(0, \boldsymbol{\rho}') \\
&= \mathcal{D}_\chi(\boldsymbol{\alpha}\mathcal{D}, \boldsymbol{\rho}').
\end{aligned} \tag{2.145}$$

We will also use the relations

$$\mathcal{D}_\phi(\boldsymbol{\alpha}D, \boldsymbol{\rho}') = \langle [\phi(\boldsymbol{\alpha}D + \boldsymbol{\rho}') - \phi(\boldsymbol{\rho}')]^2\rangle. \tag{2.146}$$

and

$$\mathcal{D}(\boldsymbol{\alpha}D, \boldsymbol{\rho}') = \mathcal{D}_\phi(\boldsymbol{\alpha}D, \boldsymbol{\rho}') + \mathcal{D}_\chi(\boldsymbol{\alpha}D, \boldsymbol{\rho}'). \tag{2.147}$$

Use of eq. 2.138 with $\alpha = 1$, $\beta = i$, $A = \chi(\boldsymbol{\rho}, \boldsymbol{\rho}'', z) + \chi(\boldsymbol{\rho}, \boldsymbol{\rho}', z)$, and $B = \phi(\boldsymbol{\rho}, \boldsymbol{\rho}'', z) - \phi(\boldsymbol{\rho}, \boldsymbol{\rho}', z)$ and the above results allows the average intensity to be expressed as

$$\langle E(\boldsymbol{\rho})\, E^{*}(\boldsymbol{\rho})\rangle = \frac{E^2}{(\lambda z)^2}\int d\boldsymbol{\rho}''\int d\boldsymbol{\rho}'\, E(\boldsymbol{\rho}'')\, E(\boldsymbol{\rho}') \times \exp\left[\frac{i2\pi}{\lambda z}(\boldsymbol{\rho}\cdot\boldsymbol{\alpha}D) - \mathcal{D}(\boldsymbol{\alpha}D, \boldsymbol{\rho}')/2\right].$$

The normalized expected value of the intensity is

$$I(\boldsymbol{\rho}) = \left(\frac{4}{\pi D}\right)^2 \int d\boldsymbol{\rho}'' \int d\boldsymbol{\rho}'\, E(\boldsymbol{\rho}'')\, E(\boldsymbol{\rho}') \exp\left[\frac{i2\pi}{\lambda z}(\boldsymbol{\rho}\cdot\boldsymbol{\alpha}D) - \mathcal{D}(\boldsymbol{\alpha}D, \boldsymbol{\rho}')/2\right], \tag{2.148}$$

which leads to an expression for the Strehl ratio of

$$SR = \left(\frac{4}{\pi D}\right)^2 \int d\boldsymbol{\rho}'' \int d\boldsymbol{\rho}'\, E(\boldsymbol{\rho}'')\, E(\boldsymbol{\rho}') \exp\left[-\mathcal{D}(\boldsymbol{\alpha}D, \boldsymbol{\rho}')/2\right]. \tag{2.149}$$

If the source distribution in the aperture is uniform, then, $E(\boldsymbol{\rho}) = E\,W(\boldsymbol{\rho})$, where

$$W(\boldsymbol{\rho}) = U(D/2 - |\boldsymbol{\rho}|). \tag{2.150}$$

If the structure function is a function of $\boldsymbol{\rho}'$, then the integral over the four aperture coordinates must be performed. If the amplitude is constant over the aperture, the coordinate transformations $\boldsymbol{\rho}' = \boldsymbol{\rho}'$ and $\boldsymbol{\alpha} = (\boldsymbol{\rho}'' - \boldsymbol{\rho}')/D$ result in

$$I(\boldsymbol{\rho}) = \left(\frac{4}{\pi D}\right)^2 \int_0^{2\pi} d\theta_\alpha \int_0^1 \alpha d\alpha \int_0^{2\pi} d\theta_\rho \int_0^{D/2} \rho' d\rho' \times W(\boldsymbol{\rho}' + \boldsymbol{\alpha}D)\, W(\boldsymbol{\rho}') \exp\left[\frac{i2\pi}{\lambda z}[\boldsymbol{\rho}\cdot\boldsymbol{\alpha}D] - \mathcal{D}(\boldsymbol{\alpha}D, \boldsymbol{\rho}')/2\right]. \tag{2.151}$$

2.5.1 Structure function dependent on aperture position

In this section some relations are developed for use when the structure function depends on position. This will be used in the calculation of the Strehl ratio for a tracked beam.

The function $W(\boldsymbol{\rho}')$ is equal to unity within a circle of diameter $D/2$ centered on the origin. The only time the integrand has a non-zero value is when the argument of $W(\boldsymbol{\rho}' - \boldsymbol{\alpha}D)$ is less than $D/2$. Therefore, the product of the two functions can be replaced by a unit step function to give

$$I(\boldsymbol{\rho}) = \left(\frac{4}{\pi D}\right)^2 \int_0^{2\pi} d\theta_\alpha \int_0^1 \alpha d\alpha \int_0^{2\pi} d\theta_\rho \int_0^{D/2} \rho' d\rho' \times U(D/2 - |\boldsymbol{\rho}' + \boldsymbol{\alpha}D|) \exp\left\{\frac{i2\pi}{\lambda z}[\boldsymbol{\rho}\cdot\boldsymbol{\alpha}D] - \mathcal{D}(\boldsymbol{\alpha}D, \boldsymbol{\rho}')/2\right\}. \tag{2.152}$$

The Strehl ratio in this case is

$$SR = \left(\frac{4}{\pi D}\right)^2 \int_0^{2\pi} d\theta_\alpha \int_0^1 \alpha d\alpha \int_0^{2\pi} d\theta_\rho \int_0^{D/2} \rho' d\rho' \times U(D/2 - |\boldsymbol{\rho}' + \boldsymbol{\alpha}D|) \exp\left\{-\mathcal{D}(\boldsymbol{\alpha}D, \boldsymbol{\rho}')/2\right\}. \tag{2.153}$$

In performing the numerical integration, we have found that the convergence properties of eq. 2.149 are better than eq. 2.153.

The often used assumption that the structure function is a function only of the difference of positions is not true for some cases of interest, the most common being when the tilt is subtracted from the phase. The phase variance will be higher in the aperture center than at the edge. These problems are more difficult to solve because the integral over $\boldsymbol{\alpha}'$ cannot be performed analytically; therefore, there is an additional two-dimensional integral to be performed numerically.

To show that the resulting field can be significantly affected by a phase variance that varies with position, I will use a pathological case. On an aperture let the phase variance be zero out to the diameter D_o and very large from D_o to D. The average phase variance is very large and one would get a very small intensity if only the average phase variance were used in the expression. For the actual distribution there is no contribution to the integral if either $\boldsymbol{\rho}'$ or $\boldsymbol{\rho}''$ is in the annulus where the phase variance is very large. The intensity on axis is equal to $(D_o/D)^2$ of the intensity with no phase variance over the aperture. This answer is significantly different from that assuming an average phase variance.

The structure function contains the phase difference at two points. Because of this, any long range phase correlations will cancel. Therefore, even though the phase variance with infinite outer scale is infinite, the structure function is finite. The phase subtraction is not the same as piston removal. Very often in systems that use a return from some beacon to drive an adaptive-optics system, there is a tracker that removes tilt, and the Strehl ratio with tilt removed is what is sought. The expression for the structure function above can be modified by subtracting the tilt term in eq. 3.27 to give

$$\mathcal{D}\left(\boldsymbol{\alpha}D,\boldsymbol{\rho}'\right)=0.2073\,k_0^2\int_0^L dz\,C_n^2(z)\int d\boldsymbol{\kappa}\,f(\kappa)F(\boldsymbol{\kappa})$$
$$\times\left[2\left[1-\cos\left(\gamma\boldsymbol{\kappa}\cdot\boldsymbol{\alpha}D\right)\right]-\frac{4J_2(\gamma\kappa D/2)}{\gamma\kappa D/2}(2\rho'/D)\cos(\theta'-\varphi)\sin\left(\gamma\boldsymbol{\kappa}\cdot\boldsymbol{\alpha}D\right)\right], \tag{2.154}$$

where θ' is the angle in $\boldsymbol{\rho}'$ space. Calculation of the Strehl ratio with a position-dependent structure function is illustrated in Sec. 7.5.

One can also consider the effect of using a servo system that does not remove all the tilt. Make the coordinate transformations in $\boldsymbol{\kappa}$ space used in Sec. 2.4 and introduce the servo response in the manner given there. The resulting formula is the structure function with the effects of the tracking servo system with response $F_f(\omega)$ included.

$$\mathcal{D}\left(\boldsymbol{\alpha} D, \boldsymbol{\rho}'\right) = 0.2073\, k_0^2 \int_0^L dz\, C_n^2(z) \left\{ \int d\boldsymbol{\kappa}\, f(\kappa) F(\boldsymbol{\kappa}) 2\left[1 - \cos\left(\gamma \boldsymbol{\kappa} \cdot \boldsymbol{\alpha} D\right)\right] - \frac{1}{\pi v^2(z)} \int_0^\infty d\omega F_f(\omega) \int_0^\infty dc\, \frac{cU(c-1)}{\sqrt{c^2-1}} \frac{4J_2(\gamma\omega c D/2v(z))}{\gamma\omega c D/2v(z)} \times (2\rho'/D)\cos(\theta' - \varphi) \sin\left(\gamma \boldsymbol{\kappa} \cdot \boldsymbol{\alpha} D\right) F(\boldsymbol{\kappa}) \right\}, \tag{2.155}$$

where in the last line of the formula $\boldsymbol{\kappa}$ has to be replaced by

$$\boldsymbol{\kappa} = \mathbf{i} \frac{\omega}{v(z)} + \mathbf{j} \frac{\omega}{v(z)} \sqrt{c^2 - 1}. \tag{2.156}$$

2.5.2 Structure function independent of aperture position

Let us now address the simpler case in which the variance is independent of position, the structure function can be represented by a relation that only depends on the difference in position of two points, and can be written as

$$\begin{bmatrix} \mathcal{D}_\phi\left(\boldsymbol{\alpha} D, \boldsymbol{\rho}'\right) \\ \mathcal{D}_\chi\left(\boldsymbol{\alpha} D, \boldsymbol{\rho}'\right) \end{bmatrix} = \begin{bmatrix} \mathcal{D}_\phi\left(\boldsymbol{\alpha} D\right) \\ \mathcal{D}_\chi\left(\boldsymbol{\alpha} D\right) \end{bmatrix} = 2 \begin{bmatrix} \langle \phi^2(0) \rangle - \langle \phi\left(\boldsymbol{\alpha} D\right)\, \phi(0) \rangle \\ \langle \chi^2(0) \rangle - \langle \chi\left(\boldsymbol{\alpha} D\right)\, \chi(0) \rangle \end{bmatrix}, \tag{2.157}$$

where this structure function is defined in eq. 2.123 as

$$\mathcal{D}\left(\mathbf{d}\right) = 0.2073\, k_0^2 \int_0^L dz\, C_n^2(z) \int d\boldsymbol{\kappa}\, f(\kappa) F\left(\gamma \boldsymbol{\kappa}\right)\, 2\left[1 - \cos\left(\boldsymbol{\kappa} \cdot \mathbf{d}\right)\right]. \tag{2.158}$$

In this next section the Strehl ratio for two common beam shapes will be calculated: a top-hat distribution that has a constant amplitude across an aperture of diameter D and a Gaussian distribution whose field has fallen by $1/e$ from the peak at the radius W_0. I will prove an important relation that can be used more generally: the Strehl ratio for the two cases is the same for large diameters if $D = 2\sqrt{2} W_0$.

Strehl ratio for a top-hat beam

For the simpler case of a uniform variance and uniform intensity over a circular aperture, the integral over the sum coordinate, $\boldsymbol{\alpha}'$, can be performed analytically in the following manner. Express the original coordinates in terms of new ones as $\boldsymbol{\rho}'' = \boldsymbol{\alpha}' D + \boldsymbol{\alpha} D/2$, and $\boldsymbol{\rho}' = \boldsymbol{\alpha}' D - \boldsymbol{\alpha} D/2$. The expected value of the intensity divided by the intensity with no turbulence can be written as

$$I\left(\boldsymbol{\rho}\right) = \int d\boldsymbol{\alpha}\, \exp\left[\frac{i2\pi}{\lambda z}\left(\boldsymbol{\rho} \cdot \boldsymbol{\alpha} D\right) - \mathcal{D}\left(\boldsymbol{\alpha} D\right)/2\right] \times \int d\boldsymbol{\alpha}'\, W\left(\boldsymbol{\alpha}' D + \boldsymbol{\alpha} D/2\right)\, W\left(\boldsymbol{\alpha}' D - \boldsymbol{\alpha} D/2\right). \tag{2.159}$$

The function $W(\mathbf{x})$ is unity anywhere in a circle of diameter D centered on $\mathbf{x}$. Integration over the two overlapping circles $W\left(\boldsymbol{\alpha}' D + \boldsymbol{\alpha} D/2\right) W\left(\boldsymbol{\alpha}' D - \boldsymbol{\alpha} D/2\right)$ can easily be performed as shown by *Fried* (1967). The result is

$$\int d\boldsymbol{\alpha}' W\left(\boldsymbol{\alpha}' D + \boldsymbol{\alpha} D/2\right) W\left(\boldsymbol{\alpha}' D - \boldsymbol{\alpha} D/2\right) = K(\alpha) = \frac{16}{\pi}\left[\cos^{-1}(\alpha) - \alpha\left(1-\alpha^2\right)^{1/2}\right] U(1-\alpha), \quad (2.160)$$

where $U(x)$ is the Heaviside unit step function defined in eq. 1.20. With this result the normalized intensity is given by

$$I(\boldsymbol{\rho}) = \frac{1}{2\pi}\int d\boldsymbol{\alpha}\, K(\alpha) \exp\left[i k_0 D\, \boldsymbol{\rho}\cdot\boldsymbol{\alpha}/z - \mathcal{D}(\boldsymbol{\alpha} D)/2\right]. \quad (2.161)$$

If the structure function is isotropic, the integration in the aperture over angle can be performed to give

$$I(\rho) = \int_0^1 d\alpha\, \alpha\, K(\alpha)\, J_0\left(\frac{k_0\, \rho D \alpha}{z}\right) \exp\left[-\frac{\mathcal{D}(\alpha D)}{2}\right]. \quad (2.162)$$

The Strehl ratio, the most common description of the performance of an optical system, is given by the value of normalized intensity evaluated at $\rho = 0$.

$$SR = \frac{1}{2\pi}\int d\boldsymbol{\alpha}\, K(\alpha) \exp\left[-\frac{\mathcal{D}(\alpha D)}{2}\right]. \quad (2.163)$$

When the structure function is isotropic, the integration over angle in the aperture can be performed to yield

$$SR = \int_0^1 d\alpha\, \alpha\, K(\alpha)\, \exp\left[-\frac{\mathcal{D}(\alpha D)}{2}\right]. \quad (2.164)$$

Mellin transform techniques are of limited usefulness in evaluating this integral. The integral can be put in the form

$$SR = \frac{1}{2\pi i}\frac{8}{\sqrt{\pi}}\int ds\, \frac{x^{-s}}{s+2}\Gamma\begin{bmatrix} s/2+\frac{3}{2} \\ s/2+3 \end{bmatrix} \mathcal{M}\left[\exp\left(-\frac{\mathcal{D}(\alpha D)}{2}\right)\right]. \quad (2.165)$$

The only structure function for which the Mellin transform can be evaluated analytically is when the structure function is a power of the argument. That is the case for uncorrected turbulence and for the effect of tilt on the Strehl ratio. Those problem are solved analytically in Chap. 8. For other problems the Strehl ratio must be evaluated numerically as illustrated in Sec. 8.5.

Eq. 2.164 can be written as

$$SR = \exp\left(-\sigma^2\right) \int_0^1 d\alpha\, \alpha\, K(\alpha)\, \exp\left[\langle\phi(\alpha D)\, \phi(0)\rangle + \langle\chi(\alpha D)\, \chi(0)\rangle\right], \quad (2.166)$$

where the total variance is

$$\sigma^2 = \left\langle \phi^2(z) \right\rangle + \left\langle \chi^2(z) \right\rangle . \tag{2.167}$$

If phase and log-amplitude have a short correlation distance, then the exponential term in the integrand can be replaced by unity to give

$$SR = \exp\left(-\sigma^2\right). \tag{2.168}$$

If amplitude fluctuations are small, as they are for many situations, this becomes the extended Maréchal approximation

$$SR \approx \exp\left(-\sigma_\phi^2\right), \tag{2.169}$$

where σ_ϕ^2 is the phase variance. The validity of this approximation is extended for anisoplanatic effects in Sec. 8.3.

If phase variance is small compared to unity and is not strongly correlated at different points, one obtains the Maréchal approximation

$$SR \approx 1 - \sigma_\phi^2. \tag{2.170}$$

For some problems the correlation distance is not small, and the above approximation is accurate only for variances that are less than 0.1. For instance, for uncorrected turbulence there is considerable energy at long wavelengths, which causes a long length correlation. For anisoplanatism problems the difference between the two waves will greatly reduce the long wavelength turbulence effect; therefore, the Maréchal approximation should be valid for smaller Strehl ratios for those types of problems.

Strehl ratio for a gaussian beam

For a Gaussian beam, the field is given by

$$E\left(\boldsymbol{\rho}, z\right) = \frac{A}{1 + i\alpha\, z} \exp\left[i k_0 z - \frac{k_0 \alpha\, \rho^2}{2(1 + i\alpha\, z)}\right], \tag{2.171}$$

where

$$\alpha = \alpha_r + i\, \alpha_i = \lambda/\pi W_o^2 + i/R_o. \tag{2.172}$$

The parameter R_o is the radius of beam curvature at the source. It is equal to infinity for a collimated beam. For convenience let $e = k_0\, \alpha/(2(1 + i\alpha\, z))$.

The equivalent of eq. 2.149 for a Gaussian beam is

$$SR = C \int d\boldsymbol{\rho}'' \int d\boldsymbol{\rho}'\, E\left(\boldsymbol{\rho}'', z\right) E\left(\boldsymbol{\rho}', z\right) \exp\left\{-\mathcal{D}\left[(\boldsymbol{\rho}'' - \boldsymbol{\rho}'), \boldsymbol{\rho}'\right]/2\right\}, \tag{2.173}$$

where C is a constant that will be chosen to give a SR of unity when there is no turbulence. Substitute in the Gaussian field and use eq. 2.139 and eq. 2.140 with $\alpha \to \alpha'$ and $\alpha' \to \alpha''$ to avoid confusion with the α in e to obtain

$$SR = C' \int d\boldsymbol{\alpha}' \int d\boldsymbol{\alpha}'' \exp\left[-\mathcal{D}\left(\boldsymbol{\alpha}', \boldsymbol{\rho}'\right)/2\right] \exp\left[-2e\left(\alpha''^2 + \alpha'^2/4\right)\right]. \quad (2.174)$$

If the structure function only depends on the magnitude of α', then the two angular integrations and the integration over α'' can be performed to obtain

$$SR = C'' \int_0^\infty \alpha' d\alpha' \exp\left[-\mathcal{D}\left(\boldsymbol{\alpha}', \boldsymbol{\rho}'\right)/2\right] \exp\left(-e\alpha'^2/2\right). \quad (2.175)$$

For no turbulence, where the structure function is zero, the last integration can be performed. Setting the result equal to unity, one obtains $C'' = e$; therefore; the Strehl ratio is

$$SR = e \int \alpha' d\alpha' \exp\left[-\mathcal{D}\left(\boldsymbol{\alpha}', \boldsymbol{\rho}'\right)/2\right] \exp\left(-e\,\alpha'^2/2\right). \quad (2.176)$$

For normal turbulence in which the structure function is

$$\mathcal{D}\left(\boldsymbol{\alpha}'\right) = 6.88\left(\alpha'/r_o\right)^{5/3}, \quad (2.177)$$

the Strehl ratio is

$$SR = e \int \alpha' d\alpha' \exp\left[-3.44\left(\alpha'/r_o\right)^{5/3}\right] \exp\left(-e\,\alpha'^2/2\right). \quad (2.178)$$

For plane waves the coherence diameter r_0 is equal to

$$r_0 = \left(0.423\, k_0^2\, \mu_0\right)^{-3/5}. \quad (2.179)$$

Make the substitutions $x = e\alpha'^2/2$ and $y = er_o^2/2 * 3.44^{6/5}$ to obtain

$$SR = \int_0^\infty \frac{dx}{x}\, x \exp\left[-\left(x/y\right)^{5/6}\right] \exp\left(-x\right). \quad (2.180)$$

With the same methods that are used to derive the Strehl ratio for the top-hat in the Chap. 7 express the Strehl ratio as

$$SR = \frac{6}{5}\frac{1}{2\pi\, i} \int_C ds\ \Gamma[s+1,\ -6s/5]\, y^{-s}. \quad (2.181)$$

The solution can be written by inspection as a Fox H-function using eq. 1.39 to give

$$SR = \frac{6}{5} H_{0,0}^{1,1}\left[y \middle| \begin{matrix}(0,1)\\ \left(0, \frac{6}{5}\right)\end{matrix}\right]. \quad (2.182)$$

The integral will also be evaluated to give a power series since there are no commercial programs to plot the H-function. Since $\Delta = -1/5$, the integral can be closed in the right-half plane. Encircled poles are located at $s = 5n/6$, for $n = 0, 1, 2, \ldots$. Residues at the enclosed poles give the following convergent series

$$SR = \sum_{n=0}^{\infty} \frac{(-1)^n}{n!}\, \Gamma[1 + 5n/6] \left(\frac{e r_o^2}{3.44^{6/5} 2} \right)^{-5n/6}. \tag{2.183}$$

For small values of the coherence diameter this series converges slowly, and an asymptotic series is more convenient. For this case one can show that the steepest-descent contribution has exponential decay; therefore, the asymptotic solution is equal to the sum of pole residues on the left side of the integration path. For small coherence diameters only the first pole at $s = -1$ contributes significantly. The first term of the asymptotic series is

$$SR \sim 6\Gamma[6/5] y/5. \tag{2.184}$$

It is this relation that will be the basis for the definition of the equivalent diameter of a beam wave. If one is in the near field, then

$$e = \frac{k_0 \alpha}{2(1 + i\,\alpha\, z)} \approx \frac{k_0 \alpha}{2}. \tag{2.185}$$

For this case

$$SR \sim \left(\frac{r_o}{2\sqrt{2}\, W_0} \right)^2, \tag{2.186}$$

where W_0 is the $1/e^2$ beam radius. Therefore, the diameter for a beam wave that corresponds to the diameter for uniform illumination is

$$D_e = 2\sqrt{2}\, W_0. \tag{2.187}$$

This relationship is only true in the asymptotic limit of small coherence diameters. In Fig. 2.8 the difference between the Strehl ratio for a Gaussian and a top-hat beam normalized to the Strehl ratio of a top-hat beam is plotted. One sees that the maximum error in determining the Strehl ratio of a Gaussian beam from the relation for a top-hat beam is that the calculated value is as much as 11% too low.

It will be shown when the Zernike modes of a Gaussian beam are found that this relation applies more generally than just for the Strehl ratio.

At a radius $\sqrt{2}W_0$ on the Gaussian wave the field is $\exp(-2) = 0.1353$ of its value in the center, giving an intensity of $\exp(-4) = 0.01832$ of the peak value.

The convergent series can be rewritten in terms of this equivalent diameter as

$$SR = \sum_{n=0}^{\infty} \frac{(-1)^n}{n!}\, \Gamma[1 + 5n/6]\, (1.10)^{5n/6} \left(\frac{D_e}{r_o} \right)^{-5n/3}. \tag{2.188}$$

The first few terms of this series are

$$SR = 1 - 1.018 \left(\frac{D_e}{r_o} \right)^{5/3} + 0.8818 \left(\frac{D_e}{r_o} \right)^{10/3} - 0.7029 \left(\frac{D_e}{r_o} \right)^{5} \cdots \tag{2.189}$$

To obtain more terms of the asymptotic series, the integral can be closed in the left-half plane. Encircled poles are located at $s = -1 - n$, for $n = 0, 1, 2, \ldots$.

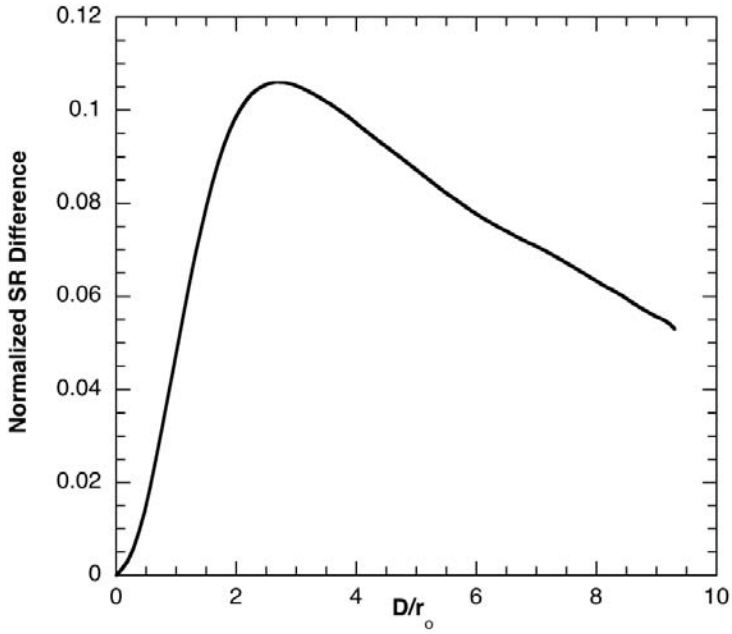

Figure 2.8. Normalized difference of the exact value of the Strehl ratio for a Gaussian beam and that calculated using the top-hat expression with the substitution $D_e = 2\sqrt{2}\,W_0$. The actual Strehl ratio for a Gaussian beam can be as much as 11% higher than that calculated using the top-hat expression.

$$SR \sim \sum_{n=0}^{N} \frac{(-1)^n}{n!} \frac{\Gamma[6/5 + 6n/5]}{\Gamma[6/5]} \left(\frac{r_o}{D_e}\right)^{2+2n}. \tag{2.190}$$

The first few terms of the series are

$$SR \sim \left(\frac{r_o}{D_e}\right)^2 - 1.353 \left(\frac{r_o}{D_e}\right)^4 + 2.024 \left(\frac{r_o}{D_e}\right)^6 - 3.238 \left(\frac{r_o}{D_e}\right)^8. \tag{2.191}$$

REFERENCES

1. Chernov, L. A., *Wave Propagation in a Random Media, Dover Publications*, Inc., New York, (1960).
2. Fante, R., L., *Progress in Optics* (Edited by Wolf, E.) North-Holland, Amsterdam, (1985).
3. Fante, R. L., Electromagnetic Beam Propagation in Turbulent Media, Proc. of IEEE, **63**, (1975) pp. 1669–1692.
4. Frehlich, R., Laser Scintillation Measurements of the Temperature Spectrum in the Atmospheric Surface Layer, Journal of the Atmospheric Sciences, **49**, (1992) pp. 1494–1509.

5. Fried, D. L., "Optical Heterodyne Detection of an Atmospherically Distorted Signal Wave Front", Proc. IEEE, **55**, (1967) pp. 57–67.
6. Goodman, J. W., *Statistical Optics*, John Wiley & Sons, Inc., New York,(1985).
7. Greenwood, D. P., Tarazano, D. O., "A Proposed Form for the Atmospheric Microtemperature Spatial Spectrum in the Input Range", RADC-TR-74-19 (ADA 776294/1GI) (Rome Air Development Center, 1974).
8. Gurvich, A. S., Time, N. S., Turovtseva, V. F., Turchin, V. F., *Reconstruction of the temperature fluctuation spectrum of the atmosphere from optical measurements*, Izvestiya, Atmospheric and Oceanic Physics, (1974).
9. Hill, R. J., Clifford, S. F., "Modified spectrum of atmospheric temperature fluctuations and its application to optical propagation", *J. Opt. Soc. Am.*, **68**, (1978) pp. 892–899.
10. Ishimaru, A., *Wave Propagation and Scattering in Random Media*, Academic Press, New York, 1978.
11. Ishimaru, A., "Fluctuations of a beam wave propagating through a locally homogeneous medium", Radio Sci., **4**, (1969) pp. 293–305.
12. Kaimal, J. C., Izumi, Y., Cote, O. R., Quart. J. *Roy. Meteorol. Soc.*, **98**, (1972) p. 563.
13. Kolmogorov, A. N.," Dissipation of energy in locally isotropic turbulence", *Doklady Akad. Nauk. SSSR*, **32**, (1941) p. 16.
14. Langhaar, H. L., *Dimensional analysis and Theory of Models*, John Wiley & Sons, Inc., Huntington, New York, (1980).
15. Milonni, P. W. Eberly, J. H. *Lasers* John Wiley & Sons, Inc., (1988).
16. Obukhov, A. M., "On the distribution of energy in the spectrum of turbulent flow", *Doklady Akad. Nauk SSSR*, **32**, (1941) p. 19.
17. Schmeltzer, R. A., "Means, Variances, and Covariances For Laser Beam Propagation Through A Random Medium", *Quart. Appl. Math.*, **24**, (1967) pp. 339–354.
18. Schonfeld, J. F., "Linearized theory of thermal-blooming phase-compensation instability with realistic adaptive-optics geometry", *J. Opt. Soc. Am. B*, **9**, (1992) pp. 1803–1812.
19. Strohbehn, J. W., *Laser Beam Propagation in the Atmosphere*, Springer-Verlag, Berlin, (1978).
20. Tatarski, V. I., *Wave Propagation In a Turbulent Medium*, Dover Publications, Inc., New York, (1961).
21. Tatarski, V. I., *The Effects Of The Turbulent Atmosphere On Wave Propagation*, U. S. Department Of Commerce, (1971).
22. Tatarski, V. I., Zavorotnyi, V. U.,"Wave propagation in random media with fluctuating turbulent parameters", *J. Opt. Soc. Am. A*, **2**, (1985) pp. 2069–2076.

Chapter 3

Filter Functions

In the last chapter expressions for phase and log-amplitude variances were derived. These expressions contained an aperture filter function. In this chapter explicit filter functions are derived for many cases of interest. First, those needed to calculate variances of any Zernike mode on an unobscured circular aperture are found. Next, expressions to find piston and tilt on an annular aperture are derived.

Filter functions required to determine the effect of either a finite-size source or receiver on the scintillation are derived. The filter function to be used when both the receiver and source are finite in size is also given.

Often in adaptive-optics systems the phase produced by a focused beam of finite size is used to correct an outgoing collimated beam. The source of the focused beam may not be coaxial with the outgoing beam. Filter functions that apply for each of these cases are derived.

All filter functions are given assuming the wave is collimated and infinite in extent. These filter functions can be applied to focused or finite beams by changing the transverse coordinate to γ times the transverse coordinate, where γ is the propagation parameter defined in eq. 2.74 for a source at $z = 0$, and in eq. 2.77 for a source at $z = L$.

New filter functions can be created from existing complex filter functions by taking the absolute value squared of their difference. This technique is used to find the filter function that applies to the performance of an adaptive-optics system. This technique is used mainly in the next chapter.

Filter functions derived in this chapter are for circular apertures, which are the most commonly encountered. Filter functions for other shapes can be derived with similar methods.

Generally, one can use the filter functions for the variance. For some problems that have several effects present, one is required to start with the expressions for phase and log-amplitude and apply the filter functions before the variance is found. The method and two examples illustrating it are given at the end of the chapter.

To evaluate various integrals, I shall need some Bessel function relations. The recurrence relations for Bessel functions are

$$\frac{d\left[r^p J_p(ar)\right]}{dr} = ar^p\, J_{p-1}(ar), \text{ and} \tag{3.1}$$

$$\frac{d}{dr}\left[\frac{J_p(ar)}{r^p}\right] = -\frac{a}{r^p}\, J_{p+1}(ar). \tag{3.2}$$

Two important special cases are

$$\frac{d\left[r\, J_1(ar)\right]}{dr} = ar\, J_0(ar), \text{ and} \tag{3.3}$$

$$\frac{d}{dr}\left[J_0(ar)\right] = -a\, J_1(ar). \tag{3.4}$$

I also use the following integrals where n is an integer

$$J_n(r) = \frac{i^{-n}}{2\pi}\int_0^{2\pi} d\varphi\, \cos(n\varphi)\exp\left[i\, r\cos(\varphi)\right] = \frac{1}{2\pi}\int_0^{2\pi} d\varphi \cos\left[r\cos(\varphi) + n\varphi\right], \tag{3.5}$$

and

$$\int_0^{2\pi} d\varphi\, \sin(n\varphi)\exp\left[i\, r\cos(\varphi)\right] = 0. \tag{3.6}$$

3.1 Circular Aperture Modes

One often is interested in obtaining weighted averages of the phase or log-amplitude over a receive aperture. The weights typically are polynomials, normally referred to as "modes". Commonly, the receive aperture is an unobscured circle or an annulus. In this section unobscured apertures are considered. Filter functions for an annulus are found in a similar fashion in the next section. Modes are defined for a Gaussian beam in the next chapter.

Consider the Zernike modes that were defined in a very useful way by *Noll* (1976). His expressions are for an aperture of unit diameter, and they are modified here to apply to an aperture of diameter D. The definition of the x and y components of the Zernike polynomials are

$$Z_{m,n}(\rho,\theta)_x = \sqrt{n+1}\, R_n^m\,(2\rho/D)\,\sqrt{2}\cos(m\theta)\,, \text{ and} \tag{3.7}$$

$$Z_{m,n}(\rho,\theta)_y = \sqrt{n+1}\, R_n^m\,(2\rho/D)\,\sqrt{2}\sin(m\theta)\,, \tag{3.8}$$

for $m \neq 0$. For $m = 0$ one uses

$$Z_{0,n}(\rho,\theta) = \sqrt{n+1}\, R_n^0\,(2\rho/D)\,. \tag{3.9}$$

The radial function is given by

$$R_n^m\,(2\rho/D) = \sum_{q=0}^{(n-m)/2} \frac{(-1)^q}{q\,!}\frac{(n-q)!\,(2\rho/D)^{n-2q}}{[(n+m)/2-q]!\,[(n-m)/2-q]!}. \tag{3.10}$$

There are requirements that $m \leq n$, and that $n - m$ be even.

These polynomials are of interest because they correspond to the common optical aberrations. $Z_{0,0}(\rho,\theta)$ is piston, $Z_{1,1}(\rho,\theta)_x$ and $Z_{1,1}(\rho,\theta)_y$ are the two components of tilt, $Z_{0,2}(\rho,\theta)$ is focus, and $Z_{2,2}(\rho,\theta)_x$ and $Z_{2,2}(\rho,\theta)_y$ are the two components of astigmatism, $Z_{1,3}(\rho,\theta)_x$ and $Z_{1,3}(\rho,\theta)_y$ are the two components of coma, and $Z_{0,4}(\rho,\theta)$ is third-order spherical distortion.

Of particular interest are the modes for piston

$$Z_{0,0}(\rho,\theta) = 1, \tag{3.11}$$

and tilt

$$Z_{1,1}(\rho,\theta)_x = \frac{4\rho}{D}\cos(\theta), \tag{3.12}$$

$$Z_{1,1}(\rho,\theta)_y = \frac{4\rho}{D}\sin(\theta). \tag{3.13}$$

These modes are orthonormal. The normalization of the Zernike modes was chosen so that

$$\frac{4}{\pi D^2}\int d\boldsymbol{\rho}\, Z_{n,m}^2(\rho,\theta)\, W(\boldsymbol{\rho}) = 1. \tag{3.14}$$

The aperture function $W(\boldsymbol{\rho})$, defined in eq. 2.150, is equal to unity inside the aperture and zero outside. Expressed in terms of the unit step, it is

$$W(\boldsymbol{\rho}) = U(D/2 - |\boldsymbol{\rho}|). \tag{3.15}$$

The Fourier transforms of Zernike polynomials defined by using eq. 2.99

$$G(\boldsymbol{\kappa}) = \frac{4}{\pi D^2}\int d\boldsymbol{\rho}\, W(\boldsymbol{\rho})\, Z_{m,n}(\rho,\theta)\exp(i\boldsymbol{\kappa}\cdot\boldsymbol{\rho}), \tag{3.16}$$

are equal to

$$\left.\begin{matrix} G_{m,n}(\boldsymbol{\kappa})_x \\ G_{m,n}(\boldsymbol{\kappa})_y \\ G_{0,n}(\boldsymbol{\kappa}) \end{matrix}\right\} = \sqrt{n+1}\,\frac{2J_{n+1}(\kappa D/2)}{\kappa D/2}\left\{\begin{matrix} (-1)^{(n-m)/2} i^n \sqrt{2}\cos(m\varphi), \\ (-1)^{(n-m)/2} i^n \sqrt{2}\sin(m\varphi), \\ (-1)^{n/2}\,(m=0). \end{matrix}\right. \tag{3.17}$$

These are the *complex filter functions* for extracting Zernike modes. *Note that the direction of the Zernike mode is in the direction of* κ. The absolute value squared of these, referred to simply as *filter functions*, are

$$\left.\begin{matrix} F_{m,n}(\boldsymbol{\kappa})_x \\ F_{m,n}(\boldsymbol{\kappa})_y \\ F_{0,n}(\boldsymbol{\kappa}) \end{matrix}\right\} = (n+1)\left[\frac{2J_{n+1}(\kappa D/2)}{\kappa D/2}\right]^2\left\{\begin{matrix} 2\cos^2(m\varphi), \\ 2\sin^2(m\varphi), \\ 1\,(m=0). \end{matrix}\right. \tag{3.18}$$

Piston and tilt filter functions are of particular interest. Two representations of these filter functions are given. For different problems, one or the other representation is appropriate. For piston, the first representation gives the filter function that extracts phase variance due to piston. In the second representation, the filter function extracts variance of the stroke of a flat mirror that

produces this piston by reflection. For tilt, the first filter function extracts phase variance due to tilt, and the second extracts the variance of the corresponding angular displacement in real space. The condition $n = m = 0$ gives *the piston phase-variance filter function*

$$F(\boldsymbol{\kappa}) = \left[\frac{2J_1(\kappa D/2)}{\kappa D/2}\right]^2 . \tag{3.19}$$

To obtain the representation that extracts the mean-square piston stroke, the filter function has to be divided by the wavenumber squared. *The filter function to find piston stroke variance is thus*

$$F(\boldsymbol{\kappa}) = \left(\frac{1}{k_0}\right)^2 \left[\frac{2J_1(\kappa D/2)}{\kappa D/2}\right]^2 . \tag{3.20}$$

This filter function can be used to calculate effects such as aperture averaging of scintillation, which affects the twinkling of stars and planets, because piston is basically a simple aperture average.

The terms $n = m = 1$ gives *the filter function to determine tilt phase variance*

$$\left.\begin{matrix} F_x(\boldsymbol{\kappa}) \\ F_y(\boldsymbol{\kappa}) \\ F(\boldsymbol{\kappa}) \end{matrix}\right\} = \left[\frac{4J_2(\kappa D/2)}{\kappa D/2}\right]^2 \left\{\begin{matrix} \cos^2(\varphi) \ , \\ \sin^2(\varphi) \ , \\ 1. \end{matrix}\right. \tag{3.21}$$

The three terms are the x, y, and total tilt phase variance.

The filter function for variance of tilt angle in real space is a factor of $(4/k_0\,D)^2$ times the phase-variance filter function. *The filter function to determine tilt angle variance is*

$$\left.\begin{matrix} F_x(\boldsymbol{\kappa}) \\ F_y(\boldsymbol{\kappa}) \\ F(\boldsymbol{\kappa}) \end{matrix}\right\} = \left(\frac{16}{k_0 D}\right)^2 \left[\frac{J_2(\kappa D/2)}{\kappa D/2}\right]^2 \left\{\begin{matrix} \cos^2(\varphi) \ , \\ \sin^2(\varphi) \ , \\ 1 \ . \end{matrix}\right. \tag{3.22}$$

The local or final diameter must be inserted in $k_0 D$ depending on the problem.

Often one wants the average phase variance on an aperture with some Zernike modes removed. This will be found by first calculating the phase variance at any point in the aperture, which is needed for some problems such as those concerning the structure function, and then averaging this expression over the aperture.

Consider the case where the phase is multiplied by a filter function $G(\boldsymbol{\kappa})$ that arises from anisoplanatism. From the definition above $G_{n,m}(\gamma\boldsymbol{\kappa})$ is either purely real or imaginary. For this case

$$\begin{aligned}\hat{F}'(\gamma\boldsymbol{\kappa}) &= |G(\boldsymbol{\kappa})|^2 \left|\exp(i\gamma\boldsymbol{\kappa}\cdot\boldsymbol{\rho}) - \sum_{n,m} G_{n,m}(\gamma\boldsymbol{\kappa}) Z_{n,m}(\rho,\theta)\right|^2 \\ &= F(\boldsymbol{\kappa})\left(1 - 2\cos(\gamma\boldsymbol{\kappa}\cdot\boldsymbol{\rho}) \sum_{n,m} \operatorname{Re} G_{n,m}(\gamma\boldsymbol{\kappa}) Z_{n,m}(\rho,\theta)\right. \\ &\quad - 2\sin(\gamma\boldsymbol{\kappa}\cdot\boldsymbol{\rho}) \sum_{n,m} \operatorname{Im} G_{n,m}(\gamma\boldsymbol{\kappa}) Z_{n,m}(\rho,\theta) \\ &\quad \left. + \sum_{n,m}\sum_{o,p} G_{n,m}(\gamma\boldsymbol{\kappa}) G^*_{o,p}(\gamma\boldsymbol{\kappa}) Z_{n,m}(\rho,\theta) Z_{o,p}(\rho,\theta)\right). \end{aligned} \tag{3.23}$$

This is the filter function that multiplies the phase expression to obtain phase with some Zernike modes removed if the phase is not averaged over the aperture. When the integration in $\boldsymbol{\kappa}$ space is performed, the cross product terms with different values of m integrate to zero. However, for the same m the cross product terms do not integrate to zero, which is the indication that the Zernike modes are not statistically independent.

The mode function for piston and tilt are given, since they are the most important. For piston

$$G_{0,0}(\gamma\boldsymbol{\kappa})\, Z_{0,0}(\boldsymbol{\rho}) = \frac{2J_1(\gamma\kappa D/2)}{\gamma\kappa D/2}. \tag{3.24}$$

For the x component of tilt

$$G_{1,1}(\gamma\boldsymbol{\kappa})_x\, Z_{1,1}(\rho,\theta)_x = i\frac{16J_2(\gamma\kappa D/2)}{\gamma\kappa D/2}(\rho/D)\cos(\theta)\cos(\varphi), \tag{3.25}$$

and for the y component of tilt

$$G_{1,1}(\gamma\boldsymbol{\kappa})_y\, Z_{1,1}(\rho,\theta)_y = i\frac{16J_2(\gamma\kappa D/2)}{\gamma\kappa D/2}(\rho/D)\sin(\theta)\sin(\varphi). \tag{3.26}$$

As a reminder, θ is the angle in real space and φ is the angle in $\boldsymbol{\kappa}$ space. For the total tilt

$$G_{1,1}(\gamma\boldsymbol{\kappa})\, Z_{1,1}(\rho,\theta) = i\frac{16J_2(\gamma\kappa D/2)}{\gamma\kappa D/2}\frac{\rho}{D}\cos(\theta-\varphi) = i\frac{16J_2(\gamma\kappa D/2)}{\gamma\kappa D/2}\frac{\boldsymbol{\rho}\cdot\boldsymbol{\kappa}}{D\kappa}. \tag{3.27}$$

The filter function to remove piston when there is no aperture averaging is

$$F(\gamma\boldsymbol{\kappa}) = 1 - 2\cos(\gamma\boldsymbol{\kappa}\cdot\boldsymbol{\rho})\left[\frac{2J_1(\gamma\kappa D/2)}{\gamma\kappa D/2}\right] + \left[\frac{2J_1(\gamma\kappa D/2)}{\gamma\kappa D/2}\right]^2. \tag{3.28}$$

The filter function to remove tilt when there is no aperture averaging is

$$F(\gamma\boldsymbol{\kappa}) = 1 - 32\cos(\theta-\varphi)\cos(\gamma\boldsymbol{\kappa}\cdot\boldsymbol{\rho})\left[\frac{\rho J_2(\gamma\kappa D/2)}{\gamma\kappa D^2/2}\right] + \left[\frac{16\rho J_1(\gamma\kappa D/2)}{\gamma\kappa D^2/2}\cos(\theta-\varphi)\right]^2. \tag{3.29}$$

Let us now find the aperture-averaged phase variance with some Zernike modes removed. In that case one needs to integrate the filter function over the entire aperture of area A to obtain

$$\hat{F}(\gamma\boldsymbol{\kappa}) = \frac{\int d\boldsymbol{\rho}\,\hat{F}'(\gamma\boldsymbol{\kappa})}{A} = F'(\gamma\boldsymbol{\kappa})\left[1 - \sum_{n,m} F_{n,m}(\gamma\boldsymbol{\kappa})\right], \tag{3.30}$$

where eq.2.99 and the orthonomality of the Zernike modes on the aperture were used.

The phase variance that results from this filter function is the total phase variance minus the variance of each of the Zernike modes that are to be removed. For instance, the filter function to find the aperture-averaged variance with piston removed is

$$F(\gamma\boldsymbol{\kappa}) = \left[1 - \sum_{n,m=0}^{0,0} F_{n,m}(\gamma\boldsymbol{\kappa})\right] = 1 - \left[\frac{2J_1(\gamma\kappa D/2)}{\gamma\kappa D/2}\right]^2. \tag{3.31}$$

For piston and tilt removal the filter function is

$$F(\gamma\boldsymbol{\kappa}) = 1 - \left[\frac{2J_1(\gamma\kappa D/2)}{\gamma\kappa D/2}\right]^2 - \left[\frac{4J_2(\gamma\kappa D/2)}{\gamma\kappa D/2}\right]^2. \tag{3.32}$$

One cannot use these last two equations in calculating the structure function with some Zernike modes removed because for the structure function the modes are not integrated over the aperture. One approach is to use an orthogonal decomposition into Karhunen-Loève polynomials which are *statistically* independent. The lowest order Karhunen-Loève polynomials are close in shape to the Zernike polynomials. *Wang* and *Markey* (1978) show that assuming Zernike modes are statistically independent results in errors of as much as 10%.

Rather than doing that, we will find an expression for the structure function with some Zernike modes removed. The structure function is

$$\mathcal{D}_\phi(\boldsymbol{\alpha}D, \boldsymbol{\rho}) = \langle[\phi(\boldsymbol{\rho}) - \phi(\boldsymbol{\alpha}D + \boldsymbol{\rho})]^2\rangle. \tag{3.33}$$

Let $A(\boldsymbol{\rho})$ represent the sum of Zernike modes that need to be removed

$$A(\boldsymbol{\rho}) = \sum_{n,m} G_{n,m}(\gamma\boldsymbol{\kappa})\, Z_{n,m}(\rho,\theta). \tag{3.34}$$

Let the phase without the Zernike modes removed be $f(\boldsymbol{\rho})$

$$\begin{aligned}&\mathcal{D}_\phi(\boldsymbol{\alpha}D,\boldsymbol{\rho}) = \langle[f(\boldsymbol{\rho}) - A(\boldsymbol{\rho}) - f(\boldsymbol{\rho}+\boldsymbol{\alpha}D) + A(\boldsymbol{\rho}+\boldsymbol{\alpha}D)]^2\rangle \\ &= \langle[f(\boldsymbol{\rho}) - f(\boldsymbol{\rho}+\boldsymbol{\alpha}D)]^2\rangle - \langle[A(\boldsymbol{\rho}) - A(\boldsymbol{\rho}+\boldsymbol{\alpha}D)]^2\rangle \\ &+ 2\langle\{f(\boldsymbol{\rho}) - A(\boldsymbol{\rho}) - [f(\boldsymbol{\rho}+\boldsymbol{\alpha}D) - A(\boldsymbol{\rho}+\boldsymbol{\alpha}D)]\}\,[A(\boldsymbol{\rho}+\boldsymbol{\alpha}D) - A(\boldsymbol{\rho})]\rangle.\end{aligned} \tag{3.35}$$

We need to calculate these three terms to obtain the structure function. Often we want to remove tilt, and for this case use eq. 3.27 to obtain

$$[A(\boldsymbol{\rho}) - A(\boldsymbol{\rho}+\boldsymbol{\alpha}D)]^2 = 7.190\left(\frac{\gamma D}{r_0}\right)^{5/3}\alpha^2. \tag{3.36}$$

Let us now give the filter function for another type of tilt. The Zernike component of tilt is also referred to as Z-tilt. Some tilt sensors respond to this quantity, while others respond to the centroid position of the focused aperture distribution, a quantity that is closer to gradient tilt. The definition of G-tilt phase is

$$\text{G-tilt} = \frac{4}{\pi D^2}\int d\boldsymbol{\rho}\,\nabla_t\Phi(\boldsymbol{\rho}), \tag{3.37}$$

where the integration is over the circular aperture and ∇_t is the transverse gradient. G-tilt, in a geometric sense, is equal to the average ray direction, corresponding to the average phase gradient over the aperture. One can calculate this in transform space by multiplying the piston component of phase by $i\kappa/k_0$. *The filter function to find gradient-tilt angle variance is thus*

$$\left.\begin{matrix}F_x(\boldsymbol{\kappa})\\F_y(\boldsymbol{\kappa})\\F(\boldsymbol{\kappa})\end{matrix}\right\} = \left(\frac{4}{k_0 D}\right)^2 J_1^2(\kappa D/2)\begin{cases}\cos^2(\varphi)\ ,\\ \sin^2(\varphi)\ ,\\ 1\ .\end{cases} \tag{3.38}$$

The filter function to calculate phase variance of G-tilt is obtained by using the same arguments as before. *The filter function to find the phase variance due to gradient tilt is thus*

$$\left.\begin{matrix}F_x(\boldsymbol{\kappa})\\F_y(\boldsymbol{\kappa})\\F(\boldsymbol{\kappa})\end{matrix}\right\} = J_1^2(\kappa D/2)\begin{cases}\cos^2(\varphi)\ ,\\ \sin^2(\varphi)\ .\\ 1\ .\end{cases} \tag{3.39}$$

3.2 Piston and Tilt on an Annulus

As with a filled-in circular aperture, the complex filter function for Zernike tilt on an annulus is the Fourier transform of the aperture function for tilt. For tilt in the x-direction, the filter function is

$$G_x(\kappa) = \int d\boldsymbol{\rho}\,g_x(\boldsymbol{\rho})\exp(i\boldsymbol{\kappa}\cdot\boldsymbol{\rho}) = a\int d\boldsymbol{\rho}\,x\,\exp(i\boldsymbol{\kappa}\cdot\boldsymbol{\rho}), \tag{3.40}$$

where a is a normalizing factor, and the integration is over an annulus with inner diameter D_i and outer diameter D. Note that $g_x(\boldsymbol{\rho}) = ax$. The angular and radial integrations can be performed with eq. 3.5 and eq. 3.1 to give

$$G_x(\kappa) = \frac{\pi a \cos(\varphi)}{4}\left[\frac{D^3 J_2(\kappa D/2)}{\kappa D/2} - \frac{D_i^3 J_2(\kappa D_i/2)}{\kappa D_i/2}\right], \tag{3.41}$$

where φ is the angle in κ space. To get the correct constant assume that a pure x-tilt is applied, i.e., let the phase be

$$\phi(\boldsymbol{\rho}) = b\,x.$$

The tilt angle in real space is b/k_0. Therefore,

$$b/k_0 = \int d\boldsymbol{\rho}\, g_x(\boldsymbol{\rho})\varphi(\boldsymbol{\rho}) = a\,b\int d\boldsymbol{\rho}\, x^2 = \frac{\pi a\, b\,(D^4 - D_i^4)}{64}.$$

This gives $a = 64/\pi k_0\,(D^4 - D_i^4)$.

The filter function is the absolute magnitude squared of the complex filter function. *The filter function to find the x-component of Zernike-tilt angle variance on an annulus is given by*

$$F_x(\kappa) = \left[\frac{16/k_0 D}{1-(D_i/D)^4}\right]^2 \left[\frac{J_2(\kappa D/2)}{\kappa D/2} - \left(\frac{D_i}{D}\right)^3 \frac{J_2(\kappa D_i/2)}{\kappa D_i/2}\right]^2 \cos^2(\varphi). \tag{3.42}$$

The complex filter function for the x-component of gradient tilt on an annular aperture can be found in exactly the same way to obtain

$$G_x(\kappa) = \frac{1}{\left[1-(D_i/D)^2\right]}\left[\frac{2J_1(\kappa D/2)}{\kappa D/2} - \frac{2J_1(\kappa D_i/2)}{\kappa D_i/2}\right]\frac{i\kappa}{k_0}\cos(\varphi). \tag{3.43}$$

The filter function of G-tilt angle in the x-direction is

$$F_x(\kappa) = \left\{\frac{4/k_0 D}{1-(D_i/D)^2\}}\right\}^2 \left[J_1(\kappa D/2) - \frac{D_i}{D}J_1(\kappa D_i/2)\right]^2 \cos^2(\varphi). \tag{3.44}$$

The y component of tilt has the cosine replaced by a sine. The total tilt has the cosine replaced by unity.

The filter function for tilt variance is obtained from the filter function for tilt. Given the tilt T on an annulus, the phase variance (now referring to averaging over the aperture) due to this tilt, which can be arbitrarily taken to be in the x direction, is

$$\sigma_T^2 = \frac{1}{A}\int d\boldsymbol{\rho}\,(k_0\mathbf{T}\cdot\boldsymbol{\rho})^2 = \frac{k_0^2 T^2}{A}\int_{D_i/2}^{D/2} d\rho\,\rho^3 \int_0^{2\pi} d\theta\,\cos^2(\theta) = \frac{T^2 k_0^2}{16}\left(D^2 + D_i^2\right).$$

Therefore, *the filter function for total tilt phase variance on an annulus is*

$$F(\kappa) = \left[\frac{16}{1+(D_i/D)^2}\right]\left[\frac{J_2(\kappa D/2)}{\kappa D/2} - \left(\frac{D_i}{D}\right)^3 \frac{J_2(\kappa D_i/2)}{\kappa D_i/2}\right]^2. \tag{3.45}$$

As before, one obtains the $x\,(y)$ component by multiplying this expression by $\cos^2(\varphi)\ \left(\sin^2(\varphi)\right)$.

The piston filter functions can be found in the same manner. The Zernike piston on an annulus is the Fourier transform of the aperture function, i.e.,

$$G_s(\kappa) = a \int d\boldsymbol{\rho}\, \exp\left(i\boldsymbol{\kappa}\cdot\boldsymbol{\rho}\right),$$

where a is a normalizing factor, and the integration is over the annulus. The angular and radial integrations can be performed with eq. 3.5 and eq. 3.3 to give

$$G(\kappa) = \pi a\,\left[D\,J_1(\kappa D/2) - D_i\,J_1(\kappa D_i/2)\right]. \tag{3.46}$$

To get the normalizing constant a assume that a pure piston is applied, i.e., let the phase be $\phi(\boldsymbol{\rho}) = b$. The piston in mirror stroke is b/k_0, so

$$b/k_0 = a\,b \int d\boldsymbol{\rho} = \pi\,a\,b\left(D^2 - D_i^2\right)/4.$$

Therefore, $a = 4/\pi\,k_0\,(D^2 - D_i^2)$. The complex filter function is

$$G(\kappa) = \frac{2}{k_0\left[1-(D_i/D)^2\right]}\left[\frac{J_1(\kappa D/2)}{\kappa D/2} - \left(\frac{D_i}{D}\right)^2 \frac{J_1(\kappa D_i/2)}{\kappa D_i/2}\right]. \tag{3.47}$$

The filter function is the absolute magnitude squared of the complex filter function. *The filter function for piston stroke variance on an annulus is given by*

$$F(\kappa) = \left\{\frac{2}{k_0\left[1-(D_i/D)^2\right]}\right\}^2 \left[\frac{J_1(\kappa D/2)}{\kappa D/2} - \left(\frac{D_i}{D}\right)^2 \frac{J_1(\kappa D_i/2)}{\kappa D_i/2}\right]^2. \tag{3.48}$$

Given the piston P on the aperture, the average phase variance due to piston is

$$\sigma_P^2 = \frac{1}{A}\int d\boldsymbol{\rho}\,(k_0\,P)^2 = k_0^2\,P^2,$$

where A is the aperture area. Therefore, one finds the filter function to obtain the piston phase variance by multiplying the filter function for the piston by k_0^2. *The filter function for piston phase variance on an annulus is given by*

$$F(\kappa) = \left[\frac{2}{1-(D_i/D)^2}\right]^2 \left[\frac{J_1(\kappa D/2)}{\kappa D/2} - \left(\frac{D_i}{D}\right)^2 \frac{J_1(\kappa D_i/2)}{\kappa D_i/2}\right]^2. \tag{3.49}$$

3.3 Finite Apertures and Focal Anisoplanatism

I derive filter functions for two types of problems that are analyzable in a similar fashion. The analysis is a generalization of the two-wave problem considered in Chap. 2. Here the source is allowed to be finite in size.

The first type of filter function is for either a distributed source or a finite-size receive aperture that produces phase and scintillation levels in a receiver that can be very different from those of a point source or point receiver. For instance, the finite angular size of a planet causes it to have much lower scintillation than a star.

The second type of filter function applies to adaptive-optics systems. Often in the operation of an adaptive-optics system, the beacon source or reflector is either a point or a distributed source, and the corrected signal is a collimated beam. The important question that arises in this case is: How much do path differences between a beacon and corrected beam affect phase variance on the corrected beam? Variances due to this effect vary with position within the outgoing aperture. For that reason a structure function that varies solely with the difference between aperture positions does not exist. Nevertheless, one can still calculate average variance over the outgoing aperture to derive a filter function that gives the average phase variance on the aperture.

First, I consider a distributed source and finite receive aperture as shown in Fig. 3.1. This geometry applies to the physically interesting cases of reflection from a corner-cube array or a diffuse plate, or return from a planet. Let us direct our attention to problems in which the turbulence-induced effects on rays going from various source to receiver points is the most important effect, rather than problems in which the source phase is important. This assumption applies to aperture averaging of scintillation or to estimating the average wavefront slope from a distributed source.

For this case, the distance between a ray parallel to the z-axis (direction of propagation) that passes through $\boldsymbol{\rho}$ on the receive aperture and a ray from aperture point $\boldsymbol{\rho}$ to the source point $\boldsymbol{\rho}'$ is

$$\mathbf{d} = \frac{z}{L}\left(\boldsymbol{\rho} - \boldsymbol{\rho}'\right). \tag{3.50}$$

This anisoplanatic shift from one point in the source plane to one point in the receive plane can be inserted into expressions for phase and log-amplitude in eq. 2.96 and eq. 2.97 to obtain

$$\begin{bmatrix} \chi R(L) \\ \phi R(L) \end{bmatrix} = k_0 \int_0^L dz \int d\nu(\boldsymbol{\kappa}, z) \begin{bmatrix} \sin\left[P\left(\gamma, \kappa, z\right)\right] \\ \cos\left[P\left(\gamma, \kappa, z\right)\right] \end{bmatrix} \exp(i\boldsymbol{\kappa} \cdot \boldsymbol{\rho}) \exp\left[i\boldsymbol{\kappa} \cdot \left(\boldsymbol{\rho} - \boldsymbol{\rho}'\right) \frac{z}{L}\right].$$

Let us consider a finite-size source, where intensity $S\left(\boldsymbol{\rho}'\right)$ can vary with position, and a finite-size receiver. To set up the correct expression for the error due to a finite beacon, one must understand the measurement process. A point beacon will radiate to the aperture, and its wavefront tilt will be measured

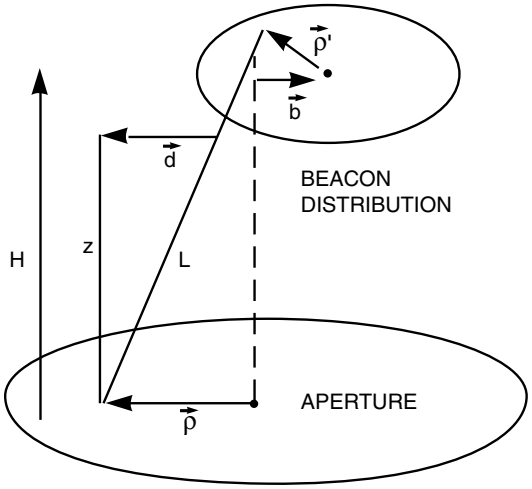

Figure 3.1. Geometry of a distributed source and finite size aperture.

with the wavefront sensor. There will be some average tilt of the beacon that will be removed when the system is aligned. The beacon wavefront will have a turbulence-induced tilt in a subaperture that will be measured and imposed on the outgoing wavefront. Any displacement between the direction of the outgoing wave and the beacon will result in an anisoplanatic error.

Consider another point beacon, incoherent with the first, that propagates toward the receive aperture. It also has a tilted wavefront, which may be different than that of the first point beacon. Since that source is incoherent with the first, because of the way wavefront sensors measure tilt, the tilts add with a weighting depending on the power of the individual point beacons. Therefore, the error from several incoherent beacons is the weighted sum of the beacon intensities multiplied by the individual anisoplanatic errors. This sum can be turned into an integral for a distributed beacon. Similar arguments apply to the intensity.

The resultant expressions one obtains by integrating over the source and aperture and normalizing to the total source intensity are

$$\begin{bmatrix} \chi R(L) \\ \phi R(L) \end{bmatrix} = k_0 \int_0^L dz \int d\nu\,(\boldsymbol{\kappa}, z) \begin{bmatrix} \sin\left[P\,(\gamma, \kappa, z)\right] \\ \cos\left[P\,(\gamma, \kappa, z)\right] \end{bmatrix}$$
$$\times \frac{\int d\boldsymbol{\rho} \int d\boldsymbol{\rho}'\, S\,(\boldsymbol{\rho}') \exp\left[i\boldsymbol{\kappa} \cdot \boldsymbol{\rho}\left(1 - \frac{z}{L}\right)\right] \exp\left(i\boldsymbol{\kappa} \cdot \boldsymbol{\rho}'\, \frac{z}{L}\right)}{A_A \int d\boldsymbol{\rho}'\, S\,(\boldsymbol{\rho}')}, \tag{3.51}$$

where A_A is the aperture area. When the integration over the receive aperture is performed, one obtains by factorization *the filter function for a finite size receiver and a finite size source with nonuniform intensity*

$$F\,(\boldsymbol{\kappa}) = \left\{ 2 \frac{J_1\left[\kappa D\,(1 - z/L)\,/2\right]}{\kappa D\,(1 - z/L)\,/2} \right\}^2 \frac{\left| \int d\boldsymbol{\rho}'\, S\,(\boldsymbol{\rho}') \exp\left(-i\boldsymbol{\kappa} \cdot \boldsymbol{\rho}'\, \frac{z}{L}\right) \right|^2}{\left| \int d\boldsymbol{\rho}'\, S\,(\boldsymbol{\rho}') \right|^2}, \tag{3.52}$$

where D is the aperture diameter. If source intensity is constant, then the integrations in eq. 3.52 can be performed yielding *the filter function for a finite size receiver and uniform circular source as*

$$F(\boldsymbol{\kappa}) = \left\{ 2\frac{J_1\left[\kappa D\left(1 - z/L\right)/2\right]}{\kappa D\left(1 - z/L\right)/2} \right\}^2 \left[2\frac{J_1\left(\kappa D_s\, z/2L\right)}{\kappa D_s\, z/2L} \right]^2, \tag{3.53}$$

where D_s is the source diameter. From this relation special cases can be found. *The filter function for a uniform, circular source located at a distance L, and a point receiver is*

$$F(\boldsymbol{\kappa}) = \left[2\frac{J_1\left(\kappa D_s\, z/2L\right)}{\kappa D_s\, z/2L} \right]^2. \tag{3.54}$$

The filter function for a finite size receive aperture with a point source located at a distance L is

$$F(\boldsymbol{\kappa}) = \left[2\frac{J_1\left(\kappa D\left(1 - z/L\right)/2\right)}{\kappa D\left(1 - z/L\right)/2} \right]^2. \tag{3.55}$$

If the point source is located at infinity, then the filter function for a finite size receiver is

$$F(\boldsymbol{\kappa}) = \left[2\frac{J_1\left(\kappa D/2\right)}{\kappa D/2} \right]^2. \tag{3.56}$$

These filter functions are used in Sec. 7.8.

Similarly, the filter function for a Gaussian intensity distribution with $1/e$ radius of R, $S(\boldsymbol{\rho}) = 1/\left(\pi R^2\right)\exp[-(\rho/R)^2]$, gives a filter function

$$F(\boldsymbol{\kappa}) = \left\{ 2\frac{J_1\left[\kappa D\left(1 - z/L\right)/2\right]}{\kappa D\left(1 - z/L\right)/2} \right\}^2 \left\{ \exp[-(\kappa R z/2L)^2] \right\}^2. \tag{3.57}$$

In an adaptive-optics system the beacon source is often small, and the transmitted beam is collimated. Rays from the small source do not sample exactly the same turbulence as that of the collimated beam; this results in a distortion on the collimated beam after it traverses the atmosphere. This effect is referred to as *focal anisoplanatism*. The phase difference arises from an offset of collimated and focused rays in the aperture. To find the filter function in this case start with eq. 2.119

$$\sigma^2_{\phi R} = 0.2073\, k_0^2 \int_0^L dz\, C_n^2(z) \int d\boldsymbol{\kappa}\, f(\kappa) \left| \exp\left(\gamma_1 \boldsymbol{\kappa}\right) - \exp\left(\gamma_2 \boldsymbol{\kappa}\right) \right|^2. \tag{3.58}$$

For a distributed source the incoming wave must be integrated over the beacon distribution. Consider the path difference between a ray parallel to the propagation direction that passes through the receiver at $\boldsymbol{\rho}$ and a ray that also passes through $\boldsymbol{\rho}$ that originates from a point in the distributed source whose center is offset from the receive aperture center by $\mathbf{b}$. The isoplanatic difference is $\exp\left(i\boldsymbol{\kappa}\cdot\boldsymbol{\rho}\right)\exp\left\{i\boldsymbol{\kappa}\cdot\left[\boldsymbol{\rho}\left(1 - z/L\right) + \left(\boldsymbol{\rho}' + \mathbf{b}\right)z/L\right]\right\}$.

To find the phase at any point in the receive aperture, the phase expression must be integrated over the normalized source distribution. Thus, the anisoplanatic difference phase is

$$\phi R(L) = k_0 \int_0^L dz \int d\nu\,(\boldsymbol{\kappa}, z)\,\cos\left[P\,(\gamma, \kappa, z)\right]$$
$$\times \left[\exp\left(i\boldsymbol{\kappa}\cdot\boldsymbol{\rho}\right) - \frac{\int d\boldsymbol{\rho}'\,S\,(\boldsymbol{\rho}')\exp\left\{i\boldsymbol{\kappa}\cdot\left[\boldsymbol{\rho}\,(1-z/L) + (\boldsymbol{\rho}'+\mathbf{b})\,z/L\right]\right\}}{\int d\boldsymbol{\rho}'\,S\,(\boldsymbol{\rho}')}\right].$$

The filter function is the absolute value squared of the term after the cosine

$$F\,(\boldsymbol{\kappa}) = \left|1 - \frac{\int d\boldsymbol{\rho}' S\,(\boldsymbol{\rho}')\exp\left\{i\boldsymbol{\kappa}\cdot\left[-\boldsymbol{\rho}z/L + (\boldsymbol{\rho}'+\mathbf{b})\,z/L\right]\right\}}{\int d\boldsymbol{\rho}'\,S\,(\boldsymbol{\rho}')}\right|^2. \tag{3.59}$$

If the beacon is a uniform circular source, then the integrations can be carried out early to give

$$F\,(\boldsymbol{\kappa}) = 1 - 2\,\frac{2\,J_1(D_s h)}{D_s\,h}\cos\left[\boldsymbol{\kappa}\cdot z\,(\mathbf{b}-\boldsymbol{\rho})/L\right] + \left[2\frac{J_1\,(D_s\,h)}{D_s\,h}\right]^2, \tag{3.60}$$

where $h = \kappa\,z/2\,L$.

The phase variance is not the same everywhere in the receive aperture. The filter function above can be used to find the phase variance at any point in the aperture. Most of the time we are interested in the aperture-averaged phase variance. To find this filter function, the previous filter function is averaged over the aperture with eq. 3.5 to give

$$F\,(\boldsymbol{\kappa}) = 1 - 2\,\frac{2\,J_1\,(D_s\,h)}{D_s\,h}\frac{2\,J_1\,(D\,h)}{D\,h}\cos\left(\boldsymbol{\kappa}\cdot\frac{z\mathbf{b}}{L}\right) + \left[2\frac{J_1\,(D_s\,h)}{D_s\,h}\right]^2. \tag{3.61}$$

If there are no other filter functions in the problem that depend on the angle in κ-space, then the integral over angle can be performed; this leads to *the filter function for focal anisoplanatism with a uniform circular source offset* $\mathbf{b}$ *from boresight*

$$F\,(\boldsymbol{\kappa}) = 1 - 2\,\frac{2\,J_1(D_s\,h)}{D_s\,h}\frac{2\,J_1(D\,h)}{D\,h}J_0\left(\frac{\kappa b z}{L}\right) + \left[2\frac{J_1(D_s\,h)}{D_s\,h}\right]^2. \tag{3.62}$$

The aperture-averaged filter function for focal anisoplanatism with a uniform circular source on boresight is

$$F\,(\boldsymbol{\kappa}) = 1 - 2\,\frac{2\,J_1(D_s\,h)}{D_s\,h}\frac{2\,J_1(D\,h)}{D\,h} + \left[2\frac{J_1\,(D_s\,h)}{D_s\,h}\right]^2. \tag{3.63}$$

If the source diameter is zero, then one obtains *the aperture-averaged filter function for focal anisoplanatism with circular symmetry for a point source with no offset as*

$$F(\boldsymbol{\kappa}) = 2\left[1 - 2\frac{J_1(D\,h)}{D\,h}\right]. \tag{3.64}$$

To find the piston or tilt component of focal anisoplanatism when the beacon has finite size, one starts with the expression for these components for a single source point in eq. 2.118

$$\begin{aligned}\phi(\boldsymbol{\rho}, L) &= k_0 \int_0^L dz' \int d\nu(\boldsymbol{\kappa}, z') \\ &\times \left[\cos\left[P(\gamma_1, \kappa, z')\right] \exp\left(i\gamma_1 \boldsymbol{\kappa}\cdot\boldsymbol{\rho}\right) - \cos\left[P(\gamma_2, \kappa, z')\right] \exp\left(i\gamma_2 \boldsymbol{\kappa}\cdot\boldsymbol{\rho}\right)\right].\end{aligned} \tag{3.65}$$

and integrates over the source distribution.

Allowing for an offset of the beams and setting $\gamma_1 = 1$ and $\gamma_2 = 1 - z/L$, the isoplanatic term is multiplied by a piston or tilt aperture function and integrated over the source aperture to obtain

$$\begin{aligned}\phi R(L) &= k_0 \int_0^L dz' \int d\nu(\boldsymbol{\kappa}, z) \cos\left[P(\gamma, \kappa, z)\right] \\ &\times \int d\boldsymbol{\rho}' \int d\boldsymbol{\rho}\, g(\boldsymbol{\rho}) \left(\exp\left(i\boldsymbol{\kappa}\cdot\boldsymbol{\rho}\right) - \frac{S(\boldsymbol{\rho}') \exp\left\{i\boldsymbol{\kappa}\cdot\left[\boldsymbol{\rho}\left(1 - \frac{z}{L}\right) + (\boldsymbol{\rho}' + \mathbf{b})\frac{z}{L}\right]\right\}}{\int d\boldsymbol{\rho}'\, S(\boldsymbol{\rho}')}\right).\end{aligned}$$

The aperture integration is evaluated to obtain an expression for a single source point at $\boldsymbol{\rho}'$ as

$$F(\boldsymbol{\kappa}) = 4\left|\frac{\nu\, J_\nu(a)}{a} - \exp\left(i\boldsymbol{\kappa}\cdot\mathbf{b}\frac{z}{L}\right)\frac{\nu\, J_\nu(e)}{e}\frac{\int d\boldsymbol{\rho}'\, S(\boldsymbol{\rho}') \exp\left(i\boldsymbol{\kappa}\cdot\boldsymbol{\rho}'\, z/L\right)}{\int d\boldsymbol{\rho}'\, S(\boldsymbol{\rho}')}\right|^2, \tag{3.66}$$

where $a = \kappa D/2$, $e = \kappa D(1 - z/L)/2$, $\nu = 1$ for piston, and $\nu = 2$ for tilt. If the source distribution is uniform, then integrations over $\boldsymbol{\rho}'$ are readily evaluated to obtain the total piston or tilt. *Thus, the filter function to find the piston or tilt component of focal anisoplanatism with a uniform circular source offset* $\mathbf{b}$ *from boresight is*

$$F(\boldsymbol{\kappa}) = \left|\frac{2\nu\, J_\nu(a)}{a} - \exp\left(i\boldsymbol{\kappa}\cdot\mathbf{b}\frac{z}{L}\right)\frac{2\nu\, J_\nu(e)}{e}\frac{2\, J_1(D_s\, h)}{(D_s\, h)}\right|^2. \tag{3.67}$$

The filter function to find the piston or tilt component of focal anisoplanatism with a uniform circular source on boresight is

$$F(\boldsymbol{\kappa}) = \left[\frac{2\nu\, J_\nu(a)}{a} - \frac{2\nu\, J_\nu(e)}{e}\frac{2\, J_1(D_s\, h)}{(D_s\, h)}\right]^2. \tag{3.68}$$

If the source size goes to zero, the filter function for the Zernike modes reduces to eq. 2.117.

3.4 Adaptive-Optics Systems

If the conjugate of the amplitude and phase of the received wave were applied to the outgoing beam, then the resulting beam would be perfectly corrected. Presently, most adaptive-optics systems only apply the conjugate of the phase.

In a phase-conjugate adaptive-optics system, a beacon beam is propagated downward through the atmosphere, and the phase impressed on the beam by atmospheric turbulence is measured by a phase sensor. The conjugate of the measured phase is applied at the origin to an outgoing beam along a propagation path that is displaced by a distance $\mathbf{d}$ from the beacon path. To calculate system performance, one has to calculate the residual phase or log-amplitude on the wave after correction. One finds the filter function by calculating the behavior of the system for a single phase screen at $z = z'$ and integrating over the turbulence distribution.

Consider a single phase screen at z' of strength $d\nu\left(\boldsymbol{\kappa}, z'\right) dz'$. The phase-related quantity measured at the origin from the downward propagating beacon with the diffraction parameter in eq. 2.83 is

$$d\nu\left(\boldsymbol{\kappa}, z'\right) \cos\left(\kappa^2 z'/2k_0\right) dz'.$$

An adaptive-optics system applies the negative of this phase to a scoring beam. The phase or log-amplitude at $z = L$ is made up of two phase components. The first is due to the measured phase that is impressed at the origin, which is propagated a distance L. The second is caused by the phase screen through which the wave passes. This second component propagates a distance $L - z$, and can have an isoplanatic component. The scintillation on the beam above the turbulence is also caused by two phase components: the first due to the phase screen and the second due to the phase at the origin produced by the adaptive-optics system.

In this case the formula for variance is a modification of the standard formula because the effect of the sinusoid and cosinusoid is included in the filter function. The formula for variance is

$$\begin{bmatrix} \sigma^2_{\phi R} \\ \sigma^2_{\chi R} \\ \sigma^2_R \end{bmatrix} = 0.2073\, k_0^2 \int_0^L dz\, C_n^2(z) \int d\boldsymbol{\kappa}\, f(\kappa) \begin{bmatrix} F'_\phi\left(\gamma\boldsymbol{\kappa}\right) \\ F'_\chi\left(\gamma\boldsymbol{\kappa}\right) \\ F'_t\left(\gamma\boldsymbol{\kappa}\right) \end{bmatrix} F\left(\gamma\boldsymbol{\kappa}\right). \tag{3.69}$$

The complex filter function associated with this process is

$$\begin{bmatrix} G'_\phi\left(\gamma\boldsymbol{\kappa}\right) \\ G'_\chi\left(\gamma\boldsymbol{\kappa}\right) \end{bmatrix} = \begin{bmatrix} \cos\left(a\,L\right)\cos\left(a\,z\right) - \exp(i\,\boldsymbol{\kappa}\cdot\mathbf{d})\cos\left[a\left(L-z\right)\right] \\ \sin\left(a\,L\right)\cos\left(a\,z\right) - \exp(i\,\boldsymbol{\kappa}\cdot\mathbf{d})\sin\left[a\left(L-z\right)\right] \end{bmatrix}, \tag{3.70}$$

where $a = \gamma\kappa^2/2k_0$. The filter function to obtain the phase and log-amplitude variances is the absolute value squared of the complex filter function given by

$$\begin{bmatrix} F'_\phi\left(\gamma\boldsymbol{\kappa}\right) \\ F'_\chi\left(\gamma\boldsymbol{\kappa}\right) \\ F'_t\left(\gamma\boldsymbol{\kappa}\right) \end{bmatrix} = \begin{bmatrix} \left|\cos\left(a\,L\right)\cos\left(a\,z\right) - \exp\left(i\,\boldsymbol{\kappa}\cdot\mathbf{d}\right)\cos\left[a\left(L-z\right)\right]\right|^2 \\ \left|\sin\left(a\,L\right)\cos\left(a\,z\right) - \exp\left(i\,\boldsymbol{\kappa}\cdot\mathbf{d}\right)\sin\left[a\left(L-z\right)\right]\right|^2 \\ \sin^2(a\,z) + 2\cos^2(a\,z)\left[1 - \cos\left(\boldsymbol{\kappa}\cdot\mathbf{d}\right)\right] \end{bmatrix}, \tag{3.71}$$

where the total variance is the sum of the phase and the log-amplitude variances given by $F_t'(\gamma\boldsymbol{\kappa})$ is

$$F_t'(\gamma\boldsymbol{\kappa}) = F_\phi'(\gamma\boldsymbol{\kappa}) + F_\chi'(\gamma\boldsymbol{\kappa}). \tag{3.72}$$

The total variance was obtained with the trigonometric identities

$$\cos(A+B) = \cos(A)\cos(B) - \sin(A)\sin(B), \text{ and}$$

$$\sin(A+B) = \sin(A)\cos(B) + \cos(A)\sin(B).$$

If the offset is zero, the filter function reduces to

$$\begin{bmatrix} F_\phi'(\gamma\boldsymbol{\kappa}) \\ F_\chi'(\gamma\boldsymbol{\kappa}) \\ F_t'(\gamma\boldsymbol{\kappa}) \end{bmatrix} = \begin{bmatrix} \sin^2(\gamma\kappa^2 L/2k_0)\ \sin^2(\gamma\kappa^2 z/2k_0) \\ \cos^2(\gamma\kappa^2 L/2k_0)\ \sin^2(\gamma\kappa^2 z/2k_0) \\ \sin^2(\gamma\kappa^2 z/2k_0) \end{bmatrix}. \tag{3.73}$$

One obtains the aperture-related variances by inserting this into eq. 3.69. Note that the residual total filter function is the same as the one for amplitude variance. Therefore, the residual variance on a perfect phase conjugate adaptive-optics system is that due to the amplitude variance of the received wave.

3.5 Structure Function for a Distributed Beacon

The displacement to put into the structure function when there is only one ray is clear; however, when there is a distributed source it is not clear where the integral over the source distribution should be placed relative to the other integrals. It is incumbent to go back to the initial definition of the phase and the structure function to develop the correct expression that applies in this case.

If we solve one problem, then you can use it as a guide to solve new problems. Let us consider a finite sized beacon of diameter D_s and develop the structure function for that case.

Consider the phase received at $\boldsymbol{\rho}$ in the aperture plane from a small area of the beacon that has a displacement of $\mathbf{d}$ relative to the beam that is to be transmitted. Let the transmitted beam have a different value of γ than the received beam. The differential phase received is derived from eq. 2.106 as

$$\begin{aligned}\phi(\boldsymbol{\rho}) = k_0 \int_0^L dz' \int d\nu(\boldsymbol{\kappa}, z') \\ \times \left\{\exp(i\gamma_1 \boldsymbol{\kappa}\cdot\boldsymbol{\rho})\cos[P(\gamma_1,\kappa,z')] - \exp(i\gamma_2\boldsymbol{\kappa}\cdot(\mathbf{d}+\boldsymbol{\rho}))\cos[P(\gamma_2,\kappa,z')]\right\}.\end{aligned} \tag{3.74}$$

Adding up the phase contributions from a distributed source with intensity $S(\boldsymbol{\rho}')$, one obtains

$$\phi(\boldsymbol{\rho}) = k_0 \int_0^L dz' \int d\nu(\boldsymbol{\kappa}, z') \left\{ \exp(i\gamma_1 \boldsymbol{\kappa}\cdot\boldsymbol{\rho}) \cos[P(\gamma_1, \kappa, z')] \right.$$
$$\left. - \frac{\int d\boldsymbol{\rho}'\, S(\boldsymbol{\rho}') \exp(i\boldsymbol{\kappa}\cdot\boldsymbol{\rho} z/L)}{\int d\boldsymbol{\rho}'\, S(\boldsymbol{\rho}')} \exp(i\gamma_2 \boldsymbol{\kappa}\cdot\boldsymbol{\rho}') \cos[P(\gamma_2, \kappa, z')] \right\}. \quad (3.75)$$

If $S(\boldsymbol{\rho})$ is uniform over a circle of radius $D_s/2$, then for the term in braces

$$I = \exp(i\gamma_1 \boldsymbol{\kappa}\cdot\boldsymbol{\rho}) \cos[P(\gamma_1, \kappa, z')]$$
$$- \frac{8\exp(i\gamma_2 \boldsymbol{\kappa}\cdot\boldsymbol{\rho})}{D_s^2} \int_0^{D_s/2} \rho'\, d\rho' \int_0^{2\pi} d\theta\, \exp(i\gamma_2 \boldsymbol{\kappa}\cdot a\boldsymbol{\rho}') \cos[P(\gamma_2, \kappa, z')]. \quad (3.76)$$

Integrating over angle and then over radius, one obtains

$$I = \exp(i\gamma_1 \boldsymbol{\kappa}\cdot\boldsymbol{\rho}) \cos[P(\gamma_1, \kappa, z')] - \frac{2J_1(\kappa h)}{\kappa h} \exp(i\gamma_2 \boldsymbol{\kappa}\cdot\boldsymbol{\rho}) \cos[P(\gamma_2, \kappa, z')],$$

where $h = \gamma_2 D_s z/2L$.

For the case where the transmitted beam is also focused at L, $\gamma_1 = \gamma_2 = \gamma = 1 - z/L$, then

$$I = \exp(i\gamma \boldsymbol{\kappa}\cdot\boldsymbol{\rho}) \cos[P(\gamma, \kappa, z')] \left[1 - \frac{2J_1(\kappa h)}{\kappa h}\right]. \quad (3.77)$$

The phase variance for this particular case is

$$\langle \phi(\boldsymbol{\rho}) \phi^*(\boldsymbol{\rho}) \rangle = \left\langle k_0^2 \int_0^L dz' \int d\nu(\boldsymbol{\kappa}', z') \int_0^L dz'' \int d\nu(\boldsymbol{\kappa}'', z') \right.$$
$$\times \cos[P(\gamma, \kappa', z')] \cos[P(\gamma, \kappa'', z'')]$$
$$\left. \times \left[1 - \frac{2J_1(\kappa' h)}{\kappa' h}\right] \left[1 - \frac{2J_1(\kappa'' h)}{\kappa'' h}\right] \right\rangle. \quad (3.78)$$

The expression can be simplified in the same manner as was done in the last chapter to obtain for the phase variance

$$\sigma_\phi^2 = 0.2073\, k_0^2 \int_0^L dz\, C_n^2(z) \int d\boldsymbol{\kappa}\, f(\kappa) \left[1 - \frac{2J_1(\kappa h)}{\kappa h}\right]^2 \cos^2[P(\gamma, \kappa, z)]. \quad (3.79)$$

This can be integrated over angle in $\boldsymbol{\kappa}$ space to give

$$\sigma_\phi^2 = 1.303\, k_0^2 \int_0^L dz\, C_n^2(z) \int_0^\infty \kappa\, d\kappa\, f(\kappa) \left[1 - \frac{2J_1(\kappa h)}{\kappa h}\right]^2 \cos^2[P(\gamma, \kappa, z)]. \quad (3.80)$$

We will consider the case where a does not depend on the receiving aperture position $\boldsymbol{\rho}$. For instance, this applies to the case where the propagating beam is focused at the beacon for which $a = z/L$. Note that the variance is constant over the aperture, allowing the simpler expression to be used to calculate the Strehl ratio.

The structure function is given in eq. 2.157 as

$$\begin{bmatrix} \mathcal{D}_\phi(\boldsymbol{\alpha} D, \boldsymbol{\rho}') \\ \mathcal{D}_\chi(\boldsymbol{\alpha} D, \boldsymbol{\rho}') \end{bmatrix} = \begin{bmatrix} \mathcal{D}_\phi(\boldsymbol{\alpha}\mathcal{D}) \\ \mathcal{D}_\chi(\boldsymbol{\alpha}\mathcal{D}) \end{bmatrix} = 2 \begin{bmatrix} \langle\phi^2(0)\rangle - \langle\phi(\boldsymbol{\alpha} D)\ \phi(0)\rangle \\ \langle\chi^2(0)\rangle - \langle\chi(\boldsymbol{\alpha} D)\ \chi(0)\rangle \end{bmatrix}. \tag{3.81}$$

The expression for the correlation function of phase is

$$\begin{aligned} C_\phi(\boldsymbol{\alpha} D) = \langle\phi(0)\phi^*(\boldsymbol{\alpha} D)\rangle = \Bigg\langle k_0^2 \int_0^L dz' \int d\nu(\boldsymbol{\kappa}', z') \int_0^L dz'' \int d\nu(\boldsymbol{\kappa}'', z') \\ \times \cos(\gamma\boldsymbol{\kappa}' \cdot \boldsymbol{\alpha} D) \cos[P(\gamma, \kappa', z')] \cos[P(\gamma, \kappa'', z'')] \\ \times \left[1 - \frac{2J_1(\kappa' h)}{\kappa' h}\right] \left[1 - \frac{2J_1(\kappa'' h)}{\kappa'' h}\right] \Bigg\rangle. \end{aligned} \tag{3.82}$$

This can be simplified to obtain

$$\begin{aligned} C_\phi(\boldsymbol{\alpha} D) = 0.2073\, k_0^2 \int_0^L dz\, C_n^2(z) \int d\boldsymbol{\kappa}\, f(\kappa) \left[1 - \frac{2J_1(\kappa h)}{\kappa h}\right]^2 \\ \times \cos(\gamma\boldsymbol{\kappa} \cdot \boldsymbol{\alpha} D) \cos^2[P(\gamma, \kappa, z)]. \end{aligned} \tag{3.83}$$

This can be integrated over angle in $\boldsymbol{\kappa}$ space to give

$$\begin{aligned} C_\phi(\boldsymbol{\alpha} D) = 1.303\, k_0^2 \int_0^L dz\, C_n^2(z) \int_0^\infty \kappa\, d\kappa\, f(\kappa) \left[1 - \frac{2J_1(\kappa h)}{\kappa h}\right]^2 \\ \times J_0(\gamma\kappa\alpha D) \cos^2[P(\gamma, \kappa, z)]. \end{aligned} \tag{3.84}$$

The correlation function of the amplitude has the cosine squared term replaced by a sine squared term. The total structure function, which is the sum of the phase and amplitude structure functions, is equal to

$$\begin{aligned} \mathcal{D}(\boldsymbol{\alpha} D) &= \mathcal{D}_\phi(\boldsymbol{\alpha} D) + \mathcal{D}_\chi(\boldsymbol{\alpha} D) \\ &= 2.606\, k_0^2 \int_0^L dz\, C_n^2(z) \int_0^\infty \kappa d\kappa\, f(\kappa) \left[1 - \frac{2J_1(\kappa D_s z/2L)}{\kappa D_s z/2L}\right]^2 \\ &\times [1 - J_0(\gamma\kappa\alpha D)]. \end{aligned} \tag{3.85}$$

If one wanted to find the Strehl ratio with some Zernike modes removed, then one would modify the above structure functions as the one in eq. 3.35 was modified. The structure function then would be a function of $\boldsymbol{\rho}$.

3.6 Developing New Variance Filter Functions

In the previous sections filter functions to apply to the variance, $F(\boldsymbol{\kappa})$, were developed. These are effective for many of the problems that one encounters; however, sometimes one has to deal with a more complicated situation where it is not clear what filter function should be applied. In those cases it is necessary to start with the expression for phase and log-amplitude given in (2.105) and apply a filter function, $G(\boldsymbol{\kappa})$. After doing that, the expression for the variance can often be written by inspection, since the same steps that were originally used to go from the phase and log-amplitude to their variances apply. One then has the filter function for the variance, $F(\boldsymbol{\kappa}) = G(\boldsymbol{\kappa}) G^*(\boldsymbol{\kappa})$, that applies to this problem.

Two examples of applying that technique to a particular problem are illustrated. First consider the tilt variance that would be obtained using an adaptive-optics system that is designed to send a focused beam to a target where the phase is measured from a distributed beacon at the focal point. The tilt is measured with respect to the center of the beacon distribution. To attack this problem, start with the expression for the phase in eq. 2.105

$$\phi R(L) = k_0 \int_0^L dz' \int d\nu\,(\boldsymbol{\kappa}, z')\, G(\gamma\,\boldsymbol{\kappa}) \cos\left[P(\gamma, \kappa, z')\right], \tag{3.86}$$

and insert the filter functions for tilt for a point source from eq. 3.22 and anisoplanatic offset from eq. 2.122, where the separation is a maximum at L and is equal to $\mathbf{d}$. It is a linear function of the distance from the aperture.

The tilt direction as determined from the definition of the Zernike modes in $\boldsymbol{\kappa}$ space is in the direction of $\boldsymbol{\kappa}$. The expression for the total anisoplanatic tilt jitter with the diffraction term neglected, i.e. $\cos\left[P(\gamma, \kappa, z')\right] = 1$ is

$$\mathbf{t}_i = \frac{16}{D} \int_0^L dz' \int d\nu\,(\boldsymbol{\kappa}, z') \left[\frac{4J_2(\gamma\kappa D/2)}{\gamma\kappa D/2}\right] \left[1 - \exp\left(i\boldsymbol{\kappa}\cdot\mathbf{d}z/L\right)\right] \frac{\boldsymbol{\kappa}}{\kappa}, \tag{3.87}$$

where D is the diameter of the receiving aperture.

Consider a distributed beacon. First, I will write down the expressions for the vector tilt from a differential area of the beacon. Next, I will integrate the tilt over the beacon area, then I will evaluate the expected value of the variance of the tilt. The exponential term in the above equation for a distributed beacon becomes

$$\exp\left(i\boldsymbol{\kappa}\cdot\mathbf{d}\right) \rightarrow \frac{1}{A} \int d\mathbf{r} f(\mathbf{r}) \exp\left(i\boldsymbol{\kappa}\cdot\mathbf{r}z/L\right), \tag{3.88}$$

where A is the weighted area of the beacon $A = \int d\mathbf{r} f(\mathbf{r})$ and $f(\mathbf{r})$ is its distribution in space. The sensor integrates the tilt from each sensor area. The exponential can be written as

$$B(\theta, z) = \frac{1}{A} \int d\mathbf{r} f(\mathbf{r}) \exp\left[i\kappa r\cos(\theta - \phi)z/L\right], \tag{3.89}$$

where the angle of $\boldsymbol{\kappa}$ with respect to the x-axis is φ, and the angle of the differential beacon component with respect to the x-axis is ϕ.

This expression is substituted into eq. 3.87, then it is multiplied by its complex conjugate, and its expected value is found. The steps to perform these operations are exactly the same as those previously used to find the variances, and the result is

$$\begin{bmatrix} \sigma_{\parallel}^2 \\ \sigma_{\perp}^2 \\ \sigma^2 \end{bmatrix} = 0.2073 \int_0^L dz\, C_n^2(z) \int d\boldsymbol{\kappa} \begin{bmatrix} \cos^2(\varphi) \\ \sin^2(\varphi) \\ 1 \end{bmatrix} \kappa^{-11/3} \times \left(\frac{16}{D}\right)^2 \left[\frac{J_2(\gamma\kappa D/2)}{\gamma\kappa D/2}\right]^2 |1 - B(\varphi, z)|^2 , \tag{3.90}$$

where σ^2 is the total variance, which is equal to the sum of the parallel and perpendicular variances. For any beacon distribution this expression can be evaluated to obtain the tilt variances in the two directions.

Let us consider a symmetrical beacon. Rotating the beacon produces no change in this case. If the beacon is a uniformly illuminated circle of radius R, then the exponential term is

$$B(\varphi, z) = \frac{1}{\pi R^2} \int_0^R \int_0^{2\pi} d\phi\, r dr \exp\left[i\kappa r \cos(\phi) z/L\right]. \tag{3.91}$$

The ϕ integration can be performed to give for this term

$$B(\varphi, z) = \frac{2}{R^2} \int_0^R r dr J_0(\kappa R z/L). \tag{3.92}$$

The radial integration can be performed to give

$$B(\varphi, z) = \frac{2J_1(\kappa R z/L)}{\kappa R z/L}. \tag{3.93}$$

For small values of the argument $J_1(x) \approx x/2$, $B(\varphi, z)$ approaches 1 when the beacon radius gets very small, thus causing the value for tilt anisoplanatism in eq. 3.90 to approach zero, as it should.

Notice that this does not depend on φ. Substituting this into eq. 3.90, one obtains

$$\begin{bmatrix} \sigma_{\parallel}^2 \\ \sigma_{\perp}^2 \\ \sigma^2 \end{bmatrix} = 0.2073 \int_0^L dz\, C_n^2(z) \int d\boldsymbol{\kappa} \begin{bmatrix} \cos^2(\varphi) \\ \sin^2(\varphi) \\ 1 \end{bmatrix} \kappa^{-11/3} \times \left(\frac{16}{D}\right)^2 \left[\frac{J_2(\gamma\kappa D/2)}{\gamma\kappa D/2}\right]^2 \left[1 - \frac{2J_1(\kappa R z/L)}{\kappa R z/L}\right]^2 . \tag{3.94}$$

This expression is the same as the one to calculate the tilt variance except for the presence of the last term in brackets. For large values of the beacon radius, the second Bessel function in the last bracketed term approaches zero, and the

term in brackets approaches unity. Therefore, for very large beacon sizes the tilt approaches the value from uncorrected turbulence. For small values of the radius $J_1(x) \approx x/2$, thus causing the value for tilt anisoplanatism to approach zero, as it should.

This expression can be evaluated numerically. Below the expression is evaluated analytically.

Let $a = \gamma DL/2zR$. The θ integration can be performed to give

$$\begin{bmatrix} \sigma_{\parallel}^2 \\ \sigma_{\perp}^2 \\ \sigma^2 \end{bmatrix} = \frac{105.1}{D^{1/3}} \begin{bmatrix} 1/2 \\ 1/2 \\ 1 \end{bmatrix} \int_0^L dz\, C_n^2(z)\, \gamma^{5/3} \times \int_0^\infty dx\, x^{-14/3} J_2^2(x) \left[\frac{2J_1(x/a)}{x/a} - 1 \right]^2. \tag{3.95}$$

Notice that the variance is the same in both directions. This expression is the same as the one for tilt variance if the Bessel function term in the second brackets is eliminated.

The x integration can be performed by Mellin transform techniques or with Mathematica, then the z integration can be performed to determine the jitter introduced by a finite-sized beacon. To perform the x integration write the integral as the sum of two integrals

$$\int_0^\infty dx\, x^{-14/3} J_2^2(x) \left[\frac{2J_1(x/a)}{x/a} - 1 \right]^2 = I_1 + I_2, \tag{3.96}$$

where

$$I_1/2 = -\int_0^\infty dx\, x^{-14/3} J_2^2(x) \left[\frac{2J_1(x/a)}{x/a} - 1 \right], \tag{3.97}$$

and

$$I_2 = \int_0^\infty dx\, x^{-14/3} J_2^2(x) \left\{ \left[\frac{2J_1(x/a)}{x/a} \right]^2 - 1 \right\}. \tag{3.98}$$

I_1 and I_2 can be evaluated to give separate solutions for small and large values of the parameter

$$\begin{aligned} I_1 = {} & 0.1156 \left\{ 1 - {}_3F_2 \left[\tfrac{23}{6}, -\tfrac{11}{6}, \tfrac{1}{6}; -\tfrac{4}{3}, 2; \left(\frac{1}{4a^2} \right) \right] \right\} \\ & + 0.001768 a^{-14/3} {}_3F_2 \left[-\tfrac{3}{2}, \tfrac{1}{2}, \tfrac{5}{2}; \tfrac{10}{3}, \tfrac{13}{3}; \left(\frac{1}{4a^2} \right) \right], \quad a > 1/2, \end{aligned} \tag{3.99}$$

and

$$I_1 = -0.1158 + 0.1165a^{1/3}{}_3F_2\left[-\tfrac{5}{6}, \tfrac{1}{6}, \tfrac{5}{2}; 3, 5; 4a^2\right], \quad a < 1/2. \tag{3.100}$$

$$\begin{aligned} I_2 = \; & 0.05788\left\{-1 + {}_4F_3\left[-\tfrac{23}{6}, -\tfrac{11}{6}, \tfrac{1}{6}, \tfrac{3}{2}; -\tfrac{4}{3}, 2, 3; \left(\frac{1}{a^2}\right)\right]\right\} \\ & - 0.006168a^{-14/3}{}_4F_3\left[-\tfrac{3}{2}, \tfrac{1}{2}, \tfrac{5}{2}, \tfrac{23}{6}; \tfrac{10}{3}, \tfrac{13}{3}, \tfrac{16}{3}; \left(\frac{1}{a^2}\right)\right], \; a > 1, \end{aligned} \tag{3.101}$$

and

$$\begin{aligned} I_2 = \; & -0.05788 + 0.05404{}_4F_3\left[-\tfrac{11}{6}, -\tfrac{5}{6}, \tfrac{1}{6}, \tfrac{5}{2}; -\tfrac{1}{3}, 3, 5; a^2\right] \\ & 0.002698{}_4F_3\left[-\tfrac{1}{2}, \tfrac{1}{2}, \tfrac{3}{2}, \tfrac{23}{6}; \tfrac{7}{3}, \tfrac{13}{3}, \tfrac{19}{3}; a^2\right], \quad a < 1. \end{aligned} \tag{3.102}$$

To see the effect of a finite size beacon, in Fig. 3.2 the tilt is plotted versus beacon radius for the Clear1 turbulence model with the platform at 12 km, the range to the target at 400 km, the aperture diameter at 1 meter, and the target height at 60 km. The tilt jitter is of the order of 100 microradians for a beacon size of 50 cm.

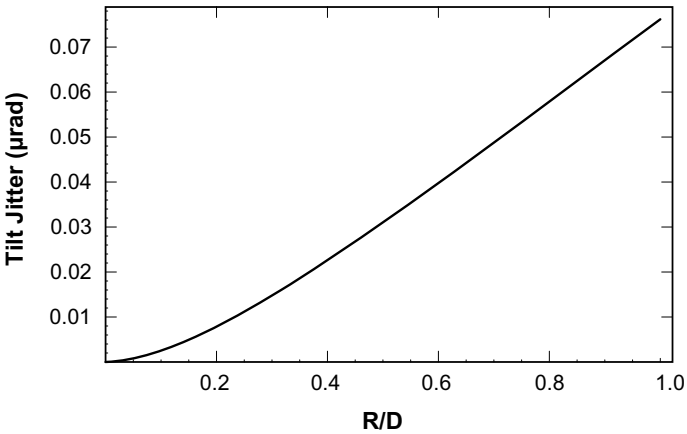

Figure 3.2. Tilt jitter due to a finite beacon of radius R measured in an aperture of diameter D for the Clear1 turbulence model with the platform at 12 km, a target range of 400 km, an aperture 1-meter receiver diameter, and a target height of 60 km.

The second example that is considered is a scenario in which an illuminator beam on a platform is directed at a target, and the target return is imaged to choose a track point. The illuminator beam is then kept as steadily as possible on this track point. A beacon beam is then sent to the target, and its return is used to control an adaptive-optics mirror off which a scoring beam is directed at the target.

To get the maximum amount of energy on the target, it is important to make higher-order corrections as accurately as possible, which is achieved by not having any anisoplanatic offset for the scoring beam. In addition, the distortion measured on the beacon is applied as quickly as possible. The only delay is due to the processing time t_p of the beacon measurements needed to generate a change in the shape of the deformable mirror.

To have maximum energy density on the target, the scoring beam is pointed in the same direction as the beacon beam, which implies that the separation of the beacon beam from the scoring beam on the target is $\mathbf{v}_t\tau$ where $\mathbf{v}_t$ is the velocity of the target and τ is the sum of the processing delay and the two-way propagation time from platform to target $\tau = t_p + 2L/c$, where L is the distance between target and platform, and c is the speed of light.

Given the aim point of the scoring beam, this selection then determines where the beacon must be placed to satisfy the requirement that there be no tilt anisoplanatism between the beacon and scoring beams. The separation between the illuminator and beacon beams is no longer an independent parameter, and there can be tilt anisoplanatism between the beams.

One would like to reduce this anisoplanatism, and several options have been considered for controlling the beam pointing. One proposal is to use the information about the illuminator beam pointing to reduce this effect. The illuminator tilt that is measured is a combination of tilt due to movement of the platform, whose velocity is $\mathbf{v}_p$, and due to turbulence-induced tilt. If one were to use the delayed illuminator turbulence-induced tilt information that corresponds to the present path of beacon propagation, then the tilt anisoplanatism due to target motion is minimized, which has the potential to reduce the beacon jitter.

In another option the measured beacon tilt is immediately used to direct the scoring beam. That approach could suffer greater anisoplanatism than the one using the delayed illuminator tilt.

Another option has been proposed to reduce tilt anisoplanatism. The returning beacon has a tilt that can be measured by the wavefront sensor. This tilt is a combination of the deterministic angular change of the platform due to its motion in the two-way transit time of the beacon and due to the different turbulence encountered by the outgoing and returning beams.

With no platform motion, there is no useful information in the tilt measured by the waveform sensor since the outgoing and incoming beacon paths are the same, which causes the outgoing turbulence-induced tilt to cancel the incoming turbulence-induced tilt; hence, the turbulence-induced tilt is not sensed. This is not exactly true since the target is finite in size, part of the beacon beam does not strike the target, which can cause a tilt to be sensed by the returning beam. I will neglect that effect in this analysis. For a moving platform, some tilt will be sensed even if the target were infinite in extent. One of the options I will examine is the effect of applying the turbulence-induced tilt from the beacon return to the scoring beam to see if that reduces the scoring-beam jitter.

Scintillation will affect the jitter; that will not be considered here.

To answer the question of whether using the beacon tilt reduces the jitter, I will find the relative rms anisoplanatic tilt jitter between the illuminator and scoring beam for each option. To find the effectiveness of each option we need to determine the magnitude of $< |\mathbf{t}_d - a\mathbf{t}_b|^2 >$ for any value of a, where $\mathbf{t}_d$ is the tilt jitter between the illuminator and scoring beams with no correction for beacon tilt, and $\mathbf{t}_b$ is the turbulence-induced tilt of the beacon.

To attack this problem start with the expression for the phase in eq. 2.105

$$\phi R(L) = k_0 \int_0^L dz' \int d\nu\left(\boldsymbol{\kappa}, z'\right) G\left(\gamma\,\boldsymbol{\kappa}\right) \cos\left[P\left(\gamma, \kappa, z'\right)\right], \tag{3.103}$$

and insert the filter functions for tilt from eq. 3.17 and anisoplanatic offset from eq. 2.122 to obtain for the total anisoplanatic tilt jitter between the beacon and illuminator with no correction

$$\mathbf{t}_d = k_0 \int_0^L dz' \int d\nu\left(\boldsymbol{\kappa}, z'\right) \left[\frac{4J_2\left(\kappa D/2\right)}{\kappa D/2}\right] \left[1 - \exp\left(i\boldsymbol{\kappa}\cdot\mathbf{d}\right)\right] \cos\left[P\left(\gamma, \kappa, z'\right)\right] \frac{\boldsymbol{\kappa}}{\kappa}. \tag{3.104}$$

This expression applies when the beacon tilt is not used.

For convenience latter let

$$B = \left[1 - \exp\left(i\boldsymbol{\kappa}\cdot\mathbf{d}\right)\right]. \tag{3.105}$$

For the option of using the beacon tilt, the anisoplanatic tilt caused by the offset between the illuminator and scoring paths $\mathbf{d}$ is modified by having a fraction of the tilt measured on the returned beacon subtracted from this tilt. The beacon tilt is caused by the platform motion and the turbulence motion due to the wind during the propagation time, which results in a path difference $\mathbf{d}_b$ through the frozen turbulence between the outgoing and returning beacon. The expression for this tilt is the same form as the illuminator-scoring beam tilt. Form the difference of the uncorrected anisoplanatic tilt and a fraction of the beacon tilt to obtain

$$\mathbf{t}_d - a\mathbf{t}_b = k_0 \int_0^L dz' \int d\nu\left(\boldsymbol{\kappa}, z'\right) \left[\frac{4J_2\left(\kappa D/2\right)}{\kappa D/2}\right] A \cos\left[P\left(\gamma, \kappa, z'\right)\right] \frac{\boldsymbol{\kappa}}{\kappa}, \tag{3.106}$$

where

$$A = 1 - \exp\left(i\boldsymbol{\kappa}\cdot\mathbf{d}\right) - a\left[1 - \exp\left(i\boldsymbol{\kappa}\cdot\mathbf{d}_b\right)\right]. \tag{3.107}$$

To obtain the tilt variance, one multiplies this tilt expression by its complex conjugate and then finds its expected value. I will sketch the derivation of the result for the case of not using the beacon tilt. It will be shown that the case of using the beacon tilt is a combination of expressions from the first option.

The entire derivation will not be given here; however, the term with the offset will be examined since its form is needed for the second option. In the derivation one finds that

$$BB^* = [1 - \exp(i\boldsymbol{\kappa} \cdot \mathbf{d})][1 - \exp(-i\boldsymbol{\kappa} \cdot \mathbf{d})] = 2[1 - \cos(\boldsymbol{\kappa} \cdot \mathbf{d})]. \quad (3.108)$$

If the variance is found by using the same procedure as was followed in Chap. 2, then one obtains the expression for tilt anisoplanatism that is given in Sec. 7.6.

Consider now the second option. The term comparable to the one just evaluated given in eq. 3.107 is written as

$$A = 1 - \exp(ib) - a[1 - \exp(if)], \quad (3.109)$$

where

$$b = \boldsymbol{\kappa} \cdot \mathbf{d}, \quad (3.110)$$

and

$$f = \boldsymbol{\kappa} \cdot \mathbf{d}_b. \quad (3.111)$$

It is easy to show that

$$AA^* = 2(1-a)[1 - \cos(b)] - 2a(1-a)[1 - \cos(f)] + 2a[1 - \cos(b - f)]. \quad (3.112)$$

Since the three terms are each of the same form as those in the analysis for the first option in eq. 3.108, the tilt jitter variance corrected for beacon tilt can be written as the sum of three terms, each of which is a tilt anisoplanatic variance term with different displacements

$$T_{corrected} = (1 - a)T(\mathbf{d}) - a(1 - a)T(\mathbf{d}_b) + aT(\mathbf{d} - \mathbf{d}_b). \quad (3.113)$$

Notice that if no correction is applied, that is $a = 0$, then the expression reduces to the first term, which is the tilt with no correction. With $a = 1$ the expression becomes

$$T_{corrected} = T(\mathbf{d} - \mathbf{d}_b). \quad (3.114)$$

For any situation one can find the value of a that minimizes the tilt.

REFERENCES

1. Noll, R. J., "Zernike polynomials and atmospheric turbulence", *J. Opt. Soc. Am.*, **3**, (1976) pp. 207–21.
2. Wang, J. Y., Markey, J. K., "Modal compensation of atmospheric turbulence phase distortion", *J. Opt. Soc. Am.*, **68**, (1978) pp. 78–87.

Chapter 4

Zero-Parameter Problems

In the second chapter I derived general formulas that enable one to write phase and log-amplitude variances, power spectral densities, and Strehl ratios as integrals. Different cases differ only in the appearance of different filter functions. In the last chapter explicit filter functions were derived for a variety of problems. With the use of these filter functions, integrands contain the following functions: $\sin(x)$, $\cos(x)$, $\sin^2(x)$, $\cos^2(x)$, $J_\nu(x)$, $J_\nu(x)\,J_\mu(x)$, $J_\nu^2(x)$, $\exp(x)$, $(1+x)^{-p}$, $(x-1)^{-p}\,U(x-1)$, and $K(x)$.

The Mellin transforms of these functions are given in Table 1.1. (Integrals containing $\cos^2(x)$ are evaluated by substituting $1-\sin^2(x)$.) *Therefore,* **all** *problems in which the phase or log-amplitude variances are wanted and in which the filter functions in Chap. 3 and the turbulence spectra given in Chap. 2 can be used are solvable by Mellin transform techniques.*

In this chapter problems of electromagnetic-wave propagation in turbulence that can be solved by table lookup are addressed. The following expressions are found: (1) variances of the Zernike tilt of collimated and focused waves, (2) gradient tilt variance, (3) variance of the difference between Zernike and gradient tilt, (4) beam movement at a target due to tilt, (5) angle-of-arrival jitter of a tracked target, (6) scintillation of collimated and focused waves, (7) phase variance of a system with temporal filtering, and (8) total variance with a phase-only adaptive-optics system with and without a beacon offset. These examples illustrate how easily solutions are obtained once the technique described in this book is mastered.

The Mellin transform technique is particularly well suited to evaluate integrals obtained in wave propagation in turbulence, because the integrand term x^{-s} matches the form of the turbulence spectrum in the most important region — the inertial subrange. Results are expressed as moments of the turbulence distribution in altitude. After defining the full and partial moments, I express their values analytically for the Hufnagel-Valley turbulence model. Other frequently used turbulence models are also defined.

4.1 Turbulence Models and Moments

Several different models are commonly used to represent effects of atmospheric turbulence. The Hufnagel-Valley model is based on one proposed by *Hufnagel* (1974) from measurements made by *Bufton* et al. (1972), and modified by *Valley* (1980) to include ground level turbulence. It is

$$C_n^2(h) = 0.00594\left(\frac{W}{27}\right)^2\left(10^{-5}\times h\right)^{10}\exp\left(-\frac{h}{1000}\right) + 2.7\times 10^{-16}\exp\left(-\frac{h}{1500}\right) + A\exp\left(-\frac{h}{100}\right), \tag{4.1}$$

where W is the pseudo-wind, and A is a parameter that is usually set equal to 1.7×10^{-14}, and h is in meters. The turbulence is usually assumed to be zero above 30 km. The turbulence strength is usually changed by a variation of the W term. For instance, the HV-21 model has the above value for A, and W is equal to 21. This model is sometimes referred to as the $\mathrm{HV}_{5/7}$ model since the coherence diameter is about 5 cm, and the isoplanatic angle is about 7 μrad for a wavelength of 0.5 μm.

The full moments, which are defined for propagation from the ground to space, are

$$\mu_m \equiv \int_0^\infty dz\, C_n^2(z)\, z^m = \sec^{m+1}(\xi)\int_0^\infty dh\, C_n^2(h)\, h^m, \tag{4.2}$$

where ξ is the zenith angle. *Notice that the zenith dependence is contained in the turbulence moments.* For constant turbulence along L, the moments are

$$\mu_m = C_n^2\, L^{(m+1)}/(m+1). \tag{4.3}$$

The integrations can be performed for the Hufnagel-Valley model to give

$$\mu_m = \int_0^\infty dz\, C_n^2(z)\, z^m = \sec^{m+1}(\xi)\left\{5.94\times 10^{-20+3m}\,(W/27)^2\,\Gamma\left[m+11\right] + 4.05\times 10^{-13}\Gamma\left[m+1\right](1500)^m + A\times 100^{m+1}\Gamma\left[m+1\right]\right\}. \tag{4.4}$$

For propagation to a distance L, which is at a height H, so that $L = \sec(\xi)\, H$, define the partial moments in the following way

$$\mu_m^+(L) \equiv \int_L^\infty dz\, C_n^2(z)\, z^m = \sec^{m+1}(\xi)\int_H^\infty dh\, C_n^2(h)\, h^m, \quad \text{and} \tag{4.5}$$

$$\mu_m^-(L) \equiv \int_0^L dz\, C_n^2(z)\, z^m = \sec^{m+1}(\xi)\int_0^H dh\, C_n^2(h)\, h^m. \tag{4.6}$$

Using the lower- and upper-incomplete gamma functions, which are

$$\gamma\left[b+1,x\right]=\int_0^x dy\, y^b \exp(-y), \quad \text{and} \quad \Gamma\left[b+1,x\right]=\int_x^\infty dy\, y^b \exp(-y), \tag{4.7}$$

one can find the partial moments of turbulence as

$$\mu_m^+(L)=\int_L^\infty dz\, C_n^2(z)\, z^m = \sec^{m+1}(\xi)\left\{\frac{5.94}{10^{20-3m}}\left(\frac{W}{27}\right)^2 \Gamma\left[m+11,\frac{H}{1000}\right]\right.$$
$$\left.+4.05\times 10^{-13}\Gamma\left[m+1,\frac{H}{1500}\right](1500)^m + A\times 100^{m+1}\Gamma\left[m+1,\frac{H}{100}\right]\right\}; \tag{4.8}$$

$$\mu_m^-(L)=\int_0^L dz\, C_n^2(z)\, z^m = \sec^{m+1}(\xi)\left\{\frac{5.94}{10^{20-3m}}\left(\frac{W}{27}\right)^2 \gamma\left[m+11,\frac{H}{1000}\right]\right.$$
$$\left.+4.05\times 10^{-13}\gamma\left[m+1,\frac{H}{1500}\right](1500)^m + A\times 100^{m+1}\gamma\left[m+1,\frac{H}{100}\right]\right\}. \tag{4.9}$$

The above formulas apply to a flat earth model. For propagation at low elevation angles, the curvature of the earth must be taken into account. In that case for propagation from a platform at h_p to a receiver at range at z, the value of height in the turbulence profile must be replaced by

$$h(z)=-R_E+\left[(h_p+R_E)^2+z^2+2z\,(h_p+R_E)\sin(el)\right]^{1/2}, \tag{4.10}$$

where el is the elevation angle, and R_E is the earth radius, 6.4×10^6 m.

For this case the turbulence moment is

$$\mu_m=\int_0^\infty dz\, C_n^2(h(z))\, z^m. \tag{4.11}$$

It can be useful to express results in terms of coherence diameter and isoplanatic angle. Define the coherence diameter r_o as

$$r_0=\left[0.423k_0^2\int_0^L dz\, C_n^2(z)\gamma^{5/3}\right]^{-3/5}. \tag{4.12}$$

and the isoplanatic angle θ_o as

$$\theta_0=\left[2.91k_0^2\int_0^L dz\, C_n^2(z)z^{5/3}\right]^{-3/5}. \tag{4.13}$$

This can be expressed as

$$\theta_0^{-5/3} = 2.91\, k_0^2\, \mu_{5/3}^{-}(L). \tag{4.14}$$

For an infinite plane wave for which $\gamma = 1$, one obtains

$$r_0^{-5/3} = 0.423\, k_0^2\, \mu_0^{-}(L). \tag{4.15}$$

For a spherical wave focused at $z = 0$ for which $\gamma = z/L$, one obtains

$$r_{0s}^{-5/3} = 0.423\, k_0^2\, \mu_{5/3}^{-}(L) L^{-5/3}. \tag{4.16}$$

Both the coherence diameter and isoplanatic angle vary as the six-fifths power of wavelength. As shown in Sec. 8.1 this definition of coherence diameter comes naturally from consideration of the beam size. As shown in Sec. 8.4.1 the isoplanatic angle is the characteristic angle that affects the Strehl ratio.

In addition to the Hufnagel-Valley model, the SLC Day and Night models are often used. $C_n^2(z)$ is usually assumed to be zero above 20.5 km for both models. The SLC Day model, also called SLCSAT Day, is based on the day-time *Miller-Zieske* profile (1979), which can be approximated by a set of power-law segments as:

$$\begin{aligned} C_n^2(z) &= 3.96 \times 10^{-13}/z^{1.05}, && 18.5 \le z \le 232 \\ &= 1.3 \times 10^{-15}, && 232 \le z \le 880 \\ &= 8.87 \times 10^{-7}/z^3, && 880 \le z \le 7220 \\ &= 2.0 \times 10^{-16}/z^{0.5}, && 7220 \le z \le 20500. \end{aligned} \tag{4.17}$$

The units of $C_n^2(z)$ are $m^{-2/3}$ and the altitude is in meters. The SLC Night model, which differs from the SLC Night model at lower altitudes, is given by:

$$\begin{aligned} C_n^2(z) &= 5.0 \times 10^{-15}, && z \le 18.5 \\ &= 2.875 \times 10^{-12}/z^2, && 18.5 \le z \le 110 \\ &= 2.5 \times 10^{-16}, && 110 \le z \le 1500 \\ &= 8.87 \times 10^{-7}/z^3, && 850 \le z \le 7000 \\ &= 2.0 \times 10^{-16}/z^{0.5}, && 7000 \le z \le 20500. \end{aligned} \tag{4.18}$$

Another turbulence profile that is regularly used is the Clear1-night profile, which is given by

$$\begin{aligned} \log 10\,[C_n^2(z)] &= -10.7025 - 4.3507z + 0.8141z^2, && 1.23\,\mathrm{km} \le \mathrm{z} \le 2.13\,\mathrm{km} \\ &= -16.2897 + 0.0335z - 0.0134z^2, && 2.13\,\mathrm{km} \le \mathrm{z} \le 10.34\,\mathrm{km} \\ &= -17.0577 - 0.0449z - 0.0005z^2 \\ &\quad + 0.6181 \exp\left\{-0.5\,[(z - 15.5617)/3.4666]^2\right\}, && 10.34\,\mathrm{km} \le \mathrm{z}. \end{aligned} \tag{4.19}$$

In this model z is given in kilometers.

These turbulence models apply for optical propagation. At radar wavelengths, moisture in the air causes the turbulence profile to differ from the above models. Measurements indicate that the turbulence strength typically is 10 to 100 times the above values. Even higher values have been measured, levels of 10^{-12} from ground level to 4 km have been reported. The spatial spectrum of this turbulence is not known.

Table 4.1. Coherence diameter and isoplanatic angle for a wavelength of 0.5 μm and moments of Hufnagel-Valley turbulence models for propagation from the ground to 30 kilometers. The turbulence moments are in mks units, and the units of the n^{th} moment are $\mathrm{m}^{n+1/3}$.

	HV-21	HV-35	HV-54	HV-72
r_0(cm)	4.96	4.67	4.18	3.70
$\theta_o(\mu\mathrm{rad})$	6.90	3.95	2.40	1.71
μ_0	2.23×10^{-12}	2.47×10^{-12}	2.97×10^{-12}	3.64×10^{-12}
$\mu_{-1/3}$	5.50×10^{-13}	5.60×10^{-13}	5.83×10^{-13}	6.14×10^{-13}
$\mu_{5/6}$	5.45×10^{-10}	1.08×10^{-9}	2.24×10^{-9}	3.80×10^{-9}
μ_1	2.21×10^{-9}	4.76×10^{-9}	1.03×10^{-8}	1.76×10^{-8}
$\mu_{5/3}$	8.97×10^{-7}	2.20×10^{-6}	5.06×10^{-6}	8.91×10^{-6}
μ_2	1.91×10^{-5}	4.97×10^{-5}	1.16×10^{-4}	2.04×10^{-4}
μ_3	2.32×10^{-1}	6.30×10^{-1}	1.49	2.64
$\mu_{11/3}$	1.32×10^{2}	3.62×10^{2}	8.58×10^{2}	1.52×10^{3}
μ_4	3.18×10^{3}	8.75×10^{3}	2.08×10^{4}	3.69×10^{4}
$\mu_{14/3}$	1.91×10^{6}	5.29×10^{6}	1.25×10^{7}	2.23×10^{7}
μ_5	4.74×10^{7}	1.31×10^{8}	3.11×10^{8}	5.53×10^{8}
μ_6	7.55×10^{11}	2.09×10^{12}	4.97×10^{12}	8.84×10^{12}

Table 4.1 contains various useful moments for several turbulence models in mks units. Values of coherence diameters and isoplanatic angles in the table are for a wavelength of 0.5 μm. The HV-21 and SLCSAT Day models are plotted versus altitude in Fig. 4.1.

4.2 Tilt and Piston for Collimated and Focused Beams

Tilt jitter is one of the most significant effects of turbulence. Tilt of a mirror is described by a Zernike tilt, and that measured by a centroid sensor is closely approximated by gradient tilt. The calculation of Zernike tilt is considered first. Since this is a single wave problem, eq. 2.112 applies. In calculations of the tilt

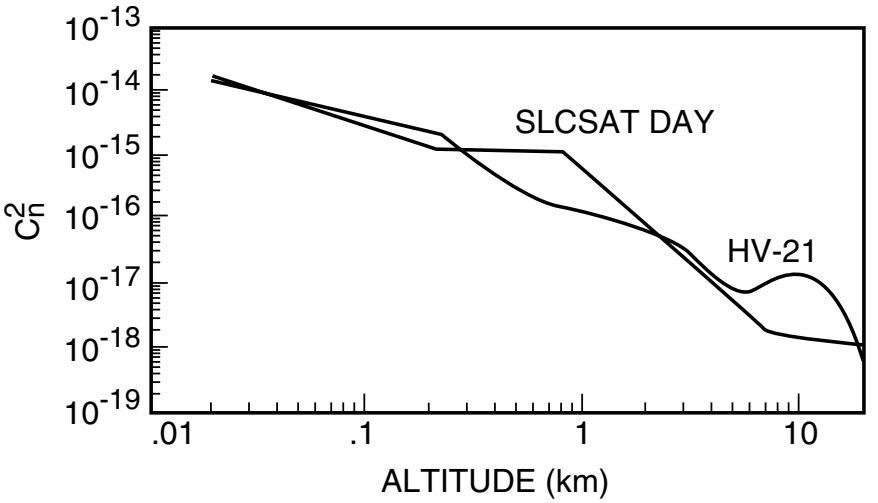

Figure 4.1. Plots of the Hufnagel-Valley 21 and SLCSAT DAY models of turbulence versus altitude. The units of turbulence strength are $m^{-2/3}$.

here and in the next two sections it will be assumed that diffraction effects are not important, thereby allowing the cosine term to be replaced by unity. The effect of diffraction on tilt is considered in Sec. 7.5. I show that as long as one is well within the Fresnel distance, effects of diffraction are negligible. If inner- and outer-scale effects are neglected, the Kolmogorov spectrum given in eq. 2.35 applies. With the filter function for two-axis Zernike tilt given in eq. 3.22 one obtains for the tilt angle variance

$$T_Z^2 = 0.2073\, k_0^2 \int_0^L dz\; C_n^2(z) \int d\boldsymbol{\kappa}\; \kappa^{-11/3} \left(\frac{16}{k_0 D}\right)^2 \left[\frac{J_2\left(\gamma\kappa D/2\right)}{\gamma\kappa D/2}\right]^2. \qquad (4.20)$$

The diameter that must be used in the term $16/k_0 D$ is the final aperture diameter. The phase variance due to local turbulence is added along the propagation path, and it is only at the aperture that the phase is converted into a tilt. The integrand in the second integral does not depend on the angle in kappa space. Integration over this angle, and substitution of $x = \gamma\kappa D/2$ yields

$$\begin{aligned} T_Z^2 &= \frac{105.1}{D^{1/3}} \int_0^L dz\, C_n^2(z)\, \gamma^{5/3} \int_0^\infty \frac{dx}{x}\, x^{-11/3} J_2^2(x) \\ &= \frac{105.1}{2\sqrt{\pi} D^{1/3}} \int_0^L dz\, C_n^2(z)\, \gamma^{5/3}\, \Gamma\left[\begin{matrix} s/2+2,\; -s/2+\frac{1}{2} \\ -s/2+3,\; -s/2+1 \end{matrix}\right]\Bigg|_{s=-\frac{11}{3}} \\ &= \frac{105.1}{2\sqrt{\pi} D^{1/3}} \int_0^L dz\, C_n^2(z)\, \gamma^{5/3}\, \Gamma\left[\begin{matrix} \frac{1}{6},\; \frac{7}{3} \\ \frac{29}{6},\; \frac{17}{6} \end{matrix}\right]. \end{aligned}$$

The x integration is equal to the Mellin transform given in eq. 1.52 evaluated at $s = -11/3$. The composite gamma function defined in eq. 1.19 is equal to the ratio of four individual gamma functions. The composite gamma function above is equal to 0.2052. This gives for the two-axis tilt variance

$$T_Z^2 = \frac{6.08}{D^{1/3}} \int_0^L dz\, C_n^2(z)\, \gamma^{5/3}. \tag{4.21}$$

For an infinite collimated beam, γ is equal to unity. For this case the integration over z can be performed with the turbulence moments given in eq. 4.2. *The 2-axis Z-tilt angle jitter variance is*

$$T_Z^2 = \frac{6.08\,\mu_0}{D^{1/3}} = 0.3641 \left(\frac{D}{r_0}\right)^{5/3} \left(\frac{\lambda}{D}\right)^2, \tag{4.22}$$

where the coherence diameter is defined in eq. 4.15.

The separate x and y tilt variances are half this value.

$$T_{Zx}^2 = T_{Zy}^2 = T_Z^2/2. \tag{4.23}$$

Because the variance is proportional to the zeroth moment of turbulence, it varies as the secant of the zenith angle, $\sec(\xi)$. Notice that the tilt variance goes to infinity as the diameter goes to zero. This singularity is removed in Sec. 5.3 by introducing a finite inner scale. For a 0.6-m diameter aperture and HV-21 turbulence, the rms tilt is 4 μrad at zenith. This is much larger than the diffraction-limited beam size of 1 μrad at 0.5 μm, and it causes considerable smearing of a star image.

If the turbulence is constant along the path of length L, the two-axis tilt variance is

$$T_Z^2 = \frac{6.08\, C_n^2 L}{D^{1/3}}. \tag{4.24}$$

If the wave originated as a point source propagating from the ground to space, the value of γ would be equal to z/L. *The tilt angle variance of a point source on the ground as viewed from space is*

$$T_Z^2 = \frac{6.08\,\mu_{5/3}}{D^{1/3} L^{5/3}} = \frac{0.169\,\lambda^2}{D^{1/3} L^{5/3} \theta_o^{5/3}}. \tag{4.25}$$

This tilt also decreases the resolution of an imaging system in space. Since the tilt is correlated from one point to another, the resolution can be improved by the use of short-exposure images or by tracking the image during the exposure.

By dividing the tilt variance value by the factor $(4/k_0\, D)^2$ given after eq. 3.21 and using the relation in eq. 4.15, one can obtain the phase variance. *The tilt phase variance averaged over the aperture is*

$$\sigma_T^2 = 0.380\,\mu_0\, k_0^2\, D^{5/3} = 0.899 \left(\frac{D}{r_0}\right)^{5/3}. \tag{4.26}$$

Total and piston phase variances are infinite for Kolmogorov turbulence. Their difference, which is piston-removed phase variance, is finite, and it is found with the relation for phase variance given in eq. 2.112 and the filter function for piston phase variance given in eq. 3.19. For a collimated beam it is

$$\sigma_{PR}^2 = 0.2073\, k_0^2 \int_0^L dz\; C_n^2(z) \int d\boldsymbol{\kappa}\; \kappa^{-11/3} \left\{ 1 - \left[\frac{2\, J_1(\kappa D/2)}{\kappa D/2} \right]^2 \right\}.$$

The angle and axial integrations can be evaluated, and when the substitution $x = \kappa D/2$ is made one obtains

$$\sigma_{PR}^2 = 1.64\, D^{5/3} \mu_0 k_0^2 \int_0^\infty \frac{dx}{x}\, x^{-11/3} \left[\frac{x^2}{4} - J_1^2(x) \right] = -\frac{1.64}{2\sqrt{\pi}}\, \mu_0 k_0^2\, D^{5/3}\, \Gamma \left[\begin{matrix} -\frac{5}{6}, \frac{7}{3} \\ \frac{23}{6}, \frac{17}{6} \end{matrix} \right].$$

The integral of individual functions in the integrand does not converge if the exponent of the power of x that multiplies dx/x is less than -2. However, because $x^2/4$ is the first term of a power series of $J_1^2(x)$, the integral can be analytically continued and converges for the exponent in the range -2 to -4, since the residues at two poles cancel as in the derivation of eq. 1.22. Thus the integral is simply the Mellin transform of the squared Bessel function in eq. 1.52 evaluated at $s = -11/3$. The value of the composite gamma function is -0.9438. *Thus, the phase variance with piston removed is*

$$\sigma_{PR}^2 = 1.033 \left(\frac{D}{r_0} \right)^{5/3}. \tag{4.27}$$

Since piston and tilt are orthogonal on a circular aperture, *the phase variance with piston and tilt removed is the difference of* eq. *4.27 and* eq. *4.26, i.e.,*

$$\sigma_{PTR}^2 = 0.134 \left(\frac{D}{r_0} \right)^{5/3}. \tag{4.28}$$

These piston- and tilt-variance relationships are often used to get a first cut at system performance. Tilt variance is 87% of the piston-removed phase variance. For this reason adaptive-optics systems are usually designed to have a separate tilt mirror to limit the dynamic range of deformable mirror motion that responds only to the tilt-removed phase. If turbulence to be corrected can be so large that one can have $D/r_0 = 10$, then the rms piston-and-tilt-removed phase standard deviation is 2.49 rads or 0.397 waves. This value can be used to estimate the dynamic range of actuator motion required in the deformable mirror.

In a similar fashion, the phase variance can be found for any Zernike mode. This result is given in eq. 6.170.

4.3 Gradient Tilt

In an exactly analogous fashion, the two-axis G-tilt integral is found with the filter function given in eq. 3.38 and the general formula in eq. 2.112, to obtain

$$T_G^2 = 0.2073\, k_0^2 \int_0^L dz\, C_n^2(z) \int d\boldsymbol{\kappa}\; \kappa^{-11/3} \left(\frac{4}{k_0 D}\right)^2 J_1^2\,(\gamma \kappa D/2). \tag{4.29}$$

After the same integrations, substitutions, and Mellin transforms as above, one obtains for a collimated beam

$$T_G^2 = \frac{6.564\,\mu_0}{D^{1/3} 2\sqrt{\pi}}\, \Gamma\left[\begin{matrix}\frac{1}{6},\, \frac{4}{3} \\ \frac{17}{6},\, \frac{11}{6}\end{matrix}\right] = \frac{5.675\,\mu_0}{D^{1/3}} = 0.3399 \left(\frac{D}{r_0}\right)^{5/3} \left(\frac{\lambda}{D}\right)^2. \tag{4.30}$$

This gives a tilt that is 3.5% lower than Z-tilt. This is the same result obtained by *Ellerbroek* (1984) and *Tatarski* (1971).

4.4 Difference Between Gradient and Zernike Tilt

Sometimes a target position is measured with a centroid sensor that responds essentially to G-tilt. The pointing system uses tilt from this sensor to direct a beam at a target by tilting a mirror that changes the Z-tilt of the wave. It is of interest to know what residual tilt jitter is expected at the target even if this process is performed perfectly. This problem was analyzed by *Yura* and *Tavis* (1985) and given the name *centroid anisoplanatism*. The variance of the difference between G-tilt and Z-tilt is found with the filter functions for G- and Z-tilt given by the square roots of the expressions in eq. 3.22 and eq. 3.38. Insert these into eq. 2.117, which determines the variance of two collimated waves that have different aperture functions, to obtain

$$T_D^2 = 0.2073\, k_0^2 \int_0^L dz\, C_n^2(z) \int d\boldsymbol{\kappa}\; \kappa^{-11/3} \left(\frac{4}{k_0 D}\right)^2 \left[\frac{4 J_2(\kappa D/2)}{\kappa D/2} - J_1(\kappa D/2)\right]^2. \tag{4.31}$$

If the bracket is expanded, one obtains three terms. Two are the sum of Zernike and Gradient tilts. The third can be evaluated with the Mellin transform in eq. 1.53, to obtain

$$T_D^2 = \frac{6.564\,\mu_0}{2\sqrt{\pi} D^{1/3}} \left(16\, \Gamma\left[\begin{matrix}\frac{1}{6},\, \frac{7}{3} \\ \frac{29}{6},\, \frac{17}{6}\end{matrix}\right] + \Gamma\left[\begin{matrix}\frac{1}{6},\, \frac{4}{3} \\ \frac{17}{6},\, \frac{11}{6}\end{matrix}\right] - 8\, \Gamma\left[\begin{matrix}\frac{1}{6},\, \frac{7}{3} \\ \frac{23}{6},\, \frac{17}{6}\end{matrix}\right]\right).$$

If the gamma functions are evaluated directly, then one requires five-place accuracy to achieve three-place accuracy in the final answer, since the terms in braces almost cancel. Rather than doing that, one uses the recurrence relation for gamma functions to show that

$$T_D^2 = \frac{6.564\,\mu_0}{2\sqrt{\pi} D^{1/3}}\, \Gamma\left[\begin{matrix}\frac{1}{6},\, \frac{4}{3} \\ \frac{17}{6},\, \frac{11}{6}\end{matrix}\right] \left(\frac{4608}{4301} + 1 - \frac{384}{187}\right).$$

This is equal to

$$T_D^2 = \frac{0.102\,\mu_0}{D^{1/3}} = 0.0061 \left(\frac{D}{r_0}\right)^{5/3} \left(\frac{\lambda}{D}\right)^2 . \tag{4.32}$$

Beamwidth of a diffraction-limited system is $1.2\,\lambda/D$; therefore, there is a one-third of a beamwidth jitter when the aperture diameter is six times the coherence diameter. This tilt jitter would be observable only if the image or outgoing beam were significantly corrected for other effects of turbulence. It was shown by *Herrmann* (1981) that the major difference between the two tilts is due to coma distortion. If an adaptive-optics system corrected most of this distortion, centroid anisoplanatism would be greatly reduced.

4.5 Zernike Mode Variance

The variance of any Zernike mode with Kolmogorov turbulence can be obtained by inserting the filter function for Zernike modes in eq. 3.18 into the general phase variance formula eq. 2.112

$$\left.\begin{matrix} Z_{(m,n)_x} \\ Z_{(m,n)_y} \\ Z_{0,n} \end{matrix}\right\} = 0.2073\,k_0^2 \int_0^L dz\; C_n^2(z) \int d\boldsymbol{\kappa}\; \kappa^{-11/3} \left\{\begin{matrix} F_{m,n}\left(\boldsymbol{\kappa}\right)_x \\ F_{m,n}\left(\boldsymbol{\kappa}\right)_y \\ F_{0,n}\left(\boldsymbol{\kappa}\right) \end{matrix}\right. . \tag{4.33}$$

The integration over angle gives the same result for all three components. Each variance is denoted by Z_n. Substitution of $x = \gamma\,\kappa\,D/2$ yields

$$\begin{aligned} Z_n &= 0.1641 D^{5/3}(n+1)k_0^2 \int_0^L dz\, C_n^2(z)\,\gamma^{5/3} \int_0^\infty \frac{dx}{x}\, x^{-11/3} J_{n+1}^2(x) \\ &= \frac{0.08205 D^{5/3}(n+1)k_0^2}{\sqrt{\pi}} \int_0^L dz\, C_n^2(z)\,\gamma^{5/3}\, \Gamma\left[\begin{matrix} s/2+n+1,\; -s/2+\frac{1}{2} \\ -s/2+n+2,\; -s/2+1 \end{matrix}\right]\Bigg|_{s=-\frac{11}{3}} \\ &= 0.04130 D^{5/3} k_0^2 \int_0^L dz\, C_n^2(z)\,\gamma^{5/3} \Gamma\left[\begin{matrix} -\frac{5}{6}+n,\; \frac{7}{3} \\ \frac{23}{6}+n,\; \frac{17}{6} \end{matrix}\right] . \end{aligned} \tag{4.34}$$

For a collimated beam the Zernike phase variance is equal to

$$Z_n = 1.0945(n+1)\Gamma\left[\begin{matrix} -\frac{5}{6}+n,\; \frac{7}{3} \\ \frac{23}{6}+n,\; \frac{17}{6} \end{matrix}\right] \left(\frac{D}{r_0}\right)^{5/3} . \tag{4.35}$$

The phase variance of each tilt component is $0.449(D/r_0)^{5/3}$, for each of the three second-order Zernike modes of focus and the two axes of astigmatism it is $0.0232(D/r_0)^{5/3}$, and for each of the four third-order distortions it is $0.00619(D/r_0)^{5/3}$.

4.6 Piston and Tilt of a Gaussian Beam

Modes for a Gaussian beam are derived, and these are shown to be in excellent agreement with expressions for top-hat beams if D is replaced by $2\sqrt{2}w_0$. This was the relationship that gave the same Strehl ratio in the large diameter limit for a top hat and Gaussian beam.

A normalized Gaussian field without diffraction can be expressed as

$$\text{Field} = \frac{1}{\pi w_0^2} \exp\left(-\frac{\rho^2}{w_0^2}\right). \tag{4.36}$$

The field is normalized so that the integration of the field over all space is equal to unity.

$$\int d\boldsymbol{\rho} \frac{1}{\pi w_0^2} \exp\left(-\frac{\rho^2}{w_0^2}\right) = 1. \tag{4.37}$$

The modes of a Gaussian beam will now be defined. One must decide how the infinite extent of the beam should be handled. A reasonable assumption is to weight the mode function by the field amplitude at that point. I will show that this assumption gives results that are consistent with a top-hat field over a diameter D.

With this assumption, the filter function for the piston of a Gaussian wave is the Fourier transform of the field times the mode function, which for piston is unity. This gives

$$G(\boldsymbol{\kappa}) = \int d\boldsymbol{\rho} \, \frac{1}{\pi w_0^2} \exp\left(-\frac{\rho^2}{w_0^2}\right) \exp\left[i\boldsymbol{\kappa}\cdot\boldsymbol{\rho}\right] = \exp\left(-\kappa^2 w_0^2/4\right). \tag{4.38}$$

This was evaluated by breaking the integral into one over ρ_x and one over ρ_y. Each of these integrals yields the same result.

The piston filter function applicable for a Gaussian beam is

$$F(\boldsymbol{\kappa}) = G(\boldsymbol{\kappa}) G^*(\boldsymbol{\kappa}) = \exp\left(-\kappa^2 w_0^2/2\right). \tag{4.39}$$

The equation for the phase and log-amplitude of a Gaussian beam that is the analogy of eq. 2.112 is

$$\begin{bmatrix} \sigma^2_{\phi R} \\ \sigma^2_{\chi R} \end{bmatrix} = 0.2073\, k_0^2 \int_0^L dz\, C_n^2(z) \int d\boldsymbol{\kappa}\, f(\kappa) \begin{bmatrix} \cos^2\left[P(\gamma,\kappa,z)\right] \\ \sin^2\left[P(\gamma,\kappa,z)\right] \end{bmatrix} \times \exp\left(-\kappa^2 w_0^2/2\right) \hat{F}(\gamma\boldsymbol{\kappa}). \tag{4.40}$$

Using the Gaussian filter function, one can find the phase variance with piston removed as

$$\sigma^2_{PR} = 0.2073\, k_0^2 \int_0^L dz\; C_n^2(z) \int d\boldsymbol{\kappa}\; \kappa^{-11/3} \left(1 - \exp\left[-\kappa^2 w_0^2/2\right]\right). \tag{4.41}$$

Integrate over the angle and z, and make the substitution $x = w_0\kappa$ to obtain

$$\sigma_{PR}^2 = 1.303\, k_0^2\, \mu_0\, w_0^{5/3} \int_0^\infty dx\; x^{-8/3} \left[1 - \exp\left(-x^2/2\right)\right]. \tag{4.42}$$

The integral is equal to 1.87; use eq. 4.15 to obtain

$$\sigma_{PR}^2 = 5.77 \left(\frac{w_0}{r_0}\right)^{5/3}. \tag{4.43}$$

Using the substitution $D = 2\sqrt{2}w_0$ one obtains for the piston-removed phase variance of a top-hat beam

$$\sigma_{PR}^2 = 1.02 \left(\frac{D}{r_0}\right)^{5/3}. \tag{4.44}$$

The same result derived directly for a top-hat beam in eq. 4.28 has a coefficient of 1.033. The results are almost identical, which helps to justify the weighting used.

As additional evidence to support the weighting, I will derive the gradient tilt of a Gaussian beam. For a Gaussian beam it is reasonable to assume that the tilt is the average of the local tilt in the beam. This is the G-tilt phase. It is given by

$$\text{G-tilt} = \int d\boldsymbol{\rho}\; \nabla_t \Phi\left(\boldsymbol{\rho}\right). \tag{4.45}$$

In Fourier space the transverse gradient produces a factor of $i\kappa$ times the gradient filter function just as the case for the top-hat beam. To obtain the tilt from the phase slope divide by k_0. The G-tilt filter function applicable for a Gaussian beam is

$$G\left(\boldsymbol{\kappa}\right) = \frac{i\kappa}{k_0} \exp\left(-\kappa^2 w_0^2/4\right), \tag{4.46}$$

which gives

$$F\left(\boldsymbol{\kappa}\right) = G\left(\boldsymbol{\kappa}\right) G^*\left(\boldsymbol{\kappa}\right) = \frac{\kappa^2}{k_0^2} \exp\left(-\kappa^2 w_0^2/2\right). \tag{4.47}$$

Therefore, the G-tilt variance is

$$\sigma_{G-Tilt}^2 = 0.2073 \int_0^L dz\; C_n^2(z) \int d\boldsymbol{\kappa}\; \kappa^{-11/3} \kappa^2 \exp\left(-\kappa^2 w_0^2/2\right). \tag{4.48}$$

Integrate over the angle and z, and make the substitution $x = w_0\kappa$ to obtain

$$\sigma_{G-Tilt}^2 = 1.303 \mu_0 / w_0^{1/3} \int_0^\infty dx\; x^{-2/3} \exp\left(-x^2/2\right). \tag{4.49}$$

The integral is equal to 3.124. Therefore, the G-tilt variance is equal to

$$\sigma_{G-Tilt}^2 = 4.071 \mu_0 / w_0^{1/3}. \tag{4.50}$$

Making the substitution $D = 2\sqrt{2}w_0$, one obtains

$$\sigma_{G-Tilt}^2 = 5.76\, \mu_0 / D^{1/3}. \tag{4.51}$$

The coefficient given in eq. 4.30 for tilt of a top-hat beam is 5.675. Again the correspondence is very close.

4.7 Beam Movement at a Target

Turbulence causes the beam boresight to move at a target. This movement is found for a source on the ground projected into space, and vice versa. Tilt causes a beam to change position on a target as shown in Fig. 4.2. In this problem one obtains the filter function by finding an expression for the beam movement on target for a given local tilt, and then taking the absolute value squared. It is

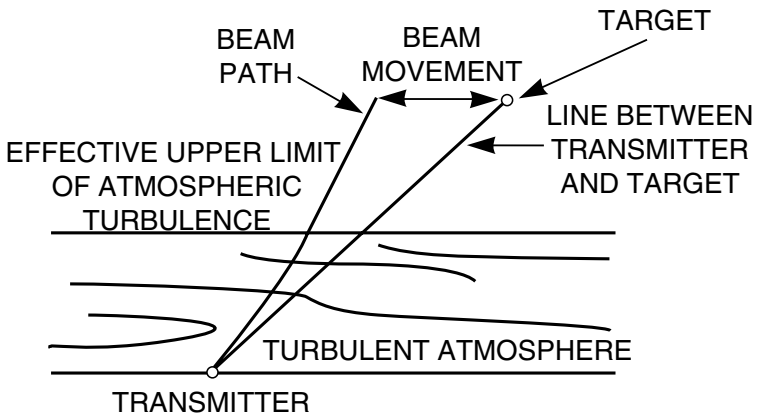

Figure 4.2. Beam movement at a target board.

assumed that scintillations are small, and the beam is not broken up. If there are significant scintillations, these will increase the movement calculated here. Far field effects decrease the movement. It is also assumed that diffraction is unimportant; therefore, a ray-optics calculation is adequate. With these assumptions, the amount of beam jitter at a target at L from turbulence at z is equal to the product of the local tilt and the distance over which it acts, $L - z$. Therefore, the tilt filter function for this problem is

$$F(\boldsymbol{\kappa}) = (L-z)^2 \left(\frac{16}{k_0 \gamma D}\right)^2 \left[\frac{J_2(\gamma \kappa D/2)}{\gamma \kappa D/2}\right]^2 . \tag{4.52}$$

One must use the local diameter, which is given by γD, to find the local tilt to multiply by the lever arm. The one-axis variance of beam movement is

$$X^2 = 0.2073\, k_0^2 \int_0^L dz\, C_n^2(z) \int d\boldsymbol{\kappa}\, \kappa^{-11/3} (L-z)^2 \left(\frac{16}{k_0 \gamma D}\right)^2 \left[\frac{J_2(\gamma \kappa D/2)}{\gamma \kappa D/2}\right]^2 . \tag{4.53}$$

This expression can be evaluated for the collimated case, for which case $\gamma = 1$, to give

$$X^2 = \frac{6.08}{D^{1/3}} \left(L^2 \mu_0 - 2\, L\, \mu_1 + \mu_2\right). \tag{4.54}$$

For distances at which the target is well above the turbulence, the first term in brackets is dominant; this gives the physically reasonable result that rms movement is rms tilt times distance. For a target at 100 km with HV-21 turbulence and a 60-cm aperture, the rms beam movement is 40 cm.

If turbulence is constant along the path, one finds

$$X^2 = \frac{2.03\, L^3 C_n^2}{D^{1/3}}. \tag{4.55}$$

This functional dependence with constant turbulence is the same as that reported in *Fante* (1980) where the fourth moment of the field was used to calculate the beam displacement. The coefficient found by Fante was 1.92 in that case. A Gaussian beam, as calculated by *Prokhorov* et al. (1975), gives the same dependence with the coefficient equal to 1.6. The advantage of the approach here is that the answer is arrived at in a straightforward manner, and the expression given in eq. 4.54 applies for turbulence that can vary in space. For the beam focused at the target board, for which case $\gamma = (L - z)/L$, the movement variance is

$$X^2 = \frac{6.08 L^2}{D^{1/3}} \int_0^L dz\, C_n^2(z)(1 - z/L)^{5/3}. \tag{4.56}$$

For constant turbulence along the path, this can be integrated to give

$$X^2 = \frac{2.03 L^3 C_n^2}{D^{1/3}} \left(\frac{9}{8}\right). \tag{4.57}$$

The movement variance is 112% that of a collimated beam, and the rms movement is 106% that of a collimated beam.

For a source in space, the same argument as above gives a filter function

$$F(\boldsymbol{\kappa}) = z^2 \left(\frac{16}{k_0 \gamma D}\right)^2 \left[\frac{J_2(\gamma \kappa D/2)}{\gamma \kappa D/2}\right]^2. \tag{4.58}$$

Variance of the beam movement for a collimated beam propagated from space to ground is

$$X^2 = \frac{6.08\, \mu_2}{D^{1/3}}. \tag{4.59}$$

This movement is equal to 1.2 cm for the HV-21 model with a 0.6-m aperture. Thus it is much easier to hit a target on the ground from space with a laser beam than vice versa.

4.8 Angle-of-Arrival Jitter

Suppose a tracking system is doing a perfect job of keeping a laser beam centered on a target. There will still be an angle-of-arrival jitter of the laser beam at the target because the beam has to traverse the atmosphere differently as turbulence

changes. This is illustrated in Fig. 4.3. This jitter can cause movement of a beam relayed from a mirror at the space target to another object if the relay mirror is not tilted to compensate for this effect.

The statement that a target is being perfectly tracked means that, at each turbulence realization, the beam movement due to the tilted tracking mirror is exactly canceled out by the displacement caused by the atmospheric turbulence tilt. The mirror and atmospheric tilts are not the same since the lever arm differs for the two tilts.

The angle-of-arrival tilt will be calculated for a turbulence screen at z. If dT_o is the mirror tilt needed to compensate for the displacement due to the turbulence-induced tilt, dT, then one obtains for perfect tracking

$$L\,dT_o - (L - z)\,dT = 0; \tag{4.60}$$

therefore,

$$dT_o = (1 - z/L)\,dT. \tag{4.61}$$

The residual tilt at the target dT_t is the tilt through turbulence minus the mirror tilt. This results in the angle-of-arrival jitter

$$dT_t = dT - dT_o = z\,dT/L. \tag{4.62}$$

Therefore, the filter function for angle-of-arrival jitter is the tilt filter function

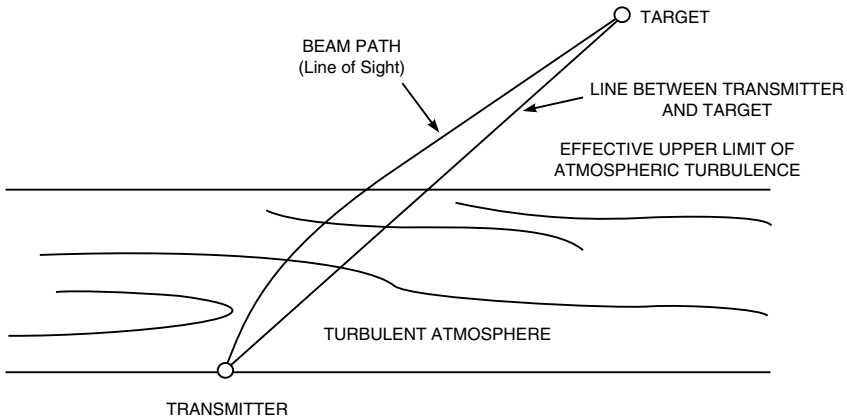

Figure 4.3. Angle-of-arrival jitter of a beam at a target that is being perfectly tracked by a ground system.

multiplied by z/L, which gives for the variance of angle-of-arrival tilt jitter the filter function

$$F(\boldsymbol{\kappa}) = \left(\frac{z}{L}\right)^2 \left(\frac{16}{k_0 \gamma D}\right)^2 \left[\frac{J_2(\gamma\,\kappa\,D/2)}{\gamma\,\kappa\,D/2}\right]^2. \tag{4.63}$$

As in the last section, one must use the local tilt, which is why a γ appears in $1/k_o D$. Remember that γ is equal to unity for a collimated beam, γ is equal to

$1-z/L$ for a beam focused at the target, and γ is equal to z/L for a point source on the ground. Substitution of this filter function into eq. 2.112 and evaluation of the κ integral gives

$$T_t^2 = \frac{6.08}{D^{1/3}L^2}\int_0^L dz\, C_n^2(z) z^2 \gamma^{-1/3}. \tag{4.64}$$

One obtains for a collimated wave

$$T_t^2 = 6.08\,\frac{\mu_2}{D^{1/3}\,L^2}. \tag{4.65}$$

For a 0.6-m system with a target at 300-km range and HV-21 turbulence, the rms tilt is 39 nrads.

For a beam focused at the object, the tilt variance is

$$T_t^2 = \frac{6.08}{D^{1/3}\,L^2}\int_0^L dz\, C_n^2\,(z)\, z^2\,(1-z/L)^{-1/3}\,. \tag{4.66}$$

If the target is well above the turbulence, then the angle-of-arrival tilt jitter is almost equal to that of a collimated beam.

For a point source on the ground, γ is equal to z/L; the angle-of-arrival variance at a target in space is

$$T_t^2 = 6.08\,\frac{\mu_{5/3}}{D^{1/3}\,L^{5/3}}. \tag{4.67}$$

For a 0.6-m target aperture at 300-km range and HV-21 turbulence, the rms tilt is 69.4 nrads.

This problem was also analyzed by *Tyler* (1985). His results are in the form of curves that are derived from a numerical integration.

4.9 Scintillation for Collimated and Focused Beams

First-order Rytov theory expressions that are derived for scintillation are valid when the log-amplitude variance values that are 0.25 or less, which is well below the saturation value of 0.3—0.4. The variance of log-intensity is four times the value of variance of log-amplitude.

In this section the scintillation is calculated for the infinite beam case that applies to a point source or a large collimated beam. When the Fresnel number is in the range from 0.01 to 10, then the finite beam analysis in Chap. 10 should be employed.

To calculate scintillation of a wave that propagates from 0 to L with inner and outer scale neglected, again use eq. 2.112 with the diffraction parameter given in eq. 2.77, to obtain

$$\sigma_\chi^2 = 0.2073\, k_0^2 \int_0^L dz\, C_n^2(z) \int d\boldsymbol{\kappa}\; \kappa^{-11/3} \sin^2\left[\frac{\gamma \kappa^2 (L-z)}{2k_0}\right]. \tag{4.68}$$

The log-amplitude variance is often referred to as the Rytov number. Sometimes the variance of the log-intensity is referred to as the Rytov variance. If propagation were from L to 0, then $L - z$ should be replaced by z in the last equation to obtain

$$\sigma_\chi^2 = 0.2073\, k_0^2 \int_0^L dz\, C_n^2(z) \int d\boldsymbol{\kappa}\; \kappa^{-11/3} \sin^2\left(\frac{\gamma \kappa^2 z}{2k_0}\right). \tag{4.69}$$

As explained in Sec. 2.3, to compare this form with expressions obtained by others such as *Hufnagel* (1978), one must make the substitution $\kappa \to \kappa/\gamma$.

With a change in variables $x^2 = \gamma \kappa^2 z/2k_0$ in the last integration, it can be evaluated by using eq. 1.50 with the result that for propagation from L to 0 one obtains

$$\sigma_\chi^2 = 0.5631\, k_0^{7/6} \int_0^L dz\, C_n^2(z)\, (\gamma z)^{5/6}\,. \tag{4.70}$$

For a plane wave, for which $\gamma = 1$, the standard result for scintillation of a wave propagating from space to the ground is obtained

$$\sigma_\chi^2 = 0.5631\, k_0^{7/6} \mu_{5/6}. \tag{4.71}$$

This varies as $\sec^{11/6}(\xi)$. It is the scintillation observed from a star and is equal to 0.059 for the HV-21 model at 0.5 μm wavelength and zero zenith angle. Even though this value is small, it produces significant scintillation. Since the variance of log-intensity is four times that of the log-amplitude; its value is 0.236. Since the log-intensity distribution is Gaussian, the one-sigma fluctuation of the intensity is about $\pm 20\%$ of the mean.

The expression for the variance of the log-intensity for plane-wave propagation from L to 0 is

$$\sigma_{lnI}^2 = 2.25\, k_0^{7/6} \mu_{5/6}. \tag{4.72}$$

If the turbulence strength is constant along the path, then the log-amplitude variance for a plane wave is equal to

$$\sigma_\chi^2 = 0.3071\, k_0^{7/6} C_n^2 L^{11/6}. \tag{4.73}$$

For the log-intensity, the value is

$$\sigma_{lnI}^2 = 1.23\, k_0^{7/6} C_n^2 L^{11/6}. \tag{4.74}$$

Return to the expression in eq. 4.68 for propagation from 0 to L. Integrating over angle and making the substitution $x^2 = \gamma \kappa^2 (L-z)/2k_0$, one obtains

$$\sigma_\chi^2 = 0.731\, k_0^{7/6} \int_0^L dz\, C_n^2(z)(L-z)^{5/6}\gamma^{5/6} \int_0^\infty \frac{dx}{x}\, x^{-5/3} \sin^2\left(x^2\right).$$

Using the Mellin transform in eq. 1.50 evaluated at $s = -5/3$, for propagation from 0 to L one obtains

$$\sigma_\chi^2 = 0.5631\, k_0^{7/6} \int_0^L dz\, C_n^2(z)(L-z)^{5/6}\gamma^{5/6}. \tag{4.75}$$

This must be integrated numerically in general. For a receiver well above the turbulence, the approximate value of σ_χ^2 for a plane wave, for which $\gamma = 1$, is

$$\sigma_\chi^2 \approx 0.5631\, k_0^{7/6} \mu_0\, L^{5/6}. \tag{4.76}$$

This varies as $\sec(\xi)$. The log-amplitude variance is greater than unity for ranges larger than 2.5 km for a propagation wavelength of 0.5 μm and for a typical turbulence strength of $10^{-14} m^{-2/3}$. Therefore, scintillation of a beam projected a modest distance along the ground or to space will be saturated.

The above expression has the scintillation increasing without bound as L increases. This does not happen because at long ranges the Fresnel number is small and the point source case is approached. In that region $\gamma = z/L$ in eq. 4.75 and the dependence on L cancels.

As pointed out in the introduction, expressions for the phase variance are usually valid even for saturated scintillation. However, if the particular application requires detailed knowledge of the amplitude profile as, for instance, in using the amplitude profile as a tracker input, then the results based on the Rytov approximation are invalid. One must use either a wave-optics simulation or a theoretical approach that works with saturated scintillation.

For a point source on the ground for which $\gamma = z/L$, the scintillation observed in space, where L is much larger than the height to which turbulence extends, is approximately equal to

$$\sigma_\chi^2 \approx 0.5631\, k_0^{7/6} \mu_{5/6}. \tag{4.77}$$

This is the same scintillation level seen on the ground from a collimated beam from space that was derived above. If the turbulence is constant along the path, then the scintillation for this case is

$$\sigma_\chi^2 = 0.5631\, k_0^{7/6} C_n^2 \int_0^L dz\, (L-z)^{5/6} \left(\frac{z}{L}\right)^{5/6} = 0.5631\, k_0^{7/6} C_n^2 L^{11/6} B\left(\frac{11}{6}, \frac{11}{6}\right), \tag{4.78}$$

where $B\left(\frac{11}{6}, \frac{11}{6}\right)$ is a Beta function whose value for this case is 0.2205. Therefore, for constant turbulence along the path, the variance for a spherical wave propagating from a focus at $z = 0$ to a receiver at L is

$$\sigma_\chi^2 = 0.124\, k_0^{7/6} L^{11/6} C_n^2. \tag{4.79}$$

This is about a factor of 2.5 lower than the plane wave result in eq. 4.73 for constant turbulence. Similarly, for a point source in space propagating towards the ground, one obtains

$$\sigma_\chi^2 = 0.5631\, k_0^{7/6} \int_0^L dz\, C_n^2(z) \frac{(L-z)^{5/6} z^{5/6}}{L^{5/6}}. \tag{4.80}$$

For a point source at L well above turbulence, the scintillation is the same as that for a plane wave propagating from space, as would be expected. This result is given in eq. 4.71.

4.10 Phase Variance with Finite Servo Bandwidth

Greenwood (1977) derived the phase variance of an adaptive-optics system with finite temporal servo bandwidth with either a one-pole filter or an infinitely sharp filter. All other errors are neglected. Residual rms-phase error from a finite frequency response is calculated here with the same servo filter treated by Greenwood. Consider the following filter,

$$F_f(\omega) = \left| 1 - \frac{1}{1 + i\ (\omega/\omega_{3dB})^n} \right|^2. \tag{4.81}$$

The single-pole filter case corresponds to $n = 1$, and the sharp cutoff case corresponds to $n = \infty$. Insert this filter into eq. 2.134 with diffraction neglected. Putting the result into eq. 2.133, and considering propagation from L_1 to L_2, one obtains

$$\sigma_\phi^2 = 0.8295\, k_0^2 \int_{L_1}^{L_2} dz\, C_n^2(z) \frac{v^{5/3}(z)}{\omega_{3dB}^{5/3}} \int_0^\infty \frac{dx}{x} \frac{x^{2n-5/3}}{1+x^{2n}} \int_0^\infty \frac{dc}{c} \frac{U(c-1)c^{-5/3}}{\sqrt{c^2-1}},$$

where $x = \omega/\omega_{3dB} = f/f_{3dB}$.

Using the Mellin transform in eq. 1.54 with $p = 1$, the relation in eq. 1.9 with $p = 2n$, and the identity $\Gamma[s]\,\Gamma[1-s] = \pi/\sin(\pi\, s)$, one obtains

$$\int_0^\infty \frac{dx}{x} \frac{x^{2n-5/3}}{1+x^{2n}} = \frac{\pi}{2n\, \sin(5\pi/6n)}.$$

Using the Mellin transform in eq. 1.56 with $a = 1/2$, and the relation in eq. 1.19 with $p = 2$, one obtains

$$\int_0^\infty \frac{dc}{c} \frac{U(c-1)c^{-5/3}}{\sqrt{c^2-1}} = \frac{\sqrt{\pi}}{2}\, \Gamma\left[\begin{matrix} \frac{4}{3} \\ \frac{11}{6} \end{matrix}\right] = 0.8413.$$

With these results, the phase variance is

$$\sigma_\phi^2 = \left(\frac{f_G}{f_{3dB}}\right)^{5/3} = \frac{0.051\, k_0^2\, v_{5/3}}{f_{3dB}^{5/3}\, n\, \sin\left(5\pi/6n\right)}, \tag{4.82}$$

where the velocity moment is defined by

$$v_m = \int_{L_1}^{L_2} dz\, C_n^2(z)\, v^m(z) = \sec\left(\xi\right) \int_{H_1}^{H_2} dh\, C_n^2(h)\, v^m(h), \tag{4.83}$$

where $v(z)$ is the velocity perpendicular to the propagation direction.

For propagation between any two points, the integration is over the propagation path, and the velocity is the component transverse to the path. For a single-pole filter ($n=1$) one finds the characteristic frequency, sometimes referred to as the Greenwood frequency, is

$$f_G = 0.254\, k_0^{6/5}\, v_{5/3}^{3/5}. \tag{4.84}$$

For a sharp cutoff filter, the limit of the phase variance as n gets very large is found from L'Hospital's rule. This gives the same form for the Greenwood frequency; however, the coefficient is lower. In this case

$$f_G = 0.0945\, k_0^{6/5}\, v_{5/3}^{3/5}. \tag{4.85}$$

These are the same results obtained by *Greenwood* (1977).

4.11 Variances for Beams Corrected by Adaptive Optics

If an adaptive-optics system applies the conjugate in both amplitude and phase of the beacon, then an outgoing wave propagating in a direction exactly opposite to the beacon would be perfectly corrected. This result can be derived from the reciprocity relations for wave propagation. Most adaptive-optics systems apply only the conjugate of phase, and the direction of the outgoing beam may be offset from that of the beacon. For that case the filter function given in eq. 3.73 applies, and the residual log-amplitude and phase variances, after correction by an adaptive-optics system, are given by eq. 3.69 with $F\left(\gamma\,\kappa\right) = 1$ as

$$\begin{bmatrix}\sigma^2_{\phi c}\\ \sigma^2_{\chi c}\end{bmatrix} = 0.2073\,k_0^2\int_0^L dz\,C_n^2(z)\int d\boldsymbol{\kappa}\,\kappa^{-11/3} \times\begin{bmatrix}|\cos(a\,L)\cos(a\,z)-\exp(i\,\boldsymbol{\kappa}\cdot\mathbf{d}\,)\cos[a\,(L-z)]\,|^2\\ |\sin(a\,L)\cos(a\,z)-\exp(i\,\boldsymbol{\kappa}\cdot\mathbf{d}\,)\sin[a\,(L-z)]\,|^2\end{bmatrix}, \tag{4.86}$$

where $a=\gamma\kappa^2/2k_0$. Let us first consider the case in which the offset between the outgoing and beacon beams $\mathbf{d}$ is zero. The variance in this case is

$$\begin{bmatrix}\sigma^2_{\phi c}\\ \sigma^2_{\chi c}\end{bmatrix} = 0.2073\,k_0^2\int_0^L dz\,C_n^2(z)\int d\boldsymbol{\kappa}\,\kappa^{-11/3}\begin{bmatrix}\sin^2(a\,z)\sin^2(a\,L)\\ \sin^2(a\,z)\cos^2(a\,L)\end{bmatrix}. \tag{4.87}$$

A simple relation can be found by the addition of the two variances to obtain

$$\sigma^2_{\phi c}+\sigma^2_{\chi c} = 0.2073\,k_0^2\int_0^L dz\,C_n^2(z)\int d\boldsymbol{\kappa}\,\kappa^{-11/3}\,\sin^2\left(\frac{\gamma\kappa^2 z}{2k_0}\right). \tag{4.88}$$

Note that the angle integration in the last two equations can be performed in κ space to obtain a factor of 2π. The last equation is the one obtained for scintillation of either a point or focused source propagating towards the ground that was analyzed in Sec. 4.7, and the result for a collimated beam is

$$\sigma^2_{\phi c}+\sigma^2_{\chi c} = 0.5631\,k_0^{7/6}\,\mu_{5/6} = \sigma^2_{\chi}. \tag{4.89}$$

Therefore, total variance is equal to the variance of the scintillation on the beacon. This expression includes the effect of diffraction, and is valid for distributed turbulence.

The corrected beam in a phase-only adaptive-optics system can be distorted by several causes. Here the distortion in a system that has an anisoplanatic error produced by an offset of the outgoing beam by θ from the beacon is considered. The filter function for the total beam distortion is given in eq. 3.71 as

$$F_t'(\gamma\boldsymbol{\kappa}) = \sin^2\left(\frac{\gamma\kappa^2 z}{2\,k_0}\right)+2\cos^2\left(\frac{\gamma\kappa^2 z}{2\,k_0}\right)[1-\cos(\boldsymbol{\kappa}\cdot\mathbf{d}\,)]. \tag{4.90}$$

The first term is the same one encountered with correctly aligned beams, and its variance is given in eq. 4.89. It will be assumed that diffraction is negligible, which enables the first cosine to be replaced by unity. To find the total distortion with an angular offset θ for which $d=\theta\,z$, use the expression for the variances in eq. 3.69 with outer and inner scale effects neglected. Sum the phase and log-amplitude variances and integrate over angle to obtain for the total variance of a corrected offset beam

$$\sigma^2_{co} = \sigma^2_{\chi}+0.2073\;(4\,\pi)\,k_0^2\int_0^L dz\,C_n^2(z)\int_0^\infty\frac{d\kappa}{\kappa}\;\kappa^{-5/3}\,[1-J_0(\kappa\theta z)]. \tag{4.91}$$

The integral can be evaluated with the Mellin transform in eq. 1.51 and the definition of isoplanatic angle in eq. 4.14 to obtain

$$\sigma_{co}^2 = \sigma_\chi^2 + (\theta/\theta_o)^{5/3} . \tag{4.92}$$

The angle-dependent variance is equal to the variance of angular anisoplanatism that is derived in Sec. 8.4.2.

REFERENCES

1. Bufton, J. L., Minott, P. O., Fitzmaurice, M. W., Titterton, P. J., "Measurements of Turbulence Profiles in the Troposphere",*J. Opt. Soc. Am.*, **62**, (1972) pp. 1068–1070.
2. Ellerbroek, B. L., "The Temporal Dependence of Turbulence-Induced Line-of-Sight Jitter as Measured by a Wavefront Gradient Sensor", *tOSC Report No. TR-572* (the Optical Sciences Company, Placentia, California, 1984).
3. Fante, R. L., "Electromagnetic Beam Propagation in Turbulent Media: An Update", Proc. of IEEE, **68**, (1980) pp. 1424–1443.
4. Greenwood, D. P., "Bandwidth specifications for adaptive optics systems", *J. Opt. Soc. Am.*, **67**, (1977) pp. 390–393.
5. Herrmann, J., "Cross Coupling and aliasing in modal wave-front estimation", *J. Opt. Soc. Am.*, **71**, (1981) 989–992.
6. Hufnagel, R. E., *Digest of Topical Meeting on Optical Propagation Through Turbulence* (Optical Society of America, Washington, D. C., 1974).
7. Hufnagel, R. E., *The Infrared Handbook* (Edited by Wolfe, W.L. & Zeiss, G.J.) 6-18 (Environmental Research Institute of Michigan, Michigan, 1978).
8. Miller, M. G., Zieske, P. L., "Turbulence Environmental Characterization", *RADC-TR- 79-131 (Rome Air Development Center*, Griffiss Air Force Base, N. Y., 1979).
9. Prokhorov, A. M., Bunkin, F. V., Gochelashvily, K. S., Shishov, V. I., "Laser Irradiance Propagation in Turbulent Media", Proc. of IEEE, **63**, (1975) pp. 790–811.
10. Tatarski, V. I., *The Effects Of The Turbulent Atmosphere On Wave Propagation*, U. S. Department Of Commerce, (1971).
11. Tyler, G. A., "The Magnitude of Angle-of-Arrival Jitter in Ground to Relay Mirror Propagation for Various Turbulence Models", *tOSC No. TR-6213* (The Optical Sciences Company, 1985).
12. Valley, G. C., "Isoplanatic degradation of tilt correction and short-term imaging syste", *Appl. Opt.*, **19**, (1980) pp. 574–577.
13. Yura, H. T., Tavis, M. T., "Centroid anisoplanatism", *J. Opt. Soc. Am. A*, **2**, (1985) pp. 765–773.

Chapter 5

Integral Evaluation with Mellin Transforms

In this chapter I continue the development of techniques for evaluating the wavenumber integrals in turbulence propagation theory. With appropriate normalization, the wavenumber (κ) integration can be expressed in a standard form depending only on zero, one, or more parameters. If no parameters are present, the integration is performed simply by table lookup as was done in the last chapter. The one parameter case requires a transformation of the integral into the complex plane that is subsequently evaluated by pole-residue techniques. Details of this process are considered in this chapter. Integrals with more than one parameter are evaluated by extensions of this technique and are considered in Chap. 10. Tatarski considered the evaluation of one-parameter integrals in which inner scale was finite. He expanded the function that multiplies the decaying exponential, which contains the inner scale, into a Taylor series, and integrated term by term. Since the integral over each term of the power series converges absolutely, this method is valid. Tatarski expressed the resulting power series as a hypergeometric function. His approach does not always work with zero inner scale and restricts the range of problems that can be solved. This limitation does not apply to the technique discussed here. The integrals evaluated here are of the form

$$I = \int_0^\infty dx\, x^a\, f\left(b\, x^c\right)\, g\left(d\, x^e\right), \tag{5.1}$$

where $f(x)$ and $g(x)$ are Meijer's G-functions, a special case of which are generalized hypergeometric functions. The only restriction on $a, b, c, d,$ and e is that the integral converges. Sometimes it will be required that $d^c/b^e \neq 1$.

A powerful method for evaluating these integrals is described by *Marichev* (1983). His method applies to all integrals whose integrand is the product of two generalized hypergeometric functions and a power of the integration variable. He shows that the integral, which can be transformed into a Mellin-Barnes integral in the complex plane, can be expressed as a finite sum of generalized hypergeometric functions or, equivalently, as a Meijer G-function.

He puts integrals into a standard form to which *Slater's* (1966) theorem applies. This is convenient for some problems and is also used here. However, for other problems this approach is not always convenient. The calculation of the

Strehl ratio in turbulence in Chap. 8 is an example. The Strehl ratio for uncorrected turbulence can be written as the sum of six generalized hypergeometric functions of the form ${}_6F_{11}[\,]$. This form is not convenient for either obtaining physical insight or in numerical evaluation. For these cases, I short circuit the step of transforming the integrand into standard form, since I can obtain the answer as a more convenient infinite series.

The parameters in the integrand can be less than or greater than unity. For small parameter values the Taylor series is useful, and for large values an asymptotic solution is sometimes applicable. Each of these solutions is obtained in a straightforward manner. The Taylor series can be expressed as generalized hypergeometric functions. For the problems considered in this book, the solutions will be given both as generalized hypergeometric and power series.

In this chapter the theory of using Mellin transforms to obtain both Taylor series and asymptotic solutions is given. The formulas are a generalization of those given by *Marichev* (1983) and apply to cases where coefficients of the complex variable in gamma functions need not be unity. I discuss examples with repeated poles in the complex plane, which give rise to characteristic logarithmic terms.

Computer algebra programs can often be used to obtain the evaluation of integrals that result in generalized hypergeometric functions. With these programs it is no longer necessary to use the Mellin transform techniques to obtain these functions. However, at the present time these programs do not provide the asymptotic solution. Often there are numerical difficulties in evaluating these functions for some parameter ranges. In the table at the end of this chapter formulas are given to obtain the asymptotic solution.

5.1 Integral Evaluation with One Parameter

The Mellin transform pair is given by

$$h(x) \rightarrow H(s) \equiv M\left[h\left(x\right)\right] \equiv \int_0^\infty \frac{dx}{x}\, h(x)\, x^{\,s}, \quad \text{and} \tag{5.2}$$

$$h(x) = \frac{1}{2\pi i} \int_C ds\, H(s)\, x^{-s}. \tag{5.3}$$

The integral in eq. 5.2 only converges when the value of s is within certain limits. The integration path in the inverse transform goes from $\eta - i\infty$ to $\eta + i\infty$, and the value of the real part of s along the integration path is determined by convergence properties of the function.

The Mellin transform of any function that can be expressed as a generalized hypergeometric function times a power of the integration variable is a ratio of gamma functions as discussed in Sec. 1.3. This category includes most common functions such as algebraic, exponential, trigonometric, inverse trigonometric,

hyperbolic, logarithmic, complete elliptic, sine and cosine integrals, error functions, incomplete gamma, parabolic cylinder, Gegenbauer polynomials, Hermite, Laguerre, Whittaker, Legendre, Bessel, and other orthogonal functions. The Mellin transform of these functions and others are given in Appendix A.

Marichev (1983) lists 1200 Mellin transforms that are expressed as the ratio of gamma functions. There is also a similar list in *Prudnikov* et al. (1990). *Oberhettinger* (1974) also has an extensive list of Mellin transforms, but they are not all expressed as ratios of gamma functions. Table 1.1 contains Mellin transforms of functions that are used for problems of wave propagation in turbulence. Other transforms are in Appendix A. The range of s for which the integral converges is also given.

The Mellin transform definition and a list of Mellin transforms is all that is necessary to solve many simple problems as in Chap. 4. More complicated problems are solved with the Mellin convolution integral, which is the parallel to the Fourier convolution integral. This was derived in Sec. 1.2 as

$$h(x) = \int_0^\infty \frac{dy}{y}\, h_0(y)\, h_1(x/y) \rightarrow \mathcal{M}\left[h\left(x\right)\right] \equiv H(s) = H_0(s) H_1(s). \tag{5.4}$$

Notice the appearance of the multiplier $1/y$, and the appearance of $1/y$ in the argument of the second function. Obtaining the Mellin transform of a function in which the variable is the reciprocal of the usual variable, as required above, is trivially obtained by the replacement of s by $-s$ in the function's Mellin transform, as in eq. 1.9. The single parameter in eq. 5.4 is x or its inverse.

Using this formula one can transform the general integral given in the introduction to this chapter into an integral in the complex plane as

$$\begin{aligned} I &= \int_0^\infty dw\, w^a\, f\left(b\, w^c\right)\, g\left(d\, w^e\right) \\ &= \frac{b^{-(1+a)/c}}{e\, c} \frac{1}{2\pi\, i} \int_C ds\, \left(d^{1/e}\, b^{-1/c}\right)^s\, F\left(\frac{s+a+1}{c}\right)\, G\left(-\frac{s}{e}\right) \end{aligned} \tag{5.5}$$

for $c > 0$. When $c < 0$, the sign of the result changes. F and G are the Mellin transforms of f and g. The integration path in the complex plane has to be consistent with the restrictions on s in the individual Mellin transforms. The integral in the complex plane can always be performed with the methods to be discussed when $d\, b^{-e/c}$ is not equal to unity.

In the single parameter case, one evaluates the integral in the complex plane by closing the integration path in a clockwise or counterclockwise direction depending on the integrand. By Cauchy's residue theorem the value of the integral is $2\pi i$ times the sum of residues of the enclosed poles. *The sign of the residues for the poles going to infinity are positive whether the path is closed in a clockwise or counterclockwise direction. The change in path direction is negated by the change in sign of s in the gamma function. The sign of the residues is negative*

for poles that are on the other side of the integration path as a result of series terms being subtracted from the function.

I now develop a method for evaluating the integral as a Taylor or asymptotic series that gives an accurate answer with the fewest number of terms for the case of a a single parameter. Since each Mellin transform in eq. 5.5 is the ratio of gamma functions, the general form of the integral in the complex plane is a Mellin-Barnes integral given by

$$h(x) = \frac{1}{2\pi i} \int_{C'} ds\, x^{-s}\; \frac{\prod_{i=1}^{A} \Gamma\,[a_i + \alpha_i\, s] \prod_{j=1}^{B} \Gamma\,[b_j - \beta_j\, s]}{\prod_{k=1}^{C} \Gamma\,[c_k + \gamma_k\, s] \prod_{m=1}^{D} \Gamma\,[d_m - \delta_m\, s]}\,. \tag{5.6}$$

The terms are arranged so that all coefficients of s are positive. The poles closest to the coordinate axis and integration path for a typical integral are shown in Fig. 5.1. In general, x can be negative or complex, as it is in the beam-wave case. For infinite waves x is positive and real. This is the case considered in this chapter. The general case of complex x is treated in Chap. 8. The integration path can have all poles of a gamma function on one side of the integration path or can split its poles. In all the turbulence problems considered so far, the integration path had all the poles or all the poles but the first and rarely the second on one side of the integration path. The methods developed here allow one to evaluate the integral regardless of the pole locations.

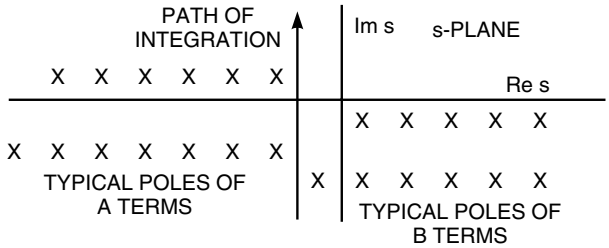

Figure 5.1. Typical integration path and pole locations for the general integral. The poles extend to infinity in both directions.

The general integral in eq. 5.6 for all the poles of an individual gamma function to one side of the integration path can be expressed as a Fox H-function, defined in eq. 1.39, as

$$h(x) = H^{B,\,A}_{A+D,\,B+C}\left[\frac{1}{x}\,\middle|\,\begin{matrix}(1-a_1,\alpha_1)\,,\ldots,(1-a_A,\ \alpha_A)\,,(d_1,\delta_1)\,,\ldots,(d_D,\delta_D)\\ (b_1,\beta_1)\,,\ldots,(b_B,\beta_B)\,,(1-c_1,\gamma_1)\,,\ldots,(1-c_C,\gamma_C)\end{matrix}\right]. \tag{5.7}$$

Since this function is not readily evaluated with current software, I generally do not express the integral in this form but as generalized hypergeometric functions.

If software becomes available to evaluate the Fox H-function, this form, which is found by inspection, would become the form of choice.

To apply Cauchy's residue theorem, the integration path must be closed at infinity. Marichev considered the conditions that allow closing the path along the infinite semicircle when the coefficients of s in the gamma functions in eq. 5.6 are unity. In this form it is easy to reduce the integrals to sums of generalized hypergeometric functions. One can obtain unity coefficients when all the coefficients of s are rational by the substitution $s = a\,y$, where a is the least common denominator of the coefficients of s. This substitution makes all the coefficients of y integers, and application of the Gauss-Legendre multiplication formula given in eq. 1.15, results in unity coefficients of y. The number of gamma functions is equal to the sum of the coefficients of y. Using that procedure, one arrives at final answers that are sometimes the sum of many high-order generalized hypergeometric functions. For some problems this form is not only lengthy to evaluate, but also it provides little physical insight. In such cases, a different procedure can be used. The coefficients of s are left as they are, and the final answer is obtained as a rapidly converging series in powers of the parameters. This method works even if the coefficients are irrational. Separate power series are obtained for large and small parameter values, while under certain conditions for large parameter values, an asymptotic solution can be obtained. For many problems one can reduce the integral to sums of a few generalized hypergeometric functions.

Pole-residue integration is the method used to evaluate these integrals. To apply this method, the integration path must be closed in the complex plane, and the value of the integral is $2\pi i$ times the sum of the residues at the enclosed poles. The only singularities of $\Gamma\left[a_i + \alpha_i\, s\right]$ are simple poles that occur when $s = -\left(n + a_i\right)/\alpha_i$ with residues equal to $(-1)^n/\alpha_i\, n\,!$. The resulting residue sum is a power series of the parameter that can be expressed as

$$h(x) = \sum_n x^{-s_n}\, G\left(s_n\right), \tag{5.8}$$

where $G\left(s_n\right)$ is the residue at the pole occurring at s_n. The summation is over all poles enclosed within the integration path. To close the path on the infinite semicircle without affecting the value of the integral, the integrand must decrease faster than $1/s$ for large values of s. Conditions for convergence along the semicircle in the left half plane are now obtained.

To determine whether the integration path can be closed in the left half plane, the asymptotic behavior of the integrand must be examined. The behavior of the gamma function for large arguments is given by Stirling's formula

$$\Gamma\left[s\right] \sim \sqrt{2\pi}\; s^{s-1\;2} \exp(-s)\left[1 + 1/(12\,s) + 1/(288\,s^2)\; + \cdots\right], \quad \left|\arg\{s\}\right| < \pi. \tag{5.9}$$

This can be used to find the asymptotic form for the gamma functions with negative coefficients of s; however, it is not valid in the entire left half plane when the gamma function argument is positive. To obtain a valid expression, the duplication formula

$$\frac{1}{\Gamma[s]} = \frac{\sin(\pi s)}{\pi}\Gamma[1-s] \tag{5.10}$$

is used to eliminate the gamma functions with positive coefficients of s; this results in an integrand of the following form

$$In = x^{-s}\pi^{A-C}\ \frac{\prod_{j=1}^{B}\Gamma[b_j-\beta_j s]\prod_{k=1}^{C}\Gamma[1-c_k-\gamma_k s]\ \sin[(c_k+\gamma_k s)\pi]}{\prod_{m=1}^{D}\Gamma[d_m-\delta_m s]\prod_{i=1}^{A}\Gamma[1-a_i-\alpha_i s]\ \sin[(a_i+\alpha_i s)\pi]}. \tag{5.11}$$

All constants are assumed to be real, and in addition, the coefficients of s are assumed to be non-negative. To examine behavior at negative infinity, the following two relations are necessary

$$\lim_{s\to-\infty}\sin[(a+\alpha s)\pi] = O\left[\exp\left(\alpha\pi\ |\mathrm{Im}\{s\}|\right)\right], \quad \text{and} \tag{5.12}$$

$$\lim_{s\to-\infty}\Gamma[s] = O\left\{\exp\left[(s-1/2)\ln(s)-s\right]\right\}. \tag{5.13}$$

The symbol O is used to denote the quantity's order of magnitude. Using these relations in the integrand, rearranging terms, and using the definitions in Table 5.1, one shows the integrand is

$$\begin{aligned} In = O\big(\exp\{&\Delta\mathrm{Re}(s)\ln|s| + (-\ln|s| - \Delta + \Delta')\,\mathrm{Re}(s) + (\nu - \Xi/2)\ln|s| \\ &+ |\mathrm{Im}(s)|\ [\Xi\arg\{-s\} + \pi(C'-A')] + \mathrm{Im}(s)\arg(-s)\}\big). \end{aligned} \tag{5.14}$$

It is assumed that the original integral converged; therefore, the sign of the exponent as the integration path goes to $\pm\infty$ along the imaginary axis does not have to be considered. The sign of the exponent must be negative for the integral along the semicircle to be negligible. There is a hierarchy of terms that determine the properties at infinity. The terms in decreasing order of importance are $\mathrm{Re}\{s\}\ln|s|$, $\mathrm{Re}\{s\}$, and $\ln|s|$. *The sign of these terms determines the direction of path closure.*

The dominant term that determines the sign of the exponent at infinity is $\Delta\mathrm{Re}\{s\}\ln|s|$. Δ is the sum of the coefficients of s in the numerator gamma functions minus those in the denominator. If $\Delta > 0$, the integral can be closed in the left half plane. A similar analysis shows that when $\Delta < 0$ the integral can be closed in the right half plane without changing the value of the integral. For both cases, a single power series that applies to all parameter values is obtained, and it converges quickly for small values of the parameter. For large parameter values the series converges slowly, and there can be numerical difficulties when one evaluates a summation composed of large terms that may alternate in sign. In this parameter regime, an asymptotic solution is appropriate, and the method to derive this solution is discussed in the next section.

If $\Delta = 0$, the term with $(-\ln|x| + \Delta')\,\mathrm{Re}\{s\}$ is the most important. Let

$$\Pi = -\ln|x| + \Delta'. \tag{5.15}$$

For $\Pi < 0$, the path can be closed in the right half plane. For $\Pi > 0$, the path can be closed in the left half plane. Typically, if $\Delta = 0$, then also $\Delta' = 0$, and in that case, for $|\,x\,| > 1$ the path can be closed in the right half plane, while for $|\,x\,| < 1$ the path can be closed in the left half plane. Here, separate power series for large and small values of x are obtained, and both converge rapidly, except possibly close to x equal to unity.

If both $\Delta = 0$ and $\Pi = 0$, the integrand behaves as

$$I = O\left[s^{(\nu - \Xi/2)}\right]. \tag{5.16}$$

For convergence on the infinite semicircle, the integrand has to decrease faster than $1/s$, and this gives the condition

$$\Omega = \nu - \Xi/2 + 1 < 0. \tag{5.17}$$

If this condition is satisfied, the integration path can be closed in either direction. If this condition is not satisfied, the path cannot be closed at infinity, and pole-residue integration cannot be used.

To illustrate the technique consider the integral

$$I = \int_0^\infty \frac{dy}{y}\; y^\mu \exp(-ay)\, J_\nu(by)\,. \tag{5.18}$$

After normalizing by letting $x = ay$, one can convert the integral into one in the complex plane with the Mellin convolution integral, the Mellin transforms in eq. 1.47 and eq. 1.51, and the relation in eq. 1.8, to give

$$I = \frac{1}{2\,a^\mu}\frac{1}{2\pi\,i}\int_C ds\,\left(\frac{2a}{b}\right)^{-s}\,\Gamma\left[\begin{matrix} s+\mu,\; -s/2+\nu/2 \\ s/2+\nu/2+1 \end{matrix}\right]. \tag{5.19}$$

With the use of eq. 1.39 the solution can be written by inspection as a Fox H-function

$$I = \frac{1}{2\,a^\mu} H_{1,\,2}^{1,\,1}\left[\left(\frac{2\,a}{b}\right)\,\middle|\,\begin{matrix}(1-\mu,\;1) \\ (\nu/2,\;1/2)\,,\;(-\nu/2,\;1/2)\end{matrix}\right]. \tag{5.20}$$

To express this as a Meijer G-function, make the substitution $s \to 2\,s$ in eq. 5.19 and use the multiplication formula in eq. 1.16 to obtain

$$I = \frac{1}{2\sqrt{\pi}}\left(\frac{2}{a}\right)^\mu \frac{1}{2\pi\,i}\int_C ds\,\left(\frac{b}{a}\right)^{2s}\,\Gamma\left[\begin{matrix} s+\mu/2,\; s+\mu/2+\frac{1}{2},\; -s+\nu/2 \\ s+\nu/2+1 \end{matrix}\right]. \tag{5.21}$$

From eq. 1.40 the solution can be written as

$$I = \frac{1}{2\sqrt{\pi}}\left(\frac{2}{a}\right)^\mu\, G_{2,\,2}^{1,\,2}\left[\left(\frac{b}{a}\right)^2\,\middle|\,\begin{matrix}1-\mu/2,\;1/2-\mu/2 \\ \nu/2,\;-\nu/2\end{matrix}\right]. \tag{5.22}$$

The solution can also be expressed as a generalized hypergeometric function. Since $\Delta = 0$ in eq. 5.21, for $b/a > 1$ close the integration path to the right and obtain pole contributions at $s = \nu/2 + n$ for $n = 0, 1, \ldots$. The value of the integral is

$$I = \frac{2^{\mu-1} b^{\nu}}{\sqrt{\pi}\, a^{\nu+\mu}} \sum_{n=0}^{\infty} \frac{(-1)^n}{n!} \left(\frac{b}{a}\right)^{2n} \Gamma\left[\begin{matrix} n + \frac{\mu+\nu}{2},\ n + \frac{\mu+\nu+1}{2} \\ n + \nu + 1 \end{matrix}\right]. \tag{5.23}$$

Use the rules in Sec. 1.3 to convert this into a generalized hypergeometric function, and use the multiplication formula to simplify the expression to

$$I = \left(\frac{b}{2\,a}\right)^{\nu} a^{-\mu} \Gamma\left[\begin{matrix} \nu + \mu \\ \nu + 1 \end{matrix}\right] {}_2F_1\left[\begin{matrix} \frac{\mu+\nu}{2}, \frac{\mu+\nu+1}{2}; \nu + 1; -\left(\frac{b}{a}\right)^2 \end{matrix}\right], \quad b > a. \tag{5.24}$$

This is the same formula as in *Gradshteyn* and *Ryzhik* (1980, eq. 6.621 #1).

When $a/b > 1$ the integration path is closed to the left, and one obtains pole contributions at $s = -n - \mu/2$, and $s = -n - \mu/2 - 1/2$ for $n = 0, 1, \ldots$. The value of the integral expressed as generalized hypergeometric functions is

$$\begin{aligned} I = {} & \frac{1}{2}\left(\frac{2}{b}\right)^{\mu} \Gamma\left[\begin{matrix} \frac{\nu+\mu}{2} \\ \frac{\nu-\mu+2}{2} \end{matrix}\right] {}_2F_1\left[\begin{matrix} \frac{\mu+\nu}{2}, \frac{\mu-\nu}{2}; \frac{1}{2}; -\left(\frac{a}{b}\right)^2 \end{matrix}\right] \\ & - \frac{a}{b}\left(\frac{2}{b}\right)^{\mu} \Gamma\left[\begin{matrix} \frac{\nu+\mu+1}{2} \\ \frac{\nu-\mu+1}{2} \end{matrix}\right] {}_2F_1\left[\begin{matrix} \frac{\mu+\nu+1}{2}, \frac{\mu-\nu+1}{2}; \frac{3}{2}; -\left(\frac{a}{b}\right)^2 \end{matrix}\right], \quad a > b. \end{aligned} \tag{5.25}$$

I now examine the convergence properties when $a = b$, in which case the integral is

$$I = \int_0^{\infty} \frac{dy}{y}\, y^{\mu} \exp(-y)\, J_{\nu}(y). \tag{5.26}$$

Equation eq. 5.17 states that the solution in eq. 5.24 converges when $\mu < 1/2$. This is equivalent to the third condition given after eq. 1.34. The integral converges even if this requirement is not satisfied; however, Mellin transform techniques do not apply. It will be shown in Chap. 10 that the single point at which the method does not apply expands to a finite volume when there is more than one parameter.

An integral can also be evaluated easily when an integrand factor has the first term of its power series subtracted. Consider, e.g.,

$$I = \int_0^{\infty} \frac{dy}{y}\, y^{\mu} \left[\exp(-ay) - 1\right] J_{\nu}(by). \tag{5.27}$$

With this change eq. 5.21 becomes

$$I = \frac{2^{\mu-1}}{\sqrt{\pi}\, a^{\mu}} \frac{1}{2\pi i} \int_C ds \left(\frac{b}{a}\right)^{s} \Gamma\left[\begin{matrix} s + \mu/2*,\ s + \mu/2 + \frac{1}{2},\ -s + \nu/2 \\ s + \nu/2 + 1 \end{matrix}\right], \tag{5.28}$$

where the asterisk indicates that the integration path falls between the first and second poles of a gamma function. The solution in this case is simply the solution above with one series term moved from the expression valid for $a > b$ to the one for $a < b$ to give

$$I = \left(\frac{b}{2\,a}\right)^{\nu} a^{-\mu}\Gamma\left[\begin{matrix}\nu+\mu\\ \nu+1\end{matrix}\right]{}_2F_1\left[\tfrac{\mu+\nu}{2},\tfrac{\mu+\nu+1}{2};\nu+1;-\left(\frac{b}{a}\right)^2\right]$$
$$-\frac{1}{2}\left(\frac{2}{b}\right)^{\mu}\Gamma\left[\begin{matrix}\frac{\nu+\mu}{2}\\ \frac{\nu-\mu+2}{2}\end{matrix}\right],\quad b > a,\ \text{and} \tag{5.29}$$

$$I = \frac{1}{2}\left(\frac{2}{b}\right)^{\mu}\Gamma\left[\begin{matrix}\frac{\nu+\mu}{2}\\ \frac{\nu-\mu+2}{2}\end{matrix}\right]\left\{{}_2F_1\left[\tfrac{\mu+\nu}{2},\tfrac{\mu-\nu}{2};\tfrac{1}{2};-\left(\frac{a}{b}\right)^2\right]-1\right\}$$
$$-\frac{a}{b}\left(\frac{2}{b}\right)^{\mu}\Gamma\left[\begin{matrix}\frac{\nu+\mu+1}{2}\\ \frac{\nu-\mu+1}{2}\end{matrix}\right]{}_2F_1\left[\tfrac{\mu+\nu+1}{2},\tfrac{\mu-\nu+1}{2};\tfrac{3}{2};-\left(\frac{a}{b}\right)^2\right],\quad a > b. \tag{5.30}$$

The first function on the right of the last equation can be expressed as another generalized hypergeometric function with the relation in eq. 1.42 to obtain

$$I = \left(\frac{a}{b}\right)^2\left(\frac{2}{b}\right)^{\mu}\Gamma\left[\begin{matrix}\frac{\nu+\mu+2}{2}\\ \frac{\nu-\mu}{2}\end{matrix}\right]{}_3F_2\left[\tfrac{\mu+\nu+2}{2},\tfrac{\mu-\nu+2}{2},1;\tfrac{3}{2},2;-\left(\frac{a}{b}\right)^2\right]$$
$$-\frac{a}{b}\left(\frac{2}{b}\right)^{\mu}\Gamma\left[\begin{matrix}\frac{\nu+\mu+1}{2}\\ \frac{\nu-\mu+1}{2}\end{matrix}\right]{}_2F_1\left[\tfrac{\mu+\nu+1}{2},\tfrac{\mu-\nu+1}{2};\tfrac{3}{2};-\left(\frac{a}{b}\right)^2\right],\quad a > b. \tag{5.31}$$

Similarly, the integral can be evaluated when the first term of the power series is subtracted from the second factor in the integrand in eq. 5.18

$$I = \int_0^{\infty}\frac{dy}{y}\ y^{\mu}\exp\left(-ay\right)\ \left[J_{\nu}\left(by\right)-\frac{1}{\Gamma\left[\nu+1\right]}\left(\frac{by}{2}\right)^{\nu}\right]. \tag{5.32}$$

In this case the asterisk is associated with the third numerator gamma function in eq. 5.21. The integral can be evaluated to give

$$I = \frac{1}{2}\left(\frac{2}{b}\right)^{\mu}\Gamma\left[\begin{matrix}\frac{\nu+\mu}{2}\\ \frac{\nu-\mu+2}{2}\end{matrix}\right]{}_2F_1\left[\tfrac{\mu+\nu}{2},\tfrac{\mu-\nu}{2};\tfrac{1}{2};-\left(\frac{a}{b}\right)^2\right]-\left(\frac{b}{2\,a}\right)^{\nu}a^{-\mu}\Gamma\left[\begin{matrix}\nu+\mu\\ \nu+1\end{matrix}\right]$$
$$-\frac{a}{b}\left(\frac{2}{b}\right)^{\mu}\Gamma\left[\begin{matrix}\frac{\nu+\mu+1}{2}\\ \frac{\nu-\mu+1}{2}\end{matrix}\right]{}_2F_1\left[\tfrac{\mu+\nu+1}{2},\tfrac{\mu-\nu+1}{2};\tfrac{3}{2};-\left(\frac{a}{b}\right)^2\right],\quad a > b,\ \text{and} \tag{5.33}$$

$$I = \left(\frac{b}{2\,a}\right)^{\nu}a^{-\mu}\Gamma\left[\begin{matrix}\nu+\mu\\ \nu+1\end{matrix}\right]\left\{{}_2F_1\left[\tfrac{\mu+\nu}{2},\tfrac{\mu+\nu+1}{2};\nu+1;-\left(\frac{b}{a}\right)^2\right]-1\right\},\quad b > a. \tag{5.34}$$

Using eq. 1.42 one can show that the last expression is

$$I = -\left(\frac{b}{2\,a}\right)^{\nu+2}a^{-\mu}\Gamma\left[\begin{matrix}\nu+\mu+2\\ \nu+2\end{matrix}\right]$$

$$\times {}_3F_2\left[\frac{\mu+\nu+2}{2}, \frac{\mu+\nu+3}{2}, 1; \nu+2, 2; -\left(\frac{b}{a}\right)^2\right], \quad b > a. \tag{5.35}$$

To summarize, if $\Delta \neq 0$, a solution is obtained for any parameter value. If $\Delta = 0$, a solution is found for all parameter values except for certain conditions, when the solution is not found for the parameter equal to unity.

5.2 Asymptotic Solutions

Asymptotic solutions are often used to obtain insight into the behavior of a solution for large parameter values and to ease the computations. There are many techniques to obtain an asymptotic solution. The Mellin transform technique is applicable to a wide variety of problems, including all turbulence problems—but by no means to all. *Wong* (1989) discusses several ways to find asymptotic solutions. He has a small section on Mellin transforms that is not as general as that presented here. Many of the examples that he solves by other techniques could be solved by the Mellin transform method. In general, Mellin transform techniques are underutilized.

When $\Delta = 0$, separate power series are obtained for small and large parameter values. Each Taylor series has good convergence properties except possibly when the parameter is equal to one, which allows them to be readily evaluated without numerical difficulties. The solution for large parameters is a convergent Taylor series. I do not refer to such a solution as an asymptotic solution. Wong calls these asymptotic series. I reserve the term asymptotic series for non- convergent series.

When $\Delta \neq 0$, a single power series is obtained, which converges slowly for large parameter values. To overcome numerical difficulties, for large parameter values an asymptotic solution is preferred. One finds the asymptotic solution not by closing the integration path at infinity, but by deforming the integration path to go through a saddle point in the direction of steepest descent as shown in Fig. 5.2. The asymptotic solution is composed of the two contributions from poles crossed in the path deformation and from the steepest-descent integration. The steepest-descent contribution can be found for complex parameters; however, this is more complicated than that for real values. The case when x is positive real is the only one considered in this chapter. The general case is considered in Chap. 8.

The value of the integral along the new integration path is found by a modification of the method of steepest descent. In this method the path is deformed from the original path to a path through a saddle point such that the function's value decreases most rapidly along the path away from the saddle point. Along this new path, the value of the integrand is a maximum at the saddle point and decreases away from it. For large parameter values, the saddle point is located at a large value of s in the complex plane. Near the saddle point one writes

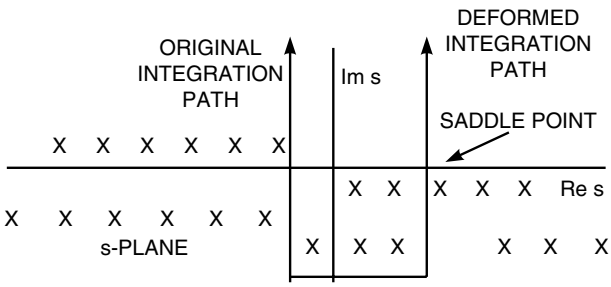

Figure 5.2. Original and deformed integration paths used to evaluate the asymptotic series.

$$I = \int_C ds\, \exp\left[f(s)\right]. \tag{5.36}$$

Write the argument of the exponent as a Taylor series given by

$$f(s) \approx f\left(s_o\right) + \frac{df\left(s_o\right)}{ds}\left(s - s_o\right) + \frac{1}{2}\frac{d^2 f\left(s_o\right)}{ds^2}\left(s - s_o\right)^2. \tag{5.37}$$

It may be shown that if the parameter is very large, then only these three terms are necessary to express the value of the integral with sufficient accuracy. At a saddle point, the value of the first derivative is zero. This condition gives equations to determine the real and imaginary parts of s_o at the saddle point. It will be seen that the contribution of derivative terms higher than the second to the integral are small compared to the second and can be normally neglected. The integral along this path is approximately that of a Gaussian function with infinite limits that is easily evaluated to give

$$I \approx \int_C ds\, \exp\left[f\left(s_o\right) + \frac{1}{2}\frac{d^2 f\left(s_o\right)}{ds^2}\left(s - s_o\right)^2\right] = \sqrt{-\frac{2\pi}{d^2 f\left(s_o\right)/ds^2}}\, \exp\left[f\left(s_o\right)\right]. \tag{5.38}$$

This is the first term of the asymptotic expansion. Additional terms can be found if desired by the inclusion of more terms in the expansion of $f(s)$ in eq. 5.37. For problems examined to date, the first term of the asymptotic series gives sufficient accuracy to get a seamless fit between the Taylor and asymptotic series. For that reason, it is the only one evaluated here.

The asymptotic value of the integral has contributions from poles crossed in the path deformation, in addition to the steepest-descent contribution. Under certain conditions, one of these two terms dominates, and the other can be neglected. If there are no poles to the right of the original integration path, the steepest-descent contribution must always be included. The pole contribution decays algebraically with the parameter. I show below that the steepest-descent contribution can vary sinusoidally, can have exponential decay, or can have exponential growth. For the sinusoidal variation, both pole and steepest-descent

contributions are important, and both must be retained. When the steepest-descent contribution decays exponentially, it can be neglected if there are any pole contributions. If the steepest-descent contribution increases exponentially, pole contributions are negligible. Conditions that allow the steepest-descent contribution to be neglected will be considered later.

The asymptotic value of the integral in eq. 5.90 is now found. Only the case $\Delta > 0$ needs to be considered. In this case, the integration path can be closed in the left half plane to obtain the convergent power series. If $\Delta < 0$, the substitution $s \to -s$ transforms the integral to one in which $\Delta > 0$, and the results derived below again apply. For the asymptotic series, the behavior of the integrand in the right half plane must be examined. As a simple case, the asymptotic series for $B = D = 0$ in eq. 5.90 will be derived first. (This case also encompasses the situation in which $B = D$, but all the poles of the B gamma functions are cancelled by poles of the denominator gamma functions. In this case the ratio of gamma functions can be replaced by a polynomial.) When there are no poles in the right-half plane, the asymptotic series does not have a branch cut in the right half plane, and the evaluation of the steepest-descent contribution is straightforward. The behavior of the integrand for large s is needed. Unlike the order of magnitude calculation previously made to determine whether the integral converges on an infinite circle, more accurate integrand estimates are required to obtain the actual value of the integral. The asymptotic form of a gamma function is

$$\Gamma\left[a_i + \alpha_i\, s\right] \sim \sqrt{2\pi}\, \exp\left[\left(a_i + \alpha_i\, s - 1/2\right)\, \ln\left(a_i + \alpha_i\, s\right) - a_i - \alpha_i\, s\right]. \tag{5.39}$$

The following approximation for the logarithm is used

$$\ln\left(a_i + \alpha_i\, s\right) = \ln\left[\alpha_i\, s\ \left(1 + a_i/\alpha_i\, s\right)\right] \approx \ln\left(\alpha_i\right) + \ln\left(s\right) + a_i/\alpha_i\, s. \tag{5.40}$$

If these are inserted into eq. 5.6 and a similar expansion is performed for the other gamma functions, one obtains

$$\begin{aligned} h\left(x\right) = \frac{\left(2\pi\right)^{\Xi/2}}{2\pi\, i} \int\limits_C ds \exp\left\{\Delta'' - \Delta'''/2\right. \\ \left. + s\left[\Delta' - \Delta - \ln\left(x\right)\right] + \ln(s)\left(\nu - \Xi/2\right) + \Delta s \ln(s)\right\}. \end{aligned} \tag{5.41}$$

The new symbols introduced above are defined in Table 5.1.

If the exponent is designated by $f(s)$, the saddle point is located at

$$\frac{df(s)}{ds} = 0 = \left[\Delta' - \Delta - \ln\left(x\right)\right] + \frac{\nu - \Xi/2}{s} + \Delta\, \left[1 + \ln\left(s\right)\right]. \tag{5.42}$$

Since $|s|$ is large (I will check this below by consistency), its value can be approximated by

$$\ln\left(s_o\right) \approx \left[\ln\left(x\right) - \Delta'\right]/\Delta, \tag{5.43}$$

which yields

$$s_o = x^{1/\Delta} \exp\left(-\Delta'/\Delta\right). \tag{5.44}$$

The value of s_o is large and positive since x is large; this agrees with the assumption that the integration path was to be moved far into the right half plane.

The second derivative is

$$\frac{d^2 f(s_o)}{ds^2} = -\frac{\nu - \Xi/2}{s_o^2} + \frac{\Delta}{s_o} \approx \frac{\Delta}{s_o}. \tag{5.45}$$

Since this is positive in the right half plane, the steepest-descent path must be in the imaginary direction as shown in Fig. 5.2 to make the quadratic term in eq. 5.37 negative. Each higher-order derivative has an increasingly higher power of s in the denominator. Therefore, the higher-order derivatives are small compared to the second, and the assumption that $f(s)$ can be accurately expressed as a constant term plus a quadratic term is valid. If these values are substituted into eq. 5.38, one obtains for the steepest-descent contribution

$$E(x) = \frac{(2\pi)^{(\Xi-1)/2}}{\sqrt{\Delta}} x^{\rho} \exp\left[-\Delta\, x^{1/\Delta} \exp\left(-\Delta'/\Delta\right) + \Delta'' - \Delta'''/2 - \rho\Delta'\right], \tag{5.46}$$

where $\rho = \left[\nu + (1-\Xi)/2\right]/\Delta$. For most problems encountered in propagation through turbulence one has the condition, $\Delta' = \Delta'' = \Delta''' = 0$. For that case one obtains the expression used by *Marichev* (1983, eq. 4.40)

$$E(x) = \frac{(2\pi)^{(\Xi-1)/2}}{\sqrt{\Delta}} x^{\rho} \exp\left(-\Delta\, x^{1/\Delta}\right). \tag{5.47}$$

This solution has an exponential decay and can be neglected if there are pole contributions.

The more general case has B and D not equal to zero in eq. 5.11. This case is more complicated since one must deal with the multi-valued nature of the asymptotic behavior of the functions. *Luke* (1969) derives expressions for this case, and a similar approach can be used to obtain the steepest-descent contribution for the case where the coefficients of s in the gamma functions are not unity. The details of this derivation are considered in Chap. 8 where x is allowed to be complex. The result for $\Lambda' \geq 0$ is

$$\begin{aligned} E(x) &= \frac{2(2\pi)^{(\Xi-1)/2}}{\sqrt{\Delta}} x^{\rho} \\ &\times \exp\left[-\Delta x^{1/\Delta} \exp\left(-\Delta'/\Delta\right) \cos\left(\pi\Lambda'/\Delta\right) + \Delta'' - \Delta'''/2 - \rho\Delta'\right] \\ &\times \cos\left[\Delta x^{1/\Delta} \exp\left(-\Delta'/\Delta\right) \sin\left(\pi\Lambda'/\Delta\right) + \pi\left(-\rho\Lambda' - \Lambda'' + \Lambda/2\right)\right]. \end{aligned} \tag{5.48}$$

Notice the factor of 2 that multiplies this expression that is not present in eq. 5.47. This is a consequence of the addition of two steepest-descent contributions that are complex conjugates of each other. In eq. 5.93 if $B = D = 0$ or, equivalently, if the argument of the second cosine is zero, then the answer

must be divided by two. If $\Lambda' < 0$, then the steepest-descent contribution has exponential decay. The decay coefficient is found with the procedure discussed in Sec. 8.2. For the simpler case that applies to many problems of interest in which

$$\Delta' = \Delta'' = \Delta''' = 0, \quad B = B', \text{ and } D = D', \tag{5.49}$$

one obtains a result equivalent to that obtained by *Marichev* (1980, eq. 4.51)

$$E(x) = \frac{2(2\pi)^{(\Xi-1)/2}}{\sqrt{\Delta}} x^{\rho} \exp\left[-\Delta x^{1/\Delta} \cos\left(\pi\Lambda/\Delta\right)\right] \times \cos\left\{\Delta x^{1/\Delta} \sin\left(\pi\Lambda/\Delta\right) + \pi\left[\left(1/2-\rho\right)\Lambda - \Lambda''\right]\right\}. \tag{5.50}$$

Designate the sum of the residues of all poles crossed in the integration path deformation by $W(x)$. The general asymptotic solution is

$$h(x) \sim W(x) + E(x). \tag{5.51}$$

The general equations necessary to obtain $E(x)$ are given in Table 5.1. In some cases, one of E or W is insignificant compared to the other. That will be obvious once the terms are evaluated. Rather than always evaluating the steepest-descent contribution, one can state conditions in which only the pole contributions are significant for the asymptotic solution. These are

$$\text{If } B' > 0 \text{ and } \Lambda'/\Delta \neq 1/2, \text{ then} \quad h\left(x\right) \sim W\left(x\right). \tag{5.52}$$

In this case the asymptotic solution has pole contributions, and the steepest-descent contribution has exponential decay, which makes it negligible.

As an example of obtaining an asymptotic series, consider the inverse transform of the function considered in eq. 1.22

$$J_0(x) - 1 = 1over2\pi i \int_C ds\, \frac{1}{2}\left(\frac{x}{2}\right)^{-s} \Gamma\begin{bmatrix} s/2* \\ -s/2+1 \end{bmatrix}. \tag{5.53}$$

Using eq. 5.94 in eq. 5.51, one obtains the pole residue at $s = 0$, and the saddle point contribution, to get

$$J_0(x) - 1 \sim \sqrt{2/\pi x}\, \cos\left(x - \pi/4\right) - 1. \tag{5.54}$$

This is the standard result.

Asymptotic solutions have useful properties that allow them to be treated almost like Taylor series, and the ones obtained here are all of the Poincaré type (*Bleistein* and *Handelsman* 1986) that have the following characteristics:

1. The error in truncation is less than the first term neglected.
2. The asymptotic series of the sum or product of two functions is equal to the sum or product of the asymptotic series of the individual functions.

3. If the asymptotic series of the integral or derivative of a function exists, it is equal to the integral or derivative of the asymptotic series of that function.
4. The asymptotic series is unique for a given function.

As the number of terms in the asymptotic series is increased, the error in the value of the integral first decreases, and after some number of terms n_o starts to increase. The value of n_o can be found from the position of the steepest-descent path for a given parameter value. In practice, one does not evaluate n_o since a few terms of the asymptotic series give an accurate result for large parameter values.

$E(x)$ is the first term of the series representation of the asymptotic series. Typically, for most problems this answer is accurate enough. If more terms of the series are required, they can be obtained with Luke's approach. This approach is complicated, and different expressions apply for different conditions on the parameters. The details of this approach will not be given here since, for all problems considered so far, the first term is sufficient to produce a region of overlap in which the values obtained from the Taylor and the asymptotic series are very close to each other.

5.2.1 Alternate method of integral evaluation

The method of evaluating integrals presented in this chapter is straightforward in concept. One finds Taylor series by closing the integration path in a direction that does not change the value of the integral. For some problems an asymptotic solution is found by the addition of the residues of poles on the other side of the integration path to a steepest-descent contribution. In Chap. 10 I will consider the evaluation of integrals in multiple complex planes. A natural approach in this more complicated scenario would be to extend the technique developed in this chapter. Unfortunately, one encounters difficulties in trying to decide which pole-contributions to include in a solution. The Mellin convolution theorem leads to gamma functions that contain the sum of complex integration variables; this results in a problematic coupling of integration paths.

Fortunately, another approach does provide a conceptually straightforward generalization to several complex planes. This approach does not rely on considering how the contours must be closed. Instead, all power series arising from poles on either side of the integration are written down. One obtains the value of the integral by choosing the correct power series. The Taylor series solution is simply the sum of those power series that converge for the parameter size of interest.

The asymptotic solution is obtained in the following manner: Express all power series in terms of the parameter or its inverse, whichever gives a positive exponent. The asymptotic series is the sum of those diverging series for which the parameter in the series is less than unity. A steepest-descent contribution must be added to the asymptotic series to obtain a complete solution.

If the integration path splits the poles of a gamma function so that p poles are on the other side of the integration path, then that summation starts at the

index equal to p. If a series that starts with the index equal to p is excluded from the solution by the criteria above, then the series with index value varying from zero to p must be added to the solution.

It is easy to see that this approach gives the same answer as that obtained with the method expounded in this chapter. In this second method, one is not concerned with how contours are closed. The series that are selected from all possible power series are those with the appropriate convergence properties. This method can be applied directly to the evaluation of integrals in multiple complex planes. It is further developed in Chap. 10 and it is used in Chaps. 11 and 12 to solve specific problems.

5.3 Multiple Poles

I show in this section that the occurrence of multiple poles, although requiring special treatment, does not pose any conceptual difficulties when one calculates the power or asymptotic series. One finds the residue at a multiple pole by expanding all integrand functions into a Laurent series centered at the multiple-pole position, by multiplying *all* the series together, and by determining the coefficient of the resulting simple pole. This is illustrated with examples that contain double and triple poles.

In turbulence theory there are typically fractional powers in integrals. The Mellin transforms of the functions encountered in turbulence theory do not have multiple poles. The poles of the transforms of functions that multiply the fractional powers are at negative integers or halfway between the negative integers. When the fractional power is introduced in the convolution theorem, the poles of the convolved functions do not coincide. I have not encountered any problems in turbulence wave propagation that have multiple poles. However, in other contexts some of the functions in the integral can have Mellin transforms that have multiple poles. For that reason, the method to evaluate integrals in which multiple poles occur is developed here. Multiple poles have been encountered in the expansion of $K_\nu(x)$ in Chap. 1.

A function that has multiple poles and occurs in elementary particle physics is the polylogarithm. The polylogarithm function of order n, $L^n(z)$, arises from an integral with a multiple pole of order n. The definition is

$$L^n(z) = \frac{1}{2\pi i}\int_C ds\,\frac{\Gamma[s,\,-s]}{(-s)^{n-1}}\,(-z)^{-s}, \quad n = 0,\ 1,\ 2,\ \ldots\,. \tag{5.55}$$

This function is discussed extensively in Marichev. Its Mellin transform is given in Appendix A.

5.3.1 Expansion of integrand functions

To calculate the residue in the presence of a multiple pole, the functions in the integrand are expanded in power series at the pole, and the coefficient of the

simple pole term is calculated. To facilitate this process, in this section two expansions of the gamma function are derived: one when the singular point is not at a pole of the gamma function; the second when it is. The function z^{-s} is also expanded in a power series.

The expansion of the gamma functions is normally expressed in terms of the logarithmic derivative of the gamma function, defined by

$$\psi(z) \equiv \frac{d \ln(\Gamma[z])}{dz} = \frac{\Gamma'[z]}{\Gamma[z]}. \tag{5.56}$$

This psi or digamma function is given in *Gradshteyn* and *Ryzhik* (1980, eq. 8.362 #1) as

$$\psi(z) = -\mathbf{C} + \sum_{n=0}^{\infty} \left(\frac{1}{n+1} - \frac{1}{z+n} \right), \tag{5.57}$$

where $\mathbf{C}$ is Euler's constant, which is equal to 0.577216... . The derivative of the last expression gives the trigamma function

$$\psi'(z) = \sum_{m=0}^{\infty} \frac{1}{(z+m)^2}. \tag{5.58}$$

The higher order derivatives are given by

$$\frac{d^n \ln(\Gamma[z])}{dz^n} \equiv \psi^{(n)}(z) = (-1)^{n+1} n! \sum_{m=0}^{\infty} \frac{1}{(z+m)^{n+1}}. \tag{5.59}$$

These expressions can be summed numerically to find the values, which are most often needed: $\psi(1) = -\mathbf{C} = -0.577216$; $\psi(0.5) = -\mathbf{C} - 2\ln(2) = -1.964$; $\psi'(-0.5) = 4 - \pi^2/2 = 8.935$; $\psi(-0.5) = 2 - \mathbf{C} - 2\ln(2) = -0.03649$; $\psi'(0.5) = \pi^2/2 = 4.935$; and $\psi'(1) = \pi^2/5 = 1.645$.

For positive z one expands

$$\Gamma[z+\varepsilon] = \Gamma[z] \left\{ 1 + \varepsilon\, \psi(z) + \varepsilon^2 \left[\psi'(z) + \psi^2(z) \right] /2 + \cdots \right\}. \tag{5.60}$$

The Gamma function $\Gamma[s]$ has a pole at $s = -N$. To find the Laurent expansion about a pole use the identity

$$\Gamma[-N+\varepsilon] = \frac{(-1)^N}{\varepsilon} \frac{\Gamma[1+\varepsilon]\,\Gamma[1-\varepsilon]}{\Gamma[1+N+\varepsilon]}. \tag{5.61}$$

This identity can be proved with the recursion relation in eq. 1.14 and the identity $\Gamma[s]\,\Gamma[1-s] = \pi/\sin(\pi s)$. If each of the three gamma functions on the right is expanded with eq. 5.61, one gets the series representation

$$\Gamma[-N+\varepsilon] = \frac{(-1)^N}{\varepsilon N!} \sum_{n=0}^{\infty} a_n(N)\, \varepsilon^n. \tag{5.62}$$

The first few coefficients of this expansion are

$$a_0(N) = 1, \quad a_1(N) = \psi(1+N), \quad \text{and} \tag{5.63}$$

$$a_2(N) = \psi'(1) + [\psi^2(1+N) - \psi'(1+N)]/2. \tag{5.64}$$

Finally the Taylor series expansion of z^{-s} about the point $s = k$ is

$$z^{-s}\Big|_{s=k+\varepsilon} = z^{-k} \sum_{n=0}^{\infty} \frac{(-1)^n}{n\,!} \left[\ln(z)\right]^n \varepsilon^n\,! = z^{-k}\left\{1 - \varepsilon \ln(z) + \frac{\varepsilon^2}{2}\left[\ln(z)\right]^2 + \cdots\right\}. \tag{5.65}$$

The integrals considered in the following examples are of the form

$$I = \frac{1}{2\pi i} \int_C ds\, F(s), \tag{5.66}$$

where the integration path and integrand are defined in each particular problem.

5.3.2 Example 1

Consider the following integrand with a double pole

$$F(s) = \frac{1}{s^2} = \Gamma\left[\begin{matrix} s,\ s \\ s+1,\ s+1 \end{matrix}\right]. \tag{5.67}$$

I seek to evaluate

$$I = \frac{1}{2\pi i} \int_C ds\, \Gamma\left[\begin{matrix} s,\ s \\ s+1,\ s+1 \end{matrix}\right]. \tag{5.68}$$

The integration path and pole location are shown in Fig. 5.3. It is obvious from the first term to the right of the equality in eq. 5.67 that there is no term that varies as $1/s$; therefore, the integral is zero. This is not obvious when the function is expressed as the ratio of gamma functions. If the gamma functions in the numerator and denominator are expanded with eq. 5.62 and eq. 5.60, the terms with $1/\varepsilon$ cancel, and no simple pole exists. Therefore, the integral is zero.

This integration in the complex plane corresponds to an integral in real space. Using the Mellin convolution integral, one finds that an integral that would give this integral in the complex plane is

$$I = \int_0^{\infty} \frac{dx}{x}\, U(1-x)\, U\left(1 - z/x\right), \quad z = 1. \tag{5.69}$$

This integral is easily evaluated to give

$$I = \int_z^1 \frac{dx}{x} = -\ln(z)\, U\left(1-z\right), \tag{5.70}$$

which is indeed equal to zero for $z = 1$.

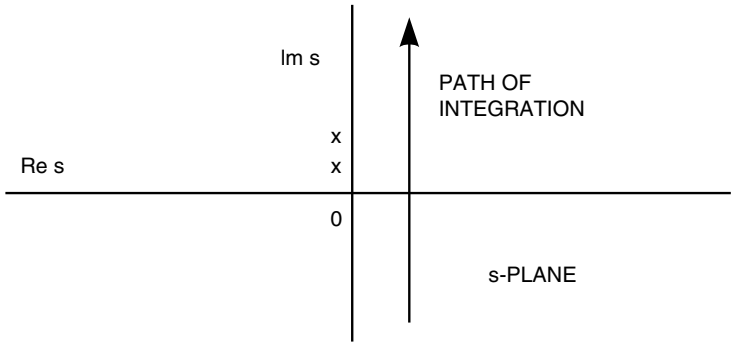

Figure 5.3. The integration path and pole location for Examples 1 and 2.

5.3.3 Example 2

Consider the slightly more complicated integrand

$$F(s) = \frac{z^{-s}}{s^2} = z^{-s}\Gamma\left[\begin{matrix} s,\ s \\ s+1,\ s+1 \end{matrix}\right]. \tag{5.71}$$

The integration path and pole location are the same as in Fig. 5.3 . Here $\Delta = 0$, and the direction of path closure depends on the magnitude of z. For $z > 1$ the integration path can be closed in the right half plane, and the value of the integral is zero. For $z < 1$ the integration path can be closed in the left half plane. If the expansions in eq. 5.62, eq. 5.60, and eq. 5.65 are used, the $1/\varepsilon$ term comes from the second term of the first equation and the second terms of the second equation. One obtains for the value of the integral

$$I = -\ln(z)\, U(1-z). \tag{5.72}$$

The integral in real space corresponding to this complex integration is the same one given in eq. 5.69.

5.3.4 Example 3

Consider the integrand

$$F(s) = \frac{\Gamma[s]}{s}\, z^{-s} = \Gamma\left[\begin{matrix} s*,\ s* \\ s+1 \end{matrix}\right] z^{-s}. \tag{5.73}$$

The asterisks appear after both numerator gamma functions because the chosen integration path passes between the first and second poles of the gamma functions. The integration path and pole location are shown in Fig. 5.4. This corresponds to the real space convolution integral

$$I = \int_0^\infty \frac{dx}{x}\ \left[\exp(-x) - 1\right]\left[1 - U(1 - z/x)\right] = \int_0^z \frac{dx}{x}\ \left[\exp(-x) - 1\right]. \tag{5.74}$$

The poles go to infinity to the left just as they do in the succeeding examples. For this example, $\Delta = 1$, and the integration path can be closed to the left for all z. All the enclosed poles are simple since the only double pole at $z = 0$ is on the right side of the integration path. The integral is equal to

$$I = -\sum_{n=1}^{\infty} \frac{(-1)^n}{n!} \frac{z^n}{n}. \tag{5.75}$$

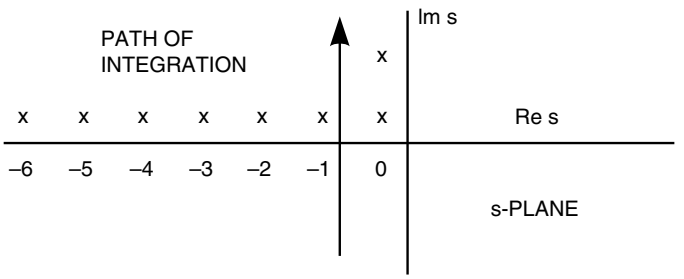

Figure 5.4. The integration path and pole location for Example 3.

For large z an asymptotic series can be found. Since $B = 0$, the steepest-descent contribution has exponential decay as given in eq. 5.92. With eq. 5.63 and eq. 5.65 for the numerator and eq. 5.60 for the denominator, the asymptotic series, which only has 3 terms in this case, is

$$I \sim \exp(-z)/z + \ln(z) + \mathbf{C}, \quad z >> 1. \tag{5.76}$$

The decaying exponential term is negligible.

5.3.5 Example 4

Consider the integrand

$$F(s) = \Gamma\left[s*, -s\right] z^{-s}. \tag{5.77}$$

The integration path and pole location are shown in Fig. 5.5. This corresponds to the real space convolution integral

$$I = \int_0^{\infty} \frac{dx}{x} \left[\exp\left(-x\right) - 1\right] \exp(-x/z). \tag{5.78}$$

Since $\Delta = \Delta' = 0$, the integration path can be closed in the left half plane when $z < 1$, and in the right half plane when $z > 1$. There is a double pole to the right at $z = 0$ that can be evaluated with eq. 5.62, eq. 5.60, and eq. 5.65. This yields

$$I = \sum_{n=1}^{\infty} \frac{(-z)^n}{n} = -\ln\left(z + 1\right), \quad z < 1, \quad \text{and} \tag{5.79}$$

$$I = \sum_{n=1}^{\infty} \frac{(-z)^{-n}}{n} + \ln(z) = -\ln(z+1) + \ln(z) = -\ln(1-1/z), \quad z > 1. \tag{5.80}$$

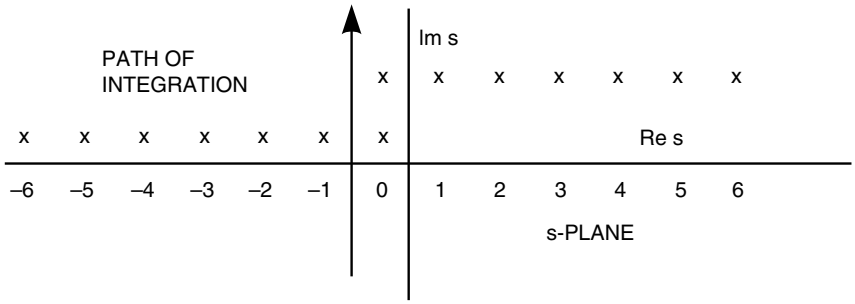

Figure 5.5. The integration path and pole location for Example 4.

5.3.6 Example 5

Consider the integrand

$$F(s) = \Gamma\left[s*, -s - N\left(*^N\right)\right] z^{-s}. \tag{5.81}$$

The $\left(*^N\right)$ term indicates that the first N terms of the power series are subtracted from the function whose Mellin transform results in that gamma function. The integration path and pole location are shown in Fig. 5.6 for the case $N = 4$. For general N this corresponds to the real space convolution integral

$$I = \int_0^{\infty} \frac{dx}{x} \left[\exp(-x) - 1\right] \left(\frac{z}{x}\right)^N \left[\exp(-x/z) - \sum_{n=0}^{N-1} \frac{1}{n!} \left(-\frac{x}{z}\right)^n\right]. \tag{5.82}$$

The value of $\Delta = \Delta' = 0$, and the direction of path closure depends on the magnitude of z. There is one double pole to the right of the integration path, N double poles to the left, and simple poles on both sides of the integration path. The result is

$$I = (-1)^N \sum_{n=1}^{N} \frac{\ln(z) + \psi(1+N-n) - \psi(1+n)}{n!\,(N-n)!} + (-z)^{N+1} \sum_{n=0}^{\infty} \frac{n!\,(-z)^n}{(N+n+1)!}, \qquad z < 1, \quad \text{and} \tag{5.83}$$

$$I = (-1)^N \frac{\psi(1) - \psi(1+N) - \ln(z)}{N!} + (-1)^N \sum_{n=0}^{\infty} \frac{n!\,(-z)^{-n-1}}{(N+n+1)!}, \quad z > 1. \tag{5.84}$$

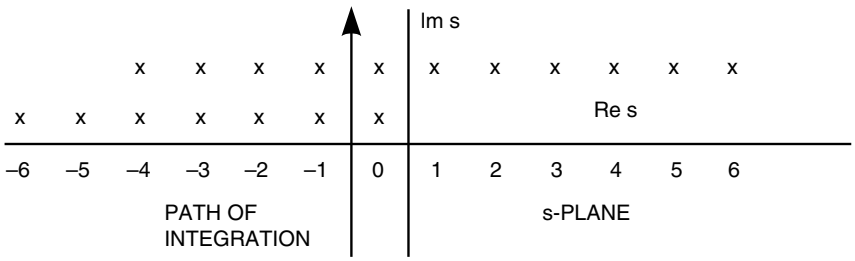

Figure 5.6. The integration path and pole location for Example 5.

5.3.7 Example 6

Consider the following integrand that has triple poles

$$F(s) = \Gamma\left[s*,\ s,\ -N - s\left(*^N\right)\right] z^{-s}. \tag{5.85}$$

The integration path and pole location are shown in Fig. 5.7 for the case $N = 4$. For this case $\Delta = 1$, and there is one triple pole to the right of the integration path, and N triple poles and an infinity of double poles to the left. Three terms in the Laurent expansions of each factor must be retained to get the complete residue at each of the triple poles. Since $\Delta = 1$, the integration path can be

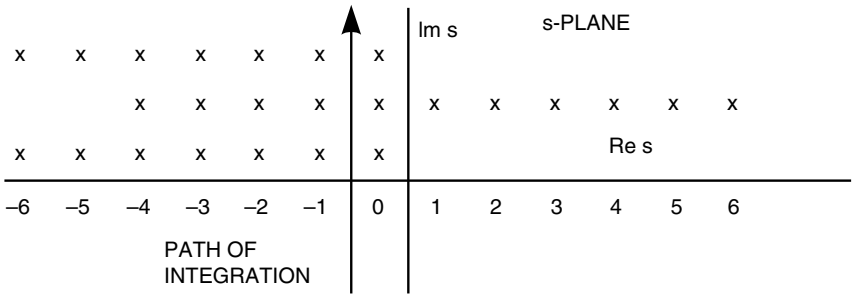

Figure 5.7. The integration path and pole location for Example 6.

closed in the left half plane. The residue at a double pole that occurs at $s = -k$, $k = N + 1,\ N + 2 \ldots$ is referred to as $R2\,(k)$ and is given by

$$R2\,(k) = \Gamma\,[k - N]\,[2\psi(1 + k) - \psi(k - N) - \ln(z)]\,\frac{z^k}{(k\,!)^2}. \tag{5.86}$$

The residue at a triple pole that occurs at $s = -1, -2, \ldots, N$ is referred to as $R3\,(k)$ and is given by

$$R3\left(k\right)=\Big\{\ln^2(z)\ /2+\ln(z)\ \left[\psi\left(1+N-k\right)-2\psi\left(1+k\right)\right]$$
$$+2\psi^2(1+k)+3\psi'(1)+\Big[\psi^2(1+N-k)-\psi'(1+N-k)\Big]/2$$
$$-\psi'(1+k)-2\psi(1+N-k)\,\psi(1+k)\Big\}\,\frac{(-1)^{N-k-1}z^k}{(k!)^2(N-k)!}. \tag{5.87}$$

The value of the integral is thus

$$I=\sum_{k=N+1}^{\infty}R2\left(k\right)+\sum_{k=1}^{N}R3\left(k\right). \tag{5.88}$$

For large values of z an asymptotic series is needed. Since the condition in eq. 5.52 applies, the asymptotic series is equal to the residues of the poles to the right of the integration path. This contains one triple pole, and the sum of the single poles at $s=n-N$, for $n=N+1,N+2\ldots$. The asymptotic series is thus

$$I\sim\frac{(-1)^{N+1}}{z}\sum_{n=0}^{\infty}\frac{(-1)^n\left(n!\right)^2}{(N+n+1)!}\,z^{-n}+\frac{z^N}{(N!)^2}\left\{\ln(z)\left[\psi(1)-2\psi(1+N)\right]+\frac{\ln^2(z)}{2}\right.$$
$$\left.+2\psi^2(1+N)+\frac{5\psi'(1)}{2}+\frac{\psi^2(1)}{2}-\psi'(1+N)-2\psi(1)\,\psi(1+N)\right\}. \tag{5.89}$$

Table 5.1 Equations to obtain the steepest-descent term $E(x)$. If $\Delta < 0$, then make the substitution $s \to -s$ before applying the equations below. In that case the parameter x becomes $1/x$.

Equation whose asymptotic value is wanted for large values of x.

$$h(x) = \frac{1}{2\pi i} \int_{C'} ds\, x^{-s}\ \frac{\prod_{i=1}^{A} \Gamma\,[a_i + \alpha_i\, s] \prod_{j=1}^{B} \Gamma\,[b_j - \beta_j\, s]}{\prod_{k=1}^{C} \Gamma\,[c_k + \gamma_k\, s] \prod_{m=1}^{D} \Gamma\,[d_m - \delta_m\, s]} \tag{5.90}$$

$$\Xi' = A + D - B - C, \quad \Xi = A + B - C - D$$

$$\Delta = \sum_{i=1}^{A} \alpha_i + \sum_{m=1}^{D} \delta_m - \sum_{j=1}^{B} \beta_j - \sum_{k=1}^{C} \gamma_k$$

$$\Delta' = \sum_{i=1}^{A} \alpha_i \ln(\alpha_i) + \sum_{m=1}^{D} \delta_m \ln(\delta_m) - \sum_{j=1}^{B} \beta_j \ln(\beta_j) - \sum_{k=1}^{C} \gamma_k \ln(\gamma_k)$$

$$\nu = \sum_{i=1}^{A} a_i + \sum_{j=1}^{B} b_j - \sum_{k=1}^{C} c_k - \sum_{m=1}^{D} d_m$$

$$A' = \sum_{i=1}^{A} \alpha_i, \quad B' = \sum_{j=1}^{B} \beta_j, \quad C' = \sum_{k=1}^{C} \gamma_k, \quad D' = \sum_{m=1}^{D} \delta_m$$

$$\rho = [\nu + (1 - \Xi)/2]\,/\Delta, \quad B'' = \sum_{j=1}^{B} b_j, \quad D'' = \sum_{m=1}^{D} d_m$$

$$\Lambda = D - B, \quad \Lambda' = D' - B', \quad \Lambda'' = D'' - B''$$

$$\Delta'' = \sum_{i=1}^{A} a_i \ln(\alpha_i) + \sum_{j=1}^{B} b_j \ln(\beta_j) - \sum_{k=1}^{C} c_k \ln(\gamma_k) - \sum_{m=1}^{D} d_m \ln(\delta_m)$$

$$\Delta''' = \sum_{i=1}^{A} \ln(\alpha_i) + \sum_{j=1}^{B} \ln(\beta_j) - \sum_{k=1}^{C} \ln(\gamma_k) - \sum_{m=1}^{D} \ln(\delta_m)$$

If $B = D = 0$ and $\Lambda' > 0$, then

$$E(x) = \frac{(2\pi)^{(\Xi-1)/2}}{\sqrt{\Delta}} x^{\rho} \exp\left[-\Delta\, x^{1/\Delta} \exp(-\Delta'/\Delta) + \Delta'' - \Delta'''/2 - \rho\Delta'\right]. \quad (5.91)$$

If $\Delta' = \Delta'' = \Delta''' = 0$, $\Lambda' > 0$ and $B = D = 0$, then

$$E(x) = \frac{(2\pi)^{(\Xi-1)/2}}{\sqrt{\Delta}} x^{\rho} \exp\left(-\Delta\, x^{1/\Delta}\right). \quad (5.92)$$

If B or $D \neq 0$ and $\Lambda' > 0$, then

$$E(x) = \frac{2(2\pi)^{(\Xi-1)/2}}{\sqrt{\Delta}} x^{\rho}$$
$$\times \exp\left[-\Delta x^{1/\Delta} \exp(-\Delta'/\Delta) \cos(\pi\Lambda'/\Delta) + \Delta'' - \Delta'''/2 - \rho\Delta'\right]$$
$$\times \cos\left[\Delta x^{1/\Delta} \exp(-\Delta'/\Delta) \sin(\pi\Lambda'/\Delta) + \pi(-\rho\Lambda' - \Lambda'' + \Lambda/2)\right]. \quad (5.93)$$

If B or $D \neq 0$ and $\Lambda' > 0$, and $\Delta' = \Delta'' = \Delta''' = 0$, $B = B'$, $D = D'$, then

$$E(x) = \frac{2(2\pi)^{(\Xi-1)/2}}{\sqrt{\Delta}} x^{\rho} \exp\left[-\Delta x^{1/\Delta} \cos(\pi\Lambda/\Delta)\right]$$
$$\times \cos\left\{\Delta x^{1/\Delta} \sin(\pi\Lambda/\Delta) + \pi\left[(1/2 - \rho)\Lambda - \Lambda''\right]\right\}. \quad (5.94)$$

If $\Lambda' \leq 0$, then $E(x)$ has exponential decay with specific values discussed in Sec. 8.2.

Table 5.2 Equations to obtain the asymptotic solution for a generalized hypergeometric function.

Express the generalized hypergeometric function as

$$
\begin{aligned}
&{}_pF_q\left[(b);(d);z\right] \\
&= \Gamma\begin{bmatrix} d_1, d_2, \ldots, d_q \\ b_1, b_2, \ldots, b_p \end{bmatrix} \frac{1}{2\pi i} \int_{C'} ds\,(-z)^{-s}\ \frac{\prod_{j=1}^{p} \Gamma\left[b_j - s\right]\Gamma\left[s\right]}{\prod_{m=1}^{q} \Gamma\left[d_m - s\right]}.
\end{aligned} \tag{5.95}
$$

For functions of the form ${}_0F_1\left[e;z\right]$, $d_1 = e$.

The asymptotic solution is a sum of pole and steepest-descent contributions

$$
{}_pF_q\left[(b);(d);z\right] \sim W(z) + E(z), \quad \text{where} \tag{5.96}
$$

$$
\begin{aligned}
W(z) &= \Gamma\begin{bmatrix} d_1, d_2, \ldots, d_q \\ b_1, b_2, \ldots, b_p \end{bmatrix} \\
&\times \sum_{k=1}^{p} \sum_{n=0}^{n_p} \frac{(-1)^n (-z)^{-n-b_k}}{n!}\ \frac{\prod_{j=1, j\neq k}^{p} \Gamma\left[b_j - b_k - n\right]\Gamma\left[b_k + n\right]}{\prod_{m=1}^{q} \Gamma\left[d_m - b_k - n\right]},
\end{aligned} \tag{5.97}
$$

and

$$
\begin{aligned}
E(-z) &= \Gamma\begin{bmatrix} d_1, d_2, \ldots, d_q \\ b_1, b_2, \ldots, b_p \end{bmatrix} \frac{2(2\pi)^{(1-\Delta)/2}}{\sqrt{\Delta}} z^{\rho} \exp\left\{-\Delta\, z^{1/\Delta} \cos\left[\pi(1 - 1/\Delta)\right]\right\} \\
&\times \cos\left\{\Delta\, z^{1/\Delta} \sin\left(\pi\left[1 - \frac{1}{\Delta}\right]\right) + \pi\left[\frac{\Delta - 1}{2\Delta} + \frac{1}{\Delta}\left(\sum_{i=1}^{p} b_i - \sum_{m=1}^{q} d_m\right)\right]\right\},
\end{aligned} \tag{5.98}
$$

where

$$
\Delta = q - p + 1, \quad \text{and} \tag{5.99}
$$

$$
\rho = \left(\sum_{1=1}^{p} b_i - \sum_{m=1}^{q} d_m + \frac{\Delta - 1}{2}\right)/\Delta. \tag{5.100}
$$

When $q = p + 1$, then $\Delta = 2$, the exponential term is equal to unity, and the steepest-descent contribution is

$$
E(-z) = \Gamma\begin{bmatrix} d_1, d_2, \ldots, d_q \\ b_1, b_2, \ldots, b_p \end{bmatrix} \frac{z^{\rho}}{\sqrt{\pi}} \cos\left\{2\, z^{1/2} + \pi\left[\frac{1}{4} + \frac{1}{2}\left(\sum_{i=1}^{p} b_i - \sum_{m=1}^{q} d_m\right)\right]\right\}. \tag{5.101}
$$

The behavior in this case is oscillatory.

REFERENCES

1. Bleistein, N., Hendelsman, R. A., *Asymptotic Expansions of Integrals*, Dover, New York, (1986).
2. Luke, Y., *The Special Functions and Their Approximations*, Academic Press, New York, (1969).
3. Marichev, O. I., *Integral Transforms of Higher Transcendental Functions*, Ellis Horwood Limited, Chichester, England, (1983).
4. Oberhettinger, F., *Tables of Mellin Transforms*, Springer-Verlag, Berlin, Germany, (1974).
5. Prudnikov, A. P., Brychkov, Y. A., Marichev, O. I., *Integrals and Series*, Gordon and Breach Science Publishers, New York, (1990).
6. Slater, L. J., *Generalized hypergeometric functions*, Cambridge University Press, London-New York, (1966).
7. Wong, R., *Asymptotic Approximations Of Integrals*, Academic Press, Inc., Boston, Ma., (1989).

Chapter 6

Examples with a Single Positive Parameter

Several interesting problems relating to wave propagation in turbulence are solved in this chapter. The Zernike tilt jitter is calculated for finite outer scale with both von Kármán and Greenwood models for outer scale effects. It is shown that outer scale significantly affects tilt even if the diameter is much smaller than the outer scale. It is shown that inner scale limits the maximum tilt that can be measured on an aperture. Tilt is calculated on an annulus, and it is shown that this tilt does not differ much from that of a filled aperture unless most of the aperture is obscured. The effect of diffraction on tilt is calculated. It is shown that tilt variance goes to half of its near-field value in the far field. The amount of tilt difference between two displaced sources is calculated. The power spectral density of tilt is found. An asymptotic series describes the behavior at high frequencies. I show that finite size sources and apertures can significantly reduce scintillation. Characteristic sizes for the source and aperture at which the reduction is significant are found. Inner scale is found to reduce the scintillation for typical inner-scale sizes. Scintillation of a beam corrected for turbulence by the use of a beacon that is displaced from the corrected beam is found. The scintillation difference between two sources in the sky is found. The phase variance of focus is found, and the correlation function of focus is calculated. The solution for anisoplanatism for any Zernike mode is then addressed. The problem of correcting turbulence with artificial beacons is addressed, and the phase variances with a point, distributed, and offset beacon are calculated.

The first few problems are solved in detail, and subsequent discussions leave out some intermediate steps that are repeated from problem to problem. This chapter illustrates how readily solutions are obtained with the algorithmic approach developed in this book. Many of these problems are difficult to solve by other means.

The solutions to many problems contain a single turbulence moment; however, for those problems in which the integration parameter is a function of the propagation coordinate, the solution is the sum of terms with different turbulence moments. For most problems considered here this does not pose a problem; however, there are cases in which the individual terms are infinite. In that case, an infinite sum of moments cannot be used, and the function in the axial integral must be evaluated at each position and multiplied by the turbulence strength.

An example of an integral in which this occurs is $\int_0^L dz\, C_n^2(z)\, \exp(-a/z)$. This integral is finite. However, if the exponential is expanded in a Taylor series, for the case in which the turbulence is non-zero at the origin, only the integral of the first term is finite. As examples of cases where this occurs in practice are the aperture-averaged scintillation considered in Sec. 6.8; the evaluation of scintillation with inner scale as treated in Sec. 6.3, if one were to consider the case of turbulence that varies along the path; and the calculation of tilt power spectral density as discussed in Sec 6.7, if the velocity were slew dominated, for which case it is proportional to z.

The answers for single parameter problems are expressed in terms of generalized hypergeometric functions. The evaluation of these expressions for particular parameters can be performed using programs such as Mathematica or Maple, which evaluate these functions. An alternative is to use the recursion relation to evaluate the generalized hypergeometric functions.

6.1 Zernike Modes and Tilt for the von Kármán Spectrum

The significant effect of outer scale on tilt jitter was pointed out by *Valley* (1979) and a solution for all Zernike modes is given by *Winker* (1991). To set up this problem, the general expression given in eq. 2.112 with diffraction and inner scale neglected is used with the filter function for Zernike tilt given in eq. 3.21, for a plane wave ($\gamma = 1$). The von Kármán turbulence spectrum given in eq. 2.26 with zero inner-scale size is used to obtain for two-axis tilt variance,

$$Z_n = 0.4146\, k_0^2 (n+1) \int_0^L dz\, C_n^2(z) \int d\boldsymbol{\kappa}\, \left(\kappa^2 + \kappa_o^2\right)^{-11/6} \left[\frac{2J_{n+1}\left(\kappa D/2\right)}{\kappa D/2}\right]^2 . \quad (6.1)$$

It is assumed that outer scale does not depend on z. The integrations over angle and z can be performed easily. Make the substitution $x = \kappa D/2$ to obtain

$$Z_n = \frac{83.38\, \mu_0\, k_0^2\, \kappa_o^{-11/3}}{D^2} \int_0^\infty \frac{dx}{x}\, J_{n+1}^2(x) \left[\left(\frac{x}{\kappa_o D/2}\right)^2 + 1\right]^{-11/6} . \quad (6.2)$$

This varies with zenith angle as $\sec(\xi)$. This expression can be converted into an integral in the complex plane with the use of the Mellin convolution integral. Define $h_0(x) = J_{n+1}^2(x)$, and $h_1(a/x) = \left[(a/x)^{-2} + 1\right]^{-11/6}$. Use the Mellin transform in eq. 1.52 for the first function. For the second, use the Mellin transform in eq. 1.54 with $q = 11/6$, and use eq. 1.9 with $p = 2$ to obtain

$$Z_n = \frac{83.38\, \mu_0\, k_0^2\, \kappa_o^{-11/3}}{4\sqrt{\pi}\, \Gamma\left[\frac{11}{6}\right] D^2}\, \frac{1}{2\pi i} \int_C ds\, \left(\frac{\kappa_o D}{2}\right)^{-s}$$

$$\times\Gamma\left[\begin{matrix} s/2+n+1,\ -s/2+\frac{1}{2},\ -s/2,\ s/2+\frac{11}{6} \\ -s/2+n+2,\ -s/2+1 \end{matrix}\right], \tag{6.3}$$

where the integration path does not split any poles of an individual gamma function. After the substitution $s \to 2s$, one obtains

$$Z_n = \frac{25\,\mu_0\,k_0^2\,\kappa_o^{-11/3}}{D^2}\frac{1}{2\pi i}\int\limits_C ds\,\left(\frac{\kappa_o D}{2}\right)^{-2s}\Gamma\left[\begin{matrix} s+n+1,\ -s+\frac{1}{2},\ -s,\ s+\frac{11}{6} \\ -s+n+2,\ -s+1 \end{matrix}\right]. \tag{6.4}$$

We will now look in detail at the tilt variance. For that case let $n = 1$ and multiply the previous equation by $(4/k_0D)^2$ to obtain

$$T_o^2 = \frac{400\,\mu_0\,\kappa_o^{-11/3}}{D^4}\frac{1}{2\pi i}\int\limits_C ds\,\left(\frac{\kappa_o D}{2}\right)^{-2s}\Gamma\left[\begin{matrix} s+2,\ -s+\frac{1}{2},\ -s,\ s+\frac{11}{6} \\ -s+3,\ -s+1 \end{matrix}\right]. \tag{6.5}$$

The only singularities of the integrand are associated with the numerator gamma functions that have poles where the argument of the gamma function is a negative integer. The poles of $\Gamma[as]$ occur at $s = -n/a$ and have a residue $(-1)^n/an!$ for $n = 0, 1, 2, \ldots$. The locations of the poles closest to the origin are shown in Fig. 6.1.

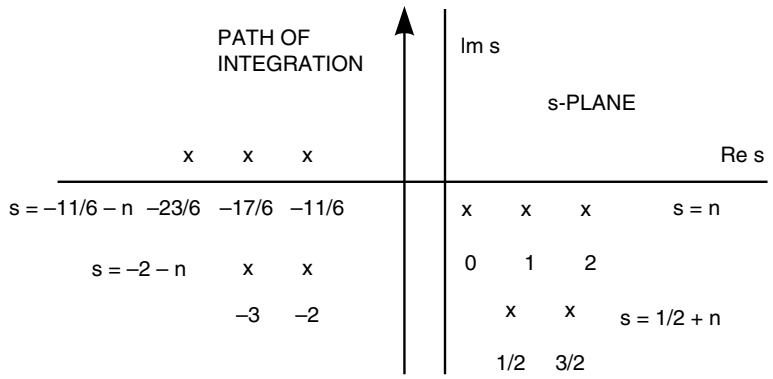

Figure 6.1. Location of the poles and integration path for determining the tilt with finite outer scale for the von Kármán turbulence spectrum.

As discussed in Chap. 5, the quantity Δ that determines the direction of path closure is the sum of the coefficients of s of the numerator gamma functions minus the sum of the coefficients of s in the denominator gamma functions. For this integral $\Delta = 2$, and the integration path can be closed in the left half plane. There are pole contributions at $s = -11/6 - n$, and $s = -2 - n$ for $n = 0, 1, 2, \ldots$. Use the definition of outer scale given in eq. 2.21 to obtain

$$T_o^2 = \frac{6.08\,\mu_0}{D^{1/3}} \left[5.18 \sum_{m=0}^{\infty} \frac{(-1)^m}{m\,!} \left\{ \left(\frac{\pi D}{L_o} \right)^{2m} \Gamma \left[\begin{matrix} -m + \frac{1}{6},\ m + \frac{7}{3},\ m + \frac{11}{6} \\ m + \frac{29}{6},\ m + \frac{17}{6} \end{matrix} \right] \right.$$

$$\left. + \left(\frac{\pi D}{L_o} \right)^{2m+1/3} \Gamma \left[\begin{matrix} m + \frac{5}{2},\ m + 2,\ -m - \frac{1}{6} \\ m + 5,\ m + 3 \end{matrix} \right] \right\} \right]. \tag{6.6}$$

This expression can be converted into the sum of two generalized hypergeometric functions with the rules in Sec. 1.3 to give

$$T_o^2 = \frac{6.08\,\mu_0}{D^{1/3}} \left\{ {}_2F_3 \left[\tfrac{11}{6}, \tfrac{7}{3}; \tfrac{5}{6}, \tfrac{29}{6}, \tfrac{17}{6}; \left(\frac{\pi D}{L_o} \right)^2 \right] \right.$$

$$\left. - 1.4234 \left(\frac{D}{L_o} \right)^{1/3} {}_2F_3 \left[2, \tfrac{5}{2}; \tfrac{7}{6}, 5, 3; \left(\frac{\pi D}{L_o} \right)^2 \right] \right\}. \tag{6.7}$$

The lowest order terms in eq. 6.6 for $D/L_o \ll 1$ are

$$T_o^2 \approx \frac{6.08\,\mu_0}{D^{1/3}} \left(1 - 1.42\,e^{1/3} + 3.70\,e^2 - 4.01\,e^{7/3} + 4.21\,e^4 - 4.00\,e^{13/3} \right), \tag{6.8}$$

where $e = D/L_o$. Tilt jitter is affected by outer scale, and the fractional decrease from the value with infinite outer scale is shown in Fig. 6.2. If outer-scale size is 100 times the aperture diameter, then the rms tilt jitter is still decreased by 15%. This decrease occurs because tilt jitter is caused mainly by long wavelength turbulence. A finite outer scale decreases turbulence at long wavelengths and, thereby, decreases tilt variance.

The first two terms in braces give a good approximation to the tilt variance if outer scale is larger than several times the aperture diameter. This is an example of how to write down the answer as a few terms of a power series. If outer-scale size were much smaller than diameter, then the series would converge slowly, and an asymptotic series would be appropriate.

In Sec. 11.4 it is shown that the difference of tilt between two closely spaced apertures separated by a distance d is little affected by the outer scale. One can use the first two series terms for the expression for tilt, T_0^2 and tilt anisoplanatism, T_d^2, to derive an expression for the outer scale as

$$L_0 = 0.35 \left[0.569(D/d)^2 - T_0^2/T_d^2 \right]^3.$$

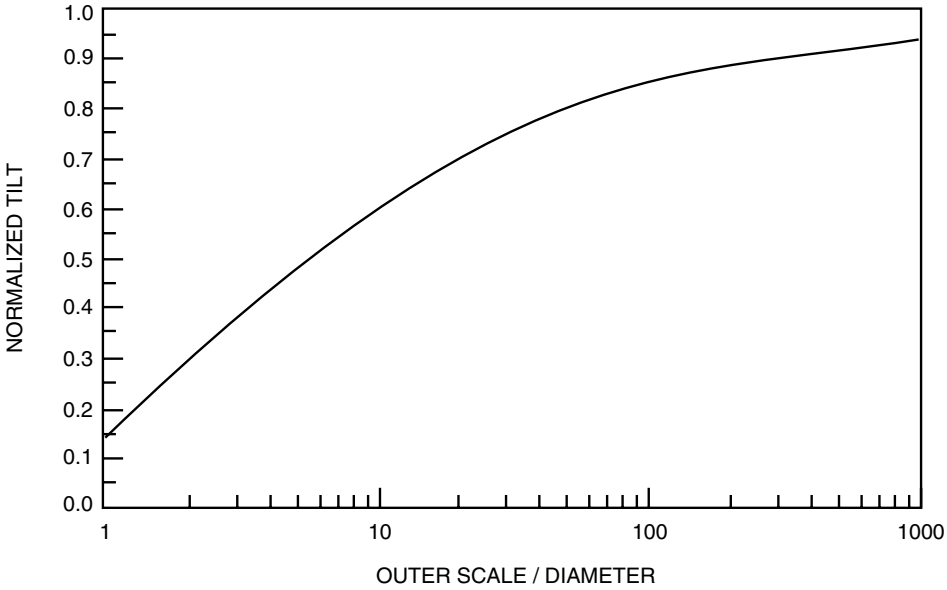

Figure 6.2. Tilt standard deviation for the von Kármán turbulence spectrum with outer scale, normalized to tilt standard deviation with infinite outer scale. Notice that there is a significant reduction of tilt even if outer scale is 100 times the diameter. This curve is independent of the turbulence distribution along the propagation path.

The variance of the Zernike modes can be expressed as

$$
\begin{aligned}
Z_n = \; & 1.512(n+1)\left(\frac{D}{r_0}\right)^{5/3}\left\{\Gamma\begin{bmatrix} n-\frac{5}{6}, \\ n+\frac{23}{6}\end{bmatrix}\,{}_2F_3\left[\tfrac{11}{6}, \tfrac{7}{3}; \tfrac{11}{6}-n, \tfrac{23}{6}+n, \tfrac{17}{6}; \left(\frac{\pi D}{L_o}\right)^2\right]\right. \\
& + 1.54\left(\frac{\pi D}{L_o}\right)^{-5/3+2n}\Gamma\begin{bmatrix} n+\frac{3}{2}, \; \frac{5}{6}-n, \; n+1 \\ 2n+3, \; n+2\end{bmatrix} \\
& \left.\times\,{}_2F_3\left[n+1, \tfrac{3}{2}+n; \tfrac{1}{6}+n, 3+2n, 2+n; \left(\frac{\pi D}{L_o}\right)^2\right]\right\}. \qquad (6.9)
\end{aligned}
$$

If one does a series expansion of this for any mode higher than tilt, then the first and second terms of the expansion come from the first function and the variance is of the form

$$Z_n = a - b\left(\frac{D}{L_0}\right)^2, \quad n > 1. \qquad (6.10)$$

For these modes the effect of outer scale decreases rapidly when the outer scale is greater than the diameter.

6.2 Tilt for the Greenwood Spectrum

The equation to find tilt variance with the Greenwood outer-scale model is the same as the one in the last section except that the spectrum in eq. 2.24 is used,

$$T_o^2 = 0.2073\, k_0^2 \int_0^L dz\, C_n^2(z) \int d\boldsymbol{\kappa}\, \left(\kappa^2 + \kappa\kappa_o\right)^{-11/6} \left(\frac{16}{k_0 D}\right)^2 \left[\frac{J_2(\kappa D/2)}{\kappa D/2}\right]^2 . \tag{6.11}$$

It is assumed again that outer scale does not depend on z. The integrations over angle and z can be performed easily. Make the substitution $x = \kappa D/2$ to obtain

$$T_o^2 = \frac{1334\, \mu_0 \kappa_o^{-11/6}}{D^4} \left(\frac{D}{2}\right)^{11/6} \int_0^\infty \frac{dx}{x}\, x^{-11/6} J_2^2(x) \left(\frac{x}{\kappa_o D/2} + 1\right)^{-11/6} . \tag{6.12}$$

This varies with zenith angle as $\sec(\xi)$. Define $h_0(x) = x^{-11/6} J_2^2(x)$, and $h_1(a/x) = \left[(a/x)^{-1} + 1\right]^{-11/6}$. Use the Mellin transform in eq. 1.52 for the first function, exploiting eq. 1.8 with $a = -11/6$. For the second function, start with (1.54) with $q = 11/6$, and use eq. 1.9 with $p = -1$. After the substitution $s \to 2s$, one obtains

$$T_o^2 = \frac{800\, \mu_0\, \kappa_o^{-11/6}}{D^4} \left(\frac{D}{2}\right)^{11/6} \frac{1}{2\pi i} \int_C ds\, \left(\frac{\kappa_o D}{2}\right)^{-2s} \times \Gamma\left[\begin{matrix} s + \frac{13}{12},\, -s + \frac{17}{12},\, -2s,\, 2s + \frac{11}{6} \\ s + \frac{47}{12},\, -s + \frac{23}{12} \end{matrix}\right], \tag{6.13}$$

where the integration path does not split any poles of an individual gamma function. Since once again $\Delta = 2$, the integration path can be closed in the left half plane, and there are pole contributions at $s = -11/12 - n/2$, and $-13/12 - n$ for $n = 0,\, 1,\, 2,\, \ldots$. Use the definition of outer scale given after eq. 2.20 to obtain

$$T_o^2 = \frac{6.08\, \mu_0}{D^{1/3}} \left\{ \sum_{n=0}^\infty \frac{(-1)^n}{n!} \left[5.18 \left(\frac{\pi D}{L_o}\right)^n \Gamma\left[\begin{matrix} -n/2 + \frac{1}{6},\, n/2 + \frac{7}{3},\, n + \frac{11}{6} \\ n/2 + \frac{29}{6},\, n/2 + \frac{17}{6} \end{matrix}\right] \right.$$
$$\left. + 15.18 \left(\frac{D}{L_o}\right)^{1/3} \Gamma\left[\begin{matrix} n + \frac{5}{2},\, 2n + \frac{13}{6},\, -2n - \frac{1}{3} \\ n + 5,\, n + 3 \end{matrix}\right] \left(\frac{\pi D}{L_o}\right)^{2n} \right] \right\}. \tag{6.14}$$

If the coefficients of s in the gamma functions in eq. 6.13 are made unity with the multiplication theorem for gamma functions given in eq 1.16, the solution can be expressed as

$$T_o^2 = \frac{6.08\,\mu_0}{D^{1/3}} \left\{ {}_3F_4 \left[\tfrac{11}{12},\ \tfrac{7}{3},\ \tfrac{17}{12};\ \tfrac{5}{6},\ \tfrac{29}{6},\ \tfrac{17}{6},\ \tfrac{1}{2};\ -\left(\frac{\pi D}{L_o}\right)^2 \right] \right.$$
$$+ 1.764 \left(\frac{D}{L_o}\right) {}_3F_4 \left[\tfrac{17}{12},\ \tfrac{23}{12},\ \tfrac{17}{6};\ \tfrac{7}{6},\ \tfrac{4}{3},\ \tfrac{3}{2}\ \tfrac{16}{3},\ \tfrac{10}{3},\ -\left(\frac{\pi D}{L_o}\right)^2 \right]$$
$$\left. - 1.848 \left(\frac{D}{L_o}\right)^{1/3} {}_3F_4 \left[\tfrac{5}{2},\ \tfrac{13}{12},\ \tfrac{19}{12};\ \tfrac{7}{6},\ 5,\ 3\ \tfrac{7}{6},\ \tfrac{2}{3},\ -\left(\frac{\pi D}{L_o}\right)^2 \right] \right\} . \quad (6.15)$$

This is plotted in Fig. 6.3.

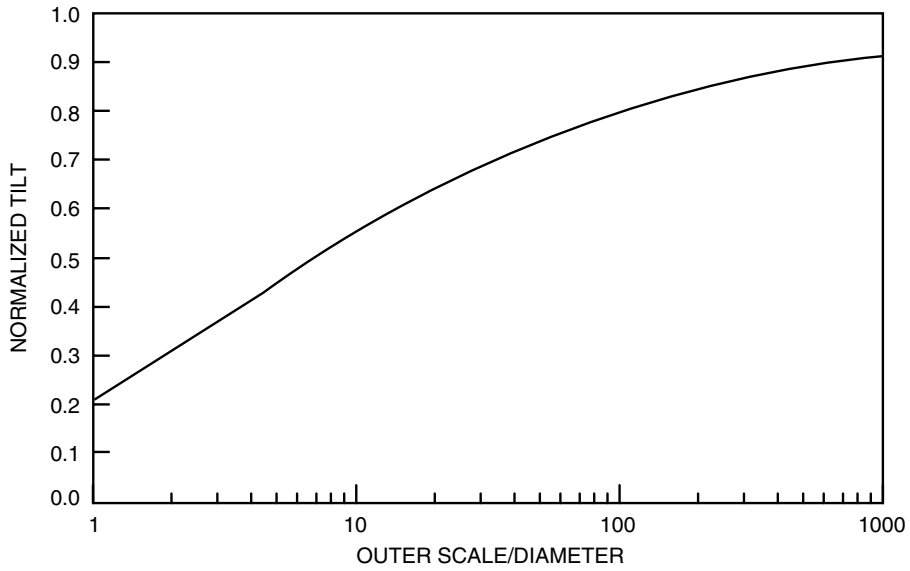

Figure 6.3. Tilt standard deviation for the Greenwood turbulence spectrum with outer scale, normalized to tilt standard deviation with infinite outer scale. Notice that there is a significant reduction of tilt even if outer scale is 100 times the diameter. This curve is independent of the turbulence distribution along the propagation path.

The lowest-order terms of the summations in eq. 6.14 for $D/L_o \ll 1$ give

$$T_o^2 \approx \frac{6.08\,\mu_0}{D^{1/3}} \left(1 - 1.85\,e^{1/3} + 1.76\,e - 5.24\,e^2 + 6.70\,e^{7/3} - 3.77\,e^3\right), \quad (6.16)$$

where $e = D/L_o$. Tilt jitter is also significantly affected by outer-scale effects for the Greenwood spectrum. The leading correction term has the 1/3 power of D/L_o in both spectra considered here; this results in a significant effect on tilt jitter even when outer scale is much larger than aperture diameter.

6.3 Tilt with Finite Inner Scale

The expression for Zernike tilt variance given in eq. 4.22 goes to infinity when the diameter goes to zero. This obviously is an incorrect physical limit; to determine the correct tilt for very small apertures, the inner scale must be included. To find this tilt, the turbulence spectrum with Tatarski's model for inner scale is used in eq. 4.34 with diffraction neglected to obtain

$$T_i^2 = \frac{105.1\,\mu_0}{D^{1/3}} \int_0^\infty \frac{dx}{x}\, x^{-11/3} J_2^2(x) \exp\left[-(x/b)^2\right], \tag{6.17}$$

where $b = \kappa_i\, D/2$, and it is assumed that the inner scale does not depend on z. This varies with zenith angle as $\sec(\xi)$. Mellin transforms in eq. 1.52 and eq. 1.47 can be used in the convolution integral, and after the substitution $s \to 2s$, one obtains

$$T_i^2 = \frac{29.64\,\mu_0}{D^{1/3}} \frac{1}{2\pi\, i} \int_C ds\, \Gamma\left[\begin{matrix} s+\frac{1}{6},\ -s+\frac{7}{3},\ -s \\ -s+\frac{29}{6},\ -s+\frac{17}{6} \end{matrix}\right] b^{-2s}. \tag{6.18}$$

The pole locations are shown in Fig. 6.4.

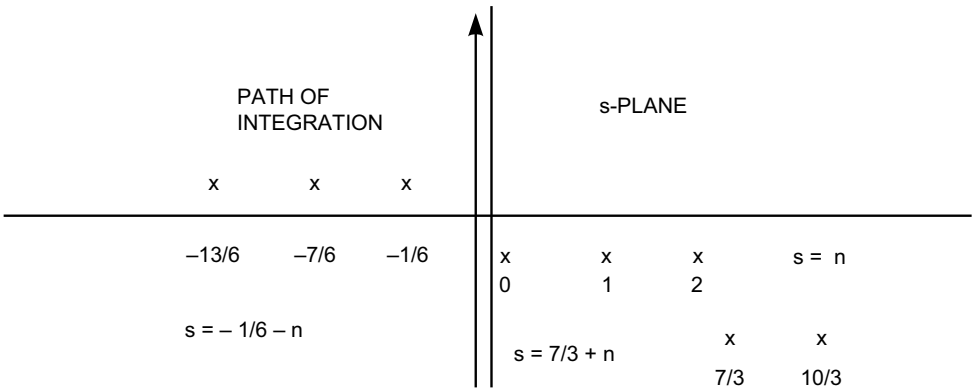

Figure 6.4. Pole location and integration path for determining the tilt with finite inner scale.

Since $\Delta = 1$, the integration path can be closed in the left half plane. There are poles at $s = -1/6 - n$, for $n = 0,\ 1,\ 2,\ \ldots$. The tilt variance is

$$T_i^2 = \frac{29.64\,\mu_0}{D^{1/3}} \sum_{n=0}^{\infty} \frac{(-1)^n}{n\,!}\, \Gamma\left[\begin{matrix} n+\frac{5}{2},\ n+\frac{1}{6} \\ n+5,\ n+3 \end{matrix}\right] \left(\frac{\pi D}{L_i}\right)^{2n+1/3}. \tag{6.19}$$

With the rules in Sec. 1.3 the solution is

$$T_i^2 = \frac{6.69\,\mu_0}{L_i^{1/3}}\, {}_2F_2\left[\frac{5}{2}, \frac{1}{6}; 5, 3; -\left(\frac{\pi D}{L_i}\right)^2\right]. \tag{6.20}$$

If inner scale is larger than diameter, then tilt variance determined only from the leading series term is

$$T_i^2 \approx \frac{6.08\,\mu_0}{(0.75L_i)^{1/3}}, \quad L_i \gg D. \tag{6.21}$$

From this solution it is seen that for inner scale large with respect to D, the tilt formula is the same as that with zero inner scale except that the diameter to place in the formula is 0.75 times the inner scale. If the inner scale is 1 millimeter, the rms tilt one would measure with a very small aperture is 12 μrads with the HV-21 turbulence distribution.

For inner scale much smaller than diameter, a case that normally occurs, the above power series converges slowly. For this case, an asymptotic solution is appropriate. The conditions given in eq. 5.52 are satisfied, which means that the asymptotic solution is simply found from the pole residues in the right half plane that are located at $s = m + 7/3$, and $s = m$ for $m = 0, 1, 2, \ldots$. This gives

$$T_i^2 \sim \frac{6.08\,\mu_0}{D^{1/3}} \sum_{m=0}^{n_o} \frac{(-1)^m}{m!} 4.875 \left\{ \Gamma \begin{bmatrix} m + \frac{1}{6}, -m + \frac{7}{3} \\ -m + \frac{29}{6}, -m + \frac{17}{6} \end{bmatrix} \left(\frac{L_i}{\pi D}\right)^{2m} \right.$$
$$\left. + 0.00479 \left(\frac{L_i}{D}\right)^{14/3} \left(\frac{L_i}{\pi D}\right)^{2m} \Gamma \begin{bmatrix} m + \frac{5}{2}, -m - \frac{7}{3} \\ -m + \frac{5}{2}, -m + \frac{1}{2} \end{bmatrix} \right\}. \tag{6.22}$$

The value to use for n_o was discussed in Sec. 5.2.

The two most significant pole contributions are at $s = 0$ and 1 in the first summation. The approximate solution from those poles is

$$T_i^2 \sim \frac{6.08\,\mu_0}{D^{1/3}} \left[1 - 0.089 \left(\frac{L_i}{D}\right)^2\right], \quad D \gg L_i. \tag{6.23}$$

The first term corresponds to the result given in eq. 4.22 where the inner scale is zero. Tilt with inner scale is plotted in Fig. 6.5.

6.4 Piston- and Tilt-Removed Phase Variance on an Annulus

Most apertures for astronomical telescopes and beam directors have a central obscuration whose diameter is 25% or less of the aperture diameter. In most analyses the effect of this obscuration is ignored because it is assumed to be small. Here it is shown explicitly that the central obscuration has little effect on piston-removed phase and tilt.

To obtain piston-removed phase variance σ_{PR}^2 on an annulus, the filter function that removes piston phase variance given in eq. 3.48 must be subtracted from unity in the standard formula in eq. 2.112 for phase variance of a single wave. This yields

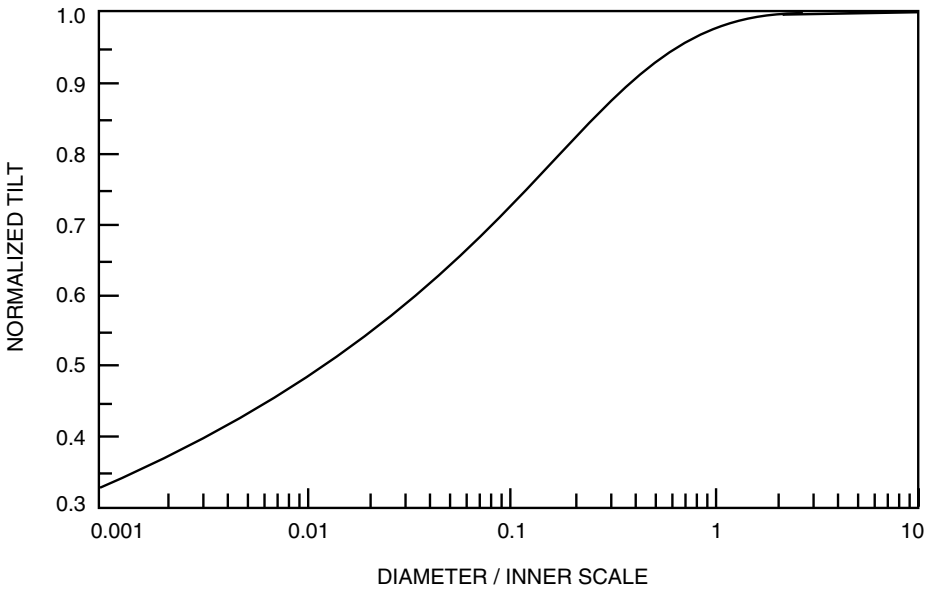

Figure 6.5. Effect of inner scale on the tilt, normalized to that with zero inner scale. This curve is independent of the turbulence distribution along the propagation path. Tilt is close to that of tilt with zero inner scale once the diameter is larger than inner scale.

$$\sigma_{PR}^2 = 0.2073\, k_0^2 \int_0^L dz\, C_n^2(z) \int d\boldsymbol{\kappa}\, \kappa^{-11/3}$$
$$\times \left\{ 1 - \frac{4}{\left[1-(D_i/D)^2\right]^2} \left[\frac{J_1(\kappa D/2)}{\kappa D/2} - \left(\frac{D_i}{D}\right)^2 \frac{J_1(\kappa D_i/2)}{\kappa D_i/2} \right]^2 \right\}. \quad (6.24)$$

For vanishingly small wavenumbers the filter function for piston approaches unity, thereby the unity term in the braces is cancelled, thus the apparent singularity at the origin in wavenumber space is cancelled. Expand the expression in braces, and rearrange terms to obtain three integrals that each converge to give

$$\sigma_{PR}^2 = \frac{5.212\,k_0^2\,\mu_0}{\left[1-(D_i/D)^2\right]^2}\int_0^\infty \frac{d\kappa}{\kappa}\,\kappa^{-5/3}\,\left(-\left\{\left[\frac{J_1(\kappa D/2)}{\kappa D/2}\right]^2-\frac{1}{4}\right\}\right.$$
$$-\left\{\left[\left(\frac{D_i}{D}\right)^2\frac{J_1(\kappa D_i/2)}{\kappa D_i/2}\right]^2-\frac{1}{4}\left(\frac{D_i}{D}\right)^4\right\}$$
$$\left.+\left[2\frac{J_1(\kappa D/2)}{\kappa D/2}\left(\frac{D_i}{D}\right)^2\frac{J_1(\kappa D_i/2)}{\kappa D_i/2}-\frac{1}{2}\left(\frac{D_i}{D}\right)^2\right]\right). \tag{6.25}$$

The first term in braces is the only term remaining when the central obscuration goes to zero, and produces the standard result in eq 4.27. The second term in braces gives the same result with a multiplier.

Let $x = \kappa D/2$, and $\beta = D_i/D$ to obtain

$$\sigma_{PR}^2 = 1.033\left(\frac{D}{r_o}\right)^{5/3}\frac{\left(1+\beta^{17/3}\right)}{\left(1-\beta^2\right)^2}+1.94\left(\frac{D}{r_o}\right)^{5/3}\frac{4}{\left(1-\beta^2\right)^2}\beta I. \tag{6.26}$$

The remaining integral to be evaluated is

$$I = \int_0^\infty \frac{dx}{x}\,x^{-11/3}\left[J_1(x)\,J_1(\beta x)-\frac{x}{2}\frac{\beta x}{2}\right]. \tag{6.27}$$

The form of this integral is not one that has been considered before. It is the product of two functions minus the product of the first terms of their series expansions. If A and B are the two functions, and a and b are the first terms of the series expansions, then the following identity will express the integral in a form that can be evaluated with the techniques that have been developed.

$$AB - ab = (A-a)(B-b) + a(B-b) + b(A-a). \tag{6.28}$$

The original integral I can now be broken up into the sum of three separate integrals that are

$$I_1 = \int_0^\infty \frac{dx}{x}\,x^{-11/3}\left[J_1(x)-\frac{x}{2}\right]\left[J_1(\beta x)-\frac{\beta x}{2}\right], \tag{6.29}$$

$$I_2 = 0.5\,\beta^{8/3}\int_0^\infty \frac{dy}{y}\,y^{-8/3}\left[J_1(y)-\frac{y}{2}\right] = -\,0.1525\,\beta^{8/3},\ \text{and} \tag{6.30}$$

$$I_3 = 0.5\,\beta\int_0^\infty \frac{dy}{y}\,y^{-8/3}\left[J_1(y)-\frac{y}{2}\right] = -\,0.1525\,\beta. \tag{6.31}$$

The last two integrals were evaluated with the Mellin transform in eq. 1.51.

Use the convolution theorem to evaluate I_1. By using eq. 1.51 and letting $s \to 2s$, one can transform I_1 into the complex plane as follows

$$I_1 = \frac{2^{-14/3}}{2\pi i} \int\limits_C ds\, \beta^{2s}\, \Gamma \begin{bmatrix} s - \frac{4}{3}*,\ -s + \frac{1}{2}* \\ -s + \frac{10}{3},\ s + \frac{3}{2} \end{bmatrix}, \tag{6.32}$$

where the asterisk indicates that the integration path passes between the first and second poles of the gamma function.

Since $\Delta = \Delta' = 0$, and $\beta < 1$, the integration path is closed to the right. The contributions of the poles at $s = 4/3$, and $s = 1/2 + n$ for $n = 1, 2, \ldots$, give

$$I_1 = 2^{-14/3} \left\{ 3.873\, \beta^{8/3} + \beta \sum_{n=1}^{\infty} \frac{(-1)^n}{n\,!} \beta^{2n} \Gamma \begin{bmatrix} n - \frac{5}{6} \\ -n + \frac{17}{6},\ n + 2 \end{bmatrix} \right\}. \tag{6.33}$$

From the rules in Sec. 1.3 this is equivalent to

$$I_1 = 0.1525\, \beta^{8/3} - 0.1525\, \beta \left({}_2F_1 \left[-\tfrac{5}{6}, -\tfrac{11}{6}; 2; \beta^2 \right] - 1 \right). \tag{6.34}$$

Therefore, the sum of the three integrals is

$$I = I_1 + I_2 + I_3 = -0.1525\, \beta\, {}_2F_1 \left[-\tfrac{5}{6}, -\tfrac{11}{6}; 2; \beta^2 \right]. \tag{6.35}$$

The piston-removed phase variance is thus

$$\sigma^2_{PR} = \frac{1.033}{(1-\beta^2)^2} \left(\frac{D}{r_o} \right)^{5/3} \left(1 + \beta^{17/3} - 1.146\, \beta^2\, {}_2F_1 \left[-\tfrac{5}{6}, -\tfrac{11}{6}; 2; \beta^2 \right] \right). \tag{6.36}$$

This is plotted in Fig. 6.6.

The expression for Zernike tilt phase variance on an annulus is obtained by inserting the filter function in eq. 3.42 into the standard formula eq. 2.112 for the phase variance of a single wave with diffraction neglected. The tilt variance in this case is thus

$$T^2_{az} = 0.2073\, k_0^2 \int\limits_0^L dz\, C_n^2(z) \int d\boldsymbol{\kappa}\ \left[\frac{16}{k_0 D\,(1-\beta^4)} \right]^2 \times \left[\frac{J_2(\kappa D/2)}{\kappa D/2} - \beta^3 \frac{J_2(\kappa \beta D/2)}{\kappa \beta D/2} \right]^2. \tag{6.37}$$

The angular and axial integrations can be performed easily, and if the square of the sum in brackets is expanded, the first term gives the Zernike tilt of a full aperture, and the second term squared is the same as the first term except it is multiplied by a constant. Making the substitution $x = \kappa D/2$, one can thus express the tilt variance as

$$T^2_{az} = \frac{6.08\, \mu_0}{D^{1/3}\,(1-\beta^4)^2} \left[1 + \beta^{23/3} - 34.55\, \beta^2 \int\limits_0^\infty \frac{dx}{x}\, x^{-11/3} J_2(x)\, J_2(\beta x) \right]. \tag{6.38}$$

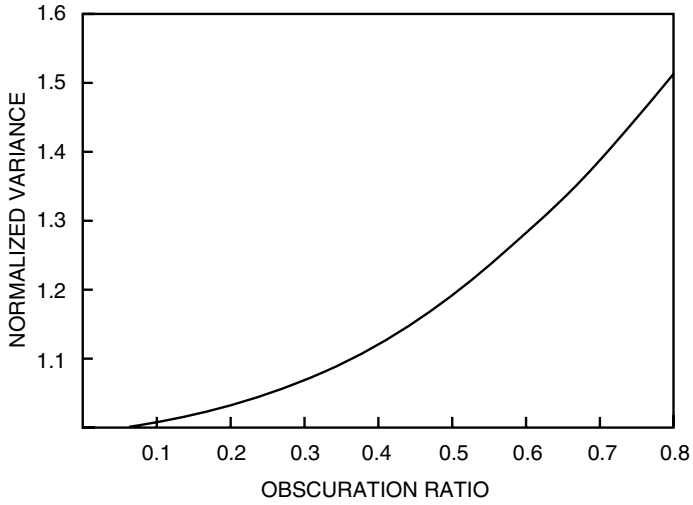

Figure 6.6. Normalized piston-removed phase variance on an annulus versus the obscuration ratio. For a typical obscuration ratio of 25% there is little change in tilt from that of a filled aperture. This curve is independent of the turbulence distribution along the propagation path.

Using the Mellin convolution theorem with the Mellin transform in eq. 1.51 and making the substitution $s \to 2s$, one obtains for the integral in eq. 6.38

$$I = \frac{2^{-14/3}}{2\pi i} \int_C ds\, \beta^{2s}\, \Gamma\left[\begin{matrix} s - \frac{5}{6},\, -s + 1 \\ -s + \frac{23}{6},\, s + 2 \end{matrix}\right]. \tag{6.39}$$

Since $\Delta = \Delta' = 0$, and the obscuration ratio is always less than 1, the integration path is closed in the right half plane. The integral is equal to the residues at $s = 1 + n$, for $n = 0,\, 1,\, 2,\, \ldots$. Tilt variance is thus equal to

$$T_{az}^2 = \frac{6.08\,\mu_0}{D^{1/3}\left(1-\beta^4\right)^2} \left\{ 1 + \beta^{23/3} - 1.36 \sum_{n=0}^{\infty} \frac{(-1)^n}{n\,!} \beta^{4+2n}\, \Gamma\left[\begin{matrix} n + \frac{1}{6} \\ -n + \frac{17}{6},\, n + 3 \end{matrix}\right] \right\}. \tag{6.40}$$

This can be expressed as a generalized hypergeometric function with the rules in Sec. 1.3,

$$T_{az}^2 = \frac{6.08\,\mu_0}{D^{1/3}\left(1-\beta^4\right)^2} \left(1 + \beta^{23/3} - 2.196\,\beta^4\, {}_2F_1\left[\tfrac{1}{6}, -\tfrac{11}{6}; 3; \beta^2\right] \right). \tag{6.41}$$

The first few terms of the solution, which give an answer accurate to better than 1% for $\beta < 0.5$, are

$$T_{az}^2 \approx 6.08\,\mu_0 \frac{\left(1 + \beta^{23/3} - 2.196\,\beta^4 + 0.2237\,\beta^6 - 0.02718\,\beta^8 - 0.0006544\,\beta^{10}\right)}{D^{1/3}\left(1-\beta^4\right)^2}. \tag{6.42}$$

Therefore, using the constant in eq. 3.45 to convert tilt angle variance to tilt phase variance, one obtains

$$\sigma_T^2 = 0.899 \left(\frac{D}{r_o}\right)^{5/3} \frac{(1+\beta^2)}{(1-\beta^4)^2} \left(1 + \beta^{23/3} - 2.196\,\beta^4\, {}_2F_1\left[\tfrac{1}{6}, -\tfrac{11}{6}; 3; \beta^2\right]\right). \quad (6.43)$$

Piston and tilt modes are orthogonal on an annulus; therefore, the phase variance with piston and tilt removed σ_{PTR}^2 is

$$\sigma_{PTR}^2 = \sigma_{PR}^2 - \sigma_T^2. \quad (6.44)$$

This is equal to

$$\sigma_{PTR}^2 = \left(\frac{D}{r_o}\right)^{5/3} \left\{ \frac{1.033}{(1-\beta^2)^2} \left(1 + \beta^{17/3} - 1.146\,\beta^2\, {}_2F_1\left[-\tfrac{5}{6}, -\tfrac{11}{6}; 2; \beta^2\right]\right) - 0.899 \left[\frac{1+\beta^2}{(1-\beta^4)^2}\right] \left(1 + \beta^{23/3} - 2.196\,\beta^4\, {}_2F_1\left[\tfrac{1}{6}, -\tfrac{11}{6}; 3; \beta^2\right]\right) \right\}. \quad (6.45)$$

The piston-and-tilt-removed phase variance is plotted in Fig. 6.7. For large obscuration ratios the terms in brackets almost cancel. To obtain an accurate answer for obscuration ratios approaching unity, the numerical constants must be replaced by their exact values, which are $1.146 \to 2^{-8/3}\sqrt{\pi}\,\Gamma\left[\frac{23}{6}\right]/\Gamma\left[\frac{7}{3}\right]$, and $2.196 \to 2^{-11/3}\sqrt{\pi}\,\Gamma\left[\frac{29}{6}\right]/\Gamma\left[\frac{7}{3}\right]$.

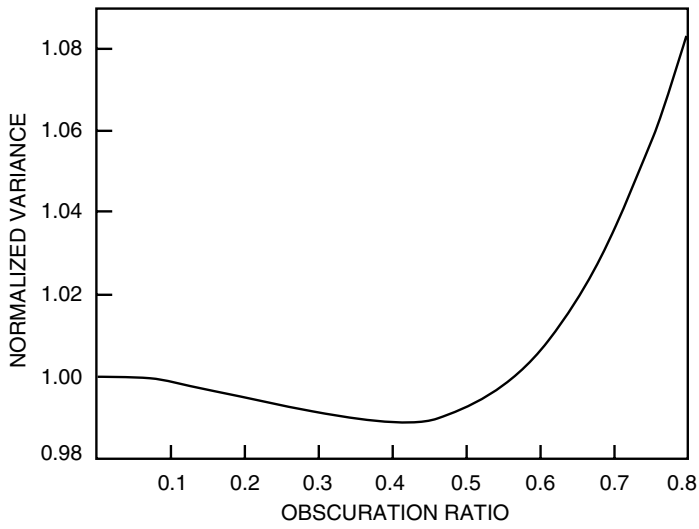

Figure 6.7. Normalized piston-and-tilt-removed phase variance on an annulus versus the obscuration ratio. For a typical obscuration ratio of 25% there is little change in variance from that of a filled aperture. This curve is independent of the turbulence distribution along the propagation path.

In a similar way gradient tilt variance can be calculated with eq. 2.112, and the filter function for gradient tilt on an annulus given in eq. 3.44, to obtain

$$T_{ag}^2 = \frac{3.317}{\left[D\left(1-\beta^2\right)\right]^2} \int_0^L dz\, C_n^2(z) \int d\boldsymbol{\kappa}\, \left[J_1\left(\kappa D/2\right) - \beta J_1\left(\kappa D_i/2\right)\right]^2 . \qquad (6.46)$$

This is evaluated in the now standard way to obtain

$$T_{ag}^2 = \frac{5.675\,\mu_0}{D^{1/3}\left(1-\beta^2\right)^2}\left(1+\beta^{11/3} - 2.156\,\beta^2\, {}_2F_1\left[\tfrac{1}{6}, -\tfrac{5}{6}; 2; \beta^2\right]\right). \qquad (6.47)$$

The first few terms of the solution, which result in an answer accurate to better than 1% for $\beta < 0.5$, are

$$T_{ag}^2 \approx 5.675\,\mu_0 \times \frac{\left(1+\beta^{11/3} - 2.156\,\beta^2 + 0.1497\,\beta^4 + 0.00485\,\beta^6 + 0.00102\,\beta^8\right)}{D^{1/3}\left(1-\beta^2\right)^2}. \qquad (6.48)$$

Normalized Zernike and gradient tilt variances are plotted in Fig. 6.8.

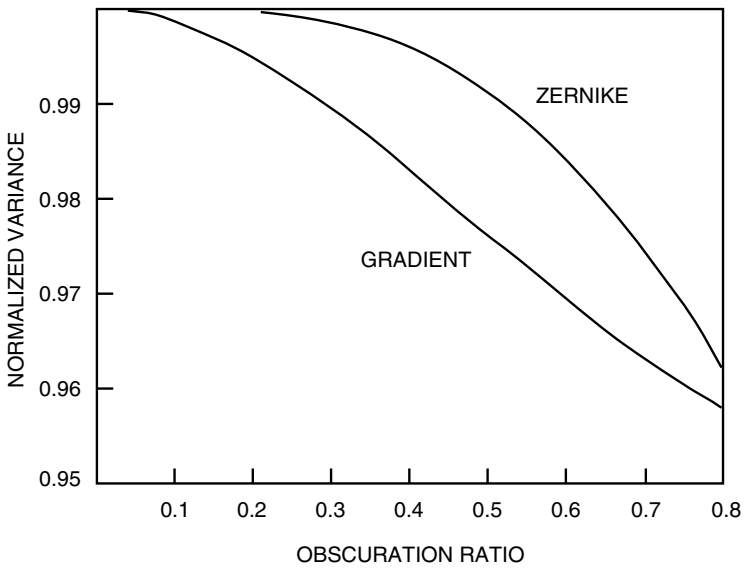

Figure 6.8. Normalized Zernike and gradient tilt variances on an annulus versus the obscuration ratio. For a typical obscuration ratio of 25% there is little change in variance from that of a filled aperture. These curves are independent of the turbulence distribution along the propagation path.

6.5 Effect of Diffraction on Tilt

As a beam propagates, it eventually spreads due to diffraction, and tilt can be affected. The effect of diffraction on Zernike tilt is obtained by not setting the cosine term equal to 1 as has been done until now. The formula for tilt of an infinite plane wave that propagates from ground to space is obtained from the standard formula for variance of a single wave given in eq. 2.112, with the filter function for Zernike tilt given in eq. 3.22, to obtain

$$T_d^2 = \frac{53.07}{D^2} \int_0^L dz\, C_n^2(z) \int d\boldsymbol{\kappa}\, \kappa^{-11/3} \left[\frac{J_2(\kappa D/2)}{\kappa D/2} \right]^2 \cos^2\left[\frac{\kappa^2 (L-z)}{2k_0} \right]. \tag{6.49}$$

Integrate over angle, let $x = \kappa D/2,$ and $y = D\sqrt{k_0/2(L-z)}$ to obtain

$$T_d^2 = \frac{105}{D^{1/3}} \int_0^L dz\, C_n^2(z) \int_0^\infty \frac{dx}{x}\, x^{-11/3} J_2^2(x) \left[1 - \sin^2(x/y)^2 \right]. \tag{6.50}$$

The first term in brackets corresponds to Zernike tilt without diffraction. With the Mellin convolution theorem, the Mellin transforms given in eq. 1.52 and eq. 1.50, and the substitution $s \to 4s$, one obtains

$$T_d^2 = \frac{6.08\,\mu_0}{D^{1/3}} \times \left\{ 1 + \frac{4.318}{\mu_0} \int_0^L dz\, C_n^2(z) \frac{1}{2\pi i} \int_C ds\, y^{-4s}\, \Gamma\left[\begin{matrix} 2s + \frac{1}{6},\, -2s + \frac{7}{3},\, -s* \\ -2s + \frac{29}{6},\, -2s + \frac{17}{6},\, s + \frac{1}{2} \end{matrix} \right] \right\}.$$

With the multiplication formula for gamma functions in eq. 1.16 one obtains for the integral over s

$$I = 2^{-25/6} \frac{1}{2\pi i} \int_C ds\, y^{-4s}\, \Gamma\left[\begin{matrix} s + \frac{1}{12},\, s + \frac{7}{12},\, -s + \frac{7}{6},\, -s + \frac{5}{3},\, -s* \\ -s + \frac{29}{12},\, -s + \frac{35}{12},\, -s + \frac{17}{12},\, -s + \frac{23}{12},\, s + \frac{1}{2} \end{matrix} \right]. \tag{6.51}$$

Since $\Delta = 2$, the integration path should be closed in the left half plane. There are poles located at $s = 0$, and $s = -1/12 - n$, and $-7/12 - n$ for $n = 0,\, 1,\, 2,\, \ldots$. The pole at zero gives a term that is minus one-half the diffraction-free term. The full result is

$$T_d^{\,2} = \frac{6.08\,\mu_0}{D^{1/3}}\left[0.5 + \frac{2.159}{\mu_0}\int_0^L dz\, C_n^2(z)\right.$$
$$\times\left(\sum_{n=0}^{\infty}\frac{(-1)^n}{n\,!}\left\{\left[\frac{k_0 D^2}{2(L-z)}\right]^{n+1/12}\Gamma\begin{bmatrix}-n+\frac{1}{2},\, n+\frac{5}{4},\, n+\frac{7}{3},\, n+\frac{1}{12}\\ n+3,\, n+2,\, -n+\frac{5}{12},\, n+\frac{5}{2},\, n+\frac{3}{2}\end{bmatrix}\right.\right.$$
$$\left.\left.\left.+\left[\frac{k_0\,D^2}{2(L-z)}\right]^{n+7/12}\Gamma\begin{bmatrix}-n-\frac{1}{2},\, n+\frac{7}{4},\, n+\frac{9}{4},\, n+\frac{7}{12}\\ n+3,\, n+2,\, -n-\frac{1}{12},\, n+\frac{5}{2},\, n+\frac{14}{3}\end{bmatrix}\right\}\right)\right]. \quad (6.52)$$

For very long ranges the first term dominates, and one finds that tilt variance is one-half that of the tilt in the near field. Use the rules in Sec. 1.3 to obtain

$$T_d^{\,2} = \frac{6.08}{D^{1/3}}\int_0^L dz\, C_n^2(z)$$
$$\times\left\{0.5 - 0.07341\left(\frac{k_0\,D^2}{(L-z)}\right)^{1/12}{}_4F_5\left[\tfrac{5}{4},\tfrac{7}{3},\tfrac{1}{2},-\tfrac{3}{2};2,3,\tfrac{1}{2},\tfrac{3}{2},\tfrac{5}{2};\left(\frac{k_0\,D^2}{2\,(L-z)}\right)^2\right]\right.$$
$$\left.+\,0.01095\left(\frac{k_0\,D^2}{(L-z)}\right)^{7/12}{}_4F_5\left[\tfrac{7}{4},\tfrac{9}{4},\tfrac{7}{12},\tfrac{13}{12};2,3,\tfrac{14}{3},\tfrac{3}{2},\tfrac{5}{2};\left(\frac{k_0\,D^2}{2\,(L-z)}\right)^2\right]\right\}. \quad (6.53)$$

When the observation plane is well above the turbulence, $L-z$ can be replaced by L in the above expression to obtain

$$T_d^{\,2} = \frac{6.08\,\mu_0}{D^{1/3}}$$
$$\times\left\{0.5 - 0.07341\left(\frac{k_0\,D^2}{L}\right)^{1/12}{}_4F_5\left[\tfrac{5}{4},\tfrac{7}{3},\tfrac{1}{2},-\tfrac{3}{2};2,3,\tfrac{1}{2},\tfrac{3}{2},\tfrac{5}{2};\left(\frac{k_0\,D^2}{2\,L}\right)^2\right]\right.$$
$$\left.+\,0.01095\left(\frac{k_0\,D^2}{L}\right)^{7/12}{}_4F_5\left[\tfrac{7}{4},\tfrac{9}{4},\tfrac{7}{12},\tfrac{13}{12};2,3,\tfrac{14}{3},\tfrac{3}{2},\tfrac{5}{2};\left(\frac{k_0\,D^2}{2\,L}\right)^2\right]\right\}. \quad (6.54)$$

Tilt is independent of wavelength at very long and short ranges. For intermediate ranges tilt can depend on wavelength.

Define the Fresnel number as

$$F_N = W_o^2/\lambda L, \quad (6.55)$$

where W_o is the beamwidth defined in eq. 2.69. In terms of F_N, the first few terms of the series solution are

$$T_d^{\,2} \approx \frac{6.08\,\mu_0}{D^{1/3}}$$
$$\times\left(0.5 + 0.3911\,F_N^{1/6} + 0.004572\,F_N^{7/6} - 0.002281\,F_N^{13/6} - 8.912\times10^{-5}\,F_N^{19/6}\right). \quad (6.56)$$

This solution converges rapidly for Fresnel numbers comparable or smaller than unity. The factor of one-half in the tilt for large ranges is due to conversion of half the phase variance into log-amplitude variance. There is a conversion back and forth between amplitude and phase scintillations. The conversion rate varies with spatial wavelength, and this results in an equipartition of variance at long ranges. For large distances the first two terms in parenthesis in eq. 6.56 provide a good estimate of tilt variance. The one-sixth power law dependence of the second term causes the variance to approach the infinite-range value slowly.

For small ranges an asymptotic solution is appropriate, and the simple poles in the right half plane that are located at $s = 7/6 + n$, and $s = 5/3 + n$ for $n = 0, 1, 2, \ldots$, and at $s = n$, for $n = 1, 2, 3, \ldots$ give an asymptotic series that is the sum of these terms plus the $E(x)$ term. Again assuming that the target is much higher than the top of the turbulence, one finds

$$T_d^2 \sim \frac{6.08\,\mu_0}{D^{1/3}} \times \left(1 + 2.159\left\{\sum_{n=0}^{n_o}\frac{(-1)^n}{n\,!}\left(\frac{2L}{k_0 D^2}\right)^{n+7/3}\Gamma\left[\begin{matrix} n+\frac{5}{2}, -n/2-\frac{7}{6} \\ -n+\frac{5}{2}, -n+\frac{1}{2}, n/2+\frac{5}{3}\end{matrix}\right] + 2\sum_{n=1}^{n_o}\frac{(-1)^n}{n\,!}\left(\frac{2L}{k_0 D^2}\right)^{2n}\Gamma\left[\begin{matrix} 2n+\frac{1}{6}, -2n+\frac{7}{3} \\ -2n+\frac{29}{6}, -2n+\frac{17}{6}, n+\frac{1}{2}\end{matrix}\right] + E\left(\frac{2L}{k_0 D^2}\right)\right\}\right). \tag{6.57}$$

The first few terms of the series, plus the E term, for $F_N \gg 1$ give

$$T_d^2 \sim \frac{6.08\,\mu_0}{D^{1/3}}\left[1 - \frac{0.7353}{F_N^2} + \frac{0.5419}{F_N^{7/3}} - \frac{0.112}{F_N^{10/3}} - \frac{0.2363}{F_N^{31/6}}\cos\left(\frac{\pi F_N}{2} + \frac{\pi}{4}\right)\right]. \tag{6.58}$$

Tilt variance normalized to the value at very short distances is plotted in Fig. 6.9 and Fig. 6.10 on linear and logarithmic scales. From this result one sees that the Fresnel number has to be very small before tilt variance drops to the far-field value. For accurate tracking one wants small deviations from the near field value; tilt variance has dropped by 5% when the Fresnel number is 3.

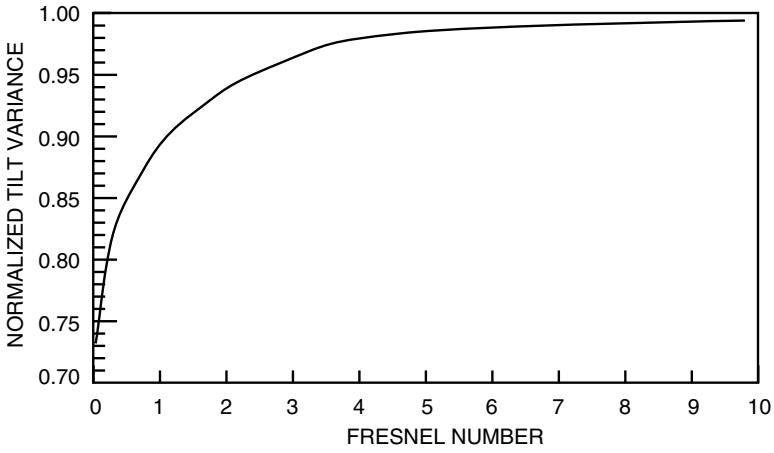

Figure 6.9. Tilt versus the Fresnel number on a linear scale. If the range is such that the Fresnel number is greater than 3, then tilt variance is within 5% of the very near field tilt variance. This curve is independent of the turbulence distribution along the propagation path.

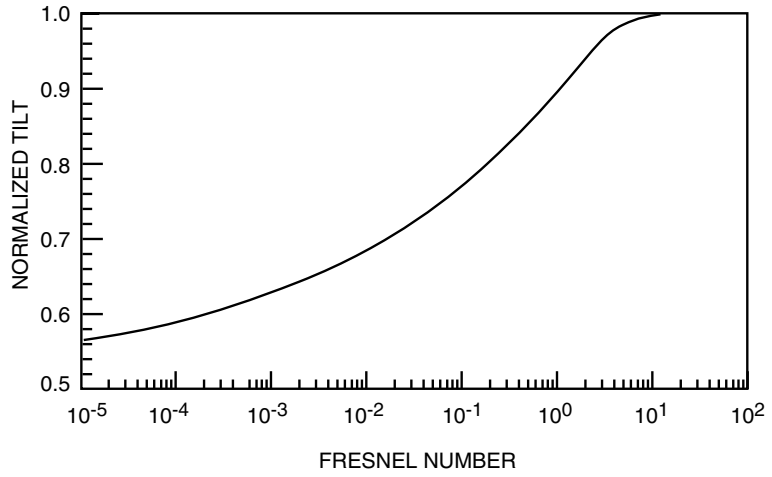

Figure 6.10. Tilt versus Fresnel number on a logarithmic scale. This plot more clearly shows tilt at low Fresnel numbers.

6.6 Tilt Anisoplanatism

Tilt anisoplanatism is the differential tilt jitter between two sources. The size of tilt anisoplanatism is of interest in many important applications. If the position of a source were measured, and a laser beam were directed at the source, there could be a jitter if the transmit aperture were not exactly aligned with the receive aperture. If a satellite were tracked, and a laser beam sent to the satellite, so that the laser beam would have to lead the perceived position of the target by an angle determined by light velocity and satellite velocity (about 50 μrads for low-altitude satellites), then this difference between the receiver and transmitter pointing angles leads to jitter of the laser beam at the target. Tilt anisoplanatism also accounts for the apparent jitter between two stars simultaneously viewed through the atmosphere. In this section I calculate Z-tilt anisoplanatism for two apertures displaced in distance or displaced in angle. In the second case, physical displacement is a function of the distance from the source. G-tilt anisoplanatism has been calculated by *Ellerbroek* and *Roberts* (1984), and one can obtain their results by using the approach illustrated below with a G-tilt rather than a Z-tilt filter function.

Tilt anisoplanatism is often much less than a beamwidth for scenarios considered in adaptive optics. When the beam is corrected, the tilt measured by sensors is closer to the Zernike tilt even for a centroid sensor, which for uncorrected beams measures a value closer to the gradient tilt (*Herrmann* 1981). For corrected beams the results obtained here are closer to values that would be measured than the G-tilt values.

To find the total value of tilt anisoplanatism and components both parallel and perpendicular to the displacement direction, eq. 2.123 with diffraction neglected is used with the filter function for Zernike tilt given in eq. 3.22. The general case will be considered so that the final formula can be applied to both collimated and focused beams. The γ factor multiplies the value of κ in the filter function for tilt, but it does not appear in the anisoplanatism term. Since the tilt is wanted at the aperture, the γ factor does not multiply the D in $1/D^2$. The resulting expression for tilt anisoplanatism is

$$\begin{bmatrix} \sigma_{\parallel}^2 \\ \sigma_{\perp}^2 \\ \sigma^2 \end{bmatrix} = 0.2073 \int_0^L dz\, C_n^2(z) \int d\boldsymbol{\kappa} \begin{bmatrix} \cos^2(\varphi) \\ \sin^2(\varphi) \\ 1 \end{bmatrix} \kappa^{-11/3} \times \left(\frac{16}{D}\right)^2 \left[\frac{J_2(\gamma\kappa D/2)}{\gamma\kappa D/2}\right]^2 2\left\{1 - \cos\left[\kappa d \cos(\varphi)\right]\right\}, \qquad (6.59)$$

where σ^2 is the total variance, which is equal to the sum of the parallel and perpendicular variances.

The angular integration can be performed with *Gradshteyn* and *Ryzhik* (1980, eq. 8.4.11 #7)

$$\int_0^{\pi} dx\, \exp\left[i\beta\cos(x)\right]\sin^{2\nu}(x) = \sqrt{\pi}\,\left(\frac{2}{\beta}\right)^{\nu}\,\Gamma\left[\nu+\tfrac{1}{2}\right]\,J_{\nu}(\beta), \quad \mathrm{Re}\left\{\nu\right\} > -\tfrac{1}{2}. \tag{6.60}$$

Use the trigonometric identity $\cos^2(\varphi) = 1 - \sin^2(\varphi)$ to express the first integral in eq. 6.59 in the form of eq. 6.60. Using eq. 3.5 one can perform the φ integration to obtain

$$\begin{bmatrix} \sigma_{\parallel}^2 \\ \sigma_{\perp}^2 \\ \sigma^2 \end{bmatrix} = \frac{667}{D^2}\int_0^L dz\, C_n^2(z) \begin{bmatrix} I_T - I_1 \\ I_1 \\ I_T \end{bmatrix}. \tag{6.61}$$

The two integrals that allows one to evaluate all three variances in kappa-space are

$$I_1 = -\int_0^{\infty} d\kappa\, \kappa^{-8/3}\, \left[\frac{J_2\left(\gamma\kappa D/2\right)}{\gamma\kappa D/2}\right]^2 \left[\frac{J_1\left(\kappa d\right)}{\kappa d} - \frac{1}{2}\right], \text{ and} \tag{6.62}$$

$$I_T = -\int_0^{\infty} d\kappa\, \kappa^{-8/3}\, \left[\frac{J_2\left(\gamma\kappa D/2\right)}{\gamma\kappa D/2}\right]^2 \left[J_0\left(\kappa d\right) - 1\right]. \tag{6.63}$$

Set $y = \kappa d$, and $x = 2d/\gamma D$, to obtain

$$\begin{bmatrix} I_1 \\ I_T \end{bmatrix} = -\frac{4d^{11/3}}{(\gamma D)^2}\int_0^{\infty}\frac{dy}{y}\begin{bmatrix} y^{-14/3}\left[J_1(y) - \frac{y}{2}\right] \\ y^{-11/3}\left[J_0(y) - 1\right] \end{bmatrix} J_2^2\left(y/x\right). \tag{6.64}$$

The Mellin transforms of the functions in brackets can be found from eq. 1.51 and eq. 1.8 with $a = -14/3$ and $-11/3$. The Mellin transform of $J_2^2(x)$ is given in eq. 1.52. After the substitution $s \to 2s$, the integrals in eq. 6.64 are transformed into

$$\begin{bmatrix} I_1 \\ I_T \end{bmatrix} = -\frac{0.0889\, d^{11/3}}{(\gamma D)^2}\frac{1}{2\pi i}\int_C ds\, \left(\frac{d}{\gamma D}\right)^{-2s} \times\Gamma\begin{bmatrix} s - \frac{11}{6}*,\, -s+2,\, s+\frac{1}{2} \\ s+3,\, s+1 \end{bmatrix}\begin{bmatrix} 1/2\Gamma\left[-s+\frac{23}{6}\right] \\ 1/\Gamma\left[-s+\frac{17}{6}\right] \end{bmatrix}. \tag{6.65}$$

The integration path and pole locations are the same for both integrals and are shown in Fig. 6.11.

Since $\Delta = \Delta' = 0$, the direction of path closure is determined by the parameter $d/\gamma D$ in the integral. Different Taylor's expansions are obtained for small and large displacements. The point in the atmosphere at which the character of the solution changes from one series to another is where the two beams just barely overlap. For $d/\gamma D < 1$, the integration path is closed to the left, and one obtains the residues of poles at $s = -1/2 - n$ for $n = 0, 1, 2, \ldots$, and $s = 11/6 - n$, for $n = 1, 2, 3, \ldots$. For $d/\gamma D > 1$, the path is closed to the

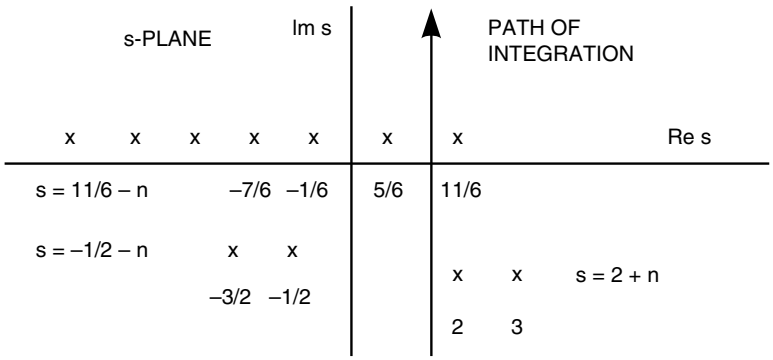

Figure 6.11. Pole location and integration path for tilt anisoplanatism.

right, and one obtains the residues of poles at $s = 2 + n$ for $n = 0, 1, 2, \ldots$, and the single pole at $s = 11/6$. The resultant values of the integrals for small displacements are

$$\begin{bmatrix} I_1 \\ I_T \end{bmatrix}_L = -\frac{0.0889\, d^{11/3}}{(\gamma D)^2}$$
$$\times \left\{ \sum_{n=1}^{\infty} \frac{(-1)^n}{n\,!} \left(\frac{d}{\gamma D}\right)^{-11/3+2n} \Gamma \begin{bmatrix} n+\frac{1}{6}, -n+\frac{7}{3} \\ n+1, -n+\frac{29}{6}, -n+\frac{17}{6} \end{bmatrix} \begin{bmatrix} \frac{0.5}{n+1} \\ 1 \end{bmatrix} \right.$$
$$\left. + \sum_{n=0}^{\infty} \frac{(-1)^n}{n\,!} \left(\frac{d}{\gamma D}\right)^{1+2n} \Gamma \begin{bmatrix} -n-\frac{7}{3}, n+\frac{5}{2} \\ n+\frac{10}{3}, -n+\frac{5}{2}, -n+\frac{1}{2} \end{bmatrix} \begin{bmatrix} \frac{0.5}{n+\frac{10}{3}} \\ 1 \end{bmatrix} \right\}, \; d < \gamma D. \quad (6.66)$$

For large displacements the integrals are equal to

$$\begin{bmatrix} I_1 \\ I_T \end{bmatrix}_U = \frac{0.0889\, d^{11/3}}{(\gamma D)^2} \left\{ \left(\frac{d}{\gamma D}\right)^{-11/3} \Gamma \begin{bmatrix} \frac{1}{6}, \frac{7}{3} \\ \frac{29}{6}, \frac{17}{6} \end{bmatrix} \begin{bmatrix} 0.5 \\ 1 \end{bmatrix} \right.$$
$$\left. - \sum_{n=0}^{\infty} \frac{(-1)^n}{n\,!} \left(\frac{d}{\gamma D}\right)^{-4-2n} \Gamma \begin{bmatrix} n+\frac{1}{6}, n+\frac{5}{2} \\ -n+\frac{5}{6}, n+5, n+3 \end{bmatrix} \begin{bmatrix} \frac{0.5}{-n+\frac{5}{6}} \\ 1 \end{bmatrix} \right\}, \quad d > \gamma D. \quad (6.67)$$

Substituting the last two results into eq. 6.64 results in

$$\begin{bmatrix}\sigma_{\parallel}^2\\ \sigma_{\perp}^2\end{bmatrix} = -\frac{29.6}{D^{1/3}}\int_0^L dz\, C_n^2(z)\gamma^{5/3}$$
$$\times\left\{\sum_{n=1}^{\infty}\frac{(-1)^n}{n\,!}\left(\frac{d}{\gamma D}\right)^{2n} \mathit{\Gamma}\begin{bmatrix} n+\frac{1}{6},\, -n+\frac{7}{3}\\ n+2,\, -n+\frac{29}{6},\, -n+\frac{17}{6}\end{bmatrix}\begin{bmatrix}2n+1\\ 1\end{bmatrix}\right.$$
$$\left.+\sum_{n=0}^{\infty}\frac{(-1)^n}{n\,!}\left(\frac{d}{\gamma D}\right)^{2n+14/3} \mathit{\Gamma}\begin{bmatrix} -n-\frac{7}{3}, n+\frac{5}{2}\\ n+\frac{13}{3}, -n+\frac{5}{2}, -n+\frac{1}{2}\end{bmatrix}\begin{bmatrix}2n+\frac{17}{3}\\ 1\end{bmatrix}\right\},\ d<\gamma D. \tag{6.68}$$

For large displacements one obtains

$$\begin{bmatrix}\sigma_{\parallel}^2\\ \sigma_{\perp}^2\end{bmatrix} = \frac{6.08}{D^{1/3}}\int_0^L dz\, C_n^2(z)\gamma^{5/3}\left\{\begin{bmatrix}1\\ 1\end{bmatrix}\right.$$
$$\left.-4.86\sum_{n=0}^{\infty}\frac{(-1)^n}{n\,!}\left(\frac{\gamma D}{d}\right)^{1/3+2n} \mathit{\Gamma}\begin{bmatrix} n-\frac{5}{6},\ n+\frac{5}{2}\\ -n+\frac{5}{6},\, n+5,\, n+3\end{bmatrix}\begin{bmatrix}2\left(n-\frac{1}{3}\right)\\ -1\end{bmatrix}\right\},\ d>\gamma D. \tag{6.69}$$

If the displacement does not depend on the propagation direction and $\gamma = 1$, then the integration over the axial coordinate can be performed. One finds that tilt variances for small displacements are

$$\begin{bmatrix}\sigma_{\parallel}^2\\ \sigma_{\perp}^2\end{bmatrix} = -\frac{29.6\,\mu_0}{D^{1/3}}$$
$$\times\left\{\sum_{n=1}^{\infty}\frac{(-1)^n}{n\,!}\left(\frac{d}{D}\right)^{2n} \mathit{\Gamma}\begin{bmatrix} n+\frac{1}{6},\, -n+\frac{7}{3}\\ n+2,\, -n+\frac{29}{6},\, -n+\frac{17}{6}\end{bmatrix}\begin{bmatrix}2n+1\\ 1\end{bmatrix}\right.$$
$$\left.+\sum_{n=0}^{\infty}\frac{(-1)^n}{n\,!}\left(\frac{d}{D}\right)^{2n+14/3} \mathit{\Gamma}\begin{bmatrix} -n-\frac{7}{3}, n+\frac{5}{2}\\ n+\frac{13}{3}, -n+\frac{5}{2}, -n+\frac{1}{2}\end{bmatrix}\begin{bmatrix}2n+\frac{17}{3}\\ 1\end{bmatrix}\right\},\ d<D. \tag{6.70}$$

For large displacements one obtains

$$\begin{bmatrix}\sigma_{\parallel}^2\\ \sigma_{\perp}^2\end{bmatrix} = \frac{6.08\,\mu_0}{D^{1/3}}\left\{\begin{bmatrix}1\\ 1\end{bmatrix}\right.$$
$$\left.-4.86\sum_{n=0}^{\infty}\frac{(-1)^n}{n\,!}\left(\frac{D}{d}\right)^{1/3+2n} \mathit{\Gamma}\begin{bmatrix} n-\frac{5}{6},\ n+\frac{5}{2}\\ -n+\frac{5}{6},\, n+5,\, n+3\end{bmatrix}\begin{bmatrix}2\left(n-\frac{1}{3}\right)\\ -1\end{bmatrix}\right\},\ d>D. \tag{6.71}$$

For very large displacements the first term is the only significant one. Tilt variance for each component for very large separations is equal to the total tilt variance of a single wave given in eq. 4.22. This is what one would expect since two uncorrelated tilts are being subtracted.

For small displacements, the first term in eq. 6.70 is the only significant term and gives

$$\begin{bmatrix} \sigma_{\parallel}^2 \\ \sigma_{\perp}^2 \end{bmatrix} \approx \frac{2.67\,\mu_0}{D^{1/3}} \left(\frac{d}{D}\right)^2 \begin{bmatrix} 3 \\ 1 \end{bmatrix}. \tag{6.72}$$

The parallel component is three times the perpendicular component of tilt variance. The value of total rms tilt is

$$T \approx \frac{3.27\,\mu_0^{1/2}}{D^{1/6}} \frac{d}{D}. \tag{6.73}$$

In some systems that propagate laser beams, a tracking system looks through a certain part of the main aperture, and the laser beam may propagate out of a different part of the aperture. This misregistration can cause a relative jitter on the laser beam if the tracked signal is used to direct it. For a 60-cm aperture with a displacement of 5 cm, the rms jitter is 442 nanoradians for an HV-21 turbulence model at zenith.

Change the summations to generalized hypergeometric functions, and convert the expression of one minus such a function into a different generalized hypergeometric function with eq. 1.42, to obtain

$$\begin{bmatrix} \sigma_{\parallel}^2 \\ \sigma_{\perp}^2 \end{bmatrix} = \frac{6.08\,\mu_0}{D^{1/3}} \left\{ \begin{bmatrix} 1.316 \left(\frac{d}{D}\right)^2 {}_5F_4\left[\frac{7}{6}, -\frac{17}{6}, -\frac{5}{6}, \frac{5}{2}, 1; -\frac{1}{3}, 3, \frac{3}{2}, 2; \left(\frac{d}{D}\right)^2\right] \\ 0.4392 \left(\frac{d}{D}\right)^2 {}_4F_3\left[\frac{7}{6}, -\frac{17}{6}, -\frac{5}{6}, 1; -\frac{1}{3}, 3, 2; \left(\frac{d}{D}\right)^2\right] \end{bmatrix} \right.$$

$$\left. + \begin{bmatrix} 2.195 \left(\frac{d}{D}\right)^{14/3} {}_4F_3\left[\frac{5}{2}, -\frac{3}{2}, \frac{1}{2}, \frac{23}{6}; \frac{17}{6}, \frac{13}{3}, \frac{10}{3}; \left(\frac{d}{D}\right)^2\right] \\ 0.388 \left(\frac{d}{D}\right)^{14/3} {}_3F_2\left[\frac{5}{2}, -\frac{3}{2}, \frac{1}{2}; \frac{13}{3}, \frac{10}{3}; \left(\frac{d}{D}\right)^2\right] \end{bmatrix} \right\}, \quad d < D, \tag{6.74}$$

and

$$\begin{bmatrix} \sigma_{\parallel}^2 \\ \sigma_{\perp}^2 \end{bmatrix} = \frac{6.08\,\mu_0}{D^{1/3}} \left\{ \begin{bmatrix} 1 \\ 1 \end{bmatrix} - \begin{bmatrix} 0.531 \left(\frac{D}{d}\right)^{1/3} {}_4F_3\left[-\frac{5}{6}, \frac{5}{2}, \frac{1}{6}, \frac{2}{3}; 5, 3, -\frac{1}{3}; \left(\frac{D}{d}\right)^2\right] \\ 0.799 \left(\frac{D}{d}\right)^{1/3} {}_3F_2\left[-\frac{5}{6}, \frac{5}{2}, \frac{1}{6}; 5, 3; \left(\frac{D}{d}\right)^2\right] \end{bmatrix} \right\},$$

$$d > D. \tag{6.75}$$

These variances vary with zenith angle as $\sec(\xi)$ if the displacement is not a function of z. They are plotted in Fig. 6.12 versus displacement.

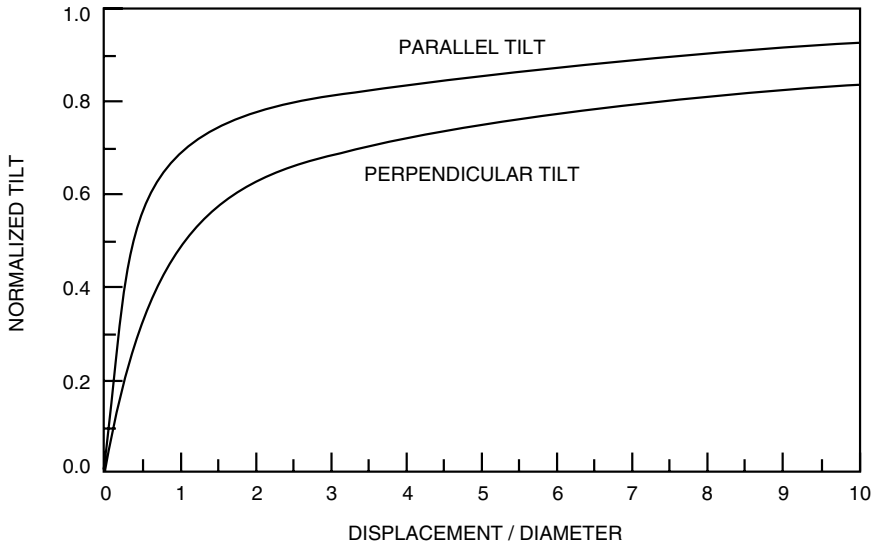

Figure 6.12. Tilt anisoplanatism versus displacement, normalized to aperture tilt. The tilt component parallel to the displacement is 1.73 times that of the perpendicular component, for small displacements. For very large displacements these components are equal. The tilt variance increases rapidly with displacement so that when the displacement is equal to the diameter, tilt variance is one-half that of a single wave. This curve is independent of the turbulence distribution along the propagation path.

For reference the expression for tilt anisoplanatism for the general case is given by

$$\begin{bmatrix} \sigma_{\parallel}^2 \\ \sigma_{\perp}^2 \end{bmatrix} = \frac{6.08}{D^{1/3}} \int_0^L dz\, C_n^2(z) \gamma^{5/3}$$
$$\left\{ \begin{bmatrix} 1.316 \left(\frac{d}{\gamma D}\right)^2 {}_5F_4 \left[\frac{7}{6}, -\frac{17}{6}, -\frac{5}{6}, \frac{5}{2}, 1; -\frac{1}{3}, 3, \frac{3}{2}, 2; \left(\frac{d}{\gamma D}\right)^2\right] \\ 0.4392 \left(\frac{d}{\gamma D}\right)^2 {}_4F_3 \left[\frac{7}{6}, -\frac{17}{6}, -\frac{5}{6}, 1; -\frac{1}{3}, 3, 2; \left(\frac{d}{\gamma D}\right)^2\right] \end{bmatrix} \right.$$
$$\left. + \begin{bmatrix} 2.195 \left(\frac{d}{\gamma D}\right)^{14/3} {}_4F_3 \left[\frac{5}{2}, -\frac{3}{2}, \frac{1}{2}, \frac{23}{6}; \frac{17}{6}, \frac{13}{3}, \frac{10}{3}; \left(\frac{d}{\gamma D}\right)^2\right] \\ 0.388 \left(\frac{d}{\gamma D}\right)^{14/3} {}_3F_2 \left[\frac{5}{2}, -\frac{3}{2}, \frac{1}{2}; \frac{13}{3}, \frac{10}{3}; \left(\frac{d}{\gamma D}\right)^2\right] \end{bmatrix} \right\}, d < \gamma D, \quad (6.76)$$

and

$$\begin{bmatrix}\sigma_{\parallel}^2\\ \sigma_{\perp}^2\end{bmatrix} = \frac{6.08}{D^{1/3}}\int_0^L dz\, C_n^2(z)\gamma^{5/3}$$
$$\left\{\begin{bmatrix}1\\ 1\end{bmatrix} - \begin{bmatrix}0.531\left(\frac{\gamma D}{d}\right)^{1/3}{}_4F_3\left[-\frac{5}{6},\frac{5}{2},\frac{1}{6},\frac{2}{3};5,3,-\frac{1}{3};\left(\frac{\gamma D}{d}\right)^2\right]\\ 0.799\left(\frac{\gamma D}{d}\right)^{1/3}{}_3F_2\left[-\frac{5}{6},\frac{5}{2},\frac{1}{6};5,3;\left(\frac{\gamma D}{d}\right)^2\right]\end{bmatrix}\right\},$$
$$d > \gamma D. \qquad (6.77)$$

If one is interested in calculating tilt anisoplanatism for two beams pointing in different directions, then displacement is a function of distance, and the axial integration results in the summation that contains various different moments of the turbulence distribution. For the Hufnagel-Valley-turbulence model these can be evaluated analytically; therefore, it is very easy to make calculations for specific turbulence levels, aperture sizes, and zenith angles.

If the displacement between the two beams is an angle θ, then the expression for tilt anisoplanatism is obtained with the substitution $d = \theta z$ in the above equations. The displacement is a small distance low in the atmosphere, however it can exceed the diameter at higher altitudes. Therefore, the solution for small displacement applies at low altitudes and that for large displacements applies at higher altitudes. The solution is a sum of a lower and upper contribution,

$$\begin{bmatrix}\sigma_{\parallel}^2\\ \sigma_{\perp}^2\end{bmatrix} = \begin{bmatrix}\sigma_{\parallel}^2\\ \sigma_{\perp}^2\end{bmatrix}_L + \begin{bmatrix}\sigma_{\parallel}^2\\ \sigma_{\perp}^2\end{bmatrix}_U. \qquad (6.78)$$

The lower contribution, with $H_c = D\cos(\xi)/\theta$, is

$$\begin{bmatrix}\sigma_{\parallel}^2\\ \sigma_{\perp}^2\end{bmatrix}_L = \frac{6.08}{D^{1/3}}\int_0^{H_c} dz\, C_n^2(z)$$
$$\times\left\{\begin{bmatrix}1.316\left(\frac{\theta z}{D}\right)^2{}_5F_4\left[\frac{7}{6},-\frac{17}{6},-\frac{5}{6},\frac{5}{2},1;-\frac{1}{3},3,\frac{3}{2},2;\left(\frac{\theta z}{D}\right)^2\right]\\ 0.4392\left(\frac{\theta z}{D}\right)^2{}_4F_3\left[\frac{7}{6},-\frac{17}{6},-\frac{5}{6},1;-\frac{1}{3},3,2;\left(\frac{\theta z}{D}\right)^2\right]\end{bmatrix}\right.$$
$$\left.+\begin{bmatrix}2.195\left(\frac{\theta z}{D}\right)^{14/3}{}_4F_3\left[\frac{5}{2},-\frac{3}{2},\frac{1}{2},\frac{23}{6};\frac{17}{6},\frac{13}{3},\frac{10}{3};\left(\frac{\theta z}{D}\right)^2\right]\\ 0.388\left(\frac{\theta z}{D}\right)^{14/3}{}_3F_2\left[\frac{5}{2},-\frac{3}{2},\frac{1}{2};\frac{13}{3},\frac{10}{3};\left(\frac{\theta z}{D}\right)^2\right]\end{bmatrix}\right\}. \qquad (6.79)$$

The upper contribution is

$$\begin{bmatrix}\sigma_{\parallel}^2\\ \sigma_{\perp}^2\end{bmatrix}_U = \frac{6.08}{D^{1/3}} \times \left\{ \mu_0^+(H_c) - \int_{H_c}^{L} dz\, C_n^2(z) \begin{bmatrix} 0.531\left(\frac{D}{\theta z}\right)^{1/3} {}_4F_3\left[-\frac{5}{6}, \frac{5}{2}, \frac{1}{6}, \frac{2}{3}; 5, 3, -\frac{1}{3}; \left(\frac{D}{\theta z}\right)^2\right] \\ 0.798\left(\frac{D}{\theta z}\right)^{1/3} {}_3F_2\left[-\frac{5}{6}, \frac{5}{2}, \frac{1}{6}; 5, 3; \left(\frac{D}{\theta z}\right)^2\right] \end{bmatrix} \right\}. \tag{6.80}$$

The upper and lower partial turbulence moments, μ_m^+ and μ_m^-, are defined in Sec. 4.1.

The turbulence above 30 km is small and is generally negligible. For small displacement angles such that H_c is higher than the uppermost turbulence, the anisoplanatic tilt variance is given solely by the lower contribution, and the leading terms of the series are

$$\begin{bmatrix}\sigma_{\parallel}^2\\ \sigma_{\perp}^2\end{bmatrix} = \frac{2.67\,\mu_2^-(H_c)}{D^{1/3}}\left(\frac{\theta}{D}\right)^2 \begin{bmatrix}3\\1\end{bmatrix} - \frac{3.68\,\mu_4^-(H_c)}{D^{1/3}}\left(\frac{\theta}{D}\right)^4 \begin{bmatrix}5\\1\end{bmatrix} + \frac{2.35\,\mu_{14/3}^-(H_c)}{D^{1/3}}\left(\frac{\theta}{D}\right)^{14/3} \begin{bmatrix}\frac{17}{3}\\1\end{bmatrix} + \cdots . \tag{6.81}$$

The total anisoplanatic tilt multiplied by the diameter is plotted versus aperture diameter for various angular separations in Fig. 6.13 for the HV-21 turbulence model. As one can observe in the figure, the plotted values decrease as the one-sixth power of the diameter for most regions of the plots. In those regions, the tilt is given with small error solely by the first term of the series. The one-term approximation applies when $\theta < D/40,000$. In this region for the HV-21 turbulence model, the total rms tilt anisoplanatism σ_T is given by

$$\sigma_T(\text{nrad}) \approx 14.2\,\theta\,(\mu\text{rad})\,\sec^{1.5}(\xi)\;/D^{7/6}.$$

Define a characteristic tilt anisoplanatic angle as the angle between two sources for which the tilt jitter is equal to one-half the diffraction-limited beam size. At this angle the jitter radius is equal to that of the perfectly corrected spot. For these small angles the first term of the expression above gives a reasonable approximation of the angle jitter, and the partial moment becomes a full moment. This characteristic tilt anisoplanatic angle θ_{Tc} is

$$\theta_{Tc} = \frac{0.184\,\lambda\,D^{1/6}}{\mu_2^{1/2}}. \tag{6.82}$$

For a HV-21 turbulence model and a 1-m diameter aperture at 0.5 μm operating wavelength the characteristic tilt anisoplanatic angle is 21 μrad.

For large angles in which the transition altitude is close to the ground, tilt variance is given solely by the upper contribution as

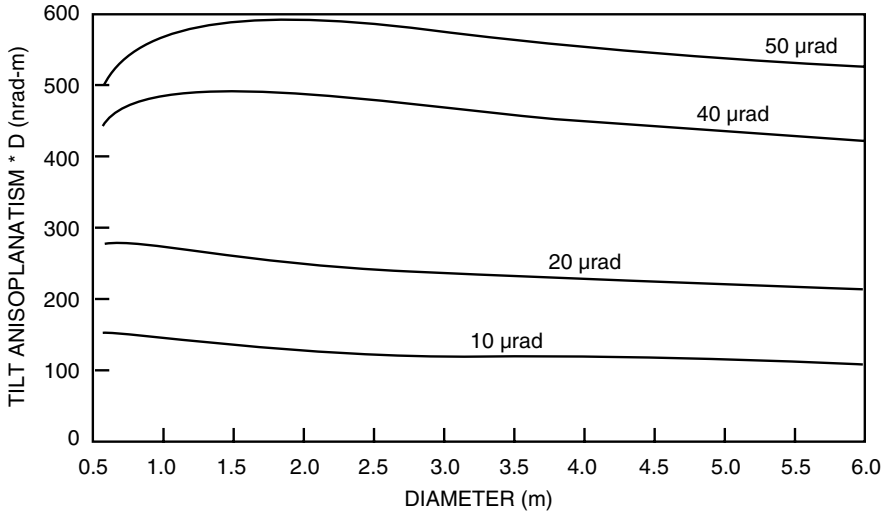

Figure 6.13. Tilt anisoplanatism at zenith times aperture diameter versus aperture diameter with the HV-21 turbulence model. Plots are given for source separations of 10, 20, 40, and 50 μrad.

$$\begin{bmatrix} \sigma_{\parallel}^2 \\ \sigma_{\perp}^2 \end{bmatrix} \approx \frac{1}{D^{1/3}} \left\{ 6.08\, \mu_0^+ (H_c) \begin{bmatrix} 1 \\ 1 \end{bmatrix} - 4.85\, \mu_{-1/3}^+ (H_c) \left(\frac{D}{\theta} \right)^{1/3} \begin{bmatrix} \frac{2}{3} \\ 1 \end{bmatrix} + 0.0205\, \mu_{-7/3}^+ (H_c) \left(\frac{D}{\theta} \right)^{7/3} \begin{bmatrix} -\frac{4}{3} \\ 1 \end{bmatrix} + \cdots \right. . \tag{6.83}$$

The leading term is twice the tilt variance of a single wave. The angular separation of the beams has to be very large before this asymptotic limit is approached.

6.7 Power Spectral Density of Tilt

In this section, the power spectral density for tilt of a collimated wave is derived. Plane-wave results have been discussed briefly in *Tatarski* (1971), and presented in more detail in *Greenwood* and *Fried* (1976) who made a simplifying assumption in order to obtain simple, analytic results. *Fields* (1983) coined the term "parallel approximation" for this simplification. One consequence of the parallel approximation is that the rate at which spectra decay at high frequencies is underestimated. *Tyler* (1986) subsequently analyzed plane-wave tilt spectra without making this approximation. However, his results remain in integral form, which has an integral over a dummy variable related to spatial frequency and an integral over altitude. In a subsequent report, *Vaughn* (1986) provided numerical techniques to solve the integrals presented by Tyler, but no solutions have been published that do not rely heavily on numerical integration. A similar approach has been used in tilt spectra associated with a point source

(spherical wave analysis). This leads to integral expressions given in *Hogge* and *Butts* (1976) and *Butts* (1980) that also must be evaluated numerically.

Power spectral density of tilt is found here with the use of the general expression for power spectral density given in eq. 2.134 and the filter function for Zernike tilt in eq. 3.22. It is assumed that one is in the near field so that the cosine term can be replaced by unity. This assumption breaks down at sufficiently high frequencies, where the exact equation must be used. The effect of including the cosine term is to lower the high-frequency spectrum. The spectral density is

$$S_T(\omega) = 2.606\, k_0^2 \omega \int_0^L dz\, \frac{C_n^2(z)}{v^2(z)} \times \int_0^\infty dc\, \frac{c\, U(c-1)}{\sqrt{c^2-1}} \left[\frac{\omega c}{v(z)}\right]^{-11/3} \left(\frac{16}{k_0 D}\right)^2 \left\{\frac{J_2\left[\omega c D/2v(z)\right]}{\omega c D/2v(z)}\right\}^2. \quad (6.84)$$

Let $x = 2v(z)/\omega D$, to give

$$S_T(\omega) = \frac{2668}{D^4 \omega^{14/3}} \int_0^L dz\, C_n^2(z)\, v^{11/3}(z) \int_0^\infty \frac{dc}{c} \frac{U(c-1)}{\sqrt{c^2-1}} J_2^2\left(\frac{c}{x}\right) c^{-11/3}. \quad (6.85)$$

To evaluate the integral over c, define the functions $h_1(x/c) = J_2^2\,(c/x)$, and $h_2(c) = U(c-1)/\sqrt{c^2-1}\, c^{-11/3}$. The integral over c can be expressed as a Mellin convolution integral with the Mellin transforms in eq. 1.52 and eq. 1.56. Let $s \to 2s$ to obtain for the c integral

$$I = \frac{1}{2} \frac{1}{2\pi i} \int_C ds\, \Gamma\left[\begin{matrix} -s+\frac{1}{2},\, s+2,\, s+\frac{7}{3} \\ -s+1,\, -s+3,\, s+\frac{17}{6} \end{matrix}\right] \left[\frac{\omega D}{2v(z)}\right]^{-2s}. \quad (6.86)$$

Since $\Delta = 2$, the integration path is closed in the left-half plane, and the contributions at the two sets of poles at $s = -2 - n$, and $s = -7/3 - n$ for $n = 0,\, 1,\, 2,\, \ldots$ give

$$I = \frac{1}{2} \sum_{n=0}^\infty \frac{(-1)^n}{n\,!} \left\{ \Gamma\left[\begin{matrix} n+\frac{5}{2},\, -n+\frac{1}{3} \\ n+3,\, n+5,\, -n+\frac{5}{6} \end{matrix}\right] \left[\omega D/2v(z)\right]^{4+2n} + \Gamma\left[\begin{matrix} n+\frac{17}{6},\, -n-\frac{1}{3} \\ n+\frac{10}{3},\, n+\frac{16}{3},\, -n+\frac{1}{2} \end{matrix}\right] \left[\omega D/2v(z)\right]^{14/3+2n} \right\}. \quad (6.87)$$

To obtain the spectral density, the velocity profile must be inserted into the above series, and the integrations along the path performed. Various velocity moments, defined in eq. 4.83, have to be calculated. The final result is a series solution for the power spectral density,

$$S_T(\omega) = 52.53\left(\frac{2}{\omega}\right)^{2/3}\sum_{n=0}^{\infty}\frac{(-1)^n}{n!}\left\{\Gamma\begin{bmatrix} n+\frac{5}{2},\ -n+\frac{1}{3} \\ n+3,\ n+5,\ -n+\frac{5}{6}\end{bmatrix}\left(\frac{\omega D}{2}\right)^{2n} v_{-2n-1/3}\right.$$
$$\left. + \Gamma\begin{bmatrix} n+\frac{17}{6},\ -n-\frac{1}{3} \\ n+\frac{10}{3},\ n+\frac{16}{3},\ -n+\frac{1}{2}\end{bmatrix}\left(\frac{\omega D}{2}\right)^{2n+2/3} v_{-2n-1}\right\}. \tag{6.88}$$

For the slew-dominated case in which the velocity is proportional to axial position, the velocity moments in the above expression are infinite. To obtain a solution for this problem, one must evaluate the power series in eq. 6.87, which is finite, and then perform the axial integration.

The low-frequency asymptote comes from the first term of the first series, and the dependence is $\omega^{-2/3}$. For large frequencies, one obtains an asymptotic series by deforming the integration path into the right half plane, thus obtaining the pole contributions at $s = -1/2 - n$ for $n = 0, 1, 2 \ldots, n_o$. The $E(x)$ term is significant in this case. It is found with eq. 5.94. Inserting this into eq. 5.51, one finds the asymptotic solution is

$$I \sim \frac{1}{2\sqrt{\pi}}\left[\frac{2v(z)}{\omega D}\right]^{3/2}\cos\left\{\left[\frac{\omega D}{v(z)}\right]-\frac{\pi}{4}\right\}$$
$$+\frac{1}{2}\sum_{n=0}^{n_o}\frac{(-1)^n}{n!}\Gamma\begin{bmatrix} n+\frac{5}{2},\ n+\frac{17}{6} \\ n+\frac{10}{3},\ -n+\frac{1}{2},\ -n+\frac{5}{2}\end{bmatrix}\left[\frac{2v(z)}{\omega D}\right]^{1+2n}. \tag{6.89}$$

The power spectral density at high frequencies is thus

$$S_T(\omega) \sim 52.53\, D^{2/3}\left(\frac{2}{\omega D}\right)^{17/3}$$
$$\times\left\{\int_0^L dz\, C_n^2(z)\frac{1}{\sqrt{\pi}}\left[\frac{2v(z)}{\omega D}\right]^{1/2} v^{14/3}(z)\cos\left\{\left[\frac{\omega D}{v(z)}\right]-\frac{\pi}{4}\right\}\right.$$
$$\left.+\sum_{n=0}^{n_o}\frac{(-1)^n}{n!}\Gamma\begin{bmatrix} n+\frac{5}{2},\ n+\frac{17}{6} \\ n+\frac{10}{3},\ -n+\frac{1}{2},\ -n+\frac{5}{2}\end{bmatrix}\left(\frac{2}{\omega D}\right)^{2n} v_{2n+14/3}\right\}. \tag{6.90}$$

The first series term, which is the high-frequency asymptote, varies as $\omega^{-17/3}$.

If velocity is constant along the path, spectral density for small values of $\omega D/2v$ is found with the rules in Sec. 1.3 as

$$S_T(\omega) = 3.453\,\frac{\mu_0 D^{2/3}}{v}\left(\frac{2v}{\omega D}\right)^{2/3}\left\{{}_2F_3\left[\tfrac{5}{2},\tfrac{1}{6};3,5,-\tfrac{2}{3};-\left(\frac{\omega D}{2v}\right)^2\right]\right.$$
$$\left.-0.5394\left(\frac{\omega D}{2v}\right)^{2/3}{}_2F_3\left[\tfrac{17}{6},\tfrac{1}{2};\tfrac{10}{3},\tfrac{16}{3},\tfrac{4}{3};-\left(\frac{\omega D}{2v}\right)^2\right]\right\}. \tag{6.91}$$

The spectral density for large values of $\omega D/2v$ is

$$S_T(\omega) = 52.53\frac{\mu_0 D^{2/3}}{v}\left(\frac{2v}{\omega D}\right)^{17/3}\left\{\frac{1}{\sqrt{\pi}}\left(\frac{2v}{\omega D}\right)^{1/2}\cos\left[\left(\frac{\omega D}{v}\right)-\frac{\pi}{4}\right]\right.$$
$$\left.+\sum_{n=0}^{n_o}\frac{(-1)^n}{n!}\,\Gamma\left[\begin{matrix} n+\frac{5}{2},\, n+\frac{17}{6} \\ n+\frac{10}{3},\, -n+\frac{1}{2},\, -n+\frac{5}{2}\end{matrix}\right]\left(\frac{2v}{\omega D}\right)^{2n}\right\}, \quad fD/v > 1. \tag{6.92}$$

Power spectral density is plotted in Fig. 6.14. The spectrum is normalized to give a value of unity when fD/v is unity. In the figure both Taylor series (first 40 terms) and asymptotic solution (first 5 terms) are plotted. For $fD/v < 1$, the asymptotic series was set equal to unity since the series is very inaccurate in that region, and above 5 the Taylor series was discarded because it becomes inaccurate with the 40-term approximation. The two series give virtually the same answer in the parameter range between 1 and 5. Notice the strong influence of the cosine term on the spectrum. If velocity is allowed to vary along the path, various cosine terms for different velocities tend to average to zero, and the spectrum does not exhibit nearly as strong an oscillatory behavior.

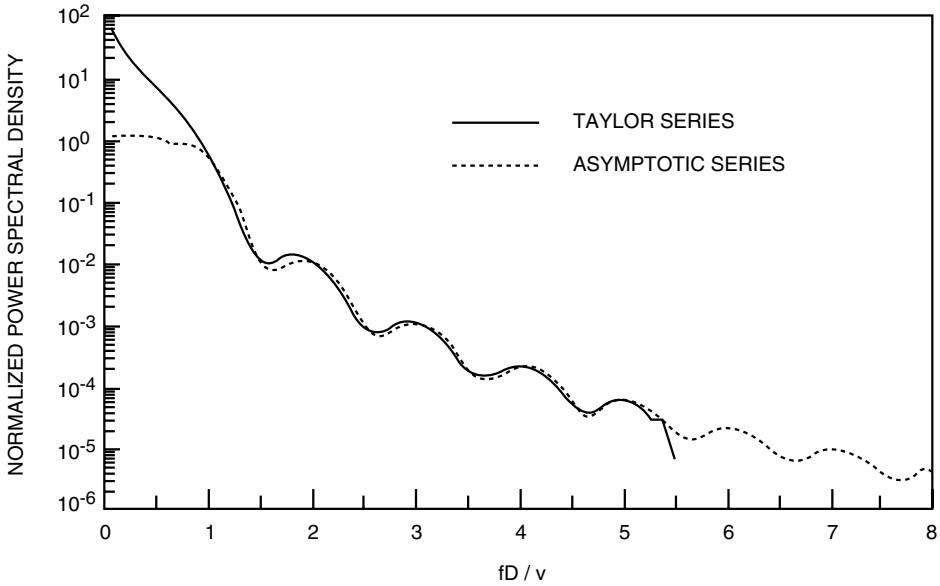

Figure 6.14. Log-linear plot of the power spectral density of tilt. The velocity and turbulence are constant along the path. Notice the agreement of asymptotic and Taylor series over a considerable range. This curve is independent of the turbulence distribution along the propagation path.

6.8 Scintillation with Finite Apertures and Sources

Scintillation in a receiver is considerably reduced from that measured with a very small aperture if the aperture is a few inches in diameter. Also, the scintillation from a finite size object such as a planet is considerably lower than that from a point source such as a star. A receiver in space, if large enough, can average the scintillation from a transmitter on the ground.

These averaging effects can be calculated with the filter function approach. In these problems one is interested in the average scintillation over an aperture or at a point receiver from a finite source. One has to average the intensity, but the statistical expressions are given in terms of the log intensity. The Rytov approximation, upon which this work is based, is valid for low levels of scintillation, and in that approximation the normalized intensity is well approximated by the log intensity. Therefore, the average of the log intensity approximates the average of the intensity. The scintillation from stars is low, and the approximation holds for that practical problem.

The exact solution was found by *Fried* (1967) for the case where the scintillation is not saturated by using a numerical integration. *Andrews* (1992) used the low scintillation approximation to obtain asymptotic results for constant turbulence with finite inner scale. His results agree with those given here.

The scintillation averaged over an aperture is obtained with the filter function in eq. 3.56 for a source at infinity that is inserted into the formula for variance given in eq. 2.112. The aperture-averaged scintillation is

$$\sigma^2_{\chi A} \approx 0.2073\, k_0^2 \int_0^L dz\, C_n^2(z) \int d\boldsymbol{\kappa}\, f(\kappa) \sin^2\left[P\left(\gamma,\kappa,z\right)\right] \left[\frac{2J_1\left(\gamma\kappa D/2\right)}{\gamma\kappa D/2}\right]^2 . \quad (6.93)$$

The diffraction parameter is $P\left(\gamma,\kappa,z\right) = \gamma\kappa^2 z/2k_0$ for propagation towards the receiver. Assuming Kolmogorov turbulence and performing the angular integration, one obtains

$$\sigma^2_{\chi A} = 1.303\, k_0^2 \int_0^L dz\, C_n^2(z) \int_0^\infty \frac{d\kappa}{\kappa}\, \kappa^{-5/3} \sin^2\left(\frac{\gamma\kappa^2 z}{2k_0}\right) \left[\frac{2J_1\left(\gamma\kappa D/2\right)}{\gamma\kappa D/2}\right]^2 . \quad (6.94)$$

Let $w^2 = \gamma\kappa^2 z/2k_0$, and $x = \sqrt{2z/\gamma D^2 k_0}$, to obtain

$$\sigma^2_{\chi A} = 2.925\, k_0^{7/6} \int_0^L dz\, C_n^2(z)\, (z\gamma)^{5/6}\, x^2 \int_0^\infty \frac{dw}{w}\, w^{-11/3} \sin^2\left(w^2\right) J_1^2\left(w/x\right). \quad (6.95)$$

The last integral can be evaluated with the Mellin transforms in eq. 1.50 and eq. 1.52. After the substitution $s \to -2s$ it is equal to

$$I = \int_0^\infty \frac{dw}{w}\, w^{-11/3}\, \sin^2\left(w^2\right)\, J_1^2(w/x)$$
$$= -\frac{1}{8}\frac{1}{2\pi i}\int_C ds\, x^{2s}\, \Gamma\left[\begin{matrix} -s/2 - \frac{11}{12}*,\ s+1,\ -s+\frac{1}{2} \\ s/2 + \frac{17}{12},\ -s+2,\ -s+1 \end{matrix}\right]. \tag{6.96}$$

Because both the sign of the integration variable and the direction of the integration path are changed, the sign of the expression remains unchanged. Since $\Delta = 1$, the integration path is closed to the left, and one obtains residues of poles at $s = -11/6$, and at $s = -n - 1$ for $n = 0,\ 1,\ 2,\ \ldots$, which gives

$$I = -\frac{1}{8}\left\{\sum_{n=0}^{\infty}\frac{(-1)^n}{n\,!}x^{-2n-2}\Gamma\left[\begin{matrix} n/2 - \frac{5}{12},\ n+\frac{3}{2} \\ -n/2 + \frac{11}{12},\ n+3,\ n+2 \end{matrix}\right] - 0.1331\, x^{-11/3}\right\}. \tag{6.97}$$

With this result the scintillation in a receiver at $z = 0$ is equal to

$$\sigma_{\chi A}^2 = -0.3656\, k_0^{7/6}\int_0^L dz\, C_n^2(z)\,(z\gamma)^{5/6}\left\{0.1331\,\left(\frac{\gamma D^2 k_0}{2z}\right)^{5/6}\right.$$
$$\left. + \sum_{n=0}^{\infty}\frac{(-1)^n}{n\,!}\left(\frac{\gamma D^2 k_0}{2z}\right)^n \Gamma\left[\begin{matrix} n/2 - \frac{5}{12},\ n+\frac{3}{2} \\ -n/2 + \frac{11}{12},\ n+3,\ n+2 \end{matrix}\right]\right\}. \tag{6.98}$$

One could express this result in terms of generalized hypergeometric functions by making the additional substitution $s \to -2s$ in eq. 6.96 and then using the Gauss-Legendre multiplication formula to obtain unity coefficients for s in all the Gamma functions. That will not be done here. For very small diameters the first series term dominates, and one obtains the point-source result.

One cannot evaluate this expression by using turbulence moments, since the negative moments are equal to infinity. In this case one obtains the scintillation by first evaluating the power series in eq. 6.98, and then performing the axial integration.

Very often the parameter in the previous equation is very large, and the answer can be approximated by the first term of the asymptotic series. The steepest-descent contribution is negligible since it has exponential decay. The pole at $s = 1/6$ gives the asymptotic contribution as

$$\sigma_{\chi A}^2 \sim \frac{4.34}{D^{7/3}}\int_0^L dz\, C_n^2(z)\,\frac{z^2}{\gamma^{1/3}}. \tag{6.99}$$

This approximate result could also be obtained by making the approximation $\sin^2(w^2) \approx w^4$ in eq. 6.95 and then evaluating the integral by table lookup.

For propagation from space to ground $\gamma = (L - z)/L$. If the source is well above the atmosphere, then this is close to unity. In this case the scintillation is equal to

$$\sigma_{\chi A}^2 \sim \frac{4.34\,\mu_2}{D^{7/3}}. \tag{6.100}$$

The aperture-averaged scintillation does not depend on the wavelength. That is the reason that no scintillation-induced color is evident in a star image as seen in a telescope. The aperture-averaged scintillation depends on the second moment of turbulence, which is close to the five-thirds moment that is needed to calculate the isoplanatic angle. By modifying the aperture function using masks in their isoplanometer, *Walters* et al. (1979) were able to closely approximate the aperture-averaged scintillation by the five-third moment of turbulence. In this manner the instrument is used to estimate isoplanatic angle.

If turbulence is constant along the path, for plane-wave propagation the variance is

$$\sigma_{\chi A}^2 \sim \frac{1.45\,C_n^2\,L^3}{D^{7/3}}. \tag{6.101}$$

Scintillation with no averaging is given in eq. 4.77 as

$$\sigma_\chi^2 = 0.5631\,k_0^{7/6}\mu_{5/6}. \tag{6.102}$$

The scintillation reduction ratio is

$$\frac{\sigma_{\chi A}^2}{\sigma_\chi^2} \sim 7.7\,\frac{\mu_2}{\mu_{5/6}\,D^{7/3}k_0^{7/6}} = 0.902\,\frac{\mu_2}{\mu_{5/6}}\left(\frac{\lambda}{D^2}\right)^{7/6} = \left(\frac{D_c}{D}\right)^{7/3}, \quad D \gg D_c, \tag{6.103}$$

where D_c is a characteristic diameter for scintillation averaging. It is given by

$$D_c = 0.957\left(\frac{\mu_2}{\mu_{5/6}}\right)^{3/7}\sqrt{\lambda}\,\sec(\xi)^{1/2}, \tag{6.104}$$

where the zenith dependence has been explicitly shown. The diameter needed for scintillation averaging increases as one moves off zenith.

For the HV-21 model of turbulence, the relevant turbulence moments are $\mu_2 = 1.91 \times 10^{-5}\mathrm{m}^{7/3}$ and $\mu_{5/6} = 5.45 \times 10^{-10}\mathrm{m}^{7/6}$. At a wavelength of 0.5 μm the characteristic diameter is 6 cm.

If turbulence is constant along the path, eq. 6.103 becomes

$$\frac{\sigma_{\chi A}^2}{\sigma_\chi^2} \sim 0.109\left(\frac{\sqrt{\lambda L}}{D/2}\right)^{7/3}, \quad D \gg \sqrt{\lambda L}. \tag{6.105}$$

This formula agrees with the power-law dependence given in *Tatarski* (1971). For this case the characteristic diameter is

$$D_c = 0.774\,\sqrt{\lambda L}. \tag{6.106}$$

One can show for constant turbulence along the path that the characteristic diameter for a spherical wave with source at $z = L$ is twice the plane-wave value.

$$D_{cSpherical} = 2D_c. \tag{6.107}$$

The formula for large diameter can be made valid for any diameter by using the interpolation formula given by *Andrews* (1992)

$$\frac{\sigma_{\chi A}^2}{\sigma_\chi^2} = \left[1 + \left(\frac{D}{D_c}\right)^2\right]^{-7/6}. \tag{6.108}$$

Sometimes one is interested in the structure of turbulence for a wave propagating from ground to space. This information can be used to determine the aperture averaging of an aperture in space or the grid spacing required to resolve the scintillation structure in a numerical propagation code. For the case of propagation from $z = 0$ to $z = L$, one must replace z with $L - z$ in eq. 6.98 to obtain

$$\sigma_{\chi A}^2 = -0.3656\, k_0^{7/6} \int_0^L dz\, C_n^2(z)\, ((L-z)\gamma)^{5/6} \left\{ 0.1331 \left(\frac{\gamma D^2 k_0}{2(L-z)}\right)^{5/6} + \sum_{n=0}^{\infty} \frac{(-1)^n}{n\,!} \left(\frac{\gamma D^2 k_0}{2(L-z)}\right)^n \Gamma \left[\begin{matrix} n/2 - \frac{5}{12},\, n + \frac{3}{2} \\ -n/2 + \frac{11}{12},\, n+3,\, n+2 \end{matrix} \right] \right\}. \tag{6.109}$$

For a point source on the ground $\gamma = z/L$ and for L well above the atmosphere so that $L - z \approx L$, one obtains

$$\sigma_{\chi A}^2 = -0.3656\, k_0^{7/6} \int_0^L dz\, C_n^2(z) z^{5/6} \left\{ 0.1331 \left(\frac{z D^2 k_0}{2L^2}\right)^{5/6} + \sum_{n=0}^{\infty} \frac{(-1)^n}{n\,!} \left(\frac{z D^2 k_0}{2L^2}\right)^n \Gamma \left[\begin{matrix} n/2 - \frac{5}{12},\, n + \frac{3}{2} \\ -n/2 + \frac{11}{12},\, n+3,\, n+2 \end{matrix} \right] \right\}. \tag{6.110}$$

The first term of the power series gives eq. 4.77, which is the scintillation in space for a point receiver, which is

$$\sigma_\chi^2 \approx 0.5631\, k_0^{7/6} \mu_{5/6}. \tag{6.111}$$

The asymptotic series for this case can be obtained from eq 6.99 by changing z to $L - z$ to obtain

$$\sigma_{\chi A}^2 \sim \frac{4.34}{D^{7/3}} \int_0^L dz\, C_n^2(z)\, \frac{(L-z)^2}{\gamma^{1/3}}. \tag{6.112}$$

For very long distances this is

$$\sigma_{\chi A}^2 \sim \frac{4.34}{D^{7/3}}\, L^{7/3} \mu_{-1/3}. \tag{6.113}$$

One can form the ratio of the aperture-averaged scintillation and that for a point receiver to find a characteristic diameter for aperture averaging as

$$D_c = 0.957\sqrt{\lambda}L \left(\frac{\mu_{-1/3}}{\mu_{5/6}}\right)^{3/7} \sec(\xi)^{-1/2}, \tag{6.114}$$

where the zenith dependence has been explicitly shown. The diameter needed for scintillation averaging decreases as one moves off zenith.

The diameter increases linearly with distance, which means that the scintillation structure is preserved; the beam structure expands linearly with distance. The structure of the scintillation has a characteristic angle given by

$$\theta_\chi = 0.957 \left(\frac{\mu_{-1/3}}{\mu_{5/6}}\right)^{3/7} \sqrt{\lambda}\sec(\xi)^{-1/2}, \tag{6.115}$$

For the HV-21 turbulence model at zenith, the characteristic angle is 35.2 μrad. A receiver in space that subtends less than this angle as viewed from the ground does not significantly reduce the scintillation. For a wave propagation code, one would have to have the mesh spacing closer than half this angle in order to capture the effect of scintillation.

Next, the case of a source of finite angular extent viewed by a point receiver is considered. In this case the filter function for a source of diameter D_s given in eq. 3.54 is rewritten in terms of the angle subtended by the source θ_s, where $\theta_s = D_s/L$. The filter function is thus

$$F(\gamma\,\boldsymbol{\kappa}) = \left[\frac{2J_1(\gamma\,\kappa\theta_s\,z/2)}{\gamma\,\kappa\theta_s\,z/2}\right]^2. \tag{6.116}$$

The analysis proceeds in the same manner as above, and with the definitions $w^2 = \gamma\kappa^2 z/2k_0$, and $x = \sqrt{2/z\theta_s^2\,k_0\,\gamma}$, one obtains eq 6.95, which is evaluated in eq. 6.96 to eq. 6.98. If the value of x is inserted into eq 6.98, one obtains

$$\sigma_{\chi A}^2 = -0.3656\,k_0^{7/6}\int_0^L dz\,C_n^2(z)\,(z\gamma)^{5/6}\left\{0.1331\left(\frac{\gamma\,z\,\theta_s^2\,k_0}{2}\right)^{5/6}\right.$$
$$\left. + \sum_{n=0}^{\infty}\frac{(-1)^n}{n\,!}\left(\frac{\gamma z\theta_s^2\,k_0}{2}\right)^n \Gamma\left[\begin{array}{c} n/2-\frac{5}{12},\, n+\frac{3}{2} \\ -n/2+\frac{11}{12}, n+3,\, n+2\end{array}\right]\right\}. \tag{6.117}$$

The leading term of the asymptotic series is

$$\sigma_{\chi A}^2 \sim \frac{4.34}{\theta_s^{7/3}}\int_0^L dz\,C_n^2(z)\,(\gamma\,z)^{-1/3}. \tag{6.118}$$

The negative moment of turbulence is finite. The leading term for scintillation from a finite source, just as for aperture averaging, does not depend on the wavelength. For propagation from space to the ground $\gamma = (L-z)/L$. If the source is well above the atmosphere, then this is close to unity. When both this is true and the source is large, the scintillation reduction ratio is

$$\frac{\sigma_{\chi A}^2}{\sigma_\chi^2} \sim 7.7 \frac{\mu_{-1/3}}{\mu_{5/6}\,\theta_s^{7/3}\,k_0^{7/6}} = 0.902 \frac{\mu_{-1/3}}{\mu_{5/6}} \left(\frac{\lambda}{\theta_s^2}\right)^{7/6} = \left(\frac{\theta_\chi}{\theta_s}\right)^{7/3}, \quad \theta_s \gg \theta_\chi, \tag{6.119}$$

where θ_χ, the characteristic angle of the source for scintillation reduction, is

$$\theta_\chi = 0.957 \left(\frac{\mu_{-1/3}}{\mu_{5/6}}\right)^{3/7} \sqrt{\lambda}\,\sec(\xi)^{-1/2}, \tag{6.120}$$

where the zenith dependence has been explicitly shown. This angle is the same as that required for a receiver to subtend in space in order to average scintillation.

For the HV-21 model the characteristic angle is equal to 35.2 μrad at a wavelength of 0.5 μm. For a planet like Venus whose apparent angular size varies between 24 and 145 μrad, there can be a significant reduction in scintillation.

If turbulence is constant along the path, the scintillation reduction factor is

$$\frac{\sigma_{\chi A}^2}{\sigma_\chi^2} \sim 2.48 \left(\frac{\lambda}{L\theta_s^2}\right)^{7/6}, \quad \theta_s \gg \sqrt{\lambda/L}. \tag{6.121}$$

The characteristic angle in this case is

$$\theta_\chi = 1.48 \sqrt{\lambda/L}. \tag{6.122}$$

6.9 Scintillation with Finite Inner Scale

The phase disturbances that results from turbulence bend the ray paths of the propagating waves. These bent rays after propagating some distance have regions of bunching and expansion, thus leading to scintillation. For close distances it is the shorter scale turbulence that affects the scintillation most significantly. Therefore, it is at short ranges that inner scale affects the scintillation most strongly, and measurements in this regime have confirmed the presence of the bump in the Hill turbulence spectrum. Most of these measurements are performed over a horizontal path for which the turbulence can be considered to be constant. I find the scintillation versus propagation distance on a collimated beam for both the Hill and Tatarski inner-scale spectra for the case in which the turbulence is constant along the propagation direction. I show the difference between their scintillation and the one with zero inner scale that for constant turbulence in eq. 4.71 is

$$\sigma_\chi^2 = 0.3071\, k_0^{7/6} L^{11/6} C_n^2. \tag{6.123}$$

Hill and *Clifford* (1978) found the scintillation for the Hill spectrum by using a numerical integration.

To obtain analytical results, use the formula for scintillation given in eq. 2.112, with the turbulence spectrum given in eq. 2.34, which has the Tatarski inner-scale spectrum. Set the outer-scale size to infinity to obtain

$$\chi_T^2 = 0.2073\, k_0^2 \int_0^L dz\, C_n^2(z) \int d\boldsymbol{\kappa}\, \kappa^{-11/3} \exp\left[-\left(\frac{\kappa^2}{\kappa_i^2}\right)\right] \sin^2\left(\frac{\kappa^2 z}{2k_0}\right). \quad (6.124)$$

The plane wave is propagated from $z = 0$ to $z = L$. Assume that the turbulence strength is constant, integrate over angle in kappa-space and along the propagation direction, to obtain

$$\chi_T^2 = -0.6513\, k_0^3 C_n^2 \int_0^\infty \frac{d\kappa}{\kappa}\, \kappa^{-11/3} \exp\left[-\left(\frac{\kappa^2}{\kappa_i^2}\right)\right] \left[\sin\left(\frac{\kappa^2 L}{k_0}\right) - \frac{\kappa^2 L}{k_0}\right]. \quad (6.125)$$

Let $y = \kappa\, (L/k_0)^{1/2}$, and $x = \kappa_i\, (L/k_0)^{1/2}$. Use the Mellin convolution theorem, the substitution $s \to 4s$, and the Legendre multiplication theorem in eq. 1.15 to obtain

$$\chi_T^2 = -0.04571\, k_0^{7/6} L^{11/6} C_n^2 \frac{1}{2\pi i} \int_C ds\, x^{-4s} \Gamma\left[\begin{matrix} s - \frac{5}{12}*,\ -s,\ -s + \frac{1}{2} \\ \frac{23}{12} - s \end{matrix}\right]. \quad (6.126)$$

Since $\Delta = 0$, the direction of path closure is determined by the parameter size. Evaluating this integral in the standard way, one obtains

$$\chi_T^2 = 0.3072\, k_0^{7/6} L^{11/6} C_n^2 \left\{ {}_2F_1\left[-\tfrac{5}{12}, -\tfrac{11}{12}; \tfrac{1}{2}; -x^{-4}\right] \right.$$
$$\left. + 6.841\ {}_2F_1\left[\tfrac{1}{12}, -\tfrac{5}{12}; \tfrac{3}{2}; -x^{-4}\right] / x^2 - 7.086\, x^{-5/3} \right\},\ x > 1, \text{ and} \quad (6.127)$$

$$\chi_T^2 = 2.177\, k_0^{7/6} L^{11/6} C_n^2\, x^{-5/3} \left\{ {}_2F_1\left[\tfrac{1}{12}, -\tfrac{5}{12}; \tfrac{3}{2}; -x^4\right] - 1 \right\},\ x < 1. \quad (6.128)$$

This is equivalent to a result given by the computer algebra program Mathematica that applies over the entire parameter range as

$$\chi_T^2 = 0.1977\, k_0^{7/6} L^{11/6} C_n^2 \frac{\left\{-11\, x^2 + 6\, (1 + x^4)^{11/12} \sin\left[11 \arctan\left(x^2\right)/6\right]\right\}}{x^2\, |\, (x^{5/3})\, |}. \quad (6.129)$$

I will now find the scintillation for the Hill spectra given in eq. 2.29. The scintillation in this case is

$$\chi_H^2 = 0.2073\, k_0^2 \int_0^L dz\, C_n^2(z)$$
$$\times \sum_{n=0}^4 a_n \int d\boldsymbol{\kappa}\, \kappa^{-11/3} (\kappa\, L_{in})^n \exp\left(-\delta\, |\kappa|\, L_{in}\right) \sin^2\left(\frac{\kappa^2 z}{2k_0}\right). \quad (6.130)$$

The constants are given by $\delta = 1.1090$, $a_0 = 1$, $a_1 = 0.70937$, $a_2 = 2.8235$, $a_3 = -0.28086$, and $a_4 = -0.08277$.

Again assume the turbulence is constant along the path, integrate over angle and propagation direction, and make the substitutions $y = \kappa\, (L/k_0)^{1/2}$, and $x = \sqrt{L/k_0}\,/\,(L_{in}\, \delta)$ to obtain

$$\chi_H^2 = -0.6513\, k_0^{7/6}\, L^{11/6}\, C_n^2 \times \sum_{n=0}^{4} \frac{a_n}{(\delta\, x)^n} \int_0^\infty \frac{dy}{y}\, y^{-11/3+n} \exp\left(-y/x\right) \left[\sin\left(y^2\right) - y^2\right]. \quad (6.131)$$

Use the Mellin convolution theorem and the substitution $s \to 4s$ to get

$$\chi_H^2 = -0.324\, k_0^{7/6}\, L^{11/6} C_n^2 \sum_{n=0}^{4} \frac{a_n}{(\delta\, x)^n} \frac{1}{2\pi i} \int_C ds\, \left(\frac{x^2}{2}\right)^{2s} \Gamma\left[\begin{matrix} -s - \frac{5}{12} + \frac{n}{4} *,\ 4s \\ \frac{23}{12} - \frac{n}{4} + s \end{matrix}\right]. \quad (6.132)$$

The multiplication theorem can be used to obtain unity coefficients in the gamma functions, in which case one obtains a solution which is the sum of four ${}_2F_1\left[\,\right]$ functions and the residue at the single pole. Rather than doing that, I give the single series solution. Since $\Delta = 2$, the integration path is closed to the left, and one obtains the contributions from the poles at $s = -5/12 + n/4$ and at $s = -m/4$ for $m = 0,\ 1,\ 2,\ \ldots$ to obtain

$$\chi_H^2 = 0.081\, k_0^{7/6}\, L^{11/6} C_n^2 \sum_{n=0}^{4} \frac{a_n}{\delta^n} \left\{ 4.514\, \Gamma\left[n - 5/3\right] \left(L_{in}\, \delta \sqrt{\frac{2\, k_0}{L}}\right)^{5/3} - \sum_{m=0}^{\infty} \frac{(-1)^m}{m\,!} \left(L_{in}\, \delta \sqrt{\frac{2\, k_0}{L}}\right)^{m+n} \Gamma\left[\begin{matrix} (n+m)/4 - \frac{5}{12} \\ -(n+m)/4 + \frac{23}{12} \end{matrix}\right] \right\}. \quad (6.133)$$

The scintillation for the Tatarski and Hill spectra versus propagation distance are plotted in Fig. 6.15. Notice the substantial difference in the scintillation, which can be used to verify the actual spectrum shape.

For small distances one can obtain an asymptotic series for the Hill spectrum. The steepest-descent contribution is exponentially small since $\Lambda' = -1$ and can be neglected. The most significant contribution is from the first pole on the left located at $s = 7/12$. The normalized scintillation for small propagation distances is

$$\chi_H^2/\sigma_\chi^2 \sim 0.90 \left(\sqrt{\lambda\, L}/L_{in}\right)^{7/3}, \quad \sqrt{\lambda\, L}/L_{in} \ll 1. \quad (6.134)$$

The first term of the relation in eq. 6.128 gives the Tatarski scintillation for small distances as

$$\chi_T^2/\sigma_\chi^2 \sim 1.22 \left(\sqrt{\lambda\, L}/L_{in}\right)^{7/3}, \quad \sqrt{\lambda\, L}/L_{in} \ll 1. \quad (6.135)$$

Both spectra produce the same functional form in the asymptotic limit although the coefficients differ.

One can find the value of the inner scale by measuring the scintillation along a path of constant turbulence with a small aperture and a large aperture of diameter, D_L. The larger aperture filters out effects of the inner scale. Take the ratio of eq. 6.134 and eq. 6.105 to find

$$L_{in} = 1.24 D_L \left(\sigma_{\chi L}^2/\sigma_\chi^2\right)^{3/7}.$$

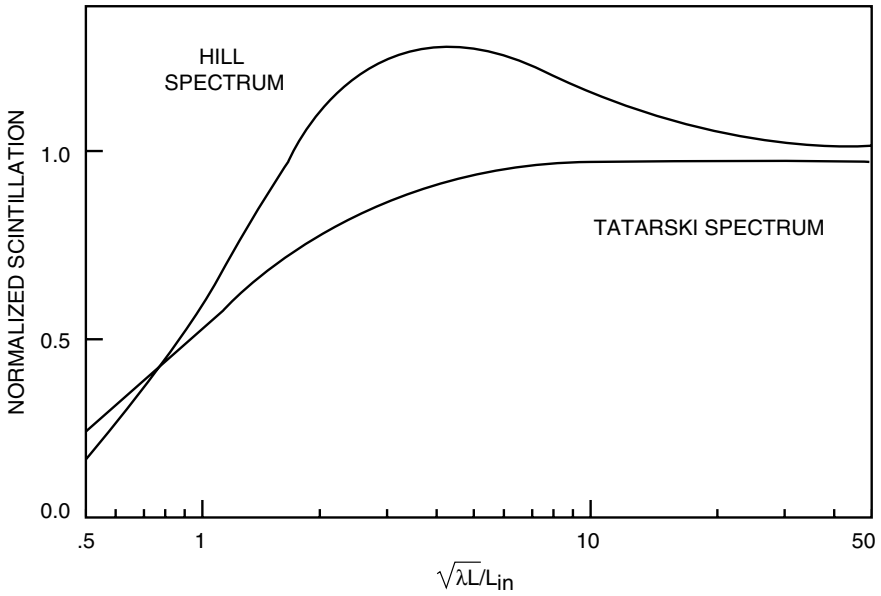

Figure 6.15. Scintillation for a collimated beam propagating over a region of constant turbulence normalized to the scintillation with zero inner scale for the Tatarski and Hill spectra of inner scale. This is plotted versus the normalized propagation distance.

6.10 Scintillation Anisoplanatism

Here, differential scintillation between two uncorrected beams that originate exoatmospherically and are displaced from each other is calculated. One application of this result is to find the scintillation difference between the components of a double star system. The second application is to the reconstruction of a diffraction-limited image of a target outside the atmosphere. In this reconstruction, which was applied by *Lynds* et al. (1976) to obtain a resolved image of Betelgeuse, the short exposure images of an object are added to each other after the brightest speckles are aligned. This procedure works only if speckles from different parts of the image are strongly correlated.

The variance of log-amplitude difference in eq. 2.123 for two offset infinite waves that propagate from $z = L$ to $z = 0$ is

$$\chi^2 = 0.2073\, k_0^2 \int_0^L dz\, C_n^2(z) \int d\boldsymbol{\kappa}\, \kappa^{-11/3}\, \sin^2\left(\frac{\gamma\kappa^2 z}{2k_0}\right) 2\left[1 - \cos\left(\gamma\boldsymbol{\kappa}\cdot\mathbf{d}\,\right)\right]. \tag{6.136}$$

Perform the angle integration and let $y = \gamma\kappa d$, and $x^2 = 2\gamma\, k_0\, d^2/z$ to obtain

$$\chi^2 = -2.606\, k_0^2 \int_0^\infty dz\, C_n^2(z)(\gamma d)^{5/3} \int_0^L \frac{dy}{y}\, y^{-5/3}\left[J_0(y) - 1\right] \sin^2\left[\left(\frac{y}{x}\right)^2\right]. \tag{6.137}$$

The last integral can be converted into one in the complex plane with the Mellin transforms in eq. 1.51 and eq. 1.50, the substitution $s \to 4s$, and the multiplication theorem for gamma functions, to give

$$I = -\frac{\sqrt{\pi}}{2^{19/3}} \frac{1}{2\pi i} \int_C ds \left(\frac{x}{4}\right)^{-4s} \Gamma \left[\begin{matrix} s - \frac{5}{12}*,\ s + \frac{1}{12},\ -s* \\ \frac{11}{12} - s,\ \frac{17}{12} - s,\ s + \frac{1}{2} \end{matrix} \right]. \tag{6.138}$$

Since $\Delta = 2$, close the integration path in the left half plane and pick up the pole contributions at $s = 0,\ 5/12 - n$ for $n = 1,\ 2,\ 3,\ \ldots$, and $-1/12 - n$ for $n = 0,\ 1,\ 2,\ \ldots$. Therefore, the scintillation difference, after the use of the rules in Sec. 1.3 to change the summation into a generalized hypergeometric function, and eq. 1.42 to reduce one minus that function to another generalized hypergeometric function, is

$$\begin{aligned} \chi^2 = {} & k_0^2 \int_0^L dz\, C_n^2(z)\, (\gamma d)^{5/3} \\ & \times \left\{ 1.457 - 0.8757 \left(\frac{\gamma k_0\, d^2}{z}\right)^{1/6} {}_2F_3 \left[\frac{1}{12}, \frac{7}{12}; \frac{3}{2}, \frac{3}{2}, 1; -\left(\frac{\gamma k_0\, d^2}{8\, z}\right)^2 \right] \right. \\ & \left. - 0.00244 \left(\frac{\gamma k_0\, d^2}{z}\right)^{7/6} {}_3F_4 \left[\frac{7}{12}, \frac{13}{12}, 1; \frac{3}{2}, \frac{3}{2}, 2, 2; -\left(\frac{\gamma k_0\, d^2}{8\, z}\right)^2 \right] \right\}. \end{aligned} \tag{6.139}$$

Consider a collimated beam for which $\gamma = 1$. For very large separations, the first pole on the right side of the integration path located at $s = 5/12$ is the main contributor. Evaluating the residue at this pole, one obtains for large path separations

$$\chi^2 \approx 2 \times 0.5631\, k_0^{7/6} \mu_{5/6}. \tag{6.140}$$

This is twice the scintillation for a point source, and it is what is expected since scintillations from the two sources are uncorrelated for large separations. The z integration in eq. 6.139 cannot be performed term by term, since after the first few terms the integral diverges at z equal to zero. Either the hypergeometric functions must be evaluated or the asymptotic solution must be used for small values of z. The integral over z of the first two terms of the general solution converge, and for two paths separated by a small angle the scintillation is

$$\chi^2 \approx 0.50\, (\theta/\theta_o)^{5/3} - 0.8757\, k_0^{13/6}\, \theta^2\, \mu_{11/6}, \quad \theta \ll \theta_o. \tag{6.141}$$

The above approximation is valid only for angles smaller than the isoplanatic angle. The scintillation increases rapidly with angle and is substantial when separation is equal to the isoplanatic angle. This is to be contrasted with tilt anisoplanatism in which tilt difference is small compared to tilt from a single object even for angles many times the isoplanatic angle. The reason for this difference is that tilt is caused by turbulence with long wavelengths, and there has to be a substantial difference in path separations to get a sizeable effect. In

contrast, small wavelength disturbances contribute most strongly to scintillation, and a small separation between paths produces significant effects.

One cannot practically use the relative scintillation difference between stars to get a direct measurement of turbulence distribution since, for reasonable star separations, several terms of the series solution are needed to get the correct scintillation, and each term contains a different turbulence moment.

6.11 Focus Anisoplanatism

It has been proposed to determine range to an airborne vehicle by using the focus component of a wavefront return from the vehicle. The concept requires that focus be measured with an error of less than 1/1000 of a wave. There are stable systematic errors such as optical aberrations of the measurement system that, hopefully, can be taken out with calibrations. There are also systematic errors that change with time such as the static focus term of the aerodynamic boundary layer that varies with angle-of-attack, altitude, and aircraft speed. There are also stochastic noise sources such as focal changes caused by the vibrations of optics and turbulence in the path. These last errors can be reduced by averaging. To calculate the effect of averaging individual focus measurements as the aircraft moves lateral to the line of sight, the focus correlation distance must be found.

I calculate the total focus variance and focus correlation distance. The focus variance is found with the filter function for focus, which is the $Z(0,2)$ Zernike mode, and is given in eq. 3.18 as

$$F(\boldsymbol{\kappa}) = 6\left[\frac{2\,J_3(\kappa D/2)}{\kappa D/2}\right]^2. \tag{6.142}$$

Insert this into eq. 2.112 for single-wave variance with diffraction neglected to get

$$\sigma_f^2 = 0.2073\,k_0^2\int_0^L dz\,C_n^2(z)\int d\boldsymbol{\kappa}\,\kappa^{-11/3}\,3\left[\frac{2J_3(\kappa D/2)}{\kappa D/2}\right]^2. \tag{6.143}$$

Integrate over axial distance and angle, and make the substitution $x = \kappa D/2$, to obtain

$$\sigma_f^2 = 9.846\,k_0^2\,\mu_0\,D^{5/3}\int_0^\infty \frac{dx}{x}\,x^{-11/3}\,J_3^2(x), \tag{6.144}$$

where μ_0 is the zeroth moment of turbulence. The value of the last integral is found with the Mellin transform in eq. 1.52 that is evaluated at $s = -11/3$, and is equal to 1.996×10^{-3}. Since the coherence diameter is $r_0^{-5/3} = 0.423\,k_0^2\,\mu_0$, the total phase variance due to focus is

$$\sigma_f^2 = 0.046\,(D/r_0)^{5/3}. \tag{6.145}$$

The focus correlation function is the variance of focus difference between two displaced apertures and is given by eq. 2.123 with the focus filter function as

$$C_f(\mathbf{d}) = 2.488\, k_0^2 \int_0^L dz\, C_n^2(z) \int d\boldsymbol{\kappa}\, \kappa^{-11/3} \left[\frac{2J_3(\kappa D/2)}{\kappa D/2}\right]^2 [1 - \cos(\boldsymbol{\kappa}\cdot\mathbf{d})]\,. \tag{6.146}$$

Assume that the displacement is constant and perpendicular to the axial direction. Perform the axial and angular integrations and make the substitutions $x = \kappa D/2$, and $y = D/2d$, to obtain

$$C_f(d) = 46.56\ (D/r_0)^{5/3} \int_0^\infty \frac{dx}{x}\, x^{-11/3} J_3^2(x)\ [1 - J_0(x/y)]. \tag{6.147}$$

Form the ratio of this quantity with the focus phase variance given in eq. 6.145 to obtain

$$R(d) = \frac{\sigma_{fd}^2}{\sigma_f^2} = 1002 \int_0^\infty \frac{dx}{x}\, x^{-11/3} J_3^2(x)\ [1 - J_0(x/y)]\,. \tag{6.148}$$

Notice that this ratio does not depend on the turbulence strength along the path.

Inserting the transforms in eq. 1.52 and eq. 1.51 into the Mellin convolution integral given in eq. 1.28, and making the substitution $s \to 2s$, one obtains

$$R(d) = -282.7\, \frac{1}{2\pi i} \int_C ds\, \left(\frac{D}{d}\right)^{-2s} \Gamma\left[\begin{matrix} s + \frac{7}{6},\, -s + \frac{7}{3},\, -s* \\ -s + \frac{35}{6},\, -s + \frac{17}{6},\, s + 1 \end{matrix}\right]. \tag{6.149}$$

Since $\Delta = \Delta' = 0$, the integration path is closed to the right for separations less than the diameter, and closed to the left for larger separations. Evaluating the pole residues at $s = 7/3 + n$ for $n = 0, 1, 2, \ldots$, and $s = n$ for $n = 1, 2, 3 \ldots$, one obtains for small displacements

$$R(d) = -282.7 \left\{ \sum_{n=1}^\infty \frac{(-1)^n}{n!} \left(\frac{d}{D}\right)^{2n} \Gamma\left[\begin{matrix} n + \frac{7}{6},\, -n + \frac{7}{3} \\ -n + \frac{35}{6},\, -n + \frac{17}{6},\, n + 1 \end{matrix}\right] \right.$$
$$\left. + \sum_{n=0}^\infty \frac{(-1)^n}{n!} \left(\frac{d}{D}\right)^{2n+14/3} \Gamma\left[\begin{matrix} n + \frac{7}{2},\, -n - \frac{7}{3} \\ -n + \frac{7}{2},\, -n + \frac{1}{2},\, n + \frac{10}{3} \end{matrix}\right] \right\}, \quad d < D. \tag{6.150}$$

For large displacements one uses the pole-residues at $s = -7/6 - n$ for $n = 0, 1, 2, \ldots$ and the single pole at $s = 0$. The result is

$$R(d) = 2 - 282.7 \sum_{n=0}^\infty \frac{(-1)^n}{n!} \left(\frac{D}{d}\right)^{2n+7/3} \Gamma\left[\begin{matrix} n + \frac{7}{2},\, n + \frac{7}{6} \\ n + 7,\, n + 4,\, -n - \frac{1}{6} \end{matrix}\right], \quad d > D. \tag{6.151}$$

Notice that as the separation gets very large, the ratio becomes 2, which is to be expected since one is subtracting two quantities that are uncorrelated. Expressed as generalized hypergeometric functions with the rules in Sec. 1.3 and eq. 1.42, one obtains

$$R(d) = 15.51 \left(\frac{d}{D}\right)^2 {}_4F_3\left[\tfrac{13}{6}, -\tfrac{23}{6}, -\tfrac{5}{6}, 1; -\tfrac{1}{3}, 2, 2; \left(\frac{d}{D}\right)^2\right] + 74.76 \left(\frac{d}{D}\right)^{14/3} {}_3F_2\left[\tfrac{7}{2}, -\tfrac{5}{2}, \tfrac{1}{2}; \tfrac{10}{3}, \tfrac{10}{3}; \left(\frac{d}{D}\right)^2\right], \quad d < D, \tag{6.152}$$

and $$R(d) = 2 + 0.03008\ (D/d)^{7/3}\, {}_3F_2\left[\tfrac{7}{2}, \tfrac{7}{6}, \tfrac{7}{6}; 7, 4; (D/d)^2\right], \quad d > D. \tag{6.153}$$

This function is plotted in Fig. 6.16. It shows that the focus term is essentially uncorrelated when the separation is one-half the aperture diameter.

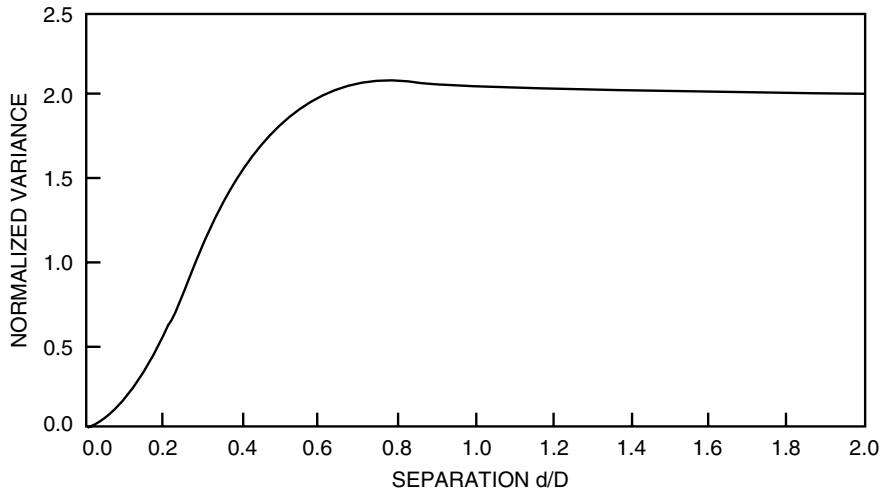

Figure 6.16. Normalized difference of the focus variance versus separation of two apertures. When the path separation is one-half the aperture diameter the focus components on the two apertures are essentially uncorrelated. This curve is independent of the turbulence distribution along the propagation path.

6.12 Zernike Anisoplanatism

Zernike anisoplanatism is the difference in the level of a Zernike mode between two sources. This difference can be the result of a difference in angle between two sources or due to a simple displacement between two apertures. Because the two apertures are looking through different turbulence, there will be a difference

in the level of each Zernike mode measured at any time. This difference will increase as the angle or displacement of the two apertures increases until the variance of the difference saturates at a level that is two times the variance of the mode measured in a single aperture.

We have considered tilt and focus anisoplanatism previously. Anisoplanatism for higher order aberrations is important in applications such as adaptive-optics systems that correct for Zernike modes rather than local parts of the aperture. It is important to determine over what angle a correction applies. It will be shown that the angle decreases as the mode order increases. Obviously, if the angle over which the correction applies is less than the resolution of the system, then the correction is worthless.

The calculation of the variance of Zernike anisoplanatism is a simple extension of the calculation performed to find the tilt anisoplanatism. The filter function for the Zernike modes is substituted for the tilt filter function into the expression for the variance of tilt anisoplanatism. The evaluation of the resulting integral follows the same path as that for tilt anisoplanatism. The result is an analytical expression given in terms of generalized hypergeometric functions.

To find the total value of Zernike anisoplanatism and both the components parallel and perpendicular to the displacement direction that is taken to be along the x-axis, eq. 2.123 with diffraction neglected is used with the filter function for a Zernike mode given in eq. 3.18. Just as for tilt anisoplanatism, one can analyze the general problem by including γ in the filter function to obtain for the phase variance

$$\begin{bmatrix} \sigma_x^2 \\ \sigma_y^2 \\ \sigma^2 \end{bmatrix}_{n,m} = 0.2073\, k_0^2 \int_0^L C_n^2(z)\, dz \int d\boldsymbol{\kappa} \begin{bmatrix} \cos^2(m\varphi) \\ \sin^2(m\varphi) \\ 1 \end{bmatrix} \times \kappa^{-11/3} (n+1) \left(\frac{2J_{n+1}(\gamma\kappa D/2)}{\gamma\kappa D/2} \right)^2 4\left[1 - \cos\left\{\kappa d \cos(\varphi)\right\}\right], \quad (6.154)$$

where σ^2 is the total variance, which is equal to the sum of the x and y variances.

The bottom term is the variance when m is equal to zero, in which case the top two terms do not apply. There are the requirements that $m \leq n$ and $n-m$ is even. Common aberrations expressed in terms of (m, n) are $(0, 0)$ is piston, $(1, 1)$ is tilt, $(0, 2)$ is focus, $(2, 2)$ is astigmatism, and $(1, 3)$ is coma. The displacement is considered to be along the x axis and the top term is the x component of the aberration. Therefore, in a more general sense the top term is the phase variance due to a movement parallel to that component of the aberration, and the middle term is a perpendicular movement.

The above equation, which has Kolmogorov turbulence, does not converge for piston; therefore, the results are not valid for $n = 0$. If a turbulence spectrum with finite outer scale is inserted into the integral, then the results would be valid for piston.

This expression gives the phase variance for a particular Zernike mode. One can use this result to obtain other information, for instance, if the expression for

tilt anisoplanatic phase variance is multiplied by $4k_0/D^2$, then one obtains the tilt variance, which is the variance of the angular jitter of a signal that arrived with that displacement.

The angular integration can not be performed in the same way as was done for tilt anisoplanatism. For this more general case the angular integration can be written as

$$\begin{aligned} I_a &= 2\int_0^{2\pi} d\,\varphi \begin{bmatrix} \cos^2(m\varphi) \\ \sin^2(m\varphi) \\ 1 \end{bmatrix} [1-\cos\{\kappa d\cos(\varphi)\}] \\ &= \int_0^{2\pi} d\,\varphi \begin{bmatrix} 1+\cos(2m\varphi) \\ 1-\cos(2m\varphi) \\ 2 \end{bmatrix} [1-\cos\{\kappa d\cos(\varphi)\}]\,. \end{aligned} \tag{6.155}$$

The integral in G & R Sec. 3.715 # 19 can be extended over the full circle to give

$$\int_0^{2\pi} \cos[\beta\cos(x)]\cos(2mx)\,dx = (-1)^m\,2\pi\;J_{2m}(\beta)\;. \tag{6.156}$$

Use this to obtain

$$\begin{aligned} \begin{bmatrix} \sigma_x^2 \\ \sigma_y^2 \\ \sigma^2 \end{bmatrix}_{n,m} &= 10.42k_0^2\,(n+1)\int_0^L dz\;C_n^2(z)\int_0^\infty \kappa^{-8/3}\,d\kappa\;\left[\frac{J_{n+1}(\gamma\kappa D/2)}{\gamma\kappa D/2}\right]^2 \\ &\quad\times\begin{bmatrix} 1-J_0(\kappa d)-(-1)^m\,J_{2m}(\kappa d) \\ 1-J_0(\kappa d)+(-1)^m\,J_{2m}(\kappa d) \\ 2\,[1-J_0(\kappa d)] \end{bmatrix}. \end{aligned} \tag{6.157}$$

There are two integrals that, when evaluated, allow one to evaluate all three integrals in kappa-space. These are

$$I_1 = -\int_0^\infty \kappa^{-8/3}\,d\kappa\;\left[\frac{J_{n+1}(\gamma\kappa D/2)}{\gamma\kappa D/2}\right]^2 J_{2m}(\kappa d), \tag{6.158}$$

and

$$I_T = -\int_0^\infty \kappa^{-8/3}\,d\kappa\;\left[\frac{J_{n+1}(\gamma\kappa D/2)}{\gamma\kappa D/2}\right]^2 [J_0(\kappa d)-1]. \tag{6.159}$$

The previous integrals expressed in terms of these two are equal to

$$\begin{bmatrix} \sigma_x^2 \\ \sigma_y^2 \\ \sigma^2 \end{bmatrix}_{n,m} = 10.42k_0^2\,(n+1)\int_0^L dz\;C_n^2(z)\begin{bmatrix} I_T+(-1)^m\,I_1 \\ I_T-(-1)^m\,I_1 \\ 2I_T \end{bmatrix}. \tag{6.160}$$

Letting $t=\kappa d$ and $x=2d/\gamma D$, one obtains

$$\begin{bmatrix} I_1 \\ I_T \end{bmatrix} = -\frac{4d^{11/3}}{(\gamma D)^2}\int_0^\infty \frac{dt}{t}t^{-11/3}\;\begin{bmatrix} J_{2m}(t) \\ J_0(t)-1 \end{bmatrix} J_{n+1}^2(t/x)\,. \tag{6.161}$$

The I_T integral is similar to the integral that was evaluated in the tilt anisoplanatism section. The top integral can be evaluated by taking the Mellin transform of $J_{2m}(t)$, which can be found from eq. 1.51 and eq. 1.8 with $a = -11/3$. The Mellin transforms of $J^2_{n+1}(t)$ is given in eq. 1.52. After the substitution $s \to 2s$, the integral can be transformed into

$$I_1 = -\frac{d^{11/3}}{2^{8/3}(\gamma D)^2\sqrt{\pi}}\frac{1}{2\pi i}\int_C ds\ \left(\frac{d}{\gamma D}\right)^{-2s} \Gamma\left[\begin{matrix} s-\frac{11}{6}+m,\ -s+n+1,\ s+\frac{1}{2} \\ -s+m+\frac{17}{6}, s+n+2,\ s+1 \end{matrix}\right]. \tag{6.162}$$

Since $\Delta = 0$, the direction of path closure is determined by the parameter $d/\gamma D$ in the integral. Different Taylor's expansions are obtained for small and large displacements. The point in the atmosphere at which the character of the solution changes from one series to another is where the two beams start to overlap. For $d/\gamma D < 1$, the integration path is closed to the left, and one obtains the residues of the poles at $s = -1/2-p$ for $p = 0, 1, 2, \ldots$, and $s = 11/6-p-m$, for $p = 0, 1, 2, \ldots$.

For $d/\gamma D > 1$, the path is closed to the right, and one obtains the residues of the poles at $s = p + n + 1$ for $p = 0, 1, 2, \ldots$.

The resultant value of the integral for small displacements, $d/\gamma D < 1$, is

$$\begin{aligned} I_{1L} = \frac{-d^{11/3}}{2^{8/3}(\gamma D)^2\sqrt{\pi}} \Bigg[& \sum_{p=0}^{\infty}\frac{(-1)^p}{p!}\left(\frac{d}{\gamma D}\right)^{-11/3+2p+2m} \\ & \times\Gamma\left[\begin{matrix} p+m+n-\frac{5}{6},\ -p-m+\frac{7}{3} \\ p+2m+1,\ -p-m+n+\frac{23}{6},\ -p-m+\frac{17}{6} \end{matrix}\right] \\ & + \sum_{p=0}^{\infty}\frac{(-1)^p}{p!}\left(\frac{d}{\gamma D}\right)^{1+2p} \Gamma\left[\begin{matrix} -p+m-\frac{7}{3},\ p+n+\frac{3}{2} \\ p+m+\frac{10}{3},\ -p+n+\frac{3}{2},\ -p+\frac{1}{2} \end{matrix}\right] \Bigg]. \end{aligned} \tag{6.163}$$

For large displacement, $d/\gamma D > 1$, the integral is equal to

$$I_{1U} = -\frac{d^{11/3}}{2^{8/3}(\gamma D)^2\sqrt{\pi}} \sum_{p=0}^{\infty} \frac{(-1)^p}{p!} \left(\frac{d}{\gamma D}\right)^{-2p-2n-2} \times \Gamma\left[\begin{matrix} p+n+m-\frac{5}{6},\ p+n+\frac{3}{2} \\ -p+m-n+\frac{11}{6},\ p+2n+3,\ p+n+2 \end{matrix}\right]. \tag{6.164}$$

The second integral is

$$I_T = \frac{-4d^{11/3}}{(\gamma D)^2} \int_0^{\infty} \frac{dy}{y}\, y^{-11/3}\, [J_0(y) - 1]\, J_{n+1}^2(y/x)\,. \tag{6.165}$$

In the Mellin transform plane this is equal to

$$I_T = -\frac{d^{11/3}}{2^{8/3}(\gamma D)^2\sqrt{\pi}} \frac{1}{2\pi i} \int_C ds\, \left(\frac{d}{\gamma D}\right)^{-2s} \Gamma\left[\begin{matrix} s-\frac{11}{6}*,\ -s+n+1,\ s+\frac{1}{2} \\ s+n+2,\ s+1, -s+\frac{17}{6} \end{matrix}\right]. \tag{6.166}$$

Since $\Delta = \Delta' = 0$, the direction of path closure is determined by the parameter $d/\gamma D$ in the integral. Different Taylor's expansions are obtained for small and large displacements. The point in the atmosphere at which the character of the solution changes from one series to another is where the two beams just barely overlap. For $d/\gamma D < 1$, the integration path is closed to the left, and one obtains the residues of poles at $s = -1/2 - p$ for $p = 0, 1, 2, \ldots$, and $s = 11/6 - p$, for $p = 1, 2, 3, \ldots$. For $d/\gamma D > 1$, the path is closed to the right, and one obtains the residues of poles at $s = p + n + 1$ for $p = 0, 1, 2, \ldots$, and the single pole at $s = 11/6$.

The resultant value of the integral for small displacements is

$$\begin{aligned} I_{TL} = -\frac{d^{11/3}}{2^{8/3}(\gamma D)^2\sqrt{\pi}} \Bigg[& \sum_{p=1}^{\infty} \frac{(-1)^p}{p!} \left(\frac{d}{\gamma D}\right)^{-11/3+2p} \\ & \times \Gamma\left[\begin{matrix} p+n-\frac{5}{6},\ -p+\frac{7}{3} \\ p+1,\ -p+n+\frac{23}{6},\ -p+\frac{17}{6} \end{matrix}\right] \\ & + \sum_{p=0}^{\infty} \frac{(-1)^p}{p!} \left(\frac{d}{\gamma D}\right)^{1+2p} \Gamma\left[\begin{matrix} -p-\frac{7}{3},\ p+n+\frac{3}{2} \\ p+\frac{10}{3},\ -p+n+\frac{3}{2},\ -p+\frac{1}{2} \end{matrix}\right] \Bigg];\ d < \gamma D\ . \end{aligned}$$

For large displacements, $d/\gamma D > 1$, the result is

$$\begin{aligned} I_{TU} = \frac{d^{11/3}}{2^{8/3}(\gamma D)^2\sqrt{\pi}} \Bigg[& \left(\frac{d}{\gamma D}\right)^{-11/3} \Gamma\left[\begin{matrix} n-\frac{5}{6},\ \frac{7}{3} \\ n+\frac{23}{6},\ \frac{17}{6} \end{matrix}\right] \\ & - \sum_{p=0}^{\infty} \frac{(-1)^p}{p!} \left(\frac{d}{\gamma D}\right)^{-2p-2n-2} \Gamma\left[\begin{matrix} p+n-\frac{5}{6},\ p+n+\frac{3}{2} \\ -p-n+\frac{11}{6},\ p+2n+3,\ p+n+2 \end{matrix}\right] \Bigg]; \\ & d > \gamma D\ . \end{aligned}$$

These results can be combined and can be written as generalized hypergeometric functions using the algorithm given in Chap. 1. For small displacements, $d/\gamma D < 1$, the result is

$$\begin{bmatrix}\sigma_x^2\\ \sigma_y^2\end{bmatrix} = 0.9259\,k_0^2 D^{5/3}\,(n+1)\int_0^L dz\,C_n^2\,(z)\,\gamma^{5/3}$$
$$\times 0.6904\left(-\Gamma\begin{bmatrix} n-\frac{5}{6}\\ n+\frac{23}{6}\end{bmatrix}\left\{{}_3F_2\left[n-\tfrac{5}{6},-n-\tfrac{17}{6},-\tfrac{11}{6};1,-\tfrac{4}{3};\left(\tfrac{d}{\gamma D}\right)^2\right]-1\right\}\right.$$
$$+26.52\left(\tfrac{d}{\gamma D}\right)^{14/3}{}_3F_2\left[n+\tfrac{3}{2},-n-\tfrac{1}{2},\tfrac{1}{2};\tfrac{10}{3},\tfrac{10}{3};\left(\tfrac{d}{\gamma D}\right)^2\right]$$
$$\mp(-1)^m\,\Gamma\begin{bmatrix} m+n-\frac{5}{6},-m+\frac{7}{3}\\ 2m+1,n-m+\frac{23}{6},\frac{17}{6}-m\end{bmatrix}\left(\tfrac{d}{\gamma D}\right)^{2m}$$
$$\times{}_3F_2\left[m+n-\tfrac{5}{6},m-n-\tfrac{17}{6},m-\tfrac{11}{6};2m+1,m-\tfrac{4}{3};\left(\tfrac{d}{\gamma D}\right)^2\right]$$
$$\mp(-1)^m\,\Gamma\begin{bmatrix} m-\frac{7}{3},n+\frac{3}{2}\\ m+\frac{10}{3},n+\frac{3}{2},\frac{1}{2}\end{bmatrix}\left(\tfrac{d}{\gamma D}\right)^{14/3}$$
$$\left.\times{}_3F_2\left[n+\tfrac{3}{2},-n-\tfrac{1}{2},\tfrac{1}{2};m+\tfrac{10}{3},-m+\tfrac{10}{3};\left(\tfrac{d}{\gamma D}\right)^2\right]\right),\quad d<\gamma D. \tag{6.167}$$

For large displacements, $d/\gamma D > 1$, the result is

$$\begin{bmatrix}\sigma_x^2\\ \sigma_y^2\end{bmatrix} = 0.9263\,k_0^2 D^{5/3}\,(n+1)\int_0^L dz\,C_n^2\,(z)\,\gamma^{5/3}$$
$$\times\left\{0.6904\;\Gamma\begin{bmatrix} n-\frac{5}{6}\\ n+\frac{23}{6}\end{bmatrix}-\Gamma\begin{bmatrix} n-\frac{5}{6},n+\frac{3}{2}\\ -n+\frac{11}{6},2n+3,n+2\end{bmatrix}\left(\tfrac{\gamma D}{d}\right)^{2n-5/3}\right.$$
$$\times{}_3F_2\left[n-\tfrac{5}{6},n+\tfrac{3}{2},n-\tfrac{5}{6};2n+3,n+2;\left(\tfrac{\gamma D}{d}\right)^2\right]$$
$$\mp(-1)^m\,\Gamma\begin{bmatrix} n+m-\frac{5}{6},n+\frac{3}{2}\\ m-n+\frac{11}{6},2n+3,n+2\end{bmatrix}\left(\tfrac{\gamma D}{d}\right)^{2n-5/3}$$
$$\left.\times{}_3F_2\left[m+n-\tfrac{5}{6},n+\tfrac{3}{2},n-m-\tfrac{5}{6};2n+3,n+2;\left(\tfrac{\gamma D}{d}\right)^2\right]\right\},\ d>\gamma D. \tag{6.168}$$

The total variance and the variance when $m = 0$ is given by either the x or the y variance with the $\pm$ terms deleted. For very large separations the x and y variances are equal to each other and are equal to the total variance (sum of the x and y components) of that Zernike component. Note that the expression for large separations diverges when $n = 0$. The only value of m that is possible is 0, since $m \le n$, which is the piston. We know that the piston variance is infinite when outer scale effects are not considered, so this result is expected.

The total variance of a Zernike component for a single wave is given by the first term in the last equation as

$$\sigma_{m,n}^2 = 0.6395\,D^{5/3}k_0^2\,(n+1)\int_0^L dz\,C_n^2\,(z)\,\gamma^{5/3}\Gamma\begin{bmatrix} n-\frac{5}{6}\\ n+\frac{23}{6}\end{bmatrix}. \tag{6.169}$$

For a collimated beam in which $\gamma = 1$, one obtains

$$\sigma_{m,n}^2 = 0.6395\,\mu_0\,k_0^2 D^{5/3}\Gamma\begin{bmatrix} n-\frac{5}{6}\\ n+\frac{23}{6}\end{bmatrix}(n+1)\,. \tag{6.170}$$

This gives the standard result for the tilt phase variance of a collimated beam

$$\sigma^2_{Tilt} = 0.380\,\mu_0\,k_0^2 D^{5/3}. \tag{6.171}$$

If there is an angular displacement between the two beams, θ, then the expression for Zernike anisoplanatism is obtained by making the substitution $d = \theta z$. For small angles the first term of the series expansion is a good approximation, and for a collimated beam gives a total variance of

$$Total\ Variance = 1.759(n+1)\Gamma\left[\begin{matrix} n+\frac{1}{6} \\ n+\frac{17}{6}\end{matrix}\right] k_o^2 D^{-1/3}\mu_2\theta^2. \tag{6.172}$$

Notice how the variance varies as the square of the angular offset for small angles.

There are many ways to define a characteristic angle. One definition allows us to gauge the effectiveness of an adaptive optics system. The angle will be defined as that which would produce the same variance as an aperture with no correction. If the anisoplanatic error is equal to or greater than the value with no correction, then it does no good to correct for that mode. With this definition, the characteristic Zernike anisoplanatic angle, θ_{nC}, is found by setting to unity the ratio of the most significant term of the total Zernike anisoplanatism for small offsets given in eq. 6.167 by the Zernike variance given in eq. 6.169 to give

$$\theta_{nC} = 0.603\,D\left(\frac{\mu_0}{\mu_2\,(n-5/6)\,(n+17/6)}\right)^{1/2}. \tag{6.173}$$

Notice that this is independent of the wavelength; therefore, for shorter wavelengths a larger number of pixels is corrected. For a HV-21 turbulence model this formula reduces to

$$\theta_{nC} = \frac{206\,D}{\sqrt{(n-5/6)\,(n+17/6)}}\,\mu rad. \tag{6.174}$$

For a 1-m diameter aperture at 0.5 μm operating wavelength, the characteristic tilt anisoplanatic angle is 258 μrad, which is considerably larger than the 21 μrad one gets when the criteria is that the anisoplanatic tilt jitter is one-half a beamwidth. When $n = 2$ the angle is 87 μrad, and for $n = 3$ the angle is 58 μrad. For large n the angle is $206D/n$ μrad; the angle gets very small at high Zernike numbers.

The angles above are the largest angles for which correcting that Zernike aberration provides any improvement in the image. For the lowest order aberrations a much smaller angle is required if one wants to approach diffraction-limited performance.

The variance of a wavefront on a 1-m diameter aperture operating at a wavelength of 0.5 μm that looks through HV-21 turbulence for the first 14 values of n are 133.7, 6.92, 1.84, 0.73, 0.35, 0.20, 0.12, 0.075, 0.050. 0.035, 0.025, 0.019, 0.014, and 0.011 μrad^2. Notice that the tilt variance far exceeds the other variances,

which is the reason why tilt must be very well corrected. The other aberrations can also contribute a significant variance. Since the variance for any Zernike aberration varies as the square of the angular offset for small offsets, one can easily determine how much the angles given above must be reduced for a particular aberration to be below a certain level. One can calculate the error for which the phase variance is under 1 rad^2 by using the first term of the series expansion to obtain

$$\theta\left(1\ rad^2\right) = 0.17\frac{\lambda D^{1/6}}{\mu_2^{1/2}\sqrt{n+1}}\Gamma\left[\begin{matrix} n+\frac{17}{6} \\ n+\frac{7}{6}\end{matrix}\right]. \tag{6.175}$$

For a 1-m diameter aperture at 0.5 μm operating wavelength, the angle for $n = 1$ is 31.5 μrad; for $n = 2$ the angle is 46.6 μrad, and for $n = 3$ the angle is 60.3 μrad. For a requirement that the error in any mode be less than 0.1 rad^2, the angle must be reduced by a factor of 3.16. A 0.1 rad^2 requirement results in very small correction angles. These angles increase as the operating wavelength increases. This formula does not apply for all n, since, as shown above, the variance never exceeds 0.1 rad^2 when $n > 7$.

6.13 Focal Anisoplanatism for Point Sources

Focal anisoplanatism refers to errors made by using a phase disturbance measured with a focused beam to correct for turbulence effects on a collimated beam. It has also been called focus anisoplanatism and cone anisoplanatism. If a point source is very far away, the error is very small. For closer sources, such as artificial beacons that are used in the 'guidestar' concept [*Gardner* et al. (1990); *Murphy* et al. (1991); *Primmerman* et al. (1991); *Fugate* et al. (1991); *Welsh* and *Gardner* (1989); *Welsh* and *Thompson* (1991)], the effect can be significant and may result in a low Strehl ratio. The phase variance from this effect is calculated in this section. First, an expression for variance is obtained that has both piston and tilt components present. Next, expressions for piston and tilt variances are obtained. If the last variances are subtracted from the total variance, then one obtains the piston-and-tilt-removed phase variances due to focal anisoplanatism.

The technique to find the variance is the same one that has been used on previous problems. The filter function for a distributed, circular, uniform beacon of diameter D_s and offset $\mathbf{b}$ that is at a range L and altitude H as given in eq. 3.62 is inserted into the formula for phase variance of a single wave given in eq. 2.112. Assume one is operating in the near field, thereby allowing the cosine term to be replaced by 1.

After doing the angle integration, one obtains for the aperture-averaged phase variance

$$\sigma_{-d}^2 = 1.303\, k_0^2 \int_0^L dz\, C_n^2(z) \int_0^\infty d\kappa\, \kappa^{-8/3}$$
$$\times \left\{ 1 - 2\frac{2\,J_1\,(a\,D_s)}{a\,D_s}\frac{2\,J_1\,(a\,D)}{a\,D} J_0\left(\frac{\kappa b z}{L}\right) + \left[\frac{2J_1\,(a\,D_s)}{a\,D_s}\right]^2 \right\}, \quad (6.176)$$

where $a = \kappa z/2L$. The subscript d on the variance refers to a distributed source. The minus subscript means that it is the component from the turbulence below the beacon. The component above the beacon will be added to this to obtain the total variance. If the d subscript is missing, it means a point source is being considered. Piston and tilt are present in σ_d^2.

This equation is the starting point for the evaluation of the total phase variance for all cases considered in this and the next two sections. The problem is solved in steps, since the results for a point source, a distributed source, and a displaced source are of interest for different situations.

The phase variance of a point source on the aperture center with piston and tilt present can be found from eq. 6.176 by setting the source diameter and displacement equal to zero to obtain

$$\sigma_-^2 = 2.606\, k_0^2 \int_0^L dz\, C_n^2(z) \int_0^\infty d\kappa\, \kappa^{-8/3} \left[1 - \frac{2J_1\,(a\,D)}{a\,D}\right]. \quad (6.177)$$

Let $x = \kappa D z/2L$ to obtain

$$\sigma_-^2 = -5.212\, k_0^2 \int_0^L dz\, C_n^2(z) \left(\frac{D\,z}{2H}\right)^{5/3} \int_0^\infty dx\, x^{-8/3-1} \left[J_1(x) - \frac{x}{2}\right]. \quad (6.178)$$

The last integral converges by analytical continuation as discussed in evaluating eq. 5.5, and its value of 0.305 is just the Mellin transform of the Bessel function given in eq. 1.51 evaluated at $s = -8/3$. The phase variance is equal to

$$\sigma_-^2 = 0.5\, k_0^2\, \mu_{5/3}^- \left(\frac{D}{L}\right)^{5/3} = \left(\frac{0.348\, D}{L\, \theta_o^-}\right)^{5/3}, \quad (6.179)$$

where the partial isoplanatic angle is defined as

$$\left(\theta_o^-\right)^{-5/3} = 2.91\, k_0^2\, \mu_{5/3}^-. \quad (6.180)$$

The phase variance results from an angular offset of the collimated and focused rays. The phase variance varies with radius; however, one can consider the average phase variance to be due to an angular offset equal to that of the ray that emanates from the point that is about 0.7 of the radius from the center. This angle is $0.348\,D/L$.

This phase variance with piston included is finite unlike the result for unfiltered turbulence, which is infinite. The infinite result comes from the zero spatial wavelength term. This infinity cancels out in the subtraction of the collimated beam phase from that of a focused beam. Even though the above result is finite, it might be possible that the major component of this variance is due to the piston, which is no practical interest. It can be shown that at satellite altitudes the piston contribution is less than 10% of the variance. At 10 km it can be as large as 20%. Therefore, the above simple expression is a reasonable zero-order approximation to phase variance. A 60-cm aperture pointed at a point source at 300 km would have the same phase variance as two beams with angular offset of 0.7 μrads. For typical isoplanatic angles, this will produce a very small variance.

Often one is interested in phase variance with piston or piston and tilt removed. The phase variance due to piston and tilt can be calculated separately and subtracted from the total phase variance to obtain these. Piston and tilt phase variances are found by using eq. 2.117 with filter functions given in eq. 3.67

$$\sigma^2_{-Z} = 0.2073\, k_0^2 \int_0^L dz\, C_n^2(z)\, 4\,\nu^2 \int d\boldsymbol{\kappa}\, \kappa^{-11/3}$$
$$\times \left\{ \frac{J_\nu\,(\kappa D/2)}{\kappa D/2} - \exp\!\left(i\,\boldsymbol{\kappa}\cdot\mathbf{b}\frac{z}{L}\right) \frac{J_\nu\,[\kappa D(1-z/L)/2]}{\kappa D(1-z/L)/2} \frac{2\,J_1\,(\kappa D_s\, z/2\,L)}{\kappa D_s\, z/2\,L} \right\}^2, \tag{6.181}$$

where D_s is the source diameter, and $\mathbf{b}$ is displacement of the source from boresight. The value of ν is 1 for piston and 2 for tilt. The subscript Z is either P or T.

First consider the case of zero source size and no offset. Perform the angular integration. The evaluation of the integral in kappa space poses some difficulty. The two terms in brackets almost cancel especially for very high beacon altitudes. If the bracket is expanded, three terms result. Two of these terms can be evaluated by table lookup. The term that is the product of the two terms must be evaluated with the Mellin convolution integral. The final answer is expanded in a power series in the parameter z/L to enable the answer to be expressed as a sum of turbulence moments. Let $\kappa D/2 = x$, and $y = 1/(1-z/L)$. The variances are equal to

$$\sigma^2_{-Z} = 1.642\, k_0^2\, \nu^2\, D^{5/3} \int_0^L dz\, C_n^2(z)\, I, \quad \text{where} \tag{6.182}$$

$$I = \int_0^\infty dx\, x^{-14/3}$$
$$\times \left\{ \left[J_\nu^2(x) - \frac{a\,x^2}{4} \right] + \left[y^2\, J_\nu^2(x/y) - \frac{a\,x^2}{4} \right] - 2\left[J_\nu(x)\; y\, J_\nu(x/y) - \frac{a\,x^2}{4} \right] \right\}.$$

The value of a is unity for piston and zero for tilt. Add the constant terms, whose sum is zero, to obtain three integrals that converge. Express the integral as the sum of three integrals

$$I = I_1 + I_2 + I_3, \tag{6.183}$$

to obtain for the first two terms

$$I_1 + I_2 = \frac{\left(1 + y^{-5/3}\right)}{2\sqrt{\pi}} \Gamma \left[\begin{matrix} -\frac{11}{6} + \nu,\ \frac{7}{3} \\ \nu + \frac{17}{6},\ \frac{17}{6} \end{matrix} \right]. \tag{6.184}$$

For piston the third integral is

$$I_3 = -2\,y \int_0^\infty \frac{de}{e}\, e^{-11/3} \left[J_1(e) J_1\left(\frac{e}{y}\right) - \frac{e}{2}\,\frac{e}{2y} \right]. \tag{6.185}$$

If $y = 1/\beta$, this is the same integral that was evaluated in eq. 6.27. Its value is

$$I_3 = -y\, 2^{-11/3} \Gamma \left[\begin{matrix} -\frac{5}{6} \\ \frac{17}{6} \end{matrix} \right] {}_2F_1\left[-\tfrac{5}{6}, -\tfrac{11}{6}; 2; (1 - z/L)^2 \right]. \tag{6.186}$$

The piston phase variance due to turbulence below the beacon is

$$\sigma_{-P}^2 = 0.5\, k_0^2\, D^{5/3} \int_0^L dz\, C_n^2(z)$$
$$\times \left\{ {}_2F_1\left[-\tfrac{5}{6}, -\tfrac{11}{6}; 2; (1 - z/L)^2 \right] - \frac{\left[1 + (1 - z/L)^{5/3} \right]}{\sqrt{\pi}\, 2^{-8/3}} \Gamma \left[\begin{matrix} \frac{7}{3} \\ \frac{23}{6} \end{matrix} \right] \right\}. \tag{6.187}$$

This can be integrated numerically; however, to express this as turbulence moments, the expression in braces is expanded in a Taylor series about the point $z/L = 0$. Some care must be taken in expanding this series to obtain a short series that is a good approximation to the exact calculation. It has been found that a good approximation to the exact result for typical turbulence models and aperture diameters is

$$\sigma_{-P}^2 \approx 0.0833\, k_0^2\, D^{5/3} \frac{\mu_2^-(H)}{L^2}. \tag{6.188}$$

The integrations can be performed for tilt to obtain

$$\sigma^2_{-T} = 0.8345\, k_0^2\, D^{5/3} \int_0^L dz\, C_n^2(z)$$
$$\times \left\{ \frac{\left[1 + (1 - z/L)^{5/3}\right]}{\sqrt{\pi}\, 2^{-11/3}} \Gamma\left[\begin{matrix}\frac{7}{3} \\ \frac{29}{6}\end{matrix}\right] - \left(1 - \frac{z}{L}\right)\, {}_2F_1\left[\frac{1}{6}, -\frac{11}{6}; 3; \left(1 - \frac{z}{L}\right)^2\right] \right\}. \quad (6.189)$$

After expansion of this Taylor series in the same way as was done for piston, the tilt variance is closely approximated by

$$\sigma^2_{-T} \approx 0.368\, k_0^2\, D^{5/3}\, \frac{\mu_2^-(H)}{L^2}. \quad (6.190)$$

The displacement can be found in the same way as in Sec. 4.5. The tilt has a lever arm of $(L - z)$ to give a displacement variance of

$$\sigma^2_{-DT} = 0.8345\, k_0^2\, D^{5/3} \int_0^L dz\, C_n^2(z)(L - z)^2$$
$$\times \left\{ \frac{\left[1 + (1 - z/L)^{5/3}\right]}{\sqrt{\pi}\, 2^{-11/3}} \Gamma\left[\begin{matrix}\frac{7}{3} \\ \frac{29}{6}\end{matrix}\right] - \left(1 - \frac{z}{L}\right)\, {}_2F_1\left[\frac{1}{6}, -\frac{11}{6}; 3; \left(1 - \frac{z}{L}\right)^2\right] \right\}. \quad (6.191)$$

Using the same approximation as for the tilt, one obtains

$$\sigma^2_{-DT} \approx 0.368\, k_0^2\, D^{5/3} \left(\mu_2^-(H) - \frac{2\mu_3^-(H)}{L} + \frac{\mu_4^-(H)}{L^2}\right). \quad (6.192)$$

If the point source beacon is located at $z = 0$, then the focal anisoplanatic tilt can be found by making the substitution $1 - z/L \to z/L$ in eq. 6.189. The approximate value of this tilt is

$$\sigma^2_{-T} \approx 0.368\, k_0^2\, D^{5/3} \left(\mu_0^-(H) - \frac{2\mu_1^-(H)}{L} + \frac{\mu_2^-(H)}{L^2}\right). \quad (6.193)$$

The piston-removed variance is

$$\sigma^2_{-PR} = \left(\frac{0.348\, D}{H\theta_o^-}\right)^{5/3} - \sigma^2_{-P}. \quad (6.194)$$

The piston-and-tilt-removed variance is

$$\sigma^2_{-PTR} = \left(\frac{0.348 D}{H\, \theta_o^-}\right)^{5/3} - \sigma^2_{-P} - \sigma^2_{-T}. \quad (6.195)$$

With the above results, a good approximation to the piston-removed phase is

$$\sigma^2_{-PR} = \left(\frac{0.348\, D}{H\theta_o^-}\right)^{5/3} - \sigma^2_{-P} \approx \frac{k_0^2\, D^{5/3}}{2} \left[\frac{\mu_{5/3}^-(H)}{L^{5/3}} - 0.167\, \frac{\mu_2^-(H)}{L^2}\right]. \quad (6.196)$$

Similarly, a good approximation to the piston-and-tilt-removed phase is

$$\sigma^2_{-PTR} = \left(\frac{0.348D}{H\,\theta_o^-}\right)^{5/3} - \sigma^2_{-P} - \sigma^2_{-T} \approx \frac{k_0^2\,D^{5/3}}{2}\left[\frac{\mu^-_{5/3}\,(H)}{L^{5/3}} - 0.903\frac{\mu_2^-\,(H)}{L^2}\right]. \tag{6.197}$$

For changes in zenith angle, when the beacon is kept at the same altitude, it is clear from the variation of each term in brackets that the zenith dependence is simply $\sec(\xi)$.

The effect of turbulence above the beacon is obtained by modifying the results in Sec. 4.2. The phase variance with piston removed is

$$\sigma^2_{+PR} = 1.033\left(D/r_0^+\right)^{5/3}, \tag{6.198}$$

where the coherence diameter looking up from the beacon altitude is

$$\left(r_0^+\right)^{-5/3} = 0.423\,k_0^2\,\mu_0^+. \tag{6.199}$$

The expression for phase variance from turbulence above the beacon with piston and tilt removed is

$$\sigma^2_{+PTR} = 0.134\,\left(D/r_0^+\right)^{5/3}. \tag{6.200}$$

The contribution due to the unsensed turbulence increases with increasing aperture size, and one will find that the beacon altitude must be increased for larger diameters in order to keep this component manageable.

The total phase variance with piston removed is

$$\sigma^2_{PR} = \sigma^2_{-PR} + \sigma^2_{+PR}. \tag{6.201}$$

The total phase variance with piston and tilt removed is

$$\sigma^2_{PTR} = \sigma^2_{-PTR} + \sigma^2_{+PTR}. \tag{6.202}$$

In Fig. 6.17 the total, piston-removed, and piston-and-tilt-removed phase variances due to turbulence below the beacon are plotted for a single beacon operating with a 60-cm diameter aperture with the HV-21 turbulence model. In Fig. 6.18 the piston-removed and piston-and-tilt-removed phase variances of the entire atmosphere are plotted for the same conditions.

6.14 Focal Anisoplanatism for Distributed Sources

The artificial beacon source is adequately approximated by a point source for very distant beacons. This, however, is a poor approximation for some closer beacons. In trying to use resonant sodium backscatter from the sodium layer at about 90 km, one wants to use as large a beacon as possible that does not significantly increase the phase variance over that of a point source. A large beacon is desirable because the return from a given area saturates at a certain power.

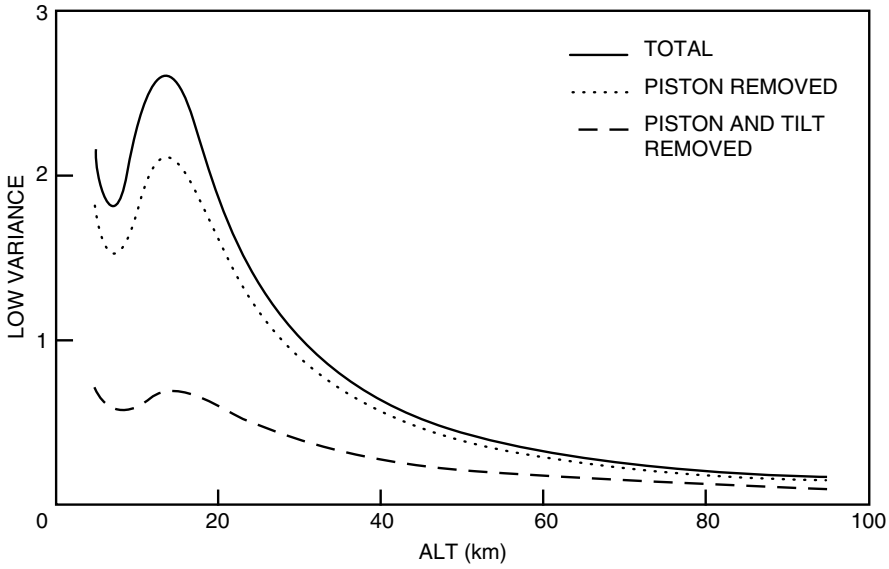

Figure 6.17. Phase variance of turbulence below the beacon for a single beacon operating with a 60-cm diameter aperture for the HV-21 turbulence model. The total, piston-removed, and tilt- and piston-removed phase variances are plotted.

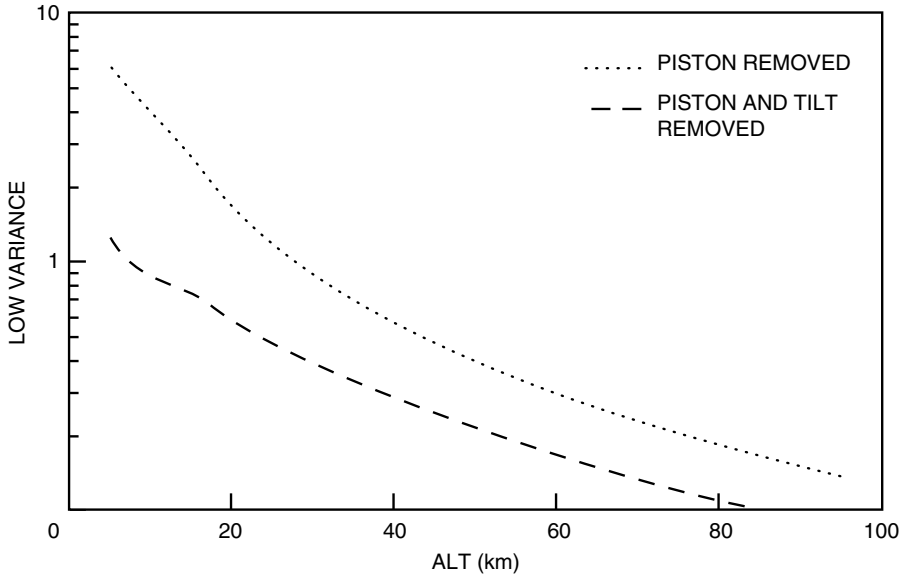

Figure 6.18. Piston-removed phase variance and piston-and-tilt-removed phase variance caused by turbulence of the entire atmosphere for a single beacon operating with a 60-cm diameter aperture for the HV-21 turbulence model.

To increase the return signal, not only must the beacon power be increased, but also, the focused spot size must be increased.

The expression for the phase variance for a distributed source centered on the aperture with piston and tilt present is found from eq. 6.176 by setting **b** equal to zero to obtain

$$\sigma^2_{-d} = 1.303\, k_0^2 \int_0^L dz\, C_n^2(z) \int_0^\infty d\kappa\, \kappa^{-8/3} \times \left\{ 1 - 8 \frac{J_1(a D_s)}{a D_s} \frac{J_1(a D)}{a D} + \left[\frac{2 J_1(a D_s)}{a D_s} \right]^2 \right\}, \tag{6.203}$$

where $a = \kappa z / 2L$. To evaluate this integral, it is written as the sum of two integrals.

Let $w = \kappa D\, z / 2\, L$, $y = \kappa D_s\, z / 2\, L$, and $x = D / D_s$, to obtain

$$\sigma^2_{-d} = 6.55 \left(\frac{0.348\, D}{L\, \theta_o^-} \right)^{5/3} (-I + J). \tag{6.204}$$

The J term is easily evaluated with eq. 1.52 to give

$$J = \frac{1}{2} \left(\frac{D_s}{D} \right)^{5/3} \int_0^\infty dy\, y^{-11/3-1} \left[J_1^2(y) - \left(\frac{y}{2} \right)^2 \right] = -0.1331 \left(\frac{D_s}{D} \right)^{5/3}. \tag{6.205}$$

The first integral is

$$I = x \int_0^\infty \frac{dw}{w}\, w^{-11/3} \left[J_1(w) J_1\left(\frac{w}{x} \right) - \frac{w}{2} \frac{w}{2x} \right]. \tag{6.206}$$

The value of I depends on x, which is not a function of z. J is also not a function of z. Therefore, the phase variance due to turbulence below the beacon depends solely on the five-thirds moment of turbulence.

The expression for I is exactly the same expression as that in eq. 6.185. Use the results of the evaluation of that integral to obtain for $D_s/D < 1$

$$\sigma^2_{-d} = \left(\frac{0.348\, D}{L\, \theta_o^-} \right)^{5/3} \left\{ {}_2F_1\left[-\tfrac{5}{6}, -\tfrac{11}{6}; 2; \left(\frac{D_s}{D} \right)^2 \right] - 0.872 \left(\frac{D_s}{D} \right)^{5/3} \right\}, \quad D_s/D < 1. \tag{6.207}$$

The first few terms of this solution are

$$\sigma^2_{-d} = \left(\frac{0.348\, D}{L\, \theta_o^-} \right)^{5/3} \left[1 - 0.872 \left(\frac{D_s}{D} \right)^{5/3} + 0.764 \left(\frac{D_s}{D} \right)^2 - 0.0177 \left(\frac{D_s}{D} \right)^4 - 0.000287 \left(\frac{D_s}{D} \right)^6 + \cdots \right], \quad D_s/D \ll 1. \tag{6.208}$$

The first three terms in brackets give a good approximation to the phase variance when $D_s/D < 1$.

When $D_s/D > 1$, the variance is

$$\sigma^2_{-d} = \left(\frac{0.348\,D_s}{L\,\theta_o^-}\right)^{5/3} \left\{-0.872 + {}_2F_1\left[-\tfrac{5}{6}, -\tfrac{11}{6}; 2; \left(\frac{D}{D_s}\right)^2\right]\right\}, \quad D_s/D > 1. \tag{6.209}$$

The first few terms of this solution are

$$\sigma^2_{-d} = \left(\frac{0.348\,D_s}{L\,\theta_o^-}\right)^{5/3} \left[0.128 + 0.764\left(\frac{D}{D_s}\right)^2 - 0.0177\left(\frac{D}{D_s}\right)^4 - 0.000287\left(\frac{D}{D_s}\right)^6 + \cdots\right], \quad D_s/D \gg 1. \tag{6.210}$$

The normalized variance is plotted in Fig. 6.19. Initially, the phase variance caused by the turbulence below the beacon decreases as source size increases, then it increases.

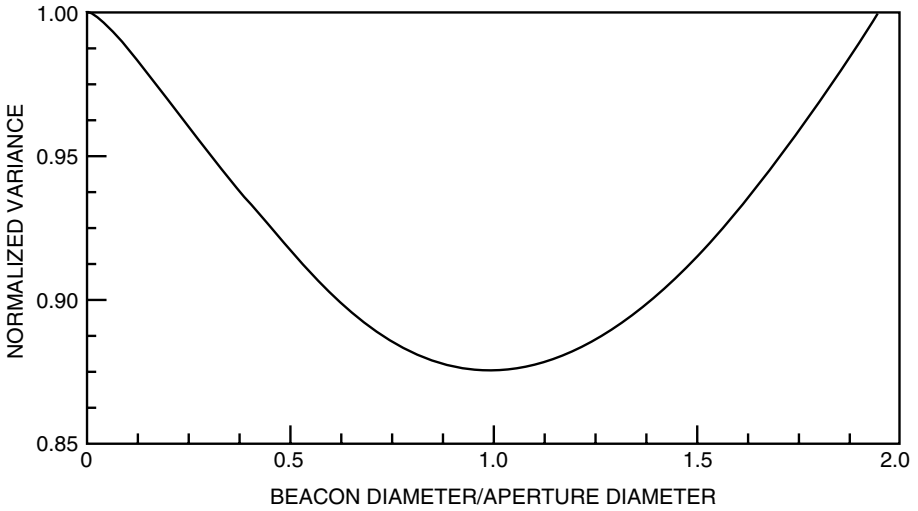

Figure 6.19. Phase variance below the beacon. Effect of beacon diameter on the phase variance due to focal anisoplanatism normalized to the phase variance due to focal anisoplanatism from a point source with piston and tilt present.

6.15 Focal Anisoplanatism for Offset Sources

The beacon may not be placed in the exact location that the correction is wanted; this results in a decreased Strehl ratio. This error can be caused by errors both in positioning the beacon and in knowing which direction to point the beacon. If a laser beam is to be projected in the point-ahead direction, which is typically about 50 μrad, there is an error made in pointing the mirrors caused by tilt anisoplanatism. This error can be as much as a microradian.

The phase variance with a point source offset from the origin is obtained by setting the source diameter equal to zero in eq. 6.176. After performing the angle integration, one obtains

$$\sigma^2_{-o} = 1.303\, k_0^2 \int_0^L dz\, C_n^2(z) \int_0^\infty d\kappa\, \kappa^{-11/3} 2 \left[1 - \frac{2J_1(\kappa D z/2L)}{\kappa D z/2L} J_0\left(\frac{\kappa b z}{L}\right)\right]. \quad (6.211)$$

The o subscript refers to an offset source. Make the substitutions $y = \kappa D z/2L$, and $x = D/2b$, to obtain

$$\sigma^2_{-o} = 2.606\, k_0^2 \left(\frac{D}{2L}\right)^{5/3} \int_0^L dz\, C_n^2(z)\, z^{5/3} \int_0^\infty \frac{dy}{y}\, y^{-5/3} \left[1 - \frac{2\,J_1\,(y)}{y} J_0\,(y/x)\right]. \quad (6.212)$$

Since the parameter in the last integral does not depend on the axial coordinate, the axial integration can be performed to give

$$\sigma^2_{-o} = 5.212\, k_0^2\, \mu^-_{5/3} \left(\frac{D}{2L}\right)^{5/3} \int_0^\infty \frac{dy}{y}\, y^{-8/3} \left[\frac{y}{2} - J_1\,(y)\; J_0\,(y/x)\right]. \quad (6.213)$$

The expression in brackets can be manipulated into two integrable terms as

$$1 - \frac{2J_1\,(y)}{y} J_0\,(y/x) = [1 - J_0\,(y/x)] + \frac{2}{y}\left[\frac{y}{2} - J_1\,(y)\right]\, J_0\,(y/x)\,. \quad (6.214)$$

The integral of the first term is evaluated by table lookup and the analytical continuation arguments used in evaluating eq. 1.22 to give

$$\sigma_1^2 = 1.118\, k_0^2\, \mu^-_{5/3} \left(\frac{2b}{L}\right)^{5/3}. \quad (6.215)$$

The last integral can be converted into an integral in the complex plane as

$$I = -\frac{2^{-11/3}}{2\pi i} \int_C ds\, \left(\frac{D}{2\,b}\right)^{-2s} \Gamma\left[\begin{matrix} s - \frac{5}{6}*,\, -s \\ -s + \frac{17}{6},\, s+1 \end{matrix}\right]. \quad (6.216)$$

Since $\Delta = 0$, the direction of path closure depends on the parameter magnitude. When the displacement is less than aperture radius, the integration path is closed to the right, and there are poles at $s = n$ for $n = 0, 1, 2, \ldots$ and at $s = 5/6$.

The last term cancels the contribution of σ_1^2. For this case, phase variance from turbulence below the beacon is

$$\sigma_{-o}^2 = -0.1293\, k_0^2\, \mu_{5/3}^- \left(\frac{D}{L}\right)^{5/3} \times \sum_{n=0}^{\infty} \frac{(-1)^n}{n\,!} \left(\frac{2b}{D}\right)^{2n} \Gamma\begin{bmatrix} n-\frac{5}{6} \\ -n+\frac{17}{6},\, n+1 \end{bmatrix}, \quad 2b/D < 1. \tag{6.217}$$

This can also be written as

$$\sigma_{-o}^2 = 0.5\, k_0^2 \mu_{5/3}^- \left(\frac{D}{L}\right)^{5/3} {}_2F_1\left[-\tfrac{5}{6}, -\tfrac{11}{6}; 1; \left(\frac{2b}{D}\right)^2\right], \quad 2b/D < 1. \tag{6.218}$$

The variance normalized to that of an on-axis source is

$$\frac{\sigma_{-o}^2}{\sigma_{-o}^2\,(b=0)} = {}_2F_1\left[-\tfrac{5}{6},\ -\tfrac{11}{6};\ 1;\ \left(\frac{2b}{D}\right)^2\right] = 1 + 6.12\left(\frac{b}{D}\right)^2 - 0.848\left(\frac{b}{D}\right)^4 + \cdots, \quad 2b/D < 1. \tag{6.219}$$

When the displacement is zero, the hypergeometric function is equal to unity, and one obtains the previous result

$$\sigma_{-o}^2\,(b=0) = 0.5\, k_0^2\, \mu_{5/3}^- \left(\frac{D}{L}\right)^{5/3}. \tag{6.220}$$

When the displacement is larger than the radius, the integration path is closed to the left, and there are poles at $s = -n + 5/6$ for $n = 1, 2, \ldots$, thus one obtains

$$\sigma_{-o}^2 = 1.293\, k_0^2\, \mu_{5/3}^- \left(\frac{D}{L}\right)^{5/3} \sum_{n=0}^{\infty} \frac{(-1)^n}{n\,!} \left(\frac{D}{2b}\right)^{2n-5/3} \Gamma\begin{bmatrix} n-\frac{5}{6} \\ -n+\frac{11}{6},\, n+2 \end{bmatrix}, \quad 2b/D > 1. \tag{6.221}$$

The variance normalized to that of an on-axis source is

$$\frac{\sigma_{-o}^2}{\sigma_{-o}^2\,(b=0)} = 1.833\left(\frac{2b}{D}\right)^{5/3} {}_2F_1\left[-\tfrac{5}{6}, -\tfrac{5}{6}; 2, \left(\frac{D}{2b}\right)^2\right], \quad 2b/D > 1. \tag{6.222}$$

The variance normalized to that with no offset is plotted in Fig. 6.20.

For larger source displacements than those plotted, one can use the approximation

$$\frac{\sigma_{-o}^2}{\sigma_{-o}^2\,(b=0)} \approx 1.833\left(\frac{2b}{D}\right)^{5/3}, \quad 2b/D > 3. \tag{6.223}$$

The phase variances in this and the last section can be used to determine the importance of beacon size and placement; however, the piston and tilt terms are included. The evaluation of the integrals to determine the phase variance with these components removed can be done by the techniques discussed in Chap. 10. The analysis is complicated and lengthy and is not given here.

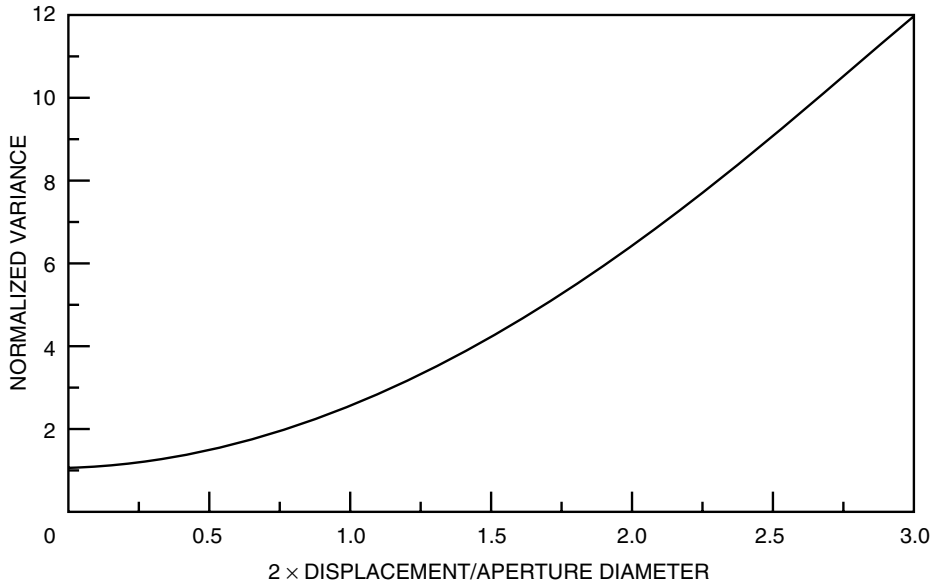

Figure 6.20. Total phase variance below the beacon for focal anisoplanatism with a displaced point source. The variance is normalized to that of a source on axis. Piston and tilt are present. It is plotted versus twice the displacement divided by the aperture diameter.

REFERENCES

1. Andrews, L. C., "Aperture-averaging factor for optical scintillation of plane and spherical waves in the atmosphere", *J. Opt. Soc. Am. A*, **9**, (1992) pp. 597–600.
2. Butts, R. R., "Spectra of Turbulence Induced Wavefront Aberrations", *AFWL-TR-80-107* (Air Force Weapons Laboratory, 1980).
3. Ellerbroek, B. L., Roberts, P. H., "Turbulence Induced Angular Separation Errors; Expected Values For the SOR-2 Experiment", *tOSC Report No. TR-613* (the Optical Sciences Company, Placentia, California, 1984).
4. Fields, D. A., "High frequency behavior of the tilt spectrum of atmospheric turbulence", *Appl. Opt.*, **22**, (1983) pp. 645–647.
5. Fried, D. L., "Aperture Averaging of Scintillation", *J. Opt. Soc. Am.*, **57**, (1967) pp. 169–175.
6. Fugate, R. Q., Fried, D. L., Ameer, G. A., Boeke, B. R., Browne, S. L., Roberts, P. H., Ruane, R. E., Tyler, G. A., Wopat, L. M., "Measurement of atmospheric distortion using scattered light from a laser guide star", *Nature*, **353**, (1991) pp. 144–146.
7. Gardner, C. S., Welsh, B. M., Thompson, L. A., "Design and Performance Analysis of Adaptive Optical Telescopes Using Laser Guide Stars", Proc. IEEE, **78**, (1990) pp. 1721–1743.

8. Gradshteyn, I. S., Ryzhik, I. M., *Table of Integrals, Series, and Products*, Academic Press, New York, (1980).
9. Greenwood, D. P., Fried, D. F., "Power spectra requirements for wave-front-compensa-tive systems", *J. Opt. Soc. Am.*", **66**, (1976) 193–206.
10. Herrmann, J., Cross Coupling and aliasing in modal wave-front estimation", *J. Opt. Soc. Am.*, **71**, (1981) pp. 989–992.
11. Hill, R. J., Clifford, S. F., "Modified spectrum of atmospheric temperature fluctuations and its application to optical propagation", *J. Opt. Soc. Am.*, **68**, (1978) pp. 892–899.
12. Hogge, C. B., Butts, R. R., "Frequency Spectra for the Geometric Representation of Wavefront Distortions Due to Atmospheric Turbulence", *IEEE Trans. Antennas Propaga.*, **24**, (1976) pp. 144–154.
13. Lynds, C. R., Worden, S. P., Harvey, J. W., "Digital Image Reconstruction Applied To Alpha Orionis", *The Astrophysical Journal*, **207**, (1976) pp. 174–180.
14. Murphy, D. V., Primmerman, C. A., Zollars, B. G., Barclay, H. T., "Experimental Demonstration of Atmospheric Compensation Using Multiple Synthetic Beacons", *Opt. Lett.*, **15**, (1991) pp. 1797–1799.
15. Primmerman, C. A., Murphy, D. V., Page, D. A., Zollars, B. G., Barclay, H. T, "Compensation of Atmospheric Optical Distortion Using a Synthetic Beacon", *Nature*, **353** (1991) pp. 141–143.
16. Tatarski, V. I., *The Effects Of The Turbulent Atmosphere On Wave Propagation*, U. S. Department Of Commerce, (1971).
17. Tyler, G. A., "The Power Spectrum for G-tilt and Z-tilt", *tOSC Report No. TR-700* (the Optical Sciences Company, Placentia, California, 1986).
18. Valley, G. C., "Long- and short-term Strehl ratios for turbulence with finite inner and outer scales", *Appl. Opt.*, **18**, (1979) pp. 984–987.
19. Vaughn, J. L., "Calculation of the Power Spectra of Z-tilt and G-tilt", *tOSC Report No. TR-710* (the Optical Sciences Company, Placentia, California, 1986).
20. Walters, D. L., Favier, D. L., Hines, J. R., "Vertical Path Atmospheric MTF Measurements", *J. Opt. Soc. Am.* **69**, (1979) pp. 828–837.
21. Welsh, B. M., Gardner, C. S., "Performance Analysis of Adaptive-Optics Systems using Laser Guide Stars and Slope Sensors", *J. Opt. Soc. Am.*, **6**, (1989) pp. 913–1923.
22. Welsh, B. M., Thompson, L. A., "Effects of Turbulence-Induced Anisoplanatism on the Imaging Performance of Adaptive-Astronomical Telescopes using Laser Guide Stars", *J. Opt. Soc. Am. A*, **8**, (1991) pp. 69–80.
23. Winker, D. M., "ffect of a finite outer scale on the Zernike decomposition of atmospheric optical turbulence", *J. Opt. Soc. Am. A*, **8**, (1991) pp. 568–1573.

Chapter 7

Strehl Ratio

Strehl ratio is an important performance measure for adaptive-optics systems. Its calculation is more complicated than that of variances. Nevertheless, it is shown below that one can obtain exact expressions for the Strehl ratio for propagation through uncorrected turbulence, and through turbulence for which all modes except tilt have been corrected. Asymptotic expressions are also obtained that apply when the distortion is high.

The effect of anisoplanatism on the Strehl is especially important. Here I consider isoplanatic effects of aperture displacement in space and angle, time delay, and chromatic offsets. A formula is obtained that is a good approximation to the Strehl ratio when it is above 0.2. Fortunately, this is the region of greatest interest in adaptive-optics system design.

For many problems one must revert to numerical techniques to find the Strehl ratio. Normally, this can be done with little difficulty; however, there are cases in which the structure function is a function of position in the aperture. Problems in which one is interested in the Strehl ratio when the tilt is removed generally fall into this category. For these cases a 7-fold integration must be performed. It is only recently that computer speed allows these integrations to be performed on even a reasonably fast computer cluster in less than a day. Examples of these types of problems are given.

7.1 Strehl Ratio for Propagation Through Turbulence

The problem of determining the on-axis intensity of a plane wave propagating through atmospheric turbulence was analyzed by *Fried* (1966), and the resultant integral was evaluated numerically. Here a compact analytic expression for the Strehl ratio is obtained. A second form expressible as an infinite series is also obtained. This second solution is more convenient, since a few series terms give an accurate answer for small levels of turbulence. An asymptotic series is obtained that is applicable when turbulence is more severe. It is shown that the first two terms of the series give an accurate result in the regime in which most astronomical telescopes operate.

Strehl ratio is the most common description of optical system performance, and it is the normalized intensity evaluated at the beam center. Its general

expression was derived in Sec. 2.5, and for an isotropic structure function it is given in eq. 2.164 as

$$SR = \int_0^1 d\alpha\, \alpha\, K(\alpha)\, \exp\left[-\mathcal{D}(\alpha D)/2\right]. \tag{7.1}$$

The integral is over a circular aperture of unit radius, $\mathcal{D}(\alpha D)$ is the structure function, α is the normalized radius that is equal to unity at the aperture edge, and $K(\alpha)$ is a constant times the optical transfer function, given by

$$K(\alpha) = \frac{16}{\pi}\left[\cos^{-1}(\alpha) - \alpha\left(1-\alpha^2\right)^{1/2}\right] U(1-\alpha), \tag{7.2}$$

where $U(x)$ is the Heaviside unit step function defined in (1.20).

The structure function is given in eq. 2.123, and for the Kolmogorov turbulence spectrum with inner and outer scale neglected is

$$\begin{aligned}\mathcal{D}(\boldsymbol{\alpha} D) &= \left\langle \left[\phi\left(\mathbf{a} + \boldsymbol{\alpha} D\right) - \phi\left(\mathbf{a}\right)\right]^2 \right\rangle \\ &= 0.4146\, k_0^2 \int_0^\infty dz\, C_n^2(z) \int d\boldsymbol{\kappa}\, \kappa^{-11/3}\left[1 - \cos\left(\boldsymbol{\kappa}\cdot\boldsymbol{\alpha} D\right)\right].\end{aligned} \tag{7.3}$$

D is the local diameter of the wave. Integrate over angle in kappa space with eq. 3.5, and perform the last integration with the relation in eq. 1.22, to obtain

$$\begin{aligned}\mathcal{D}(\alpha D) &= 2.605\, k_0^2 \int_0^\infty dz\, C_n^2(z) \int_0^\infty d\kappa\, \kappa^{-5/3-1}\left[1 - J_0\left(\kappa \alpha D\right)\right] \\ &= 2.605\, k_0^2 (\alpha D)^{5/3} \int_0^\infty dz\, C_n^2(z) \mathcal{M}\left[1 - J_0(x)\right]\Big|_{s=-5/3} = 2.91\, \mu_0 k_0^2 (\alpha D)^{5/3}.\end{aligned} \tag{7.4}$$

Write the structure function in the form

$$\mathcal{D}(\alpha D) = 6.88\, \left(\alpha D/r_0\right)^{5/3}. \tag{7.5}$$

For plane waves D is constant, and the coherence diameter r_0 is equal to

$$r_0 = \left(0.423\, k_0^2\, \mu_0\right)^{-3/5}. \tag{7.6}$$

This reproduces the standard definition of r_0.

When Strehl ratio calculations are made for values of $D/r_0 > 7$, small errors in the coefficients can produce significant differences in the calculated value of the Strehl ratio. For those cases one should substitute the more accurate values of the constants given by $6.88 \to 2(24/5\Gamma[6/5)^{5/6} = 6.88388$, $0.2073 \to 10\Gamma[5/6]/(2^{4/3}\pi^{1/2}9\Gamma[2/3]) = 0.207379$, and $r_0 = (0.42336\, k_0^2\, \mu_0)^{-3/5}$.

For spherical waves with a focus at 0, the separation of beam centers decreases toward the focus so that $D \to D\, z/L$. For this case one obtains the spherical-wave coherence diameter

$$r_{os0} = L\left(0.423\,k_0^2\,\mu_{5/3}\right)^{-3/5} = 3.18\,L\theta_o, \tag{7.7}$$

where L is the distance from the aperture at $z = L$ to the beam focus at $z = 0$, and θ_o is the isoplanatic angle defined in eq. 4.14. This equation implies that if one measured the structure function at the receiver from a point source, then one could determine the isoplanatic angle at the point source.

One can also consider the case of a wave focused at $z = L$, in which case the coherence diameter is

$$r_{osL} = \left[0.423\,k_0^2\int_0^L dz\,C_n^2(z)\,(1 - z/L)^{5/3}\right]^{-3/5}. \tag{7.8}$$

The spherical wave coherence diameter determines the system resolution. The angular resolution looking up is λ/r_{osL}, and that looking down is λ/r_{os0}. For distant sources $r_{osL} \approx r_0$, which allows r_o to be used in resolution calculations looking towards space. For HV-21 turbulence r_0 is about 5 cm at 0.5 μm. For a system looking down from 100 km above the earth the coherence diameter is 2.2 m at this wavelength, which is a factor of 44 times the resolution looking up. This is why the resolution of an imaging system looking down toward the earth is much greater than that of an imaging system on the ground looking at an object in space.

Insert the structure function into the integral for Strehl ratio to obtain

$$SR = \int_0^\infty d\alpha\,\alpha\,K(\alpha)\,\exp\left[-3.44\,(\alpha D/r_0)^{5/3}\right]. \tag{7.9}$$

Another type of coherence diameter ρ_o is sometimes used, and it is related to r_0 by $r_0 = 2.1\,\rho_0$. This coherence diameter results in a unity coefficient in the exponential when inserted into the last equation. This is the integral that was evaluated numerically by *Fried* (1966). It is analytically evaluated here. Use the Mellin convolution integral given in eq. 1.28 and the Mellin transforms in eq. 1.64 and eq. 1.47, and eq. 1.9 with $p = 5/3$, to express the Strehl ratio as

$$SR = \frac{24}{5\sqrt{\pi}}\frac{1}{2\pi i}\int_C ds\,\Gamma\begin{bmatrix} s/2 + \frac{3}{2},\ -3s/5 \\ s/2 + 3 \end{bmatrix}\left(\frac{1}{s+2}\right)\left[3.44\,(D/r_0)^{5/3}\right]^{3s/5}. \tag{7.10}$$

Let $s \to -5s/3$, and replace the fraction by a ratio of gamma functions with the recursion relation $-s + 6/5 = \Gamma\left[-s + \frac{11}{5}\right]/\Gamma\left[-s + \frac{6}{5}\right]$ to obtain

$$SR = \frac{24}{5\sqrt{\pi}}\frac{1}{2\pi i}\int_C ds\,\Gamma\begin{bmatrix} s,\ -5s/6 + \frac{3}{2},\ -s + \frac{6}{5} \\ -5s/6 + 3,\ -s + \frac{11}{5} \end{bmatrix}\left[3.44\left(\frac{D}{r_0}\right)^{5/3}\right]^{-s}. \tag{7.11}$$

The coefficients of s in the gamma functions can be made equal to unity by the substitution $s \to 6s$ and with the Gauss-Legendre multiplication theorem in eq. 1.15 to obtain

$$SR = \frac{\sqrt{0.6}}{25\pi^3}\frac{1}{2\pi i}\int_C ds\,\left[\left(\frac{6}{3.44}\right)^6\left(\frac{r_0}{D}\right)^{10}\right]^s \Gamma\left[\begin{matrix} s,\ s+\frac{1}{6},\ s+\frac{1}{3},\ s+\frac{1}{2} \\ -s+\frac{6}{5},\ -s+\frac{3}{5},\ -s+\frac{4}{5}\end{matrix}\right]$$
$$\times\Gamma\left[\begin{matrix} s+\frac{2}{3},\ s+\frac{5}{6},\ -s+\frac{1}{5},\ -s+\frac{3}{10},\ -s+\frac{1}{2},\ -s+\frac{7}{10},\ -s+\frac{9}{10},\ -s+\frac{11}{10} \\ -s+1,\ -s+\frac{6}{5},\ -s+\frac{7}{5}\end{matrix}\right]. \tag{7.12}$$

The result can be written by inspection as a Meijer G-function, which is defined in eq. 1.40, or as a Fox H-function, which is defined in eq. 1.39, as

$$SR = \frac{\sqrt{0.6}}{25\pi^3}\,G^{6,6}_{12,6}\left[\left(\frac{6}{3.44}\right)^6\left(\frac{r_0}{D}\right)^{10}\left|\begin{matrix}1,\ \frac{5}{6},\ \frac{2}{3},\ \frac{1}{2},\ \frac{1}{3},\ \frac{1}{6},\ \frac{6}{5},\ \frac{3}{5},\ \frac{4}{5},\ 1,\ \frac{6}{5},\ \frac{7}{5} \\ \frac{1}{5},\ \frac{3}{10},\ \frac{1}{2},\ \frac{7}{10},\ \frac{9}{10},\ \frac{11}{10}\end{matrix}\right.\right]$$
$$= \frac{24}{5\sqrt{\pi}}\,H^{2,1}_{1,4}\left[\frac{1}{3.44}\left(\frac{r_0}{D}\right)^{5/3}\left|\begin{matrix}(1,\,1)\,,\ \left(3,\,\frac{5}{6}\right),\ \left(\frac{11}{5},\,1\right) \\ \left(\frac{3}{2},\,\frac{5}{6}\right),\ \left(\frac{6}{5},\,1\right)\end{matrix}\right.\right]. \tag{7.13}$$

An equivalent solution, which provides more physical insight, expresses the Strehl ratio as an infinite sum in which coefficients of the integers in the arguments of the gamma functions are fractions. Since $\Delta = 1$ in eq. 7.11, the integral can be closed in the left-half plane. Encircled poles are located at $s = -n$, for $n = 0, 1, 2, \ldots$. Residues at the enclosed poles give the following convergent series

$$SR = \frac{24}{5\sqrt{\pi}}\sum_{n=0}^{\infty}\frac{(-1)^n}{n\,!}\,\Gamma\left[\begin{matrix}\frac{3}{2}+5n/6,\ n+\frac{6}{5} \\ 3+5n/6,\ n+\frac{11}{5}\end{matrix}\right]\left[3.44\left(\frac{D}{r_0}\right)^{5/3}\right]^n. \tag{7.14}$$

The first few terms of this series are

$$SR = 1 - 1.032\left(\frac{D}{r_0}\right)^{5/3} + 0.7982\left(\frac{D}{r_0}\right)^{10/3} - 0.5015\left(\frac{D}{r_0}\right)^{5} + \cdots. \tag{7.15}$$

For large diameters this series converges slowly, and an asymptotic series is more convenient. For this case one can show with eq. 5.93 that the steepest-descent contribution has exponential decay; therefore, the asymptotic solution is equal to the sum of pole residues on the left side of the integration path. The poles are at $s = 6/5$, and $s = 6n/5 + 9/5$ for $n = 0, 1, 2, \ldots$. (Remember to multiply the second set of residues by $6/5$ because the coefficient of s in the gamma function is not unity.) The gamma function that produces the pole at $s = 6/5$ only has a single contributing pole because the residues at the other poles of the gamma function are zero. The asymptotic series is

$$SR \sim \left(\frac{r_0}{D}\right)^2 - \frac{24}{5\sqrt{\pi}}\,3.44^{-9/5}\sum_{n=0}^{n_o}\frac{(-1)^n}{n\,!\left(n+\frac{1}{2}\right)}\Gamma\left[\begin{matrix}6n/5+\frac{9}{5} \\ -n+\frac{3}{2}\end{matrix}\right]3.44^{-6n/5}\left(\frac{r_0}{D}\right)^{3+2n}, \tag{7.16}$$

where n_o is a number of terms discussed in Sec. 5.2. The first few terms of this series are

$$SR \sim \left(\frac{r_0}{D}\right)^2 - 0.6159\left(\frac{r_0}{D}\right)^3 + 0.0500\left(\frac{r_0}{D}\right)^5 + 0.0132\left(\frac{r_0}{D}\right)^7 + \cdots . \quad (7.17)$$

It is this relation that was the basis for the definition of coherence diameter. For very large apertures the field on axis has the same value as would be produced by a transmitter with diameter r_0 that propagates through free space. The Strehl ratio is plotted in Fig. 7.1.

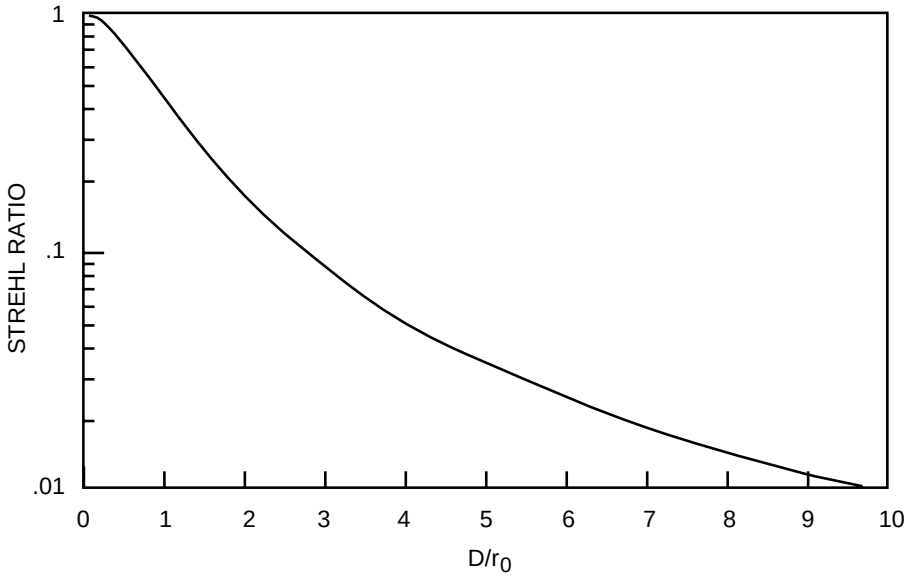

Figure 7.1. Strehl ratio for uncorrected turbulence versus D/r_0.

If one calculates the Strehl ratio using solely the first term of the asymptotic series for $D/r_0 = 2$, 5, and 10, then one obtains errors of 32%, 13%, and 6%. The use of the first two terms produces errors of 0.8%, 0.04%, and 0.005%, respectively. Therefore, the first two terms of the asymptotic expansion give a value of Strehl ratio when $D/r_0 > 2$ that has an error of less than 1%.

An approximation proposed by Andrews and Phillips that has an error of less than 6% over the entire range is

$$SR = \left(1 + (D/r_0)^{5/3}\right)^{-6/5} . \quad (7.18)$$

The phase structure function and Strehl ratio can also be found with a finite outer scale. With the von Kármán spectrum the structure function is

$$\mathcal{D}(\alpha D) = 2.605\, k_0^2 \int_0^\infty dz\, C_n^2(z) \int_0^\infty d\kappa\, \kappa \left(\kappa^2 + \kappa_0^2\right)^{-11/6} \left[1 - J_0\left(\kappa \alpha D\right)\right] . \quad (7.19)$$

After the substitution $y = \kappa_0 \alpha D$, the integrals can be evaluated to give

$$\mathcal{D}(r) = 6.88 \left(\frac{\alpha D}{r_0}\right)^{5/3} \left(0.895 \left\{\frac{\Gamma[5/6] y^{-5/3} - 2^{1/6} y^{-5/6} K_{5/6}[y]}{2\Gamma[11/6]}\right\}\right). \quad (7.20)$$

The effect of outer scale is contained in the term in braces that multiplies the structure function with infinite outer scale. This factor is plotted in Fig. 7.2. The structure function has been reduced by about 50% when the separation is 1/25 of the outer scale. Therefore, the effect of outer scale is much more dramatic on the phase structure function than the density structure function.

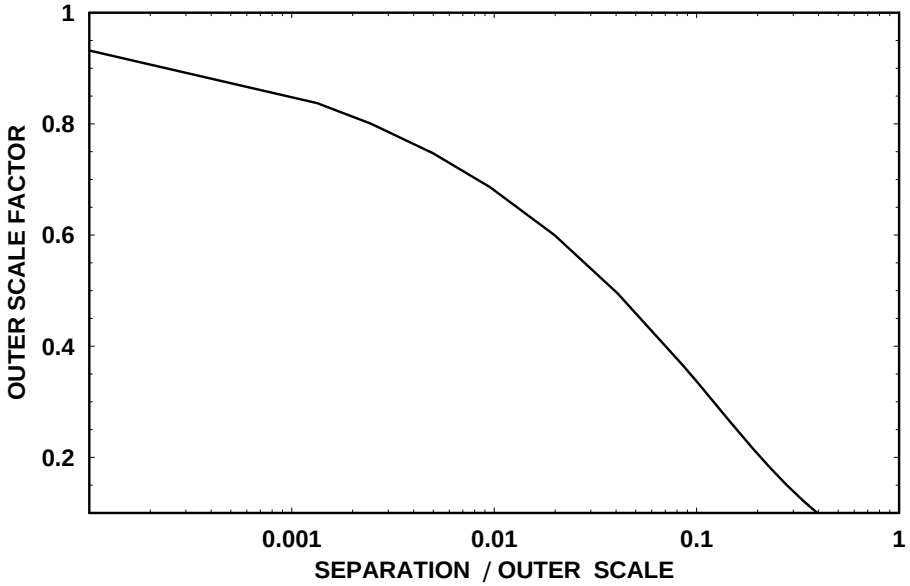

Figure 7.2. Reduction of the phase structure function versus the ratio of separation (αD) to the outer scale size.

When this structure function is inserted into the Strehl ratio expression for different ratios of the diameter to the outer scale size, one obtains the curves plotted in Fig. 7.3. There is a significant increase in the Strehl ratio for ratios of the diameter to outer scale that are expected in common situations.

To reify this effect, consider an aperture size of 1 meter with an outer scale size of 10 meters. The ratio of SR with the finite outer scale to that with infinite outer scale versus D/r_0 is plotted in Fig. 7.4. Notice that the Strehl ratio can be almost a factor of 2 higher than the case with infinite outer scale.

7.2 Strehl Ratio with Beam Jitter

Typical adaptive-optics systems correct higher-order terms; tilt is corrected by a separate tracking system and mirror. Any jitter associated with this tracking

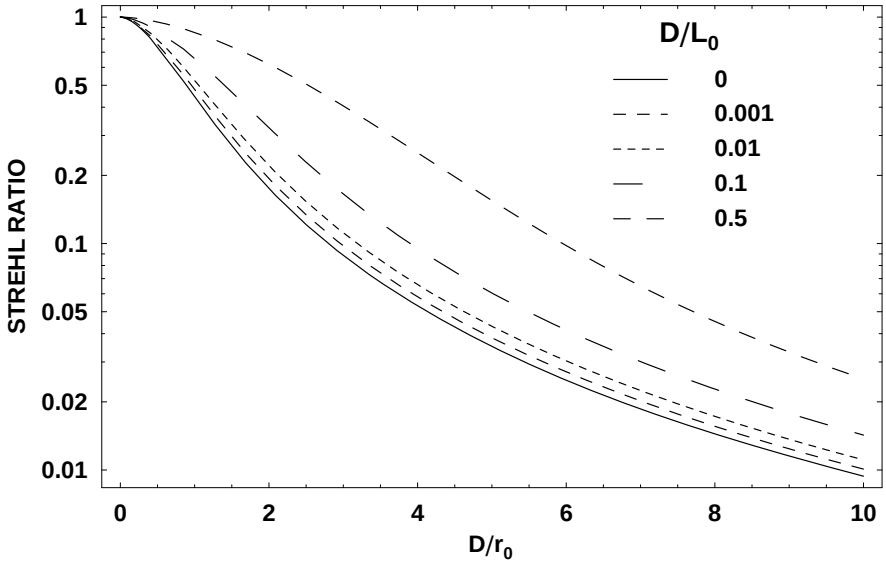

Figure 7.3. Strehl ratio versus D/r_0 for various ratios of the diameter to the outer scale size.

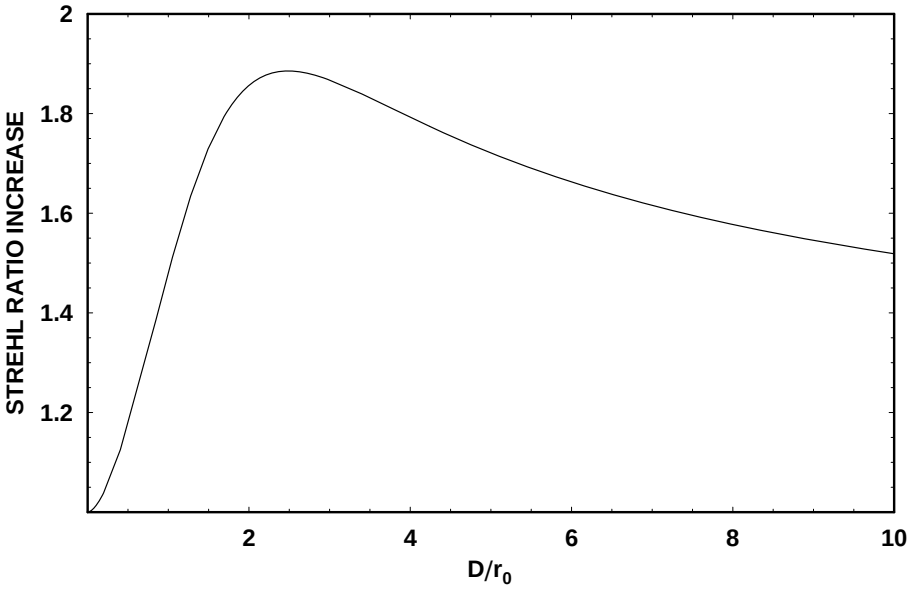

Figure 7.4. Increase in SR versus D/r_0 for $D/L_0 = 0.1$.

system reduces intensity on axis, and its effect on system resolution must be known during system design. For propagation through turbulence, jitter can be expressed as a function of turbulence strength. *Yura* and *Tavis* (1985) solved for the structure function of the difference between Zernike and gradient tilts. Many tracking systems measure gradient tilt, which is sensitive to higher-order Zernike aberrations. The difference between gradient and Zernike tilt represents an inherent source of tilt jitter in such a system and is referred to as centroid anisoplanatism. An adaptive-optics system reduces this error as explained in Sec. 4.4. Yura and Tavis presented numerical results for the Strehl ratio. They also presented a simple expression that is a reasonable approximation to the Strehl ratio. Here an analytic solution is derived for the Strehl ratio for centroid anisoplanatism and also for the Zernike and gradient tilts.

The structure function of tilt-induced phase is equal to the expected value of the square of the difference between tilt-induced phase at two points in the aperture, and is expressed as

$$\mathcal{D}(\boldsymbol{\rho}_1-\boldsymbol{\rho}_2)=\left\langle\left[\phi\left(\boldsymbol{\rho}_1\right)-\phi\left(\boldsymbol{\rho}_2\right)\right]^2\right\rangle=k_0^2\left\langle\left[\mathbf{T}\cdot\left(\boldsymbol{\rho}_1-\boldsymbol{\rho}_2\right)\right]^2\right\rangle=\frac{k_0^2\,T^2}{2}\left|\boldsymbol{\rho}_1-\boldsymbol{\rho}_2\right|^2, \tag{7.21}$$

where $\mathbf{T}$ is the two-axis tilt of a wave that is randomly distributed in angle. The structure function is solely a function of the position difference. This tilt can be due solely to tracking jitter or can be considered to be due to atmospheric turbulence. If it is due to turbulence, then it is assumed that there is an adaptive-optics system that corrects all higher order modes of wavefront distortion, which leaves tilt as the only remaining distortion. The same expression with different constants is valid for gradient and Zernike tilt and for their difference. Two-axis tilt variances for atmospheric turbulence, which are listed in eq. 4.22, eq. 4.30, and eq. 4.32, are given by

$$T^2=\frac{1}{\pi^2}\left(\frac{D}{Mr_0}\right)^{5/3}\left(\frac{\lambda}{D}\right)^2, \tag{7.22}$$

where M is equal to 0.4642, 0.4838, and 5.394 for Zernike tilt (Z-tilt), gradient tilt (G-tilt), and their difference respectively. Therefore,

$$\mathcal{D}\left(\boldsymbol{\rho}_1-\boldsymbol{\rho}_2\right)/2=D\left(\alpha D\right)/2=\alpha^2\left(\frac{D}{Mr_0}\right)^{5/3}=\alpha^2\sigma^2, \tag{7.23}$$

where $\sigma^2=\left(D/Mr_0\right)^{5/3}$. This form leads to one plot that applies to all three tilts. With this relation one can write the Strehl ratio as

$$SR=\int_0^1\alpha\,d\alpha\,K(\alpha)\exp\left(-\sigma^2\alpha^2\right). \tag{7.24}$$

To evaluate this integral use the Mellin transforms in eq. 1.64 and eq. 1.10 in the Mellin convolution integral, and let $s\rightarrow 2s$ to obtain

$$SR = -\frac{4}{\sqrt{\pi}} \frac{1}{2\pi i} \int_C ds \left(\frac{1}{s-1}\right) \Gamma\left[\begin{matrix} s,\ -s+\frac{3}{2} \\ -s+3 \end{matrix}\right] \left(\sigma^2\right)^{-s}. \tag{7.25}$$

The pole location and integration path are shown in Fig. 7.5. The recursion relation for gamma functions, $\Gamma[s] = (s-1)\,\Gamma[s-1]$, is used to simplify the integrand. The substitution $s \to s+1$ gives

$$SR = -\frac{4}{\sigma^2\sqrt{\pi}} \frac{1}{2\pi i} \int_C ds\, \Gamma\left[\begin{matrix} s*,\ -s+\frac{1}{2} \\ -s+2 \end{matrix}\right] \left(\sigma^2\right)^{-s}, \tag{7.26}$$

where the asterisk signifies that the integration path passes between the first and second poles of that gamma function.

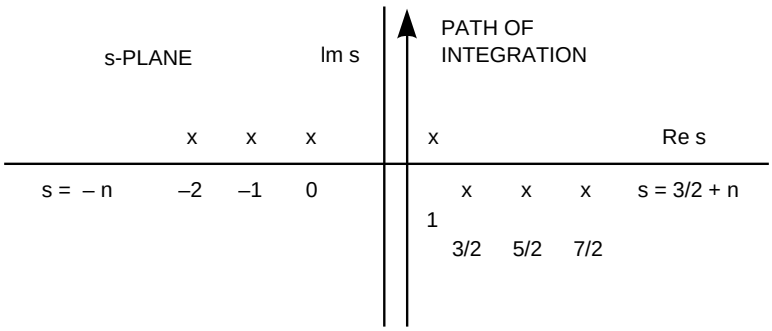

Figure 7.5. Pole location and integration path in the complex plane for the problem to determine the Strehl ratio with tilt jitter.

For this case $\Delta = 1$, and the integration path can be closed in the left-half plane. The enclosed poles are located at $s = -n$, $n = 1, 2, 3, \ldots$. The Strehl ratio given by the sum of the residues at the enclosed poles is

$$\begin{aligned} SR &= \frac{4}{\sqrt{\pi}} \sum_{n=0}^{\infty} \frac{(-1)^n}{(n+1)!} \Gamma\left[\begin{matrix} n+\frac{3}{2} \\ n+3 \end{matrix}\right] \left(\frac{D}{Mr_0}\right)^{5n/3} \\ &= {}_2F_2\left[\tfrac{3}{2}, 1; 3, 2; -\left(\frac{D}{Mr_0}\right)^{5/3}\right]. \end{aligned} \tag{7.27}$$

This can also be expressed as a confluent hypergeometric function as

$$SR = 4\left(\frac{Mr_0}{D}\right)^{5/3} \left\{1 - {}_1F_1\left[\tfrac{1}{2}; 2; -\left(\frac{D}{Mr_0}\right)^{5/3}\right]\right\}. \tag{7.28}$$

Strehl ratio is plotted for the general case in Fig. 7.6. The first few terms of this series are

$$SR = 1 - 0.25\left(\frac{D}{Mr_0}\right)^{5/3} + 0.0521\left(\frac{D}{Mr_0}\right)^{10/3} - 0.00911\left(\frac{D}{Mr_0}\right)^{5} + \cdots. \tag{7.29}$$

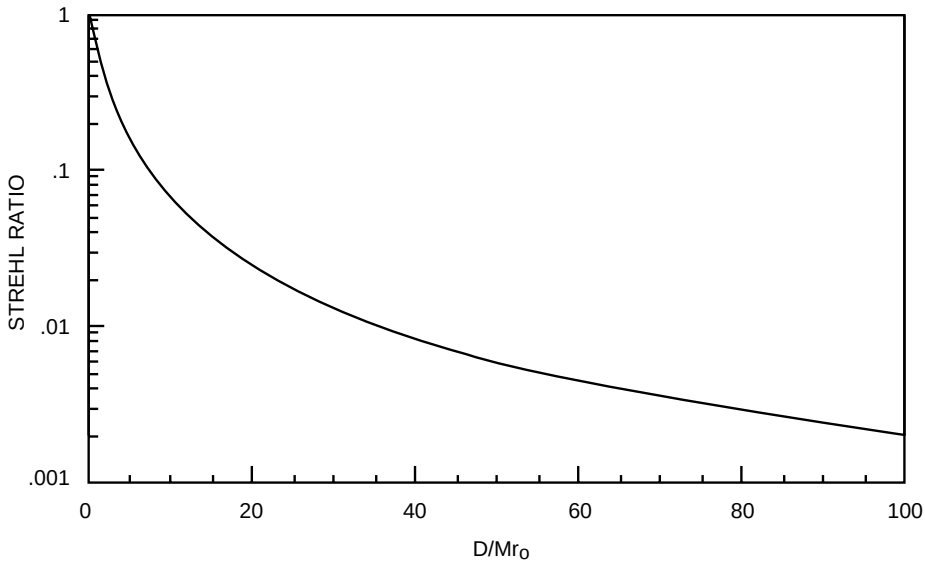

Figure 7.6. General Strehl ratio for any type of tilt. M is equal to 0.4642, 0.4838, and 5.394 for Z-tilt, G-tilt, and their difference, respectively.

For large parameter values an asymptotic solution is needed to get an approximation that is accurate with only a few terms. One could use the results in *Abramowitz* and *Stegun* (1964) for confluent hypergeometric functions or, alternatively, one can easily calculate the series. The steepest-descent contribution given by eq. 5.93 decays exponentially in this case. The asymptotic series is equal to the residues of the poles on the right side of the integration path located at $s = 0$, and $s = n + 1/2$ for $n = 0, 1, 2, \ldots$. The asymptotic series is

$$SR \sim 4\left(\frac{Mr_0}{D}\right)^{5/3} - \frac{4}{\sqrt{\pi}} \sum_{n=0}^{n_o} \frac{(-1)^n}{n\,!} \Gamma\begin{bmatrix} n+\frac{1}{2} \\ -n+\frac{3}{2} \end{bmatrix} \left(\frac{Mr_0}{D}\right)^{5n/3+5/2}. \tag{7.30}$$

The first few terms of this series are

$$SR \sim 4\left(\frac{Mr_0}{D}\right)^{5/3} - 4.51\left(\frac{Mr_0}{D}\right)^{5/2} + 1.13\left(\frac{Mr_0}{D}\right)^{25/6} + 0.423\left(\frac{Mr_0}{D}\right)^{35/6} + \cdots. \tag{7.31}$$

Yura gives an approximation

$$SR \approx \left[1 + \frac{1}{4}\left(\frac{D}{Mr_0}\right)^{5/3}\right]^{-1} = \left[1 + \left(\frac{\pi T D}{2\lambda}\right)^2\right]^{-1}. \tag{7.32}$$

One can obtain this expression by dividing unity by the sum of unity and the inverse of the first term of the asymptotic series. For very large or small diameters this approximation gives the same result as the exact calculation. For intermediate diameters this approximation gives a Strehl ratio that is too large, but not by more than 10%.

7.3 Strehl Ratio with Anisoplanatism

In adaptive-optics systems the paths of the beacon signal and the imaging or projected laser should be the same. In general, this is not possible to achieve in practice, and there is a degradation in performance caused by time delays, displacement of the two paths by translation and angle, and differences in wavelength of the beacon and measurement or projecting systems. The effect of displacement, angular mispointing, time delay, and atmospheric dispersion can each be treated as an anisoplanatic effect. In fact, if all displacements are present simultaneously, they can be combined to get a total offset of the measurement from the imaging paths. In this section, the effect of that displacement on the Strehl ratio is determined. To find the Strehl ratio, the structure function must first be determined. Use the expression for the structure function in eq. 2.123 with $d = \boldsymbol{\alpha}\mathbf{D}$ and $\mathbf{s} = \mathbf{d}(z)$.

The diameter to insert is the local diameter. The following analysis is performed for a collimated beam. To obtain expressions for a beam focused at $z = L$ one needs to make the substitution $D \to (1 - z/L)D$. If this is done, then one finds that the approximations made in this section are not valid. *The power series expansion in this section is only valid for a collimated beam.*

Using Kolmogorov turbulence one obtains for the collimated case

$$\mathcal{D}(\boldsymbol{\alpha} D) = 0.4146\, k_0^2 \int_0^\infty dz\, C_n^2(z) \int d\boldsymbol{\kappa}\, \kappa^{-11/3} \times \left[1 - \cos\left(\boldsymbol{\kappa} \cdot \boldsymbol{\alpha} D\right)\right] 2\left\{1 - \cos\left[\boldsymbol{\kappa} \cdot \mathbf{d}(z)\right]\right\}. \tag{7.33}$$

The integrand can be expanded and the trigonometric identity for the product of cosines used to get

$$I = 2 \int d\boldsymbol{\kappa}\, \kappa^{-11/3} \left(1 - \cos\left(\boldsymbol{\kappa} \cdot \boldsymbol{\alpha} D\right) - \cos\left[\boldsymbol{\kappa} \cdot \mathbf{d}(z)\right] + \cos\left\{\boldsymbol{\kappa} \cdot \left[\boldsymbol{\alpha} D + \mathbf{d}(z)\right]\right\}/2 + \cos\left\{\boldsymbol{\kappa} \cdot \left[\boldsymbol{\alpha} D - \mathbf{d}(z)\right]\right\}/2\right). \tag{7.34}$$

This expression is integrated over angle with eq. 3.5, and after rearranging terms, one obtains

$$I = 4\pi \int_0^\infty d\kappa\, \kappa^{-8/3} \left(\left\{1 - J_0\left(\kappa \alpha D\right)\right\} + \left\{1 - J_0\left[\kappa d(z)\right]\right\} - \left\{1 - J_0\left[\kappa \left|\boldsymbol{\alpha} D + \mathbf{d}(z)\right|\right]\right\}/2 - \left\{1 - J_0\left[\kappa \left|\boldsymbol{\alpha} D - \mathbf{d}(z)\right|\right]\right\}/2\right). \tag{7.35}$$

Using eq. 1.22 for each of the four terms, one obtains for the structure function

$$\mathcal{D}(\alpha D) = 2(2.91)\, k_0^2 \int_0^\infty dz\, C_n^2(z)$$
$$\times \left[(\alpha D)^{5/3} + d^{5/3}(z) - \tfrac{1}{2} \left| \boldsymbol{\alpha} D + \mathbf{d}(z) \right|^{5/3} - \tfrac{1}{2} \left| \boldsymbol{\alpha} D - \mathbf{d}(z) \right|^{5/3} \right]. \quad (7.36)$$

The sum of terms in brackets almost cancel, which causes difficulties if one tries to evaluate this integral numerically. The terms in the absolute value sign are equal to

$$\left| \boldsymbol{\alpha} D \pm \mathbf{d}(z) \right|^{5/3} = \left[(\alpha D)^2 \pm 2\alpha D\, d(z) \cos(\varphi) + d^2(z) \right]^{5/6}, \quad (7.37)$$

where φ is the angle between $\boldsymbol{\alpha}$ and $\mathbf{d}$.

This expression can be simplified and numerical difficulties eliminated with the use of Gegenbauer polynomials $C_p^\lambda(x)$. Their generating function is

$$\left(1 - 2ax + a^2\right)^{-\lambda} = \sum_{p=0}^{\infty} C_p^\lambda(x)\, a^p. \quad (7.38)$$

These functions are sometimes referred to as ultraspherical functions because they are a generalization of the Legendre polynomials $P_n(t)$ whose generating function is

$$\left(1 - 2ax + a^2\right)^{-1/2} = \sum_{p=0}^{\infty} P_p(x)\, a^p. \quad (7.39)$$

The Gegenbauer polynomials can be represented as

$$C_p^\lambda[\cos(\varphi)] = \sum_{m=0}^{p} \frac{\Gamma[\lambda + m]\ \Gamma[\lambda + p - m] \cos[(p - 2m)\varphi]}{m!\,(p-m)!\ \{\Gamma[\lambda]\}^2}. \quad (7.40)$$

A Gegenbauer polynomial that is useful in this analysis is

$$C_2^{-5/6}[\cos(\varphi)] = \tfrac{5}{6}\left[1 - \tfrac{1}{3}\cos^2(\varphi)\right]. \quad (7.41)$$

For $\alpha D > d(z)$ the terms in the structure function can be expanded in Gegenbauer polynomials. The zeroth and all odd order terms cancel. When the summation index is changed by the substitution $m \to 2m$, the result is

$$\mathcal{D}(\alpha D) = 2(2.91)\, k_0^2 \int_0^\infty dz\, C_n^2(z)$$
$$\times \left\{ d^{5/3}(z) - (\alpha D)^{5/3} \sum_{p=1}^{\infty} C_{2p}^{-5/6}[\cos(\varphi)] \left[\frac{d(z)}{\alpha D} \right]^{2p} \right\}. \quad (7.42)$$

It is this canceling of the first two terms of the power series that would cause numerical difficulties if the original integral were evaluated numerically. Define

$$d_m \equiv 2.91\ k_0^2 \int_0^\infty dz\ C_n^2(z)\, d^m(z),\ \text{and} \tag{7.43}$$

$$\sigma_\phi^2 = d_{5/3}. \tag{7.44}$$

Unlike the calculation for the Strehl ratio for uncorrected turbulence and for corrected turbulence with tilt jitter, an exact analytical solution cannot be found for anisoplanatism. Fortunately for adaptive-optics systems, the Strehl ratio should be fairly high by design, which requires the structure function to be small. This assumption allows one to retain only the first term of the Gegenbauer expansion to give

$$\mathcal{D}(\alpha D) \approx 2\sigma_\phi^2 - 2x, \tag{7.45}$$

where

$$x = d_2 \left[1 - \tfrac{1}{3}\cos^2(\varphi)\right] \tfrac{5}{6}(\alpha D)^{-1/3}. \tag{7.46}$$

I justify this single-term approximation below by showing that its value is close to the exact result. The assumption that $\alpha D > d(z)$ is not true close to the center of the aperture, but it is typically true over most of the aperture. The error in the center is ameliorated by the α factor in the integral. There will be an error, which increases with each term of the series, caused by the integration of this approximate expression over the entire aperture. In fact, because of this assumption, if the exponential is expanded in a power series, only the integral of the first six terms converges. An expansion in Gegenbauer polynomials that applies close to the aperture center can be performed, and different expansions can be used for different parts of the aperture. These integrals cannot be evaluated in simple form, which is why it is not done here. The Strehl ratio with the six-term approximation is

$$SR \approx \frac{\exp\left(-\sigma_\varphi^2\right)}{2\pi} \int d\boldsymbol{\alpha}\, K(\alpha) \left(1 + x + \frac{x^2}{2} + \frac{x^3}{6} + \frac{x^4}{24} + \frac{x^5}{120}\right). \tag{7.47}$$

If just the first term in the last parentheses is retained, the result is equivalent to the extended Maréchal approximation. It is shown below that the six-term approximation is best for aperture sizes that are normally encountered. The integrals over angle and aperture coordinate are performed analytically. The angle integral for the n^{th} term, after the use of the binomial theorem, is proportional to

$$\Phi(n) = \frac{1}{2\pi} \int_0^{2\pi} d\varphi \left[1 - \tfrac{1}{3}\cos^2(\varphi)\right]^n = \frac{1}{2\pi} \sum_{m=0}^{n} \binom{n}{n-m} 3^{-m} \int_0^{2\pi} d\varphi\, \cos^{2m}(\varphi), \tag{7.48}$$

where $$\binom{n}{n-m} = \frac{n!}{(n-m)!\,m!}. \tag{7.49}$$

Equation 4.641 #4 in *Gradshteyn* and *Ryzhik* (1980) is

$$\int_0^{\pi/2} d\varphi \, \cos^{2m}(\varphi) = \frac{\pi(2m-1)!!}{2(2m)!!}, \quad \text{where} \tag{7.50}$$

$(2m-1)!! = (2m-1)(2m-3)\ldots(3)(1)$, and $(2m)!! = (2m)(2m-2)\ldots(4)(2)$. With these relations, the angle integral is equal to

$$\Phi(n) = 1 - \sum_{m=1}^{n} \binom{n}{n-m} 3^{-m} \frac{(2m-1)!!}{(2m)!!}. \tag{7.51}$$

The needed values are $\Phi(0) = 1$, $\Phi(1) = 0.8333$, $\Phi(2) = 0.7083$, $\Phi(3) = 0.6134$, $\Phi(4) = 0.5404$, and $\Phi(5) = 0.4836$. The aperture integration for the n^{th} term is proportional to

$$Y(n) = \int_0^1 d\alpha \, \alpha^{1-n/3} K(\alpha). \tag{7.52}$$

From eq. 1.64, the needed values are $Y(0) = 1$, $Y(1) = 1.402$, $Y(2) = 2.087$, $Y(3) = 3.396$, $Y(4) = 6.419$, and $Y(5) = 16.94$. If these values are used, then the approximation to the Strehl ratio is

$$\begin{aligned} SR \approx{}& \exp\left(-\sigma_\phi^2\right) \\ &\times\left(1 + 0.9736E + 0.5133E^2 + 0.2009E^3 + 0.06970E^4 + 0.02744E^5\right), \\ & E < 0.5 \end{aligned} \tag{7.53}$$

where $E = d_2/D^{1/3}$.

As mentioned above, the Gegenbauer polynomial expansion is not valid near the center of the aperture. There is an error made in the use of this approximation for the central part of the aperture that increases with each term in the approximation. One has to determine whether this error is less or greater than the increased accuracy achieved over the remainder of the aperture by the inclusion of additional series terms. To resolve these uncertainties, I compared the Strehl ratio using various numbers of terms with the exact calculations.

I calculated the Strehl ratio numerically for the case in which the displacement does not vary with propagation distance. In Fig. 7.7 are plotted the exact Strehl ratio versus displacement for the Hufnagel-Valley 21 model of turbulence, and the Strehl ratio from eq. 7.53 for $D/r_0 = 1$ with only the unity term in brackets (Maréchal approximation), and with different numbers of terms in the brackets. This case of low turbulence is a region in which the approximation fares most poorly. The curves are plotted past their region of applicability to show how they begin to deviate from the correct values. The approximation that includes three or more terms is good out to a displacement that is one-third of the diameter, and the extended Maréchal approximation is always worse than that obtained with additional terms. The three-, four-, five-, and six-term approximations are the best.

In Fig. 7.8 and Fig. 7.9 are plotted the comparisons of the exact Strehl ratio for $D/r_0 = 5$ and 10 with the extended Maréchal approximation and the approximation derived here. The six-term approximation is the best, and it gives

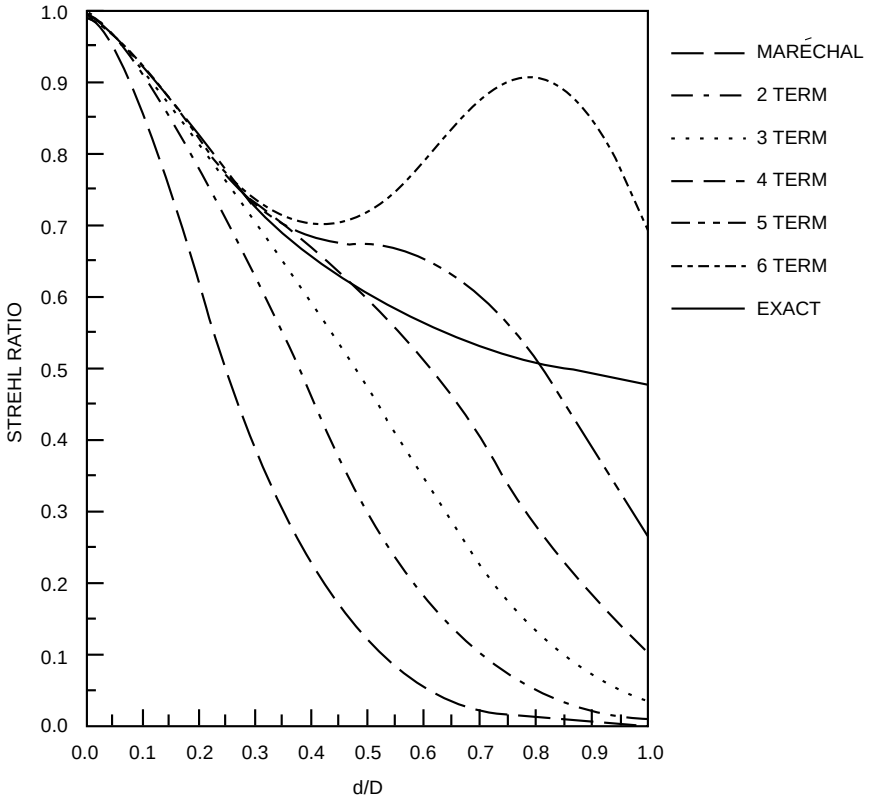

Figure 7.7. Comparison of the Maréchal and two- to six-term approximations with the exact value of Strehl ratio, for an anisoplanatic displacement, for D/r_0 equal to 1.

accurate Strehl ratio values down to values of 0.2. The six-term approximation is always best when $D/r_0 > 5$. The extended Maréchal approximation is poor. The six-term approximation gives results accurate to 1% over the first half of the range of plotted values of d/D for $D/r_0 = 5$ and 10. The error approaches 10% at the maximum values of d/D that are plotted. As the ratio of coherence diameter to aperture diameter gets smaller, the approximation improves. The close agreement between the exact results and those obtained with this approximation shows that the use of the one-term expansion in Gegenbauer polynomials was justified.

I now apply this approximate expression to calculate the Strehl ratio for various types of specific anisoplanatic effects.

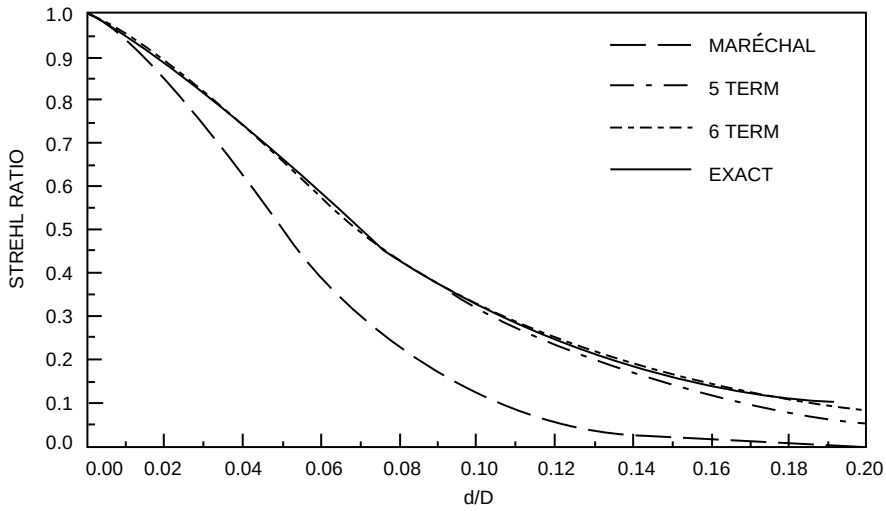

Figure 7.8. Comparison of Maréchal and five- and six-term approximations with the exact value of the Strehl ratio, with an anisoplanatic displacement that is constant along the propagation path, for D/r_0 equal to 5.

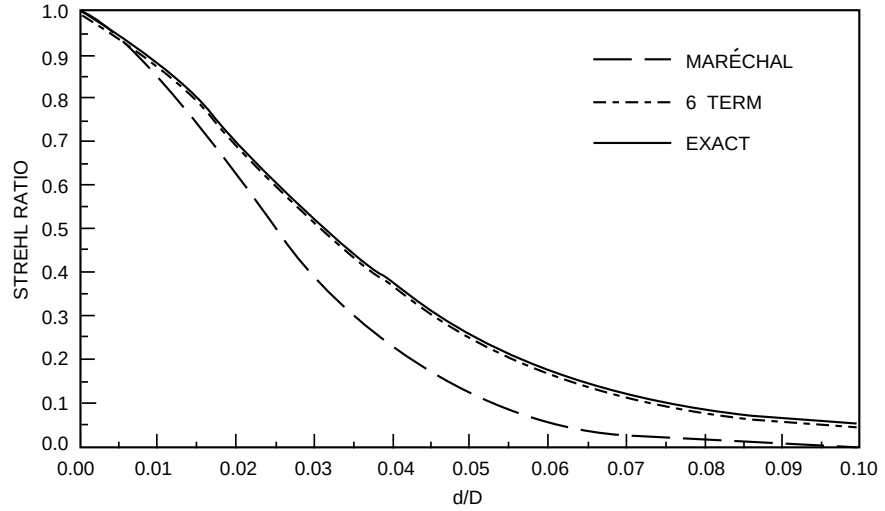

Figure 7.9. Comparison of Maréchal and six-term approximations with the exact value of the Strehl ratio, with an anisoplanatic displacement, for D/r_0 equal to 10.

7.4 Strehl Ratio for Various Anisoplanatic Effects

The Strehl ratio for various types of anisoplanatic effects is found with the expression given in eq. 7.53, and the three terms

$$E = d_2/D^{1/3}, \tag{7.54}$$

$$\sigma_\phi^2 = d_{5/3}, \text{ and} \tag{7.55}$$

$$d_m \equiv 2.91\, k_0^2 \int_0^\infty dz\, C_n^2(z)\, d^m(z). \tag{7.56}$$

7.4.1 Displacement anisoplanatism

In this simplest case of displacement anisoplanatism, which was treated in the Sec. 7.3, the displacement is constant along the propagation direction. Terms needed to find the Strehl ratio are $d(z) = d$, $d_2 = 2.91\, k_0^2\, \mu_0\, d^2$, $E = 6.88\, (d/D)^2\, (D/r_0)^{5/3}$, and $\sigma_\phi^2 = 2.91\, k_0^2\, \mu_0\, d^{5/3} = 6.88\, (d/r_0)^{5/3}$, where the turbulence moments are defined in eq. 4.2, and the coherence diameter is $r_0 = (0.423\, k_0^2\, \mu_0)^{5/3}$. The Strehl ratios are plotted in Fig. 7.8 and Fig. 7.9.

7.4.2 Angular anisoplanatism

When the propagation beam is offset by a constant angle from the direction along which turbulence is measured, the effect is called angular anisoplanatism (*Fried* 1982). It arises naturally when one is tracking a satellite target and directing a laser beam at it. Because of the finite speed of light, the laser beam has to lead the tracking direction; this results in an angular difference between the direction along which the target is tracked and the one along which the laser beam is directed. This error can be eliminated if the target has a reflector for the beacon that extends a suitable distance in the point-ahead direction. For the case of an angular error θ, one obtains

$$d(z) = \theta\, z, \tag{7.57}$$

$$d_2 = 2.91\, k_0^2\, \mu_2^*\, \theta^2, \tag{7.58}$$

$$E = 6.88\, \frac{\mu_2^*}{\mu_0} \left(\frac{\theta}{D}\right)^2 \left(\frac{D}{r_0}\right)^{5/3} = 0.68 \frac{\mu_2^*\, \mu_0^{1/5}}{\mu_{5/3}^{6/5}} \left(\frac{D}{r_0}\right)^{-1/3} \left(\frac{\theta}{\theta_0}\right)^2, \text{ and} \tag{7.59}$$

$$\sigma_\phi^2 = 2.91\, k_0^2\, \theta^{5/3} \int_0^L dz\, C_n^2(z)\, z^{5/3} = (\theta/\theta_o)^{5/3}, \tag{7.60}$$

where the relation in eq. 7.60 defines the isoplanatic angle, which is defined by $\theta_o = \left(2.91\, k_0^2\, \mu_{5/3}\right)^{-3/5}$. The turbulence moment μ_2^* is equal to μ_2 for a collimated beam and $\int_0^L dz\, C_n^2(z)\, z^2 (1 - z/L)^{-1/3}$ for a wave focused at $z = L$.

The only dependence on the particular turbulence distribution in the expression for Strehl ratio is the term $0.68\mu_2\ \mu_0^{1/5}/\mu_{5/3}^{6/5}$. This varies little with large changes in turbulence moments caused by different turbulence distributions. Its value is 1.13, 0.99, 0.88, and 0.82 for the HV-21, HV-35, HV-54, and HV-72 turbulence models respectively. Therefore, the Strehl ratio depends mainly on the ratios r_0/D and θ/θ_0 and weakly on the particular turbulence distribution.

The Strehl ratio versus offset angle for various turbulence models is plotted in Fig. 7.10 for a collimated beam directed vertically and in Fig. 7.11 for a collimated beam directed at 30 degrees off zenith.

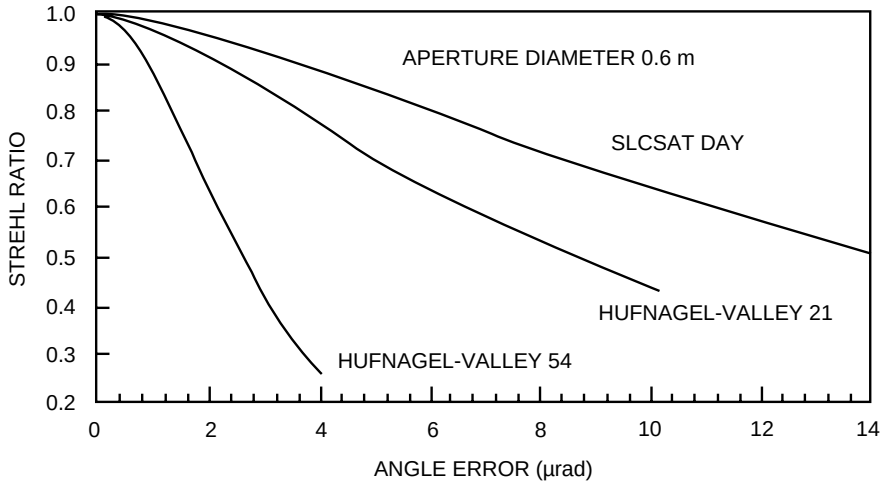

Figure 7.10. Strehl ratio of a collimated beam for angular anisoplanatic error at zenith, for various turbulence models, versus separation angle for a 0.6-m system. Upper-altitude turbulence has a strong effect on Strehl ratio.

7.4.3 Time-delay anisoplanatism

If there is a time delay τ between when turbulence is measured and a correction is applied to the deformable mirror, there is a degradation in performance as noted by *Tyler* (1984). This effect is not often thought of as an anisoplanatic effect; however, it can be treated as such. The Strehl ratio decays because the wind velocity $v(z)$ carries the turbules across the field of view. Using Taylor's frozen turbulence assumption discussed in Sec. 2.4, one obtains

$$d(z) = v(z)\tau, \tag{7.61}$$

$$d_2 = 2.91\, k_0^2 \int_0^L dz\, C_n^2(z)\, v^2(z)\, \tau^2 = (\tau/\tau_2)^2\,, \tag{7.62}$$

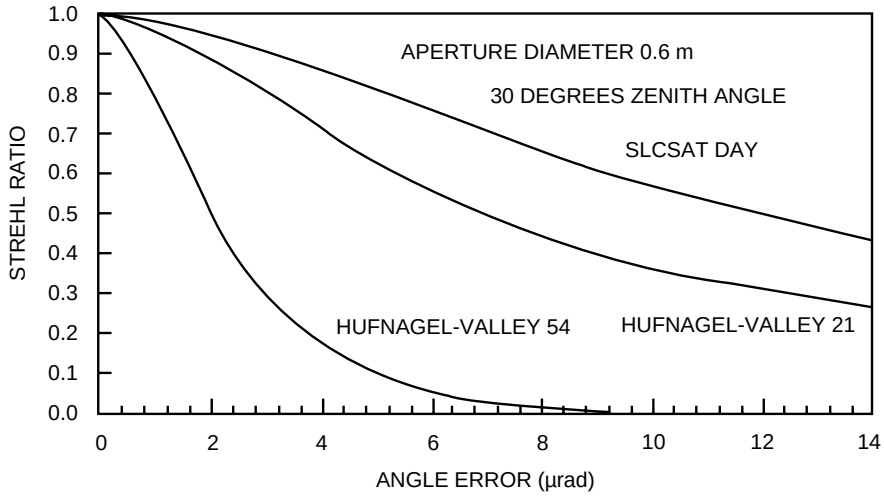

Figure 7.11. Strehl ratio of a collimated beam for angular anisoplanatism at 30 degrees from zenith for a 0.6-m system.

$$E = \frac{\tau^2}{\tau_2^2 D^{1/3}}, \quad \text{and} \tag{7.63}$$

$$\sigma_\phi^2 = 2.91\, k_0^2 \int_0^L dz\, C_n^2(z)\, v^{5/3}(z)\, \tau^{5/3} = \left(\tau/\tau_{5/3}\right)^{5/3}. \tag{7.64}$$

The temporal moment is defined as

$$\tau_m = \left[2.91\, k_0^2 \int_0^L dz\, C_n^2(z)\, v^m(z)\right]^{-3/5}. \tag{7.65}$$

The time $\tau_{5/3}$ is the characteristic time of the problem. It is related to the Greenwood frequency, defined in Sec. 4.8, by

$$f_G \tau_{5/3} = \left[\frac{0.0175}{n \sin\left(5\pi/6n\right)}\right]^{3/5}, \tag{7.66}$$

where n is the order of the filter in the servo system. For a single-pole filter $f_G\, \tau_{5/3} = 0.134$ as noted by *Fried* (1990).

The Strehl ratio is plotted in Fig. 7.12 for various turbulence models at zenith for a Bufton wind model with a ground speed of 5 m/s, and it is plotted at 30 degrees off zenith in Fig. 7.13. The Bufton wind model gives the wind versus altitude as

$$v(h) = v_g + 30\, \exp\left[-\left(\frac{h - 9400}{4800}\right)^2\right], \tag{7.67}$$

where v_g is the ground speed.

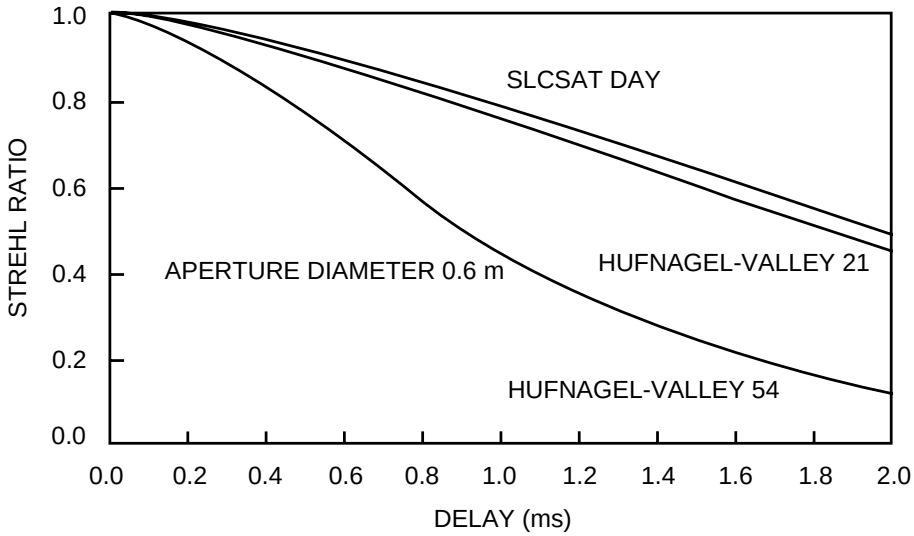

Figure 7.12. Strehl ratio versus time delay at zenith for 0.6-m system.

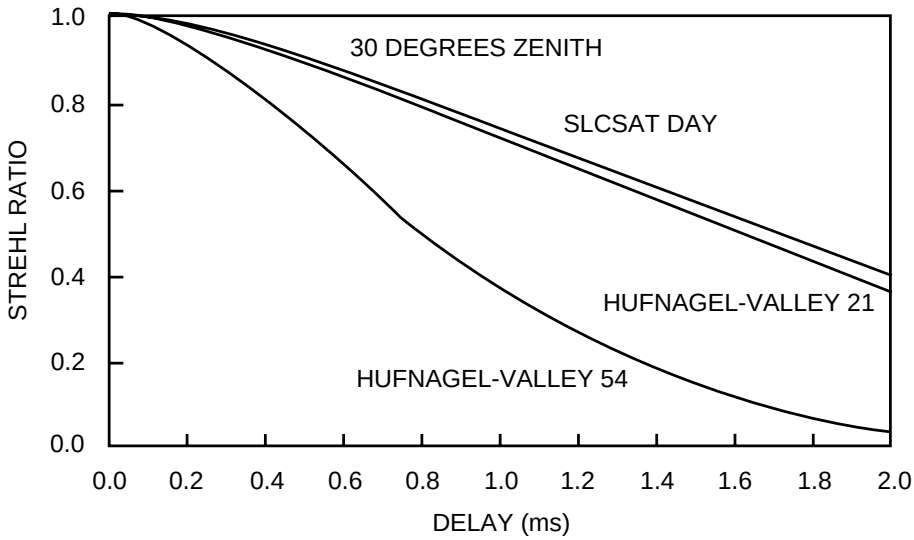

Figure 7.13. Strehl ratio versus time delay for 0.6-m system at 30 degrees zenith angle.

7.4.4 Chromatic anisoplanatism

If the beacon beam that senses the turbulence has a wavelength different from that of the laser beam that is sent out, then the two beams will follow different paths through the atmosphere because of the atmosphere's dispersive properties. The analysis given here parallels that given by *Belsher* and *Fried* (1981). Geomet-

ric optics is used to obtain the path displacement for chromatic anisoplanatism. If $n(h)$ is the refractive index seen by the first wave and $n(h) + \Delta n(h)$ is that seen by the second and if $\xi(h)$ is the zenith angle of the first and $\xi(h) + \Delta\xi(h)$ is that of the second, Snell's law, which states that $n \sin(\xi)$ is a constant, gives

$$\Delta\xi(h) = -\Delta n(h) \tan[\xi(h)]. \tag{7.68}$$

This can be integrated along the path to yield

$$\mathbf{d}_c(z) = \int_0^z dz\, \Delta\xi(h) = -\frac{\boldsymbol{\xi} \sin(\xi)\, \Delta n_0}{\xi \cos^2(\xi)} \int_0^z dz'\, \alpha(z'), \tag{7.69}$$

where Δn_0 is the difference in refractive index between the two colors at wavelengths λ_1 and λ_2 at the beginning of the path, and $\alpha(z)$ is the air density normalized to the value at sea level. The change of refractive index with wavelength has been given by *Allen* (1963) as

$$\Delta n_0 = \left(\lambda_1^2 - \lambda_2^2\right) \left[\frac{29498.1}{(146\lambda_2^2 - 1)(146\lambda_1^2 - 1)} + \frac{255.4}{(41\lambda_2^2 - 1)(41\lambda_1^2 - 1)}\right] 10^{-6}, \tag{7.70}$$

when the wavelengths are given in μm. The atmospheric density versus altitude is given in *Cole* (1965). The ratio of the atmospheric density at any altitude normalized to that at sea level was approximated by Belsher and Fried as

$$\alpha(h) = \exp\left(-1.11 \times 10^{-4} h\right), \quad h < 10\,\text{km, and}$$

$$\alpha(h) = 1.6 \exp\left(-1.57 \times 10^{-4} h\right), \quad h > 10\,\text{km}. \tag{7.71}$$

A plot of the absolute value difference in the refractive index between waves at 0.5 μm and other wavelengths is shown in Fig. 7.14. The normalized air density versus height is plotted in Fig. 7.15.

To calculate the Strehl ratio, the displacement as a function of range is found with eq. 7.68. At the target range R, the displacement is $d_c(L)$, and to hit the target squarely one must change the launching angle by $d_c(L)/L$. Thus the beam displacement along the path is

$$\mathbf{d}_c(z) = -\frac{\boldsymbol{\xi} \sin(\xi)\ \Delta n_0}{\xi\ \cos^2(\xi)} \left[\int_0^z dz'\, \alpha(z') - \frac{z}{L} \int_0^L dz'\, \alpha(z')\right]. \tag{7.72}$$

Define the integral of air density as

$$I(z) = \int_0^z dz'\, \alpha(z'). \tag{7.73}$$

This is evaluated as

$$I(z) = 9010 \left[1 - \exp\left(-1.11 \times 10^{-4} z\right)\right], \quad z < 10\,\text{km, and}$$

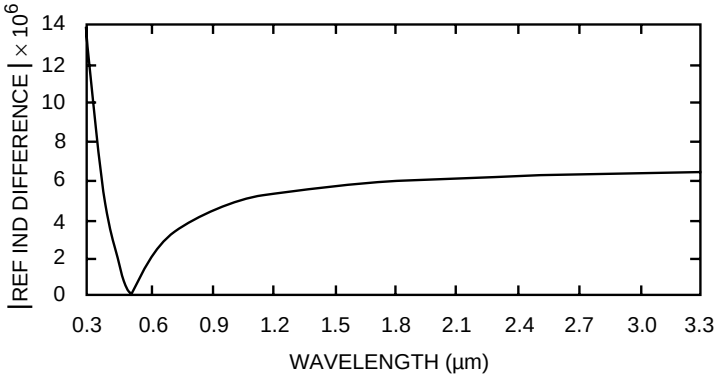

Figure 7.14. A million times the difference in refractive index between 0.5 μm and another wavelength.

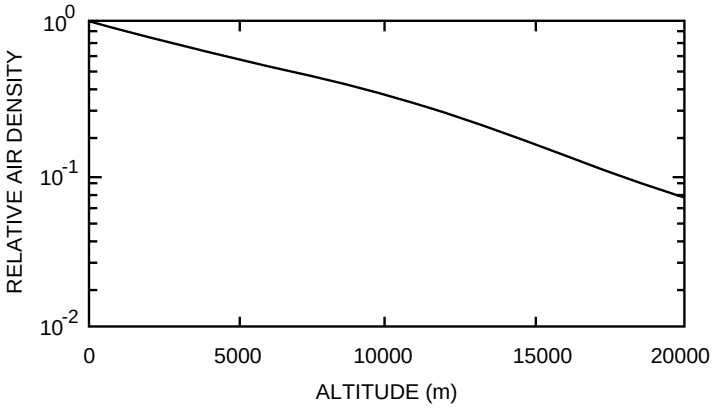

Figure 7.15. Normalized air density versus altitude.

$$I(z) = 8161 - 10\,190\,\exp\left(-1.57 \times 10^{-4} z\right), \quad z > 10\,\text{km}. \tag{7.74}$$

The moments of this displacement are

$$d_m = \left[\frac{\sin(\xi)\,\Delta n_0}{\cos^2(\xi)}\right]^m T_m, \tag{7.75}$$

where

$$T_m = 2.91\,k_0^2 \sec(\xi) \int_0^H dh\, C_n^2(h) \left[I(h) - \frac{h \sec(\xi)}{L} I(L)\right]^m. \tag{7.76}$$

H is the altitude of the target. The last term in brackets goes to zero as the range becomes infinite. A Strehl ratio comparison of a target at 300 km and one at infinity is plotted in Fig. 7.16. There is very little difference in the two results. For infinite range, the above equation reduces to

$$T_m = 2.91\, k_0^2 \sec(\xi) \int_0^H dh\, C_n^2(h)\, I^m(h). \tag{7.77}$$

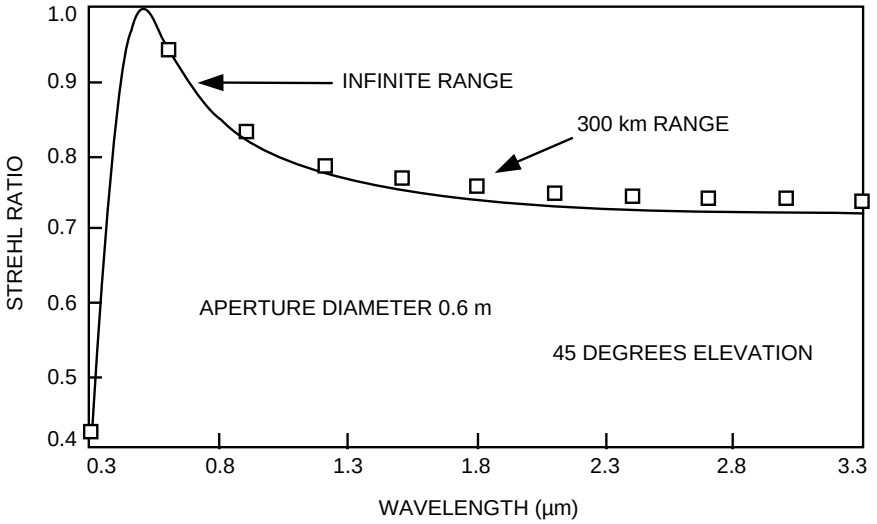

Figure 7.16. Comparison of the Strehl ratio at infinite and 300 km range versus beacon wavelength. The two results are close in value. This allows a simpler calculation for finite range problems.

The result for finite range entails a numerical calculation for each range. The infinite-range results can be calculated once for each turbulence model and used for different zenith angles. Table 7.1 contains values of T_2 and $T_{5/3}$ for various turbulence models.

Table 7.1. Values of T_2 and $T_{5/3}$ for various turbulence models. The units of T_2 are $m^{1/3}$, and $T_{5/3}$ is dimensionless.

Model	T_2	$T_{5/3}$
SLCDAY	2.706×10^{-6}	2.004×10^{-7}
SLCNIGHT	2.258×10^{-6}	1.512×10^{-7}
HV-21	6.160×10^{-6}	3.596×10^{-7}
HV-54	3.399×10^{-5}	1.867×10^{-6}
HV-72	5.949×10^{-5}	3.247×10^{-6}

The relevant quantities to calculate Strehl ratio are

$$E = \left[\frac{\sin(\xi)\, \Delta n_0}{\cos^2(\xi)}\right]^2 \frac{T_2}{D^{1/3}}, \text{ and} \tag{7.78}$$

$$\sigma_\phi^2 = \left[\frac{\sin(\xi)\,\Delta n_0}{\cos^2(\xi)}\right]^{5/3} T_{5/3}. \tag{7.79}$$

As a specific example, Fig. 7.17 contains plots of Strehl ratio for the SLCSAT day model for various elevation angles for an infinite-range target, when one beam is at 0.5-μm wavelength.

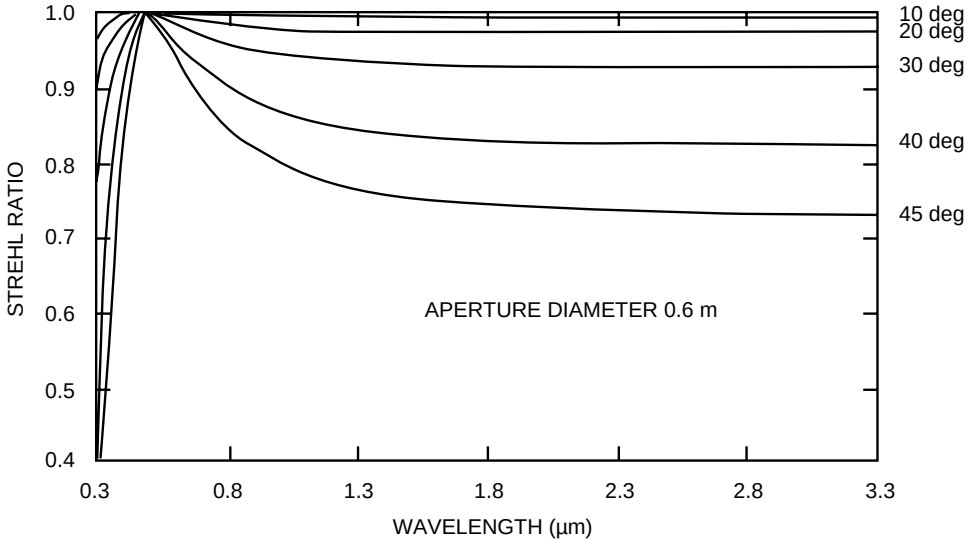

Figure 7.17. Strehl ratio for SLCSAT day turbulence with the scoring beam at 0.5 μm for a 0.6-m system and zenith angles between 10 and 45 degrees. Notice that above 45 degrees elevation angle the Strehl ratio exceeds 0.7 for the first beam at 0.5 μm and the second at any longer wavelength.

7.4.5 Combined displacement anisoplanatism

If there are several anisoplanatic effects present, with each not decreasing the Strehl ratio much, it is a common practice to multiply the Strehl ratios for the individual effects to get a combined Strehl ratio. The validity of this assumption is now examined. The total displacement that is due to a translation, an angular offset, a time delay, and a chromatic offset is

$$\mathbf{d}_t(z) = \mathbf{d} + \boldsymbol{\theta}\, z + \mathbf{v}(z)\tau + \mathbf{d}_c(z), \tag{7.80}$$

where chromatic displacement is given in eq. 7.73. The two terms necessary to calculate the Strehl ratio are $E = d_2/D^{1/3}$, and $\sigma_\phi^2 = d_{5/3}$, where

$$d_m = 2.91\, k_0^2 \int_0^\infty dz\, C_n^2(z)\, d_t^m(z).$$

Let us examine the case in which the effects of displacement, angular offset, and temporal delay are comparable. Chromatic anisoplanatism is assumed to be zero. To obtain comparable effects from the remaining three types of anisoplanatism, the angular offset in microradians is 850 times the displacement in meters. The time delay in milliseconds is 130 times the displacement in meters for the Bufton wind model with a ground speed of 5 m/sec.

In Fig. 7.18 the Strehl ratios are plotted for these effects present individually and combined for the SLCSAT Day turbulence model with a 0.6-m diameter system. It was assumed that the three vector displacements either were all in the same direction or were separated by 120 degrees. Also plotted is the product of the Strehl ratios from the individual effects. Note that the Strehl ratio for all the effects combined can be less than or greater than the Strehl ratio obtained by the common practice of multiplying individual Strehl ratios. The relative direction of the displacements is crucial. It is possible to get some cancellation if the displacements cancel. *Tyler* et al. (1982) took advantage of the vector nature of the displacement almost to eliminate the effect of chromatic anisoplanatism on an adaptive-optics system by choosing an optimal offset angle of a beacon from the propagation direction.

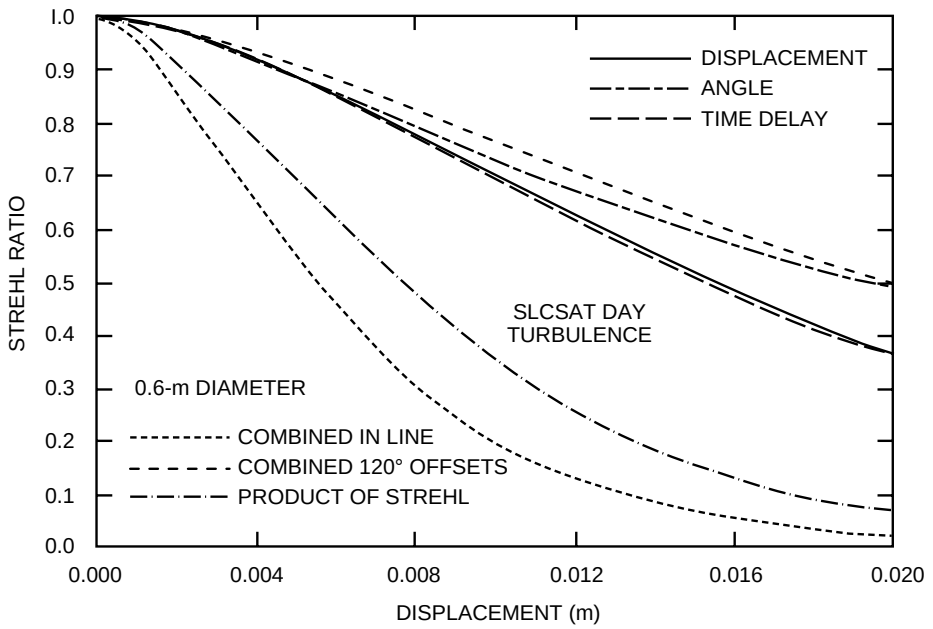

Figure 7.18. Strehl ratios for displacement, angle, and time delay anisoplanatism presented separately and combined for the SLCSAT-Day turbulence model. The displacement is constant along the propagation path. The angle offset in microradians is 850 times the displacement in meters. The time delay in milliseconds is 130 times the displacement in meters. The combined effects are for all displacements in line and at 120 degrees to each other.

7.5 Strehl Ratio Using Numerical Integration

For most of the examples considered in this book the variances of phase- and amplitude-related quantities are calculated. For some problems that is not adequate. Often one wants to know the intensity on target, for which one must calculate the Strehl ratio.

For small variances one can use the Maréchal approximation to calculate the Strehl ratio. That approximation is not valid for large variances or when the correlation function has significant range. Uncorrected turbulence is such a case where the approximation is completely inadequate. Tilt makes up 87% of the phase variance with piston removed, yet for large values of D/r_0, removing the tilt hardly affects the Strehl ratio. It was evident in the approximation in (7.17) that $SR \sim (r_0/D)^2 - 0.6159(r_0/D)^3$ rather than an exponential dependence.

Although the analytical expressions for the Strehl ratio for some problems was obtained, calculating the Strehl ratio for most problem must be done numerically, which accounts for some reluctance to find the Strehl ratio. When the Strehl ratio is calculated, usually the simpler formula that assumes that the structure function is not a function of position is used. In this case

$$SR = \frac{1}{2\pi} \int d\boldsymbol{\alpha}\, K(\alpha) \exp\left[-\frac{\mathcal{D}\left(\boldsymbol{\alpha} D\right)}{2}\right], \tag{7.81}$$

where $\boldsymbol{\alpha} D = \boldsymbol{\rho}' - \boldsymbol{\rho}$.

This is a two-fold integration. Sometimes the structure function contains an integration over the axial coordinate z, requiring a three-fold integration. If evaluating the structure function requires a calculation in $\boldsymbol{\kappa}$- or $\mathbf{x}$-space, then a four- or five-fold integration is required.

For many problems of interest, such as calculating the Strehl ratio with tilt removed, the structure function depends on position, and eq. 7.81 is not valid. One must use

$$SR = \left(\frac{4}{\pi D}\right)^2 \int d\boldsymbol{\rho}' \int d\boldsymbol{\rho}\, W\left(\boldsymbol{\rho}'\right) W\left(\boldsymbol{\rho}\right) \exp\left\{-\mathcal{D}\left([\boldsymbol{\rho}' - \boldsymbol{\rho}], \boldsymbol{\rho}'\right)\ /2\right\}. \tag{7.82}$$

In this case, there are two additional integrals over the aperture, and one must perform either a four-, five-, six-, or seven-fold integration for the cases considered above. Because of the computer resources required to do this, in the past, people have made approximations to the structure function or used eq. 7.81 when eq. 7.82 was appropriate. These approximations were made with arguments that some terms could be neglected or the aperture average structure function could be used. These arguments are not backed up with quantitative results that the approximations were valid. Because the structure function appears in an exponential and one of its factors $(D/r_0)^{5/3}$ can be large, small errors in one factor could produce large errors in the calculation.

Here, the exact calculation is performed and compared to the approximate results. Examples are given for the Strehl ratio for uncorrected turbulence, for

a finite beacon with the corrected beam focused at the beacon center, and for a finite beacon with a collimated corrected beam. The Strehl ratio is given for tilt present and removed and compared to the Maréchal approximation.

The general formula for structure function in eq. 3.35 with a quantity, $A(\boldsymbol{\rho})$, subtracted from the phase-related quantity, $f(\boldsymbol{\rho})$, is

$$\begin{aligned}\mathcal{D}_{\phi}\left(\boldsymbol{\alpha}D,\boldsymbol{\rho}\right) &= 0.207378\,k_0^2\int_0^L dz\,C_n^2(z)\int_0^{2\pi}d\varphi\int_0^{\infty}d\kappa\,\kappa^{-8/3}\\ &\quad\times\left[f(\boldsymbol{\rho})-A(\boldsymbol{\rho})-f(\boldsymbol{\rho}+\boldsymbol{\alpha}D)+A(\boldsymbol{\rho}+\boldsymbol{\alpha}D)\right]^2\\ &= \mathcal{D}_1(\boldsymbol{\alpha}D,\boldsymbol{\rho})+\mathcal{D}_2(\boldsymbol{\alpha}D,\boldsymbol{\rho})+\mathcal{D}_3(\boldsymbol{\alpha}D,\boldsymbol{\rho}).\end{aligned}\tag{7.83}$$

where the three structure functions result from the respective terms in

$$\begin{aligned}&\left[f(\boldsymbol{\rho})-A(\boldsymbol{\rho})-f(\boldsymbol{\rho}+\boldsymbol{\alpha}D)+A(\boldsymbol{\rho}+\boldsymbol{\alpha}D)\right]^2\\ &=\left[f(\boldsymbol{\rho})-f(\boldsymbol{\rho}+\boldsymbol{\alpha}D)\right]^2-\left[A(\boldsymbol{\rho})-A(\boldsymbol{\rho}+\boldsymbol{\alpha}D)\right]^2\\ &+2\left[f(\boldsymbol{\rho})-A(\boldsymbol{\rho})-\{f(\boldsymbol{\rho}+\boldsymbol{\alpha}D)-A(\boldsymbol{\rho}+\boldsymbol{\alpha}D)\}\right]\left[A(\boldsymbol{\rho}+\boldsymbol{\alpha}D)-A(\boldsymbol{\rho})\right].\end{aligned}\tag{7.84}$$

The meaning of the above equations is clear in real space. In $\boldsymbol{\kappa}$-space some of the quantities are complex. In that case the last term, which is the product of two different quantities, is calculated in the following manner

$$\frac{1}{2}[AB^*+A^*B]=\mathrm{Re}\,[AB^*].\tag{7.85}$$

Each of the three components of the structure function will be calculated separately. The first component is the structure function of the phase-related quantities. The second is the structure function of the quantity to be subtracted, and the third contains a combination of both terms.

Unlike the first two terms, the third term cannot be evaluated analytically for most problems. For instance, for turbulence with tilt removed one finds that the total structure function is equal to

$$\begin{aligned}\mathcal{D}(\boldsymbol{\alpha}D,\boldsymbol{\rho}) &= \mathcal{D}_1(\boldsymbol{\alpha}D,\boldsymbol{\rho})+\mathcal{D}_2(\boldsymbol{\alpha}D,\boldsymbol{\rho})+\mathcal{D}_3(\boldsymbol{\alpha}D,\boldsymbol{\rho})\\ &= 6.8839\left(\frac{D}{r_0}\right)^{5/3}\left(\alpha^{5/3}-1.04332\alpha^2+\alpha C\right),\end{aligned}\tag{7.86}$$

where C is a double integral that is derived in the next section.

Because of the singularity at $\kappa=0$ in some of the integrals, a Taylor series expansion is performed in κ, and the integral is evaluated analytically for small values of κ.

7.5.1 Strehl ratio for uncorrected turbulence with tilt present and removed

First, calculate the Strehl ratio for uncorrected turbulence with tilt present and removed. The structure function with tilt present is given in eq. 7.5 as

$$\mathcal{D}(\boldsymbol{\alpha} D) = \mathcal{D}_1(\boldsymbol{\alpha} D) = 6.8839\ (\alpha D/r_0)^{5/3}\,, \tag{7.87}$$

where $r_0 = (0.42336\, k_0^2\, \mu_0)^{-3/5}$. The coefficient in the coherence diameter is more accurate than the standard value of 0.423 because for large values of D/r_0 more accurate coefficients are required in the calculations. Errors in the fourth decimal place produce errors of several per cent in the Strehl ratio when $D/r_0 = 10$. As explained above, the integral expression for this term will be used.

Fried (1966) calculated the Strehl ratio for tilt present and tilt removed. He used eq. 7.81 to find the Strehl ratio with tilt present. He then made the assumption that the third component of the structure function, which is the correlation of the difference of the phase with tilt removed at two points and the tilt, is zero. This is true for the average over the aperture, but is not true without the aperture average, since tilt and the other modes are not statistically independent. The structure function he used in his calculations was

$$\mathcal{D}(\boldsymbol{\alpha} D) = 6.8839\ (\alpha D/r_0)^{5/3}\,(1 - \alpha^{1/3}). \tag{7.88}$$

With this, he found that the tilt-removed Strehl ratio was significantly improved for small values of D/r_0 with a maximum improvement of a factor of 4.3 when $D/r_0 = 3.8$. Fried actually gives the factor multiplying the $\alpha^{1/3}$ term as 1.026 (It actually is 1.04332) but he approximates it by 1. The reason he did that is because with the coefficient 1.026 the structure function is negative as α approaches one, which is physically impossible for a squared real quantity. Using the correct value of 1.04332 in the structure function, one finds that the Strehl ratio actually increases for increasing values of D/r_0 for $D/r_0 > 7$. This obviously incorrect result calls into question the accuracy of the results for lower values of D/r_0.

This problem was subsequently addressed by *Heidbreder* (1967), *Yura* (1973), *Tavis* and *Yura* (1976), and *Valley* (1979). *Valley* found that outer scale can have a significant effect of the Strehl ratio. None of these analysis treat the full problem because computer resources were not adequate at the time. Faster computers make it possible to calculate the structure function for this case.

Now calculate the three components of the structure function. To find the first component, first evaluate

$$\begin{aligned}[f(\boldsymbol{\rho}) - f(\boldsymbol{\rho} + \boldsymbol{\alpha} D)]^2 &= |\exp(\boldsymbol{\kappa}\cdot\boldsymbol{\rho}) - \exp[i\boldsymbol{\kappa}\cdot(\boldsymbol{\rho} + \boldsymbol{\alpha} D)|^2 \\ &= 2\,[1 - \cos(\boldsymbol{\kappa}\cdot\boldsymbol{\alpha} D)]\,. \end{aligned} \tag{7.89}$$

Using this result, the first term of the structure function is

$$\begin{aligned}\mathcal{D}_1\left(\boldsymbol{\alpha} D, \boldsymbol{\rho}\right) &= 0.207379\, k_0^2 \int_0^L dz\, C_n^2(z) \int_0^{2\pi} d\varphi \int_0^\infty d\kappa\, \kappa^{-8/3} 2\left[1 - \cos(\boldsymbol{\kappa}\cdot\boldsymbol{\alpha} D)\right] \\ &= 1.95935 \left(\frac{\alpha D}{r_0}\right)^{5/3} \int_0^\pi d\varphi \int_0^\infty dx\, x^{-8/3} \left\{1 - \cos[x\cos(\theta_d - \varphi)]\right\} \\ &= 6.8839 \left(\frac{\alpha D}{r_0}\right)^{5/3}, \end{aligned} \tag{7.90}$$

where use was made of the fact that if π is added to the phase, then it does not change the value of the integrand. In addition, use the definition $r_0^{-5/3} = 0.42336\, k_0^2\, \mu_0$, and let $x = \kappa\alpha D$. The value of the dot products is obtained from the definition of the angles, $\boldsymbol{\rho}\cdot\boldsymbol{\kappa}/\kappa = \rho\cos(\theta_\rho - \varphi)$, $\boldsymbol{\rho}'\cdot\boldsymbol{\kappa}/\kappa = \boldsymbol{\rho}'\cos(\theta_{\rho'} - \varphi)$, and $(\boldsymbol{\rho}' - \boldsymbol{\rho})\cdot\boldsymbol{\kappa}/\kappa = |\boldsymbol{\rho}' - \boldsymbol{\rho}|\cos(\theta_d - \varphi)$, where θ_d is the angle between $\boldsymbol{\rho}' - \boldsymbol{\rho}$ and the x-axis given by

$$\theta_d = \arctan\left[\frac{\rho'\sin(\theta_{\rho'}) - \rho\sin(\theta_\rho)}{\rho'\cos(\theta_{\rho'}) - \rho\cos(\theta_\rho)}\right]. \tag{7.91}$$

In numerically computing θ_d one needs to use an arctangent function that has a 2π range. The magnitude of the vector is

$$|\boldsymbol{\alpha} D| = |\boldsymbol{\rho}' - \boldsymbol{\rho}| = \left\{\left[\rho'\sin(\theta_{\rho'}) - \rho\sin(\theta_\rho)\right]^2 + \left[\rho'\cos(\theta_{\rho'}) - \rho\cos(\theta_\rho)\right]^2\right\}^{1/2}. \tag{7.92}$$

The value of $\mathcal{D}_2(\boldsymbol{\alpha} D, \boldsymbol{\rho})$, which is the square of the tilt difference at the two points, is obtained by using eq. 3.27

$$G_{1,1}\left(\gamma\boldsymbol{\kappa}\right) Z_{1,1}\left(\rho, \theta\right) = i\frac{16 J_2(\gamma\kappa D/2)}{\gamma\kappa D/2}\frac{\rho}{D}\cos(\theta_\rho - \varphi) = i\frac{16 J_2(\gamma\kappa D/2)}{\gamma\kappa D/2}\frac{\boldsymbol{\rho}\cdot\boldsymbol{\kappa}}{D\kappa}. \tag{7.93}$$

For the case $\gamma = 1$, this leads to

$$\begin{aligned}\left[A(\boldsymbol{\rho}) - A(\boldsymbol{\rho} + \boldsymbol{\alpha} D)\right]^2 &= \left| i\frac{16 J_2(\kappa D/2)}{\kappa D/2}\frac{\boldsymbol{\rho}\cdot\boldsymbol{\kappa}}{D\kappa} - i\frac{16 J_2(\kappa D/2)}{\kappa D/2}\frac{(\boldsymbol{\rho} + \boldsymbol{\alpha} D)\cdot\boldsymbol{\kappa}}{D\kappa}\right|^2 \\ &= \left[\frac{16 J_2(\kappa D/2)}{\kappa D/2}\frac{\boldsymbol{\alpha}\cdot\boldsymbol{\kappa}}{\kappa}\right]^2 = \left[\frac{16 J_2(\kappa D/2)}{\kappa D/2}\right]^2 \cos^2(\theta_d - \varphi), \end{aligned} \tag{7.94}$$

which inserted into the formula for the structure function gives

$$
\begin{aligned}
&\mathcal{D}_2\left(\boldsymbol{\alpha} D, \boldsymbol{\rho}\right) \\
&= -0.207378\, k_0^2 \int_0^L dz\, C_n^2(z) \int_0^{2\pi} d\varphi \left[\frac{\boldsymbol{\kappa}\cdot\boldsymbol{\alpha}}{|\kappa|}\right]^2 \int_0^{\infty} d\kappa\, \kappa^{-8/3} \left[16\alpha \frac{J_2(\kappa D/2)}{\kappa D/2}\right]^2 \\
&= -78.996\alpha^2 \left(\frac{D}{r_0}\right)^{5/3} \int_0^{\pi} d\varphi [\cos(\theta_d - \varphi)]^2 \int_0^{\infty} dx\, x^{-8/3} \left[\frac{J_2(x)}{x}\right]^2 \\
&= -7.182 \left(\frac{D}{r_0}\right)^{5/3} \alpha^2 = -6.8839 \left(\frac{\alpha D}{r_0}\right)^{5/3} 1.04334\alpha^{1/3},
\end{aligned} \tag{7.95}
$$

where $x = \kappa D/2$.

The third component is equal to

$$
\begin{aligned}
&\{f(\boldsymbol{\rho}) - A(\boldsymbol{\rho}) - [f(\boldsymbol{\rho} + \boldsymbol{\alpha} D) - A(\boldsymbol{\rho} + \boldsymbol{\alpha} D)]\}\, [A(\boldsymbol{\rho} + \boldsymbol{\alpha} D) - A(\boldsymbol{\rho})] \\
&= \mathrm{Re}\left\{\left[\exp(i\boldsymbol{\kappa}\cdot\boldsymbol{\rho}) - i16\frac{J_2(\kappa D/2)}{\kappa D/2}\frac{\boldsymbol{\rho}\cdot\boldsymbol{\kappa}}{D\kappa} - \exp(i\boldsymbol{\kappa}\cdot\boldsymbol{\rho}') + i16\frac{J_2(\kappa D/2)}{\kappa D/2}\frac{\boldsymbol{\rho}'\cdot\boldsymbol{\kappa}}{D\kappa}\right]\right. \\
&\qquad \left.\times \left[-i16\frac{J_2(\kappa D/2)}{\kappa D/2}\frac{(\boldsymbol{\rho}' - \boldsymbol{\rho})\cdot\boldsymbol{\kappa}}{D\kappa}\right]\right\}.
\end{aligned} \tag{7.96}
$$

After setting $\boldsymbol{\rho}' = \boldsymbol{\rho} + \boldsymbol{\alpha} D$ and inserting the values of the dot products, and $x = \kappa D/2$, the third component of the structure function is equal to

$$
\begin{aligned}
&\mathcal{D}_3\left(\boldsymbol{\alpha} D, \boldsymbol{\rho}\right) = 9.869 \left(\frac{D}{r_0}\right)^{5/3} \alpha \int_0^{\infty} dx\, x^{-11/3} J_2(x) \\
&\times \int_0^{\pi} d\varphi \cos(\theta_d - \varphi) \left\{\sin\left[\frac{2x}{D}\rho\cos(\theta_\rho - \varphi)\right] - 16\frac{\rho}{D}\cos(\theta_\rho - \varphi)\frac{J_2(x)}{x}\right. \\
&\left. - \sin\left[\frac{2x}{D}\rho'\cos(\theta_{\rho'} - \varphi)\right] + 16\frac{\rho'}{D}\cos(\theta_{\rho'} - \varphi)\frac{J_2(x)}{x}\right\}.
\end{aligned} \tag{7.97}
$$

If the four terms in brackets are expanded into Taylor series, then the linear terms cancel. The first non-zero term is the cubic term. The cubic terms from the first two terms and the last two terms almost cancel for small values of α. Because of this, the main contribution from this correlation term is from smaller wavelengths of turbulence and for larger values of α. The first term of the power series is

$$
\begin{aligned}
&x^{-11/3} J_2(x) \left\{\sin\left[\frac{2x}{D}\rho\cos(\theta_\rho - \varphi)\right] - 16\frac{\rho}{D}\cos(\theta_\rho - \varphi)\frac{J_2(x)}{x}\right. \\
&\left. - \sin\left[\frac{2x}{D}\rho'\cos(\theta_{\rho'} - \varphi)\right] + 16\frac{\rho'}{D}\cos(\theta_{\rho'} - \varphi)\frac{J_2(x)}{x}\right\} \\
&\approx x^{4/3}\left[\frac{\rho}{48D}\cos(\theta_\rho - \varphi) - \frac{1}{6}\left(\frac{\rho}{D}\right)^3 \cos^3(\theta_\rho - \varphi)\right. \\
&\left. - \frac{\rho'}{48D}\cos(\theta_{\rho'} - \varphi) + \frac{1}{6}\left(\frac{\rho'}{D}\right)^3 \cos^3(\theta_{\rho'} - \varphi)\right], \quad x << 1.
\end{aligned} \tag{7.98}
$$

This term is the one that Fried neglected. The remaining terms do not depend on ρ or ρ', enabling his use of the simpler expression in eq. 7.81 to calculate the Strehl ratio.

The total structure function is equal to

$$\begin{aligned}
&\mathcal{D}_{TR}(\boldsymbol{\alpha} D, \boldsymbol{\rho}) = \mathcal{D}_1(\boldsymbol{\alpha} D, \boldsymbol{\rho}) + \mathcal{D}_2(\boldsymbol{\alpha} D, \boldsymbol{\rho}) + \mathcal{D}_3(\boldsymbol{\alpha} D, \boldsymbol{\rho}) \\
&= \int_0^{\pi} d\varphi \int_0^{\infty} dx\, x^{-8/3} \Bigg[1.95935\alpha^{5/3} \{1 - \cos[x\cos(\theta_d - \varphi)]\} \\
&\quad -78.996\alpha^2 [\cos(\theta_d - \varphi)]^2 \left[\frac{J_2(x)}{x}\right]^2 \\
&\quad + 9.869\alpha \left(\cos(\theta_d - \varphi) \left\{ \sin\left[\frac{2x}{D}\rho\cos(\theta_\rho - \varphi)\right] - 16\frac{\rho}{D}\cos(\theta_\rho - \varphi)\frac{J_2(x)}{x} \right.\right. \\
&\quad \left.\left. - \sin\left[\frac{2x}{D}\rho'\cos(\theta_{\rho'} - \varphi)\right] + 16\frac{\rho'}{D}\cos(\theta_{\rho'} - \varphi)\frac{J_2(x)}{x} \right\} \right) \Bigg] . \qquad (7.99)
\end{aligned}$$

To find the exact Strehl ratio, the structure function in eq. 7.99 must be inserted into eq. 2.153. The resulting expression is

$$SR = \left(\frac{4}{\pi D}\right)^2 \int_0^{2\pi} d\theta_{\rho'} \int_0^{D/2} \rho' d\rho' \int_0^{2\pi} d\theta_\rho \int_0^{D/2} \rho d\rho \, \exp\left[-\mathcal{D}_{TR}\left(\alpha D, \boldsymbol{\rho}\right)/2\right] . \qquad (7.100)$$

This is a six-fold integration. If the problem were solved strictly in real space as suggested by *Heidbreder* (1967), then a six-fold integration is also required. Here, use the $\boldsymbol{\kappa}$-space formulation as a prelude to solve more complicated problems.

Stock and Herrmann performed the six-fold integration in real space and their results are identical to those reported here. In Fig. 7.19 is plotted the Strehl ratio on a linear scale of the uncorrected turbulence and three calculations of the Strehl ratio with tilt removed. The top most curve has the Fried approximation with the coefficient of the α^2 term equal to 1.04332. The structure function becomes negative as α approaches unity, which results in the Strehl ratio increasing at values of D/r_0 above 6. This approximation is good for $D/r_0 < 4$. The Fried approximation with the coefficient of the α^2 term equal to 1.0 gives values of the Strehl ratio that are lower than the exact result, which is also plotted. In Fig. 7.20 are the same plots on a log scale. Fig. 7.21 has the ratio of the tilt-removed Strehl ratio to that with tilt present. Notice that there is as much as a factor of 5.5 improvement.

A Strehl ratio approximation when tilt is removed valid for values of $D/r_0 < 10$ is

$$SR_{TR} = \left\{ 1 + \left[D/\left(r_0\, 4.65^{1-D/13.5r_0} \right) \right]^{5/3} \right\}^{-6/5} \qquad D/r_0 < 10. \qquad (7.101)$$

7.5.2 Strehl ratio for a finite beacon and focused corrected beam

Next, consider the case where there is a beacon at $z = L$ of diameter D_s and the outgoing beam is focused at the center of the beacon. This case applies

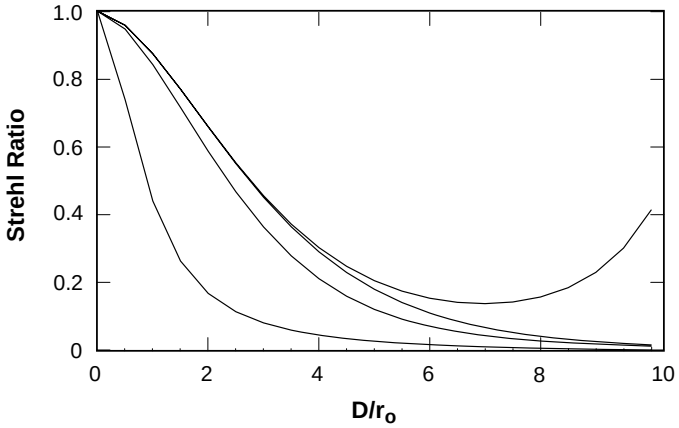

Figure 7.19. Strehl ratios for various situations versus the ratio D/r_0 plotted on a linear scale. The highest curve is for the tilt-removed Fried approximation with the coefficient of the tilt term 1.4332. The next lowest curve is the exact calculation with tilt removed. The next lowest curve is for the tilt-removed Fried approximation with the coefficient of the tilt term 1.0. The lowest curve is for uncorrected turbulence with the tilt present.

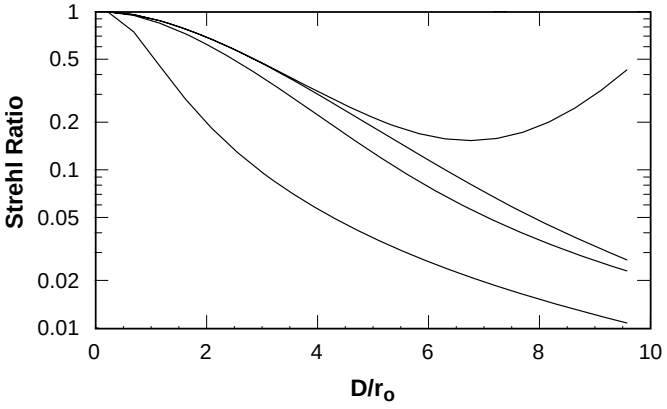

Figure 7.20. Strehl ratios for various situations versus the ratio D/r_0 plotted on a log scale. The highest curve is for the tilt-removed Fried approximation with the coefficient of the tilt term 1.4332. The next lowest curve is the exact calculation with tilt removed. The next lowest curve is for the tilt-removed Fried approximation with the coefficient of the tilt term 1.0. The lowest curve is for uncorrected turbulence with the tilt present.

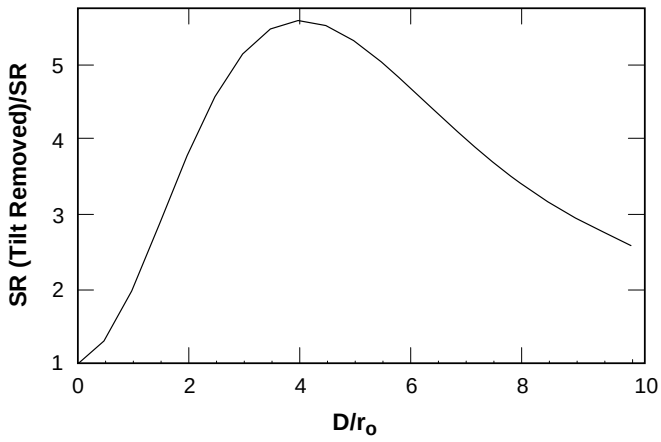

Figure 7.21. The ratio of the Strehl ratio for uncorrected turbulence with the tilt removed to that for uncorrected turbulence versus the ratio D/r_0.

to a target that is illuminated by a beacon, and the scoring beam is focused at the target. As discussed in Sec. 3.5 the finite beacon introduces a term $2J_1(\kappa D_s z/2L)/(\kappa D_s z/2L)$ in the expression for the incoming beacon signal. For this case, $\gamma = \gamma_i = 1 - z/L$ for both the incoming and the outgoing beams, and

$$\begin{aligned} f(\boldsymbol{\rho})^2 = & \left[\exp[i\gamma_i \boldsymbol{\kappa}\cdot\boldsymbol{\rho}] - \frac{2J_1(\kappa D_s z/2L)}{\kappa D_s z/2L}\exp(i\gamma_i\boldsymbol{\kappa}\cdot\boldsymbol{\rho})\right]^2 \\ & = \left[1 - \frac{2J_1(\kappa D_s z/2L)}{\kappa D_s z/2L}\right]^2 = f(\boldsymbol{\rho}+\boldsymbol{\alpha}D)^2, \end{aligned} \tag{7.102}$$

and

$$-2f(\boldsymbol{\rho})f(\boldsymbol{\rho}+\boldsymbol{\alpha}D) = -2\left[1 - \frac{2J_1(\kappa D_s z/2L)}{\kappa D_s z/2L}\right]^2 \cos(\gamma_i\boldsymbol{\kappa}\cdot\boldsymbol{\alpha}D)\,. \tag{7.103}$$

Therefore, the structure function with tilt present is given by using eq. 3.85 as

$$\begin{aligned} \mathcal{D}(\boldsymbol{\alpha}D) = & \; 0.8295\,k_0^2 \int_0^L dz\, C_n^2(z) \int_0^\pi d\varphi \int_0^\infty \kappa^{-8/3} d\kappa \\ & \times \left[1 - \frac{2J_1(\kappa D_s z/2L)}{\kappa D_s z/2L}\right]^2 [1 - \cos(\gamma_i\boldsymbol{\kappa}\cdot\boldsymbol{\alpha}D)]\,. \end{aligned} \tag{7.104}$$

The previous equation is not the total structure function, it is the structure function for phase without the diffraction term. Assume that diffraction is negligible and the scintillation is small, so the phase structure function is a good approximation to the total structure function.

Let $x = \kappa D_s z/2L$ and $e = D_s z/2L\alpha D\gamma_1$ to obtain

$$\begin{aligned}\mathcal{D}(\boldsymbol{\alpha}D) &= \mathcal{D}_1(\boldsymbol{\alpha}D) = 0.26128\, k_0^2 D_s^{5/3} \int_0^L dz\, C_n^2(z)(z/L)^{5/3} \int_0^\pi d\varphi \int_0^\infty x^{-8/3} dx \\ &\times \left[1 - \frac{2J_1(x)}{x}\right]^2 \left\{1 - \cos\left[\frac{2x}{e}\cos(\theta_d - \varphi)\right]\right\} \\ &= 0.82084\, k_0^2 D_s^{5/3} \int_0^L dz\, C_n^2(z)(z/L)^{5/3} \int_0^\infty x^{-8/3} dx \\ &\times \left[1 - \frac{2J_1(x)}{x}\right]^2 [1 - J_0(x/e)]\,. \end{aligned} \tag{7.105}$$

The integral over x can be evaluated in terms of generalized hypergeometric functions.

This structure function with tilt present does not depend on ρ, and eq. 7.81 can be used to calculate the Strehl ratio. The integrand is small for large wavelengths, and it is expected that the correlation of phase to decay rapidly with distance, which should result in the Maréchal formula being a better approximation for the Strehl ratio for small values of the parameter than for uncorrected turbulence.

The variance is equal to

$$\begin{aligned}\sigma^2 &= 0.13064\, k_0^2 D_s^{5/3} \int_0^L dz\, C_n^2(z) \left(\frac{z}{L}\right)^{5/3} \int_0^\pi d\varphi \int_0^\infty x^{-8/3} dx \left[1 - \frac{2J_1(x)}{x}\right]^2 \\ &= 0.06362\, k_0^2 (D_s/L)^{5/3} \mu_{5/3} = (\theta/9.91\theta_0)^{5/3}, \end{aligned} \tag{7.106}$$

where $\theta = D_s/L$ is the angle subtended by the beacon. This is similar to the formula for variance for an anisoplanatic offset and the Strehl ratio calculated using an angular offset of $\theta/9.91$ provides a good approximation for the Strehl ratio.

As an example of this calculation consider a transmitter at 12.2 km and a receiver 273 km away at an altitude of 20.9 km with a CLEAR1 turbulence model. Fig. 7.22 shows the Strehl ratio versus the ratio of beacon to transmit diameter. Also plotted is the result from the Maréchal formula. Notice the good agreement up to a ratio of 0.25. The third curve is the result obtained from the formula for tilt anisoplanatism. There is good agreement up to a ratio of 2.

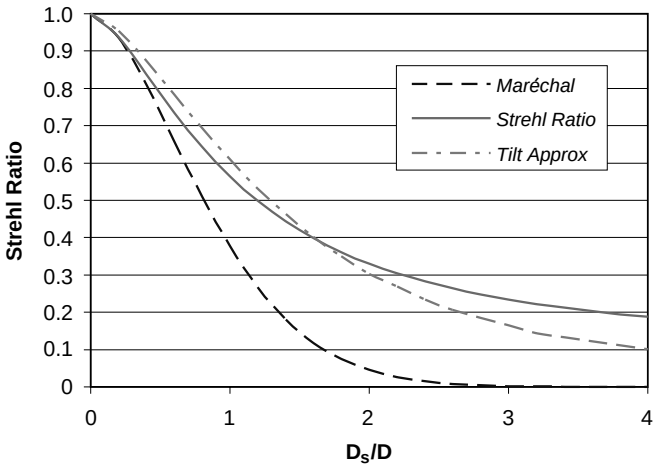

Figure 7.22. The Strehl ratio, the Maréchal approximation, and the approximation using the tilt anisoplanatic expression versus the ratio of beacon diameter to receive diameter. The transmitter is at 12.2 km and a receiver is 273 km away at an altitude of 20.9 km with a CLEAR1 turbulence model.

The square of the tilt difference at the two points is

$$
\begin{aligned}
&[A(\boldsymbol{\rho}) - A(\boldsymbol{\rho} + \boldsymbol{\alpha} D)]^2 = \left| i \frac{16 J_2(\gamma_i \kappa D/2)}{\gamma_i \kappa D/2} \frac{\boldsymbol{\rho} \cdot \boldsymbol{\kappa}}{D\kappa} \left[1 - \frac{2 J_1 (\kappa D_s z/2L)}{\kappa D_s z/2L} \right] \right. \\
&\left. - i \frac{16 J_2(\gamma_i \kappa D/2)}{\gamma_i \kappa D/2} \frac{(\boldsymbol{\rho} + \boldsymbol{\alpha} D) \cdot \boldsymbol{\kappa}}{D\kappa} \left[1 - \frac{2 J_1 (\kappa D_s z/2L)}{\kappa D_s z/2L} \right] \right|^2 \\
&= \left[\frac{16 J_2(\gamma_i \kappa D/2)}{\gamma_i \kappa D/2} \frac{\boldsymbol{\alpha} \cdot \boldsymbol{\kappa}}{\kappa} \right]^2 \left[1 - \frac{2 J_1 (\kappa D_s z/2L)}{\kappa D_s z/2L} \right]^2 \\
&= 256\, \alpha^2 \left[\frac{J_2(\gamma_i \kappa D/2)}{\gamma_i \kappa D/2} \right]^2 \left[1 - \frac{2 J_1 (\kappa D_s z/2L)}{\kappa D_s z/2L} \right]^2 \cos^2(\theta_d - \varphi). \qquad (7.107)
\end{aligned}
$$

Let $x = \kappa D_s z/2L$ and $d = z D_s / L D \gamma_i$ to obtain for the second component of the structure function

$$
\begin{aligned}
\mathcal{D}_2(\boldsymbol{\alpha} D) &= -33.444\, \alpha^2 k_0^2 D_s^{5/3} \int_0^L dz\, C_n^2(z) (z/L)^{5/3} \int_0^\pi d\varphi \cos^2(\theta_d - \varphi) \\
&\quad \times \int_0^\infty x^{-8/3} dx \left[\frac{J_2(x/d)}{x/d} \right]^2 \left[1 - \frac{2 J_1(x)}{x} \right]^2 \\
&= -52.534\, \alpha^2 k_0^2 D_s^{5/3} \int_0^L dz\, C_n^2(z) (z/L)^{5/3} \\
&\quad \times \int_0^\infty x^{-8/3} dx \left[\frac{J_2(x/d)}{x/d} \right]^2 \left[1 - \frac{2 J_1(x)}{x} \right]^2 . \qquad (7.108)
\end{aligned}
$$

The third component of the structure function is found from

$$
\begin{aligned}
&[f(\boldsymbol{\rho}) - A(\boldsymbol{\rho}) - \{f(\boldsymbol{\rho}+\boldsymbol{\alpha}D) - A(\boldsymbol{\rho}+\boldsymbol{\alpha}D)\}]\,[A(\boldsymbol{\rho}+\boldsymbol{\alpha}D) - A(\boldsymbol{\rho})] \\
&= \mathrm{Re}\left\{\left[\exp(i\gamma_i\boldsymbol{\kappa}\cdot\boldsymbol{\rho})X - i16\frac{J_2(\gamma_i\kappa D/2)}{\gamma_i\kappa D/2}\frac{\boldsymbol{\rho}\cdot\boldsymbol{\kappa}}{D\kappa}X\right.\right. \\
&\left. - \exp(i\gamma_i\boldsymbol{\kappa}\cdot\boldsymbol{\rho}')X + i16\frac{J_2(\gamma_i\kappa D/2)}{\gamma_i\kappa D/2}\frac{\boldsymbol{\rho}'\cdot\boldsymbol{\kappa}}{D\kappa}X\right] \\
&\qquad \times \left.\left[-i16\frac{J_2(\gamma_i\kappa D/2)}{\gamma_i\kappa D/2}\frac{(\boldsymbol{\rho}'-\boldsymbol{\rho})\cdot\boldsymbol{\kappa}}{\kappa D}X\right]\right\},
\end{aligned}
\tag{7.109}
$$

where

$$
X = \left[1 - \frac{2J_1\left(\kappa D_s z/2L\right)}{\kappa D_s z/2L}\right]. \tag{7.110}
$$

Using this, one finds

$$
\begin{aligned}
&\mathcal{D}_3\left(\boldsymbol{\alpha}D, \boldsymbol{\rho}\right) = 4.1805\,\alpha k_0^2 D_s^{5/3}\int_0^L dz\; C_n^2(z)(z/L)^{5/3}\int_0^\pi d\varphi\cos(\theta_d-\varphi) \\
&\times\int_0^\infty dx\, x^{-8/3}\frac{J_2(x/d)}{x/d}\left[1-\frac{2J_1\left(x\right)}{x}\right]^2\left\{\sin\left[\frac{2x\rho}{dD}\cos(\theta_\rho-\varphi)\right]\right. \\
&\left.-16\frac{\rho}{D}\cos(\theta_d-\varphi)\frac{J_2(x/d)}{x/d} - \sin\left[\frac{2x\rho'}{dD}\cos(\theta_{\rho'}-\varphi)\right]\right\},
\end{aligned}
\tag{7.111}
$$

where $x = \kappa D_s z/2L$ and $d = zD_s/LD\gamma_i$.

The total tilt-removed structure function is

$$
\begin{aligned}
&\mathcal{D}_{TR}\left(\boldsymbol{\alpha}D\right) = k_0^2\, D_s^{5/3}\int_0^L dz\, C_n^2(z)(z/L)^{5/3}\int_0^\pi d\varphi\int_0^\infty x^{-8/3}dx \\
&\times\left(0.26128\left[1-\frac{2J_1\left(x\right)}{x}\right]^2\left\{1-\cos\left[\frac{x}{e}\cos(\theta_d-\varphi)\right]\right\}\right. \\
&-33.444\alpha^2\cos^2(\theta_d-\varphi)\left[\frac{J_2\left(x/d\right)}{x/d}\right]^2\left[1-\frac{2J_1\left(x\right)}{x}\right]^2 \\
&+4.1805\,\alpha\cos(\theta_d-\varphi)\frac{J_2(x/d)}{x/d}\left[1-\frac{2J_1\left(x\right)}{x}\right]^2 \\
&\times\left\{\sin\left[\frac{2x\rho}{dD}\cos(\theta_\rho-\varphi)\right] - 16\frac{\rho}{D}\cos(\theta_d-\varphi)\frac{J_2(x/d)}{x/d}\right. \\
&\left.\left.-\sin\left[\frac{2x\rho'}{dD}\cos(\theta_{\rho'}-\varphi)\right]\right\}\right).
\end{aligned}
\tag{7.112}
$$

For the same example as plotted in Fig. 7.22, the Strehl ratio with tilt present, with tilt removed, and the tilt anisoplantic approximation are plotted in Fig. 7.23. Notice that removing tilt significantly increases the Strehl ratio for larger beacon sizes. It was found that for the several cases that were tried that the third term $\mathcal{D}_3$ only changed the Strehl ratio by at most 2%. Numerically, this is the most difficult term to calculate since the κ integration cannot be performed analytically.

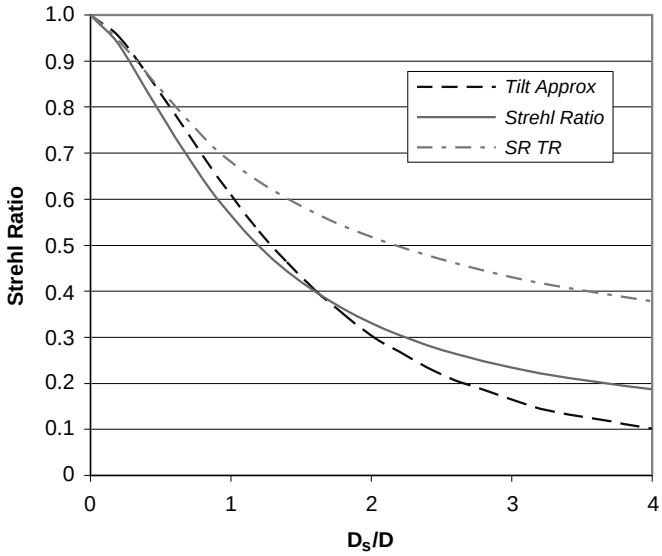

Figure 7.23. The Strehl ratio with tilt present and removed, and the approximation using the tilt anisoplanatic expression versus the ratio of beacon diameter to receive diameter. The transmitter is at 12.2 km and a receiver is 273 km away at an altitude of 20.9 km with a CLEAR1 turbulence model.

7.5.3 Strehl ratio for a finite beacon and collimated corrected beam

Next, consider the case where there is a beacon at $z = L$ of diameter D_s and the outgoing beam is collimated. This case applies to using a guidestar to correct for a telescope, or to use the guidestar to correct a beam that is collimated. The formulas that are developed are more complicated than the previous case. For this case $\gamma = \gamma_i = 1 - z/L$ for the incoming beam, and $\gamma = 1$ for the outgoing beam. For this case the phase variance term is

$$\begin{aligned} f(\boldsymbol{\rho})^2 &= \left[\exp(i\boldsymbol{\kappa}\cdot\boldsymbol{\rho}) - \frac{2J_1(x)}{x}\exp(i\gamma_i\boldsymbol{\kappa}\cdot\boldsymbol{\rho})\right]^2 \\ &= 1 - 2\frac{2J_1(x)}{x}\cos(\boldsymbol{\kappa}\cdot\boldsymbol{\rho}z/L) + \left[\frac{2J_1(x)}{x}\right]^2, \end{aligned} \tag{7.113}$$

where $x = \kappa D_s z/2L$. Notice that this term depends on $\boldsymbol{\rho}$. Similarly

$$\begin{aligned} f(\boldsymbol{\rho}+\boldsymbol{\alpha}D)^2 &= \left\{\exp[i\boldsymbol{\kappa}\cdot(\boldsymbol{\rho}+\boldsymbol{\alpha}D)] - \frac{2J_1(x)}{x}\exp\left[i\gamma_i\boldsymbol{\kappa}\cdot(\boldsymbol{\rho}+\boldsymbol{\alpha}D)\right]\right\}^2 \\ &= 1 - 2\frac{2J_1(x)}{x}\cos(\boldsymbol{\kappa}\cdot(\boldsymbol{\rho}+\boldsymbol{\alpha}D)z/L) + \left[\frac{2J_1(x)}{x}\right]^2. \end{aligned} \tag{7.114}$$

Also

$$-2f(\boldsymbol{\rho})f(\boldsymbol{\rho}+\boldsymbol{\alpha}D) = -2\left(\cos\left[\boldsymbol{\kappa}\cdot\boldsymbol{\alpha}D\right] + 2\left[\frac{2J_1(x)}{x}\right]^2\cos\left(\gamma_i\,\boldsymbol{\kappa}\cdot\boldsymbol{\alpha}D\right)\right.$$
$$\left. - \left[\frac{2J_1(x)}{x}\right]\left\{\cos\left[\,\boldsymbol{\kappa}\cdot(-\boldsymbol{\rho}z/L+\gamma_i\,\boldsymbol{\alpha}D)\right] + \cos\left[\boldsymbol{\kappa}\cdot(\boldsymbol{\rho}z/L+\;\boldsymbol{\alpha}D)\right]\right\}\right). \tag{7.115}$$

The phase variance is

$$\sigma^2 = 0.06532\,D_s^{5/3}\,k_0^2\int_0^L dz\,C_n^2(z)(z/L)^{5/3}\int_0^{\pi}d\varphi\int_0^{\infty}x^{-8/3}dx$$
$$\left\{1 - 2\frac{2J_1(x)}{x}\cos\left[\frac{2x\rho}{D_s}\cos(\theta_\rho-\varphi)\right] + \left[\frac{2J_1(x)}{x}\right]^2\right\}. \tag{7.116}$$

Integrating over angle gives

$$\sigma^2 = 0.4104\,k_0^2\,D_s^{5/3}\int_0^L dz\,C_n^2(z)(z/L)^{5/3}\int_0^{\infty}x^{-8/3}dx$$
$$\left\{1 - 2\frac{2J_1(x)}{x}J_0\left[2x\rho/D_s\right] + \left[\frac{2J_1(x)}{x}\right]^2\right\}. \tag{7.117}$$

The aperture-averaged phase variance is equal to

$$\sigma_{Ave}^2 = 0.4104\,k_0^2 D_s^{5/3}\int_0^L dz\,C_n^2(z)\,(z/L)^{5/3}\int_0^{\infty}x^{-8/3}dx$$
$$\left\{1 - 2\frac{2J_1(x)}{x}\frac{2J_1(Dx/D_s)}{Dx/D_s} + \left[\frac{2J_1(x)}{x}\right]^2\right\}. \tag{7.118}$$

The phase structure function with tilt present is found from

$$\left[f\left(\boldsymbol{\rho}+\boldsymbol{\alpha}D\right) - f\left(\boldsymbol{\rho}\right)\right]^2 = 2\left[1-\cos(\boldsymbol{\kappa}\cdot\boldsymbol{\alpha}D)\right] + 2Y^2\left[1-\cos(\gamma_i\boldsymbol{\kappa}\cdot\boldsymbol{\alpha}D)\right]$$
$$-2Y\left\{\cos(\boldsymbol{\kappa}\cdot\boldsymbol{\rho}z/L) + \cos[\boldsymbol{\kappa}\cdot(\boldsymbol{\rho}+\boldsymbol{\alpha}D)z/L]\right.$$
$$\left. - \cos[\boldsymbol{\kappa}\cdot(-\boldsymbol{\rho}z/L+\boldsymbol{\alpha}D\gamma_i)] - \cos[\boldsymbol{\kappa}\cdot(\boldsymbol{\alpha}D+\boldsymbol{\rho}z/L)]\right\}, \tag{7.119}$$

where $Y = 2J_1(\kappa D_s z/2L)/(\kappa D_s z/2L)$.

Using these relations, the structure function with tilt present is given as

$$\begin{aligned}\mathcal{D}(\boldsymbol{\alpha}D) &= \mathcal{D}_1(\boldsymbol{\alpha}D) = 0.8292\,k_0^2\int_0^L dz\,C_n^2(z)\int_0^\pi d\varphi\int_0^\infty \kappa^{-8/3}d\kappa \\ &\times\left(\left[1-\cos(\boldsymbol{\kappa}\cdot\boldsymbol{\alpha}D)\right]+\left[\frac{2J_1(\kappa D_s z/2L)}{\kappa D_s z/2L}\right]^2\left[1-\cos(\boldsymbol{\kappa}\cdot\gamma_i\boldsymbol{\alpha}D)\right]\right. \\ &-\left[\frac{2J_1(\kappa D_s z/2L)}{\kappa D_s z/2L}\right]\{\cos(\boldsymbol{\kappa}\cdot\boldsymbol{\rho}z/L)+\cos(\boldsymbol{\kappa}\cdot\boldsymbol{\rho}'z/L) \\ &\left.-\cos[\boldsymbol{\kappa}\cdot(-\boldsymbol{\rho}z/L+\gamma_i\boldsymbol{\alpha}D)]-\cos[\boldsymbol{\kappa}\cdot(\boldsymbol{\rho}z/L+\boldsymbol{\alpha}D)]\}\right). \quad (7.120)\end{aligned}$$

The dot products can be replaced by expressions that contain the cosine of angles. For instance

$$\boldsymbol{\kappa}\cdot(\boldsymbol{\rho}z/L+\gamma_i\boldsymbol{\alpha}D) = \kappa\rho z\cos(\theta_\rho-\varphi)/L+\gamma_i\kappa\alpha D\cos(\theta_d-\varphi). \quad (7.121)$$

As in the last section, the previous equation is not the structure function, it is the structure function for phase without the diffraction term. Assume that diffraction is negligible and the scintillation is small, so the phase structure function is good approximation to the total structure function. The integrand is small for large wavelengths, and it is expected that the correlation of phase to decay rapidly with distance, which should result in the Maréchal formula being a better approximation for the Strehl ratio than for uncorrected turbulence.

A comparison of the Maréchal formula and the Strehl ratio is plotted in Fig. 7.24. Note that the Strehl ratio is only slightly higher than the approximation even for values of the beacon diameter to aperture diameter of 4.

The square of the tilt difference at the two points is

$$\begin{aligned}[A(\boldsymbol{\rho})-A(\boldsymbol{\rho}+\boldsymbol{\alpha}D)]^2 &= \left|i\frac{16J_2(\kappa D/2)}{\kappa D/2}\frac{\boldsymbol{\rho}\cdot\boldsymbol{\kappa}}{D\kappa}-iY\frac{16J_2(\gamma_i\kappa D/2)}{\gamma_i\kappa D/2}\frac{\boldsymbol{\rho}\cdot\boldsymbol{\kappa}}{D\kappa}\right. \\ &\left.-i\frac{16J_2(\kappa D/2)}{\kappa D/2}\frac{(\boldsymbol{\rho}+\boldsymbol{\alpha}D)\cdot\boldsymbol{\kappa}}{D\kappa}+iY\frac{16J_2(\gamma_i\kappa D/2)}{\gamma_i\kappa D/2}\frac{(\boldsymbol{\rho}+\boldsymbol{\alpha}D)\cdot\boldsymbol{\kappa}}{D\kappa}\right|^2 \\ &= 256\,\alpha^2\left\{\frac{J_2(\kappa D/2)}{\kappa D/2}-\left[\frac{2J_1(\kappa D_s z/2L)}{\kappa D_s z/2L}\right]\frac{J_2(\gamma_i\kappa D/2)}{\gamma_i\kappa D/2}\right\}^2\cos^2(\theta_d-\varphi). \quad (7.122)\end{aligned}$$

The second component of the structure function is

$$\begin{aligned}\mathcal{D}_2(\boldsymbol{\alpha}D) &= -33.444\,\alpha^2\,k_0^2\,D^{5/3}\int_0^L dz\,C_n^2(z)\int_0^\pi d\varphi\cos^2(\theta_d-\varphi) \\ &\times\int_0^\infty x^{-8/3}dx\left[\frac{J_2(x)}{x}-\frac{2J_1(x/b)}{x/b}\frac{J_2(\gamma_i x)}{\gamma_i x}\right]^2. \quad (7.123)\end{aligned}$$

where $x=\kappa D/2$ and $b=DL/D_s z$.

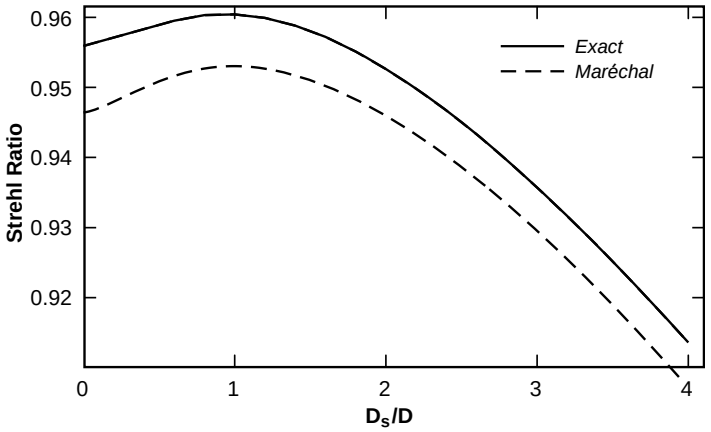

Figure 7.24. The Strehl ratio and the Maréchal approximation for a beacon of diameter D_s and a collimated scoring beam. The aperture diameter is 1 meter, the range L is 90 km, and the isoplanatic angle is 22 microradians.

Once again set the finite beacon function $Y = 2J_1(\kappa D_s z/2L)/(\kappa D_s z/2L)$. The third component of the structure function is found from

$$
\begin{aligned}
&\{f(\boldsymbol{\rho}) - A(\boldsymbol{\rho}) - [f(\boldsymbol{\rho} + \boldsymbol{\alpha}D) - A(\boldsymbol{\rho} + \boldsymbol{\alpha}D)]\}\,[A(\boldsymbol{\rho} + \boldsymbol{\alpha}D) - A(\boldsymbol{\rho})] \\
&= \mathrm{Re}\,\{[\exp(i\boldsymbol{\kappa}\cdot\boldsymbol{\rho}) - Y\exp(i\gamma_i\boldsymbol{\kappa}\cdot\boldsymbol{\rho}) - \exp(i\boldsymbol{\kappa}\cdot\boldsymbol{\rho}') + Y\exp(i\gamma_i\boldsymbol{\kappa}\cdot\boldsymbol{\rho}') \\
&\quad - i16\frac{J_2(\kappa D/2)}{\kappa D/2}\frac{\boldsymbol{\rho}\cdot\boldsymbol{\kappa}}{D\kappa} + i16Y\frac{J_2(\gamma_i\kappa D/2)}{\gamma_i\kappa D/2}\frac{\boldsymbol{\rho}\cdot\boldsymbol{\kappa}}{D\kappa} \\
&\quad + i16\frac{J_2(\kappa D/2)}{\kappa D/2}\frac{\boldsymbol{\rho}'\cdot\boldsymbol{\kappa}}{D\kappa} - i16Y\frac{J_2(\gamma_i\kappa D/2)}{\gamma_i\kappa D/2}\frac{\boldsymbol{\rho}'\cdot\boldsymbol{\kappa}}{D\kappa}\Bigg] \\
&\qquad \times(-i16)\left[\frac{J_2(\kappa D/2)}{\kappa D/2}\frac{\boldsymbol{\alpha}\cdot\boldsymbol{\kappa}}{\kappa} - \frac{YJ_2(\gamma_i\kappa D/2)}{\gamma_i\kappa D/2}\frac{\boldsymbol{\alpha}\cdot\boldsymbol{\kappa}}{\kappa}\right]\Bigg\} \\
&= 16\alpha\Bigg\{\sin(\boldsymbol{\kappa}\cdot\boldsymbol{\rho}) - Y\sin(\gamma_i\boldsymbol{\kappa}\cdot\boldsymbol{\rho}) - \sin(\boldsymbol{\kappa}\cdot\boldsymbol{\rho}') + Y\sin(\gamma_i\boldsymbol{\kappa}\cdot\boldsymbol{\rho}') \\
&\quad + 16\left[\frac{J_2(\kappa D/2)}{\kappa D/2} + Y\frac{J_2(\gamma_i\kappa D/2)}{\gamma_i\kappa D/2}\right]\alpha\cos(\theta_d - \varphi)\Bigg\} \\
&\times\left[\frac{J_2(\kappa D/2)}{\kappa D/2} - Y\frac{J_2(\gamma_i\kappa D/2)}{\gamma_i\kappa D/2}\right]\cos(\theta_d - \varphi),
\end{aligned}
\tag{7.124}
$$

Using this result, the third component of the structure function is equal to

$$\mathcal{D}_3\left(\boldsymbol{\alpha}\, D, \boldsymbol{\rho}\right) = 6.636\, \alpha k_0^2 \int_0^L dz\; C_n^2(z) \int_0^\pi d\varphi \cos(\theta_d - \varphi) \int_0^\infty d\kappa\, \kappa^{-8/3}$$
$$\times \Bigg\{ \sin(\boldsymbol{\kappa}\cdot\boldsymbol{\rho}) - Y \sin(\gamma_i \boldsymbol{\kappa}\cdot\boldsymbol{\rho}) - \sin(\boldsymbol{\kappa}\cdot\boldsymbol{\rho}') + Y \sin(\gamma_i \boldsymbol{\kappa}\cdot\boldsymbol{\rho}')$$
$$+ 16 \left[\frac{J_2(\kappa D/2)}{\kappa D/2} - Y \frac{J_2(\gamma_i \kappa D/2)}{\gamma_i \kappa D/2} \right] \alpha \cos(\theta_d - \varphi) \Bigg\}$$
$$\times \left[\frac{J_2(\kappa D/2)}{\kappa D/2} - Y \frac{J_2(\gamma_i \kappa D/2)}{\gamma_i \kappa D/2} \right]. \tag{7.125}$$

Set $x = \kappa D/2$ to obtain

$$\mathcal{D}_3\left(\boldsymbol{\alpha}\, D, \boldsymbol{\rho}\right) = 2.090\, \alpha k_0^2\, D^{5/3} \int_0^L dz\; C_n^2(z) \int_0^\pi d\varphi \cos(\theta_d - \varphi) \int_0^\infty dx\, x^{-8/3}$$
$$\times \Bigg(\sin\left(\frac{2x}{D}\rho\cos(\theta_\rho - \varphi)\right) - \left[\frac{2J_1(x/b)}{x/b}\right] \sin\left(\frac{2x}{D}\gamma_i\rho\cos(\theta_\rho - \varphi)\right)$$
$$- \sin\left(\frac{2x}{D}\rho'\cos(\theta_{\rho'} - \varphi)\right) + \left[\frac{2J_1(x/b)}{x/b}\right] \sin\left(\frac{2x}{D}\gamma_i\rho'\cos(\theta_{\rho'} - \varphi)\right)$$
$$+ 16 \left\{ \frac{J_2(x)}{x} - \left[\frac{2J_1(x/b)}{x/b}\right] \frac{J_2(\gamma_i x)}{\gamma_i x} \right\} \alpha \cos(\theta_d - \varphi) \Bigg)$$
$$\times \left\{ \frac{J_2(x)}{x} - \left[\frac{2J_1(x/b)}{x/b}\right] \frac{J_2(\gamma_i x)}{\gamma_i x} \right\}. \tag{7.126}$$

A comparison of the Strehl ratio with tilt present and tilt removed is plotted in Fig. 7.25.

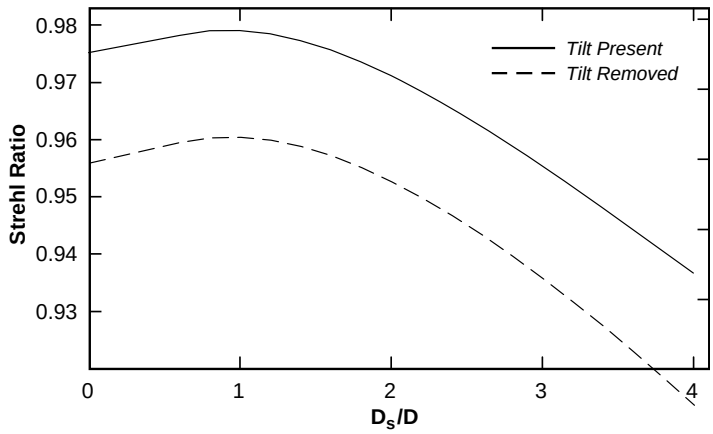

Figure 7.25. The Strehl ratio with tilt present and with tilt removed for a beacon of diameter D_s and a collimated scoring beam. The aperture diameter is 1 meter, the range L is 90 km, and the isoplanatic angle is 22 microradians.

REFERENCES

1. Abramowitz, M., Stegun, I. A., *Handbook of Mathematical Functions*, National Bureau of Standards, Washington, (1964).
2. Allen, C. W., *Astrophysical Quantities*, The Athone Press, University of London, (1963).
3. Belsher, J., Fried, D., "Chromatic Refraction Induced Pseudo Anisoplanatism", *tOSC Report No. TR-433* (the Optical Sciences Company, Placentia, California, 1981).
4. Cole, A. E., Court, A., Kantor, A. J., *Handbook of Geophysics and Space Environments*, Edited by Valley, Shea L., McGraw-Hill Book Company, Inc., New York, (1965).
5. Fried, D., "Anisoplanatism in adaptive optics", *J. Opt. Soc. Am.*, **72**, (1982) pp. 52–61.
6. Fried, D. L., "Limiting Resolution Looking Down Through the Atmosphere", *J. Opt. Soc. Am.*, **56**, (1966) pp. 1380–1384.
7. Fried, D. L., "Time-delay-induced mean-square error in adaptive optics", *J. Opt. Soc. Am. A*, **7**, (1990) pp. 1224–1225.
8. Fried, D. L., "Optical Resolution Through a Randomly Inhomogeneous Medium for Very Long and Very Short Exposures", *J. Opt. Soc. Am.*, **56**, (1966) pp. 1372–1379.
9. Fried, D. L., "Time-delay-induced mean-square error in adaptive optics", *J. Opt. Soc. Am. A*, **7**, (1990) pp. 1224–1225.
10. Gradshteyn, I. S., Ryzhik, I. M., *Table of Integrals, Series, and Products*, Academic Press, New York, (1980)
11. Heidbreder, G. R., "Image Degradation with Random Wavefront Tilt Compensation", *IEE Trans. on Antennas and Propagation*, Vol. AP-15, No. 1, (1967) pp. 90–98.
12. Stock, R, and Herrmann, J., Private communication.
13. Tyler, G., Belsher, J., Fried, D., "Amelioration of Chromatic Refraction Induced Pseudoanisoplanatism", *tOSC Report No. TR-465* (the Optical Sciences Company, Placentia, California, 1982).
14. Tyler, G. A., Turbulence-induced adaptive-optics performance degradation: evaluation in the time domain, J. Opt. Soc. Am. A, **1**, (1984) 251–262.
15. Yura, H. T., Tavis, M. T., "Centroid anisoplanatism", *J. Opt. Soc. Am. A*, 2, (1985) pp. 765–773.
16. Yura, H. T., "Short-term optical-beam spread in a turbulent medium", *J. Opt. Soc. Am.*, **63**, (1973) pp. 567–572.
17. Tavis, M. T., and Yura, H. T., "Short-term average irradiance profile of an optical beam in a turbulent medium", *Applied Optics. A*, **15**, (1976) pp. "2922–2931.
18. Valley, G. C., Long- and short-term Strehl ratios for turbulence with finite inner and outer scales",*Applied Optics. A*, **18**, (1979) pp. 984–987.

Chapter 8

Mellin Transforms with a Complex Parameter

When one analyzes beam-wave propagation through turbulence, the propagation parameter γ is complex. This causes complications when one evaluates the steepest-descent contribution to an asymptotic solution. In some problems, the spatial filter functions contain a decaying exponential times a function that grows exponentially when γ is complex. Consequently, the Mellin convolution relation must be generalized to allow for convergent integrals that contain integrands that are the product of functions that exhibit exponential growth and exponential decay. In addition, methods developed in Chap. 5 must be extended to include asymptotic results for a non-positive parameter. This requires an extension of saddle-point results to complex-parameter cases. These extensions are discussed in this chapter.

The theory of asymptotic expressions for general integrals has been considered by *Luke* (1969). *Marichev* (1983) states asymptotic results for integrals with complex parameters that apply specifically to Mellin-Barnes integrals with unity coefficients of the complex variable in the gamma functions. These results are generalized here to allow asymptotic series to be written for Mellin-Barnes integrals in which the coefficients of the complex variable are not unity. Also, the results are given in a form that is directly applicable to the evaluation of integrals encountered in turbulence problems.

8.1 Mellin-Barnes Integrals with Complex Parameters

In beam-wave analysis, the integral expression that must be evaluated is

$$h(z) = \int_0^\infty \frac{dy}{y}\, h_0(y)\, h_1\,(z/y), \tag{8.1}$$

where the parameter z in general is complex. If $z = x$, x real, the convolution integral in eq. 1.28 may be used to obtain the Mellin transform of the integral

$$h(x) = \int_0^\infty \frac{dy}{y}\, h_0(y) h_1\,(x/y) \rightarrow \mathcal{M}\,[h(x)] = H(s) = H_0(s)\, H_1(s). \tag{8.2}$$

The function $h(x)$ is written as an inverse Mellin transform that is evaluated with pole-residue methods. In the case of a complex parameter, however, the Mellin transform of one integrand function may be undefined because it exhibits exponential growth. Let that function be $h_1(x)$. It is not obvious how to apply the convolution integral in this case. *Marichev* (1983, Theorem 23) gives a generalized Parseval's equality that is applicable here. Before the statement of the theorem, it is necessary to show how to express a function with a complex parameter as a Mellin-Barnes integral.

The general integral of interest is given by eq. 5.90

$$h(z) = \frac{1}{2\pi\, i} \int\limits_{C'} ds\, z^{-s}\, \frac{\prod\limits_{i=1}^{A} \Gamma\left[a_i + \alpha_i\, s\right] \prod\limits_{j=1}^{B} \Gamma\left[b_j - \beta_j\, s\right]}{\prod\limits_{k=1}^{C} \Gamma\left[c_k + \gamma_k\, s\right] \prod\limits_{m=1}^{D} \Gamma\left[d_m - \delta_m\, s\right]}. \tag{8.3}$$

The parameter z in the above equation may, in general, be complex. In this discussion if the parameter is real, it will be represented by x. The contour C' along which the integral is normally evaluated is given by the vertical line from $\eta - i\,\infty$ to $\eta + i\,\infty$, where η is a real constant chosen to insure that the integration path lies within the strips of analyticity of the integrand functions. When the parameter is complex, however, convergence conditions may require that the integration path be closed either in the left-half-plane or the right-half-plane. This issue is discussed further by *Luke* (1969) and *Marichev* (1983). An example of this condition is provided by the Bessel function of the first kind $J_\nu(z)$. If $z = x$ is real, the Mellin-Barnes integral representation of $J_\nu(z)$ is given by

$$J_v(x) = \frac{1}{4\pi i} \int\limits_{\eta - i\infty}^{\eta + i\infty} ds\, \Gamma\begin{bmatrix} s/ + \nu/2 \\ -s/2 + 1 + \nu/2 \end{bmatrix} \left(\frac{x}{2}\right)^{-s}, \tag{8.4}$$

where $x > 0$, and $-\mathrm{Re}\,\{v\} < \eta < 3/2$. If $z = \beta\, x$ is complex, a similar integral expression may be written,

$$J_v(\beta x) = \frac{1}{4\pi i} \int\limits_{C_{-\infty}} ds\, \Gamma\begin{bmatrix} s/2 + \nu/2 \\ -s/2 + 1 + \nu/2 \end{bmatrix} \left(\frac{\beta x}{2}\right)^{-s}, \tag{8.5}$$

where the new integration path $C_{-\infty}$ is the left loop surrounding all poles of $\Gamma\left[(v + s)/2\right]$. These poles occur at $s = -v - 2n$ for $n = 0,\, 1,\, 2, \ldots$.

In problems treated in this book and encountered in analyzing the effects of turbulence, the parameters a_i, α_1, b_j, β_j, c_k, γ_k, d_m, and δ_m are all real. Therefore, all the integrand's poles occur along the real axis. This makes it possible to paraphrase *Marichev's* theorem (1983) as below:

Theorem 1. *If the following three conditions hold:*

a) for certain $x > 0$ and η, the integrals

$$\int\limits_0^\infty \frac{dy}{y}\, h_0\,(y)\; h_1(x/y),\; \frac{1}{2\pi\, i} \int\limits_{\eta - i\,\infty}^{\eta + i\,\infty} ds\, H_0(s)\, H_1(s)\, x^{-s} \tag{8.6}$$

exist;

b) $H_0(s)$ *is an analytic function of* s *without singularities for* $Re\{s\} < \eta$ *(or* $Re\{s\} > \eta$*); and*

c) $h_1(y)$ *is a function of hypergeometric type (a hypergeometric function with a power of the argument multiplying it, or such that some terms of its power series are subtracted from it) such that* $H_1(s)$ *exists with*

$$h_1(y) = \frac{1}{2\pi i} \int\limits_{L\mp\infty} ds\, H_1(s)\, y^{-s}, \tag{8.7}$$

where the integration is over the appropriate loop $L_{-\infty}$ *(or* $L_{+\infty}$*) such that all the poles of* $H_1(s)$ *are enclosed, then*

$$\int\limits_0^\infty \frac{dy}{y}\, h_0(y)\; h_1(z/y) = \frac{1}{2\pi i} \int\limits_{\eta - i\infty}^{\eta + i\infty} ds\, H_0(s)\, H_1(s)\, z^{-s}. \tag{8.8}$$

The Bessel function satisfies the conditions required for $h_1(y)$, and for complex z can have exponential growth. In practice, when conditions for the theorem are satisfied one substitutes the Mellin transforms of the functions with real parameters into the convolution integral and ignores the fact that the individual Mellin transforms may not exist for a complex parameter.

Use of this result is illustrated in Sec. 8.3 where the Mellin transform of $\exp(-\alpha x^2)\; J_v(\beta x)$ is derived for β complex.

8.2 Asymptotic Results with a Complex Parameter

As discussed in Chap. 5, when the parameter associated with a Mellin convolution is large, the series result obtained by pole-residue techniques may converge slowly. Consequently, asymptotic results are useful when accurate approximations are desired. Asymptotic expressions were obtained in Chap. 5 when the parameter was assumed to be positive real (complex argument has zero imaginary part). These results are now generalized to allow complex or negative parameters.

The general form of the Mellin-Barnes integral that must be evaluated is given in eq. 8.3. The definitions in the table at the end of this chapter are used in our analysis. One finds the asymptotic form of eq. 8.1 by deforming the original integration path so that the new path goes through all saddle points in the direction of steepest descent. The asymptotic approximation of the integral includes the pole residues picked up through path deformation. One calculates the asymptotic contribution of the deformed path by computing a steepest-descent contribution, and one finds the pole-residue contributions by changing the normal direction of contour closure as described in Chap. 5.

To find the steepest-descent contribution to the integral, one uses the asymptotic form of the integrand. The identity

$$\Gamma[\nu]\ \Gamma[1-\nu] = \pi/\sin(\pi\nu) \tag{8.9}$$

allows eq. 8.3 to be expressed so that the coefficients of s in all gamma functions are negative. The asymptotic expressions for the gamma functions,

$$\Gamma[e+\varepsilon s] \sim \sqrt{2\pi}\,\exp\left[(\varepsilon s + e - 1/2)\ln(\varepsilon s) - \varepsilon s\right], \tag{8.10}$$

where e and ε are arbitrary numbers, and the sine functions

$$\sin(\pi s) \sim \tfrac{1}{2}\exp\left[-i\pi\left(s-\tfrac{1}{2}\right)\right]$$

when $\mathrm{Im}\{s\} > 0$, and

$$\sin(\pi s) \sim \tfrac{1}{2}\exp\left[i\pi\left(s-\tfrac{1}{2}\right)\right]$$

when $\mathrm{Im}\{s\} < 0$, may be used to obtain the asymptotic form for the integral,

$$h(z) \sim -i(2\pi)^{\Xi/2-1}\int ds\,\exp[f(s)]. \tag{8.11}$$

The function in the exponent is given by

$$\begin{aligned} f(s) &= \Delta'' - \Delta'''/2 + s\left[\Delta' - \Delta - \ln(z)\right] \\ &+ \ln(s)\left(\nu - \frac{\Xi}{2} + \Delta s\right) - i\lambda\pi\left(-\Lambda'' + \Lambda/2 + s\Lambda'\right). \end{aligned} \tag{8.12}$$

This expression is valid for $-\pi < \arg\{s\} < \pi$. When $\mathrm{Im}\{s\} > 0$, then $\lambda = 1$, and when $\mathrm{Im}\{s\} < 0$, then $\lambda = -1$.

To find the steepest-descent contribution, the saddle points of $f(s)$ must be found. These are the points at which

$$\frac{df(s)}{ds} = 0 = \Delta\ln(s) + \Delta' - \ln(z) - i\lambda\pi\Lambda'. \tag{8.13}$$

Terms which depend upon $1/s$ have been dropped from this expression because at the saddle point $|s|$ is large for large $|z|$. Two cases must be considered. If a saddle point exists in the upper half plane, then the solution of eq. 8.13 for s requires $\lambda = 1$. Similarly lower-half-plane saddle points require $\lambda = -1$.

The upper-half-plane saddle point is located at

$$s_o = z^{1/\Delta}\exp\left[-\frac{1}{\Delta}\left(\Delta' - i\pi\Lambda'\right)\right], \tag{8.14}$$

and the requirement on $\arg\{z\}$ for the existence of the saddle point in the upper half-plane is

$$-\pi\Lambda' < \arg\{z\} < \pi\left(\Delta - \Lambda'\right). \tag{8.15}$$

Similarly, the lower-half-plane saddle point is located at

$$s_o = z^{1/\Delta}\exp\left[-\frac{1}{\Delta}\left(\Delta' + i\pi\Lambda'\right)\right], \tag{8.16}$$

and the corresponding restriction on $\arg\{z\}$ is

$$-\pi\left(\Delta-\Lambda'\right)<\arg\{z\}<\pi\Lambda'. \tag{8.17}$$

If $\Lambda'=0$, then for positive-real z the saddle point is located on the real axis. If $-1<\Lambda'/\Delta<0$, there is a contradiction. If one assumes the saddle point is in the upper half plane, one finds that the saddle point specified by eq. 8.14 is located in the lower half plane. A contradiction also results if one assumes that the saddle point is located in the lower half plane. The only other possibility is to assume that the saddle point is located on the real axis. For this case the sinusoid cannot be represented by their asymptotic equivalents. A simple case arises when $B=D=0$. For this case one should set $\lambda=0$ in eq. 8.12, and indeed the single saddle point is located on the real axis at

$$s_o=z^{1/\Delta}\exp\left(-\Delta'/\Delta\right). \tag{8.18}$$

One obtains the correct value for the steepest-descent contribution in this case from the final answer given in eq. 8.25 and eq. 8.26 by setting $\Lambda''=\Lambda'=\Lambda=0$ and dividing the answer by two. For the more general case of $\Lambda'<0$, eq. 8.12 becomes

$$\begin{aligned}f(s)&=\Delta''-\Delta'''/2+s\left[\Delta'-\Delta-\ln(z)\right]\\&+\ln(s)\left(\nu-\frac{\Xi}{2}+\Delta s\right)+\exp\left(ln\left\{\frac{\prod_{m=1}^{D}\sin\left[\pi\left(\delta_m s-d_m+1\right)\right]}{\prod_{j=1}^{B}\sin\left[\pi\left(\beta_j s-b_j+1\right)\right]}\right\}\right).\end{aligned} \tag{8.19}$$

The steepest-descent point in this case is located at the solution of the equation

$$\begin{aligned}s_o&=z^{1/\Delta}\exp\left(-\frac{\Delta'}{\Delta}\right)\\&\times\exp\left(\frac{\pi}{\Delta}\left\{\sum_{m=1}^{D}\delta_m\cot\left[\pi\left(\delta_m s_o+1-d_m\right)\right]-\sum_{j=1}^{B}\beta_j\cot\left[\pi\left(\beta_j s_o+1-b_j\right)\right]\right\}\right).\end{aligned} \tag{8.20}$$

The right-hand side of the equation is always positive for positive-real z; therefore, the saddle point is located in the right half plane. The equation has multiple solutions but the one closest to the origin gives the largest contribution. For this case the saddle point has exponential decay. Often knowledge of this fact allows the steepest-descent contribution to the value of the integral to be neglected compared to pole contributions. If there are no pole contributions in the right-half plane, then eq. 8.20 must be solved to find the steepest-descent contribution.

For the case in which the saddle point is on the real axis, it is located in the right half plane. Therefore, in deforming the path to pass through the saddle point, one picks up poles that were not included in the Taylor series solution.

When there are two complex saddle points, they are also located in the right half plane. To prove that, first note that all Mellin transforms have fewer or the same number of denominator gamma functions than numerator gamma functions (this stems from the requirement that the inverse transform integrand must go to zero at $\pm\infty$). Also note that for this case $\Delta' > 0$ and $\Delta > 0$. The direction of the upper-complex saddle point is determined by

$$0 < \frac{\Lambda'}{\Delta} = \frac{1}{2} - \frac{1}{2}\left(\frac{A + B - C - D}{\Delta}\right) \leq \frac{1}{2}. \tag{8.21}$$

Therefore, the saddle point specified by eq. 8.14 is located in the upper-right complex plane for positive-real z.

One finds the line integral contribution to the asymptotic form of the original integral by evaluating the steepest-descent contribution at upper- and lower-half-plane saddle points. The exponent in eq. 8.12 is expanded in a Taylor series given by

$$f(s) \approx f(s_o) + \frac{df(s_o)}{ds}(s - s_o) + \frac{1}{2}\frac{d^2 f(s_o)}{ds^2}(s - s_o)^2. \tag{8.22}$$

The magnitudes of second and higher-order derivatives at the saddle point are proportional to s_o^{1-n}, where n is the order of the derivative. Since $|s_o|$ is large, higher-order terms may be neglected. At the saddle point

$$f(s) \approx f(s_o) + \frac{1}{2}\frac{d^2 f(s_o)}{ds^2}(s - s_o)^2. \tag{8.23}$$

With this approximation and an appropriate change of variables, the integral in eq. 8.11 becomes the integral of a Gaussian function that, when evaluated, gives the following results

$$h(z) \sim E(z) = E_1(z) + E_2(z), \tag{8.24}$$

where $E_1(z)$ and $E_2(z)$ are the upper- and lower-half-plane contributions, respectively. $E_1(z)$ is given by

$$E_1(z) = \frac{(2\pi)^{(\Xi-1)/2}}{\sqrt{\Delta}} z^{\rho} \exp\left[-\rho(\Delta' - i\pi\Lambda') - \Delta z^{1/\Delta} \exp\left(\frac{-\Delta' + i\pi\Lambda'}{\Delta}\right) + \Delta'' - \frac{\Delta'''}{2} - i\pi\left(-\Lambda'' + \frac{\Lambda}{2}\right)\right] \tag{8.25}$$

when $-\pi\Lambda' < \arg\{z\} < \pi(\Delta - \Lambda')$, and $E_1(z) = 0$ otherwise. $E_2(z)$ is given by

$$E_2(z) = \frac{(2\pi)^{(\Xi-1)/2}}{\sqrt{\Delta}} z^{\rho} \exp\left[-\rho\left(\Delta' + i\pi\Lambda'\right)\right.$$
$$\left. - \Delta z^{1/\Delta} \exp\left(\frac{-\Delta' + i\pi\Lambda'}{\Delta}\right) + \Delta'' - \frac{\Delta'''}{2} + i\pi\left(-\Lambda'' + \frac{\Lambda}{2}\right)\right] \quad (8.26)$$

when $-\pi\left(\Delta - \Lambda'\right) < \arg\{z\} < \pi\Lambda'$, and $E_2(z) = 0$ otherwise.

I have actually underestimated the range of $\arg\{z\}$ over which the approximations in eq. 8.25 or eq. 8.26 are valid. It may be extended by using asymptotic approximations for the gamma function $\Gamma[\alpha]$, that are valid for other ranges of $\arg\{a\}$. When this is done, results from steepest-descent methods reported here match those obtained by *Luke* (1969) that were derived from the properties of the Meijer G function. *Marichev* (1983) summarizes these results. With this extension, eq. 8.25 can be used for $-\pi\Lambda' < \arg\{z\} < \pi\left(\Delta - \Lambda' + \varsigma\right)$, and eq. 8.26 can be used for $-\pi\left(\Delta - \Lambda' + \varsigma\right) < \arg\{z\} < \pi\Lambda'$ where $\varsigma = 1/2$ when $\Delta = 1$, and $\varsigma = 1$ when $\Delta > 1$.

To determine which terms dominate the asymptotic solution, the steepest-descent and the pole-residue portions of the asymptote must be examined. If $E(z)$ exhibits exponential growth, it will dominate the asymptote. If $E(z)$ exhibits exponential decay, and there is a pole-residue contribution to the asymptote, then the pole-residue portion is dominant. An example that illustrates the use of these techniques is given in the next section.

When the parameter z is positive real, these results reduce to the saddle-point expression given in eq. 5.93.

8.3 The Mellin Transform of an Exponential Times a Bessel Function

In this section the technique that was developed above is used to evaluate an integral with a complex parameter to illustrate how to find the pole and steepest-descent contributions in this case.

The integral expression for the Mellin transform of $\exp\left(-\alpha x^2\right) J_v\left(\beta x\right)$ is given by

$$Q(s) = \mathcal{M}\left[\exp\left(-\alpha x^2\right) J_\nu\left(\beta x\right)\right] = \int_0^\infty \frac{dx}{x} x^s \exp\left(-\alpha x^2\right) J_\nu\left(\beta x\right), \quad (8.27)$$

where β is complex, and α is real and greater than zero. This integral is of interest not only because its solution demonstrates the techniques described in this chapter, but also because it occurs in the log-amplitude and phase variance expressions for propagation in the presence of Kolmogorov turbulence through complex cascaded optical systems, referred to as ABCD systems (*Yura* and *Hanson* 1989), and in the evaluation of the scintillation in the next chapter.

In addition, one can use this transform as an intermediate step in finding the Mellin transform of $\exp(-\alpha x^2) J_v^2(\beta x)$, which is encountered in beam-wave tilt analysis.

I use the extension to the Mellin convolution integral discussed in Sec. 9.2, with the expression for the Mellin-Barnes representation of the Bessel function given in eq. 8.4, to evaluate the integral given above. Note that Mellin transforms of Bessel functions with complex arguments do not converge although they do satisfy condition (c) of the theorem in Sec. 8.2. The exponential function that appears in the integrand satisfies condition (b) of the theorem and balances the exponential growth of the Bessel function (when β is complex) with exponential decay.

As discussed in Sec. 8.1, the Mellin transform of the Bessel function to be inserted into the convolution integral is given by

$$\mathcal{M}[J_\nu(\beta x)] = \frac{1}{2}\Gamma\begin{bmatrix} s/2+\nu/2 \\ -s/2+\nu/2+1 \end{bmatrix}\left(\frac{\beta}{2}\right)^{-s}. \tag{8.28}$$

With these results, the Mellin transform in eq. 1.47, and the substitution $u \to 2u$, eq. 8.27 is equal to

$$Q(s) = \left(\frac{\alpha^{-s/2}}{2}\right)\frac{1}{2\pi i}\int_{\eta-i\infty}^{\eta+i\infty} du\,\Gamma\begin{bmatrix} -u+\frac{s}{2},\, u+\frac{\nu}{2} \\ -u+\frac{\nu}{2}+1 \end{bmatrix}\left(\frac{\beta^2}{4\alpha}\right)^{-u}, \tag{8.29}$$

where $\mathrm{Re}\{-\nu/2\} < \eta < \mathrm{Re}\{-s/2\}$. In this integral $\Delta = 1$; therefore, in order to obtain a converging series solution for the integral, the integration path is closed to the left, and one obtains the pole contributions at $u = -n - \nu/2$ for $n = 0, 1, 2, \ldots$. Pole-residue techniques applied to the integral give

$$\begin{aligned}\exp\left(-\alpha x^2\right) J_\nu(\beta x) &\to \frac{1}{2\alpha^{s/2}}\left(\frac{\beta^2}{4\alpha}\right)^{\nu/2}\sum_{n=0}^{\infty}\frac{(-1)^n}{n!}\Gamma\begin{bmatrix} s/2+\nu/2+n \\ \nu+1+n \end{bmatrix}\left(\frac{\beta^2}{4\alpha}\right)^n \\ &= \frac{1}{2\alpha^{s/2}}\left(\frac{\beta^2}{4\alpha}\right)^{\nu/2}\Gamma\begin{bmatrix} \frac{\nu+s}{2} \\ \nu+1 \end{bmatrix}{}_1F_1\left[\frac{\nu}{2}+\frac{s}{2};\nu+1;-\frac{\beta^2}{4\alpha}\right],\end{aligned} \tag{8.30}$$

for $\mathrm{Re}\{\nu+s\} > 0$, and $\alpha > 0$.

The natural parameter that results from this analysis is $\beta^2/4\alpha$. When the magnitude of this parameter is small, the series given in eq. 8.30 converges quickly, thereby only a few terms are needed to accurately approximate the transform. If the parameter magnitude is large, and an approximation for the integral is needed, the asymptotic solution for eq. 8.29 is more appropriate. The integral is closed to the right in order to pick up the pole-residue contributions. One obtains path-integral contributions to the asymptotic form by evaluating the integral with the steepest-descent methods discussed in Sec. 9.2.

The poles which contribute to the asymptotic form for the Mellin transform occur at the points $u = n + s/2$ for $n = 0, 1, 2, \ldots$. This leads to a pole-residue contribution given by

$$W = \frac{1}{2}\left(\frac{2}{\beta}\right)^s \sum_{n=0}^{n_o} \frac{(-1)^n}{n\,!}\Gamma\begin{bmatrix} n+s/2+\nu/2 \\ -n-s/2+\nu/2+1 \end{bmatrix}\left(\frac{\beta^2}{4\alpha}\right)^{-n}. \tag{8.31}$$

n_o is selected to minimize the error in the asymptotic approximation as discussed in Sec. 5.2.

Added to W are the steepest-descent components of the integral. Equations eq. 8.25 and eq. 8.26 are evaluated, and it is found that

$$E_1 = \frac{\alpha^{1-s}}{2}\left(-\frac{\beta^2}{4}\right)^{s/2-1}\exp\left(-\frac{\beta^2}{4\alpha}+\frac{i\pi\nu}{2}\right)$$
$$\text{for } 0 < \arg\left\{\beta^2/4\alpha\right\} < 3\pi/2, \text{ and} \tag{8.32}$$

$$E_2 = \frac{\alpha^{1-s}}{2}\left(-\frac{\beta^2}{4}\right)^{s/2-1}\exp\left(-\frac{\beta^2}{4\alpha}-\frac{i\pi\nu}{2}\right)$$
$$\text{for } -3\pi/2 < \arg\left\{\beta^2/4\alpha\right\} < 0. \tag{8.33}$$

These terms are dominant only when Re $\{\beta^2/4\alpha\} < 0$ in which case E_1 or E_2 exhibit exponential growth. When E_1 or E_2 have sinusoidal behavior (when Re $\{\beta^2/4\alpha\} = 0$), both W and E components must be included in the asymptotic solution. Combining these results, one obtains the following asymptotic form for the Mellin transform of $\exp(-\alpha x^2)\ J_v(\beta x)$:

$$Q(s) \sim E_1 \text{ when } \frac{\pi}{2} < \arg\left\{\beta^2/4\alpha\right\} < \frac{3\pi}{2}, \tag{8.34}$$

$$Q(s) \sim E_1 + W \text{ when } \arg\left\{\beta^2/4\alpha\right\} = \frac{\pi}{2}, \tag{8.35}$$

$$Q(s) \sim W \text{ when } -\frac{\pi}{2} < \arg\left\{\beta^2/4\alpha\right\} < \frac{\pi}{2}, \tag{8.36}$$

$$Q(s) \sim E_2 + W \text{ when } \arg\left\{\beta^2/4\alpha\right\} = -\frac{\pi}{2}, \text{ and} \tag{8.37}$$

$$Q(s) \sim E_2 \text{ when } -\frac{3\pi}{2} < \arg\left\{\beta^2/4\alpha\right\} < -\frac{\pi}{2}. \tag{8.38}$$

As a check on this result, examine the case when $s = 1$, for which results are available in the literature. Replace β by $i\delta$ (δ is still complex.) Note the identity that relates Bessel and modified Bessel functions,

$$I_\nu(z) = \exp\left(-\frac{i\pi\nu}{2}\right)J_\nu(iz), \quad \left[-\pi < \arg\{z\} \le \tfrac{\pi}{2}\right], \tag{8.39}$$

and the relation in *Gradshteyn* and *Ryzhik* (1980, eq. 9.238 #2)

$$I_\nu(x) = \frac{2^{-\nu}}{\Gamma[\nu+1]}\,x^\nu \exp(-x)\ {}_1F_1\left[\frac{1}{2}+\nu; 1+2\nu; 2x\right]. \tag{8.40}$$

Substitute these results in eq. 8.30 to give

$$\int_0^\infty \frac{dx}{x}\, x\, \exp\left(-\alpha\, x^2\right)\, I_\nu\left(\delta\, x\right) = \frac{1}{2}\sqrt{\frac{\pi}{\alpha}} \exp\left(\frac{\delta^2}{8\alpha}\right)\, I_{\nu/2}\left(\frac{\delta^2}{8\alpha}\right) \tag{8.41}$$

for $\mathrm{Re}\{\nu\} > -1$, and $\alpha > 0$. This agrees with the result given in *Gradshteyn* and *Ryzhik* (1980, eq. 6.618 #4).

If δ is real, *Gradshteyn* and *Ryzhik* (1980, eq. 8.451 #5) gives the asymptotic form for the modified Bessel function

$$I_\nu(z) \sim \frac{\exp\left(z\right)}{\sqrt{2\pi\, z}}. \tag{8.42}$$

This leads to the asymptotic form for the integral given by

$$\begin{aligned} Q(1) &= \exp\left(\frac{i\pi\,\nu}{2}\right)\, \int_0^\infty \frac{dx}{x}\, x \exp\left(-\alpha\, x^2\right)\, I_\nu\left(\delta\, x\right) \\ &\sim \frac{1}{\delta} \exp\left(\frac{\delta^2}{4\alpha}\right) \exp\left(\frac{i\pi\,\nu}{2}\right), \qquad \left|\frac{\delta^2}{\alpha}\right| >> 1. \end{aligned} \tag{8.43}$$

With these methods I can obtain asymptotic results for arbitrary values of s. For the present case $\arg\{\beta^2/4\alpha\} = \pi$, and the steepest-descent contribution dominates. One finds this by inserting eq. 8.32 into eq. 8.34 to obtain

$$Q(s) \sim \frac{\alpha^{1-s}}{2} \left(-\frac{\beta^2}{4}\right)^{s/2-1} \exp\left(-\frac{\beta^2}{4\alpha}\right) \exp\left(\frac{i\pi\,\nu}{2}\right), \qquad \left|\frac{\beta^2}{\alpha}\right| >> 1. \tag{8.44}$$

For $s = 1$ this result is identical to eq. 8.43. The case of arbitrary s is not generally available.

REFERENCES

1. Gradshteyn, I. S., Ryzhik, I. M., *Table of Integrals, Series, and Products*, Academic Press, New York,(1980).
2. Luke, Y., *The Special Functions and Their Approximations*, Academic Press, New York, (1969).
3. Marichev, O. I., *Integral Transforms of Higher Transcendental Functions*, Ellis Horwood Limited, Chichester, England, (1983).
4. Yura, H. T., Hanson, S. G., "Second order statistics for wave propagation through complex optical systems", *J. Opt. Soc. Am. A*, **6**, (1989) pp. 564–575.

Chapter 9

Finite Beam Characteristics As Examples with a Single Complex Parameter

In Chap. 2 I introduced a method for easily expressing in integral form the second moment of phase and log-amplitude related quantities for infinite collimated and focused waves propagating through turbulence. It was shown how these integrals could be evaluated using Mellin transform techniques. I extend these methods here to solve for the propagation of beam waves with Gaussian shape. Earlier results are a special case of this more general case. To express results as integrals, the approach in Chap. 2 is followed to the point where the propagation parameter γ was assumed to be real. Here γ must be complex to handle beams of finite extent. I derive the filter function for two counterpropagating or copropagating waves.

The filter function for the general case has a complex propagation parameter, which results in functions with exponential growth in the integrand. The Mellin convolution integral was generalized to this contingency in the last chapter by applying Parseval's equality. The Taylor series obtained using pole-residue integration are not more difficult to derive in this case. For large parameters I derive asymptotic expressions that have a more complicated dependence than for the infinite-wave case, because the functional form can change depending on the argument of the propagation constant in the complex plane. The method is applied to find the scintillation on a beam wave.

Recent results from computer simulations show that these results are not correct for every geometry. The restrictions on the validity of the solution are discussed. In addition, these results only apply to the case in which the beam is tracked so that its center stays on axis. Heuristic formulas that apply in the other cases for both the tracked and untracked cases are given.

9.1 Phase and Log-Amplitude Variances of Beam Waves

The derivation of the second moment expressions for beam-wave problems is the same as in Chap. 2 up to eq. 2.95. At that point the propagation parameter γ is allowed to be complex, which requires that the succeeding equations be modified. The assumptions of a beam being on axis and not varying in size that were used in the derivation of the equations for phase and log-amplitude variations do not

apply for all beam propagation scenarios. For instance, there are cases in which the tilt jitter causes a movement of the beam that is greater than the beam diameter. In that case the turbulence does not cause a small perturbation of the field. *Charnotskii* (1964) divided the propagation space into different regions with different properties. *Baker* (2006) observed that Charnotskii's D1 region is one in which the formulas developed here are incorrect and defines two parameters

$$N_L = k_0 w_0^2 / 2L \left| 1 + L/R_0 \right|, \tag{9.1}$$

and

$$N_\tau = k_0 w_0^2 / 2z_\tau \left| 1 + z_\tau/R_0 \right|, \tag{9.2}$$

where z_τ is the location or thickness of the turbulence and R_0 is the range at which the beam is focused.

In the $D1$ region where $N_\tau > 1$ and $N_L < 1$, the formulas derived here do not apply. For other regions the formulas that are derived here are valid for the case in which the beam is tracked and kept on axis.

At the end of this chapter, formulas are given that apply for both the tracked and untracked cases for all values of the two parameters. These formulas were derived heuristically by observing the output of computer code calculations for many scenarios.

The relevant equations from Chap. 2 are repeated here as eq. 9.3 to eq. 9.11 for convenience. The phase and log-amplitude are given by

$$\begin{bmatrix} i\phi\left(\boldsymbol{\rho}, z\right) \\ \chi\left(\boldsymbol{\rho}, z\right) \end{bmatrix} = \tfrac{1}{2} \left[\Phi_1(\boldsymbol{\rho}, z) \mp \Phi_1^*(\boldsymbol{\rho}, z) \right], \tag{9.3}$$

where

$$\Phi_1(\boldsymbol{\rho}, L) = \int_0^L dz' \int d\nu\left(\boldsymbol{\kappa}, z'\right) H(\boldsymbol{\kappa}, L, z') \exp\left(i\gamma \boldsymbol{\kappa} \cdot \boldsymbol{\rho}\right), \tag{9.4}$$

$$H(\boldsymbol{\kappa}, L, z) = i k_0 \exp\left[-iP\left(\gamma, \kappa, z\right)\right], \tag{9.5}$$

$k_0 = 2\pi/\lambda$, and λ is the wavelength in the propagating medium. The requirement that the refractive index is real gives

$$d\nu(\boldsymbol{\kappa}, z) = d\nu^*(-\boldsymbol{\kappa}, z). \tag{9.6}$$

For propagation from $z = 0$ to $z = L$ the diffraction parameter is given by

$$P\left(\gamma, \kappa, z\right) = \frac{\gamma \kappa^2 (L - z)}{2 k_0}, \tag{9.7}$$

and for propagation from $z = L$ to $z = 0$, the diffraction parameter is equal to

$$P\left(\gamma, \kappa, z\right) = \frac{\gamma \kappa^2 z}{2 k_0}. \tag{9.8}$$

The value of γ is

$$\gamma = \frac{1 + i\alpha\, z}{1 + i\alpha\, L} \tag{9.9}$$

for a wave propagating from $z = 0$ to $z = L$, and

$$\gamma = \frac{1 + i\alpha\,(L - z)}{1 + i\alpha\, L} \tag{9.10}$$

for a wave propagating from $z = L$ to $z = 0$.

The value of α is

$$\alpha = \alpha_r + i\,\alpha_i = \lambda/\pi\, W_o^2 + i/R_o. \tag{9.11}$$

The parameter R_o is the radius of curvature of the beam at the source. It is equal to infinity for a collimated beam. At the radius equal to W_o, the intensity has dropped to $1/e^2$ of its value on axis.

Change the sign of κ in eq. 9.4, take the complex conjugate, use eq. 9.6 and the evenness of $H\,(\boldsymbol{\kappa}, L, z)$ with respect to κ. Substitute the result and eq. 9.4 into eq. 9.3 to obtain

$$\begin{bmatrix} i\phi\,(\boldsymbol{\rho}, L) \\ \chi\,(\boldsymbol{\rho}, L) \end{bmatrix} = \int_0^L dz' \int \frac{d\nu\,(\boldsymbol{\kappa}, z')}{2} \left[H\,(\boldsymbol{\kappa}, L, z') \exp\left(i\gamma\boldsymbol{\kappa}\cdot\boldsymbol{\rho}\right) \mp H^*\,(\boldsymbol{\kappa}, L, z') \exp\left(i\gamma^*\boldsymbol{\kappa}\cdot\boldsymbol{\rho}\right)\right]. \tag{9.12}$$

These expressions apply to a single point in space. Often the aperture average of the phase times a weighting function $g\,(\boldsymbol{\rho}\,)$ is required, as in the case of tilt. For the beam wave case, the aperture averaging function does not have to be centered on the beam axis but can be displaced by a distance $\boldsymbol{\rho}$. In that case phase and log-amplitude related quantities are

$$\begin{bmatrix} i\phi R(\boldsymbol{\rho}, L) \\ \chi R(\boldsymbol{\rho}, L) \end{bmatrix} = \frac{1}{2} \int d\boldsymbol{\rho}\,' \int_0^L dz' \int d\nu\,(\boldsymbol{\kappa}, z')\; g\,(\boldsymbol{\rho}\,' - \boldsymbol{\rho}\,)$$
$$\times \left[H(\boldsymbol{\kappa}, L, z') \exp\left(i\gamma\boldsymbol{\kappa}\cdot\boldsymbol{\rho}\,'\right) \mp H^*(\boldsymbol{\kappa}, L, z') \exp\left(i\gamma^*\boldsymbol{\kappa}\cdot\boldsymbol{\rho}\,'\right)\right]. \tag{9.13}$$

Now interchange the integration order. The integral over a finite aperture converges and is recognized as the two-dimensional Fourier transform of the aperture function

$$G\,(\gamma\boldsymbol{\kappa}\,) = \int d\boldsymbol{\rho}\,'\, g\,(\boldsymbol{\rho}\,') \exp\left(i\gamma\boldsymbol{\kappa}\cdot\boldsymbol{\rho}\,'\right) \tag{9.14}$$

with the transform variable $\gamma\boldsymbol{\kappa}$. This gives

$$\begin{bmatrix} i\phi R(\boldsymbol{\rho}, L) \\ \chi R(\boldsymbol{\rho}, L) \end{bmatrix} = \frac{1}{2} \int_0^L dz' \int d\nu(\boldsymbol{\kappa}, z')$$
$$\times \left[H(\boldsymbol{\kappa}, L, z') G(\gamma \boldsymbol{\kappa}) \exp(i\gamma \boldsymbol{\kappa} \cdot \boldsymbol{\rho}) \mp H^*(\boldsymbol{\kappa}, L, z') G(\gamma^* \boldsymbol{\kappa}) \exp(i\gamma^* \boldsymbol{\kappa} \cdot \boldsymbol{\rho}) \right]. \tag{9.15}$$

Up to now only a single wave has been considered. Generalize this to the case of finding the difference between the phase and log-amplitude of two waves that can have different propagation constants. This will allow consideration of the difference between displaced counterpropagating and copropagating waves that are focused or collimated. Let the second wave be multiplied by a quantity $A(\boldsymbol{\kappa}, z)$ that can be a function of the axial coordinate and transverse wavenumber. If this multiplier is zero, one is back to the single-wave case, and if it is a complex exponential, it corresponds to anisoplanatism. Finally, let the aperture weighting factor be different for each wave. The result is

$$\begin{bmatrix} i\phi R(\boldsymbol{\rho}, L) \\ \chi R(\boldsymbol{\rho}, L) \end{bmatrix} = \frac{1}{2} \int_0^L dz' \int d\nu(\boldsymbol{\kappa}, z')$$
$$\times \{ [H_1(\boldsymbol{\kappa}, L, z') G_1(\gamma_1 \boldsymbol{\kappa}) \exp(a_1) \mp H_1^*(\boldsymbol{\kappa}, L, z') G_1(\gamma_1^* \boldsymbol{\kappa}) \exp(a_1^*)]$$
$$- A(\boldsymbol{\kappa}, z') [H_2(\boldsymbol{\kappa}, L, z') G_2(\gamma_2 \boldsymbol{\kappa}) \exp(a_2) \mp H_2^*(\boldsymbol{\kappa}, L, z') G_2(\gamma_2^* \boldsymbol{\kappa}) \exp(a_2^*)] \}, \tag{9.16}$$

where $a_n = i\gamma_n \boldsymbol{\kappa} \cdot \boldsymbol{\rho}$.

The second moment of this quantity is found by multiplying it by its complex conjugate and taking the expected value. The same manipulations as between eq. 2.107 and eq. 2.110 are applied to eliminate integrations over κ and the axial coordinate, to obtain

$$\begin{bmatrix} \sigma_{\phi R}^2(\boldsymbol{\rho}) \\ \sigma_{\chi R}^2(\boldsymbol{\rho}) \end{bmatrix} = \frac{0.2073}{4} \int_0^L dz\, C_n^2(z) \int d\boldsymbol{\kappa}\, f(\kappa)$$
$$\times \{ [H_1(\boldsymbol{\kappa}, L, z) G_1(\gamma_1 \boldsymbol{\kappa}) \exp(a_1) \mp H_1^*(\boldsymbol{\kappa}, L, z) G_1(\gamma_1^* \boldsymbol{\kappa}) \exp(a_1^*)]$$
$$- A(\boldsymbol{\kappa}, z) [H_2(\boldsymbol{\kappa}, L, z) G_2(\gamma_2 \boldsymbol{\kappa}) \exp(a_2) \mp H_2^*(\boldsymbol{\kappa}, L, z) G_2(\gamma_2^* \boldsymbol{\kappa}) \exp(a_2^*)] \}$$
$$\times \{ [H_1^*(\boldsymbol{\kappa}, L, z) G_1^*(\gamma_1 \boldsymbol{\kappa}) \exp(-a_1^*) \mp H_1(\boldsymbol{\kappa}, L, z) G_1^*(\gamma_1^* \boldsymbol{\kappa}) \exp(-a_1)]$$
$$- A^*(\boldsymbol{\kappa}, z) [H_2^*(\boldsymbol{\kappa}, L, z) G_2^*(\gamma_2 \boldsymbol{\kappa}) \exp(-a_2^*) \mp H_2(\boldsymbol{\kappa}, L, z) G_2^*(\gamma_2^* \boldsymbol{\kappa}) \exp(-a_2)] \}. \tag{9.17}$$

This is the central formula for beam-wave problems and is the analog of eq. 2.110. This expression does not simplify as nicely as its analog did for the

special cases considered in Chap. 2. Consequently, only the expression for a single beam will be treated explicitly. If there is only one beam, $A(\boldsymbol{\kappa}, z)$ is zero.

The above expression, which has two exponentials with opposite signs, can be simplified by using the evenness of $H(\boldsymbol{\kappa}, L, z)$ and $f(\kappa)$ with respect to κ and the relation $G(\gamma\boldsymbol{\kappa}) = G^*(-\gamma^*\boldsymbol{\kappa})$, which comes from the Fourier-transform definition in eq. 9.14. If in addition $G(\gamma\boldsymbol{\kappa})$ is even in κ, which it is for all filter functions considered in this book, then eq. 9.17 reduces to

$$\begin{bmatrix} \sigma^2_{\phi R}(\boldsymbol{\rho}) \\ \sigma^2_{\chi R}(\boldsymbol{\rho}) \end{bmatrix} = \frac{0.2073}{2} \int_0^L dz\, C_n^2(z) \int d\boldsymbol{\kappa}\, f(\kappa)$$
$$\times \Big(|H(\boldsymbol{\kappa}, L, z)\, G(\gamma\boldsymbol{\kappa})|^2 \exp(-2\gamma_i \boldsymbol{\kappa}\cdot\boldsymbol{\rho}) \mp \mathrm{Re}\Big\{ [H(\boldsymbol{\kappa}, L, z)]^2 G(\gamma\boldsymbol{\kappa})\, G(-\gamma\boldsymbol{\kappa}) \Big\} \Big). \tag{9.18}$$

For the Zernike modes defined in eq. 3.7 to eq. 3.10, $G(-\gamma\boldsymbol{\kappa}) = (-1)^m G(\gamma\boldsymbol{\kappa})$, where m is the order of the azimuthal mode.

In a similar manner the correlation function can be found. If the phase and amplitude related quantities in eq. 9.15 are multiplied by the same functions displaced by $\mathbf{d}$, then one obtains

$$\begin{bmatrix} B_{\phi R}(\boldsymbol{\rho},\, \mathbf{d}) \\ B_{\chi R}(\boldsymbol{\rho},\, \mathbf{d}) \end{bmatrix} = \frac{0.2073}{4} \int_0^L dz\, C_n^2(z) \int d\boldsymbol{\kappa}\, f(\kappa)$$
$$\times \Big[|H(\boldsymbol{\kappa}, L, z)\, G(\gamma\boldsymbol{\kappa})|^2 \exp(-2\gamma_i \boldsymbol{\kappa}\cdot\boldsymbol{\rho}) \left[\exp(-i\gamma\boldsymbol{\kappa}\cdot\mathbf{d}) + \exp(-i\gamma^*\boldsymbol{\kappa}\cdot\mathbf{d}) \right]$$
$$\mp \Big\{ [H(\boldsymbol{\kappa}, L, z)]^2\, G(\gamma\boldsymbol{\kappa})\, G(-\gamma\boldsymbol{\kappa}) \exp(-i\gamma\boldsymbol{\kappa}\cdot\mathbf{d})$$
$$+ [H^*(\boldsymbol{\kappa}, L, z)]^2 G(\gamma^*\boldsymbol{\kappa})\, G(-\gamma^*\boldsymbol{\kappa}) \exp(-i\gamma^*\boldsymbol{\kappa}\cdot\mathbf{d}) \Big\} \Big]. \tag{9.19}$$

From eq. 9.5 and eq. 9.7 for a wave going from $z = 0$ to L, one obtains

$$|H(\boldsymbol{\kappa}, L, z)|^2 = k_0^2 \exp\left[\gamma_i \kappa^2 (L - z)/k_0 \right], \text{ and} \tag{9.20}$$

$$\mathrm{Re}\left\{ H(\boldsymbol{\kappa}, L, z)^2 \right\} = -\mathrm{Re}\left\{ k_0^2 \exp\left[-i\gamma\kappa^2 (L - z)/k_0 \right] \right\}, \tag{9.21}$$

where γ is expressed in real and imaginary parts as

$$\gamma = \gamma_r + i\gamma_i. \tag{9.22}$$

Insert these relations into eq. 9.18 to obtain

$$\begin{bmatrix} \sigma^2_{\phi R}(\boldsymbol{\rho}) \\ \sigma^2_{\chi R}(\boldsymbol{\rho}) \end{bmatrix} = \frac{0.2073\, k_0^2}{2} \int_0^L dz\, C_n^2(z) \int d\boldsymbol{\kappa}\, f(\kappa)$$
$$\times \left[F(\gamma\boldsymbol{\kappa}) \exp(\gamma_i b) \exp(-2\gamma_i \boldsymbol{\kappa}\cdot\boldsymbol{\rho}) \pm (-1)^m \mathrm{Re}\left\{ \exp(-i\gamma b)\, G^2(\gamma\boldsymbol{\kappa}) \right\} \right], \tag{9.23}$$

where $b = \kappa^2(L-z)/k_0$, and $F(\gamma\boldsymbol{\kappa}) = G(\gamma\boldsymbol{\kappa})\,G^*(\gamma\boldsymbol{\kappa})$. For γ real this reduces to the result in eq. 2.112. The real expression in the last term can be expressed as the exponential of the real part times the cosine of the imaginary part of the argument. This form is closer to the form in eq. 2.112 when γ is real. Although it is tempting to do this, I will not, since it results in an integral with an additional parameter, thereby complicating evaluation.

On axis the variances are

$$\begin{bmatrix}\sigma^2_{\phi R}(\boldsymbol{\rho})\\ \sigma^2_{\chi R}(\boldsymbol{\rho})\end{bmatrix} = \frac{0.2073\,k_0^2}{2}\int_0^L dz\,C_n^2(z)\int d\boldsymbol{\kappa}\,f(\kappa)\exp\left(\gamma_i\kappa^2(L-z)/k_0\right)$$
$$\times\left[F(\gamma\boldsymbol{\kappa}) \pm (-1)^m\,\mathrm{Re}\left\{\exp(-i\,\gamma_r b)\,G^2(\gamma\boldsymbol{\kappa})\right\}\right]. \tag{9.24}$$

If the filter function is unity, then this reduces to a form similar to (2.112)

$$\begin{bmatrix}\sigma^2_{\phi R}\\ \sigma^2_{\chi R}\end{bmatrix} = 0.2073\,k_0^2\int_0^L dz\,C_n^2(z)\int d\boldsymbol{\kappa}\,f(\kappa)\begin{bmatrix}\cos^2[P(\gamma,\kappa,z)]\\ \sin^2[P(\gamma,\kappa,z)]\end{bmatrix}\exp\left(\frac{\gamma_i\kappa^2(L-z)}{k_0}\right). \tag{9.25}$$

In a similar way the correlation function can be expressed as

$$\begin{bmatrix}B_{\phi R}(\boldsymbol{\rho},\,\mathbf{d})\\ B_{\chi R}(\boldsymbol{\rho},\,\mathbf{d})\end{bmatrix} = \frac{0.2073\;k_0^2}{4}\int_0^L dz\,C_n^2(z)\int d\boldsymbol{\kappa}\,f(\kappa)$$
$$\times\Big[|G(\gamma\boldsymbol{\kappa})|^2\exp(\gamma_i b)\exp(-2\gamma_i\,\boldsymbol{\kappa}\cdot\boldsymbol{\rho})\left[\exp(-i\gamma\boldsymbol{\kappa}\cdot\mathbf{d}) + \exp(-i\gamma^*\boldsymbol{\kappa}\cdot\mathbf{d})\right]$$
$$\pm\Big\{\left[\exp(-i\gamma b)\right]^2 G(\gamma\boldsymbol{\kappa})\,G(-\gamma\boldsymbol{\kappa})\exp(-i\gamma\boldsymbol{\kappa}\cdot\mathbf{d})$$
$$+\left[\exp(i\gamma^* b)\right]^2 G(\gamma^*\boldsymbol{\kappa})\,G(-\gamma^*\boldsymbol{\kappa})\exp(-i\gamma^*\boldsymbol{\kappa}\cdot\mathbf{d})\Big\}. \tag{9.26}$$

If $G(\gamma\boldsymbol{\kappa})$ does not depend on angle, the angular integration can be performed readily to give

$$\begin{bmatrix}\sigma^2_{\phi R}(\boldsymbol{\rho})\\ \sigma^2_{\chi R}(\boldsymbol{\rho})\end{bmatrix} = \frac{1.303\,k_0^2}{2}\int_0^L dz\,C_n^2(z)\int_0^\infty d\kappa\,\kappa\,f(\kappa)$$
$$\times\left(F(\gamma\kappa)\exp(\gamma_i b)\,J_0(2i\gamma_i\kappa\rho) \pm (-1)^m\,\mathrm{Re}\left\{\exp(-i\gamma b)\,G^2(\gamma\kappa)\right\}\right). \tag{9.27}$$

The correlation function for this case is

$$\begin{bmatrix}B_{\phi R}(\boldsymbol{\rho},\,\mathbf{d})\\ B_{\chi R}(\boldsymbol{\rho},\,\mathbf{d})\end{bmatrix} = 0.3256\;k_0^2\int_0^L dz\,C_n^2(z)\int_0^\infty \kappa\,d\kappa\,f(\kappa)$$
$$\times\Big\{|G(\gamma\kappa)|^2\left[J_0(\kappa\,|2i\gamma_i\,\boldsymbol{\rho}-\gamma\mathbf{d}|) + J_0(\kappa\,|2i\gamma_i\,\boldsymbol{\rho}-\gamma^*\mathbf{d}|)\right]$$
$$\mp\left[\exp(-i\gamma b)\,G(\gamma\kappa)\,G(-\gamma\kappa)J_0(\gamma\kappa d)\right.$$
$$\left.+\exp(i\gamma^* b)\,G(\gamma^*\kappa)\,G(-\gamma^*\kappa)J_0(\gamma^*\kappa d)\right]\Big\}. \tag{9.28}$$

One can find the equivalent expressions for the structure function.

9.2 Power Spectral Density of Beam Waves

The derivation of power spectral density follows the same procedure that was used in Chap. 2. The arguments that lead up to eq. 2.134 also apply here, to obtain for the power spectral density of a single wave,

$$\begin{bmatrix} S_\phi(\omega) \\ S_\chi(\omega) \end{bmatrix} = 1.303\, k_0^2\, \omega \int_0^L dz\, \frac{C_n^2(z)}{v^2(z)} \int_0^\infty dc\, \frac{c\, U(c-1)}{\sqrt{c^2-1}}\, f\left[\frac{\omega\, c}{v\,(z)}\right] F_f(\omega)$$

$$\times \left(\exp\left[\frac{\gamma_i \omega^2 c^2 (L-z)}{v^2(z) k_0}\right] F\left[\frac{\gamma\, \omega\, c}{v(z)}\right] J_0\left[\frac{2 i \gamma_i \omega c \rho}{v(z)}\right] \right.$$

$$\left. \pm (-1)^m \,\mathrm{Re}\left\{ \exp\left[-i \frac{\gamma \omega^2 c^2 (L-z)}{v^2(z) k_0}\right] G^2\left[\frac{\gamma\, \omega\, c}{v(z)}\right] \right\} \right), \tag{9.29}$$

where $F_f(\omega)$ is the response of a servo system.

This reduces to the earlier results for collimated and spherical waves when the appropriate values of gamma are inserted. As with the variance, these formulas only apply to a beam that is tracked and the geometry is such that one is not in the $D1$ region. I shall not consider further the power spectral density of a beam wave.

9.3 Scintillation on Beam Waves

An adaptive-optics system requires a reference wave that propagates along the same path that is to be imaged or along which a laser beam is to be propagated. The reference wave provides information used to deform a mirror to correct for turbulence. It can be generated by an active source on the target or by a laser signal reflected from a retroreflector on the target. A minimum return energy is necessary to drive the wavefront sensor that measures the integrated turbulence distribution. For good performance the signal must also not drop out too frequently due to scintillation fades. To properly design a beacon transmitter one needs to know the intensity and scintillation for various beacon-transmitter diameters and wavelengths. Knowledge of the variation of average intensity and scintillation as one moves off the optical axis is necessary to specify the accuracy of the reference-wave tracking system. This set of problems is analyzed for collimated beams in this section.

The analysis of this problem is complicated since different effects occur as the transmitter diameter varies. For very small diameters, scintillation approaches that of a point source, and for very large diameters, the scintillation approaches that of an infinite plane wave. Scintillation of the plane wave is several orders of magnitude larger than that of a point source for typical target ranges. In the intermediate range the behavior is complicated by two factors. As the diameter gets larger the beamwidth gets smaller than the turbulence-induced-tilt jitter. In this regime there is a rapid increase in scintillation with increasing beam

diameter. For smaller apertures one finds that scintillation can decrease with increasing diameter. For intermediate size apertures, the scintillation of a beam wave on axis can be less than that of a point source.

Scintillation also varies with the distance off axis. It will be shown that the scintillation can grow rapidly as one moves away from beam boresight.

This problem has been partially analyzed by others. *Ishimaru* (1969, 1978a, 1978b) develops an expression for scintillation of a beam wave. The formula applies to the general case in which turbulence is allowed to vary along the propagation path; however, he evaluates the expression only for constant turbulence strength along the beam path. *Kinoshita* et al. (1968) also finds the scintillation for constant turbulence, but with a Gaussian correlation function. The scintillation for propagation with constant turbulence strength was found by *Fried* and *Siedman* (1967), and for ground-to-space-propagation where the turbulence is not constant by *Fried* (1967). The Kolmogorov turbulence spectrum is used in these calculations. In *Fried* (1967), the approximation is made that the target is well into the far field of the beam, which implies that the diameter cannot be large, yet the analysis is carried out to large beams, for which it is found that the scintillation decreases as the $-7/3$ power of the Gaussian beam size. It is not clear to what range of diameters this solution applies.

To obtain an expression for scintillation of a wave that propagates from ground to space, use eq. 9.27 with the aperture filter function set equal to unity to obtain

$$\sigma_\chi^2(\boldsymbol{\rho}) = 0.2073\,\pi\,k_0^2 \int_0^L dz\, C_n^2(z) \int_0^\infty d\kappa\,\kappa\, f(\kappa)$$
$$\times \left(J_0(2i\gamma_i\,\kappa\,\rho) \exp\left[\frac{\gamma_i\,\kappa^2(L-z)}{k_0}\right] - \mathrm{Re}\left\{\exp\left[i\frac{\gamma\,\kappa^2(L-z)}{k_0}\right]\right\}\right). \tag{9.30}$$

The propagation parameter is given in terms of its real and imaginary parts as

$$\gamma_r = \frac{1+\alpha^2 z\,L}{1+(\alpha\,L)^2} = \frac{F_N + F_N^{-1}\,z/L}{F_N + F_N^{-1}}, \quad \text{and} \tag{9.31}$$

$$\gamma_i = -\frac{\alpha(L-z)}{1+(\alpha\,L)^2} = -\frac{1-z/L}{F_N + F_N^{-1}}, \tag{9.32}$$

and the Fresnel number is defined to be

$$F_N = \mathrm{Re}\,(1/\alpha\,L) = \pi\,W_o^2/\lambda\,L. \tag{9.33}$$

For a collimated beam $\alpha = \lambda/\pi W_o^2$. The inner scale of turbulence with the Tatarski spectrum can be included without an increase in complexity of the expression. The spectrum given in eq. 2.34 is used with infinite outer scale. After the use of these relations, the log-amplitude variance is equal to

$$\sigma_\chi^2(\rho) = 0.2073\,\pi\,k_0^2 \int_0^L dz\, C_n^2(z) \int_0^\infty \frac{d\kappa}{\kappa}\, \kappa^{-5/3}$$
$$\times\left(J_0\left(2i\gamma_i\,\kappa\,\rho\right) \exp\left[\frac{\gamma_i\,\kappa^2(L-z)}{k_0} - \frac{\kappa^2}{\kappa_i^2}\right] - \mathrm{Re}\left\{\exp\left[-i\frac{\gamma\,\kappa^2(L-z)}{k_0} - \frac{\kappa^2}{\kappa_i^2}\right]\right\}\right). \tag{9.34}$$

Each integral diverges due to a simple pole at the origin. The residues at these two poles cancel, so the region of validity of the integral can be analytically continued, which enables these integrals to be evaluated with Mellin transforms.

The Bessel function can be left with an imaginary argument because the exponential that multiplies it causes the integrand to go to zero at infinity. As shown in the previous chapter, one can obtain the Mellin transform of this function.

Make the changes of variables $A^2 = -\gamma_i(L-z)/k_0 + 1/\kappa_i^2$, $B^2 = i\gamma(L-z)/k_0 + 1/\kappa_i^2$, and $\kappa A = x$ in the first integral, and $\kappa B = x$ in the second, and $y = A/2i\gamma_i\,\rho$. The integral is then equal to

$$\sigma_\chi^2(\rho) = 0.2073\,\pi\,k_0^2 \int_0^L dz\, C_n^2(z)$$
$$\times\left(A^{5/3}\int_0^\infty \frac{dx}{x}\, x^{-5/3} \exp\left(-x^2\right) J_0\left(x/y\right) - \mathrm{Re}\left\{ B^{5/3}\int_0^\infty \frac{dx}{x}\, x^{-5/3} \exp\left(-x^2\right)\right\}\right)$$
$$= 0.1037\,\pi\,k_0^2\,\Gamma\left[-\tfrac{5}{6}\right] \int_0^L dz\, C_n^2(z)\,\left(I_1 - I_2\right). \tag{9.35}$$

The second integral in braces with the pole contribution neglected, which is designated by the d superscript, is equal to

$$I_2^d = \frac{2}{\Gamma\left[-\frac{5}{6}\right]} \mathrm{Re}\left\{\frac{B^{5/3}}{2}\,\Gamma[s/2]|_{s=-5/3}\right\} = \mathrm{Re}\left\{B^{5/3}\right\}. \tag{9.36}$$

The Mellin convolution theorem and the substitution $s \to -2s$ in the first integral gives

$$I_1 = \frac{A^{5/3}}{\Gamma\left[-\frac{5}{6}\right]} \frac{1}{2\,\pi\,i} \int_C ds\, \left(-\frac{\gamma_i^2\,\rho^2}{A^2}\right)^{-s} \Gamma\begin{bmatrix} -s-\frac{5}{6}, s \\ -s+1 \end{bmatrix}. \tag{9.37}$$

The pole locations and integration path are shown in Fig. 9.1.

Since $\Delta = 1$, close the integration path to the left, and obtain pole contributions at $s = -n$ for $n = 0,\, 1,\, 2, \ldots$. As explained above, the residue at $s = -5/6$ is cancelled by an opposite contribution from the second integral so this pole contribution can be neglected. The integral is thus effectively equal to

$$I_1^d = \frac{A^{5/3}}{\Gamma\left[-\frac{5}{6}\right]} \sum_{n=0}^\infty \frac{1}{n\,!} \left(\frac{\gamma_i^2\,\rho^2}{A^2}\right)^n \Gamma\begin{bmatrix} n-\frac{5}{6} \\ n+1 \end{bmatrix} = A^{5/3}\,{}_1F_1\left[-\tfrac{5}{6}; 1; \frac{\gamma_i^2\,\rho^2}{A^2}\right]. \tag{9.38}$$

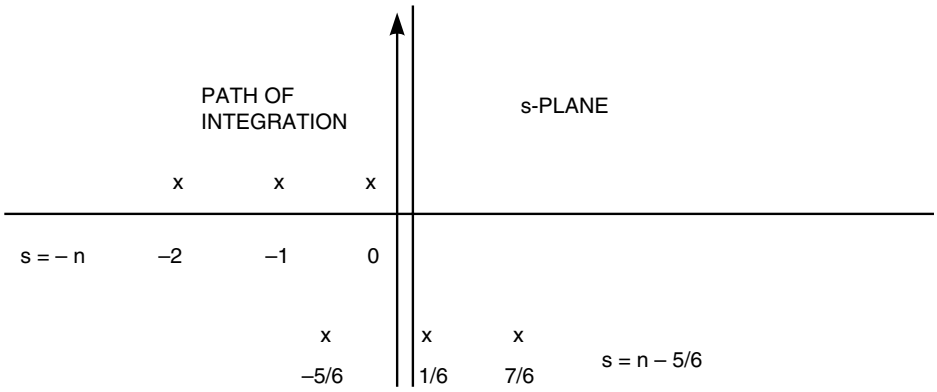

Figure 9.1. Pole locations and integration path for the beam-wave scintillation problem.

When the parameter is large, an asymptotic series is appropriate. The steepest-descent contribution given in eq. 5.94 grows exponentially; therefore, the pole contributions are negligible, and the asymptotic series is

$$I_1 \sim \frac{A^{5/3}}{\Gamma\left[-\frac{5}{6}\right]} \left(\frac{A^2}{\gamma_i^2 \rho^2}\right)^{11/6} \exp\left(\frac{\gamma_i^2\, \rho^2}{A^2}\right). \tag{9.39}$$

Using these results, one obtains for the Taylor series solution

$$\sigma_\chi^2(\rho) = \frac{2.176\, k_0^{7/6} L^{5/6}}{\left(F_N + F_N^{-1}\right)^{5/6}} \int_0^L dz\, C_n^2(z)\, (1 - z/L)^{5/3}$$

$$\times \mathrm{Re}\left\{ \left[i \frac{F_N + F_N^{-1} z/L}{(1 - z/L)} + 1 + \zeta \right]^{5/6} - (1+\zeta)^{5/6}\, {}_1F_1\left[-\tfrac{5}{6}; 1; \frac{k_0\, \rho^2/L}{\left(F_N + F_N^{-1}\right)(1+\zeta)} \right] \right\}, \tag{9.40}$$

where

$$\zeta = \frac{k_0 \left(F_N + F_N^{-1}\right)}{L \kappa_i^2\, (1 - z/L)^2}. \tag{9.41}$$

This expression is valid out to radii for which the paraxial assumption holds, which requires that $\rho^4 << L^3 \lambda$ as discussed in Sec. 2.3.

If the turbulence is constant along the propagation path, this result reduces to that obtained by Ishimaru. This also reduces to the standard results for a collimated or focused infinite wave. For a collimated infinite wave the Fresnel number is infinite, and the scintillation variance with zero inner-scale is

$$\sigma_\chi^2(\rho) = \lim_{F_N \to \infty} \frac{2.175\, k_0^{7/6}}{\left(F_N + F_N^{-1}\right)^{5/6}} \mathrm{Re}\left\{ \int_0^L dz\, C_n^2(z) \left[i\left(F_N + F_N^{-1} z/L\right)\right]^{5/6} (L-z)^{5/6} \right\}$$
$$= 2.176\, k_0^{7/6} \mathrm{Re}\left\{ i^{5/6} \right\} \int_0^L dz\, C_n^2(z)\, (L-z)^{5/6} = 0.5631\, k_0^{7/6} \int_0^L dz\, C_n^2(z)\, (L-z)^{5/6}, \tag{9.42}$$

since $\mathrm{Re}\left\{ i^{5/6} \right\} = \cos(5\pi/12) = 0.2588$. As the diameter goes to zero the Fresnel number goes to zero and one obtains

$$\sigma_\chi^2(\rho) = \lim_{F_N \to 0} \frac{2.176\, k_0^{7/6}}{\left(F_N + F_N^{-1}\right)^{5/6}} \mathrm{Re}\left\{ \int_0^L dz\, C_n^2(z) \left[i\left(F_N + F_N^{-1} z/L\right)\right]^{5/6} (L-z)^{5/6} \right\}$$
$$= 0.5631\, k_0^{7/6} \int_0^L dz\; C_n^2(z) (L-z)^{5/6}\, (z/L)^{5/6}\,. \tag{9.43}$$

The limiting expressions in eq. 9.42 and eq. 9.43 are the same as in eq. 4.75 and eq. 4.80. In this limit even though the inverse of the Fresnel number goes to infinity, it is multiplied by the altitude. For sufficiently small altitudes this limit is not valid. One requires $z \gg \pi^2 W_0^4/\lambda^2 L$ for this limit to be valid. If the turbulence contribution below that)altitude is significant, then the scintillation can differ from the limiting value.

Fig. 9.2 shows the log-amplitude variance versus Fresnel number for various target distances, normalized to scintillation of a point source given by eq. 9.43. The scintillation approaches that of a point source for small aperture sizes. As the aperture size increases, the scintillation decreases initially and then increases to approach the value for an infinite diameter source. The results plotted are correct only when $\sigma_\chi^2 < 0.5$ because above this value the Rytov approximation breaks down, and scintillation is less than that calculated above. For a system that operates at 0.5-μm wavelength with the Hufnagel-Valley 21 turbulence model, the point source scintillation is 0.059; therefore, the results when the normalized scintillation is above 4 are too high.

As the distance increases the formulas predict that the value of the scintillation in the dip gets lower. This is an incorrect result. The scintillation found from computer simulations does not have as much as a pronounced dip. The computer simulations also show that for the untracked case that the scintillation starts increasing at lower Fresnel numbers.

Scintillation with inner-scale sizes of 10 mm and zero at a target distance of 500 km are plotted versus the Fresnel number in Fig. 9.3. For larger Fresnel numbers the two curves are identical. An inner-scale size of 1 mm, a value that is often quoted as typical, produces scintillation that is virtually identical to that with zero inner scale.

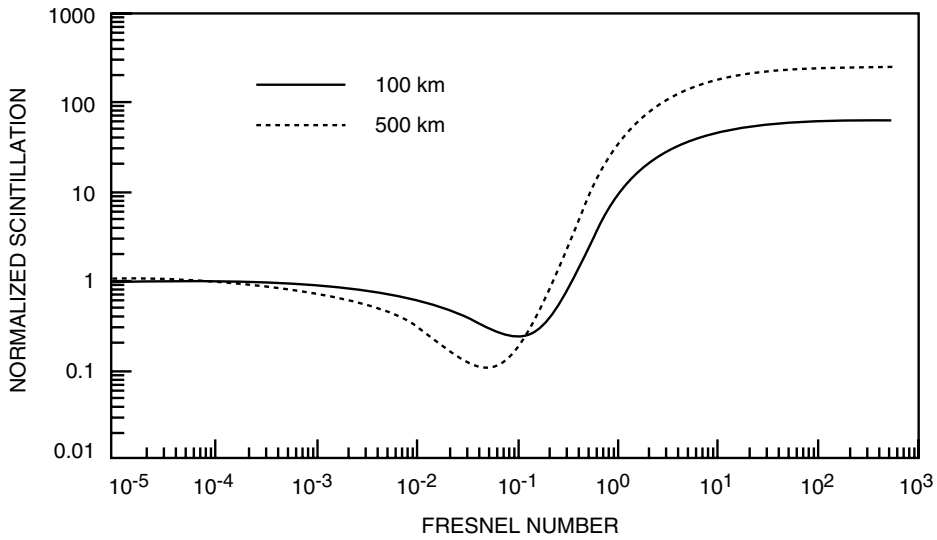

Figure 9.2. Scintillation on axis versus Fresnel number for a target at 100- and 500-km range for HV-21 turbulence. The Fresnel number is defined in eq. 9.33. The scintillation is normalized by that of a point source.

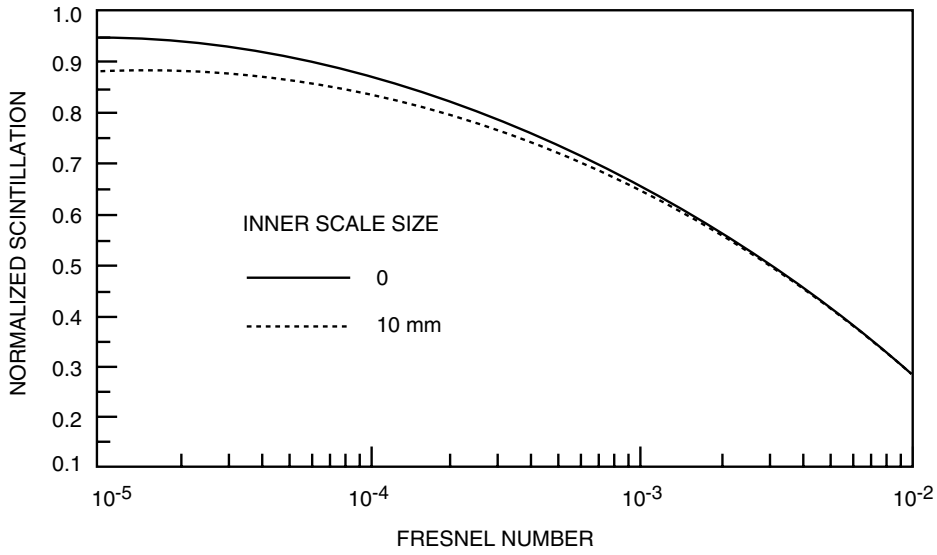

Figure 9.3. Scintillation on axis versus Fresnel number for a target at 500 km with HV-21 turbulence and inner scale of zero and 10 mm.

Scintillation as a function of distance off axis is considered for several specific cases that are close to the minimum of the scintillation curve in Fig. 9.2. Consider a target at 500 km, with a system that operates in the visible at 0.5-μm wavelength. The value of $\sqrt[4]{L^3 \lambda}$ is 500 meters; therefore, the paraxial assumption is valid to about 50 meters off axis. For beam radii of 0.625, 1.25, and 2.5 cm, the beam waist at 500 km is 12, 6, and 3 meters, respectively. Fig. 9.4 shows the scintillation out to those radii for these three cases. Notice that even though scintillation on axis is smaller for a 2.5-cm beam, it increases more rapidly away from beam center than for beams that started off with smaller beam waists at the transmitter. These results can be used to do a tradeoff in a beacon illumination system between tracking accuracy versus laser power required to get an intensity above a certain level at a space target.

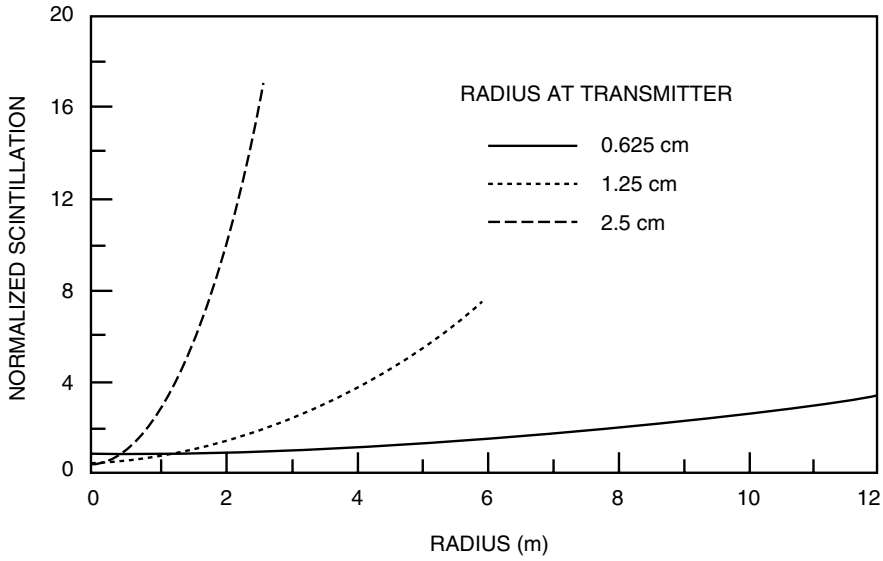

Figure 9.4. Normalized scintillation versus distance from the beam center at a 500 km target for various transmitted beam sizes, for the HV-21 turbulence model. The increase of scintillation with distance off axis is a strong function of beam size.

9.4 Heuristic Scintillation Formulas

As mentioned, the beam-wave formulas that were derived do not apply to all situations. Expressions for the variance of scintillation for the tracked and untracked case were derived by observing the output of many computer runs. The process of doing that is contained in Parenti et al. (2005). These formulas apply even in saturated scintillation.

The scintillation for the untracked case is

$$\sigma_I^2 = \frac{\sqrt{[\sigma_I^2]_{FF}^2 + [\sigma_I^2]_{NF}}}{1 + \exp\left[-3r_0/w_0\right][\sigma_I^2]_{NF}}. \tag{9.44}$$

If the object is tracked, then the phase distortion is the figure distortion. The scintillation for the tracked case with the focus at the target is

$$\left[\sigma_I^2\right]_{fig} = \frac{\sqrt{[\sigma_I^2]_{FF}^2 + [\sigma_I^2]_{NF,fig}}}{1 + \exp\left[-3r_0/w_0\right][\sigma_I^2]_{NF,fig}}, \tag{9.45}$$

where

$$\left[\sigma_I^2\right]_{FF} = 2.25k_0^{7/6}\int_0^L dz\; z^{5/6}(1-z/L)^{5/6}\left[1 + 1.39(1-z/L)\frac{k_0 w_0^2}{z}\right]^{-7/6} C_n^2(z), \tag{9.46}$$

$$\left[\sigma_I^2\right]_{NF} = 0.550k_0^2 w_0^{5/3}\int_0^L dz\; (1-z/L)^{5/3} C_n^2(z), \tag{9.47}$$

and

$$\left[\sigma_I^2\right]_{NF,fig} = 0.0234k_0^{14/5} w_0^{7/3}\left[\int_0^L dz\; (1-z/L)^{5/3} C_n^2(z)\right]^{7/5}. \tag{9.48}$$

For both cases of tilt present and removed the intensity variance approaches unity as the diameter gets very large.

REFERENCES

1. Charnotskii, M. I., "Asymptotic analysis of finite beam scintillation in a turbulent medium", *Waves Random Media*, **4**, (1994) pp. 243–273.
2. Baker, G. J., "Scintillation of a Ground-to-Space Laser Illuminator", *J. Opt. Soc. Am. A*, **57**, (1967) pp. 980–983.
3. Fried, D., "Scintillation of a Ground-to-Space Laser Illuminator", *J. Opt. Soc. Am.*, **57**, (1967) pp. 980–983.
4. Fried, D., Seidman, J., "Laser-Beam Scintillation in the Atmosphere", *J. Opt. Soc. Am.*, **57**, (1967) pp. 181–185.
5. Ishimaru, A., "Fluctuations of a beam wave propagating through a locally homogeneous medium", *Radio Sci.*, **4**, (1969) pp. 293–305.
6. Ishimaru, A., *Laser Beam Propagation in the Atmosphere* (Edited by Strohbehm, J.W.) Springer-Verlag, Berlin, (1978).

7. Ishimaru, A., *Wave Propagation and Scattering in Random Media*, Academic Press, New York, (1978).
8. Kinoshita, Y., Asakura, T., Suzuki, M.,"Fluctuation Distribution of a Gaussian Beam Propagating Through a Random Medium", *J. Opt. Soc. Am.*, **58**, (1968) pp. 798–807.
9. Parenti, R. R., Sasiela, R. J.,"Distribution Models for Optical Scintillation Due to Atmospheric Turbulence", *Lincoln Laboratory Technical Report TR-1108*, (12 Dec. 2005).

Chapter 10

Mellin Transforms in N Complex Planes

In Chaps. 4 and 6 Mellin transform techniques were used to solve problems of wave propagation through turbulence in which there was zero or one parameter. Here, that technique is generalized to allow one to solve problems with any number of parameters. Analytical solutions that are easily evaluated are obtained for problems that have previously been considered analytically intractable and for which only numerical results are available. The method to obtain the solution in integral form by the insertion of the transverse spatial filter functions into the standard formula for variances is exactly the same as that discussed in Chap. 2. This process produces a three-dimensional integral over the transverse spatial-transform coordinates and the propagation path. The integration over angle in transform space can usually be performed analytically. The integration over the magnitude of the spatial transform coordinate in which there are two or more parameters in the integrand is addressed in this chapter. I show that it can be evaluated to give a series solution. The remaining integration over the propagation path can be performed term by term in most cases. For some cases the infinite series terms after the axial integration are infinite, in which cases one must evaluate the integration along the propagation direction first.

The integration over the magnitude of the transform coordinate is the one that is difficult. For some problems, more than one parameter remains in the integrand after a normalization of the variables. For N parameters, this integral can be transformed into an integral in N complex planes with the Mellin convolution integral extended to N functions given in eq. 1.30 as

$$h\left(x_1,\ldots,x_N\right)=\int_0^\infty \frac{dy}{y}\,h_0(y)\prod_{j=1}^{N}h_j\left(x_j/y\right)\rightarrow M\left[h\left(x_1,\ldots,x_N\right)\right]$$
$$=H_0\left(s_1+s_2+\cdots+s_N\right)\prod_{j=1}^{N}H_j\left(s_j\right)=H\left(s_1,s_2,\ldots,s_N\right). \tag{10.1}$$

The original integral is equal to an integration in N complex planes given by

$$h\left(x_1,\ldots,x_N\right)=\frac{1}{\left(2\pi i\right)^N}\int_{C_1}\cdots\int_{C_N}ds_1\cdots ds_N\,H\left(s_1,s_2,\ldots,s_N\right)x_1^{-s_1}\ldots x_N^{-s_N}. \tag{10.2}$$

For the problems that are considered here, the function $H(s_1, s_2, \ldots, s_N)$ is the product of ratios of gamma functions. The evaluation of integrals of this type is an area of mathematics that is not well developed. Pole-residue integration cannot easily be applied in problems; also, the steepest-descent contributions for the asymptotic series have been evaluated only for limited conditions. Because the complex variables appear either alone or in sums, however, *Shelton* and *I* (1993) have been able to extend pole-residue integration into this new area. I show how to evaluate these integrals and develop Taylor series and asymptotic solutions. The technique to select which power series apply for different parameter regimes is new.

If a function in the integrand of the original integral has the first term of its power series subtracted from it, the integration path moves over one pole as it did in the single-parameter case. This property eliminates difficulties one encounters in evaluating some integrals numerically. Deciding which pole residues contribute is more difficult than in the single-parameter case; however, procedures are given to make those decisions.

The solution for multiparameter problems is reduced to a technique that is straightforward, in principle, but may be algebraically lengthy. The types of problems it is possible to solve with this technique often are very difficult to solve with standard methods.

I begin by introducing the necessary background. First, the convergence properties of multiple infinite series are examined. Next, I show that Cauchy's residue theorem can be extended into N complex planes for integrands that contain the product of ratios of gamma functions. The value of the integral depends on the residues at points at which there is a confluence of N poles. After all the possible power series are written down, which corresponds to all ways of closing contours, those that are pertinent to the parameter range of interest are selected with a simple procedure that relies on the convergence properties of the series. The justification for this approach is given in the next section where it is shown that if a power series converged, then the integration path could have been closed to enclose the poles that led to that power series.

This procedure is demonstrated on a "toy" problem in which the integrand is a product of three unit step functions. A second "toy" problem in which the integrand is the product of three exponentials is subsequently solved. In this example one clearly sees why the power series solution sometimes is valid in a parameter region that is smaller than the convergence region of the integral. This example is also used to illustrate how to evaluate integrals in which the integrand functions have terms of their power series subtracted from them.

It is straightforward to write down the solution as convergent power series. This is a complete solution to the problem. Sometimes these solutions converge slowly and require great accuracy for individual series terms; however, computer algebra programs in which one can specify the accuracy of calculation are suitable for this purpose. For faster convergence and to obtain insight into how the solution varies with the parameters, an asymptotic solution is appropriate. It is easy to find the asymptotic series. The technique to obtain the steepest-descent

contribution is more complicated than that for a single complex plane (*Bleistein* and *Handelman* 1986; *Dingle* 1973). Methods to find the asymptotic series and saddle-point contributions are developed here. Restricting the class of integrals to Mellin-Barnes integrals with certain restrictions on functions allows one to obtain readily evaluated expressions for the saddle-point contribution to the asymptotic form of the integral. Results on saddle-point contributions available in the literature are not directly applicable here because the integrals are generally not in the standard form assumed in traditional saddle-point treatments. In addition, in problems considered here, saddle-point contributions are not only necessary when all parameters in the original integral are large, but may also be required when one or more of the parameters are small. The reason behind this phenomenon is discussed in Sec. 10.4.

The form of the solutions, which is composed of the sum of multiple infinite summations, looks complicated. However, because typically few terms are necessary to get an answer that is accurate to 1%, these solutions are easy to evaluate using the recursion relations for the summations. The examples in this book were evaluated on a personal computer.

10.1 Convergence of Multi-Parameter Series

The convergence properties of power series obtained by pole-residue integration are used in Sec. 10.3 in criteria to decide whether to include a particular series in the solution. For that reason these properties are important. The conditions for convergence of multiple series are more complex than those for a single series. Books on advanced calculus discuss multiple integrals; however, they normally do not discuss multiple series. When there is a discussion (*Whittaker and Watson*) it is general, such as the statement of Pringsheim's theorem that if the sum exists, then the sum by rows and columns gives the same results. This is not useful for the purpose of this section. Specific convergence criteria that apply to series encountered in turbulence problems are developed below.

First, consider the double series

$$F(x,y) = \sum_{n=0}^{\infty} \sum_{m=0}^{\infty} A_{m,n}\, x^m y^n. \tag{10.3}$$

The series coefficients, as found by pole-residue techniques, are of the form

$$A_{m,n} = \prod_i \Gamma\left[a_i + u_i m + v_i n\right] / \Gamma\left[a_i\right], \tag{10.4}$$

where the coefficients u_i and v_i are typically either 1, -1, or 0. One achieves this form from the normal form by moving gamma functions in the denominator into the numerator with the identity $1/\Gamma\left[1-s\right] = \Gamma\left[s\right] \sin\left(\pi s\right)/\pi$. Some solutions can have the sign of $A_{m,n}$ alternate in one or both indices. If the series converges absolutely, this alternating series also converges.

The form of the coefficients in eq. 10.4 is a special case of the general function with arbitrary integer coefficients studied by *Horn* (1889). This function can be generalized to N variables, in which case the coefficients of the power series are of the form

$$A_{n_1,\ldots,\,n_N} = \prod_i \Gamma\left[a_i + c_{i1}n_1 + \cdots + c_{iN}n_N\right] / \Gamma\left[a_i\right]. \tag{10.5}$$

This is also the form of the coefficients of the residues for the typical N-parameter case. Horn derived general convergence criteria for multiple series, which are discussed for double series by *Erdélyi* (1981, p. 227) and for multiple series in *Exton* (1978, p. 30). I give here the criteria for a double series, followed by the general criteria.

The criteria for convergence give two regions of parameter space, and the region of convergence is the space within the intersection of the two regions. The first region comes from the requirement that the series must converge when one of the indices is zero. The second region results from a rearrangement of the series terms so that one obtains an infinite sum of a finite sum of terms for which the sum of the indices is the same. The two series that result are

$$F(x,y) = \sum_{n=0}^{\infty}\sum_{p=0}^{n} A_{n-p,\,p}\,x^{n-p}y^{p} = \sum_{m=0}^{\infty}\sum_{p=0}^{m} A_{p,\,m-p}\,x^{p}y^{m-p}. \tag{10.6}$$

The ratio test, which requires each successive term to decrease in the limit as the index goes to infinity, is applied to each series. In the series in eq. 10.6 it is applied to each term of the second series. To express the result in a convenient form define the functions

$$\frac{A_{m+1,\,n}}{A_{m,\,n}} = P_1(m,n), \quad \text{and} \quad \frac{A_{m,\,n+1}}{A_{m,\,n}} = P_2(m,n), \tag{10.7}$$

where it is required that these be algebraic functions, a condition that is satisfied if the coefficients of the indices (m and n) in the gamma functions are integers. Also, define

$$\Phi_1(m,n) = \lim_{\varepsilon\to\infty} P_1(\varepsilon m, \varepsilon n), \quad \text{and} \quad \eta = |y| = 1/\left|\Phi_2(0,1)\right|. \tag{10.8}$$

The first region in the $x-y$ plane is a rectangle in the quadrant in which both variables are positive. Two sides of the rectangle are formed from the x and y axes and the origin. The other two sides are the two lines

$$\xi = |x| = 1/\left|\Phi_1(1,0)\right|, \quad \text{and} \quad \eta = |y| = 1/\left|\Phi_2(0,1)\right|. \tag{10.9}$$

The second region is a surface that includes the origin and the x and y axes and is bounded by the surface that is defined by the parametric equations

$$\xi = |x| = 1/\Phi_1(m,n), \quad \text{and} \quad \eta = |y| = 1/\Phi_2(m,n). \tag{10.10}$$

This second surface may be identical to the rectangle defined above or may be a subregion of the rectangle.

For problems solved by Mellin transform techniques, the region defined by eq. 10.9 is a unit square. The parametric equations are always of the form

$$\xi = |x| = \frac{(m+n)^k}{m^k}, \quad \text{and} \quad \eta = |y| = \frac{(m+n)^k}{n^k}, \tag{10.11}$$

where k is an integer that can be positive or negative. The equation of the bounding surface is

$$|x|^{1/k} + |y|^{1/k} = 1. \tag{10.12}$$

For positive k this region lies within the unit square; therefore, it determines the region of convergence. For parameter values that lie between this curve and the unit square no analytical solutions can be found with this method.

For negative k the unit square lies within this region; therefore, the series converges if the magnitude of both parameters is less than unity. Solutions for all parameter values except possibly those on the boundary of the unit square are obtained in this case.

To summarize the convergence criteria for two variables, define $\Omega_2(\Omega_1)$ as the sum of all coefficients of $n(m)$ in the numerator gamma functions minus the sum of those in the denominator. A factorial function is equivalent to a gamma function in this definition. I refer to $\Omega_2(\Omega_1)$ as the "net factorial power" of $n(m)$. From the criteria above, the following statements are evident. If $\Omega_2(\Omega_1)$ is negative, the series converges for all values of $x(y)$. If $\Omega_2(\Omega_1)$ is negative, and $\Omega_1(\Omega_2)$ is zero, then the series converges for all values of $x(y)$ and for $y(x)$ less than unity. All these series are Taylor series. If either Ω_2 or Ω_1 is positive, then the series does not converge for any finite values of x or y. These series are asymptotic series. The only complicated case occurs when $\Omega_1 = \Omega_2 = 0$. In this case the convergence criteria vary from problem to problem. Examples of this case are considered in the next section and in Chap. 11.

In a similar manner as in the single complex plane case, one can define quantities Δ_{s_1} and Δ_{s_2} that are the sum of coefficients of s_1 and s_2 in the numerator gamma functions minus the sum of coefficients of the denominator gamma functions in an integral. The condition $\Delta_{s_1} = \Delta_{s_2} = 0$ corresponds to the case $\Omega_1 = \Omega_2 = 0$.

For the general case, a summation with p variables is

$$F(x_1, \ldots, x_p) = \sum_{n_1=0}^{\infty} \cdots \sum_{n_p=0}^{\infty} A_{n_1,\ldots,n_p} x_1^{n_1} \cdots x_p^{n_p}. \tag{10.13}$$

Define

$$\frac{A_{n_1,\ldots,n_{q-1},(n_q+1),n_{q+1},\ldots,n_p}}{A_{n_1,\ldots,n_q,\ldots,n_p}} = P_q(n_1, \ldots, n_p), \text{ and} \tag{10.14}$$

$$\Phi_q(n_1, \ldots, n_q, \ldots, n_p) = \lim_{\varepsilon \to \infty} P_q(\varepsilon n_1, \ldots, \varepsilon n_p), \quad q = 1, 2, \ldots, p. \tag{10.15}$$

The space within the intersection of two regions is again the region of convergence. The first region is a hyper-rectangle formed by the origin, the positive part of the coordinate axes, and a bounding hyperplane given by

$$\xi_q = |x_q| = 1/\left|\Phi_q(0, \ldots, 1, \ldots, 0)\right|, \quad q = 1, 2, \ldots, p. \tag{10.16}$$

Only the q^{th} term in parenthesis is not equal to zero.

The second region is a hypersurface that includes the origin, the coordinate axes, and a bounding surface that is defined by the parametric equations

$$\xi_q = |x_q| = 1/\Phi_q\left(n_1, \ldots, n_p\right), \; q = 1, 2, \ldots, p. \tag{10.17}$$

The region of convergence equivalent to the one in eq. 10.12 is

$$|x_1|^{1/k} + |x_2|^{1/k} + \cdots + |x_p|^{1/k} = 1. \tag{10.18}$$

These regions are found for a particular problem in Sec. 11.3.

Criteria for convergence of functions that are not Horn functions, a case that does not occur in the examples in this book, can be developed with the approach developed by *Slater* (1966) that is used to find the convergence regions of the four Appell functions.

The results on convergence can be used to show that if a power series converges, then the integration path can be closed to include the poles that lead to that power series. This result is proved for two complex planes. The proof is easily generalized to N complex planes.

10.2 Path Closure at Infinity

In this section I show that if the power series converges, then the integration path could have been closed at infinity to encircle the poles that generate the power series. Consider the general form of the integral in two complex planes

$$I = \frac{1}{(2\pi i)^2} \int_C ds \int_C dt \, x^{-s} y^{-t} \, F\,(s,t)\,, \tag{10.19}$$

where s and t are the two complex variables. To be able to close the contour at negative infinity for the two complex variables, one requires the contribution of the line integral at infinity to be zero, i.e.,

$$\lim_{\substack{s \to -\infty \\ t \to -\infty}} x^{-s} y^{-t} \, F\,(s,t)\; s\, t = 0. \tag{10.20}$$

If $F\,(s,t)$ has more gamma functions in both complex variables in the denominator than in the numerator, then it is easy to show that eq. 10.20 is true. If $F\,(s,t)$ has more gamma functions in the t complex variable in the denominator than in the numerator and the same number for s, then the series converges if $x < 1$. This is shown with l'Hospital's rule, which gives

$$\lim_{s\to-\infty} x^{-s}\, s = \lim_{s\to-\infty} \frac{s}{x^s} = \lim_{s\to-\infty} \frac{1}{\ln(x)\; x^s} = 0. \tag{10.21}$$

Since the limit in this equation is zero, one can close the integration path along an infinite semicircle in the left half plane about the poles that contribute to the series.

The only complicated case is the one in which there are the same number of gamma functions in each variable in the numerator and denominator. Consider the case when the infinite series results from poles in the left half plane for both complex variables. The integrand for large values of the complex variables, for the case of the integrand composed of the ratio of gamma functions, is given by

$$\lim_{\substack{s\to-\infty \\ t\to-\infty}} x^{-s} y^{-t}\, F(s,t)\; s\, t = \lim_{\substack{m\to\infty \\ n\to\infty}} x^m y^n \left\{ \Gamma \begin{bmatrix} m+n \\ m,\, n \end{bmatrix} \right\}^k m\, n = 0, \tag{10.22}$$

where k is an integer that can be positive or negative. For convergence, the mildest restrictions on x and y are that they are both less than unity. There can be constants added to the arguments of the gamma functions. These constants do not affect the limits; therefore, for notational convenience they are not explicitly displayed. For large index values one obtains from Stirling's approximation to the gamma function

$$\Gamma \begin{bmatrix} m+n \\ m,\, n \end{bmatrix} \sim A \frac{(m+n)^{m+n}}{m^m n^n}, \tag{10.23}$$

where A is a factor that does not affect convergence at infinity.

There are two cases to consider, one in which one index goes to ∞ with the other remaining finite, and one in which both indices go to ∞. Suppose n goes to ∞ and m remains finite, then

$$\lim_{n\to\infty} x^m y^n \left\{ \Gamma \begin{bmatrix} m+n \\ m,\, n \end{bmatrix} \right\}^k m\, n = A \frac{\exp(mk)\, x^m}{m^{mk-1}} \lim_{n\to\infty} y^n n^{mk+1}. \tag{10.24}$$

I made use of the relation

$$\lim_{n\to\infty} (1 + m/n)^n = \exp(m). \tag{10.25}$$

If k is negative, then the limit in eq. 10.24 is obviously zero for $|y| < 1$. For k positive, one has

$$\begin{aligned} \lim_{n\to\infty} y^n n^{mk+1} &= \lim_{n\to\infty} \frac{n^{mk+1}}{y^{-n}} = \lim_{n\to\infty} \frac{(mk+1)\, n^{mk}}{-\ln(y)\; y^{-n}} \\ &= \ldots = \lim_{n\to\infty} \frac{(mk+1)!}{(-1)^{mk+1} \ln^{mk+1}(y)\; y^{-n}} = 0. \end{aligned} \tag{10.26}$$

Consider the case in which both indices go to ∞. I will let $m = n$. With the form given in eq. 10.22 series convergence requires

$$y^{1/k} = 1 - x^{1/k} - \delta, \tag{10.27}$$

where δ is a small positive number. One obtains

$$\lim_{\substack{s\to-\infty \\ t\to-\infty}} x^{-s} y^{-t} F(s,t)\; s\, t = A \lim_{n\to\infty} n^2 \left[4^k x \left(1 - x^{1/k} - \delta\right)^k \right]^n. \tag{10.28}$$

The maximum value of the expression, which one finds by setting the derivative of the term in braces equal to zero, occurs at $x_{Max} = (1/2)^k$. Inserting this into the above expression, one finds

$$\lim_{\substack{s\to-\infty \\ t\to-\infty}} x^{-s} y^{-t} F(s,t)\; s\, t = A \lim_{n\to\infty} n^2 (1 - 2\,\delta)^{k\,n} = \lim_{n\to\infty} \frac{n^2}{\exp(2\,\delta\,k\,n)} = 0. \tag{10.29}$$

Therefore, the contributions along the infinite paths in the two complex variables are zero, and one could close the integration path at infinity without affecting the value of the integral.

The infinite series coefficients are the values of the residues of the integrand at the pole locations. It may turn out that many of those residues are zero, which is the case when a gamma function in the denominator is of the form $\Gamma[1 - n - m]$. For that case only the $n = m = 0$ term contributes. Notice that the proof above depended only on the indices in the gamma functions and not on any constants added to them. Therefore, when calculating whether to include a series one must determine if the series is of a convergent form rather than whether it actually converges. A series of convergent form is defined to be one in which the parameters lie within the convergent region defined in eq. 10.9 for the two complex-plane case and eqs. 10.16—10.17 for the general case.

10.3 Integration in Multiple Complex Planes

The space of several complex variables can be very complicated geometrically, and much of the recent work has been concerned with the validity of basic concepts in complex geometries. For problems in which the Mellin transform theorem applies, the only singularities of the integrand are poles of finite order and branch cuts. To evaluate these integrals only the simplest concepts are necessary. One can obtain the residues at the poles with Cauchy's integral formula on polydisks. A polydisk $P(\mathbf{a}, \mathbf{r})$ is the space in the N-dimensional complex plane $\mathbb{C}^N$ that is analogous to the unit circle in one complex plane. It has a multiradius $\mathbf{r} = (r_1, \ldots, r_N)$ centered at $\mathbf{a}$ and is defined by the condition

$$P(\mathbf{a}, \mathbf{r}) = \left\{ z \in \mathbb{C}^N, \quad |z_j - a_j| < r_j, \quad 1 \le j \le N \right\}. \tag{10.30}$$

An example of a polydisk in two complex planes is represented in Fig. 10.1.

The extension of the Cauchy pole-residue integral theorem given in *Range* (1986, p. 8) to the polydisk is

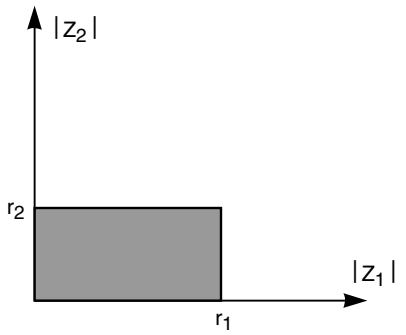

Figure 10.1. Representation of a polydisk in the space of the absolute value of each complex variable.

$$f(z_1, z_2, \ldots, z_N) = \frac{1}{(2\pi i)^N} \int_{C_1} \ldots \int_{C_N} ds_1 \ldots ds_N \frac{f(s_1, s_2, \ldots, s_N)}{(s_1 - z_1) \ldots (s_N - z_N)}, \quad z \in P, \tag{10.31}$$

where the contour encloses all poles, and the function $f(s_1, s_2, \ldots, s_N)$ is holomorphic (has no singularities) in the integration region. For Mellin transform problems there are poles that depend on the individual complex variables as above, and poles that have the sum of the variables. The method to evaluate these is to expand the integrand in partial fractions in which there are N independent poles in the denominator of each term. The terms with the sum of the variables is converted into the above form by a change of a single variable

$$s_{N+1} = s_1 + s_2 + \cdots + s_N. \tag{10.32}$$

Since the Wronskian of the transformation is unity, this new variable is treated just like the others.

The method to evaluate an integral in which the integrand is a ratio of gamma functions multiplied by a power of the integration variable is first considered for two complex planes. The generalization of this result to more complex planes is obvious. The partial fraction expansion is equivalent to one choosing from the set of all possible poles the pairs of poles in which the variables are independent. A gamma function has an infinite number of simple poles that occur at the points where the gamma function's argument has a negative integer value. For integrands that contain the product of gamma functions, one must consider all sets of pole pairs (2-poles) formed by gamma functions whose arguments are linearly independent in the two complex variables. The complete solution is the sum of all pole residues for these sets of 2-poles that are contained in the closed integration path. To determine which poles are enclosed in the integration path is not obvious for the multiple complex-plane geometry.

I will generally evaluate the complex-contour integration by simultaneously performing the integration over N-complex planes. As an example I will first evaluate the integral traditionally and then with the method espoused here. As

shown above, if one writes down the power series resulting from the evaluation at the multiple poles, then the series that should be included are the ones that converge, since the contour path could be closed at infinity thereby encircling those poles without affecting the value of the integral. As a "toy" problem, consider the integration of a product of unit step functions given by

$$\begin{aligned} I &= d \int_0^\infty \frac{dx}{x}\, x^d\, U(a-x)\; U(x-b)\; U(x-c) \\ &= 0 \;\text{ if } a < b \text{ or } \; a < c, \\ &= a^d - c^d \;\text{ if } a > b, \;\; a > c, \text{ and } c > b, \\ &= a^d - b^d \;\text{ if } a > b, \;\; a > c, \text{ and } b > c\,. \end{aligned} \tag{10.33}$$

$U(x)$ is unity for $x > 0$ and zero for $x < 0$. Convert this into an integral in two complex planes with the convolution integral in eq. 10.1, the inverse transform relation in eq. 10.2 and the Mellin transforms in eq. 1.59 and eq. 1.60, to obtain

$$\begin{aligned} I &= \frac{d\,a^d}{(2\pi i)^2} \int_{C_1}\int_{C_2} ds_1\, ds_2 \left(\frac{b}{a}\right)^{-s_1} \left(\frac{c}{a}\right)^{-s_2} \Gamma\begin{bmatrix} s_1+s_2+d,\; s_1,\; s_2 \\ s_1+s_2+d+1,\; s_1+1,\; s_2+1 \end{bmatrix} \\ &= \frac{d\,a^d}{(2\pi i)^2} \int_{C_1}\int_{C_2} ds_1\, ds_2 \left(\frac{b}{a}\right)^{-s_1} \left(\frac{c}{a}\right)^{-s_2} \frac{1}{(s_1+s_2+d)\; s_1\, s_2} \\ &= \frac{a^d}{(2\pi i)^2} \int_{C_1}\int_{C_2} ds_1\, ds_2 \left(\frac{b}{a}\right)^{-s_1} \left(\frac{c}{a}\right)^{-s_2} \\ &\qquad \times \left[\frac{1}{s_1\, s_2} - \frac{1}{(s_1+s_2+d)\; s_1} - \frac{1}{(s_1+s_2+d)\; s_2}\right]. \end{aligned} \tag{10.34}$$

The last form of the integrand is used in the traditional evaluation of the integral. The integration path as determined from the individual Mellin transforms is such that if one closed the path in the negative half plane in each complex plane, then one would include all poles. If $a < b$ or $a < c$, at least one of the integration paths must be closed in the right half plane of s_1 or s_2, and one obtains zero. If $a > b$ and $a > c$, perform the s_2 integration first, and obtain contributions from one pole in each of the first two terms and from two poles of the third term. For two of the terms the s_1 integration can be subsequently performed since $a > b$ and $a > c$ to give

$$I = a^d - b^d + \frac{c^d}{2\pi i} \int_{C_1} ds_1 \left(\frac{c}{b}\right)^{s_1} \left(\frac{1}{s_1+d} - \frac{1}{s_1}\right). \tag{10.35}$$

If $c < b$, the integration path is closed to the right, and the integral does not have any contribution. If $c > b$, the integration path is closed to the left, and both poles contribute. The net result is that one obtains the result in eq. 10.33.

Next, the solution is found by the method developed in this book by listing the three possible power series that are solutions of the complex integration that appear in the first line of eq. 10.34 and by choosing those that converge. Since information is required on the convergence of the series, the full power series are written down even if all the terms but the first have a coefficient of zero. The locations of the 2-poles that contribute are:

$$\begin{array}{l}(1)\ \ s_1 = -n;\ s_2 = -m;\ \text{therefore,}\ \ s_1 = -n;\ s_2 = -m,\\ (2)\ \ s_1 + s_2 + d = -m;\ \ s_1 = -n;\ \text{therefore,}\ \ s_1 = -n;\ \ s_2 = n - m - d,\ \text{and}\\ (3)\ \ s_1 + s_2 + d = -n;\ s_2 = -m;\ \text{therefore,}\ \ s_1 = -n + m - d;\ \ s_2 = -m.\end{array} \tag{10.36}$$

This leads to the following three double series:

$$I_1 = d\,a^d\,S\,(0,0)\left(\frac{b}{a}\right)^n\left(\frac{c}{a}\right)^m \Gamma\left[\begin{matrix}-m-n+d\\ 1-m,\ 1-n,\ 1-n-m+d\end{matrix}\right] = a^d, \tag{10.37}$$

$$I_2 = d\,a^d\,S\,(0,0)\left(\frac{b}{c}\right)^n\left(\frac{c}{a}\right)^{m+d} \Gamma\left[\begin{matrix}n-m-d\\ 1-m,\ 1-n,\ 1+n-m-d\end{matrix}\right] = -c^d, \tag{10.38}$$

$$I_3 = d\,a^d\,S\,(0,0)\left(\frac{b}{a}\right)^{n+d}\left(\frac{c}{b}\right)^m \Gamma\left[\begin{matrix}m-n-d\\ 1-m,\ 1-n,\ 1-n+m-d\end{matrix}\right] = -b^d. \tag{10.39}$$

I have introduced a notation to keep the equation size manageable. In the above equations and many subsequent equations I use

$$S\,(p_1, \ldots,\, p_k) = \sum_{n_1=p_1}^{\infty} \cdots \sum_{n_k=p_k}^{\infty} \frac{(-1)^{n_1+\cdots+n_k}}{n_1! \cdots n_k!}. \tag{10.40}$$

If the series is asymptotic in any variable, then an a is inserted next to the number that represents the lower limit.

As explained at the end of Sec. 10.2, even if a series is truncated because terms of the series are zero, one must still apply the convergence criteria given in Sec. 10.1 to determine if a given series should be included in the solution for particular parameter values. The convergence criterion in Sec. 10.1 requires $a > b$ and $a > c$ for I_1 to be included, $c > b$ and $a > c$ for I_2 to be included, and $a > b$ and $b > c$ for I_3 to be included. Include only those series that converge in the region of convergence to obtain the same result as in eq. 10.33.

The method discussed here replaces considerations of contour closure necessary in the usual treatment of complex-contour integrals with a criterion based upon series convergence. In the physical problems this results in a tremendous simplification. When the Mellin transform of products of more than three hypergeometric functions are sought, the resulting complex contour integral may contain two or more complex variables of integration. The geometric considerations necessary to determine the direction of contour closure rapidly become very cumbersome especially as three or more complex variables are introduced.

Replacing this often intractable requirement with an algebraic basis for determining the proper solution provides a method for easily solving these otherwise difficult integrals. In addition, this technique may be used to find the asymptotic series for an integral of Mellin type. The asymptotic forms are enumerated as part of the solution process for convergent series solutions; this requires only the occasional addition of a steepest-descent contribution.

To apply this method to find the convergent and asymptotic series, the series that result from pole-residue evaluation are written such that the exponents that appear in the power series are positive. By this I mean, for example, that if I have double series in indices m and n, the parameters in the power series are raised to the powers m and n rather than $-m$ and $-n$. *All possible infinite series are enumerated and the Taylor series solution is the sum of those series that converge for the parameter range of interest. Parameters that appear in these power series may have magnitudes greater than 1. When an approximation is desired that contains only a few terms, in these cases an asymptotic approximation should be used. One obtains this by examining all possible series and retaining those that contain parameters with all magnitudes less than 1. The asymptotic approximation appropriate for a particular parameter range is the sum of those series that contain series parameters that are less than unity. A steepest-descent contribution must be added when any Taylor series are excluded because their parameters have magnitudes greater than 1.* This leads to a straightforward way to evaluate the integral that no longer requires explicit consideration of the direction of contour closure in a $2N$-dimensional space.

Using this method to evaluate the integral given by eq. 10.34, one must write down all combinations of two independent poles, which are called 2-poles, evaluate the residue at each of these 2-poles, and sum the contributions of the enclosed 2-poles. Let the integral be a product of factors in which there are n_1 poles that contain only the first variable, n_2 poles with only the second, and n_3 poles with the sum of the two variables. The number of potential infinite series in the solution is equal to the total number of ways that two poles can be picked from the total number of poles—$A = (n_1 + n_2 + n_3)(n_1 + n_2 + n_3 - 1)$, minus the number of ways in which two poles could be chosen solely from each of the three categories. Therefore, the total number of 2-poles for the two complex-plane case is

$$\begin{aligned} N_t &= 0.5\left[A - n_1(n_1 - 1) - n_2(n_2 - 1) - n_3(n_3 - 1)\right] \\ &= n_1 n_2 + n_1 n_3 + n_3 n_2. \end{aligned} \tag{10.41}$$

The last form of the equation, in which there is the product of every combination of the number of each complex variable with one deleted, also applies to cases where there are more than two complex planes.

In the discussion that follows, a Taylor series is defined to be a series that converges. An asymptotic series is a series that diverges as the number of terms in the series gets arbitrarily large. For some problems the solution contains two Taylor series, one of which applies when the parameter is less than unity and the

other when the parameter is greater than unity. Some authors, i.e., *Wong* (1989), call this second series an asymptotic series. In this book the term asymptotic series is only applied to a divergent series.

A second "toy" problem is solved to illustrate two important concepts. First I show that the restricted region of validity of the solution as compared to the region of convergence of the integral results from the power series form of the solution. The same integral is then evaluated with terms of the power series subtracted from the integrand functions to illustrate that these integrals pose no conceptual difficulties. Consider an integral that contains the product of three exponentials

$$I = \int_0^\infty du\, \exp(-u) \exp(-x\,u) \exp(-y\,u). \tag{10.42}$$

For $1 + x + y > 0$ this is easily solved to give

$$I = \frac{1}{1 + x + y}. \tag{10.43}$$

To evaluate this with Mellin transform techniques, use the Mellin convolution theorem with the Mellin transform in eq. 1.47 to obtain

$$I = \frac{1}{(2\pi i)^2} \int_{C_1} \int_{C_2} ds_1\, ds_2\, \Gamma[s_1 + s_2 + 1,\, -s_1,\, -s_2]\, x^{s_1} y^{s_2}. \tag{10.44}$$

Since $n = m = p = 1$, eq. 10.41 states that there are three sets of 2-poles in the integrand. These three 2-poles are:

$$\begin{array}{ll} (1) & -s_1 = -n;\ -s_2 = -m, \\ (2) & s_1 + s_2 + 1 = -m;\ -s_1 = -n, \text{ and} \\ (3) & s_1 + s_2 + 1 = -n;\ -s_2 = -m. \end{array} \tag{10.45}$$

These 2-poles lead to the following powers of the parameters and powers of the factorial of the summation indices in the summation:

$$\begin{array}{lll} (1) & x^n y^m \left(n!\right)^0 \left(m!\right)^0, & \\ (2) & x^n y^{-n-m-1} \left(n!\right)^0 \left(m!\right)^0 = & y^{-m-1} \left(\dfrac{x}{y}\right)^n F\left(0,0\right), \text{ and} \\ (3) & x^{-n-m-1} y^m \left(n!\right)^0 \left(m!\right)^0 = & x^{-n-1} \left(\dfrac{y}{x}\right)^m F\left(0,0\right). \end{array} \tag{10.46}$$

New parameters were formed in the second and third terms that are combinations of the original parameters. The constant terms added to the exponent do not affect series convergence and will be suppressed in subsequent problems. The powers of the factorials represent the behavior of the terms of the summation as the index goes to infinity. The powers of these factorials were previously defined as Ω. I have introduced the notation

$$F\left(\Omega_1, \ldots, \Omega_k\right) = \left(n_1!\right)^{\Omega_1} \ldots \left(n_k!\right)^{\Omega_k}. \tag{10.47}$$

The three double sums that result from the evaluation of the integral at these three 2-poles are:

$$I_1 = S\,(0,0)\ \Gamma[1+n+m]\,x^n\,y^m, \tag{10.48}$$

$$I_2 = S\,(0,0)\ \Gamma[1+n+m]\,\left(\frac{x}{y}\right)^n\,y^{-m},\ \text{and} \tag{10.49}$$

$$I_3 = S\,(0,0)\ \Gamma[1+n+m]\,x^{-n}\left(\frac{y}{x}\right)^m. \tag{10.50}$$

The definition of $S\,(0,0)$ was introduced in the last example. In this example $\Omega_1 = \Omega_2 = 0$ for all three series; therefore, the three series are Taylor series. Their convergence depends on the sizes of the parameters. The parameters x and y can be either less than or greater than unity. To be specific, assume that $1 > x > y$. To find the region of convergence of I_1 note that

$$\Phi_1\,(m,n) = \frac{n+m}{m}, \quad \text{and} \quad \Phi_2\,(m,n) = \frac{n+m}{n}. \tag{10.51}$$

Therefore, the first criterion for the region of convergence gives the unit square. The parametric equations obtained from the second criterion for the region of convergence are

$$\xi = \frac{m}{m+n}, \quad \text{and} \quad \eta = \frac{n}{m+n}. \tag{10.52}$$

The variable m and n can be eliminated from these two equations, which leads to the condition $\eta + \xi < 1$. Therefore, this double series converges when $x + y < 1$. This is sometimes true for the assumed relation between the parameters as shown in Fig. 10.2. From the same criteria one finds that I_2 converges when $1 + x < y$, and I_3 converges when $1 + y < x$. These last two conditions are never satisfied with the assumed relations between the parameters. Since these series do not converge, they are not included in the solution.

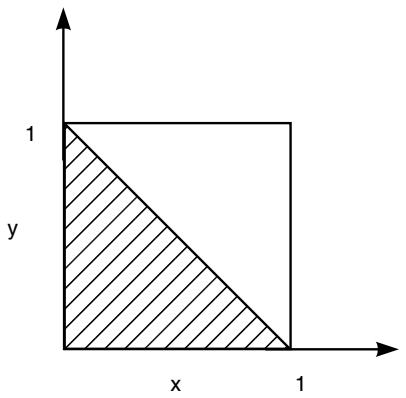

Figure 10.2. Hatched area is the parameter region in which the power series converges.

The value of the integral is

$$I = \int_0^\infty du\, \exp(-u) \exp(-x\,u) \exp(-y\,u) = S\,(0,0)\ \Gamma[1+n+m]\, x^n y^m, \quad x+y < 1. \tag{10.53}$$

If the ordering of the magnitudes of 1, x, and y were chosen differently, then one of the other power series would have been selected.

To show the equivalence of the direct result in eq. 10.43 with this double infinite series, note that for $x + y < 1$, one obtains

$$I = \frac{1}{1+x+y} = \sum_{n=0}^{\infty} (-1)^n\,(x+y)^n\,. \tag{10.54}$$

This can be expressed as a double series by using the binomial theorem when $x > y$ to obtain

$$I = \sum_{n=0}^{\infty} \sum_{m=0}^{n} (-1)^n x^n \left(\frac{y}{x}\right)^m \frac{n\,!}{(n-m)\,!\,m\,!}. \tag{10.55}$$

If one changes variables to $m \to m'$ and $n \to n' + m'$ with $m \le n$, then the summation reduces to the result given in eq. 10.53 that was obtained with Mellin transform techniques. Therefore, the Mellin transform method produces the correct result although it was expressed as an infinite series rather than a simple function as in the direct integration. In general, one would not recognize the double series that was obtained as being equivalent to the simple function. The conditions on the parameters are more restrictive than the requirement that $1 + x + y > 0$ as obtained by the direct integration. This is a direct result of the requirement that the solution be expressible as a double series, and results from the restriction on the expansion to obtain the series in eq. 10.54.

From this example, one learns that in solving problems of this type, the conditions obtained to get an answer, even though they are correct, may be too restrictive. An answer exists for other parameter values, but it cannot be expressed as a double series. To find a solution in those regions, specialized techniques that are peculiar to individual integrals are used (*Gervois* and *Navelet* 1985, 1986).

The fact that an answer is not in the most compact form and expressible in terms of simple functions is not a major deficiency because more complicated problems cannot, in general, be expressed as elementary functions. If the original function that is represented by the double summation can be found, then the region in which the solution applies can be extended. To do this one must invert two power series in succession. I am unaware of any general techniques to do this.

Up to now it has been assumed that the integration path has all poles of each gamma function on one side. For this case all summations start at the index equal to zero. There is an additional complication that arises when a summation does not start at zero. In the single complex plane case if there is a

term of the form $\sum_{n=b}^{\infty} D_n x^n$ that applies when x is less than unity, then $\sum_{n=0}^{b-1} D_n x^n$ must be added to the series that applies when x is greater than unity. This is easily generalizable to the case of two complex planes. Consider first the case where one series starts at zero, and the other starts at the index equal to unity. This series can be represented as

$$B_1 = \sum_{n=1}^{\infty} \sum_{m=0}^{\infty} A_{mn} x^n y^m \tag{10.56}$$

and applies when x and y are less than unity. In parallel to the single complex plane case, when x is greater than unity and y is less than unity, the term

$$B_2 = \sum_{m=0}^{\infty} A_{m0} y^m \tag{10.57}$$

must be added to the solution. Similarly, for the other index starting at unity, assume the series

$$C_1 = \sum_{n=0}^{\infty} \sum_{m=1}^{\infty} A_{mn} x^n y^m \tag{10.58}$$

applies when x and y are less than unity. When x is less than unity and y is greater than unity, then

$$C_3 = \sum_{n=0}^{\infty} A_{0n} x^n \tag{10.59}$$

must be added to the solution.

In the most general case both indices can start at a non-zero value. Assume the expression that applies when x and y are less than unity is

$$A_1 = \sum_{n=a}^{\infty} \sum_{m=b}^{\infty} A_{mn} x^n y^m. \tag{10.60}$$

When x is greater than unity and y is less than unity, then

$$A_2 = \sum_{n=0}^{a-1} \sum_{m=b}^{\infty} A_{mn} x^n y^m \tag{10.61}$$

must be added to the solution. When x is less than unity and y is greater than unity, then

$$A_3 = \sum_{n=a}^{\infty} \sum_{m=0}^{b-1} A_{mn} x^n y^m \tag{10.62}$$

must be added to the solution. When x and y are greater than unity, then

$$A_4 = \sum_{n=0}^{a-1} \sum_{m=0}^{b-1} A_{mn} x^n y^m \tag{10.63}$$

must be added to the solution. All possible solutions in which the summations do not start at zero are summarized in Table 10.1. For each set of parameter

Table 10.1. Expressions to include for different parameter ranges when the indices m and n do not start at zero.

x	y	Terms to include
<1	<1	$A_1\ B_1\ C_1$
>1	<1	$A_2\ B_2$
<1	>1	$A_3\ C_3$
>1	>1	A_4

values for a given pole set, only one of the tabulated series is included in the solution. If the indices m and n start at zero, then none of these additional expressions is included.

To illustrate this, consider a modified version of the integral considered in the previous example

$$I = \int_0^\infty du\, \exp(-u)\,[\exp(-x\,u) - 1]\exp(-y\,u). \tag{10.64}$$

This integral transforms into

$$I = \frac{1}{(2\pi i)^2}\int_{C_1}\int_{C_2} ds_1\, ds_2\, \Gamma\left[s_1 + s_2 + 1,\, -s_1*,\, -s_2\right]\, x^{s_1} y^{s_2}, \tag{10.65}$$

where * means that the integration path passes between the first and second poles of that gamma function. The three 2-poles are:

$$\begin{array}{ll} (1) & -s_1 = -n*;\ -s_2 = -m, \\ (2) & s_1 + s_2 + 1 = -m;\ -s_1 = -n*, \text{ and} \\ (3) & s_1 + s_2 + 1 = -n;\ -s_2 = -m. \end{array} \tag{10.66}$$

The asterisk indicates that the summation index starts at 1. The solution contains the same summation as in the first example except that the n summation starts at 1. There is a potential to pick up one term of the second summation; however, that is added to the solution when $y > 1$ and $y/x > 1$. Since that is not the case being considered, this term is not added to the solution. Therefore, the value of this integral is

$$I = S\,(1,0)\ \Gamma[1 + n + m]\, x^n y^m = \frac{1}{1 + x + y} - \frac{1}{1 + y}, \quad x + y < 1. \tag{10.67}$$

This is the same result that is obtained from direct integration.

If unity is also subtracted from the last exponential in eq. 10.64, then the answer is obtained in a similar manner. Consider the following integral

$$I = \int_0^\infty du\, \exp(-u)\,[\exp(-x\,u) - 1]\,[\exp(-y\,u) - 1]\,. \tag{10.68}$$

This transforms into

$$I = \frac{1}{(2\pi i)^2} \int_{C_1} \int_{C_2} ds_1\, ds_2\, \Gamma\left[s_1 + s_2 + 1,\, -s_1*,\, -s_2*\right] x^{s_1} y^{s_2}. \tag{10.69}$$

The three 2-poles are:

$$\begin{array}{ll} (1) & -s_1 = -n*;\ -s_2 = -m*\,, \\ (2) & s_1 + s_2 + 1 = -m;\ -s_1 = -n*,\ \text{and} \\ (3) & s_1 + s_2 + 1 = -n;\ -s_2 = -m*\,. \end{array} \tag{10.70}$$

The solution contains the same summation as in the first example except that the n and m summations both start at 1. Again there is a potential to pick up one term of the second and third summations; however, the first term of the second is added to the solution when $x > 1$ and $y/x > 1$, and the first term of the third is added to the solution when $y > 1$ and $y/x > 1$. Since these are not the cases being considered, these terms are not added to the solution. The value of this integral is thus

$$I = S\,(1,1)\ \Gamma[1 + n + m]\, x^n y^m = \frac{1}{1+x+y} - \frac{1}{1+y} - \frac{1}{1+x} + 1, \quad x + y < 1\ . \tag{10.71}$$

This is the same result that is obtained from direct integration. In these examples no terms from the other series appeared in the solution.

The problem of being unable to represent the solution to an integral for all parameter ranges surfaces in various fields. For instance, one can show (*Jackson* 1962) that the electric potential in space caused by an infinitely thin conducting disc of radius a with a charge q is

$$V\,(\rho, z) = q \int_0^\infty dk\, \frac{\sin\,(k\,a)}{k\,a} \exp\,(-k\,z)\, J_0\,(k\,\rho)\,. \tag{10.72}$$

One can evaluate this integral with the methods developed in the chapter to obtain a solution as a double series. This series does not converge for some ratios of the parameters close to unity. For this case a solution that applies for all space is available in *Gradshteyn* and *Ryzhik* (1980, eq. 6.752 #1) as

$$V\,(\rho, z) = \frac{q}{a}\, \sin^{-1}\left(\frac{2a}{\sqrt{(\rho - a)^2 + z^2} + \sqrt{(\rho + a)^2 + z^2}}\right). \tag{10.73}$$

The above result was obtained with eq. 3.5 to convert the Bessel function into an integral over angle, the evaluation of the integral over k, followed by the evaluation of the integral over angle. This technique does not work if the index of the Bessel function is different than unity or if the power of the integration variable in the integrand is other than -1. I know of no general procedures to convert double power series into such complicated functional relations.

10.3.1 Evaluation procedure for N complex planes

The procedure to obtain Taylor series solutions in more than two complex planes is easily extended from the procedure given above. After all possible power series are determined, choose only those series that converge for the parameter range of interest. With this procedure it is straightforward to obtain Taylor series for very complicated integrals. Examples of the application this procedure to 3 and N complex planes are given in Sec. 11.3.

10.4 Asymptotic Solution in Two or More Complex Planes

In general, different Taylor (convergent) series may be readily obtained for various parameter regimes. For many problems this solution is adequate. For other problems, the Taylor series converge slowly for some parameter regimes, and it is desirable to obtain asymptotic solutions in these regimes.

The procedure to obtain the series that converge most rapidly is rather simple; write down the series terms that correspond to every pole set in the entire complex plane in a form such that the parameters have positive exponents, and choose only those series for which the parameter magnitude is less than unity. If a Taylor series convergent for the parameter magnitudes over the range of interest is excluded because of this procedure, then an asymptotic solution that consists of an asymptotic series and a steepest-descent contribution must be included. Normally this will be obvious because the procedure will automatically require the inclusion of an asymptotic series. In some cases, however, no asymptotic series will be called for because the coefficients in the asymptotic series are all zero. In these cases, the steepest-descent contribution by itself is the asymptotic form for the excluded Taylor series.

It is possible to have the sum of Taylor and asymptotic solutions for the same range of parameter values. This is a consequence of the fact that the integrand's decomposition into the partial-fraction expansion as given in eq. 10.34 results in a sum of functions. Some of the functions may contribute a Taylor series, and some may contribute an asymptotic form to the final solution. This procedure is applied in Sec. 11.4—11.7.

The technique to obtain asymptotic expressions for an integral in a single complex plane discussed in Chaps. 5 and 8 is extended here to obtain steepest-descent contributions for integrals in two or more complex planes. A simple case to evaluate occurs in the parameter regime where the power series is convergent in one parameter and asymptotic in the other. In that case the integration in the complex variable that leads to the convergent series is performed first, followed by the evaluation of the asymptotic solution for the second integral. The result is a sum of power series that are the ones that would be chosen from all possible power series by the application the rules of the last section. In addition, one needs to obtain the steepest-descent contribution.

The situation is more complicated when the parameter regime is such that both power series are asymptotic and a change of variables cannot be made to make one integral result in a convergent series. I show that when the complex variables are not strongly coupled that one can still perform the integrations serially.

I will now discuss the general case. As for a single complex plane, the integration path of the complex variables is deformed so that all saddle points of the integrand are crossed in the directions of steepest descent. The asymptotic expression for the integral is given by the sum of the contributions of poles crossed as a result of the path deformation, and the contribution of the path integral along the steepest-descent path. The asymptotic series are found with the procedure discussed in the last section. In this section the method to find the steepest-descent contribution is discussed.

For a single-complex-plane case the steepest-descent contribution was found by a modification of the normal method in which one is concerned with evaluating integrals of the form

$$I(\lambda) = \int_C ds\, g(s) \exp[-\lambda f(s)]\,, \tag{10.74}$$

where λ is large. The difference in the application of this technique for Mellin transform problems is that there is no large quantity that is immediately evident. It was shown in Chap. 5 when the parameter was large that the second derivative of $f(s)$ was much larger than the higher order derivatives at the saddle point with the result that the procedure essentially reduced to the normal steepest-descent procedure. For more than one complex plane a similar procedure is attempted. It is found that it does not work in general; however, for a class of problems one can find the steepest-descent contribution by the simple process of evaluating integrals in each complex plane in sequence. This special case occurs often in practice, and it applies to every turbulence problem discussed in the next chapter. The only case for which a general method to obtain the asymptotic solution for two complex planes is not available is when there is a steepest-descent contribution that must be retained for the first integration no matter which integral is performed first.

To develop this method, I will discuss the standard problem of steepest descent in two variables, then I will modify those results to apply to Mellin transform problems. The integral to be evaluated with the normal method is

$$I(\lambda) = \int_{C_2} ds_2 \int_{C_1} ds_1\, g(s_1, s_2) \exp[-\lambda f(s_1, s_2)]\,. \tag{10.75}$$

We will recast the Mellin convolution integral into this form. The general form for the inverse Mellin transform integral in two complex planes is

$$h(x_1, x_2) = \frac{1}{(2\pi i)^2} \int_{C_2} \int_{C_1} ds_1\, ds_2\, H_0(s_1 + s_2)\; H_1(s_1)\, H_2(s_2)\, x_1^{-s_1}\, x_2^{-s_2}, \tag{10.76}$$

where the paths C_1 and C_2 represent a sheet in 4-space that must be contained within the hyper-volumes where $H_0(s_1+s_2)$, $H_1(s_1)$, and $H_2(s_2)$ are analytic. In the one complex-plane case, asymptotic results are needed only when the parameter magnitude $|x|$ is large. In two complex planes, asymptotic analysis is more complicated for the following reason: Expansion of the integral in eq. 10.76 into a form that allows the use of pole-residue methods was discussed in Sec. 10.2. Pole-residue integration produces terms that each contain the product of a holomorphic function and a function with one simple pole for each complex variable. The resultant power series may contain a factor $x_1^{n+m}x_2^{-m}$ that reduces to $(x_1/x_2)^n x_1^m$. The ratio $|x_1/x_2|$ may be large even though $|x_1|$ and $|x_2|$ are small. This type of possibility demonstrates the potential need for asymptotic analysis even when both $|x_1|$ and $|x_2|$ are small. Three distinct cases are possible: $|x_1|$ and $|x_2|$ are small, $|x_1|$ is small (large) and $|x_2|$ is large (small), and $|x_1|$ and $|x_2|$ are large.

In problems discussed in this book, the integrand may be expressed as the ratio of products of gamma functions

$$H_0(s_1+s_2)\,H_1(s_1)\,H_2(s_2) = \left\{ \frac{\prod_{j=1}^{A_1} \Gamma[a_{1,j}+s_1] \prod_{j=1}^{B_1} \Gamma[b_{1,j}-s_1]}{\prod_{j=1}^{C_1} \Gamma[c_{1,j}+s_1] \prod_{j=1}^{D_1} \Gamma[d_{1,j}-s_1]} \right\}$$
$$\times \left\{ \frac{\prod_{j=1}^{A_2} \Gamma[a_{2,j}+s_2] \prod_{j=1}^{B_2} \Gamma[b_{2,j}-s_2]}{\prod_{j=1}^{C_2} \Gamma[c_{2,j}+s_2] \prod_{j=1}^{D_2} \Gamma[d_{2,j}-s_2]} \right\}$$
$$\times \left\{ \frac{\prod_{j=1}^{A_3} \Gamma[a_{3,j}+s_1+s_2] \prod_{j=1}^{B_3} \Gamma[b_{3,j}-s_1-s_2]}{\prod_{j=1}^{C_3} \Gamma[c_{3,j}+s_1+s_2] \prod_{j=1}^{D_3} \Gamma[d_{3,j}-s_1-s_2]} \right\} . \tag{10.77}$$

The coefficients of s_1, s_2, and s_1+s_2 are unity in the above expression, unlike the more general case considered in the single-parameter case. If integrals that contain noninteger, rational coefficients must be evaluated, make the substitution $s \to us$ where u is the least common denominator of the coefficients, and use the Gauss-Legendre multiplication theorem to expand the gamma functions until all the coefficients are unity.

Define the following quantities:

$$\Delta_n = A_n + D_n - B_n - C_n \quad \text{for } n = 1,\ 2,\ 3, \text{ and} \tag{10.78}$$

$$\Delta_{s_n} = \Delta_n + \Delta_3 \quad \text{for } n = 1,\ 2. \tag{10.79}$$

These Δ's play an important role in the determination of the asymptotic properties of the integral. If $\Delta_{s_1} = \Delta_{s_2} = 0$, no asymptotic form for $h(x_1, x_2)$ is necessary. As in the one-dimensional case, path closure is determined by the

magnitude of the parameters x_1 and x_2, and a rapidly converging series always results in the parameter regime in which the series converges. If either Δ_{s_1} or Δ_{s_2} is less than zero, then a change of variables $s_1 \to -s_1$ and / or $s_2 \to -s_2$ should be used to rewrite the integral so that these Δ's are greater than or equal to zero.

The identity $\Gamma[s]\,\Gamma[1-s] = \pi \csc(\pi s)$ is used to rewrite gamma functions that contain $-s_1$, $-s_2$, and $-(s_1+s_2)$ in terms of gamma functions that contain s_1, s_2, and s_1+s_2. This allows the use of an asymptotic expansion for all gamma functions that is valid in the sector where the phase of the argument of the gamma function is greater than $-\pi$ and less than π. Because the integrand's behavior at large values of s_1 and s_2 is of interest, the gamma functions are replaced with the asymptotic equivalent given as

$$\Gamma[a+s] \sim \sqrt{2\pi}\exp\left[(s+a-1/2)\ln(s)-s\right]. \tag{10.80}$$

The asymptotic form for the sine terms obtained through application of the previously discussed identity is also used. One must use different representations for the sine terms depending upon the sign of the imaginary part of the sine's argument.

If $\mathrm{Im}\{\pi s\} > 0$, then

$$\sin(\pi s) \sim \tfrac{1}{2}\exp\left[-i\pi\left(s-\tfrac{1}{2}\right)\right]. \tag{10.81}$$

Similarly, if $\mathrm{Im}\{\pi s\} < 0$, then

$$\sin(\pi s) \sim \tfrac{1}{2}\exp\left[i\pi\left(s-\tfrac{1}{2}\right)\right]. \tag{10.82}$$

Incorporate the sign of $i\pi$ into quantities λ as in Sec. 8.1, one for each s_1, s_2, and s_1+s_2. This leads to six conditions that require separate treatment as tabulated in Table 10.2.

Table 10.2. Conditions on the imaginary parts of s_1, s_2, and s_1+s_2 that require separate treatment.

Case 1	$\mathrm{Im}\{s_1\}>0$	$\mathrm{Im}\{s_2\}>0$	$\mathrm{Im}\{s_1+s_2\}>0$	$\lambda_1=1$	$\lambda_2=1$	$\lambda_3=1$
Case 2	$\mathrm{Im}\{s_1\}<0$	$\mathrm{Im}\{s_2\}<0$	$\mathrm{Im}\{s_1+s_2\}<0$	$\lambda_1=-1$	$\lambda_2=-1$	$\lambda_3=-1$
Case 3a	$\mathrm{Im}\{s_1\}>0$	$\mathrm{Im}\{s_2\}<0$	$\mathrm{Im}\{s_1+s_2\}>0$	$\lambda_1=1$	$\lambda_2=-1$	$\lambda_3=1$
Case 3b	$\mathrm{Im}\{s_1\}>0$	$\mathrm{Im}\{s_2\}<0$	$\mathrm{Im}\{s_1+s_2\}<0$	$\lambda_1=1$	$\lambda_2=-1$	$\lambda_3=-1$
Case 4a	$\mathrm{Im}\{s_1\}<0$	$\mathrm{Im}\{s_2\}>0$	$\mathrm{Im}\{s_1+s_2\}>0$	$\lambda_1=-1$	$\lambda_2=1$	$\lambda_3=1$
Case 4b	$\mathrm{Im}\{s_1\}<0$	$\mathrm{Im}\{s_2\}>0$	$\mathrm{Im}\{s_1+s_2\}<0$	$\lambda_1=-1$	$\lambda_2=1$	$\lambda_3=-1$

Cases 1, 2, 3, and 4 correspond to different quadrants in 4-space. The distinctions in Case 3 (a and b) and in Case 4 (a and b) arise because of the possibility that Im (s_1+s_2) may be positive or negative in each instance.

Combining the exponential form of the gamma functions with the logarithm of the parameters x_1 and x_2 one obtains

$$h\left(x_1, x_2\right) = \left(2\pi\right)^{\left(\left[\Xi_1+\Xi_2+\Xi_3\right]/2-2\right)} \int_{C_1}\int_{C_2} ds_1\, ds_2\, \exp\left[f(s_1, s_2\,)\right], \tag{10.83}$$

where

$$\begin{aligned} f\left(s_1, s_2\right) = \sum_{j=1}^{2} \Big\{ &\left(\nu_j - \Xi_j\,/2 + \Delta_j\, s_j\right)\, \ln\left(s_j\right) - s_j \ln\left(x_j\right) - \Delta_j\, s_j \\ &- i\,\pi\,\lambda_j \left[\Lambda_j'' + \Lambda_j\left(s_j + \tfrac{1}{2}\right)\right]\Big\} + \left[\nu_3 - \Xi_3/2 + \Delta_3(s_1 + s_2)\right] \ln\left(s_1 + s_2\right) \\ &- \Delta_3\left(s_1 + s_2\right) - i\,\pi\,\lambda_3\, \left[\Lambda_3'' + \Lambda_3\left(s_1 + s_2 + \tfrac{1}{2}\right)\right], \end{aligned} \tag{10.84}$$

$$\Xi_n = A_n + B_n - C_n - D_n, \tag{10.85}$$

$$\nu_n = \sum_{j=1}^{A_n} a_{n,j} + \sum_{j=1}^{B_n} b_{n,j} - \sum_{j=1}^{C_n} c_{n,j} - \sum_{j=1}^{D_n} d_{n,j}, \tag{10.86}$$

$$\Lambda_n = B_n - D_n, \quad \text{and} \tag{10.87}$$

$$\Lambda_n'' = \sum_{j=1}^{B_n} b_{n,j} - \sum_{j=1}^{D_n} d_{n,j}, \tag{10.88}$$

for $n = 1$ to 3. The contributions of the sine terms, that depend upon the quadrant of the saddle point, are contained in the terms dependent upon λ_n.

The first step in one's calculating the integral's steepest-descent value is to locate the saddle points of $f\left(s_1, s_2\right)$. These points occur at $(\tilde{s}_1, \tilde{s}_2)$ where

$$0 = \left.\frac{\partial f\left(s_1, s_2\right)}{\partial\, s_1}\right|_{(s_1,s_2\,)=\,(\tilde{s}_1,\tilde{s}_2)} \text{and} \quad 0 = \left.\frac{\partial f\left(s_1, s_2\right)}{\partial\, s_2}\right|_{(s_1,s_2\,)=(\tilde{s}_1,\tilde{s}_2)}. \tag{10.89}$$

This gives the two equations

$$\begin{aligned} \frac{\partial f\left(s_1, s_2\right)}{\partial s_1} \approx &- \ln\left(x_1\right) + \Delta_1 \ln\left(s_1\right) + \Delta_3 \ln\left(s_1 + s_2\right) \\ &+ i\,\pi\left[\lambda_1\left(B_1 - D_1\right) + \lambda_3\left(B_3 - D_3\right)\right] \\ &+ \frac{\nu_1 - \Xi_1/2}{s_1} + \frac{\nu_3 - \Xi_3/2}{s_1 + s_2}, \text{ and} \end{aligned} \tag{10.90}$$

$$\frac{\partial f(s_1,s_2)}{\partial s_2} \approx -\ln(x_2) + \Delta_2 \ln(s_2) + \Delta_3 \ln(s_1+s_2) + i\pi\left[\lambda_2(B_2-D_2)+\lambda_3(B_3-D_3)\right] + \frac{\nu_2-\Xi_2/2}{s_2} + \frac{\nu_3-\Xi_3/2}{s_1+s_2}. \tag{10.91}$$

Another set of partial derivatives that is necessary to evaluate saddle-point contributions are given by

$$\frac{\partial^2 f(s_1,s_2)}{\partial^2 s_1} = \alpha(s_1,s_2) \approx \frac{\Delta_1}{s_1} + \frac{\Delta_3}{s_1+s_2} - \frac{\nu_1-\Xi_1/2}{s_1^2} - \frac{\nu_3-\Xi_3/2}{(s_1+s_2)^2}, \tag{10.92}$$

$$\frac{\partial^2 f(s_1,s_2)}{\partial^2 s_2} = \beta(s_1,s_2) \approx \frac{\Delta_2}{s_2} + \frac{\Delta_3}{s_1+s_2} - \frac{\nu_2-\Xi_2/2}{s_2^2} - \frac{\nu_3-\Xi_3/2}{(s_1+s_2)^2}, \tag{10.93}$$

$$\text{and} \quad \frac{\partial^2 f(s_1,s_2)}{\partial s_1 \partial s_2} = \gamma(s_1,s_2) \approx \frac{\Delta_3}{s_1+s_2} - \frac{\nu_3-\Xi_3/2}{(s_1+s_2)^2}. \tag{10.94}$$

At the saddle point, Taylor's theorem may be used to show that $f(s_1,s_2)$ is given by

$$f(s_1,s_2) \approx f(\tilde{s}_1,\tilde{s}_2) + \frac{(s_1-\tilde{s}_1)^2}{2}\alpha(\tilde{s}_1,\tilde{s}_2) + \frac{(s_2-\tilde{s}_2)^2}{2}\beta(\tilde{s}_1,\tilde{s}_2) + (s_1-\tilde{s}_1)(s_2-\tilde{s}_2)\gamma(\tilde{s}_1,\tilde{s}_2). \tag{10.95}$$

Only terms up to quadratic order in s_1 and s_2 are kept. As in the case of a single complex variable, higher-order terms will generally not contribute significantly to the integral. The first term in the expansion given above does not depend upon the integration variables and may be moved outside the integral. The remaining integral is evaluated along the paths of steepest descent, i.e., along the paths where the imaginary part of $f(s_1,s_2)$ is constant. The result is a two-dimensional analog of the Gaussian integral that is obtained by the application of steepest-descent techniques to an integral over a single complex variable.

First restrict ourselves to the case when Δ_1, Δ_2, and Δ_3 are all positive. In that case when $|x_1|$ and $|x_2|$ are large, the saddle points occur where $|s_1|$, $|s_2|$, and $|s_1+s_2|$ are large. This fact allows one to neglect terms with the square of the complex variables in the denominators of eqs. 10.92—10.94. The final result of this manipulation is

$$h(x_1,x_2) \sim (2\pi)^{[(\Delta_1+\Delta_2+\Delta_3)/2-1]} \frac{\exp\left[f(\tilde{s}_1,\tilde{s}_2)\right]}{\sqrt{\alpha(\tilde{s}_1,\tilde{s}_2)\,\beta(\tilde{s}_1,\tilde{s}_2) - \gamma^2(\tilde{s}_1,\tilde{s}_2)}}. \tag{10.96}$$

The term under the square root can be expressed as

$$\alpha(\tilde{s}_1,\tilde{s}_2)\,\beta(\tilde{s}_1,\tilde{s}_2) - \gamma^2(\tilde{s}_1,\tilde{s}_2) = \frac{\Delta_1\Delta_2}{\tilde{s}_1\tilde{s}_2} + \frac{\Delta_1\Delta_3}{\tilde{s}_1(\tilde{s}_1+\tilde{s}_2)} + \frac{\Delta_2\Delta_3}{(\tilde{s}_1+\tilde{s}_2)\tilde{s}_2}. \tag{10.97}$$

This term is referred to as Hesse's determinant, and can be generalized to N complex variables (*Ishimaru* 1991).

If Δ_1, Δ_2, and Δ_3 are all positive, then one can find the saddle points. The second derivatives are large, and the steepest-descent contribution can be found. This typically is a difficult procedure because the equations to be solved are nonlinear.

For many integrals to be evaluated and all the problems in turbulence that I have considered, a simpler procedure applies. Looking at the Mellin transform tables, one sees that the sums of the coefficients of s in the numerator minus those in the denominator are either positive or zero. One could possibly obtain a negative sum by finding the Mellin transform of the inverse of the variable. However, for turbulence problems and many integrals, the functions do not have the inverse of the argument, and the quantities Δ_1, Δ_2, and Δ_3 are not all positive. First, assume that they are all nonzero and arrange the functions so that Δ_3 is negative. Because of the difference in sign, a large parameter size does not guarantee that the second derivatives given in eqs. 10.92—10.94 are large or even positive. It is not clear that there is a steep saddle point in this case that allows the line integral to be approximated by an integration along a short segment. I will not discuss this case further.

A case that often occurs in practice is the one in which one of the Δ's is zero. The signs of the complex variables can be changed if necessary so that the other two Δ's are positive. The functions can be arranged in the integral so that the Δ that is zero is Δ_3. In this case the saddle point is approximately located at

$$s_1 \approx x_1^{1/\Delta_1}, \quad \text{and} \quad s_2 \approx x_2^{1/\Delta_2}. \tag{10.98}$$

In this case if x_1 is large, then s_1 is large, and if x_2 is large, then s_2 is large. The derivatives higher than second order are much smaller than the second order ones. The steepest-descent results in eq. 10.96 apply. Notice that in eq. 10.97 only one of the three terms on the right is non-zero. The denominator term has the product of the two non-zero Δ's. This suggests that the double integral might be broken into the product of two single integrals. Thus examine $f(s_1, s_2)$ in eq. 10.84. With $\Delta_3 = 0$, the only term that couples the two complex variables is $\ln(s_1 + s_2)$. As in the single complex plane case, the dominant term in this exponential function are terms of the form $s \ln(s)$. There are two terms of that form due to Δ_1 and Δ_2, and the coupling term is small compared to these terms. Since I am only interested in calculating the first term of the steepest-descent contribution, this coupling is neglected, and the double integral is performed as a cascade of two single integrals.

When one of the Δ's is zero, the three cases of relative parameter magnitude are all treated similarly to obtain the steepest-descent contribution. In the first case where the magnitudes of both parameters are small, the integral over one of the two complex variables is evaluated to obtain the pole contributions. One or more of the resulting power series depend on the ratio of the parameters. For only those series in which this ratio can be large is the second integral examined

to obtain solely the steepest-descent contributions. For the second case, when one parameter is large and the other small, the integration over the complex variable associated with the large variable is performed first to obtain only the steepest-descent contribution. The remaining integral is performed with pole-residue techniques. Doing the integration in this order reduces the amount of algebra. In the final case both parameters are large. One obtains the steepest-descent contribution to the double integral by first evaluating the asymptotic solution to the first integral. This includes both the asymptotic series and the steepest-descent contribution. The second integral is then evaluated to obtain only the steepest-descent contribution from each series, and the steepest-descent contribution and asymptotic series for the steepest-descent result of the first integration.

In actuality the functions do not have to be arranged so that when one of the Δ's is zero it is Δ_3. Suppose Δ_2 is zero. By making the substitutions $s_1 + s_2 \rightarrow s_2$ and $s_2 \rightarrow s_1 + s_2$ one can make the same arguments as above. Therefore, the integrals can be evaluated one at a time as long as any of the Δ's is zero. *In fact, even though it was assumed that the coefficients of s in the gamma functions were unity in the derivation of eq. 10.96, for the case in which the integration is performed sequentially, the coefficients of s can be arbitrary.* This procedure is illustrated in Secs. 11.4 to 11.7.

A similar analysis applies for more than two complex planes when one of the Δ's is zero. Arrange the functions in the integrand so that the Δ associated with the sum of the N complex variables is zero. The function in the exponential, $f(s_1, s_2, \ldots s_N)$, can again be approximated by the sum of terms that each depend on a single complex variable, thereby allowing one to perform the integration as a cascade of integrals.

If two of the Δ's are zero, that implies that either Δ_{s_1} or Δ_{s_2} is zero. In this case the series in one of the variables is a convergent series with a net factorial of zero. The asymptotic series has to be found in only one variable. One of Poincaré's theorems on asymptotic series given in Sec. 5.2 states that the integral of asymptotic series is equal to the asymptotic series of the integral. Therefore, the asymptotic solution can be found for the integral whose complex variable has the non-zero value of Δ_s, and the remaining integral can be evaluated with pole-residue techniques. This applies even if Δ_1, Δ_2, and Δ_3 are all positive.

Above I showed that if Δ_1, Δ_2, and Δ_3 are all positive and both parameters are large, then it is not possible in general to obtain a steepest-descent contribution to the integral. If only one of the parameters is large, then an asymptotic solution can be found for one variable and pole-residue integration performed for the second. This can be generalized to the case of N parameters. Define Δ_1 to Δ_{N+1} as in eq. 10.78. If all these Δ's are positive and only one parameter is large, then one evaluates the integral by obtaining the steepest-descent contribution of the complex variable associated with the large parameter followed by evaluating the remaining multiple integral by the method described in this chapter.

The results of this chapter are now summarized. To evaluate an integral with N parameters, one must first determine the locations of the N-poles and the power series associated with them. The Taylor series solution is simply the sum of those series that converge in the parameter regime of interest. Conditions for convergence are given in this chapter. An exact convergent solution is always obtained except for certain parameter regimes when more than one of the Δ's is zero. In those parameter regimes no valid solution is obtained.

If terms of the power series are subtracted from some integrand functions, then the summations do not start at zero. Criteria for the inclusion of additional partial series in the solution were developed.

If some of the series converge slowly, it is often possible to obtain an asymptotic solution for the integral. This solution is composed of a sum of series plus a steepest-descent contribution. To find the series solution, express all power series such that the parameters in the series are raised to a positive exponent. The asymptotic series part of the solution is simply the sum of all series that have all parameters in the summation less than unity for the parameter regime of interest.

The steepest-descent contribution can be found for those cases in which the integrals can be arranged so that either the result of the first integration is a rapidly convergent series for the parameter range of interest or one of the Δ's is zero. For these cases one finds the steepest-descent part of the solution by performing the integrals sequentially. There are several ways in which the first integral can result in a convergent series:

1. The result of the first integration is a rapidly convergent series regardless of the size of the parameter when either Δ_{s_1} or Δ_{s_2} is zero. In this case separate power series are obtained for small and large parameters.
2. If neither Δ_{s_1} nor Δ_{s_2} is zero, then the order of the integrals sometimes may be arranged so that the single power series that results from the first integration converges rapidly for the parameter range of interest. In this case, the steepest-descent contribution is found when the second integral is subsequently evaluated.
3. If neither Δ_{s_1} nor Δ_{s_2} is zero but $\Delta_1 = \pm\Delta_2$, then by making the substitutions $s \to \mp s$, $t \to s + t$, and $s + t \to t$ one obtains $\Delta_{s_1} = 0$. This has now been reduced to the first case.

For cases where a steepest-descent contribution cannot be found by sequential evaluation of the integrals in the complex plane and all the Δ's are positive, one can obtain that contribution by solving the nonlinear equations given in this section. For the remaining cases it is not clear that an asymptotic solution with a single-term, steepest-descent contribution can be found that gives an accurate approximation to the integral.

REFERENCES

1. Bleistein, N., Hendelsman, R. A., *Asymptotic Expansions of Integrals*, Dover, New York, (1986).
2. Dingle, R. B., *Asymptotic Expansions: Their Derivation and Interpretation*, Academic Press, London, (1973).
3. Erdélyi, A., *Higher Transcendental Functions*, Robert E. Kieger Publishing Company, Malabar, Florida, (1981).
4. Exton, H., *Multiple Hypergeometric Functions and Applications*, John Wiley & Sons, Chichester, England (1978).
5. Gervois, A., Navelet, H., "Integrals of three Bessel functions and Legendre functions. I", *J. Math. Phys.*, **26**, (1985) pp. 633–644.
6. Gervois, A., Navelet, H., "Integrals of three Bessel functions and Legendre functions. II", *J. Math. Phys.*, **27**, (1986) pp. 688–695.
7. Gradshteyn, I. S., Ryzhik, I. M., *Table of Integrals, Series, and Products*, Academic Press, New York, (1980).
8. Horn, J., "Ueber die Convergenz der hypergeometrischen Reihen zweier und dreier veränderlichen", *Math. Ann.*, **34**, (1889) pp. 544–600.
9. Ishimaru, A., *Electromagnetic Wave Propagation, Radiation, and Scattering*, Prentice Hall, Englewood Cliffs, New Jersey, (1991).
10. Jackson, J. D., *Classical Electromagnetics*, John Wiley & Sons, Inc., New York, (1962).
11. Range, R. M., *Holomorphic Functions and Integral Representations in Several Complex Variables*, Springer-Verlag, Berlin, Germany, (1986).
12. Sasiela, R. J., Shelton, J. D., "Mellin transform methods applied to integral evaluation: Taylor series and asymptotic approximations", *J. Math. Phys.*, **34**, (1993) pp. 2572–2617.
13. Slater, L. J., *Generalized hypergeometric functions*, Cambridge University Press, London-New York, (1966).
14. Wong, R., *Asymptotic Approximations Of Integrals*, Academic Press, Inc., Boston, Ma., (1989).
15. Whittaker, E. T., Watson, G. N., *A Course of Modern Analysis*, Cambridge University Press, Inc., Cambridge, England (1980).

Chapter 11

Integral Evaluation with N Parameters

The mathematical technique developed in the last chapter is used to find analytical solutions to seven problems. The first three are purely mathematical problems, and the last four are problems related to turbulence.

The first three examples have solutions that are in integral tables. The same solution and range of applicability is obtained with the Mellin transform method. The second problem, which contains a product of three Bessel functions, has applicability in the calculation of the correlation coefficients of various modes on a circular aperture. The third example has an integrand that contains a sinusoid and the product of Bessel functions. Two cases are considered; in the first there are three Bessel functions and in the second there are N. This example is the only one given in this book that illustrates how to use the technique in more than two complex planes.

For the first four problems asymptotic solutions are not required. In the last three problems they are required. It may not be necessary to use asymptotic solutions for certain applications since if enough Taylor series terms are used they can provide a sufficiently accurate answer. In the calculation of the power spectral density in Sec. 6.7 a 40-term Taylor series was sufficient to calculate the spectrum to large frequencies. The asymptotic solution does have one advantage over the Taylor series in that the dependence on parameters is clearly evident.

Four problems in wave propagation in turbulence are solved. These problems were chosen to illustrate the various techniques one must use to obtain asymptotic solutions under different conditions. The first three are generalizations of problems solved earlier in the book. It is shown that these solutions approach the former solutions at the proper limits. These three solutions determine the effect of outer scale on tilt anisoplanatism, the effect on tilt variance with both inner-scale and outer-scale effects present, and the tilt power spectral density with outer-scale effects. The fourth solution gives phase structure and correlation functions with inner and outer scale effects. These solutions demonstrate one of the most valuable assets of this technique. From the first term that couples the two effects, one can determine when the coupling starts to affect the result. From this term, one can determine when coupling can be neglected. The specific form of the coupling is difficult to ascertain when numerical methods are used to evaluate the integral.

For notational convenience, in two-complex-plane problems the two complex variables are designated s and t rather than s_1 and s_2. The notation introduced in the last chapter is used extensively in this chapter. For convenience it is repeated here.

$$S\left(p_1, \ldots, p_k\right) = \sum_{n_1=p_1}^{\infty} \cdots \sum_{n_k=p_k}^{\infty} \frac{(-1)^{n_1+\cdots+n_k}}{n_1! \cdots n_k!}. \tag{11.1}$$

If an a is placed next to the limit, it indicates that the series is asymptotic and only a finite number of terms should be summed. The argument of $S\left(p_1, \ldots, p_k\right)$ has the n limit first followed by the m limit. Sometimes when there are multiple series, the summations are separated by other terms. In that case there will be two terms of the form $S(0)$, and I will add either an n or an m subscript to make it clear which summation is first.

The other function gives the factorial behavior of series terms as the summation index goes to infinity.

$$F\left(\Omega_1, \ldots, \Omega_k\right) = \left(n_1!\right)^{\Omega_1} \cdots \left(n_k!\right)^{\Omega_k}. \tag{11.2}$$

11.1 An Integral with Two Bessel Functions and a Sinusoid

This first example is chosen because the value of the integral is a particularly simple expression. Consider the integral in *Gradshteyn* and *Ryzhik* (1980, eq. 6.711 # 3)

$$I = \int_0^{\infty} du\, u^{\nu-\mu-2} J_\mu(au)\, J_\nu(bu)\, \sin(cu) = \frac{2^{\nu-\mu-1} a^\mu b^{-\nu} c\, \Gamma[\nu]}{\Gamma[\mu+1]}, \tag{11.3}$$

with $a > 0$, $b > 0$, $b - a > c > 0$, and $0 < \mathrm{Re}\{\nu\} < \mathrm{Re}\{\mu\} + 3$. The last condition results from the requirement that the integral must converge at the upper and lower limits.

Without loss of generality, the functions can be arranged so that $a < b$. This integral is put into the standard form by the following transformations $au = y$, $y = a/b$, and $z = a/c$, to give

$$I = a^{-\nu+\mu+1} \int_0^{\infty} \frac{dx}{x}\, x^{\nu-\mu-1} J_\mu(x)\, J_\nu\left(\frac{x}{y}\right) \sin\left(\frac{x}{z}\right).$$

This can be converted into an integral in two complex planes with the Mellin transforms in eq. 1.51 and eq. 1.48 and the Mellin convolution integral given in eq. 1.31. After the substitutions $s \to 2s$ and $t \to 2t$, one obtains

$$I = \frac{\sqrt{\pi}}{2} \left(\frac{a}{2}\right)^{1-\nu+\mu} \frac{1}{(2\pi i)^2} \int_{C_1} \int_{C_2} ds\, dt \left(\frac{a}{b}\right)^{-2s} \left(\frac{a}{c}\right)^{-2t}$$

$$\times\Gamma\left[\begin{array}{c} s+t+\nu/2-1/2,\ -s+\nu/2,\ -t+1/2 \\ -s-t-\nu/2+\mu+3/2,\ s+1+\nu/2,\ t+1 \end{array}\right].$$

Since $\Delta_s = \Delta_t = 0$, there is no asymptotic series.

The technique discussed in Chap. 10 is used to evaluate this integral. The locations of the 2-poles are:

$$\begin{array}{ll} (1) & -t+1/2=-m\,;\ -s+\nu/2=-n, \\ (2) & -s+\nu/2=-n\,;\ s+t+\nu/2-1/2=-m, \text{ and} \\ (3) & -t+1/2=-m\,;\ s+t+\nu/2-1/2=-n. \end{array} \tag{11.4}$$

To determine which 2-pole contributions must be retained, the above relations are used to find the power-law dependence of the parameters for large values of m and n. If the exponents have m and n indices in the same exponent, one must separate the terms by defining new parameters. This statement is made clearer when one performs this process for the three sets of two-poles to give:

$$\begin{array}{ll} (1) & \left(\dfrac{b}{a}\right)^{2n}\left(\dfrac{c}{a}\right)^{2m}F(0,0), \\ (2) & \left(\dfrac{b}{c}\right)^{2n}\left(\dfrac{a}{c}\right)^{2m}F(0,0), \text{ and} \\ (3) & \left(\dfrac{a}{b}\right)^{2n}\left(\dfrac{c}{b}\right)^{2m}F(0,0). \end{array} \tag{11.5}$$

As discussed in Chap. 10 the values of Ω_1 and Ω_2 in $F(\Omega_1, \Omega_2)$ are the values of the exponent of the factorial function. These are referred to as the "net factorial power", and they determine the series type. If both values are non-positive, then the series is a Taylor series, otherwise it is an asymptotic series. The parameters with a single index in the exponent are the natural parameters of the problems, and are independent of initial substitutions made to put the integral into the canonical form. The constant terms in the exponents do not affect series convergence and, therefore, the direction of path closure, and have not been displayed explicitly. The three power series are Taylor series that apply to different parameter ranges. The range of applicability of the various series is given in Table 11.1.

Table 11.1. Range of applicability of various series.

2–Pole Set	Solution Type	Parameter Range
1	Taylor	$b < a\ c < a$
2	Taylor	$b < c\ a < c$
3	Taylor	$a < b\ c < b$

From the condition $b - a > c > 0$ the first two series diverge, in which case only the third series is convergent, and the integral is equal to

$$I = \sqrt{\pi}\frac{a^{\mu}\, c}{b^{\nu}\, 2^{2-\nu+\mu}} S\,(0,0) \left(\frac{a}{b}\right)^{2n} \left(\frac{c}{b}\right)^{2m} \Gamma\left[\begin{matrix} m+n+\nu \\ n+\mu+1, -m-n+1, m+3/2 \end{matrix}\right]. \tag{11.6}$$

The term $\Gamma[-m-n+1]$ in the denominator is infinite at all n and m except $m = n = 0$. Therefore, all residues vanish except those at $m = n = 0$. The single series term gives the result in eq. 11.3. The particular value of the power of x produces this simple form for the result. The expression is more complicated for a general exponent in the original integral, and this method can be used to get a double-series solution for this case. This will not be pursued here since this type of series is illustrated in the next example.

One must examine the convergence region of this solution. Since the net factorial power for both summation indices is zero, one has to use the criteria for convergence of the power series given in Sec. 10.2. Even though terms other than the first are zero, in order to get the first term, one had to close the integration path at infinity to encompass all terms of this series; therefore, the convergence criteria must be applied as if all series terms are non-zero. Equation 10.8 gives $\Phi_1(m,n) = (m+n)^2/m^2$, and $\Phi_2(m,n) = (m+n)^2/n^2$. From eq. 10.9 one finds the first of the two regions is a rectangle with sides of unity length. The parametric equations given by eq. 10.10 are $\xi = |x| = m^2/(m+n)^2$, and $\eta = |y| = n^2/(m+n)^2$. These equations satisfy the relation $\sqrt{x} + \sqrt{y} < 1$.

Since $x = (a/b)^2$ and $y = (c/b)^2$, one requires that $a/b + c/b < 1$. The area in the x–y plane defined by this condition is contained within the unit square; therefore, this more restrictive condition defines the region of convergence. From this, one obtains the same condition as that in the integral tables given by $b - a > c$.

11.2 An Integral with Three Bessel Functions

Consider the following integral whose value is needed to evaluate the Zernike covariance matrix

$$I = \int_0^{\infty} \frac{d\omega}{\omega}\, \omega^d J_{\mu}(a\omega)\, J_{\nu}(b\omega)\, J_{\rho}(c\omega). \tag{11.7}$$

This integral is tabulated in *Gradshteyn and Ryzhik* (1980, eq. 6.578 # 1). The condition for convergence at the lower limit is $\mu+\nu+\rho+d > 0$. For convergence at the upper limit one requires $\mathrm{Re}\,\{d\} < 5/2$. Without loss of generality, one can arrange the Bessel functions so that $c > b > a$. With this last condition the only region in parameter space for which a solution is required is the hatched region of Fig. 11.1.

Watson (1934) considered this integral but was unable to evaluate it. *Bailey* (1936) found its value when $a + b < c$, which is in the integral table, and is the result derived below.

Evaluate the integral by letting $x = c\omega$ to give

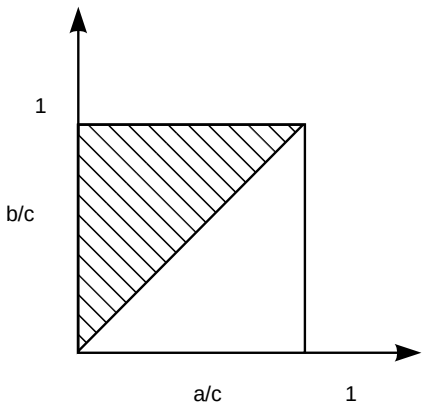

Figure 11.1. Hatched area is the parameter region in which a solution is required for the integral of 3 Bessel functions.

$$I = c^{-d} \int_0^\infty \frac{dx}{x}\, x^d\, J_\rho(x)\, J_\mu\left[x/\left(c/a\right)\right]\; J_\nu\left[x/\left(c/b\right)\right].$$

Use the generalized Mellin convolution theorem and the Mellin transform in eq. 1.51, and make the substitutions $s \to 2s$, and $t \to 2t$, to write the integral in the s and t complex planes as

$$I = \frac{2^{d-1}}{c^d} \frac{1}{(2\pi i)^2} \int_{C_1} \int_{C_2} ds\, dt\, \left(\frac{c}{b}\right)^{-2s} \left(\frac{c}{a}\right)^{-2t}$$

$$\times \Gamma\begin{bmatrix} s+t+(d+\rho)/2,\ -s+\nu/2,\ -t+\mu/2 \\ -s-t+(\rho-d)/2+1,\ s+\nu/2+1,\ t+1+\mu/2 \end{bmatrix}.$$

Since $\Delta_s = \Delta_t = 0$, there is no asymptotic series. The 2-poles are located at:

1) $s+t+(d+\rho)/2 = -n\,;\ -s+\nu/2 = -m,$
2) $s+t+(d+\rho)/2 = -m\,;\ -t+\mu/2 = -n,$ and
3) $-s+\nu/2 = -n\,;\ -t+\mu/2 = -m.$

These 2-poles lead to terms of the type:

$$(1)\quad \left(\frac{c}{a}\right)^{2n} \left(\frac{b}{a}\right)^{2m} F(0,0)\,,$$

$$(2)\quad \left(\frac{a}{b}\right)^{2n} \left(\frac{c}{b}\right)^{2m} F(0,0)\,, \text{ and}$$

$$(3)\quad \left(\frac{b}{c}\right)^{2n} \left(\frac{a}{c}\right)^{2m} F(0,0)\,.$$

These three sets of 2-poles give three Taylor series that are applicable for different parameter ranges, given in Table 11.2.

Table 11.2. Range of applicability of various series for the problem in which the product of three Bessel functions is integrated.

2–Pole Set	Solution Type	Parameter Range
1	Taylor	$c < a\ b < a$
2	Taylor	$a < b\ c < b$
3	Taylor	$b < c\ a < c$

For the case being considered in which $c > b > a$, the power series that corresponds to the third pole set is the only one applicable, and the solution is

$$I = \frac{2^{d-1}a^{\mu}b^{\nu}}{c^{d+\mu+\nu}} S\left(0,0\right) \left(\frac{b}{c}\right)^{2n} \left(\frac{a}{c}\right)^{2m}$$

$$\times \Gamma\left[\begin{matrix} m+n+\left(\nu+\rho+\mu+d\right)/2 \\ -m-n+\left(\rho-\nu-\mu-d\right)/2+1,\ m+1+\mu,\ n+1+\nu \end{matrix}\right].$$

The summation can be written as an Appell function of the fourth kind to get exactly the same result as in the integral tables

$$I = \frac{2^{d-1}a^{\mu}b^{\nu}}{c^{d+\mu+\nu}} \Gamma\left[\begin{matrix} \left(\nu+\rho+\mu+d\right)/2 \\ 1-\left(\nu-\rho+\mu+d\right)/2,\ 1+\nu,\ 1+\mu \end{matrix}\right]$$

$$\times F_4\left[\frac{\left(\nu+\rho+\mu+d\right)}{2}, \frac{\left(\nu-\rho+\mu+d\right)}{2}, 1+\mu, 1+\nu; \left(\frac{a}{c}\right)^2, \left(\frac{b}{c}\right)^2\right]. \quad (11.8)$$

Since the net factorial power for both summation indices is zero, one has to examine the convergence criteria of the power series in this case. The analysis to find the region of convergence proceeds exactly as in the last section, and the parametric equations are identical. Since in this problem $x = (b/c)^2$, and $y = (a/c)^2$, one obtains the same condition as in the integral tables $a + b < c$. The two potential regions of convergence represented by the above inequality and the unit square are shown in Fig. 11.2. Both hatched regions are ones in which the power series does not apply even though the parameters are less than one. The horizontally hatched region is half the area of interest as depicted in Fig. 11.1. In that region $1/2 < c/2b < 1$. For parameter values in this region, the integration path cannot be closed around the poles, and the above technique does not give an answer even though the integral converges. *Gervois* and *Navelet* (1985, 1986) gave results in the horizontally hatched region for special values of the order of the Bessel function and exponent in the integration. The analytic value of the integral for arbitrary parameter values is not known.

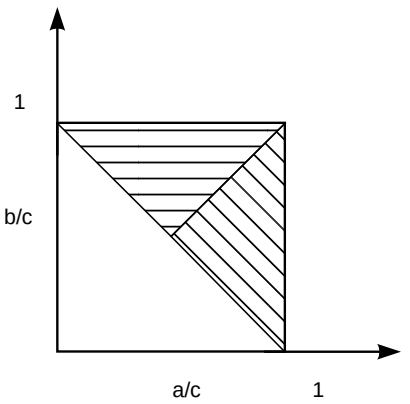

Figure 11.2. Regions in which the power series has different convergence properties for the integral of 3 Bessel functions.

11.3 Example in Three and N Complex Planes

As an example of the technique in three complex planes, an integral similar to the first example, whose value has a particularly simple form, is worked out. By examining the steps in obtaining this solution, one can obtain by inspection the result of the integration in N complex planes. Consider the following integral

$$\begin{aligned} I &= \int_0^\infty du\, u^{\nu-\mu-\lambda-2}\, J_\nu(bu)\, \sin(cu)\, J_\mu(au)\, J_\lambda(du) \\ &= \frac{2^{\nu-\mu-\lambda-1}\, b^{-\nu}\, \Gamma[\nu]\, c\, a^\mu\, d^\lambda}{\Gamma[\mu+1]\, \Gamma[\lambda+1]}, \end{aligned} \tag{11.9}$$

with $a > 0$, $b > 0$, $d > 0$, $b > a + c + d > 0$, and $0 < \mathrm{Re}\,\{\nu\} < \mathrm{Re}\,\{\mu + \lambda\} + 3.5$. The last condition results from the convergence requirement at the upper and lower limits.

Without loss of generality, functions can be arranged so that $a < b$ and $d < b$. This integral is converted into standard form by the following transformations $au = x$, $y = a/b$, $z = a/c$, and $w = a/d$, to give

$$I = a^{-\nu+\mu+\lambda+1} \int_0^\infty \frac{dx}{x}\, x^{\nu-\mu-\lambda-1} J_\mu(x)\, J_\nu\left(\frac{x}{y}\right)\, \sin\left(\frac{x}{z}\right)\, J_\lambda\left(\frac{x}{w}\right).$$

This can be converted into an integral in three complex planes with the Mellin transforms in eq. 1.51 and eq. 1.48 and the Mellin convolution integral given in eq. 1.31. The third complex variable is r.

After the substitutions $s \to 2s$, $r \to 2r$, and $t \to 2t$, one obtains

$$I = \sqrt{\pi} a^{-\nu+\mu+\lambda+1} 2^{-2+\nu-\mu-\lambda} \frac{1}{(2\pi i)^3} \int_{C_1}\int_{C_2}\int_{C_3} ds\, dt\, dr \left(\frac{a}{b}\right)^{-2s} \left(\frac{a}{c}\right)^{-2t} \left(\frac{a}{d}\right)^{-2r}$$

$$\times \Gamma\left[\begin{matrix} s+t+r+\nu/2-\lambda/2-1/2,\ -s+\nu/2,\ -t+1/2,\ -r+\lambda/2 \\ -s-t-r-\nu/2+\lambda/2+\mu+3/2,\ s+1+\nu/2,\ t+1,\ r+1+\lambda/2 \end{matrix}\right].$$

The technique discussed in the last chapter is used to evaluate this integral. The locations of the 3-poles are:

$$(1) \quad -t+\frac{1}{2} = -m\,;\ -s+\frac{\nu}{2} = -n\,;\ -r+\frac{\lambda}{2} = -p,$$

$$(2) \quad -s+\frac{\nu}{2} = -n\,;\ s+t+r+\nu/2-\frac{\lambda}{2}-\frac{1}{2} = -m\,;\ -r+\frac{\lambda}{2} = -p,$$

$$(3) \quad -t+\frac{1}{2} = -m\,;\ s+t+r+\frac{\nu}{2}-\frac{\lambda}{2}-\frac{1}{2} = -n\,;\ -r+\lambda/2 = -p, \text{ and}$$

$$(4) \quad s+t+r+\frac{\nu}{2}-\frac{\lambda}{2}-\frac{1}{2} = -p\,;\ -s+\frac{\nu}{2} = -n\,;\ -t+\frac{1}{2} = -m.$$

To determine which 3-pole contributions must be retained, the above relations are used to find the power-law dependence of the variables for large values of m, n, and p, which are:

$$(1) \quad \left(\frac{b}{a}\right)^{2n} \left(\frac{c}{a}\right)^{2m} \left(\frac{d}{a}\right)^{2p} F(0,0,0)\,,$$

$$(2) \quad \left(\frac{b}{c}\right)^{2n} \left(\frac{a}{c}\right)^{2m} \left(\frac{d}{c}\right)^{2p} F(0,0,0)\,,$$

$$(3) \quad \left(\frac{a}{b}\right)^{2n} \left(\frac{c}{b}\right)^{2m} \left(\frac{d}{b}\right)^{2p} F(0,0,0)\,, \text{ and}$$

$$(4) \quad \left(\frac{b}{d}\right)^{2n} \left(\frac{c}{d}\right)^{2m} \left(\frac{a}{d}\right)^{2p} F(0,0,0)\,.$$

All four lead to Taylor series that converge for different parameter ranges. It will be required that $c < b$, and since $a < b$ and $d < b$, only the third Taylor series converges so that the integral is equal to

$$I = \sqrt{\pi} a^{\mu}\, c\, 2^{-2+\nu-\mu-\lambda}\, b^{-\nu}\, d^{\lambda} S(0,0,0) \left(\frac{a}{b}\right)^{2n} \left(\frac{c}{b}\right)^{2m} \left(\frac{d}{b}\right)^{2p}$$

$$\times \Gamma\left[\begin{matrix} m+n+p+\nu \\ n+\mu+1,\ -m-n-p+1,\ m+3/2,\ p+\lambda+1 \end{matrix}\right]. \qquad (11.10)$$

The term $\Gamma[-m-n-p+1]$ in the denominator is infinite at all n, m, and p except for $m = n = p = 0$. Therefore, all poles have zero residue except the

3-pole at $m = n = p = 0$. The one term that remains gives the same result as that in eq. 11.9. The particular form of the power of x produces the simple form for the result, and the expression is more complicated for a general exponent.

As before, because the net factorial power for the three summation indices is zero, one has to examine the criteria for convergence of Sec. 10.2. Equation 10.15 gives $\Phi_1(m,n,p) = (m+n+p)^2/m^2$, $\Phi_2(m,n,p) = (m+n+p)^2/n^2$, and $\Phi_3(m,n,p) = (m+n+p)^2/p^2$. From eq. 10.17 one finds that the hyper-rectangle of possible convergence has sides of unity length. The parametric equations to determine the second convergence criterion are $\xi = |x| = n^2/(m+n+p)^2$, $\eta = |y| = m^2/(m+n+p)^2$, and $\phi = |z| = p^2/(m+n+p)^2$.These conditions require $\sqrt{x} + \sqrt{y} + \sqrt{z} < 1$.

Since $x = (a/b)^2$, $y = (c/b)^2$, and $z = (d/b)^2$, then $b > c + a + d$. The volume in the x–y–z plane defined by this condition is contained within the hyper-rectangle; therefore, this more restrictive condition defines the convergence region. The above result agrees with the special case of the integral in *Prudnikov* et al. (1990, eq. 7 of Sec. 2.12.44) when one notes that

$$J_{1/2}(cx) = \sqrt{\frac{2}{\pi\, cx}}\sin(cx)\,. \tag{11.11}$$

The extension of this technique to evaluate integrals with more Bessel functions, which require more than three complex planes, is obvious. The result is

$$\begin{aligned} I &= \int_0^\infty du\, u^{\left(\nu-2-\sum_{i=1}^{N} a_i\right)} J_\nu(bu)\sin(cu)\prod_{i=1}^{N} J_{a_i}(d_i u) \\ &= 2^{\left(\nu-1-\sum_{i=1}^{N} a_i\right)} \frac{c}{b^\nu}\Gamma[\nu]\prod_{i=1}^{N}\frac{d_i^{a_i}}{\Gamma[1+a_i]}\,. \end{aligned} \tag{11.12}$$

For convergence at the lower and upper limits, one requires

$$0 < \mathrm{Re}\{\nu\} < \mathrm{Re}\left\{\sum_{i=1}^{N} a_i\right\} + \frac{N+5}{2}. \tag{11.13}$$

The convergence criteria are easily extended into N-complex planes to obtain $b > c + \sum_{i=1}^{N} d_i$. This integration formula also agrees with the special case of the above-mentioned integral in *Prudnikov* et al. (1990).

11.4 Effect of Outer Scale on Tilt Anisoplanatism

Tilt anisoplanatism with an infinite outer scale was considered in Sec. 6.6. Here this problem is solved with a finite outer turbulence scale for the von Kármán spectrum. I will show that outer scale's effect is not as significant here as its effect on tilt in Sec. 6.1. The equivalent of eq. 6.59 with outer-scale effects included is

$$\begin{bmatrix} \sigma_{\parallel}^2 \\ \sigma_{\perp}^2 \\ \sigma^2 \end{bmatrix} = 0.4146 \left(\frac{16}{D}\right)^2 \int_0^L dz\, C_n^2(z) \int d\boldsymbol{\kappa} \begin{bmatrix} \cos^2(\varphi) \\ \sin^2(\varphi) \\ 1 \end{bmatrix}$$

$$\times \left(\kappa^2 + \kappa_o^2\right)^{-11/6} \left[\frac{J_2\,(\kappa D/2)}{\kappa D/2}\right]^2 \left\{1 - \cos\left[\kappa d \cos\left(\varphi\right)\right]\right\}. \qquad (11.14)$$

Let $w = \kappa d$, $y = 2\pi d/L_o$, and $x = 2d/D$, and integrate over angle. The equivalent of eq. 6.65 is

$$\begin{bmatrix} I_1 \\ I_T \end{bmatrix} = -\frac{4\,d^{11/3}}{D^2} \int_0^\infty \frac{dw}{w} \begin{bmatrix} w^{-14/3}\left[J_1(w) - \frac{w}{2}\right] \\ w^{-11/3}\left[J_0(w) - 1\right] \end{bmatrix} J_2^2\left(w/x\right) \left[1 + (y/w)^2\right]^{-11/6}.$$

Using the Mellin convolution theorem with the Mellin transforms in eq. 1.51, eq. 1.52, and eq. 1.54, and making the substitutions $s \to 2s$ and $t \to 2t$, one can convert this into an integral in two complex planes as

$$\begin{bmatrix} I_1 \\ I_T \end{bmatrix} = \frac{-0.0945\,d^{11/3}}{D^2} \frac{1}{(2\pi i)^2} \int_{C_1}\int_{C_2} ds\,dt \left(\frac{\pi d}{L_o}\right)^{-2s} \left(\frac{d}{D}\right)^{-2t}$$

$$\times \Gamma \begin{bmatrix} s + t - \frac{11}{6}*,\ -t + 2,\ t + \frac{1}{2},\ s,\ -s + \frac{11}{6} \\ t + 3,\ t + 1 \end{bmatrix} \begin{Bmatrix} \frac{1}{2\Gamma\left[-s-t+\frac{23}{6}\right]} \\ \frac{1}{\Gamma\left[-s-t+\frac{17}{6}\right]} \end{Bmatrix}.$$

The asterisk indicates that the integration path passes between the first and second poles of that gamma function.

The list of 2-poles are:

(1) $-s + \frac{11}{6} = -m\,;\ t + \frac{1}{2} = -n,$
(2) $-s + \frac{11}{6} = -m\,;\ -t + 2 = -n,$
(3) $-s + \frac{11}{6} = -m\,;\ s + t - \frac{11}{6} = -n*,$
(4) $s = -m\,;\ \frac{1}{2} + t = -n,$
(5) $s = -m\,;\ -t + 2 = -n,$
(6) $s = -m\,;\ \ s + t - \frac{11}{6} = -n*$
(7) $t + \frac{1}{2} = -n\,;\ \ s + t - \frac{11}{6} = -m*,$ and
(8) $-t + 2 = -n\,;\ \ s + t - \frac{11}{6} = -m*\,.$

The values of m and n are integers that vary between 0 and ∞. The asterisk after a term means that the index varies between 1 and ∞ on one side of the

integration path, and is equal to 0 on the other. The general terms of the various possible series are:

$$(1) \quad \left(\frac{L_o}{\pi d}\right)^{2m} \left(\frac{d}{D}\right)^{2n} F(0,2)\,,$$

$$(2) \quad \left(\frac{L_o}{\pi d}\right)^{2m} \left(\frac{d}{D}\right)^{2n} F(0,2)\,,$$

$$(3) \quad \left(\frac{L_o}{\pi D}\right)^{2m} \left(\frac{d}{D}\right)^{2n*} F(0,2)\,,$$

$$(4) \quad \left(\frac{\pi d}{L_o}\right)^{2m} \left(\frac{d}{D}\right)^{2n} F(0,-2)\,,$$

$$(5) \quad \left(\frac{\pi d}{L_o}\right)^{2m} \left(\frac{D}{d}\right)^{2n} F(0,-2)\,,$$

$$(6) \quad \left(\frac{d}{D}\right)^{2n*} \left(\frac{\pi D}{L_o}\right)^{2m} F(0,-2)\,,$$

$$(7) \quad \left(\frac{L_o}{\pi D}\right)^{2n} \left(\frac{\pi d}{L_o}\right)^{2m*} F(2,-2)\,, \text{ and}$$

$$(8) \quad \left(\frac{\pi D}{L_o}\right)^{2n} \left(\frac{\pi d}{L_o}\right)^{2m*} F(-2,-2)\,.$$

This process produces the parameters that are relevant to the problem. The new parameter introduced above is $\pi D/L_o$. In this analysis, this ratio as well as $\pi d/L_o$ is considered to be less than 1. To determine which pole residues must be included, the rule given in the last chapter must be applied. These results are summarized in Table 11.3. Series 1, 2, 3, and 7 are asymptotic series that apply when the displacement or diameter is much greater than the outer-scale size. I am not interested in this parameter range; therefore, these series are discarded. For $d/D < 1$, Series 4 for all m and n, and Series 6 for all m and n greater than 0 contribute. For $d/D > 1$, Series 5 for all n and m, and Series 6 for $n = 0$ and all m contribute. Series 8 contributes for all ranges of d/D for all n and for m greater than 0. Series 6 corresponds to a series of type B_1 in Table 10.1 and the term with $n = 0$ must be added to the solution when $d/D > 1$.

Since the only relevant series are Taylor series, steepest-descent contributions do not have to be added to the solution. With these properties the value of the integral for small displacements, $d/D < 1$, can be expressed as

Table 11.3. Series ranges of applicability for most rapid convergence, for the problem where the effect of outer scale on tilt anisoplanatism is found.

2–Pole Set	Solution Type	Parameter	Range
1	Asymp	$\pi D/L_o > 1$	$d < D$
2	Asymp	$\pi d/L_o > 1$	$d < D$
3	Asymp	$\pi D/L_o > 1$	$d < D$
4	Taylor	$\pi d/L_o < 1$	$d < D$
5	Taylor	$\pi d/L_o < 1$	$d > D$
6	Taylor	$\pi D/L_o < 1$	$d < D$
7	Asymp	$\pi D/L_o > 1$	$\pi d/L_o < 1$
8	Taylor	$\pi D/L_o < 1$	$\pi d/L_o < 1$

$$\begin{bmatrix} I_1 \\ I_T \end{bmatrix} = \frac{-0.0945\, d^{11/3}}{D^2}$$
$$\times\Bigg\{ S(0,0)\left(\frac{\pi d}{L_o}\right)^{2m}\left(\frac{d}{D}\right)^{2n+1} \Gamma\begin{bmatrix} -m-n-\frac{7}{3},\, n+\frac{5}{2},\, m+\frac{11}{6} \\ -n+\frac{5}{2},\, -n+\frac{1}{2},\, n+m+\frac{10}{3} \end{bmatrix}\begin{bmatrix} \frac{0.5}{n+m+\frac{10}{3}} \\ 1 \end{bmatrix}$$
$$+ S(1,0)\left(\frac{\pi D}{L_o}\right)^{2m}\left(\frac{d}{D}\right)^{-\frac{11}{3}+2n} \Gamma\begin{bmatrix} n-m+\frac{1}{6},\, m-n+\frac{7}{3},\, m+\frac{11}{6} \\ -n+m+\frac{29}{6},\, -n+m+\frac{17}{6},\, n+1 \end{bmatrix}\begin{bmatrix} \frac{0.5}{n+1} \\ 1 \end{bmatrix}$$
$$+\left(\frac{D}{d}\right)^4 S(0,1)\left(\frac{\pi d}{L_o}\right)^{2m+\frac{1}{3}}\left(\frac{\pi D}{L_o}\right)^{2n} \Gamma\begin{bmatrix} n+\frac{5}{2},\, -m-n-\frac{1}{6},\, m+n+2 \\ n+5,\, n+3,\, m+1 \end{bmatrix}\begin{bmatrix} \frac{0.5}{m+1} \\ 1 \end{bmatrix}\Bigg\}. \tag{11.15}$$

For large displacements, $d/D > 1$, the integral is equal to

$$\begin{bmatrix} I_1 \\ I_T \end{bmatrix} = \frac{-0.0945\, d^{11/3}}{D^2}\Bigg\{\left(\frac{D}{d}\right)^4 S(0,1)\left(\frac{\pi d}{L_o}\right)^{2m+1/3}\left(\frac{\pi D}{L_o}\right)^{2n}$$
$$\times\Gamma\begin{bmatrix} n+\frac{5}{2},\, -m-n-\frac{1}{6},\, m+n+2 \\ n+5,\, n+3,\, m+1 \end{bmatrix}\begin{bmatrix} \frac{0.5}{m+1} \\ 1 \end{bmatrix}$$
$$+ S(0,0)\left(\frac{\pi d}{L_o}\right)^{2m}\left(\frac{d}{D}\right)^{-4-2n} \Gamma\begin{bmatrix} -m+n+\frac{1}{6},\, n+\frac{5}{2},\, m+\frac{11}{6} \\ n+5,\, n+3,\, m-n+\frac{5}{6} \end{bmatrix}\begin{bmatrix} \frac{0.5}{m-n+\frac{5}{6}} \\ 1 \end{bmatrix}$$
$$-\left(\frac{D}{d}\right)^{11/3} S(0)\left(\frac{\pi D}{L_o}\right)^{2m} \Gamma\begin{bmatrix} -m+\frac{1}{6},\, m+\frac{7}{3},\, m+\frac{11}{6} \\ m+\frac{29}{6},\, m+\frac{17}{6} \end{bmatrix}\begin{bmatrix} 0.5 \\ 1 \end{bmatrix}\Bigg\}. \tag{11.16}$$

If the outer scale goes to infinity, only terms with $m = 0$ in the first two summations for large or small displacements contribute, and these expressions reduce to the ones in which the outer scale was neglected in eq. 6.67 and eq. 6.70.

For relatively small displacements, $d/D < 1$, the tilt variance is

$$\begin{bmatrix}\sigma_\parallel^2\\ \sigma_\perp^2\end{bmatrix} = \frac{-31.5\,\mu_0}{d^{1/3}}$$
$$\times\Bigg\{S(0,0)\left(\frac{\pi d}{L_o}\right)^{2m}\left(\frac{d}{D}\right)^{2n+5}\Gamma\begin{bmatrix}-m-n-\frac{7}{3},\ n+\frac{5}{2},\ m+\frac{11}{6}\\ -n+\frac{5}{2},-n+\frac{1}{2},n+m+\frac{13}{3}\end{bmatrix}\begin{bmatrix}2n+2m+\frac{17}{3}\\ 1\end{bmatrix}$$
$$+S\,(1,0)\left(\frac{\pi D}{L_o}\right)^{2m}\left(\frac{d}{D}\right)^{2n+1/3}\Gamma\begin{bmatrix}n-m+\frac{1}{6},\ m-n+\frac{7}{3},\ m+\frac{11}{6}\\ -n+m+\frac{29}{6},-n+m+\frac{17}{6},n+2\end{bmatrix}\begin{bmatrix}2n+1\\ 1\end{bmatrix}$$
$$+S\,(0,1)\left(\frac{\pi d}{L_o}\right)^{2m+1/3}\left(\frac{\pi D}{L_o}\right)^{2n}\Gamma\begin{bmatrix}n+\frac{5}{2},-m-n-\frac{1}{6},m+n+2\\ n+5,\ n+3,\ m+2\end{bmatrix}\begin{bmatrix}2m+1\\ 1\end{bmatrix}\Bigg\}. \tag{11.17}$$

The most significant terms for small displacements are the $n = 1$, $m = 0$, and the $n = 1$, $m = 1$ terms of the second summation, which give

$$\begin{bmatrix}\sigma_\parallel^2\\ \sigma_\perp^2\end{bmatrix} \approx \frac{2.67\mu_0}{D^{1/3}}\left(\frac{d}{D}\right)^2\begin{bmatrix}3\\ 1\end{bmatrix}\left[1-20.6\left(\frac{D}{L_o}\right)^2+27.4\left(\frac{D}{L_o}\right)^{7/3}\right]. \tag{11.18}$$

The first term is the same as that in eq. 6.72 in which outer scale was neglected. In Sec. 6.1 where tilt with outer scale was considered, outer scale had a significant effect on tilt because the leading term had the ratio of diameter to outer scale raised to the inverse one-third power. Here, the effect is small if the outer-scale size is significantly greater than the diameter because the leading term is the inverse second power of that ratio. The physical reason this occurs is that for small relative aperture displacements the two apertures see the same tilt from long-wavelength turbulence, which cancels when the tilts are subtracted from each other. Mathematically, this subtraction results from the requirement that the third summation starts at $m = 1$ rather than 0. The term that was eliminated has the one-third power-law dependence on outer scale.

Plots of tilt for various ratios of outer scale to diameter are given in Fig. 11.3 and Fig. 11.4 for the parallel and perpendicular components of tilt anisoplanatism, respectively. When outer scale is 100 times the diameter, the curve is virtually identical to that for infinite outer scale, and is not plotted on the graph. This is in contrast to the result for tilt with outer scale as seen in Fig. 6.2, for which tilt is reduced by 15% for the same ratio of outer scale to diameter.

11.5 Tilt with Inner and Outer Scale

Tilt with outer scale was found in Sec. 6.1 and with inner scale in Sec. 6.3. Here tilt with both effects present is found. The integral expression for tilt with non-zero inner and finite outer scale can be found from eq. 6.1 by the insertion of the Tatarski inner-scale term to obtain

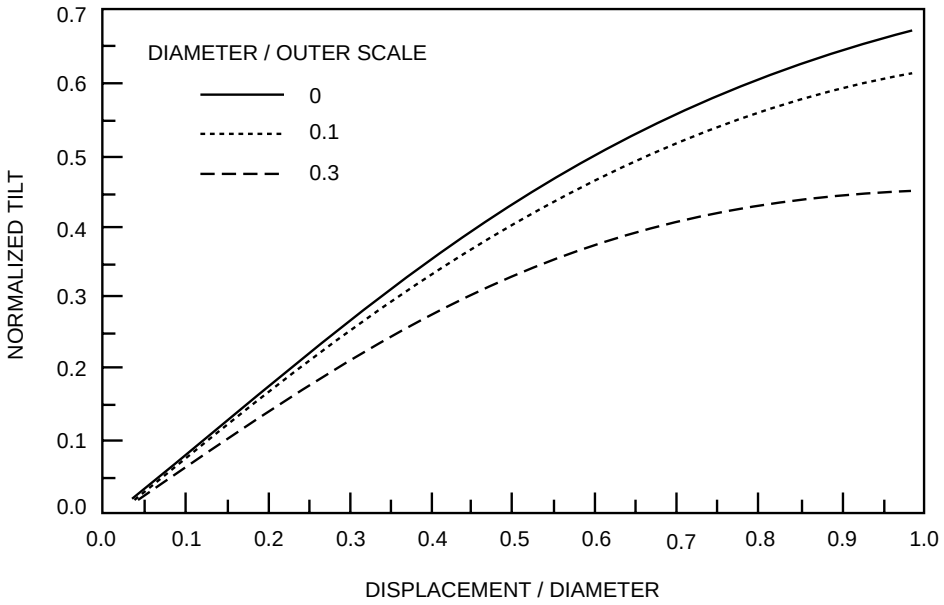

Figure 11.3. Tilt parallel to the displacement, versus displacement, for various outer-scale sizes, normalized to the tilt on the aperture.

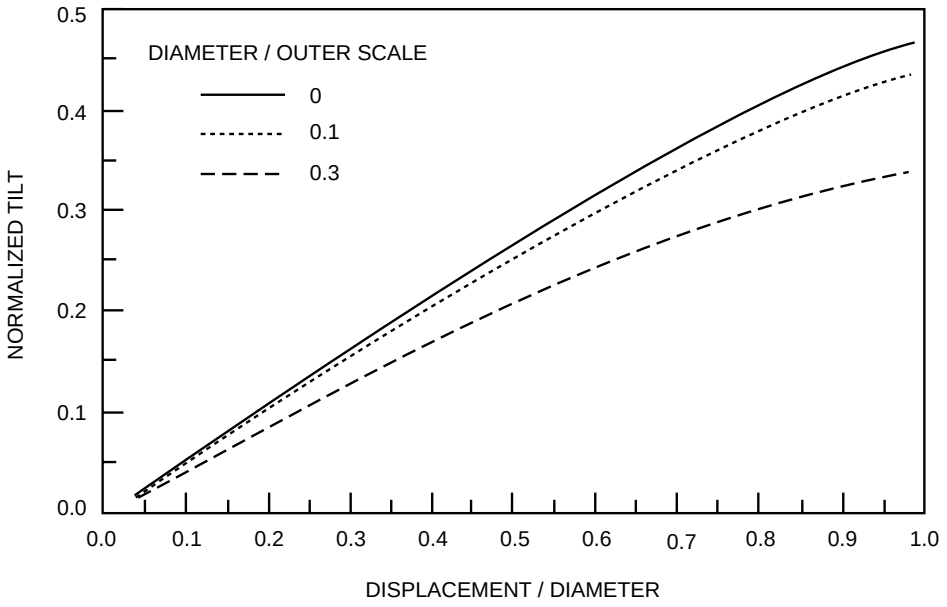

Figure 11.4. Tilt perpendicular to the displacement, versus displacement, for various outer-scale sizes, normalized to the tilt on the aperture.

$$T_o^2 = 0.2073\, k_0^2 \int_0^L dz\, C_n^2(z) \int d\boldsymbol{\kappa}\, \left(\kappa^2 + \kappa_o^2\right)^{-11/6} \left(\frac{16}{k_0 D}\right)^2$$
$$\times \left[\frac{J_2(\kappa D/2)}{\kappa D/2}\right]^2 \exp\left(-\kappa^2/\kappa_i^2\right). \tag{11.19}$$

The integrations over angle and z can easily be performed. The substitution $x = \kappa D/2$ gives

$$T_o^2 = \frac{1334\,\mu_0}{D^4\,\kappa_o^{11/3}} \int_0^\infty \frac{dx}{x}\, J_2^2(x) \left[\left(\frac{x}{\kappa_o D/2}\right)^2 + 1\right]^{-11/6} \exp\left\{-\left[x/\left(\kappa_i D/2\right)\right]^2\right\}.$$

Using the Mellin convolution integral and the Mellin transforms given by eq. 1.52, eq. 1.54, and eq. 1.47, and making the substitutions $s \to 2s$ and $t \to 2t$, one obtains

$$T_o^2 = \frac{400\,\mu_0\,\kappa_o^{-11/3}}{D^4} \frac{1}{(2\pi i)^2} \int_{C_1}\int_{C_2} ds\, dt\, \left(\frac{\kappa_o D}{2}\right)^{-2s} \left(\frac{\kappa_i D}{2}\right)^{-2t}$$
$$\times \Gamma\left[\begin{matrix} s+t+2,\ -s-t+\frac{1}{2},\ -s,\ s+\frac{11}{6},\ -t \\ -s-t+3,\ -s-t+1 \end{matrix}\right]. \tag{11.20}$$

From eq. 10.77 one finds that $\Delta_s = 2$, and $\Delta_t = 1$. There are 8 sets of 2-poles that are given by:

(1) $s+t+2 = -n\,;\ -s = -m,$
(2) $s+t+2 = -n\,;\ s+\frac{11}{6} = -m,$
(3) $s+t+2 = -n\,;\ -t = -m,$
(4) $-s-t+\frac{1}{2} = -n\,;\ -s = -m,$
(5) $-s-t+\frac{1}{2} = -n\,;\ s+\frac{11}{6} = -m,$
(6) $-s-t-\frac{1}{2} = -n\,;\ -t = -m,$
(7) $-s = -n\,;\ -t = -m,$ and
(8) $s+\frac{11}{6} = -n\,;\ -t = -m.$

This leads to terms of the type:

(1) $\left(\frac{L_o}{L_i}\right)^{2m} \left(\frac{\pi D}{L_i}\right)^{2n} F(-1,1),$

(2) $\left(\frac{L_i}{L_o}\right)^{2m} \left(\frac{\pi D}{L_i}\right)^{2n} F(-1,-1),$

(3) $\left(\frac{L_i}{L_o}\right)^{2m} \left(\frac{\pi D}{L_o}\right)^{2n} F(-2,-1),$

(4) $\left(\frac{L_o}{L_i}\right)^{2m} \left(\frac{L_i}{\pi D}\right)^{2n} F(1,1),$

$$(5) \quad \left(\frac{L_i}{L_o}\right)^{2m} \left(\frac{L_i}{\pi D}\right)^{2n} F(1,-1),$$

$$(6) \quad \left(\frac{L_i}{L_o}\right)^{2m} \left(\frac{L_o}{\pi D}\right)^{2n} F(2,-1),$$

$$(7) \quad \left(\frac{L_o}{\pi D}\right)^{2n} \left(\frac{L_i}{\pi D}\right)^{2m} F(2,1), \text{ and}$$

$$(8) \quad \left(\frac{\pi D}{L_o}\right)^{2n} \left(\frac{L_i}{\pi D}\right)^{2m} F(-2,1).$$

The Taylor series solution is the sum of the second and third series. This converges slowly for normal parameter values, and the solution is not expressed in this form. Instead, a solution that contains asymptotic series that gives an accurate answer with the fewest number of terms is found.

Table 11.4 contains the range of applicability of the various series. Terms 1, 2, 4, 6, and 7 apply only when the outer scale is less than the diameter or the inner scale, or if the inner scale is larger than the diameter. Therefore, these are not included in the solution of interest. The only terms that are appropriate in the case in which outer scale is larger than the diameter and also inner scale is less than the diameter are 3, 5, and 8.

Table 11.4. Series ranges of applicability for most rapid convergence, for the problem in which the effect of inner and outer scale on the tilt is found.

2–Pole Set	Solution Type	Parameter	Range
1	Asymp	$L_i > L_o$	$L_i/\pi D > 1$
2	Taylor	$L_i < L_o$	$L_i/\pi D > 1$
3	Taylor	$L_i < L_o$	$L_o/\pi D > 1$
4	Asymp	$L_i > L_o$	$L_i/\pi D < 1$
5	Asymp	$L_i < L_o$	$L_i/\pi D < 1$
6	Asymp	$L_i < L_o$	$L_o/\pi D < 1$
7	Asymp	$L_i/\pi D < 1$	$L_o/\pi D < 1$
8	Asymp	$L_i/\pi D < 1$	$L_o/\pi D > 1$

These asymptotic and Taylor series lead to

$$
\begin{aligned}
T_o^2 \sim{}& \frac{6.08\,\mu_0}{D^{1/3}} \\
&\times\left\{5.18\,S\left(0,0\right)\left(\frac{\pi D}{L_o}\right)^{2n+1/3}\left(\frac{L_i}{L_o}\right)^{2m}\Gamma\left[\begin{matrix} n+\frac{5}{2},\, n+m+2,\, -n-m-\frac{1}{6} \\ n+5,\, n+3 \end{matrix}\right]\right. \\
&+5.18\,S\left(0,0a\right)\left(\frac{\pi D}{L_o}\right)^{2n}\left(\frac{L_i}{\pi D}\right)^{2m}\Gamma\left[\begin{matrix} m-n+\frac{1}{6},\, n-m+\frac{7}{3},\, n+\frac{11}{6} \\ n-m+\frac{29}{6},\, n-m+\frac{17}{6} \end{matrix}\right] \\
&+0.0248\,S\left(0a,0\right)\left(\frac{L_i}{D}\right)^{14/3}\left(\frac{L_i}{L_o}\right)^{2m}\left(\frac{L_i}{\pi D}\right)^{2n} \\
&\left.\times\Gamma\left[\begin{matrix} n+\frac{5}{2},\, m+\frac{11}{6},\, -n-m-\frac{7}{3} \\ -n+\frac{5}{2},\, -n+\frac{1}{2} \end{matrix}\right]\right\}. \qquad (11.21)
\end{aligned}
$$

The steepest-descent contribution must be added to these asymptotic series. The technique discussed in Sec. 10.4 is used to determine this part of the solution. As seen from eq. 11.20, the parameter associated with the complex variable s is small, and the parameter $\pi D/L_o$ associated with the complex variable t is large. Since $\Delta_1 = 0$, the complex integral is evaluated sequentially with the evaluation of the steepest-descent contribution over the variable t and normal, pole-residue evaluation over the variable s. Equation 11.20 is rewritten as

$$
\begin{aligned}
T_o^2 = {}& \frac{400\,\mu_0\kappa_o^{-11/3}}{D^4}\,\frac{1}{2\pi i}\int\limits_{C_1} ds\,\left(\frac{\kappa_o D}{2}\right)^{-2s}\Gamma\left[-s\right] \\
&\times\frac{1}{2\pi i}\int\limits_{C_2} dt\,\left(\frac{\kappa_i D}{2}\right)^{-2t}\Gamma\left[\begin{matrix} s+t+2,\, -s-t+\frac{1}{2},\, -t,\, s+\frac{11}{6} \\ -s-t+3,\, -s-t+1 \end{matrix}\right]. \qquad (11.22)
\end{aligned}
$$

Using eq. 5.94 to evaluate the steepest-descent contribution, one finds that it has exponential decay and can be neglected compared to the pole contributions. This exponential decay was the same behavior found in Sec. 6.3 when the inner scale was much smaller than the diameter. Therefore, the solution in eq. 11.21 is the complete solution.

If inner scale goes to zero, the only terms left are the $m=0$ terms of the first and last summations, which reduce to the series obtained in eq. 6.6. If the outer scale goes to infinity, the only terms left are the $n = 0$ term of the first series, and the $m = 0$ term of the third series, which reduce to the series obtained in eq. 6.22. A plot of the change in variance, divided by the variance with zero inner-scale size, is given in Fig. 11.5.

11.6 Power Spectrum of Tilt with Outer Scale

The temporal power spectrum of Zernike tilt with infinite outer-scale size was found in Sec. 6.7. When finite outer scale is considered, a two-dimensional com-

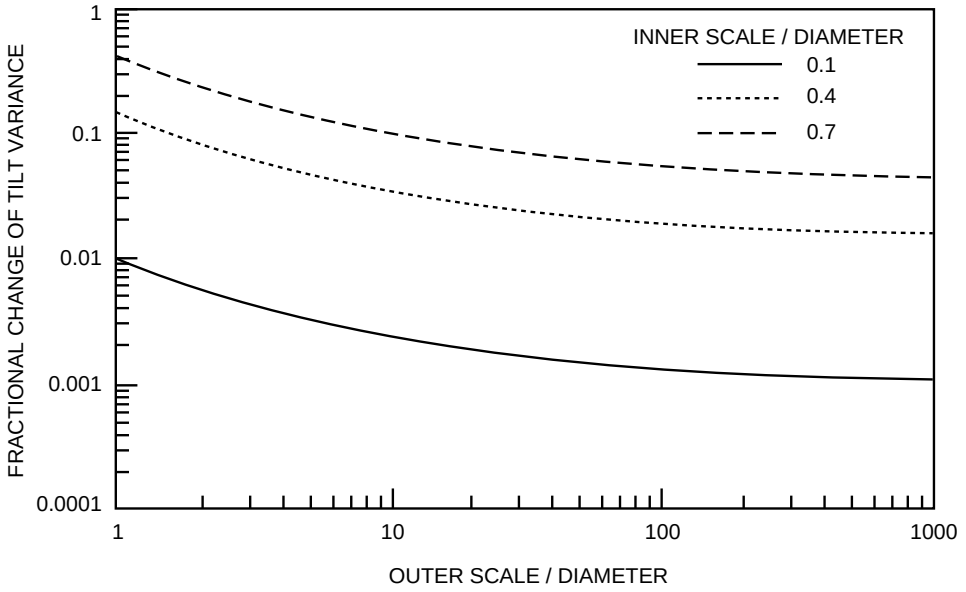

Figure 11.5. Fractional change of the tilt variance versus the ratio of the outer-scale size to the diameter, with various inner-scale sizes. Notice that the effect of inner scale is to change the scaling of the curves. There is little change in shape. This occurs because inner and outer scale operate at opposite ends of the turbulence spectrum and their effects are almost independent.

plex integral must be evaluated to compute the tilt power spectral density. The integral that must be evaluated has the general form given in eq. 6.84 except that the spectrum has outer scale included and is equal to

$$S_T(\omega) = 2.606\, k_0^2 \omega \int_0^L dz\, \frac{C_n^2(z)}{v^2(z)} \times \int_0^\infty c\, dc\, \frac{U(c-1)}{\sqrt{c^2-1}}\, \cos^2\left[\frac{\gamma\, \omega^2\, c^2 z}{2 v^2(z) k_0}\right] f\left[\frac{\omega\, c}{v(z)}\right] F\left[\frac{\gamma\, \omega\, c}{v(z)}, z\right]. \tag{11.23}$$

One neglects diffraction by setting the cosine term equal to unity. The collimated beam case is considered for which $\gamma = 1$. The filter function for tilt is given in eq. 3.21. Change variables by letting $x = 2\, v(z)/\omega\, D$, and $y = v(z)\, \kappa_o/\omega$. The tilt spectrum is expressed as

$$S_T(\omega) = \frac{2668}{\omega\, D^4\, \kappa_o^{11/3}} \int_0^L dz\, C_n^2(z) \int_0^\infty \frac{dc}{c}\, \frac{U(c-1)}{\sqrt{c^2-1}}\, J_2^2\left(\frac{c}{x}\right) \left[1 + \left(\frac{c}{y}\right)^2\right]^{-11/6}. \tag{11.24}$$

With the generalized Mellin convolution integral and the Mellin transforms in eq. 1.56, eq. 1.52, and eq. 1.54, and after the substitution $s \to -2s$ and $t \to -2t$, the integral over c transforms into

$$I = \frac{1}{2\Gamma[11/6]} \frac{1}{(2\pi i)^2} \int_{C_1} \int_{C_2} ds\, dt\, \Gamma\begin{bmatrix} s+2,\ -s+\frac{1}{2},\ t,\ -t+\frac{11}{6},\ s+t+\frac{1}{2} \\ -s+1,\ -s+3,\ s+t+1 \end{bmatrix} \times \left[\frac{\omega D}{2v(z)}\right]^{-2s} \left[\frac{L_o\,\omega}{2\pi\, v(z)}\right]^{-2t}.$$

From the definition in eq. 10.79, $\Delta_s = 2$, and $\Delta_t = 0$. There are eight sets of 2-poles that can contribute to I:

(1) $s+2 = -m\,;\ t = -n,$
(2) $-s+1/2 = -m\,;\ t = -n,$
(3) $s+2 = -m\,;\ -t+11/6 = -n,$
(4) $-s+1/2 = -m\,;\ -t+11/6 = -n,$
(5) $s+t+1/2 = -m\,;\ t = -n,$
(6) $s+t+1/2 = -m\,;\ -t+11/6 = -n,$
(7) $s+2 = -m\,;\ s+t+1/2 = -n,$ and
(8) $-s+1/2 = -m\,;\ s+t+1/2 = -n.$

For each of these cases, the 2-poles lead to power series that contain terms which vary as:

(1) $\left[\frac{\omega D}{2v(z)}\right]^{2m} \left[\frac{L_o\,\omega}{2\pi\, v(z)}\right]^{2n} F(0,-2)\,,$

(2) $\left[\frac{2v(z)}{\omega D}\right]^{2m} \left[\frac{L_o\,\omega}{2\pi\, v(z)}\right]^{2n} F(0,2)\,,$

(3) $\left[\frac{\omega D}{2v(z)}\right]^{2m} \left[\frac{2\pi\, v(z)}{L_o\,\omega}\right]^{2n} F(0,-2)\,,$

(4) $\left[\frac{2v(z)}{\omega D}\right]^{2m} \left[\frac{2\pi\, v(z)}{L_o\,\omega}\right]^{2n} F(0,2)\,,$

(5) $\left[\frac{\omega D}{2v(z)}\right]^{2m} \left(\frac{L_o}{\pi\, D}\right)^{2n} F(2,-2)\,,$

(6) $\left[\frac{\omega D}{2v(z)}\right]^{2m} \left(\frac{\pi\, D}{L_o}\right)^{2n} F(-2,-2)\,,$

(7) $\left(\frac{\pi\, D}{L_o}\right)^{2m} \left[\frac{L_o\,\omega}{2\pi\, v(z)}\right]^{2n} F(0,-2)\,,$ and

(8) $\left(\frac{L_o}{\pi\, D}\right)^{2m} \left[\frac{L_o\,\omega}{2\pi\, v(z)}\right]^{2n} F(0,2)\,.$

Table 11.5 summarizes the series type and the parameter range over which the series should be used to obtain a solution that requires the least number of series terms to obtain an accurate answer.

Table 11.5. Properties of series solutions and ranges of applicability for most rapid series convergence in the problem in which the temporal power spectrum of tilt with outer scale is found.

2–Pole Set	Solution Type	Parameter	Range
1	Taylor	$2\pi v(z)/\omega L_o > 1$	$2v(z)/\omega D > 1$
2	Asymp	$2\pi v(z)/\omega L_o > 1$	$2v(z)/\omega D < 1$
3	Taylor	$2\pi v(z)/\omega L_o < 1$	$2v(z)/\omega D > 1$
4	Asymp	$2\pi v(z)/\omega L_o < 1$	$2v(z)/\omega D < 1$
5	Asymp	$\pi D/L_o > 1$	$2v(z)/\omega D > 1$
6	Taylor	$\pi D/L_o < 1$	$2v(z)/\omega D > 1$
7	Taylor	$2\pi v(z)/\omega L_o > 1$	$\pi D/L_o < 1$
8	Asymp	$2\pi v(z)/\omega L_o > 1$	$\pi D/L_o > 1$

Here I assume that $D/L_o << 1$, which results in eliminating the contribution of asymptotic series 2, 5, and 8. The remaining 5 series fall into three parameter regimes:

1. For low frequencies, $\omega < 2\pi v(z)/L_o$, terms 1, 6, and 7 provide Taylor series. The natural parameters in eq. 11.24 are given by $\omega D/2v(z)$ and $L_o\omega/2\pi v(z)$.
2. At mid-frequencies, $2\pi v(z)/L_o < \omega < 2v(z)/D$, terms 3 and 6 provide Taylor series.
3. At high frequencies, $\omega > 2v(z)/D$, terms 3 and 6 continue to provide the Taylor series solution for the spectrum although they converge slowly. The asymptotic series from term 4 and the steepest-descent contribution may be used in this regime rather than the slowly converging Taylor series to approximate the spectrum with only a few series terms.

The steepest-descent contribution to the asymptotic form of I is obtained with the use of the procedure explained in Sec. 10.4. Since $\Delta_2 = \Delta_3 = 0$, the integral is evaluated sequentially. Accordingly, the integral in eq. 11.24 is rewritten as

$$E = \frac{1}{2\Gamma[11/6]}\,\frac{1}{2\pi i}\int\limits_{C_2} dt\,\Gamma\left[t,\ -t+\tfrac{11}{6}\right]\left[\frac{L_o\,\omega}{2\pi v(z)}\right]^{-2t} I_2, \tag{11.25}$$

where

$$I_2 = \frac{1}{2\pi i}\int\limits_{C_1} ds\,\Gamma\left[\begin{matrix} s+2,\ -s+\frac{1}{2},\ s+t+\frac{1}{2} \\ -s+1,\ -s+3,\ s+t+1 \end{matrix}\right]\left[\frac{\omega D}{2v(z)}\right]^{-2s}. \tag{11.26}$$

Equation eq. 5.94 is used to show that

$$I_2 \sim \frac{1}{\sqrt{\pi}}\left[\frac{2v(z)}{\omega D}\right]^{3/2}\cos\left[\frac{\omega D}{v(z)}-\frac{\pi}{4}\right]. \tag{11.27}$$

In this problem I_2 does not depend upon t, and the evaluation of eq. 11.25 is trivial. Because $\Delta_t = 0$ and $L_o\omega/2\pi\, v(z) > 1$, the contour in eq. 11.25 is closed to the right, and pole residues are evaluated at the points $t = m + 11/6$. This gives a series result that can be expressed as a generalized hypergeometric function with the rules in Sec. 1.3 as

$$E \sim \frac{\kappa_o^{11/3}/\sqrt{2/\pi}}{D^{3/2}\Gamma(11/6)} \left[\frac{v(z)}{\omega}\right]^{31/6} \cos\left[\frac{\omega D}{v(z)} - \frac{\pi}{4}\right] S\,(0)\, \Gamma\Big[m + \tfrac{11}{6}\Big] \left[\frac{2\pi\, v(z)}{L_o\omega}\right]^{2m}$$

$$\sim \frac{\kappa_o^{11/3}}{D^{3/2}} \sqrt{\frac{2}{\pi}} \left[\frac{v(z)}{\omega}\right]^{31/6} \cos\left[\frac{\omega D}{v(z)} - \frac{\pi}{4}\right] {}_1F_0\left[\frac{11}{6}; -\left[\frac{2\pi\, v(z)}{L_o\,\omega}\right]^2\right]. \qquad (11.28)$$

With the identity given in eq. 1.67, this becomes

$$E \sim \frac{\kappa_o^{11/3}}{D^{3/2}} \sqrt{\frac{2}{\pi}} \left[\frac{v(z)}{\omega}\right]^{31/6} \left\{1 + \left[\frac{2\pi\, v(z)}{L_o\omega}\right]^2\right\}^{-11/6} \cos\left[\frac{\omega D}{v(z)} - \frac{\pi}{4}\right]. \qquad (11.29)$$

Using pole residues to evaluate series 1, 3, 4, 6, and 7 combined with the result given above leads to the expressions that follow for the power spectral density of tilt with finite outer scale.

For $\omega < 2\pi v(z)/L_o$, after the interchange of m and n in the first summation,

$$S_T(\omega) = \frac{88.64}{\kappa_o^{2/3}} S\,(0,0) \left(\frac{\pi D}{L_o}\right)^{2n} v_{-2m-1}$$

$$\times \left\{ \Gamma\left[\begin{matrix} n + \frac{5}{2},\, m - n + \frac{1}{3},\, -m + n + \frac{3}{2} \\ -m + \frac{1}{2},\, n + 3,\, n + 5 \end{matrix}\right] \left(\frac{L_o\omega}{2\pi}\right)^{2m} \right.$$

$$\left. + \left(\frac{\pi D}{L_o}\right)^{2/3} \Gamma\left[\begin{matrix} n + \frac{11}{6},\, m + n + \frac{17}{6},\, -m - n - \frac{1}{3} \\ -m + \frac{1}{2},\, m + n + \frac{10}{3},\, m + n + \frac{16}{3} \end{matrix}\right] \left(\frac{\omega D}{2}\right)^{2m} \right\}. \qquad (11.30)$$

The contribution from Series 1 does not appear here because the coefficients in this series are all zero. The n^{th} velocity moment defined in eq. 4.83 is expressed as v_n in these results. For $2\pi v(z)/L_o < \omega < 2v(z)/D$ one obtains

$$S_T(\omega) = \frac{52.53\, D^{2/3}}{\Gamma[11/6]} \left(\frac{2}{\omega D}\right)^{2/3} S\,(0,0) \left(\frac{\omega D}{2}\right)^{2m}$$

$$\times \left\{ \Gamma\left[\begin{matrix} m + \frac{5}{2},\, n + \frac{11}{6},\, -m + n + \frac{1}{3} \\ m + 3,\, m + 5,\, -m + n + \frac{5}{6} \end{matrix}\right] \left(\frac{2\pi}{L_o\omega}\right)^{2n} v_{-2m+2n-1/3} \right.$$

$$\left. + \Gamma\left[\begin{matrix} n + \frac{11}{6},\, m + n + \frac{17}{6},\, -m - n - \frac{1}{3} \\ -m + \frac{1}{2},\, m + n + \frac{10}{3},\, m + n + \frac{16}{3} \end{matrix}\right] \left(\frac{\omega D}{2}\right)^{2/3} \left(\frac{\pi D}{L_o}\right)^{2n} v_{-2m-1} \right\}. \qquad (11.31)$$

For $\omega > 2v(z)/D$, eq. 11.30 provides a slowly converging Taylor series solution. The asymptotic solution for the power spectral density in this regime is given by

$$S_T(\omega) \sim \frac{52.53\, D^{2/3}}{\Gamma[11/6]} \left(\frac{2}{\omega D}\right)^{17/3}$$
$$\times \left\{ \int_0^L dz\, C_n^2(z) \frac{\Gamma[11/6]}{\sqrt{\pi}} \left[\frac{2\,v(z)}{\omega D}\right]^{1/2} \frac{v(z)^{14/3} \cos\left[\omega D/v(z) - \frac{\pi}{4}\right]}{\left[1 + (2\pi v(z)/L_o\,\omega)^2\right]^{11/6}} \right.$$
$$\left. + S(0,0a)\Gamma\begin{bmatrix} m+\frac{5}{2},\, n+\frac{11}{6},\, m+n+\frac{17}{6} \\ -m+\frac{1}{2}, -m+\frac{5}{2}, m+n+\frac{10}{3} \end{bmatrix} \left(\frac{2}{\omega D}\right)^{2m} \left(\frac{2\pi}{L_o\omega}\right)^{2n} v_{2m+2n+14/3} \right\}. \tag{11.32}$$

At low frequencies, $\omega < 2\pi v(z)/L_o$, the tilt spectrum is flat, or stated equivalently, the spectrum is proportional to ω^0. In the mid-range of frequencies, $2\pi v(z)/L_o < \omega < 2v(z)/D$, the tilt spectrum is proportional to $\omega^{-2/3}$. This regime corresponds to the low-frequency portion of the tilt spectrum in the absence of outer-scale effects. At high frequencies, $\omega > 2v(z)/D$, the tilt spectrum is proportional to $\omega^{-17/3}$ as is the case when outer scale is neglected. In the limit as L_o grows large and outer scale no longer influences the tilt spectrum, eq. 11.30 and eq. 11.31 reduce to the expressions for tilt spectrum without outer scale derived in Sec. 6.7.

For a constant velocity (independent of altitude), the tilt spectrum for the three frequency regimes is given by the following equations. For $\omega < 2\pi v(z)/L_o$,

$$S_T(\omega) = \frac{88.64\,\mu_0}{v\,\kappa_o^{2/3}} S\,(0,0) \left(\frac{\pi D}{L_o}\right)^{2n}$$
$$\times \left\{ \Gamma\begin{bmatrix} n+\frac{5}{2},\, m-n+\frac{1}{3},\, -m+n+\frac{3}{2} \\ -m+\frac{1}{2},\, n+3,\, n+5 \end{bmatrix} \left(\frac{L_o\omega}{2\pi\, v}\right)^{2m} \right.$$
$$\left. + \left(\frac{\pi D}{L_o}\right)^{2/3} \Gamma\begin{bmatrix} n+\frac{11}{6},\, m+n+\frac{17}{6},\, -m-n-\frac{1}{3} \\ -m+\frac{1}{2},\, m+n+\frac{10}{3},\, m+n+\frac{16}{3} \end{bmatrix} \left(\frac{\omega D}{2v}\right)^{2m} \right\}. \tag{11.33}$$

For $2\pi v/L_o < \omega < 2v/D$,

$$S_T(\omega) = \frac{52.53\,\mu_0\, D^{2/3}}{v\,\Gamma[11/6]} S\,(0,0)$$
$$\times \left\{ \Gamma\begin{bmatrix} m+\frac{5}{2},\, n+\frac{11}{6},\, -m+n+\frac{1}{3} \\ m+3,\, m+5,\, -m+n+\frac{5}{6} \end{bmatrix} \left(\frac{\omega D}{2v}\right)^{2m-2/3} \left(\frac{2\pi\, v}{L_o\omega}\right)^{2n} \right.$$
$$\left. + \Gamma\begin{bmatrix} n+\frac{11}{6},\, m+n+\frac{17}{6},\, -m-n-\frac{1}{3} \\ -m+\frac{1}{2},\, m+n+\frac{10}{3},\, m+n+\frac{16}{3} \end{bmatrix} \left(\frac{\omega D}{2v}\right)^{2m} \left(\frac{\pi D}{L_o}\right)^{2n} \right\}. \tag{11.34}$$

For $\omega > 2v/D$, eq. 11.33 provides a slowly converging Taylor series solution. The asymptotic solution for the power spectral density in this regime is given by

$$S_T(\omega) \sim \frac{52.53\,\mu_0\,D^{2/3}}{v}\left(\frac{2\,v}{\omega\,D}\right)^{17/3}\left\{\frac{1}{\sqrt{\pi}}\left(\frac{2\,v}{\omega\,D}\right)^{1/2}\frac{\cos\left(\omega\,D/v-\frac{\pi}{4}\right)}{\left[1+(2\pi\,v/L_o\omega)^2\right]^{11/6}}\right.$$
$$\left.+\frac{S\,(0,0a)}{\Gamma\,[11/6]}\Gamma\begin{bmatrix} m+\frac{5}{2},\, n+\frac{11}{6},\, m+n+\frac{17}{6} \\ -m+\frac{1}{2},\, -m+\frac{5}{2},\, m+n+\frac{10}{3}\end{bmatrix}\left(\frac{2\,v}{\omega\,D}\right)^{2m}\left(\frac{2\pi\,v}{L_o\,\omega}\right)^{2n}\right\}. \tag{11.35}$$

The power spectral density is plotted in Fig. 11.6 as a function of $f\,D/v$ for several values of the parameter D/L_o. The curves have been normalized so that the power spectral density at $f\,D/v = 1$ is unity for infinite outer scale. These spectra are similar to the spectra without outer scale given in Fig. 6.14 except that the spectrum saturates below the frequency $\omega = 2\pi\,v/L_o$ due to outer-scale effects. Because it was assumed that $L_o > D$, outer scale has little impact on the high-frequency portion of the tilt spectrum.

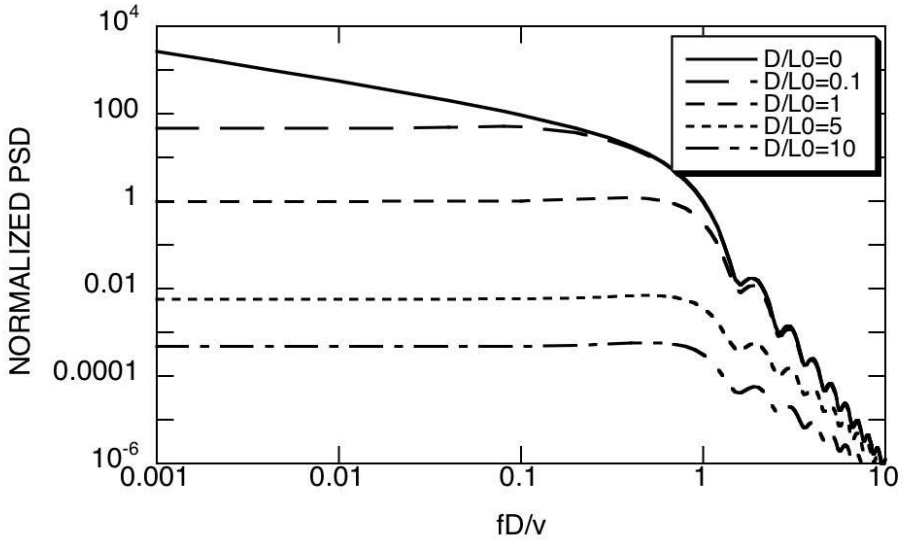

Figure 11.6. Normalized tilt power spectral density with the assumption of a constant wind velocity and several ratios of outer-scale size to aperture diameter. Smaller outer scale causes a lowering and leveling off of the spectral power at lower frequencies.

11.7 Structure and Correlation Functions with Inner and Outer Scales

In Sec. 11.6 the impact of non-zero inner and finite outer scale on tilt variance was examined. Inner and outer scales also influence the phase variance of a wave that has propagated through turbulence. For example, if infinite outer scale in Kolmogorov turbulence is assumed, the phase variance is unbounded, and if finite outer scale in Kolmogorov turbulence is assumed, the phase variance is finite. Unfortunately, the inclusion of inner and outer scale in turbulence calculations often leads to integrals that are difficult to evaluate. This is one of the reasons to assume that the outer scale is infinite and to work around the problem of infinite phase. Structure functions are often used in calculations rather than correlation functions for this reason. As shown in this section, Mellin transform methods can be used to solve for both structure and correlation functions with inner and outer scale. First, one derives the structure function, after which solving for the phase correlation function is a simple extension.

The expression for the structure function in eq. 2.123 with the turbulence spectrum in eq. 2.34 is

$$\mathcal{D}\left(\mathbf{d}\right) = 0.4146\, k_0^2 \int_0^L dz\, C_n^2(z) \times \int d\boldsymbol{\kappa}\, \left(\kappa^2 + \kappa_o^2\right)^{-11/6} \exp\left(-\kappa^2/\kappa_i^2\right) \cos^2\left[\frac{\kappa^2(L-z)}{2k_0}\right] \left[1 - \cos\left(\boldsymbol{\kappa}\cdot\mathbf{d}\right)\right]. \tag{11.36}$$

Furthermore, it is assumed that turbulence is in the near field of the receiver; therefore, the $\cos^2$ term may be set to unity. The integral over angle in κ space may be performed to give

$$\mathcal{D}\left(d\right) = 2.605\, k_0^2 \int_0^L dz\, C_n^2(z) \int_0^\infty d\kappa\, \kappa\, \left(\kappa^2 + \kappa_o^2\right)^{-11/6} \exp\left(-\kappa^2/\kappa_i^2\right) \left[1 - J_0(\kappa\, d)\right]. \tag{11.37}$$

The integral over κ is evaluated with Mellin transform techniques. In order to generalize the results, the exponent $-11/6$ is replaced with $-\alpha/2$. For Kolmogorov turbulence, $\alpha = 11/3$. After the change of variables $q = \kappa d$, $x = d\kappa_i$, and $y = d\kappa_o$, the integral over κ becomes

$$Q = \frac{1}{d^2\kappa_o^\alpha} \int_0^\infty \frac{dq}{q}\, q^2 \left[1 - J_0\left(q\right)\right] \exp\left[-(q/x)^2\right] \left[1 + (q/y)^2\right]^{-\alpha/2}.$$

With standard Mellin transform techniques, this integral is converted into a contour integral over two complex planes with the transforms in eq. 1.47, eq. 1.51, and eq. 1.54, and the substitutions $s \to -2s$ and $t \to -2t$ to obtain

$$Q = \frac{-2}{d^2 \Gamma\left[\alpha/2\right] \kappa_o^\alpha} \frac{1}{(2\pi i)^2} \int_{C_1} \int_{C_2} ds\, dt \left(\frac{x}{2}\right)^{-2s} \left(\frac{y}{2}\right)^{-2t}$$
$$\times \Gamma \begin{bmatrix} s+t+1*,\ -s,\ -t,\ t+\alpha/2 \\ -s-t \end{bmatrix}.$$

The * indicates that the contour of integration is shifted to the left by one pole location. In this problem, $\Delta_s = 1$, and $\Delta_t = 2$. The two-poles associated with the integrand are located at:

$$\begin{array}{ll} (1) & s+t+1 = -m*;\ -s = -n, \\ (2) & s+t+1 = -n*;\ -t = -m, \\ (3) & s+t+1 = -n*;\ \alpha/2+t = -m, \\ (4) & -s = -n;\ -t = -m, \text{ and} \\ (5) & -s = -n;\ \alpha/2+t = -m. \end{array}$$

The range of the integers m and n are from 0 to ∞. The asterisk after an index indicates that the range of that index is 1 to ∞ for one series and 0 to ∞ for the other. These relations lead to terms of the form:

$$\begin{array}{ll} (1) & \left(\frac{\pi d}{L_o}\right)^{2m*} \left(\frac{L_i}{L_o}\right)^{2n} F\left(-1,-2\right), \\ (2) & \left(\frac{L_o}{L_i}\right)^{2m} \left(\frac{\pi d}{L_i}\right)^{2n*} F\left(-1,1\right), \\ (3) & \left(\frac{L_i}{L_o}\right)^{2m} \left(\frac{\pi d}{L_i}\right)^{2n*} F\left(-1,-1\right), \\ (4) & \left(\frac{L_o}{\pi d}\right)^{2m} \left(\frac{L_i}{\pi d}\right)^{2n} F\left(1,2\right), \text{ and} \\ (5) & \left(\frac{\pi d}{L_o}\right)^{2m} \left(\frac{L_i}{\pi d}\right)^{2n} F\left(1,-2\right). \end{array} \tag{11.38}$$

The sum of Taylor series 1 and 3 gives the complete solution for all parameter values. The Taylor series solution, however, converges slowly when $L_i/\pi < d < L_o/\pi$, and even more slowly when $d > L_o/\pi$. To ease computational requirements, I seek asymptotic approximations when $d > L_i/\pi$ that allow me to approximate the structure function with only a few terms. The approximations also more clearly illustrate the functional dependence of the structure function on parameters $\pi d/L_i$, $\pi d/L_o$, and L_i/L_o in the regimes where many terms from the Taylor series are required. One can determine the parameter regimes where asymptotic approximations are useful by examining Table 11.6.

There are three regimes in this problem. In the first regime where $d < L_i/\pi$, Taylor series 1 and 3 converge rapidly. In the second regime that occurs when $L_i/\pi < d < L_o/\pi$, Taylor series 1, asymptotic series 5, and a steepest-descent component should be used to obtain accurate estimates with a few terms. In

Table 11.6. Series ranges of applicability for most rapid convergence for structure function with inner and outer scale present.

2–Pole Set	Solution Type	Parameter Range	
1	Taylor	$L_i < L_o$	$\pi d < L_o$
2	Asymp	$L_i > L_o$	$\pi d < L_i$
3	Taylor	$L_i < L_o$	$\pi d < L_i$
4	Asymp	$\pi d > L_i$	$\pi d > L_o$
5	Asymp	$\pi d > L_i$	$\pi d < L_o$

the third regime, where $d > L_o/\pi$, asymptotic series 4 and a steepest-descent component provide a good approximation to the structure function. Because the inner-scale size L_i is always less than the outer-scale size L_o, the series that corresponds to the second pole set in the table never contributes. The series that results from the evaluation of the residues at 2-poles 1, 3, 4, and 5 are given below:

$$Q_1 = \frac{-2\pi^2\kappa_o^{-\alpha}}{L_o^2\,\Gamma\left[\alpha/2\right]} S\left(0,1\right)\left(\frac{L_i}{L_o}\right)^{2n}\left(\frac{\pi\,d}{L_o}\right)^{2m}\Gamma\left[\begin{matrix} m+n+1,\ -m-n+\alpha/2-1 \\ m+1 \end{matrix}\right],$$

$$Q_3 = \frac{-2\pi^2\left(d/2\right)^{\alpha}}{L_i^2\,\Gamma\left[\alpha/2\right]} S\left(1,0\right)\left(\frac{L_i}{L_o}\right)^{2m}\left(\frac{\pi\,d}{L_i}\right)^{2n-\alpha}\Gamma\left[\begin{matrix} -m+n-\alpha/2+1,\ m+\alpha/2 \\ n+1 \end{matrix}\right],$$

$$Q_4 = \frac{-2\,\kappa_o^{-\alpha}}{d^2\,\Gamma\left[\alpha/2\right]} S\left(0a,0a\right)\left(\frac{L_i}{\pi\,d}\right)^{2n}\left(\frac{L_o}{\pi\,d}\right)^{2m}\Gamma\left[\begin{matrix} m+n+1,\ m+\alpha/2 \\ -m-n \end{matrix}\right] = 0,$$

and

$$Q_5 = \frac{-2\,\left(d/2\right)^{\alpha}}{d^2\,\Gamma\left[\alpha/2\right]} S\left(0a,0\right)\left(\frac{L_i}{\pi\,d}\right)^{2n}\left(\frac{\pi\,d}{L_o}\right)^{2m}\Gamma\left[\begin{matrix} -m+n-\alpha/2+1,\ m+\alpha/2 \\ m-n+\alpha/2 \end{matrix}\right].$$

Because $\Gamma[-m-n]$ is infinite for all m and n, Q_4 is equal to zero. I must also be concerned with the B_2 and C_3 terms discussed in Sec. 10.3 and defined in eq. 10.57 and eq. 10.59. In the second and third regimes, the third set of two-poles contributes a series of type B_2. The first set of two-poles contributes a series of type C_3 in the third regime. These terms are given by

$$B_2 = \frac{-2\pi}{\Gamma\left[\alpha/2\right]\cos\left(\pi\,\alpha/2\right)}\left(\frac{L_i}{2\pi}\right)^{\alpha}\left(\frac{\pi}{L_i}\right)^{2}\exp\left(\frac{L_i}{L_o}\right)^{2}, \quad \text{and} \tag{11.39}$$

$$C_3 = \frac{-2}{\Gamma\left[\alpha/2\right]}\left(\frac{L_o}{2\pi}\right)^{\alpha}\left(\frac{\pi}{L_o}\right)^{2}\sum_{n=0}^{\infty}\left(-1\right)^{n}\,\Gamma\left[-n+\alpha/2-1\right]\left(\frac{L_i}{L_o}\right)^{2n}. \tag{11.40}$$

The steepest-descent contributions to the asymptotic forms for the integral must be calculated for the second and third regimes. Since $\Delta_2 = 0$, the steepest-descent contribution is found by sequential evaluation of the two-dimensional integral.

In the second regime, x is large and y is small. The integral may be rewritten as

$$\tilde{Q} = \frac{-2\,\kappa_o^{-\alpha}}{d^2\,\Gamma\,[\alpha/2]}\frac{1}{(2\pi i)^2}\int\limits_{C_1} dt\,\left(\frac{y}{2}\right)^{-2t}\Gamma\,[-t,\,t+\alpha/2] \times \int\limits_{C_2} ds\,\left(\frac{x}{2}\right)^{-2s}\Gamma\left[\begin{matrix}s+t+1*,\,-s\\ -s-t\end{matrix}\right]. \tag{11.41}$$

The tilde over Q is used to acknowledge the fact that pole contributions may be counted more than once as a result of our separating the integrations over s and t. As I noted before, multiple counting of poles residues is not a concern when the saddle-point solution is being sought since pole residues are neglected. Using eq. 5.94 one finds that the steepest-descent contribution has exponential decay and can be neglected compared to the pole contributions in this parameter regime.

The steepest-descent contribution in the third parameter regime is now calculated. Both $x/2$ and $y/2$ are greater than one, which requires the full asymptotic solution for the first integral. There are pole contributions at $t = n$ for $n = 0,\,1,\,2,\,\ldots$ as well as a steepest-descent contribution. Exponentially decaying terms are retained since there is no pole contribution in this region for the correlation function. The result of the evaluation of the t integration is

$$\tilde{Q}=\frac{-2\,\kappa_o^{-\alpha}}{d^2\Gamma\,[\alpha/2]}\frac{1}{2\pi i}\int\limits_{C_2} ds\,\left(\frac{x}{2}\right)^{-2s}\left[S(0a)\left(\frac{y}{2}\right)^{-2n}\Gamma[n+\alpha/2]\,\Gamma\left[\begin{matrix}s+n+1*,\,-s\\ -s-n\end{matrix}\right] + \sqrt{\pi}\,\Gamma\,[-s]\left(\frac{y}{2}\right)^{2\,s+(\alpha+1)/2}\exp\,(-y)\right]. \tag{11.42}$$

For the first term $\Delta_s = 1$, and the parameter $x/2$ is large. The steepest-descent contribution is obtained from eq. 5.94. In the last term $\Delta_s = -1$; therefore, let $s \to -s$ making $\Delta_s = 1$. The parameter y/x is small, and the integration path is closed to the left. There are pole contributions at $s = -m$ for $m = 0,\,1,\,2,\ldots$. Adding all these contributions gives the steepest-descent contribution as

$$Q \sim -\frac{\kappa_o^{-\alpha}}{\Gamma\,[\alpha/2]}\left\{\frac{\kappa_i^2\,S(0a)}{2\,\exp\left[(\pi\,d/L_i)^2\right]}\left(\frac{\pi\,L_o d}{L_i^2}\right)^{2n} + \frac{2\sqrt{\pi}\,(\pi\,d/L_o)^{(\alpha+1)/2}}{d^2\exp\left[(L_i/L_o)^2+\kappa_o d\right]}\right\}. \tag{11.43}$$

Collecting all the results from this section and assuming that the inner- and outer-scale lengths do not change with altitude and performing the integration over z, one obtains the final expression for the structure function given by the following: Regime 1 ($d < L_i/\pi$)

$$\mathcal{D}(d) = \frac{-51.42\, k_0^2\, \mu_0}{\Gamma\left[\alpha/2\right]\, \kappa_o^{\alpha}}$$

$$\times \left\{ \left(\frac{1}{L_o}\right)^2 S\left(0,1\right) \left(\frac{L_i}{L_o}\right)^{2n} \left(\frac{\pi d}{L_o}\right)^{2m} \Gamma\left[\begin{matrix} m+n+1,\ -m-n-1+\alpha/2 \\ m+1 \end{matrix}\right] \right.$$

$$\left. + \left(\frac{1}{L_i}\right)^2 \left(\frac{L_i}{L_o}\right)^{\alpha} S\left(1,0\right) \left(\frac{L_i}{L_o}\right)^{2m} \left(\frac{\pi d}{L_i}\right)^{2n} \Gamma\left[\begin{matrix} -m+n-\alpha/2+1, m+\alpha/2 \\ n+1 \end{matrix}\right] \right\}. \tag{11.44}$$

Regime 2 ($L_i/\pi < d < L_o/\pi$)

$$\mathcal{D}(d) \sim \frac{-51.42\, k_0^2\, \mu_0}{\Gamma\left[\alpha/2\right]}$$

$$\times \left\{ \left(\frac{1}{L_o}\right)^2 \kappa_o^{-\alpha} S\left(0,1\right) \left(\frac{L_i}{L_o}\right)^{2n} \left(\frac{\pi d}{L_o}\right)^{2m} \Gamma\left[\begin{matrix} m+n+1,\ -m-n-1+\alpha/2 \\ m+1 \end{matrix}\right] \right.$$

$$\left. + \left(\frac{1}{\pi\, d}\right)^2 \left(\frac{d}{2}\right)^{\alpha} S(0a,0) \left(\frac{L_i}{\pi\, d}\right)^{2n} \left(\frac{\pi d}{L_o}\right)^{2m} \Gamma\left[\begin{matrix} -m+n-\alpha/2+1, m+\alpha/2 \\ m-n+\alpha/2 \end{matrix}\right] \right\}. \tag{11.45}$$

Regime 3 ($d > L_o/\pi$)

$$\mathcal{D}(d) \sim \frac{k_0^2\, \mu_0}{\Gamma\left[\alpha/2\right]\, \kappa_o^{\alpha}} \left\{ \frac{51.42}{L_o^2} S_n(0) \Gamma\left[-n-1+\alpha/2\right] \left(\frac{L_i}{L_o}\right)^{2n} \right.$$

$$\left. -1.30\, \kappa_i^2\, \exp\left[-\left(\pi\, d/L_i\right)^2\right] S(0a) \left(\frac{\pi\, L_o d}{L_i^2}\right)^{2n} - \frac{9.23\ \left(\pi\, d/L_o\right)^{(\alpha+1)/2}}{d^2\, \exp\left[\left(L_i/L_o\right)^2 + \kappa_o d\right]} \right\}. \tag{11.46}$$

The first term in Regime 2 comes from the B_2 term from the third set of two-poles. In Regime 3, the terms are the B_2 and C_3 components from Series 3 and 1, respectively. The steepest-descent contributions have been neglected here since they decay exponentially with increasing d and contribute negligibly to the final solution.

It may be shown that in the limit as $L_o \to \infty$, *Tatarski's* (1961) result for the structure function with inner scale is reproduced. For this case $\alpha = 11/3$. A plot of the structure function for several values of L_i/L_o is shown in Fig. 11.7. Note

that in Regime 2, which spans the range from $\pi d/L_o = L_i/L_o$ to $\pi d/L_o = 1$, the structure function has a 5/3-power-law dependence. In Regime 1, which occurs where $\pi d/L_o < L_i/L_o$, there is a power-law dependence of 2. The structure function approaches a constant equal to twice the phase variance in Regime 3.

Let us look at the case in which $\alpha = 11/3$, $d < L_0/\pi$, and the inner scale is zero. The expression for Regime 2 reduces to

$$\mathcal{D}(d) \sim \frac{-51.42\, k_0^2\, \mu_0}{\Gamma\,[11/6]} \left\{ \left(\frac{1}{L_o}\right)^2 \kappa_o^{-11/3} \sum_{m=1}^{\infty} \frac{(-1)^m}{m!} \left(\frac{\pi d}{L_o}\right)^{2m} \Gamma[-m + 5/6] \right.$$

$$\left. + \left(\frac{1}{\pi d}\right)^2 \left(\frac{d}{2}\right)^{11/3} \sum_{m=0}^{\infty} \frac{(-1)^m}{m!} \left(\frac{\pi d}{L_o}\right)^{2m} \Gamma[-m - 5/6] \right\}. \tag{11.47}$$

Using the series expansion for the modified Bessel function of the third kind given in eq. 1.25, one can show that this formula reduces to the previously derived formula for the structure function given in eq. 7.20.

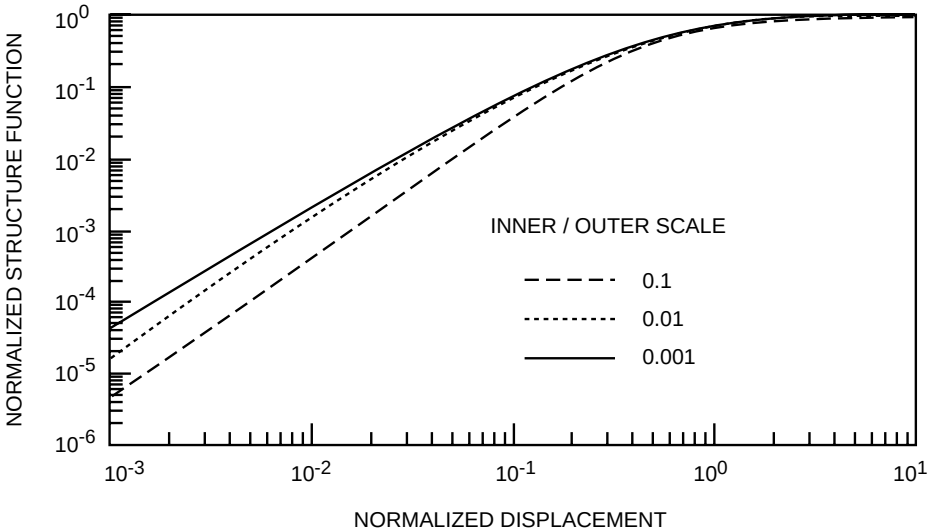

Figure 11.7. Structure function for several values of L_i/L_o. The structure function has been normalized by twice the variance and has been plotted against the normalized displacement, $\pi d/L_o$. Notice that as the inner scale gets smaller, the structure function increases at small separations because the turbulence increases at the smaller scales.

Because a finite outer scale is included in this problem, the variance is bounded, and a phase correlation function may be computed. One can obtain this result from the previous derivation by noting that the correlation function defined in eq. 2.124 is given by

$$\mathcal{B}_\phi(d) = 2.605\, k_0^2 \int_0^L dz\, C_n^2(z) \int_0^\infty d\kappa\, \kappa \left(\kappa^2 + \kappa_o^2\right)^{-11/6} \exp\left(-\kappa^2/\kappa_i^2\right) J_0(\kappa d)/2. \tag{11.48}$$

This differs from the expression for the structure function given in eq. 11.38 in the factor associated with the Bessel function. As a result, the two-dimensional contour integral expression for the structure function eq. 11.38 may be used with slight modification. Analytic continuation need not be used to get the Mellin transform of the factor that contains the Bessel function, and the asterisks in eq. 11.38 should be eliminated. The subsequent analysis is identical except that summation indices for terms due to the first and second set of two-poles range from 0 to ∞ for both m and n, and there are no terms due to the B_2 and C_3 components.

The expression for the phase correlation function becomes:
Regime 1 ($d < L_i/\pi$)

$$\mathcal{B}_\phi(d) = \frac{25.71\, k_0^2\, \mu_0}{\Gamma[\alpha/2]\, \kappa_o^\alpha}$$

$$\times \left\{ \left(\frac{1}{L_o}\right)^2 S(0,0) \left(\frac{L_i}{L_o}\right)^{2n} \left(\frac{\pi d}{L_o}\right)^{2m} \Gamma\begin{bmatrix} m+n+1,\ -m-n-1+\alpha/2 \\ m+1 \end{bmatrix} \right.$$

$$\left. + \left(\frac{1}{L_i}\right)^2 \left(\frac{L_i}{L_o}\right)^\alpha S(0,0) \left(\frac{L_i}{L_o}\right)^{2m} \left(\frac{\pi d}{L_i}\right)^{2n} \Gamma\begin{bmatrix} -m+n-\alpha/2+1, m+\alpha/2 \\ n+1 \end{bmatrix} \right\}. \tag{11.49}$$

Regime 2 ($L_i/\pi < d < L_o/\pi$)

$$\mathcal{B}_\phi(d) \sim \frac{25.71\, k_0^2\, \mu_0}{\Gamma[\alpha/2]\, \kappa_o^\alpha}$$

$$\times \left\{ \left(\frac{1}{L_o}\right)^2 S(0,0) \left(\frac{L_i}{L_o}\right)^{2n} \left(\frac{\pi d}{L_o}\right)^{2m} \Gamma\begin{bmatrix} m+n+1,\ -m-n-1+\alpha/2 \\ m+1 \end{bmatrix} \right.$$

$$\left. + \left(\frac{1}{\pi d}\right)^2 \left(\frac{\pi d}{L_o}\right)^\alpha S(0a,0) \left(\frac{L_i}{\pi d}\right)^{2n} \left(\frac{\pi d}{L_o}\right)^{2m} \Gamma\begin{bmatrix} -m+n-\alpha/2+1, m+\alpha/2 \\ m-n+\alpha/2 \end{bmatrix} \right\}. \tag{11.50}$$

Regime 3 ($d > L_o/\pi$)

$$\mathcal{B}_\phi(d) \sim -\frac{k_0^2\, \mu_0}{\Gamma[\alpha/2]\, \kappa_o^\alpha}$$

$$\times \left\{ 0.65\, \kappa_i^2 \exp\left[-(\pi d/L_i)^2\right] S(0a) \left(\frac{\pi L_o d}{L_i^2}\right)^{2n} + \frac{4.62\ (\pi d/L_o)^{(\alpha+1)/2}}{d^2\, \exp\left[(L_i/L_o)^2 + \kappa_o d\right]} \right\}. \tag{11.51}$$

The steepest-descent contributions in Regime 2 have been discarded because of their negligible contribution. Note that in Regime 3 the only contribution comes from steepest-descent terms. A plot of the correlation function for the same parameter ranges used for the structure function in Fig. 11.7 is given in Fig. 11.8 for $\alpha = 11/3$. How L_i/L_o affects the correlation function is less obvious than its effect on the structure function.

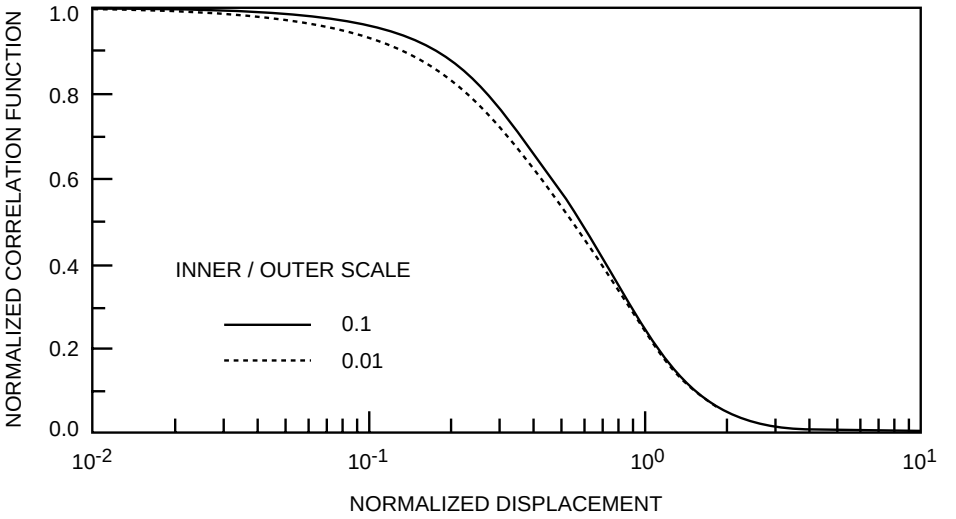

Figure 11.8. Normalized phase correlation function for several values of L_i/L_o. The correlation function has been plotted against the normalized displacement $\pi d/L_o$. As inner scale increases, the displacement must be larger to get the same reduction in correlation.

REFERENCES

1. Bailey, W. N., "Some Infinite Integrals Involving Bessel Functions", Proc. London Math. Soc., **40**, (1936) pp. 37–48.
2. Gervois, A., Navelet, H., "Integrals of three Bessel functions and Legendre functions. I", *J. Math. Phys.*, **26**, (1985) pp. 633–644.
3. Gradshteyn, I. S., Ryzhik, I. M., *Table of Integrals, Series, and Products*, Academic Press, New York, (1980).
4. Prudnikov, A. P., Brychkov, Y. A., Marichev, O. I., *Integrals and Series*, Gordon and Breach Science Publishers, New York, (1990).
5. Tatarski, V. I., *Wave Propagation In a Turbulent Medium*, Dover Publications, Inc., New York, (1961).
6. Watson, G. N., "An Infinite Integral Involving Bessel Functions", *Journal London Math Soc.*, **9**, (1934) pp. 16–22

Chapter 12

Beam Shape

Propagating a wave through turbulence not only reduces the Strehl ratio, but also changes the beam shape. Mellin transform techniques can be used to calculate the beam shape using the same technique as previously applied. Determining the beam shape simply adds another parameter to an integral. The beam profile after propagating through uncorrected turbulence, or through a medium with turbulence-induced beam jitter present, or with anisoplanatic effects can all be represented as special cases of a general integral. Results from evaluating the general integral are used to find the average beam profiles for the three specific cases.

12.1 General Formula for Beam Shape

A framework for finding the beam profile for any ratio of coherence diameter to aperture diameter is developed here. The starting point for obtaining the beam profile with uncorrected turbulence is the general expression for the normalized beam shape with isotropic turbulence in eq. 2.162 and the structure function for uncorrected turbulence given in eq. 7.7. This gives

$$I(\rho) = \int_0^1 d\alpha\, \alpha K(\alpha)\, J_0\left(\frac{k_0\, \rho D \alpha}{z}\right) \exp\left[-3.44\, \left(\frac{\alpha D}{r_o}\right)^{5/3}\right]. \tag{12.1}$$

Similar integrals are required to determine the beam shape both with tilt jitter and with anisoplanatism. To evaluate the three beam shapes at the same time, use the fact that $K(\alpha)$ is zero for $\alpha > 1$ to define

$$P(\rho, \nu, q, g) = \int_0^\infty \frac{d\alpha}{\alpha}\, \alpha^{2+\nu}\, K(\alpha)\, J_0\left(\frac{k_0\, \rho D \alpha}{z}\right) \exp\left(-g^q\, \alpha^q\right), \tag{12.2}$$

where for the case of uncorrected turbulence

$$I(\rho) = P\left(\rho, 0, 5/3, \frac{3.44^{3/5} D}{r_o}\right). \tag{12.3}$$

This integral will be evaluated by using the Mellin transform techniques in two complex planes developed in Chap. 10. Let $x = z/k_0\rho D$, and $y = 1/g$. Using the Mellin convolution integral and the Mellin transforms in eq. 1.64, eq. 1.51, and eq. 1.47, one can transform the integral into

$$P(\rho,\nu,q,g) = \frac{4}{q\sqrt{\pi}}\frac{1}{(2\pi i)^2}\int_{C_1}\int_{C_2} ds\,dt\;(2x)^{-s}\,y^{-t}$$
$$\times\frac{1}{(s+t+\nu+2)}\Gamma\left[\begin{matrix}\frac{s+t+\nu}{2}+\frac{3}{2},\,-s/2,\,-t/q\\ \frac{s+t+\nu}{2}+3,\,s/2+1\end{matrix}\right].$$

Let $s \to 2s$, and $t \to 2t$, and use the recursion relation

$$\frac{1}{(s+t+\nu/2+1)} = \frac{\Gamma[s+t+\nu/2+1]}{\Gamma[s+t+\nu/2+2]}$$

to obtain

$$P(\rho,\nu,q,g) = \frac{8}{q\sqrt{\pi}}\frac{1}{(2\pi i)^2}\int_{C_1} ds\int_{C_2} dt\;(2x)^{-2s}\,y^{-2t}$$
$$\times\Gamma\left[\begin{matrix}s+t+\nu/2+\frac{3}{2},\,s+t+\nu/2+1,\,-s,\,-2t/q\\ s+t+\nu/2+3,\,s+t+\nu/2+2,\,s+1\end{matrix}\right].$$

To evaluate this integral, 2-poles must be listed, and these are:

(1) $s+t+\nu/2+\frac{3}{2} = -m;\ -s = -n,$
(2) $s+t+\nu/2+1 = -m;\ -s = -n,$
(3) $s+t+\nu/2+\frac{3}{2} = -m;\ -2t/q = -n,$
(4) $s+t+\nu/2+1 = -m;\ -2t/q = -n,$ and
(5) $-s = -n;\ -2t/q = -m.$

These lead to terms of the form:

(1) $\left(\frac{1}{g}\right)^{2m}\left(\frac{k_0\rho D}{2gz}\right)^{2n}(m!)^{2/q}(n!)^{2/q-2},$

(2) $\left(\frac{1}{g}\right)^{2m}\left(\frac{k_0\rho D}{2gz}\right)^{2n}(m!)^{2/q}(n!)^{2/q-2},$

(3) $\left(\frac{2z}{k_0\rho D}\right)^{2m}\left(\frac{2zg}{k_0\rho D}\right)^{qn}(m!)^{2}(n!)^{q-1},$

(4) $\left(\frac{2z}{k_0\rho D}\right)^{2m}\left(\frac{2zg}{k_0\rho D}\right)^{qn}(m!)^{2}(n!)^{q-1},$ and

(5) $\left(\frac{k_0\rho D}{2z}\right)^{2n} g^{qm}(m!)^{-1}(n!)^{-2}.$

Table 12.1. Region in which the series have most rapid convergence for the general problem of finding the beam shape with uncorrected turbulence, tilt jitter, or anisoplanatism.

2–Pole Set	Solution Type	Parameter	Range
1	Asymp	$g > 1$	$2gz > k_0 \rho D$
2	Asymp	$g > 1$	$2gz > k_0 \rho D$
3	Asymp	$2gz < k_0 \rho D$	$k_0 \rho D > 2z$
4	Asymp	$2gz < k_0 \rho D$	$k_0 \rho D > 2z$
5	Taylor	$g < 1$	$k_0 \rho D < 2z$

The series in n can be a Taylor or an asymptotic series depending on the value of q. The ranges of applicability of the 5 double series to get the most rapid convergence are given in Table 12.1.

As described in Chap. 10 these series are useful for different parameter ranges. The single Taylor series gives a solution that is applicable for all parameter ranges and is a complete solution to the problem. It is given by

$$P(\rho, \nu, q, g) = \frac{4}{\sqrt{\pi}} S(0,0) \left(\frac{k_0 \rho D}{2z} \right)^{2n} \frac{g^{qm}}{n!} \times \left(\frac{1}{n + mq/2 + \nu/2 + 1} \right) \Gamma \begin{bmatrix} n + mq/2 + \nu/2 + \frac{3}{2} \\ n + mq/2 + \nu/2 + 3 \end{bmatrix}. \tag{12.4}$$

Because of the presence of the term $(n!)^2\, m!$ in the denominator, the above series converges rapidly even for relatively large distances off the beam axis and can be used rather than the asymptotic series. For instance, if the parameter $k_0 \rho D/2z$ is equal to 10, then the error in using 30 terms of the series is one part in 10^5 of the value on axis.

For some parameter ranges a large number of terms is necessary to get an accurate answer. In these regions an asymptotic series may be more convenient. The asymptotic series given by the second and first set of 2-poles is

$$P(\rho, \nu, q, g)_{AS} \sim \frac{8}{q\sqrt{\pi}} S(0a) \left(\frac{k_0 \rho D}{2zg} \right)^{2n} \left\{ \left(\frac{1}{g} \right)^{\nu+2} \sqrt{\pi} \Gamma \left[2n/q + \nu/q + 2/q \right] + S_m(0) \frac{1}{\left(m + \frac{1}{2} \right)} \left(\frac{1}{g} \right)^{2m+\nu+3} \Gamma \begin{bmatrix} 2n/q + 2m/q + \nu/q + 3/q \\ -m + \frac{3}{2} \end{bmatrix} \right\}. \tag{12.5}$$

Since $\Delta_3 = 0$, the steepest-descent contribution is found by sequential evaluation of the two-dimensional integral. In the regime in which the above equation applies, integrate eq. 12.4 first over s assuming that x is large, and then integrate over t assuming y is small. The result is equal to zero.

The asymptotic solution given by the third and fourth set of 2-poles is

$$P(\rho,\nu,q,g)_{AS}\sim\frac{4}{\sqrt{\pi}}S(0a)\left(\frac{2g\,z}{k_0\,\rho\,D}\right)^{nq}\left\{\left(\frac{2z}{k_0\,\rho\,D}\right)^{\nu+2}\sqrt{\pi}\Gamma\begin{bmatrix}nq/2+\nu/2+1\\-nq/2-\nu/2\end{bmatrix}\right.$$
$$\left.-S_m(0a)\,\frac{1}{\left(m+\frac{1}{2}\right)}\left(\frac{2z}{k_0\,\rho\,D}\right)^{2m+\nu+3}\Gamma\begin{bmatrix}m+nq/2+\nu/2+\frac{3}{2}\\-m+\frac{3}{2},\,-m-nq/2-\nu/2-\frac{1}{2}\end{bmatrix}\right\}. \tag{12.6}$$

The steepest-descent contribution that is found by integrating eq. 12.4 first over t assuming that y is large, then over s assuming x is small, is

$$P(\rho,\nu,q,g)_{SD}=-\frac{32}{\pi}\left(\frac{z}{k_0\,\rho\,D}\right)^3\sin\left(\frac{k_0\,\rho\,D}{z}\right)\exp\left[-\left(\frac{g}{2}\right)^q\right]. \tag{12.7}$$

12.2 Beam Shape for Uncorrected Turbulence

For the specific case of uncorrected turbulence, the beam shape is given in eq. 12.3 as $P\left(\rho,0,5/3,3.44^{3/5}D/r_o\right)$. The range of applicability of the series is obtained by inserting the parameters into Table 12.1 to give the ranges in Table 12.2.

Table 12.2. Region in which the series have most rapid convergence for uncorrected turbulence.

2–Pole Set	Solution Type	Parameter	Range
1	Asymp	$0.4765r_o < D$	$k_0\,\rho r_o < 4.197\,z$
2	Asymp	$0.4765r_o < D$	$k_0\,\rho r_o < 4.197\,z$
3	Asymp	$k_0\,\rho r_o > 4.197\,z$	$k_0\,\rho D > 2\,z$
4	Asymp	$k_0\,\rho r_o > 4.197\,z$	$k_0\,\rho D > 2\,z$
5	Taylor	$0.4765r_o > D$	$k_0\,\rho D < 2\,z$

The Taylor series solution for this case that applies for all turbulence values and distances from the axis is

$$I(\rho)=\frac{4}{\sqrt{\pi}}\,S(0,0)\frac{1}{n\,!}\left(\frac{k_0\,\rho D}{2z}\right)^{2n}\left[3.44\left(\frac{D}{r_o}\right)^{5/3}\right]^m$$
$$\times\left(\frac{1}{n+5m/6+1}\right)\Gamma\begin{bmatrix}n+5m/6+\frac{3}{2}\\n+5m/6+3\end{bmatrix}. \tag{12.8}$$

Notice that the only way turbulence enters the expression is in the form of the coherence diameter.

It is instructive to consider the solution for infinite r_o. That can be done by examining the solution above, or alternatively, by evaluating the integration over t in eq. 12.4 and only evaluating the pole at $t = 5m/6$. Set $m = 0$ to obtain

$$I(\rho) = \frac{1}{2\pi i} \int_C ds \, \frac{2}{\sqrt{\pi}} \, \Gamma \left[\begin{matrix} s/2, -s/2 + \frac{3}{2} \\ -s/2 + 2, -s/2 + 3 \end{matrix} \right] \left(\frac{k_0 \rho D}{2z} \right)^s . \tag{12.9}$$

From eq. 1.52, one sees that this integral produces an Airy pattern given by

$$I(\rho) = \left[J_1 \left(\frac{k_0 \rho D}{2z} \right) \Big/ \left(\frac{k_0 \rho D}{4z} \right) \right]^2 . \tag{12.10}$$

The beamwidth in the plots in this chapter is the value of radius that results in a zero value for the intensity. The argument is 3.8 at this radius, and the normalizing function to convert the arguments of the function into beamwidths is $1.22 \rho D / \lambda z$.

The beam profiles versus axial position of a wave that propagated through turbulence with values of D/r_o of 0, 0.5, 0.7, and 1 are plotted in Fig. 12.1. The beam shape is similar for all cases out to the beamwidth that is plotted. If the beamwidth increased by the inverse of the square root of the Strehl ratio, then the normalized half-power beamwidths would be 1, 1.15, 1.28, and 1.60 for these cases. The beamwidths are 1, 1.11, 1.23, and 1.56, which are close to the above values.

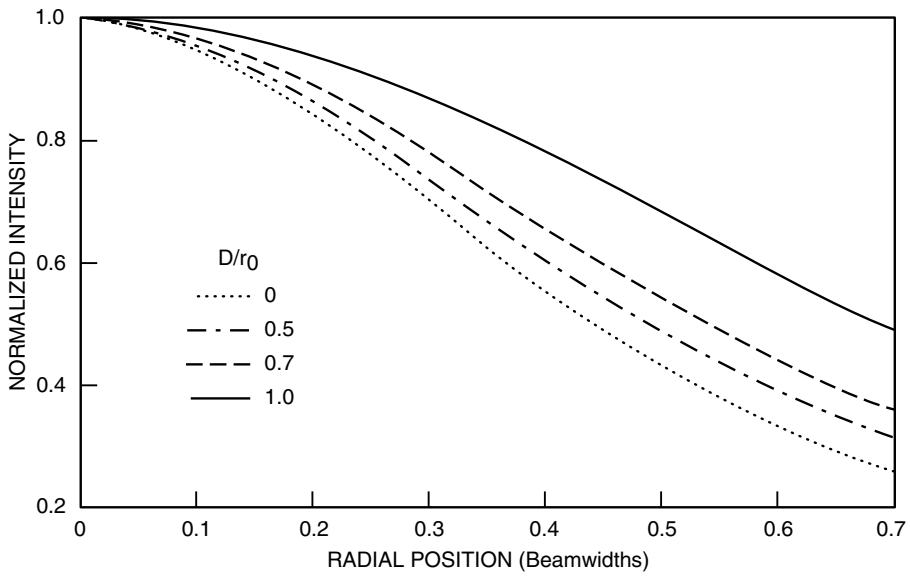

Figure 12.1. Beam shape of a wave that propagated through turbulence with the ratio D/r_o equal to 0, 0.5, 0.7, and 1.0.

Only a few terms of the Taylor series are necessary to get an accurate answer for low turbulence and small distances from the axis. For stronger turbulence conditions or larger distances off axis, asymptotic solutions are easier to evaluate. The asymptotic series in eq. 12.5 are applicable when the coherence diameter is much less than the aperture diameter, and the angle off-axis is less than the diffraction-limited size of an aperture of diameter r_o. These are given by

$$I(\rho) \sim \frac{24}{5\sqrt{\pi}} S(0) \frac{1}{n!} \left(\frac{0.238\, r_o\, k_0\, \rho}{z} \right)^{2n} \left\{ \left(\frac{0.4765\, r_o}{D} \right)^2 \sqrt{\pi} \Gamma \left[6n/5 + \tfrac{6}{5} \right] \right.$$

$$\left. - S_m(0) \frac{1}{\left(m + \frac{1}{2} \right)} \left(\frac{0.4765\, r_o}{D} \right)^{2m+3} \Gamma \begin{bmatrix} 6n/5 + 6m/5 + \frac{9}{5} \\ -m + \frac{3}{2} \end{bmatrix} \right\}. \quad (12.11)$$

For the second and fourth sets of poles the only value of m that gives a non-zero contribution is $m = 0$. The third and fourth double series in eq. 12.4 and the steepest-descent contribution in eq. 12.4 gives the asymptotic solution that is applicable for large distances from the axis. These expressions are

$$I(\rho) \sim \frac{4}{\sqrt{\pi}} S(0a) \left(\frac{4.197\, z}{r_o k_0 \rho} \right)^{5n/3} \left\{ \left(\frac{2z}{k_0 \rho D} \right)^2 \sqrt{\pi} \Gamma \begin{bmatrix} 5n/6 + 1 \\ -5n/6 \end{bmatrix} \right.$$

$$\left. - S_m(0a) \frac{1}{\left(m + \frac{1}{2} \right)} \left(\frac{2z}{k_0 \rho D} \right)^{2m+3} \Gamma \begin{bmatrix} m + 5n/6 + \frac{3}{2} \\ -m + \frac{3}{2},\ -m - 5n/6 - \frac{1}{2} \end{bmatrix} \right\}$$

$$- \frac{32}{\pi} \left(\frac{z}{k_0 \rho D} \right)^3 \sin \left(\frac{k_0 \rho D}{z} \right) \exp \left[- \left(\frac{3.44^{3/5} D}{2\, r_o} \right)^{5/3} \right]. \quad (12.12)$$

Two curves are plotted in Fig. 12.2. One is the beam shape with turbulence; the other is the beam shape for a wave with no turbulence that was transmitted from an aperture with a diameter equal to the coherence diameter. The horizontal axis is distance normalized to the beamwidth so that a value of unity corresponds to the first zero of the Airy pattern of an unperturbed beam. Notice that the shapes of the two profiles are close to each other when the intensity is above 0.2 of the value on axis.

12.3 Beam Shape with Tilt Jitter

There are some occasions when the higher-order Zernike modes of turbulence are well corrected, yet tilt jitter remains. One can use an artificial beacon to correct for higher-order turbulence terms as discussed in Secs. 6.12–6.14. This beacon provides no information on the jitter of the source. Since tilt jitter is several microradians, it must be well corrected to prevent significant tilt smearing of the image. One technique of reducing the jitter is to track a bright source close to the object to be corrected. There is some tilt remaining that results from

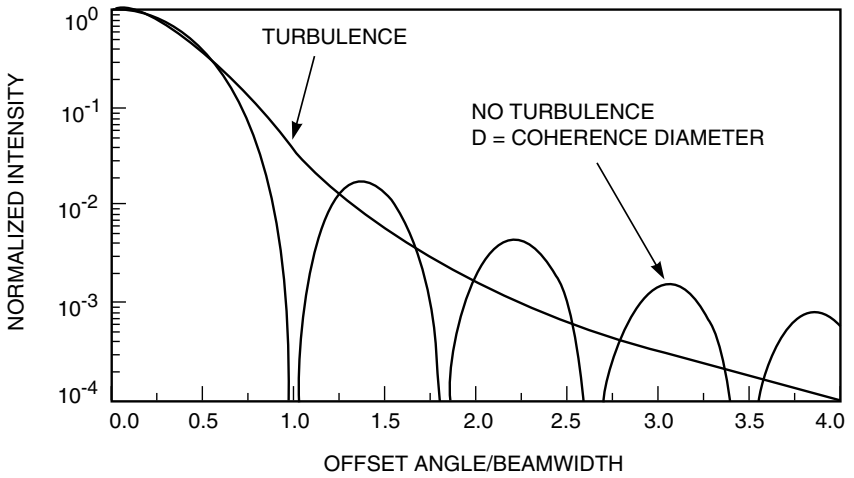

Figure 12.2. Beam shape with and without turbulence. Notice how closely the average beam profile in turbulence is approximated down to a normalized intensity of 0.2 by a diffraction-limited beam profile transmitted from a coherence-diameter sized aperture.

the angular offset of the guide star that will degrade the image. In another scenario, which is not common, one can correct for turbulence in an adaptive-optics system and track on the uncorrected image. This results in a tilt jitter due to the difference of gradient and Zernike tilt, which is referred to as centroid anisoplanatism by *Yura* and *Tavis* (1980). Tilt jitter affects the beam shape, and it is shown that it basically increases its area by a factor equal to the inverse of the reduction in Strehl ratio.

The expression for beam shape with tilt jitter is given by substituting the structure function in eq. 7.23 into eq. 2.162 to obtain

$$\begin{aligned} I(\rho) &= K(\alpha) J_0\left(\frac{k_0 \rho D \alpha}{z}\right) \exp\left[-\alpha^2 \left(\frac{D}{M r_o}\right)^{5/3}\right] \\ &= P\left(\rho, 0, 2, \left(\frac{D}{M r_o}\right)^{5/6}\right). \end{aligned} \tag{12.13}$$

M is equal to 0.4642, 0.4838, and 5.394 for Zernike tilt (Z-tilt), gradient tilt (G-tilt), and their difference respectively. The ranges of applicability of the series are obtained by inserting the parameters into Table 12.1 to give the ranges in Table 12.3.

The Taylor series good for all radii and turbulence strengths is

$$I(\rho) = \frac{4}{\sqrt{\pi}} S(0,0) \frac{1}{n!} \left(\frac{k_0 \rho D}{2z}\right)^{2n} \left(\frac{D}{M\, r_o}\right)^{5m/3} \left(\frac{1}{n+m+1}\right) \Gamma\left[\begin{matrix} n+m+\frac{3}{2} \\ n+m+3 \end{matrix}\right]. \tag{12.14}$$

Table 12.3. Region in which the series have most rapid convergence for beam shape with beam jitter.

2–Pole Set	Solution Type	Parameter	Range
1	Asymp	$Mr_o < D$	$(Mr_o)^{5/6} k_0 \rho D^{1/6} < 2z$
2	Asymp	$Mr_o < D$	$(Mr_o)^{5/6} k_0 \rho D^{1/6} < 2z$
3	Asymp	$k_0 \rho D > 2z$	$(Mr_o)^{5/6} k_0 \rho D^{1/6} > 2z$
4	Asymp	$k_0 \rho D > 2z$	$(Mr_o)^{5/6} k_0 \rho D^{1/6} > 2z$
5	Taylor	$Mr_o > D$	$k_0 \rho D < 2z$

Notice that the only way turbulence enters the formulas is in the form of the coherence diameter as was the case for uncorrected turbulence. The beam shape is plotted in Fig. 12.3 for D/Mr_o equal to 0, 1, 2, and 3 versus the beamwidth $1.2\lambda z/D$. The normalized beamwidths are 1, 1.09, 1.30, and 1.58 for these cases. If the beamwidth varied as the inverse of the square root of the Strehl ratio, they would be 1, 1.12, 1.37, and 1.66, which are close to the actual values. This

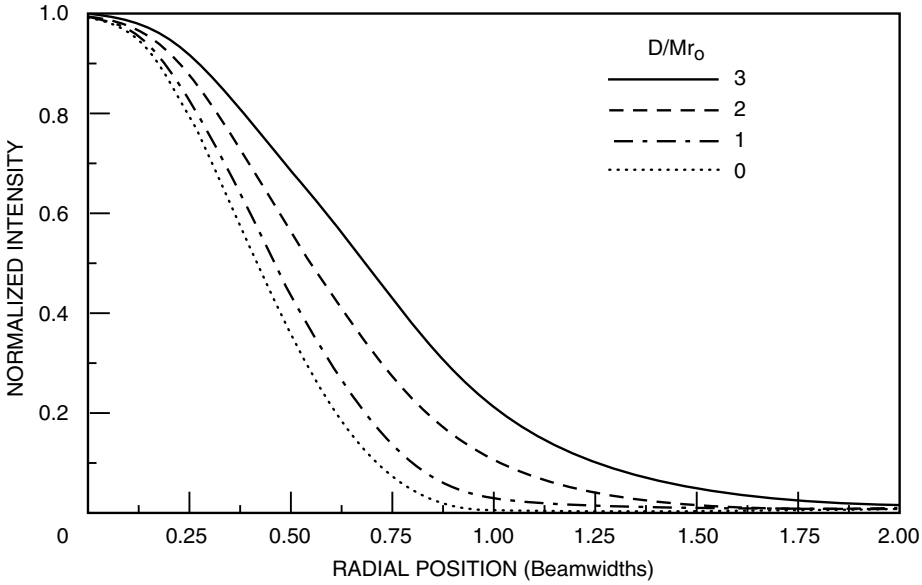

Figure 12.3. Beam shape of a wave that propagated through turbulence with the ratio D/Mr_o equal to 0, 1, 2, and 3 that has all distortions except tilt corrected.

expression reduces to an Airy pattern if the coherence diameter becomes infinite. The asymptotic series that applies when the angle off-axis is much less than the diffraction-limited size of an aperture of diameter D and the coherence diameter is smaller than the aperture diameter is given in eq. 12.5 as

$$I(\rho) \sim \frac{4}{\sqrt{\pi}} S(0) \left[\frac{D^{1/6} k_0 \rho}{2z} \left(M r_o \right)^{5/6} \right]^{2n}$$
$$\times \left\{ \left(\frac{M r_o}{D} \right)^{5/3} \sqrt{\pi} - S_m(0a) \frac{1}{n! \left(m + \frac{1}{2} \right)} \left(\frac{M r_o}{D} \right)^{5m/3+3} \Gamma \begin{bmatrix} n+m+\frac{3}{2} \\ -m+\frac{3}{2} \end{bmatrix} \right\}. \tag{12.15}$$

The asymptotic solution that applies when the angle off-axis is much greater than the diffraction-limited size of an aperture of diameter D is given in eq. 12.6 and eq. 12.7 as

$$I(\rho) \sim \frac{4}{\sqrt{\pi}} S(0a) \left[\frac{r_o k_0 \rho}{2z} \left(\frac{D}{M r_o} \right)^{5/6} \right]^{2n} \left\{ \left(\frac{2z}{k_0 \rho D} \right)^2 \sqrt{\pi} \Gamma \begin{bmatrix} n+1 \\ -n \end{bmatrix} \right.$$
$$\left. - S_m(0a) \frac{1}{\left(m + \frac{1}{2} \right)} \left(\frac{2z}{k_0 \rho D} \right)^{2m+3} \Gamma \begin{bmatrix} m+n+\frac{3}{2} \\ -m+\frac{3}{2}, \, -m-n-\frac{1}{2} \end{bmatrix} \right\}$$
$$- \frac{32}{\pi} \left(\frac{z}{k_0 \rho D} \right)^3 \sin \left(\frac{k_0 \rho D}{z} \right) \exp \left[-\frac{1}{4} \left(\frac{D}{M r_o} \right)^{5/3} \right]. \tag{12.16}$$

The Taylor series expression given in eq. 12.14 reduces to the Strehl ratio given in eq. 7.32 if it is evaluated on axis. The ratio of beam intensity on axis with tilt jitter to that with all turbulence for very high turbulence levels is

$$\frac{I(Jitter)}{I(Turbulence)} = 4 M^{5/3} \left(\frac{D}{r_o} \right)^{1/3}, \qquad D >> r_o. \tag{12.17}$$

The same result is also obtained by taking the ratio of Strehls in eq. 7.31 and eq. 7.17.

12.4 Beam Shape with Anisoplanatism

Next, the more complicated problem of finding the beam shape with anisoplanatism is solved. I expand the exponential in the integral into a series of Gegenbauer polynomials as was done in the calculation of Strehl ratio. For this reason, the range of applicability of this calculation is the same as that for the calculation of Strehl ratio. The beam profile calculation is valid when the displacements at the altitudes that contribute most to the reduction in Strehl ratio are less than 0.3 of the beam diameter. Fortunately, for adaptive-optics systems, that is often the region of greatest interest. The starting point is the expression for the beam profile given in eq. 2.161, repeated here

$$I(\boldsymbol{\rho}) = \frac{1}{2\pi} \int d\boldsymbol{\alpha} \, K(\alpha) \exp \left[i k_0 D \boldsymbol{\rho} \cdot \boldsymbol{\alpha} / z - \mathcal{D}(\boldsymbol{\alpha} D) / 2 \right]. \tag{12.18}$$

The integration is over the unit circle. The structure function is the same as that used for Strehl ratio. It is again expanded into Gegenbauer polynomials, and only the first term is retained. If the exponential is expanded into a power series as was done before, the expression equivalent to that given in eq. 7.47 is

$$I(\boldsymbol{\rho}) \approx \frac{\exp\left(-\sigma_\varphi^2\right)}{2\pi} \int d\boldsymbol{\alpha}\, K(\alpha)\, \exp\left(i k_0 D \boldsymbol{\rho} \cdot \boldsymbol{\alpha}/z\right) \times \left(1 + x + \frac{x^2}{2} + \frac{x^3}{6} + \frac{x^4}{24} + \frac{x^5}{120}\right), \tag{12.19}$$

where x is the same quantity as defined in eq. 7.46 and repeated here

$$x = \tfrac{5}{6} d_2 \left[1 - \tfrac{1}{3}\cos^2(\varphi)\right] (\alpha D)^{-1/3}. \tag{12.20}$$

The integration over angle is not as straightforward as before since there is an additional term in the exponential that also depends on angle. Rather than performing a complicated calculation, at this point I make an approximation. The angular dependence of x is weak, especially for the lower-order terms. I will replace the angular expression in x by the values averaged over angle that were calculated for the Strehl ratio. This eliminates any angular dependence of the beam profile; therefore, the calculations below give the beam profile averaged over angle. The angular integration can then be evaluated to get a Bessel function for the exponential term. Define

$$Q(\nu) = \frac{1}{P(0,\nu,0,0)} \int_0^1 \frac{d\alpha}{\alpha}\, \alpha^{v+2}\, K(\alpha)\, J_0(k_0 \rho D \alpha/z) = \frac{P(\rho,\nu,0,0)}{P(0,\nu,0,0)}, \tag{12.21}$$

where $P(0,\nu,0,0)$ is found from eq. 12.4 as

$$P(0,\nu,0,0) = \frac{4}{\sqrt{\pi}} \frac{1}{(\nu/2+1)} \Gamma\begin{bmatrix} \nu/2 + \frac{3}{2} \\ \nu/2 + 3 \end{bmatrix}. \tag{12.22}$$

With these definitions, the beam profile is

$$I(\rho) \approx \exp\left(-\sigma_\varphi^2\right) \left[Q(0) + 0.9736 E Q\left(-\tfrac{1}{3}\right) + 0.5133 E^2 Q\left(-\tfrac{2}{3}\right) + 0.2009 E^3 Q(-1) + 0.06970 E^4 Q\left(-\tfrac{4}{3}\right) + 0.02744 E^{\,5} Q\left(-\tfrac{5}{3}\right)\right]. \tag{12.23}$$

The value of $Q(\nu)$ is obtained from the evaluation $P(\rho,\nu,0,0)$. Substituting the values of the parameters into Table 12.1, one obtains Table 12.4 for the ranges of applicability of the series.

Table 12.4. Region in which the series have most rapid convergence for beam shape with anisoplanatism for which $g = 0$.

2–Pole Solution Set	Type	Parameter Range	
1	Asymp	$0 < 1$	$k_0 \rho D > g z$
2	Asymp	$0 > 1$	$k_0 \rho D > g z$
3	Asymp	$k_0 \rho D > 0$	$k_0 \rho D > 2 z$
4	Asymp	$k_0 \rho D > 0$	$k_0 \rho D > 2 z$
5	Taylor	$0 < 1$	$k_0 \rho D < 2 z$

Since the conditions for Series 1 and 2 cannot be satisfied, these series do not apply for this problem. The Taylor series solution obtained from eq. 12.4 is

$$\begin{aligned} Q(\nu) &= (\nu/2+1)\Gamma\begin{bmatrix}\nu/2+3\\ \nu/2+\frac{3}{2}\end{bmatrix} \\ &\quad \times S(0)\,\frac{1}{n!\,(n+1+\nu/2)}\Gamma\begin{bmatrix}n+\frac{3}{2}+\nu/2\\ n+3+\nu/2\end{bmatrix}\left(\frac{k_0\rho D}{2z}\right)^{2n} \\ &= {}_2F_3\left[\frac{3}{2}+\nu/2, 1+\nu/2; 3+\nu/2, 2+\nu/2, 1; -\left(\frac{k_0\rho D}{2z}\right)^2\right]. \end{aligned} \tag{12.24}$$

For large radii, an asymptotic solution is needed. This series is obtained from eq. 12.6 and eq. 12.7 as

$$\begin{aligned} Q(\nu) &\sim (\nu/2+1)\Gamma\begin{bmatrix}\nu/2+3\\ \nu/2+\frac{3}{2}\end{bmatrix} \\ &\quad \times\left\{S(0)\,\frac{-1}{\left(m+\frac{1}{2}\right)}\Gamma\begin{bmatrix}m+\frac{3}{2}+\nu/2\\ -m-\frac{1}{2}-\nu/2,\ -m+\frac{3}{2}\end{bmatrix}\left(\frac{2z}{k_0\rho D}\right)^{2m+3+\nu}\right. \\ &\quad \left. +\sqrt{\pi}\Gamma\begin{bmatrix}\nu/2+1\\ -\nu/2\end{bmatrix}\left(\frac{2z}{k_0\rho D}\right)^{\nu+2} - \frac{8}{\sqrt{\pi}}\left(\frac{z}{k_0\rho D}\right)^3 \sin\left(\frac{k_0\rho D}{z}\right)\right\}. \end{aligned} \tag{12.25}$$

The beam pattern can be plotted for various types of anisoplanatism by insertion of the appropriate values of E and σ_ϕ^2 which were derived in Secs. 7.4.1—7.4.5. The beam pattern is plotted for angular anisoplanatism in Figs. 12.4 and 12.5 for various values of offset angles. Notice how the dips in the Airy pattern fill in as anisoplanatism increases, and the power gets redistributed to larger radial distances. In Fig. 12.6 the curves are normalized to unity at zero radius for angular offsets of 0, 9, and 18 μrad. The intensity on axis for these three cases is 1, 0.7, and 0.45, and they reach a normalized intensity of 0.5 at 0.423, 0.435, and 0.494 beamwidths, respectively. If anisoplanatism causes the peak to spread by an amount proportional to the inverse of the square root of the Strehl ratio, then the half power points would occur at 0.423, 0.505, and 0.630 beamwidths.

The beamwidth of the central core is narrower for these anisoplanatism levels that indicates that the effect of small offsets is to decrease the power on axis without a substantial affect on the near-axis beamwidth. Small angular anisoplanatic errors mainly affect the high spatial spectral components, which scatter energy out to large angles, thus they produce a distribution with a narrow peak and a low plateau of energy that extends much further out.

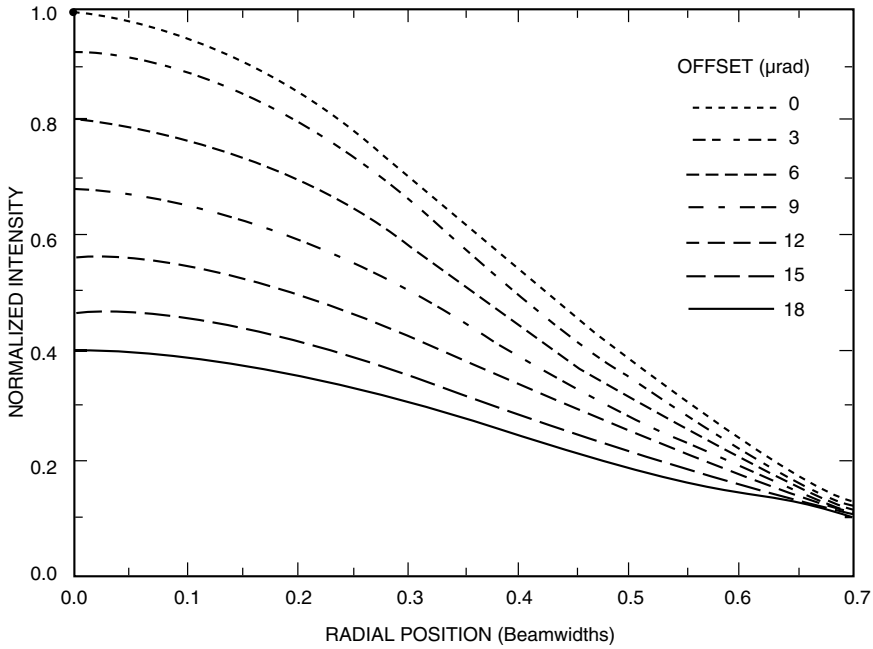

Figure 12.4. Beam shape close to the beam axis with angular anisoplanatism for a 0.6-m aperture at zenith for the SLCSAT day model. The intensity is normalized to that with no turbulence.

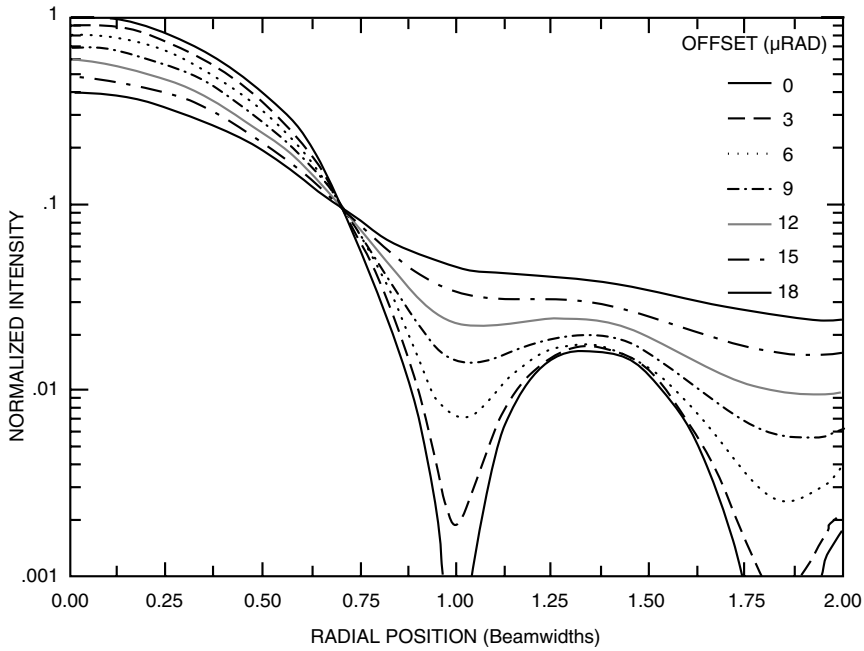

Figure 12.5. Beam shape with angular anisoplanatism for a 0.6-m aperture at zenith for the SLCSAT day model. The intensity is normalized to that with no turbulence.

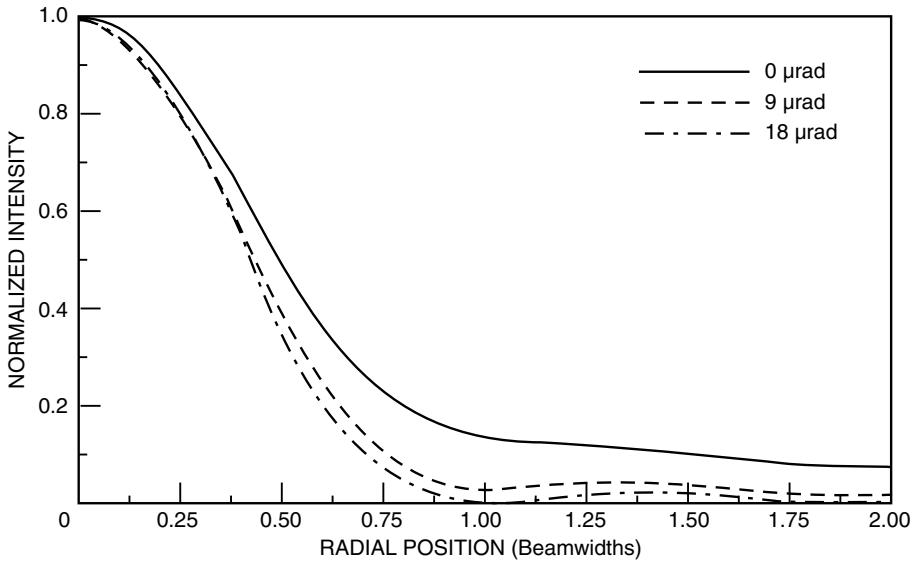

Figure 12.6. Beam shape with angular anisoplanatism for a 0.6-m aperture at zenith for the SLCSAT day model with offset of 0, 9, and 18 μrad. The intensity is normalized to unity on axis.

REFERENCES

1. Yura, H. T., Tavis, M. T.,"Centroid anisoplanatism",*J. Opt. Soc. Am. A*, **2**, (1985) pp. 765–773.

Appendix A

Additional Mellin Transforms

This table contains Mellin transforms to supplement the ones at the end of Chap. 1. These are still a small fraction of the transforms that are listed in *Marichev* (1983). The special functions that are not commonly used are defined in Appendix B. The value of n is an integer in the transforms below.

$$h(x) \qquad \to M\left[h(x)\right] \equiv H(s) = \int_0^\infty \frac{dx}{x}\; h(x)\, x^s \tag{A.1}$$

$$\frac{1}{1-x} \to \pi \Gamma \begin{bmatrix} s,\, 1-s \\ s+\frac{1}{2},\, \frac{1}{2}-s \end{bmatrix}, \qquad 0 < \mathrm{Re}\left\{s\right\} < 1 \tag{A.2}$$

$$|1-x|^{-p} \to \frac{\pi}{\Gamma\left[p\right] \cos\left(\pi p/2\right)} \Gamma \begin{bmatrix} s,\, p-s \\ s+(1-p)/2,\, (1+p)/2-s \end{bmatrix},$$
$$0 < \mathrm{Re}\left\{s\right\} < \mathrm{Re}\left\{p\right\} < 1 \tag{A.3}$$

$$\left[x^2 + 2x\cos\left(\pi b\right) + 1\right]^{-1} \to -\frac{\pi}{\sin\left(\pi b\right)} \Gamma \begin{bmatrix} s,\; 1-s \\ s\,b-b,\; 1+b-s\,b \end{bmatrix}$$
$$0 < \mathrm{Re}\left\{s\right\} < 2\,, \quad |b| < 1 \tag{A.4}$$

$$\sin\left(x + b\pi\right) \to \sqrt{\pi}\, 2^{s-1} \Gamma \begin{bmatrix} s/2,\, s/2+\frac{1}{2} \\ s/2+b,\, 1-b-s/2 \end{bmatrix}, \qquad 0 < \mathrm{Re}\left\{s\right\} < 1 \tag{A.5}$$

$$\cos\left(x + b\pi\right) \to \sqrt{\pi}\, 2^{s-1} \Gamma \begin{bmatrix} s/2,\, s/2+\frac{1}{2} \\ s/2+b+\frac{1}{2},\, \frac{1}{2}-b-s/2 \end{bmatrix}, \qquad 0 < \mathrm{Re}\left\{s\right\} < 1 \tag{A.6}$$

$$\sin^{2n-1}\left(x\right) \to \frac{\sqrt{\pi}}{4^{n-s/2}} \sum_{k=0}^{n-1} (-1)^{n+k-1} \frac{(2n-1)!}{k\,!\,(2\,n-k-1)!}\, (2\,n-2\,k-1)^{-s}$$
$$\times \Gamma \begin{bmatrix} s/2+\frac{1}{2} \\ 1-s/2 \end{bmatrix}, \qquad |\mathrm{Re}\left\{s\right\}| < 1 \tag{A.7}$$

$$\sin^{2n}(x) \to 2^{-2n}\sqrt{\pi}\sum_{k=0}^{n-1}(-1)^{n+k}\frac{(2n)!}{k!\,(2n-k)!}(n-k)^{-s}\Gamma\left[\begin{matrix}s/2\\ \frac{1}{2}-s/2\end{matrix}\right],$$
$$-2<\mathrm{Re}\{s\}<0 \tag{A.8}$$

$$\cos^{2n-1}(x) \to 4^{s/2-n}\sqrt{\pi}\sum_{k=0}^{n-1}\frac{(2n-1)!}{k!\,(2n-k-1)!}(2n-2k-1)^{-s}\Gamma\left[\begin{matrix}s/2\\ \frac{1}{2}-s/2\end{matrix}\right],$$
$$0<\mathrm{Re}\{s\}<1 \tag{A.9}$$

$$\cos^{2n}(x)-1 \to 2^{-2n}\sqrt{\pi}\sum_{k=0}^{n-1}\frac{(2n)!}{k!\,(2n-k)!}(n-k)^{-s}\Gamma\left[\begin{matrix}s/2\\ \frac{1}{2}-s/2\end{matrix}\right],$$
$$-2<\mathrm{Re}\{s\}<0 \tag{A.10}$$

$$\ln(x)\,U(1-x) \to \Gamma\left[\begin{matrix}s,\,-s\\ 1+s,\,1-s\end{matrix}\right],\quad 0<\mathrm{Re}\{s\} \tag{A.11}$$

$$\ln(x)\,U(x-1) \to -\Gamma\left[\begin{matrix}s,\,-s\\ 1+s,\,1-s\end{matrix}\right],\quad 0>\mathrm{Re}\{s\} \tag{A.12}$$

$$\ln(1+x) \to -\Gamma[s,\,-s],\qquad -1<\mathrm{Re}\{s\}<0 \tag{A.13}$$

$$\ln|1-x| \to -\pi\,\Gamma\left[\begin{matrix}s,\,-s\\ s+\frac{1}{2},\,\frac{1}{2}-s\end{matrix}\right],\quad -1<\mathrm{Re}\{s\}<0 \tag{A.14}$$

$$\frac{\ln(x)}{x-1} \to \Gamma[s,\,s,\,1-s,\,1-s],\quad 0<\mathrm{Re}\{s\}<1 \tag{A.15}$$

$$\frac{\ln(x)}{x+1} \to -\pi\,\Gamma\left[\begin{matrix}s,\,s,\,1-s,\,1-s\\ s+\frac{1}{2},\,\frac{1}{2}-s\end{matrix}\right],\quad 0<\mathrm{Re}\{s\}<1 \tag{A.16}$$

$$L^n(-x) \to (-s)^{1-n}\,\Gamma[s,\,-s],\qquad -1<\mathrm{Re}\{s\}<0 \tag{A.17}$$

$$\sinh[v\,\mathrm{arcsinh}(x)] \to \frac{v\,\cos(\pi\,v/2)}{4\sqrt{\pi}}\,\Gamma\left[\begin{matrix}s/2+\frac{1}{2},\,v/2-s/2,\,-v/2-s/2\\ 1-s/2\end{matrix}\right],$$
$$-1<\mathrm{Re}\{s\}<-|\mathrm{Re}\{v\}| \tag{A.18}$$

$$\mathrm{arcsin}(x)\,U(1-x) \to \frac{\pi}{4}\,\Gamma\left[\begin{matrix}s/2\\ s/2+1\end{matrix}\right]+\frac{\sqrt{\pi}}{4}\,\Gamma\left[\begin{matrix}s/2+\frac{1}{2},\,-s/2\\ s/2+1,\,1-s/2\end{matrix}\right],\ -1<\mathrm{Re}\{s\} \tag{A.19}$$

$$\arccos(x)\,U(1-x) \to -\frac{\sqrt{\pi}}{4}\,\Gamma\left[\begin{matrix} s/2+\frac{1}{2},\, -s/2 \\ s/2+1,\, 1-s/2 \end{matrix}\right], \qquad 0 < \mathrm{Re}\{s\} \tag{A.20}$$

$$\arctan(x) \to \frac{1}{4}\,\Gamma\left[\begin{matrix} s/2+\frac{1}{2},\, \frac{1}{2}-s/2,\, -s/2 \\ 1-s/2 \end{matrix}\right], \qquad -1 < \mathrm{Re}\{s\} < 0 \tag{A.21}$$

$$K(x) \to \frac{\pi}{4}\,\Gamma\left[\begin{matrix} s/2,\, \frac{1}{2}-s/2 \\ s/2+\frac{1}{2},\, 1-s/2 \end{matrix}\right], \qquad 0 < \mathrm{Re}\{s\} < 1 \tag{A.22}$$

$$K(ix) \to \frac{1}{4}\,\Gamma\left[\begin{matrix} s/2,\, \frac{1}{2}-s/2,\, \frac{1}{2}-s/2 \\ 1-s/2 \end{matrix}\right], \qquad 0 < \mathrm{Re}\{s\} < 1 \tag{A.23}$$

$$K\left(\sqrt{1-x}\right)U(1-x) \to \frac{\pi}{2}\,\Gamma\left[\begin{matrix} s,\, s \\ s+\frac{1}{2},\, s+\frac{1}{2} \end{matrix}\right], \qquad 0 < \mathrm{Re}\{s\} \tag{A.24}$$

$$E\left(\sqrt{1-x}\right)U(1-x) \to \frac{\pi}{2}\,\Gamma\left[\begin{matrix} s,\, s+1 \\ s+\frac{1}{2},\, s+\frac{3}{2} \end{matrix}\right], \qquad 0 < \mathrm{Re}\{s\} \tag{A.25}$$

$$E\left(\frac{1}{\sqrt{1+x}}\right)\frac{1}{\sqrt{1+x}} \to \Gamma\left[\begin{matrix} s,\, s+1,\, \frac{1}{2}-s \\ s+\frac{1}{2} \end{matrix}\right], \qquad 0 < \mathrm{Re}\{s\} < 1/2 \tag{A.26}$$

$$Ei(-x) \to -\,\Gamma\left[\begin{matrix} s,\, s \\ s+1 \end{matrix}\right], \qquad 0 < \mathrm{Re}\{s\} \tag{A.27}$$

$$\exp(x)\,Ei(-x) \to -\,\Gamma[s,\, s,\, 1-s], \qquad 0 < \mathrm{Re}\{s\} < 1 \tag{A.28}$$

$$Si(x) \to -\frac{\sqrt{\pi}}{4}2^s\,\Gamma\left[\begin{matrix} s/2,\, s/2+\frac{1}{2} \\ s/2+1,\, 1-s/2 \end{matrix}\right], \qquad -1 < \mathrm{Re}\{s\} < 0 \tag{A.29}$$

$$si(x) \to -\frac{\sqrt{\pi}}{4}2^s\,\Gamma\left[\begin{matrix} s/2,\, s/2+\frac{1}{2} \\ s/2+1,\, 1-s/2 \end{matrix}\right], \qquad 0 < \mathrm{Re}\{s\} < 2 \tag{A.30}$$

$$Ci(x) \to \frac{\sqrt{\pi}}{4}2^s\,\Gamma\left[\begin{matrix} s/2,\, -s/2 \\ 1-s/2,\, \frac{1}{2}-s/2 \end{matrix}\right], \qquad 0 < \mathrm{Re}\{s\} < 2 \tag{A.31}$$

$$\mathrm{Erf}(x) \to \frac{1}{2\sqrt{\pi}}\,\Gamma\left[\begin{matrix} s/2+\frac{1}{2},\, -s/2 \\ 1-s/2 \end{matrix}\right], \qquad -1 < \mathrm{Re}\{s\} < 0 \tag{A.32}$$

$$\exp\left(-x^2\right)\mathrm{Erf}(ix) \to \frac{i}{2}\,\Gamma\left[\begin{matrix} s/2+\frac{1}{2},\, \frac{1}{2}-s/2 \\ 1-s/2 \end{matrix}\right], \qquad 1 > |\mathrm{Re}\{s\}| \tag{A.33}$$

$$\mathrm{Erfc}(x) \to \frac{1}{2\sqrt{\pi}}\,\Gamma\left[\begin{matrix} s/2+\frac{1}{2},\, s/2 \\ s/2+1 \end{matrix}\right], \qquad 0 < \mathrm{Re}\{s\} \tag{A.34}$$

$$\exp\left(x^2\right)\mathrm{Erfc}(x) \to \frac{1}{2\pi}\,\Gamma\left[s/2+\tfrac{1}{2},\, s/2,\, \tfrac{1}{2}-s/2\right], \qquad 0 < \mathrm{Re}\{s\} < 1 \tag{A.35}$$

$$S(x) \to -\frac{2^s}{4}\,\Gamma\left[\begin{matrix} s/2+\frac{3}{4},\, s/2 \\ s/2+1,\, \frac{3}{4}-s/2 \end{matrix}\right], \qquad -3/2 < \mathrm{Re}\{s\} < 0 \tag{A.36}$$

$$C(x) \to -\frac{2^s}{4}\,\Gamma\left[\begin{matrix} s/2+\frac{1}{4},\, s/2 \\ s/2+1,\, \frac{1}{4}-s/2 \end{matrix}\right], \qquad -1/2 < \mathrm{Re}\{s\} < 0 \tag{A.37}$$

$$\gamma[a,\, x] \to \Gamma\left[\begin{matrix} s+a,\, -s \\ 1-s \end{matrix}\right], \qquad -\mathrm{Re}\{a\} < \mathrm{Re}\{s\} < 0 \tag{A.38}$$

$$\Gamma[a,\, x] \to \Gamma\left[\begin{matrix} s+a,\, s \\ s+1 \end{matrix}\right], \qquad \mathrm{Re}\{s\} > -\mathrm{Re}\{a\},\, 0 < \mathrm{Re}\{s\} \tag{A.39}$$

$$\exp\left(-x^2/4\right)\, D_\nu(x) \to 2^{s/2+\nu/2-1/2}\,\Gamma\left[\begin{matrix} s/2,\, s/2+\frac{1}{2} \\ s/2+(1-\nu)/2 \end{matrix}\right], \quad 0 < \mathrm{Re}\{s\} \tag{A.40}$$

$$\exp\left(x^2/4\right) D_\nu(x) \to \left[2^{-s/2+\nu/2+3/2}\sqrt{\pi}\,\Gamma[-\nu]\right]^{-1}$$
$$\times\Gamma\left[s/2,\, s/2+\tfrac{1}{2},\, -\nu/2-s/2\right], \quad 0 < \mathrm{Re}\{s\} < -\mathrm{Re}\{\nu\} \tag{A.41}$$

$$N_\nu(x) \to \frac{2^s}{2}\Gamma\left[\begin{matrix} s/2+\nu/2,\, s/2-\nu/2 \\ s/2-(1+\nu)/2,\, (3+\nu)/2-s/2 \end{matrix}\right],$$
$$|\,\mathrm{Re}\{\nu\}\,| < \mathrm{Re}\{s\} < 3/2 \tag{A.42}$$

$$H_\nu(x) \to \frac{2^s}{2}\Gamma\left[\begin{matrix} s/2+(1+\nu)/2,\, (1-\nu)/2-s/2 \\ 1+\nu/2-s/2,\, 1-\nu/2-s/2 \end{matrix}\right],$$
$$\mathrm{Re}\{s\} < 3/2, \;\; -1 < \mathrm{Re}\,\{s+\nu\} < 1 \tag{A.43}$$

$$s_{u,\nu}(x) \to 2^{s/2+u-2}\,\Gamma\left[\frac{u-\nu+1}{2},\, \frac{u+\nu+1}{2}\right]$$
$$\times\Gamma\left[\begin{matrix} s/2+(u+1)/2, (1-u)/2-s/2 \\ 1-\nu/2-s/2,\, 1+\nu/2-s/2 \end{matrix}\right],$$
$$|\mathrm{Re}\{s+u\}| < 1, \mathrm{Re}\{s\} < 3/2 \tag{A.44}$$

$$\exp(-x)\; I_\nu(x) \to \frac{2^{-s}}{\sqrt{\pi}}\,\Gamma\left[\begin{matrix} s+\nu,\, \frac{1}{2}-s \\ 1+\nu-s \end{matrix}\right], \qquad \mathrm{Re}\{\nu\} < \mathrm{Re}\{s\} < 1/2 \tag{A.45}$$

$$\exp(-x)\, K_\nu(x) \to 2^{-s}\sqrt{\pi}\Gamma\left[\begin{matrix} s+\nu,\, s-\nu \\ s+\frac{1}{2} \end{matrix}\right], \qquad |\,\mathrm{Re}\{\nu\}\,| < \mathrm{Re}\{s\} \tag{A.46}$$

$$\exp(x)\,K_\nu(x) \to \frac{2^{-s}\cos(\pi\nu)}{\sqrt{\pi}}\Gamma\left[s+\nu,\, s-\nu,\, \tfrac{1}{2}-s\right],$$
$$|\mathrm{Re}\{\nu\}| < \mathrm{Re}\{s\} < 1/2 \tag{A.47}$$

$$P_n(2x-1)\,U(1-x) \to \Gamma\begin{bmatrix} s,\, s \\ s+n+1,\, s-n \end{bmatrix}, \quad 0 < \mathrm{Re}\{s\} \tag{A.48}$$

$$P_n(2x-1)\,U(x-1) \to \Gamma\begin{bmatrix} -n-s,\, 1+n-s \\ 1-s,\, 1-s \end{bmatrix}, \qquad -n > \mathrm{Re}\{s\} \tag{A.49}$$

$$P_n(x)\,U(1-x) \to \frac{1}{2}\Gamma\begin{bmatrix} s/2,\, s/2+\frac{1}{2} \\ s/2+(1-n)/2,\, s/2+1+n/2 \end{bmatrix}, \quad 0 < \mathrm{Re}\{s\} \tag{A.50}$$

$$P_n(x)\,U(x-1) \to \frac{1}{2}\Gamma\begin{bmatrix} (1+n)/2-s/2,\, -n/2-s/2 \\ 1-s/2,\, \frac{1}{2}-s/2 \end{bmatrix}, \quad -n > \mathrm{Re}\{s\} \tag{A.51}$$

$$(1-x)^{-1/2}\,U(1-x)\,T_n(2x-1) \to \sqrt{\pi}\,\Gamma\begin{bmatrix} s,\, s+\frac{1}{2} \\ s+\frac{1}{2}-n,\, s+\frac{1}{2}+n \end{bmatrix},$$
$$0 < \mathrm{Re}\{s\} \tag{A.52}$$

$$(1-x)^{1/2}\,U(1-x)\,U_n(2x-1) \to \sqrt{\pi}\,\frac{n+1}{2}\,\Gamma\begin{bmatrix} s,\, s-\frac{1}{2} \\ s+\frac{3}{2}+n,\, s-\frac{1}{2}-n \end{bmatrix},$$
$$0 < \mathrm{Re}\{s\} \tag{A.53}$$

$$(x-1)^{1/2}\,U(x-1)\,U_n(2x-1) \to \sqrt{\pi}\,\frac{n+1}{2}\,\Gamma\begin{bmatrix} \frac{3}{2}+n-s,\, -\frac{1}{2}-n-s \\ 1-s,\, \frac{3}{2}-s \end{bmatrix},$$
$$-1/2-n > \mathrm{Re}\{s\} \tag{A.54}$$

$$H_n(x)\exp(-x/2) \to 2^{n-1}\,\Gamma\begin{bmatrix} s/2,\, s/2+\frac{1}{2} \\ s/2+(1-n)/2 \end{bmatrix}, \qquad 0 < \mathrm{Re}\{s\} \tag{A.55}$$

$$L_n^a(x)\,\exp(-x) \to \frac{1}{n!}\,\Gamma\begin{bmatrix} s,\, 1+n+a-s \\ 1+a-s \end{bmatrix}, \qquad 0 < \mathrm{Re}\{s\} \tag{A.56}$$

$$C_n^{\lambda}\left(2x-1\right)U\left(1-x\right)\left(1-x\right)^{\lambda-1/2}\rightarrow\frac{\left(2\lambda\right)_n}{n!}\Gamma\left[\lambda+\tfrac{1}{2}\right]$$
$$\times\Gamma\left[\begin{matrix}s,\ s-\lambda+\frac{1}{2}\\ s+\lambda+n+\frac{1}{2},\ s-\lambda-n+\frac{1}{2}\end{matrix}\right],\quad 0<\mathrm{Re}\left\{s\right\},\ \mathrm{Re}\left\{\lambda\right\}>-1/2 \tag{A.57}$$

$$C_n^{\lambda}\left(2x-1\right)U\left(x-1\right)\left(x-1\right)^{\lambda-1/2}\rightarrow\frac{\left(2\lambda\right)_n}{n!}\Gamma\left[\lambda+\tfrac{1}{2}\right]$$
$$\times\Gamma\left[\begin{matrix}\frac{1}{2}-n-\lambda-s,\ \frac{1}{2}+n+\lambda-s\\ 1-s,\ \lambda+\frac{1}{2}-s\end{matrix}\right],$$
$$1/2-n-\mathrm{Re}\left\{\lambda\right\}>\mathrm{Re}\left\{s\right\},\mathrm{Re}\left\{\lambda\right\}>-1/2 \tag{A.58}$$

$$P_n^{(a,b)}\left(2x-1\right)U\left(1-x\right)\left(1-x\right)^{a}\rightarrow\frac{\Gamma\left[a+n+1\right]}{n!}$$
$$\times\Gamma\left[\begin{matrix}s,\ s-b\\ s+a+n+1,\ s-b-n\end{matrix}\right],\qquad 0<\mathrm{Re}\left\{s\right\},\ \mathrm{Re}\left\{a\right\}>-1 \tag{A.59}$$

$$P_n^{(a,b)}\left(2x-1\right)U\left(x-1\right)\left(x-1\right)^{a}\rightarrow\frac{\Gamma\left[a+n+1\right]}{n!}$$
$$\times\Gamma\left[\begin{matrix}1+n+b-s,\ -a-b-s\\ 1+b-s,\ 1-s\end{matrix}\right],\mathrm{Re}\left\{s\right\}<-n-\mathrm{Re}\left\{a\right\},\mathrm{Re}\left\{a\right\}>-1 \tag{A.60}$$

$$P_{\nu}^{u}\left(2x-1\right)U\left(1-x\right)\left(1-x\right)^{-u/2}\rightarrow\Gamma\left[\begin{matrix}s+u/2,\ s-u/2\\ s+\nu+1-u/2,\ s-\nu-u/2\end{matrix}\right],$$
$$\mathrm{Re}\left\{s\right\}>\left|\mathrm{Re}\left\{u\right\}\right|/2,\ \mathrm{Re}\left\{u\right\}<1 \tag{A.61}$$

$$P_{\nu}^{u}\left(2x-1\right)U\left(x-1\right)\left(x-1\right)^{-u/2}\rightarrow\ \Gamma\left[\begin{matrix}u/2-\nu-s,\ u/2+1+\nu-s\\ 1+u/2-s,\ 1-u/2-s\end{matrix}\right],$$
$$\mathrm{Re}\left\{s\right\}<1+\mathrm{Re}\left\{u/2\right\}+\mathrm{Re}\left\{\nu\right\},\ \mathrm{Re}\left\{s\right\}<\mathrm{Re}\left\{u/2\right\}-\mathrm{Re}\left\{\nu\right\},\ \mathrm{Re}\left\{u\right\}<1 \tag{A.62}$$

$$\left(1+x\right)^{-u/2}Q_{\nu}^{u}\left(1+2x\right)\rightarrow\frac{\exp\left(i\pi u\right)}{2}$$
$$\times\Gamma\left[\begin{matrix}s+u/2,\ s-u/2,\ \nu+1+u/2-s\\ s+\nu+1-u/2\end{matrix}\right],$$
$$\left|\mathrm{Re}\left\{u\right\}\right|/2<\mathrm{Re}\left\{s\right\}<1+\mathrm{Re}\ \left\{\nu+u/2\right\} \tag{A.63}$$

$$ {}_1F_1\left[a;c;-x\right] \rightarrow \Gamma\left[\begin{matrix} c \\ a \end{matrix}\right] \Gamma\left[\begin{matrix} a-s,\, s \\ c-s \end{matrix}\right], \qquad 0 < \mathrm{Re}\left\{s\right\} < \mathrm{Re}\left\{a\right\} \tag{A.64} $$

$$ \exp\left(-x\right) {}_1F_1\left[a;c;x\right] \rightarrow \Gamma\left[\begin{matrix} c \\ c-a \end{matrix}\right] \Gamma\left[\begin{matrix} c-a-s,\, s \\ c-s \end{matrix}\right], $$

$$ 0 < \mathrm{Re}\left\{s\right\} < \mathrm{Re}\left\{c-a\right\} \tag{A.65} $$

$$ \Psi\left[a,c;x\right] \rightarrow \frac{1}{\Gamma\left[a,\, 1+a-c\right]} \Gamma\left[s,\, s+1-c,\, a-s\right], $$

$$ \mathrm{Re}\left\{c-1\right\} < \mathrm{Re}\left\{s\right\} < \mathrm{Re}\left\{a\right\},\, 0 < \mathrm{Re}\left\{s\right\} \tag{A.66} $$

$$ \exp\left(-x\right) \Psi\left[a,c;x\right] \rightarrow \Gamma\left[\begin{matrix} s,\, s+1-c \\ s+a+1-c \end{matrix}\right],\ \mathrm{Re}\left\{c-1\right\} < \mathrm{Re}\left\{s\right\},\, 0 < \mathrm{Re}\left\{s\right\} \tag{A.67} $$

$$ \exp\left(-x/2\right) M_{a,u}\left(x\right) \rightarrow \Gamma\left[\begin{matrix} 2u+1 \\ a+u+\frac{1}{2} \end{matrix}\right] \Gamma\left[\begin{matrix} s+u+\frac{1}{2},\, a-s \\ u+\frac{1}{2}-s \end{matrix}\right], $$

$$ -\mathrm{Re}\left\{u-1/2\right\} < \mathrm{Re}\left\{s\right\} < \mathrm{Re}\left\{a\right\} \tag{A.68} $$

$$ \exp\left(-x/2\right) W_{a,u}\left(x\right) \rightarrow \Gamma\left[\begin{matrix} s+u+\frac{1}{2},\, s+\frac{1}{2}-u \\ s+1-a \end{matrix}\right], \quad \mathrm{Re}\left\{s\right\} < 1/2 + \left|\mathrm{Re}\left\{u\right\}\right| \tag{A.69} $$

$$ \exp\left(x/2\right) W_{a,u}\left(x\right) \rightarrow \frac{1}{\Gamma\left[\frac{1}{2}-u-a,\, \frac{1}{2}+u-a\right]} $$

$$ \times\Gamma\left[s-u+\tfrac{1}{2},\, s+\tfrac{1}{2}+u, -a-s\right],\ -1/4 + \left|\mathrm{Re}\left\{u\right\}\right| < \mathrm{Re}\left\{s\right\} < -\left|\mathrm{Re}\left\{a\right\}\right| \tag{A.70} $$

$$ {}_1F_1\left[a,b;c;-x\right] \rightarrow \Gamma\left[\begin{matrix} c \\ a,\, b \end{matrix}\right] \Gamma\left[\begin{matrix} a-s,\, b-s,\, s \\ c-s \end{matrix}\right], $$

$$ 0 < \mathrm{Re}\left\{s\right\} < \mathrm{Re}\left\{a\right\}, \mathrm{Re}\left\{s\right\} < \mathrm{Re}\left\{b\right\} \tag{A.71} $$

$$ Ai\left(z\right) \rightarrow \frac{3^{s/3}}{6\pi\, 3^{1/6}} \Gamma\left[s/3+\tfrac{1}{3},\, s/3\right], \quad \mathrm{Re}\left\{s\right\} > 0 \tag{A.72} $$

Appendix B

Transcendental Functions

Below are the definitions of functions whose Mellin transforms are given in App. A. If an expression contains gamma functions, it is not valid for arguments that give an infinite result. For functions of the form ${}_2F_1\left[a,b;c,z\right]$ the expression is only valid when $|z|<1$.

Polylogarithm

$$L^n\left(z\right)=\sum_{k=1}^{\infty}\frac{z^k}{k^n}\qquad |z|<1 \tag{B.1}$$

Complete elliptic integral of the second kind

$$E\left(k\right)=\int_0^{\pi/2}d\varphi\sqrt{1-k^2\sin^2\left(\varphi\right)}=\frac{\pi}{2}\,{}_2F_1\left[-\tfrac{1}{2},\tfrac{1}{2};1;k^2\right] \tag{B.2}$$

Elliptic integral of the first kind

$$K\left(k\right)=\int_0^{\pi/2}\frac{d\varphi}{\sqrt{1-k^2\sin^2\left(\varphi\right)}}=\frac{\pi}{2}\,{}_2F_1\left[\tfrac{1}{2},\tfrac{1}{2};1;k^2\right] \tag{B.3}$$

Exponential integral

$$Ei\left(x\right)=\int_{-\infty}^{x}dt\,\frac{\exp\left(t\right)}{t}=-\exp\left(x\right)\Psi\left[1,1;-x\right],\quad x<0 \tag{B.4}$$

Lower Sine integral

$$Si\left(x\right)=\int_0^{x}dt\,\frac{\sin\left(t\right)}{t} \tag{B.5}$$

Upper Sine integral

$$si\left(x\right)=Si\left(x\right)-\frac{\pi}{2}=-\int_x^{\infty}dt\,\frac{\sin\left(t\right)}{t} \tag{B.6}$$

Cosine integral

$$Ci\,(x) = -\int_x^\infty dt\,\frac{\cos\,(t)}{t} \tag{B.7}$$

Error function

$$\mathrm{Erf}\,(x) = \frac{2}{\sqrt{\pi}}\int_x^\infty dt\,\exp\left(-t^2/2\right) = \frac{2x}{\sqrt{\pi}}\,{}_1F_1\left[-\tfrac{1}{2};\tfrac{3}{2};-x^2\right] \tag{B.8}$$

Complementary error function

$$\mathrm{Erfc}\,(x) = 1-\mathrm{Erf}\,(x) = \frac{\exp\,(-x^2)}{\sqrt{\pi}}\,\Psi\left[-\tfrac{1}{2},\tfrac{1}{2};x^2\right] \tag{B.9}$$

Fresnel sine integral

$$S\,(x) = \frac{1}{\sqrt{2\,\pi}}\int_0^x dt\,\frac{\sin\,(t)}{\sqrt{t}} \tag{B.10}$$

Fresnel cosine integral

$$C\,(x) = \frac{1}{\sqrt{2\,\pi}}\int_0^x dt\,\frac{\cos\,(t)}{\sqrt{t}} \tag{B.11}$$

Lower incomplete gamma function

$$\gamma\,[a,\,x] = \frac{x^a}{a}\,{}_1F_1\,[a;a+1;-x]\,,\quad \mathbf{Re}\,\{a\} > 0 \tag{B.12}$$

Upper incomplete gamma function

$$\Gamma\,[a,\,x] = \exp\,(-x)\,\Psi\,[1-a,1-a;x] \tag{B.13}$$

Parabolic cylinder function

$$D_\nu\,(x) = 2^{\nu/2}\exp\left(-z^2/4\right)\Psi\left[-\nu/2,\tfrac{1}{2};z^2/2\right] \tag{B.14}$$

Bessel function of the second kind or Neumann function

$$\begin{aligned} N_\nu\,(z) = &-\frac{1}{\pi}\left(\frac{z}{2}\right)^{-\nu}\Gamma\,[\nu]\,{}_0F_1\left[1-\nu;-z^2/4\right] \\ &-\frac{1}{\pi}\cos\,(\pi\,\nu)\left(\frac{z}{2}\right)^{\nu}\Gamma\,[-\nu]\,{}_0F_1\left[1+\nu;-z^2/4\right] \end{aligned} \tag{B.15}$$

Struve function

$$H_\nu(z) = \frac{2}{\sqrt{\pi}} \left(\frac{2}{z}\right)^{\nu+1} \frac{1}{\Gamma\left[\nu + \frac{3}{2}\right]} {}_1F_2\left[1; \tfrac{3}{2}, \nu + \tfrac{3}{2}; -z^2/4\right] \tag{B.16}$$

Lommel function

$$s_{u,\nu}(z) = \frac{z^{u+1}}{(u-\nu+1)(u+\nu+1)} {}_1F_2\left[1; (u-\nu+3)/2, (u+\nu+3)/2; -z^2/4\right] \tag{B.17}$$

Bessel function of imaginary argument

$$I_\nu(z) = \left(\frac{z}{2}\right)^\nu \frac{1}{\Gamma[\nu+1]} {}_0F_1\left[\nu+1; z^2/4\right] \tag{B.18}$$

Bessel Function of the Third Kind or Macdonald or Kelvin function

$$K_\nu(z) = \frac{1}{2}\left(\frac{z}{2}\right)^\nu \Gamma[-\nu] {}_0F_1\left[\nu+1; z^2/4\right] + \frac{1}{2}\left(\frac{z}{2}\right)^{-\nu} \Gamma[\nu] {}_0F_1\left[1-\nu; z^2/4\right] \tag{B.19}$$

Legendre polynomials

$$P_n(z) = \frac{2^{-n}}{n!}\frac{d^n}{dz^n}\left(z^2-1\right)^n = {}_2F_1\left[-n, 1+n;, 1; \frac{1-z}{2}\right] \tag{B.20}$$

Chebyshev or Tchebcheff polynomial of the first kind

$$T_n(z) = \cos[n \arccos(z)] = {}_2F_1[-n, n; 1/2; (1-z)/2] \tag{B.21}$$

Chebyshev polynomial of the second kind

$$U_n(z) = \frac{\sin[(n+1)\arccos(z)]}{\sqrt{1-z^2}} = (n+1) {}_2F_1[-n, n+2; 3/2; (1-z)/2] \tag{B.22}$$

Hermite polynomials

$$H_n(z) = (-1)^n \exp\left(z^2\right) \frac{d^n}{dz^n} \exp\left(-z^2\right) = 2^{2n} z {}_1F_1\left[(1-n)/2; \tfrac{3}{2}; z^2\right] \tag{B.23}$$

Laguerre polynomials

$$L_n^a(z) = \frac{\exp(z) z^{-a}}{n!}\frac{d^n}{dz^n}\left[\exp(-z) z^{n+a}\right] = \Gamma\left[\begin{matrix} a+n+1 \\ a+1,\ n+1 \end{matrix}\right] {}_1F_1[-n; a+1; z] \tag{B.24}$$

Gegenbauer polynomials

$$C_p^\lambda(z) = \Gamma\left[\begin{matrix} 2\lambda+p \\ 2\lambda,\ p+1 \end{matrix}\right] {}_2F_1\left[-p, p+2\lambda; \lambda+\tfrac{1}{2}; \frac{1-z}{2}\right] \tag{B.25}$$

Jacobi polynomials

$$P_n^{(a,b)}(z) = \Gamma\left[\begin{matrix} a+n+1 \\ a+1,\ n+1 \end{matrix}\right] {}_2F_1\left[-n, n+a+b+1; 1-a; \frac{1-z}{2}\right] \tag{B.26}$$

Associated Legendre function of the first kind

$$P_\nu^u(z) = \left(\frac{z+1}{z-1}\right)^{u/2} \frac{1}{\Gamma[1-u]} {}_2F_1\left[-\nu, 1+\nu; 1-u; \frac{1-z}{2}\right], \ |\arg(z\pm 1)| < \pi \tag{B.27}$$

Associated Legendre function of the second kind

$$\begin{aligned} Q_\nu^u(z) &= 2^{-\nu-1}\,\Gamma\left[\begin{matrix} u+\nu+1 \\ \nu+\frac{3}{2} \end{matrix}\right] \exp(iu\pi)\,\sqrt{\pi}\,z^{-u-\nu-1}\left(z^2-1\right)^{u/2} \\ &= {}_2F_1\left[(u+\nu+1)/2, (u+\nu+2)/2; \nu+3/2; 1/z^2\right], \\ &\qquad |\arg(z\pm 1)| < \pi, \ \ |\arg z| < \pi \end{aligned} \tag{B.28}$$

Tricomi function

$$\Psi[a,c;x] = \Gamma\left[\begin{matrix} 1-c \\ a-c+1 \end{matrix}\right] {}_1F_1[a;c;z] + z^{1-c}\Gamma\left[\begin{matrix} c-1 \\ a \end{matrix}\right] {}_1F_1[a-c+1; 2-c; z] \tag{B.29}$$

Degenerate Whittaker hypergeometric function

$$M_{b,u}(z) = \exp(-z/2)\, z^{u+1/2} = {}_1F_1[1/2-b+u; 2u+1; z] \tag{B.30}$$

Airy function

$$\begin{aligned} Ai(z) &= \frac{1}{\pi}\int_0^\infty dw\, \cos\left(w^3/3 + w\,z\right) = \frac{z^{1/2}}{\pi\sqrt{3}} K_{1/3}\left(2z^{3/2}/3\right) \\ &= \frac{\Gamma\left[\frac{1}{3}\right]}{\pi\ 3^{1/6}} {}_0F_1\left[\tfrac{2}{3}; z^3/9\right] + \frac{\Gamma\left[-\frac{1}{3}\right]}{\pi\ 3^{5/6}}\, z\ {}_0F_1\left[\tfrac{4}{3}; z^3/9\right] \end{aligned} \tag{B.31}$$

Index

Richard J. Sasiela was a member of the Technical Staff at MIT/Lincoln Laboratory from 1969 until his death in March 2007. He received a PhD in Electrophysics from the Polytechnic Institute of Brooklyn. He contributed to improving radar systems and measurements and spent 9 years at the Ronald Reagan radar site in the Marshall Islands. Other interests included signal processing, image recognition, safety systems for airports, and the propagation of optical and radar beams through the turbulence in the atmosphere. His later research interests dealt with amplitude statistics of beam propagation and their effect on optical communications systems.